

DETERMINATION OF TRACE ELEMENTS IN
IRON-MANGANESE OXIDE COATINGS BY LASER
ABLATION ICP-MS FOR ENVIRONMENTAL
MONITORING/MINERAL EXPLORATION

CENTRE FOR NEWFOUNDLAND STUDIES

**TOTAL OF 10 PAGES ONLY
MAY BE XEROXED**

(Without Author's Permission)

SHELDON RICHARD HUELIN



**DETERMINATION OF TRACE ELEMENTS IN IRON-MANGANESE OXIDE
COATINGS BY LASER ABLATION ICP-MS FOR ENVIRONMENTAL
MONITORING/MINERAL EXPLORATION**

By

Sheldon Richard Huelin, B.Sc. (Hons)

*A Thesis Submitted to the School of Graduate Studies
in Partial Fulfilment of the Requirements for the Degree
of Master of Science*

*Environmental Science Programme
Memorial University of Newfoundland*

April, 2005

St. John's

Newfoundland



Library and
Archives Canada

Bibliothèque et
Archives Canada

Published Heritage
Branch

Direction du
Patrimoine de l'édition

0-494-06640-7

395 Wellington Street
Ottawa ON K1A 0N4
Canada

395, rue Wellington
Ottawa ON K1A 0N4
Canada

Your file *Votre référence*

ISBN:

Our file *Notre référence*

ISBN:

NOTICE:

The author has granted a non-exclusive license allowing Library and Archives Canada to reproduce, publish, archive, preserve, conserve, communicate to the public by telecommunication or on the Internet, loan, distribute and sell theses worldwide, for commercial or non-commercial purposes, in microform, paper, electronic and/or any other formats.

The author retains copyright ownership and moral rights in this thesis. Neither the thesis nor substantial extracts from it may be printed or otherwise reproduced without the author's permission.

AVIS:

L'auteur a accordé une licence non exclusive permettant à la Bibliothèque et Archives Canada de reproduire, publier, archiver, sauvegarder, conserver, transmettre au public par télécommunication ou par l'Internet, prêter, distribuer et vendre des thèses partout dans le monde, à des fins commerciales ou autres, sur support microforme, papier, électronique et/ou autres formats.

L'auteur conserve la propriété du droit d'auteur et des droits moraux qui protègent cette thèse. Ni la thèse ni des extraits substantiels de celle-ci ne doivent être imprimés ou autrement reproduits sans son autorisation.

In compliance with the Canadian Privacy Act some supporting forms may have been removed from this thesis.

Conformément à la loi canadienne sur la protection de la vie privée, quelques formulaires secondaires ont été enlevés de cette thèse.

While these forms may be included in the document page count, their removal does not represent any loss of content from the thesis.

Bien que ces formulaires aient inclus dans la pagination, il n'y aura aucun contenu manquant.


Canada

ABSTRACT

Abstract

Iron-manganese oxide coatings can form on a wide range of geologic samples and they have the inherent geochemical ability to adsorb elements and thus potentially act as tools for mineral exploration and environmental monitoring. In this study the concentrations of elements present in Fe-Mn oxide coatings were determined using Laser Ablation-Inductively Coupled Plasma-Mass Spectrometry (LAM-ICP-MS). The potential of Fe-Mn oxide coatings for environmental monitoring was assessed at three study sites located on the island of Newfoundland. Additionally, annual accretion at one study site was also examined to further understand coating accretion as a function of time.

Useful analytical results were obtained using a data normalisation scheme which set the sum of $\text{MnO}_2 + \text{Fe}_2\text{O}_3$ in the coating to 100%. Quantification of an internal standard was investigated using an Electron Microprobe and Scanning Electron Microscope. However this was not successful because of sample heterogeneity and the thinness of the coating. The acquired samples underwent a simple sample preparation procedure, and were analysed using optimised operating conditions.

For the mineral exploration and environmental monitoring aspect of this study, four study locations with a wide range of sample sites were selected; Tilt Cove, Betts Cove, Robinsons River, and Rennies River. Water samples were collected along with the Fe-Mn oxide coatings. The waters were analysed for dissolved oxygen, pH, conductivity,

temperature, and 46 elements using ICP-MS. Multivariate statistics, in the form of Principal Component Factor Analysis (PCFA) was performed on the data. Graphical display of the Factor scores from the PCFA produced sample groupings that were related to both geologic and environmental inputs. For the water PCFA, variable loadings were related to the local geology and environmental conditions along with the affinity of the element. The loading of variables in each Factor for the Fe-Mn oxide coating data was related to the adsorption of the element either on the MnO_2 or Fe_2O_3 phase with most elements except Cr and Cu displaying preferential adsorption to MnO_2 . Elemental Fe-Mn oxide coating concentrations were a function of the elements affinity (chalcophile, lithophile, or siderophile), pH of the environment, stream water concentration, and amount of the two oxide phases present. Even with these complications, LA-ICP-MS analysis of Fe-Mn oxides was able to identify areas of heavy metal pollution and suggest geologic inputs.

Accretion of Fe-Mn oxide coatings was examined on an annual basis by placing artificial substrates (streak plates, cement, and polished pebbles) in Rennie's River, St. John's, Newfoundland at seven sampling sites and allowing the coatings to collect for periods of time from three months to one year with samples acquired every 3 months. Water samples were also collected and measured for most of the same variables as the oxide coatings. For the Fe-Mn oxide coatings, two Factors resulted from the PCFA. A plot of the Factor scores showed four groups of samples based on location, and time of

sampling. Coating concentrations did not match any of the expected trends based on stream chemistry or coating properties. This is explained by a model of coating accretion suggesting that high amounts of Fe_2O_3 and metals coprecipitate for the initial stage of coating formation and greater amounts were adsorbed in the later stages.

ACKNOWLEDGEMENTS

I would first and foremost like to thank my supervisor's, Dr. Derek Wilton and Dr. Henry Longerich for their support, wisdom, and guidance over the past 3 years. Both have been there for me for all the obstacles, trials, and tribulations during my course of study. They have been extremely generous with their time, always making themselves available when I had any questions or concerns. They bestowed upon me a tremendous amount of knowledge and expertise that I will be forever thankful for.

I would also like to thank and acknowledge the following people at the Department of Earth Science, Memorial University of Newfoundland, for their time, expertise, and energy. Mike Tubrett, ICP-MS facility manager, thanks for all of the suggestions throughout this study, and for teaching me about the technique of LA-ICP-MS. Pam King, analytical geochemist, for helping me locate and order lab supplies. Lakmali Hewa, for showing me sample preparation and analysis for the water samples collected in this project and for answering any questions that I had about the ICP-MS. Michael Schaeffer for the electron microprobe work and Lisa Lee for the scanning electron microscope work. Dr. George Jenner for making suggestions during the early stages of this thesis. Thanks to all of the Earth Science Department Faculty and Staff that made the past 3 years a very pleasant and memorable experience.

Dr. Brian Fryer of the Great Lakes Institute for Environmental Research at the University of Windsor for his helpful inputs for the data acquisition and other valuable areas of my thesis.

The Environmental Science Academic Unit have also been a great help over the course of my study. Special thanks go to Dr. Moire Wadleigh and Dr. Niall Gogan for comments and suggestions about this study and the course-work aspect of my Masters. Also, Dr. Leonard Lye is thanked for help in the statistical analysis of the acquired data. I am also thankful to Coasts Under Stress who employed me as a part-time researcher and funded certain parts of my study.

Fellow students in the Earth Science Department that have been there to listen and talk to me which aided in me keeping my sanity at times. These include but are not limited to Michelle Huminicki, Pat Collins, Kehinde Adetona, Ayse Cakiroglu, Susan Strowbridge, Tammy Perry, Glenn Penny, and Carolyn Burr ridge. To friends that I have made in the Field Hall Graduate residence, such as Anas El Aneed, Zhang Lei, and Mike Kelly I thank you also. To all of my friends to all of my friends outside of these areas such as Jayne Simmons, Louis Barry, Desmond Legge, and Trevor Snow, thanks for being there all of the time.

Finally I would like to say that no amount of thanks could show how much my brother, Shawn, and parents, Richard and Lorraine, meant to me over this period of time. Thank you for all of your support and encouragement throughout my Masters degree. Thanks for listening to me and supporting me when I became discouraged.

TABLE OF CONTENTS

Chapter 1: Introduction

1.1 Overview	1-1
1.2 Iron Manganese Oxide Coatings	1-4
1.2.1 Formation	1-5
1.2.2 Adsorption	1-7
1.2.3 Mineral Exploration/Environmental Opportunities	1-8
1.3 Previous Work with Fe-Mn Oxides	1-10
1.3.1 Accretion Rates	1-10
1.3.2 Laser Ablation and Fe-Mn Oxides	1-12
1.4 Location	1-17
1.4.1 Rennies River Water System	1-17
1.4.2 Tilt Cove/Betts Cove Geology	1-19
1.4.2.1 Tilt Cove Mineralization	1-22
1.4.2.2 Tilt Cove Mining	1-23
1.4.2.3 Betts Cove Mineralization	1-25
1.4.2.4 Betts Cove Mining	1-26
1.4.2.5 Acid Mine Drainage at Betts Cove and Tilt Cove	1-25
1.4.3 Robinson's River Study Area	1-29

Chapter 2: Experimental, Field Sampling and Laboratory Procedures

2.1 Annual Accretion	2-1
2.1.1 Annual Accretion Setup	2-1
2.1.2 Water Sampling	2-2
2.1.3 Annual Accretion Study Area	2-3
2.1.4 Substrate Collection	2-6
2.2 Mineral Exploration/Environmental Monitoring	2-7
2.2.1 Study Areas	2-7
2.3 Stream Water Analysis	2-13

2.4 LA-ICP-MS Analysis	2-16
2.4.1 Imaging System and Stage Control	2-17
2.4.2 Laser Setup	2-17
2.4.3 LA-ICP-MS Data Acquisition	2-20

Chapter 3: LA-ICP-MS Quantification and Data Analysis

3.1 LA-ICP-MS Internal Standard	3-1
3.1.1 EM and SEM Analysis	3-1
3.1.2 EM Results	3-2
3.2 LA-ICP-MS Data Reduction	3-6
3.3 LA-ICP-MS Optimization	3-8
3.3.1 Results of LA-ICP-MS Optimization	3-10
3.4 LA-ICP-MS Results	3-12
3.5 Stream Water Results	3-22
3.5.1 Statistical Analysis of Waters Results	3-24
3.6 Statistical Analysis of LA-ICP-MS Data	3-33
3.6.1 PCFA of Fe-Mn Oxide Formation Data	3-41

Chapter 4: Discussion

4.1 Stream Water PCFA	4-1
4.1.1 Water PCFA Factor 1	4-1
4.1.2 Water PCFA Factor 2	4-10
4.1.3 Water PCFA Factor 3	4-13
4.1.4 Water PCFA Factor 4	4-17
4.2 LA-ICP-MS PCFA	4-21
4.2.1 Fe-Mn Oxide Coating PCFA Factor 1	4-21
4.2.2 Fe-Mn Oxide Coating PCFA Factor 2	4-32
4.2.3 Fe-Mn Oxide Coating PCFA Factor 3	4-36

4.3 Fe-Mn Oxide Formation PCFA	4-37
4.3.1 Group 1	4-38
4.3.2 Group 2	4-41
4.3.3 Mature <i>versus</i> Fresh Fe-Mn Oxide Coatings	4-47
4.3.4 Model for Fe-Mn Oxide Formation	4-49
4.3.5 Metal Accumulation at Rennies River	4-52

Chapter 5: Conclusions

5.1 LA-ICP-MS	5-1
5.2 Stream Water Samples	5-1
5.3 Fe-Mn Oxide Coatings	5-2
5.4 Future Work	5-5

References

References	R-1
------------	-----

Appendix 1

A1.1 Electron Microprobe Data	A1-1
A1.2 LA-ICP-MS Optimization	A1-9

Appendix 2

A2.1 Stream Water Results for Elements	A2-1
A2.2 Stream Water Results for pH, dissolved oxygen, conductivity	A2-29

Appendix 3

A3 Stream Water Box Plots and Scatter Plots

A3-1

Appendix 4

A4 LA-ICP-MS Intensity (cps) Values

A4-1

Appendix 5

A5 Fe-Mn Oxide Coating Concentrations

A5-1

Appendix 6

A6 Fe-Mn Oxide Coating Box Plots and Scatter Plots

A6-1

LIST OF TABLES

Table 1.1 Element affinities for Fe-oxide and Mn-oxide.	1-8
Table 2.1 HP4500+ quadrupole ICP-MS operating conditions for water analysis.	2-14
Table 2.2 Incident power of different beam constrictor diameters.	2-18
Table 2.3 LA-ICP-MS operating condition.	2-21
Table 3.1 Calculated means (avg), standard deviations (std), and relative standard deviations (rsd) of elemental concentrations for traverses done on a streak plate, polished pebble, cement sphere, and pebble collected from site S2 in May, 2002.	3-4
Table 3.2 Calculated means (avg), standard deviations (std), and relative standard deviations (rsd) of elemental concentrations (ppm) determined by LA-ICP-MS for traverses done on TCS 13.1.2 (* = Concentration in %).	3-11
Table 3.3 Element concentrations (wt%) determined by SEM for three analyses of TCPS 3.1.1-3.2.2.	3-14
Table 3.4 Pearson-R correlation coefficients and associated p-values (bottom of cell) for MR14B08 analysis and MR14B09 analysis.	3-16
Table 3.5 Median values of concentrations determined by LA-ICP-MS for streak plates placed in the Rennies River study area at sites SJS1, SJS6A, and SJS6B for 3, 6, 9, and 12 months.	3-18
Table 3.6 Means(wt%), standard deviations, and relative standard deviations determined on a 60-point traverse of a streak plate by electron microprobe.	3-19
Table 3.7 Factor loadings and eigenvalues obtained from unrotated PCFA for log-transformed element concentrations in water samples.	3-33
Table 3.8 Elements, along with their main oxidation state in the environment, and ionic radius, that were initially tried in the PCFA.	3-39
Table 3.9 Factor loadings and eigenvalues obtained from unrotated PCA for log-transformed element concentrations in pebble samples.	3-40

Table 3.10 Factor loadings and eigenvalues from unrotated PCFA for log-transformed element concentrations in the coatings that formed on the artificial substrates. 3-44

Table 4.1 Elements that loaded high in Fe-Mn oxide coating Factor 1 along with their common oxidation state in the environment and ionic radius. 4-27

Table 4.2 Elements that loaded high in Factor 2 along with their common oxidation state in the environment and ionic radius. 4-33

Table 4.3 Pearson's-R correlation coefficients between elements that loaded high in Fe-Mn oxide Factor 2 and the MnO_2 and Fe_2O_3 phases of Fe-Mn oxide coatings. 4-35

Table 4.4 Elements that loaded high in Factor 1 and Factor 2 for the annual accretion samples along with their common oxidation state in the environment, ionic radius and affinity. 4-39

Table 4.5 Pearson's-R correlation coefficients calculated between elements in Factor 1 and Factor 2 of the artificial substrate PCFA and MnO_2 and Fe_2O_3 . 4-48

Table 4.6 Element concentrations determined by LA-ICP-MS in Fe-Mn oxide coatings present on pebbles collected from the streambed and artificial substrates located at site SWS1 in Rennies River, St. John's, NL. 4-50

Table 4.7 Pearson-R correlation coefficients between analyte water and Fe-Mn oxide coating concentrations for samples taken from all sites in Rennies River. 4-51

LIST OF FIGURES

Figure 1.1 Map of Newfoundland showing study areas	1-34
Figure 1.2 Geologic map of the St. John's study area.	1-35
Figure 1.3 Geologic map of the Tilt Cove study area.	1-36
Figure 1.4 Geologic map of the Betts Cove study area.	1-37
Figure 1.5 Geologic map of the Robinsons River study area.	1-38
Figure 1.6 Bay St. George sub-basin stratigraphic column with thickness of each Formation in metres.	1-39
Figure 2.1 Map of the St. John's study area showing sampling locations.	2-24
Figure 2.2 Map of the Tilt Cove study area showing sampling locations.	2-25
Figure 2.3 Map of the Betts Cove study area showing sampling locations.	2-26
Figure 2.4 Map of the Robinsons River study area showing sampling locations.	2-27
Figure 2.5 LA-ICP-MS schematic.	2-28
Figure 3.1 Electron microprobe schematic.	3-45
Figure 3.2 Photographs of iron-manganese oxide coatings present on a pebble taken from the streambed at (a) site SJS2 and (b) site SJS6A.	3-46
Figure 3.3 Results for the LA-ICP-MS optimisation run with analyses 1-4 done at a focal height of 200 μm and analyses 4-8 done at a focal height of 400 μm for (a) Al_2O_3 and SiO_2 and (b) Cd, Ba, La, and Pb.	3-47
Figure 3.4(a) TCPS 8.1.2 and (b) TCPS 8.2.1 intensity (cps) vs. time (s) plot for Al, Si, Mn, and Fe determined by LA-ICP-MS.	3-48
Figure 3.5 Normality plot for intensity values of (a) ^{62}Ni (cps) and (b) log transformed values of ^{62}Ni (cps).	3-49

Figure 3.6 Scatter plots for analysis (a) MR14B08, sample TCPS 8.1.2, and (b) MR14B09, sample TCPS 8.2.1 for the analytes ^{27}Al , ^{29}Si , ^{55}Mn , and ^{57}Fe determined by LA-ICP-MS. 3-50

Figure 3.7 Intensity (cps) vs. time (s) plots for the streak plate substrate taken from site SJS6A at; (a) three months, (b) six months, (c) nine months, and (d) twelve months for the elements ^{27}Al , ^{29}Si , ^{55}Mn , and ^{57}Fe determined by LA-ICP-MS. 3-51

Figure 3.8 Photographs of iron-manganese oxide coatings present on a streak plate substrate taken from site SJS6A at; (a) three months, (b) six months, (c) nine months, and (d) twelve months. 3-52

Figure 3.9 Photographs of iron-manganese oxide coatings present on a streak plate substrate taken from site SJS6A after; (a) six months, (b) nine months, and site SJS6B after (c) six months, and, (d) nine months. 3-53

Figure 3.10(a) Scree plot obtained from PCFA of elements in water samples from all four study areas; (b) plot of Factor 1 vs. Factor 2 that were obtained from PCFA of elements in water samples. 3-54

Figure 3.11 Normality plot for (a) Ag (ppm) and (b) log transformed Ag (ppm). 3-55

Figure 3.12(a) Scree plot obtained from PCFA of elements in Fe-Mn oxide coating samples from all four study areas; (b) plot of Factor 3 vs. Factor 1 and Factor 2 vs. Factor 1 that were obtained from PCFA of elements in Fe-Mn oxide coatings. 3-56

Figure 3.13 Normality plot for (a) Pb (ppm) and (b) log transformed values of Pb (ppb) for LA-ICP-MS analysis of Fe-Mn oxide coating samples on annual accretion samples collected from Rennies River. 3-57

Figure 3.14 (a) Scree plot and (b) plot of Factor 1 vs. Factor 2; both obtained from PCFA of elements in Fe-Mn oxide coatings that formed on the substrates placed in Rennies River. 3-58

Figure 4.1(a) Plot of log concentration (ppb) of Co, Cu, Zn, and Cd, and pH values in water samples from the Tilt Cove sampling sites; (b) photograph of the Tilt Cove study area outlining sampling sites. 4-54

Figure 4.2(a) Plot of log concentration (ppb) of Co, Cu, Zn, and Cd, and pH values of water samples from the Betts Cove sampling sites; (b) photograph of the Betts Cove polluted study area outlining the polluted sampling sites. 4-55

Figure 4.3 Plot of log concentration (ppb) of Li, Mg, Ca, Mn, Fe, and Cs, and conductivity (mS/cm) for water samples from the (a) Tilt Cove and (b) Betts Cove study areas. 4-56

Figure 4.4(a) Sampling site SJWS1 located in Nagles Hill Brook, and (b) site SJWS6B at the outlet of Kelly's Brook. 4-57

Figure 4.5 Plot of log concentration (ppb) of Al and Ni, pH and dissolved oxygen (mg/L) readings for the (a) Betts Cove and (b) Tilt Cove study areas. 4-58

Figure 4.6 Plot of log concentration (ppb) of Rb and Ba, and pH readings for the (a) Tilt Cove and (b) Betts Cove study areas. 4-59

Figure 4.7 Plot of log concentration (ppb) of As and Ce, and pH readings for the (a) Tilt Cove (b) Betts Cove study areas. 4-60

Figure 4.8 Plot of (a) log dissolved oxygen (mg/l) values and (b) log U (ppb) vs. sampling site for all study areas. 4-61

Figure 4.9 Plot of log transformed concentrations from water samples (ppb, solid line) and Fe-Mn oxide coatings (ppm, dashed line) for (a) Sr and Ba and (b) La and Ce from the Tilt Cove study area. 4-62

Figure 4.10 Plot of log transformed concentrations from water samples (ppb, solid line) and Fe-Mn oxide coatings (ppm, dashed line) for (a) Sr and Ba and (b) La, Ce, and Y from the Betts Cove study area. 4-63

Figure 4.11 Plot of log transformed concentrations from water samples (ppb, solid line) and Fe-Mn oxide coatings (ppm, dashed line) for (a) iron along with pH and dissolved oxygen readings (mg/L) and (b) chromium, copper, and pH(mg/L) for the Tilt Cove study area. 4-64

Figure 4.12 Plot of log transformed concentrations from water samples (ppb, solid line) and Fe-Mn oxide coatings (ppm, dashed line) for (a) iron, pH, and dissolved oxygen (mg/L), and (b) chromium, copper, and pH levels from Betts Cove. 4-65

Figure 4.13 Plot of log transformed concentrations of (a) Fe_2O_3 (wt%) and (b) Cu (ppm) on Fe-Mn oxide coatings present on stream pebbles collected from Rennies River at three month intervals from March 2002 to March 2003. 4-66

Figure 4.14 Plot of log transformed concentrations from water samples (ppb, solid line) and Fe-Mn oxide coatings (ppm, dashed line) for Co, Ni, and pH levels from (a) Tilt Cove, and (b) Betts Cove. 4-67

Figure 4.15 Plot of log transformed concentrations from water samples (ppb, solid line) and Fe-Mn oxide coatings (ppm, dashed line) for Zn, Cd, and pH levels from (a) Tilt Cove, and (b) Betts Cove. 4-68

Figure 4.16 Plot of log transformed concentrations from water samples (ppb, solid line) and Fe-Mn oxide coatings (ppm, dashed line) for As and pH levels from (a) Tilt Cove, and (b) Betts Cove. 4-69

Figure 4.17 Plot of log transformed concentrations of Co, Ni, Zn, As, Cd (ppm) and MnO_2 (wt%) in Fe-Mn oxide coatings from (a) Tilt Cove and (b) Betts Cove. 4-70

Figure 4.18 Plot of log transformed concentrations from Fe-Mn oxide coating samples (a) Ba, Th (ppm), and MnO_2 (wt%) from Tilt Cove and (b) Sr, Th (ppm), and MnO_2 (wt%) from Rennies River. 4-71

Figure 4.19(a) Plot of Ni(ppm) and (b) Ba(ppm) concentrations for Fe-Mn oxide coatings on artificial substrates taken from Rennies River from March 2002 to March 2003 at three month intervals. 4-72

Figure 4.20(a) Boxplot of Fe_2O_3 concentrations (wt%) for Fe-Mn oxide coatings on artificial substrates, (b) Plot of Fe_2O_3 concentrations for (wt%) samples taken from SJPS6B vs. time 4-73

Figure 4.21(a) Plot of Cr concentrations (ppm) and (b) plot of Th concentrations (ppm) for Fe-Mn oxide coatings on artificial substrates taken from SJPS6B at three month intervals over a 12 month period. 4-74

Figure 4.22(a) Plot of MnO_2 concentrations (wt%) for Fe-Mn oxide coatings on artificial substrates taken from SJPS1 for a 12 month period; (b) plot of MnO_2 concentrations (wt%) for samples taken from SJPS6A. 4-75

Figure 4.23(a) Boxplot of log V (ppm) vs. month and (b) log Pb (ppm) vs. month for artificial substrate samples taken from Rennies River over a 1-year period from March, 2002, to March, 2003. 4-76

Figure 4.24(a) Scatter plot of log MnO₂ (wt%) vs. log Ba (ppm) and (b) log MnO₂ (wt%) vs. log Sr(ppm) for artificial substrate samples taken from Rennies River over a 1-year period from March, 2002, to March, 2003. 4-77

Figure 4.25 Intensity (cps) vs. time (s) plots for the cement substrate taken from site SJS1 at; (a) three months, (b) six months, (c) nine months, and (d) twelve months for the elements ²⁷Al, ²⁹Si, ⁵⁵Mn, and ⁵⁷Fe determined by LA-ICP-MS. 4-78

Figure 4.26 Photographs of iron-manganese oxide coatings present on a cement substrate taken from site SJS6A after 3 months of coating accretion (a) before and (b) after LA-ICP-MS analysis; and from site SJS1 after 6 months of coating accretion (c) before and (d) after LA-ICP-MS analysis. 4-79

Figure 4.27 Intensity (cps) vs. time (s) plots for the streak plate taken from site SJS1 after three months analyzed by LA-ICP-MS for (a) ²⁷Al, ²⁹Si, ⁵⁵Mn, and ⁵⁷Fe, (b) ⁴⁷Ti, ⁵¹V, ⁵³Cr, ⁶²Ni, ⁶⁵Cu, (c) ⁶⁷Zn, ⁸⁶Sr, ⁸⁹Y, ¹³⁷Ba, ¹⁴⁰Ce, (d) ²⁰⁸Pb, ²⁰⁹Bi, ²³²Th, and ²³⁸U. 4-80

Figure 4.28 Intensity (cps) vs. time (s) plots for the cement substrate taken from site SJS1 after three months analyzed by LA-ICP-MS for (a) ²⁷Al, ²⁹Si, ⁵⁵Mn, and ⁵⁷Fe, (b) ⁴⁷Ti, ⁵¹V, ⁵³Cr, ⁶²Ni, ⁶⁵Cu, (c) ⁶⁷Zn, ⁸⁶Sr, ⁸⁹Y, ¹³⁷Ba, ¹⁴⁰Ce, (d) ²⁰⁸Pb, ²⁰⁹Bi, ²³²Th, and ²³⁸U. 4-81

Figure 4.29 Plot of (a) log temperature (°C), (b) log dissolved oxygen (mg/L) and (c) log pH vs. time for water samples taken from Rennies River over a 1-year period from March, 2002, to March, 2003. 4-82

Figure 4.30 Artificial substrate samples along with pebbles (located on upper right of glass dish) taken from Rennies River at sites (a) SJS1 and (b) SJS6A at three month intervals from March 2002 to March 2003. 4-83

Figure 4.31 Diagram modified from Robinson (1981) that illustrates the proposed model for trace metal scavenging by Fe-Mn oxides in a stream. 4-84

1. Introduction

1.1 Overview

The major goal of mineral exploration is to determine anomalous concentrations (*i.e.* concentrations above background levels) of elements in geologic materials that suggest the presence of mineralization. Environmental monitoring is also concerned with anomalous concentrations, and geologic media may also be used to trace sources of pollution. In freshwater fluvial systems, iron-manganese (Fe-Mn) oxide coatings on stream pebbles have the potential to act as both a mineral exploration and environmental monitoring tool.

Iron-manganese oxides are recognized in ocean environments as important scavengers of heavy metals (Gadde and Laitinen, 1974). Their role in freshwater environments seems to be equally important as they occur on a variety of geologic materials. These coatings have a strong affinity for many elements over a wide range of pH, acting like “sponges” for the trapping of heavy metals (Thompson *et al.*, 1992). They have large surface areas that enhance their scavenging abilities (Blaistrieri and Chao, 1990). Fe-Mn oxide coatings can elucidate the major and trace metal distribution of a particular stream, which in turn can be related to local geology and environmental inputs (Robinson, 1981).

For pebble coatings to be useful tools for heavy metal monitoring in fluvial systems, however, high quality analysis of their metal contents is required. In the past, partial digestion of the coatings has most often been used (Carpenter and Hayes, 1978;

Cerling and Turner, 1982; Dong *et al.*, 2001, 2002; Gulson *et al.*, 1992; Robinson, 1984). Procedures for partial dissolution, however, have associated problems such as being time consuming. For example, in the procedure reported by Carpenter *et al.* (1978), the authors used a two-step digestion procedure that involved placing the pebbles in unheated hydroxylamine hydrochloride for two hours to dissolve the Mn component of the Fe-Mn oxide and then placing the pebbles in heated HCl for 2 hours to remove the Fe-component. Other problems encountered with partial digestion involve leaching of the substrate and high detection limits for some elements (Thompson *et al.*, 1992). Because of these difficulties, analysis using microanalytical tools such as Laser Ablation-Inductively Coupled-Mass Spectrometry (LA-ICP-MS) has also been used. This is a low cost, rapid technique with simple sample preparation and low detection limits that has been used in the analysis of a variety of geologic samples (Günther *et al.*, 2000). Previous work by Coish (1993, 2000), Hale *et al.* (1984), and Thompson *et al.* (1992), suggested that laser ablation of Fe-Mn oxide coatings could be a viable technique for detecting either mineralized areas or the release of various pollutants into a stream environment. They concluded however that future studies required the determination of the actual concentrations of elements as opposed to relative values in the coatings.

There are still many aspects of Fe-Mn oxide coatings that need to be understood before their analysis becomes a routine analytical tool, ranging from adsorption mechanisms to fundamental mineralogy. One of the most important areas requiring further study is annual accretion, since reports are in serious contradiction. Carpenter and

Hayes (1978, 1980) found that coatings formed in just 36 days on ceramic plates, and within a year, levels of metals on the plates were one third of that of surrounding rocks, thus suggesting at least a yearly formation. Carpenter *et al.* (1975) empirically observed that in the winter months, coating formation decreased with decreases in pH and dissolved oxygen, suggesting the possibility of seasonal dissolution and reformation of the coatings. Consequently, the coatings could reflect either long term or short term stream conditions. This is very important especially for environmental monitoring where past contamination events may be erased by dissolution. There have been only two studies carried out using Fe-Mn oxide coatings on stream pebbles as environmental monitors (Coish, 1993, 2000), whereas there have been a multitude of studies using these coatings as mineral exploration tools. Clearly, more development work is needed.

There were three main objectives to this study. The first objective was to determine the concentrations of elements present in Fe-Mn oxide coatings by LAM-ICP-MS while optimising conditions for analysis. Secondly, annual accretion would be examined to determine the time frame of coating accretion. Finally, the role of Fe-Mn oxide coatings as environmental monitors would be assessed at three study sites located on the island of Newfoundland.

1.2 Iron Manganese Oxide Coatings

Iron-manganese oxide coatings form as thin (< 1 mm thick), layered structures on fluvial geologic material ranging from silt to boulders (Nowlan, 1976). These coatings have two distinct phases, a Mn-oxide (black) and a Fe-oxide (red) phase with the colour of a coating related to the relative amounts of the two oxides present (Whitney, 1975). Coatings with similar quantities of both oxides appear reddish-black.

The actual coating consists of accumulated iron-manganese oxide layers. These are usually amorphous but some may have a low degree of crystallinity containing the phases goethite ($\text{FeO}(\text{OH})$), birnessite ($\text{Na}_4\text{Mn}_{14}\text{O}_{27} \cdot 9 \text{H}_2\text{O}$), and todorokite ($(\text{Mn}, \text{Mg}, \text{Ca}, \text{Ba}, \text{K}, \text{Na})_2\text{Mn}_3\text{O}_{12} \cdot \text{H}_2\text{O}$) (Chao, 1984). As coatings age, the degree of crystallinity increases (Förstner and Wittman, 1979). Iron-manganese oxide coatings also contain trapped organic material, silt, clay, and absorbed water. Particular attention has been paid to the organic material, which is very complex due to its humic nature, as it can scavenge metals from solutions (Robinson, 1984).

Living organisms can also be present on these coatings. These include photosynthetic organisms, microbes, and epifauna such as larvae and crustaceae which have a chemical affect on coating formation (Filipek *et al.*, 1981). For example, the photosynthesizers are able to induce an increase in pH and redox potential near the rock surface by removing carbon dioxide and adding oxygen, which then aids in the precipitation of Mn and Fe oxides on the pebbles.

1.2.1 Formation

The formation of Fe-Mn oxide coatings begins with natural or anthropogenic iron and manganese ions entering the aquatic system through both ground and surface water (Förstner and Wittmann, 1979). Natural sources may be from the weathering of primary and secondary minerals whereas anthropogenic sources can involve drainage sources such as mine tailings, debris eroded from mine dumps, and runoff from urban areas (Chao, 1984). One mechanism for coating formation begins with Mn and Fe in groundwater as the reduced states Mn (II) and Fe (II). When they enter an oxygenated aquatic environment (neutral to alkaline pH), Fe (II) and Mn (II) are oxidized to less soluble $\text{Fe}_2\text{O}_3 \cdot (\text{H}_2\text{O})_x$ and MnO_x , which then precipitates on the streambed material. The coatings will continue to form as long as there is sufficient oxygen, iron, and manganese flowing toward the coating (Robinson, 1981).

One of the most important variables which controls the formation of these coatings is pH. Minimum pH values have been determined for the precipitation of iron and manganese oxides. Brown ferric hydroxide precipitates from water at pH values of 4.5 and at higher pH if the aerated waters contain concentrations of Fe greater than 0.01 ppm (Theobald *et al.*, 1963). Manganese hydroxide precipitates when the pH exceeds approximately 8. It is also important that the oxidation process of Fe^{2+} to Fe^{3+} takes a few hours at pH = 5, but at pH = 7, it takes only a few minutes. Oxidation rates of both iron and manganese increase by a factor of 100 for each pH unit increase, with manganese requiring a much higher pH for equivalent rates of oxidation (Morgan and Stumm, 1964).

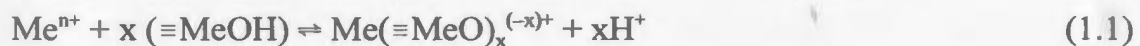
Regionally, coating formation is favoured in humid temperate-to-tropical environments where chemical weathering is most intense, where there is porous or permeable rock or overburden, and where there is widespread seepage of groundwater from springs (Carpenter and Hayes, 1979). They may be absent in areas with sluggish drainage such as swamps and marshes, due to the low dissolved oxygen contents and higher acidities (Carpenter and Hayes, 1979). Locally, formation is favoured in moderate to swift flowing shallow portions of streams, probably since the water is well oxygenated (Whitney, 1975). Deposits are also best developed on boulders and pebbles, and not on the sand and silt (Carpenter *et al.*, 1975). One possible reason for this is that pebbles and boulders are more stationary in the swift flowing areas where coating formation is favoured, whereas the sand and silt fractions can be easily transported.

Some of the most favourable sites of formation for Fe-Mn coatings include areas where the neutralization of acidic waters takes place, such as acid mine drainage, the confluence of rivers with different pH values, the surface of carbonate minerals such as calcite where there is a microzone of higher pH, and in the mixing zones of acid river water with basic seawater. The latter was shown in a study of the Mullica River by Coonley *et al.* (1971). When water from the upper reaches of this system was mixed in a bottle with water from the bay, a brown precipitate settled out within a few minutes. This was probably due to an increase in both ionic strength and pH.

1.2.2 Adsorption

Upon arrival in the stream, metals can be absorbed and partitioned into either organic or inorganic phases, depending on the chemical and geologic setting, with iron-manganese oxide coatings being the important inorganic phases. Oxide coatings have strong affinities for most elements over a range of pH, acting as “sponges” for the trapping of heavy metals (Thompson *et al.*, 1992). The actual scavenging of heavy metals by the oxide coatings occurs through several mechanisms: (1) coprecipitation, (2) adsorption, (3) surface complex formation, (4) ion exchange, and (5) penetration of the crystal lattice (Chao and Theobald, 1976). Coprecipitation can occur under certain conditions where the Fe and Mn oxides are precipitated from solution along with other metals. Mechanisms (2)-(5) are closely interrelated.

The actual physio-chemical process of the above-mentioned mechanisms involves protons being lost or acquired by the iron-manganese oxides, resulting in a positive or negative surface whereby cations and anions are attracted and scavenged from solution (Thompson *et al.*, 1992). It is shown by the following reaction (Chao and Theobald, 1976):



In the equation, Me is the metal ion to be adsorbed, ($\equiv\text{MeOH}$) and ($\equiv\text{MeO}$) are the oxide surface sites. This model explains the pH dependence of the adsorption of metal

ions and that the amount adsorbed is found to increase with pH (Loganathan and Burau, 1973).

The scavenging abilities of iron and manganese ions are not equal (Förstner and Wittman, 1979). Generally, manganese oxides have a greater ability to adsorb metals than iron-oxides from solution although a few elements are adsorbed better by the Fe-rich part of the coating (Rose *et al.*, 1985). Also, each oxide phase shows preferential adsorption of different elements, as shown in Table 1.1.

Table 1.1 Element affinities for Fe-oxide and Mn-oxide (Rose *et al.*, 1979).

	Mn-oxides	Fe-oxides
Greatest	Cu ²⁺	Pb ²⁺
	Co ²⁺	Cu ²⁺
	Mn ²⁺	Zn ²⁺
	Zn ²⁺	Ni ²⁺
	Ni ²⁺	Cd ²⁺
	Ba ²⁺	Co ²⁺
	Sr ²⁺	Sr ²⁺
	Ca ²⁺	Mn ²⁺
Least	Mg ²⁺	

1.2.3 Mineral Exploration/Environmental Opportunities

What makes Fe-Mn oxide coatings such excellent geochemical and environmental monitors is that they are able to accurately represent stream chemistry (Robinson, 1981). For example, if the concentration of a particular element is high in the stream, then it will likewise be elevated in the coating. This in turn relates to the local geology and/or sources of pollution. Iron-manganese oxide coatings have the ability to

provide an accurate metal history for a stream environment. Also, the coatings concentrate metals which leads to analytical advantages when compared to taking stream water samples where many trace metals could potentially be below detection limit. It has been estimated that the metal composition of approximately 1 km² of land area can be adequately represented by only 1 µg of pebble coating (Hale *et al.*, 1984).

Iron and manganese oxides on different media have been employed in soil and stream sediment surveys in the past (Gulson *et al.*, 1992). They have been applied to such things as the exploration for porphyry copper, base metal, and gold deposits. Iron-manganese oxide coatings on stream pebbles offer several advantages over other media types. Traditionally the fine fraction of sediment (minus 80 or minus 100 mesh) has been used (Whitney, 1975). This offers the advantage of having easily measurable quantities of metals for a small sample, but it has several disadvantages. Difficulties include obtaining samples from swift flowing streams, especially those with little or no sediment and the loss of substantial amounts of fines during sampling. But, the greatest problem is obtaining reproducible samples from a site. This may be due to size and density sorting of the fines in the stream because during intense periods of precipitation, when stream discharge increases, there can be a redistribution of existing fines and/or the addition of new material which changes the sample composition (Carpenter *et al.*, 1975). On the other hand, stream pebbles do not have these problems. It has also been suggested that pebbles are also considered to be more sensitive to mineralization than the minus 80-mesh fraction (Carpenter *et al.*, 1978).

1.3 Previous Work with Fe-Mn Oxides

The use of iron and manganese oxides as environmental and geochemical monitors has been reviewed in several reports and studies over the last thirty years, in which some important aspects have been studied (Carpenter *et al.*, 1975, 1978; Carpenter and Hayes, 1978, 1980; Cerling and Turner, 1982; Coish, 1993, 2000; Filipek *et al.*, 1981; Robinson, 1981; Hale *et al.*, 1984; Thompson *et al.*, 1992). The features of the studies that are of most relevance to this report are accretion rates and laser ablation analysis.

1.3.1 Accretion Rates

A study by Carpenter *et al.* (1975) based on empirical observations in the southeastern United States suggested that there were seasonal differences in the formation of coatings. They noticed periods of active growth from April to November, whereas during the winter months there was a decline in the thickness and abundance of coatings present on the streambed material. Some of the boulders below the air-water interface showed an absence of coatings, probably due to anoxic conditions induced by deciduous leaves that clogged the streams. Establishment of anoxic conditions often begins with dissolved oxygen being consumed by decaying leaves which leads to a decrease in pH and Eh. It has been shown in low pH environments that there is no metal adsorption by the oxides and conversely various elements are released (Drever, 1988). Another possible reason for lack of coatings is that there is a decrease in CO₂ production

in the upper horizon soils, therefore chemical weathering by carbonic acids will be decreased resulting in lower concentrations of Fe, Mn, and other metals in the water (Carpenter *et al.*, 1975).

Accretion rates were also studied in Georgia (Carpenter and Hayes, 1978, 1980) and in Tennessee (Cerling and Turner, 1982). Carpenter and Hayes (1978) examined Fe-Mn oxide formation rates in the Magruder mine area in Lincoln County, Georgia. Here there was a pronounced Cu-Zn-Pb sediment anomaly due to weathering of mineralized areas and from contamination by mill tailings and smelter slags. The authors placed streak plates (commonly used in mineralogical tests) on concrete construction blocks in pools of the stream at depths of 0.3-0.5 m at sites upstream and downstream of the Magruder mine. When they were detached from the blocks 36 days later, most of them had a brownish-black precipitate. The coatings on the plates were then dissolved with HCl and the resulting solution was analysed for Mn, Fe, Cu, Zn, and Pb using atomic absorption spectrometry (AAS). The accreted coatings had considerably higher concentrations of Mn and Fe than Cu, Zn, and Pb indicating the presence of mineralization within a 36-day period.

Another study by Carpenter and Hayes (1980) looked at annual accretion rates of Fe-Mn oxides on streak plates in Turkey Creek, Georgia. All of the plates were removed from the stream at weekly to biweekly intervals for a period of one year. Pebbles were also obtained to compare amounts of metals on the pebbles with amounts on the plates. For both the pebbles and the plates, the Mn-rich component was removed with hydroxyl-

amine hydrochloride solution and the Fe-rich portion was removed with 3% oxalic acid. Both solutions were analysed for Mn, Fe, Co, Zn, Cu, and Ni. Results showed that isolated spots formed in just a few weeks enlarged, darkened, and coalesced with time until a continuous black film formed after 5-7 months. Results indicated that for most samples, the metal/Fe or Mn ratios of coatings on the plates matched or were similar to pebbles found in the stream. It was also observed that there was three times as much metal per unit area on the rock coating than on the plates.

Another study by Cerling and Turner (1982) looked at formation of Fe-Mn coatings on gravel and glass plates in White Oak Creek, a small watershed in eastern Tennessee. In this study, heavy plate glass (15 x 15 x 0.5 cm) was placed in the stream at eight locations for approximately three months. Sequential extractions were performed on the plates that were covered by coatings and it was found that Mn:Fe ratios of the coatings were not simply related to Mn:Fe ratios in the water. Of the eight locations, only two had Fe-Mn oxide coatings, one showed loss of Fe-Mn rich coatings by dissolution, and the remaining results suggested the importance of abrasion.

1.3.2 Laser Ablation and Fe-Mn Oxides

There have been a variety of studies on the interaction of metals with iron-manganese oxide coatings on fluvial sediment, such as adsorption of metals (Robinson, 1981), partitioning of metals (Carpenter *et al.*, 1978; Filipek *et al.*, 1981), and the application of coatings for stream sediment geochemical surveys (Carpenter *et al.*,

1975). As previously mentioned, stream pebbles were found to be the most suitable media for geochemical surveys and environmental monitoring, thus studies that used stream sediment may be superseded by a better technique. Another negative aspect of the earlier studies is that they involved dissolution or chemical leaching. Dissolution procedures for oxide coatings are often unsuitable for the determination of certain elements such as As (Hale *et al.*, 1984). Chemical leaching can discriminate chemically active phases, but it may also leach elements from the substrate as well as from the coating (Thompson *et al.*, 1992). This technique is also limited to elements that can be maintained in the leachate solution. Furthermore, separation of the coating from the substrate for preparation of a powder for total analysis is extremely difficult. The partial digestion procedures are typically time consuming and labour intensive, with many steps in the procedure which are vulnerable to contamination.

To avoid these problems, analysis of Fe-Mn oxide coatings can be carried out using Laser Ablation Microprobe-Inductively Coupled Plasma-Mass Spectrometry (LA-ICP-MS). The process begins with the laser ablating a portion of the coating on a pebble with the ablated material being carried to the ICP-MS where a wide range of isotopes can be determined. With this technique, there is minimal sample preparation, a potential spatial resolution of less than 5 μm , and a dry plasma that offers reduced spectral interferences (Veinott, 2001). This technique also offers detection limits of 1 ppb for some elements with the possibility of lower detection limits when large volume pits and a more limited set of elements are used (Longerich, 2001).

There has been some work completed with iron-manganese oxide coatings of stream pebbles using laser ablation systems. Hale *et al.* (1984) used a Laser Ablation-Inductively Coupled Plasma-Emission Spectrometer (LA-ICP-ES) for analysis of 1 cm diameter pebbles from the Allen drainage basin, in Southwest England. Samples were collected in the active courses of the streams at 200-250 m intervals throughout the drainage basin. One pebble per site was examined along with 30-40 g of fine sediment. The samples were analysed for Fe, Zn, Mn, Pb, V, and As. Results obtained from laser ablation closely matched those of selective leaching of the coatings and it was concluded that this technique was suitable for geochemical surveys.

Thompson *et al.* (1992) used a Laser Ablation-Inductively Coupled Plasma-Atomic Emission Spectrometer (LA-ICP-AES) for analysis of stream pebbles (0.5-1.0 cm diameter) from a 750 km² area in northwest Wales. Samples were collected from the surface of the stream bed, in the active part of the stream channel. At each site, 10 pebbles were collected and air dried prior to analysis. These coatings were analysed for more than 30 elements and results indicated that there were clear variations between sites for at least 12 elements. Variations in the composition of the pebble coating were related to the underlying geology, especially the mineralization. They concluded that this technique was valid for mineral exploration.

Two of the most relevant studies to this current research project are by Coish (1993, 2000) who collected pebbles in Newfoundland streams and analysed them with the LA-ICP-MS system at Memorial University of Newfoundland (MUN). Coish's first

study used sampling sites located in the St. John's and Carbonear areas. The Rennies River system and its two tributaries, Leary's Brook and Nagles Hill Brook, were selected because they represented a fresh water source that drains through the St. John's area. Streams flowing north then east out of Silver Pond in the Carbonear area were selected because they represented a pristine environment that exhibits natural base metal anomalies. For all sites sampled, stream waters, sediment, and pebbles were collected and the pH and conductivity were also recorded. Partial dissolution was carried out on the stream pebbles with analysis by solution ICP-MS. Also analysis using LA-ICP-MS were performed. For the Rennies River system, mixed results were obtained. That is, in some sites, relationships were apparent among the three types of media, whereas at others, relationships were absent. For the streams in the Carbonear area, variability was also found and the area of base metal mineralization was detected. It was concluded that analysis of stream pebble coatings by LA-ICP-MS seemed promising but partial dissolution gave more reliable results. Reasons for some of the variability were the short time used for ablation and elemental determinations, not enough spots being ablated on the pebbles, and also the procedure of using intensity ratios can lead to long term inaccuracies. A more detailed study was suggested.

The rationale for Coish's second study was to determine the relative accuracy of LA-ICP-MS analysis of stream pebble coatings compared to ICP-MS solution analysis. The study areas included: (1) Rocky Pond, which is located in northeastern Newfoundland, and drains the Duder Lake gold prospects, (2) Country Brook, which is

located on the Hermitage Peninsula of southern Newfoundland and flows from a small pond located at the base of the Winter Hill Pb-Zn volcanogenic massive sulphide deposit, and (3) streams located downwind from the Come-By-Chance oil refinery comprised the environmental aspect of this study. Here, substantial quantities of vanadium and chromium were released into the environment from refinery emissions. Similar to the earlier study by Coish (1993), water and pebble samples were taken at each sampling location. Stream pebbles were analysed by both partial dissolution and LA-ICP-MS. Partial dissolution gave better results compared to LA-ICP-MS for all three areas. In the Rocky Pond/Duder Lake area, the partial dissolution analysis was more reliable at indicating gold mineralization than the LA-ICP-MS analysis, the latter depicted gold at a lower intensity. In the Winter Hill Study area, similar results were found for the detection of mineralization using partial digestion and LA-ICP-MS. For the Come-By-Chance oil refinery area, the analysis using LA-ICP-MS defined enrichment in V, Ni, Fe, Zn, Pb, and S, for up to 1.5-2 km away from the stack, but the enrichments were not as intense as those obtained using the partial dissolution analysis. The main recommendations for future studies using Fe-Mn oxide coated pebbles were that it was important to be able to determine the concentration of elements in Fe-Mn oxide coatings. The paradigm of ratioing an element's intensity in counts per second (cps) to Fe cps made comparisons between data sets difficult. Also, larger volumes of coating should be ablated because this should make the anomalies more easily observed.

In the above mentioned studies on laser ablation, the actual concentration of various metals in the coatings were not determined. Hale *et al.* (1984) normalized the raw data to the Fe or Mn value of the same sample. Thompson *et al.* (1992), and Coish (1993, 2000) followed a similar method. The problem with normalized values is that they make comparisons between different studies difficult. Also, since there was no concentration calculation using a technique such as external calibration with a naturally occurring internal standard, the multiplicative effects of matrix, drift, and quantity of sample ablated are not corrected (Longerich, 2001).

1.4 Location

1.4.1 Rennies River Water System

The primary study area for this project was the Rennies River water system (Figure 1.1 and Figure 1.2). This is located in the St. John's region, which is a metropolitan area with a population of approximately 150,000 located on the Avalon Peninsula of the island of Newfoundland. Geologically it is located within the Avalon tectonostratigraphic zone (Catto and St. Croix, 1998). The Rennies River water system has a freshwater source that is considered unpolluted and drains through a metropolitan area, where there is pollution on a variety of scales (Coish, 1993).

Underlying the St. John's area of the Avalon peninsula are resistant Late Proterozoic sandstones, siltstones and shales (Catto and St. Croix, 1998). On the river banks of the Rennies River system, vegetation and surficial deposits are present that limit

bedrock exposure throughout the drainage area, although outcrops do occur along the streambed. The local geology of the St. John's study area consists of the Late Proterozoic St. John's and Conception Groups between which the boundary is not well defined (King, 1990). The St. John's Group comprises the Fermeuse and the Trepassey Formations. The former unit consists of interbedded white to brown sandstones (3-10 cm) and tuffaceous siltstone and shale (30-100 cm). The middle facies consists of remobilised black shales with slump folds of shale and sandstone. Shale and thinly laminated siltstone and sandstone compose the uppermost facies. The Trepassey Formation underlies the Fermeuse Formation, this contact between them is a gradual transition to beds (10-30 cm) of green grey sandstone, tuffaceous siltstone, and grey-black shale. The Conception Group comprises the Mistaken Point Formation; beneath the Trepassey formation, are green and purple argillaceous siltstones and fine grained sandstones, that make up the Hibbs Cove member of the Mistaken Point Formation. Iron and manganese stainings suggest groundwater movement along fractures in these rocks. Finally there is the Middle Cove member which makes up the lower part of the Mistaken Point formation which consists of tuffaceous muscone-siltstone, graded siliceous turbiditic sandstone and interbedded siltstone, chert, and tuff.

Late Wisconsinian glacial deposits are present in the St. John's area with a thicknesses that rarely exceed 2 m (Catto and St. Croix, 1998). The glacio-sediment is present through most of St. John's where it is < 2 m thick over the bedrock in most locations.

1.4.2 Tilt Cove/Betts Cove Geology

The Tilt Cove and Betts Cove sites are located on the Baie Verte Peninsula (Figure 1.1, Figure 1.3, and Figure 1.4) in central Newfoundland near the boundary between the Humber and Dunnage tectonostratigraphic zones (Strong, 1984). The Betts Cove ophiolite provides a geologic record of marginal ocean basin evolution (Bédard *et al.*, 2000).

The Tilt Cove and Betts Cove study areas are above sea level along a rugged coastline with steep cliffs at elevations of 100 to 200 metres (Al, 1990). The Tilt Cove study area is situated in a linear north-northwest trending valley and is surrounded by high hills (Maddox, 2001). At the centre of this valley, is Winsor Lake, which is surrounded by a few houses along a dirt road (Riggs, 2002). The Betts Cove study area is in a rather rough terrain. An abandoned mine site is on a hillside that has a relief of about 140 m and is located approximately 1.5 km inland. The landscape inland from both locations is hilly with a maximum relief of about 200 m. This region has been extensively glaciated (Squires, 1981), producing west and northwest barrens, rounded hilltops, and shallow valleys that have thin moraine coatings with marshes and small ponds.

There are three main stratigraphic units exposed at the Tilt Cove and Betts Cove sites (Strong, 1984). These are the Betts Cove ophiolite, the Cape St. John Group, and the Snooks Arm Group. The Betts Cove ophiolite is an example of a low TiO₂ ophiolite which has unusual chemical characteristics including extremely low (< 0.20 wt.%)

contents of Zr, Y, and REE in the basalts. The preserved oceanic crustal section of the Betts Cove ophiolite has a maximum stratigraphic thickness of 4320 m with outcrops to the southwest and east of Winsor Lake. There is also a completely preserved section at Betts Cove (Al, 1990; Bédard *et al.*, 2000).

The Betts Cove ophiolite comprises ultramafic rocks and these occupy a belt that ranges from 100 to 750 m wide over a distance of 6 km (Strong and Saunders, 1988). The lithologies range from black massive serpentinite that have preserved banded harzburgite textures, to strongly foliated rusty-weathering yellow talc-carbonate. The ultramafic rocks are either faulted against, or overlain by the Cape St. John Group in the Tilt Cove area. In the Betts Cove area, the upper contact of the ultramafic member has a complex transition zone with alternating layers of pyroxenite and gabbro that eventually become gabbro (Upadhyay and Strong, 1973).

The gabbroic rocks, with a maximum thickness of 330 m, are faulted out through most of the ophiolite belt (Strong and Saunders, 1988). The gabbro ranges from pegmatitic to fine-grained and ascending through the unit, the gabbros are cut by diabase dikes (Strong and Saunders, 1988). This marks the transitional contact with the sheeted dyke unit, which has a maximum thickness of 1.6 km, with almost 100% dikes. It is very well developed in the Betts Cove mine area where it has a stratigraphic thickness of 1.6 km and 4.5 km width perpendicular to the dykes thinning to the north (Bédard *et al.*, 1999). Most of the dykes in the Tilt Cove/Betts Cove are considered to be of boninitic composition.

The transition to the pillow lava unit, which is the most extensive of all the members with a thickness of up to 1.5 km (south of Betts Cove), is marked by dike swarms cutting the pillow lavas (Strong and Saunders, 1988). In the Tilt Cove area, the contact is a steep scarp which may be a fault separating it from the talc carbonates and serpentinites of the ultramafic units. In the Betts Cove area, they are mainly faulted towards the sheeted dyke complex and are well exposed in the Betts Head area (Upadhyay and Strong, 1973).

The Betts Head Formation is a transitional unit linking the Betts Cove ophiolite with the overlying Snooks Arm Group (Bédard *et al.*, 2000). It represents the autochthonous cover to the ophiolite and is associated with the oceanic crust. It consists of olivine + chromite + orthopyroxene boninitic pillow lavas. The lavas are composed of two types: low Ti and intermediate Ti.

Conformably overlying the ophiolite is the Snooks Arm Group which consists of basalt and mafic pyroclastic rocks (Al, 1990). In Tilt Cove/Betts Cove, there are three formations within the Snooks Arm Group that outcrop; these are (oldest to youngest) Mount Misery, the Scrape Point, and the Bobby Cove formations (Bédard *et al.*, 2000).

The Mount Misery Formation has well formed pillow lavas that grade into an altered massive flow complex, breccia zones and sill-like intrusions (Bédard *et al.*, 2000). In the Tilt Cove area, Betts Head lavas are interbedded with the Mount Misery lavas. The Scrape Point Formation is made up of two parts, there is a sedimentary member and an overlying volcanic member. Green turbiditic to tuffaceous sandstone and laminated

siliceous siltstone having minor conglomerate and ironstone make up the sedimentary member. The volcanic member has basal sheet flows that grade up to a section that has Fe and Ti rich tholeiitic basalt pillow lavas.

The Bobby Cove Formation has an average thickness of 500 m to the west and is 16 km long, consisting primarily of pyroxene-andesite agglomerate, tuff, and graywacke, with minor amounts of thinly bedded variably coloured chert, argillite, and minor conglomerate (Cousineau and Béhard, 2000).

Unconformably overlying the Snooks Arm Group is the Cape St. John Group (Strong and Saunders, 1988). This is a subaerial sequence, with a thickness of 3500 m and is the youngest volcanic assemblage in the area (Neale *et al.*, 1975). It is exposed in the cliffs north of Winsor Lake and can be followed eastward to Beaver Cove (Strong and Saunders, 1988). It consists of basalts, silicic ash-flow tuffs, and sandstones. At the base of the group, there is a gold-bearing, magnetite-rich iron formation. This is related to the chalcopyrite-bearing massive pyrite. Intrusive breccias occur as dikes, plugs, and diatremes and contain the same clasts as the pyroclastics.

1.4.2.1 Tilt Cove Mineralization

The mines at Tilt Cove were Cyprus-type, ophiolite hosted volcanogenic copper sulphide deposits (Bédard *et al.*, 2000). The deposits are hosted by the Ordovician Snooks Arm Group (Kanehira and Bachinski, 1967) and occur within a 400 m thick zone of massive and pillowed basalt and basalt breccia (Bédard *et al.*, 2000). The ore-bearing

lavas and breccia units are overlain by a thick sedimentary sequence that belongs to the Sedimentary Member of the Scrape Point Formation.

Two mines have operated at Tilt Cove, the East and West Mines (Figure 1.3) (Bédard *et al.*, 2000). The East mine consisted of several smaller ore bodies including the low-grade stockwork “A” zone, the massive Cliff zone, and further east, the Main zone. In the West zone, the deposit consisted mainly of disseminated and stringer chalcopyrite and pyrite mineralization in a steeply dipping pipe-like body; the actual ore zone is contained within massive and pillowed mafic lavas and breccia. The Tilt Cove deposits have a simple chemistry with copper as the important economic element. Gold grade is typically low with some concentrations in the 1-2 ppm range. Nickel ranges from 8 to 1370 ppb, and cobalt ranges from 8 to 1990 ppb. Arsenic for the most part has low concentrations, but some samples have concentrations near 500 ppb.

1.4.2.2 Tilt Cove Mining

The Tilt Cove copper mines operated from 1864-1917, and from 1957-1967. A smelter facility operated there from 1888-1892 (Hibbard, 1983). During the lifetime of the mine, about 7.4 million tonnes of ore were extracted with the greatest production occurring from 1957-1967 when 6.7 million tonnes of ore were removed (Bédard *et al.*, 2000). During the early life of the mine, the ore grade was 4 to 12% Cu, but during the final 10 years of operation, the grade decreased to 2% (Strong and Saunders, 1988). Gold

was also mined, with approximately 42,000 oz produced during the last episode of mining.

The Tilt Cove deposit was discovered in 1857 by Smith McKay (Hibbard, 1983) who developed the Union Mining Company with C. F. Bennett. The West Mine opened on July 27, 1864. Mining began with horizontal adits to remove ore, and as the surface ore became depleted, the miners went deeper into the hillside (Martin, 1983). Nickel was also extracted, with a total 416 tons of ore removed from the West mine from 1869-1876, and in 1870. At that time Tilt Cove accounted for 5% of world nickel production (Martin, 1983).

In 1955, several new large ore bodies were discovered in what was the East and West Mines. The Maritime Mining Corporation Limited produced ore from August 1957 to June 1967. Closure was due to exhaustion of reserves and collapse of the West Mine (Hibbard, 1983). During this period of mining operation, flotation methods were used to concentrate the ore, and one years worth of tailings were deposited on-land southeast of Winsor Lake, which was covered with topsoil (Maddox, 2001). Tailings here have grades of up to 0.3% Cu and greater than 0.5% Zn. Also, 5 to 6 million tons of tailings were slurried via pipeline to the southwest of Tilt Cove Harbour following this work. These tailings have concentrations of Cu less than 0.2% and Zn 0.3 to 0.4% (Maddox, 2001).

1.4.2.3 Betts Cove Mineralization

The Betts Cove deposit is the most polymetallic occurrence in the area containing elevated concentrations of zinc, gold, and minor lead (Béhard *et al.*, 2000). Traces of galena, PbTe, and AgTe are present also. Twenty-one grab samples obtained from dumps in the mine area gave Cu concentrations of 0.19 to 20.02%, and Zn concentrations of 0.02 to 20.54% (Strong and Saunders, 1988). One sample had a significant Pb concentration of 1.08%, four samples had Au greater than 10 ppm, while silver ranged from 10.1 to 39.5 ppm.

The Betts Cove mine outcrops are in a complex transition zone between the sheeted dyke unit and the Betts Head Formation lavas (Figure 1.4) (Béhard *et al.*, 2000). Detailed mapping reveals that the majority of the sulfide concentration occurs along the contact between the sheeted dikes and overlying pillow lavas (Upadhyay and Strong, 1973). The mineralization in the pillow lavas has maximum concentrations in the spaces between the pillows. Of the sulfide minerals, pyrite is most abundant, followed by chalcopyrite and sphalerite.

The high grade massive ore is only present in dumps and cannot be seen in the outcrop, because it is buried in a caved-in area (Béhard *et al.*, 2000). The massive ore consisted of brecciated pyrite with chalcopyrite, sphalerite, and a range of gold sulphide minerals.

1.4.2.4 Betts Cove Mining

The Betts Cove deposits were discovered in 1860 and mined between 1875 and 1885 producing 130,000 tons of hand-picked ore with an average grade of 10% copper, along with 2,450 tons of pyrite (Upadhyay and Strong, 1973).

Mining began on the Betts Cove Mine site in the spring of 1875 with copper being first discovered and removed near Betts Head. By September, the mine had exported 6000 tons of copper ore to Swansea (Martin, 1983). In total the mine site comprised six shafts with some of them reaching 150 feet below the surface. Support for the mine was maintained by copper-rich pillars.

The first ore smelters in Newfoundland were installed in Betts Cove in 1876 (Martin, 1983). The smelter sat on the west side of the mine site and consisted of six cupola blast furnaces that were able to produce a mixture of 20-30% copper. More than 75,000 tons of ore was removed from Betts Cove between 1875 and 1878 which lead to the establishment of a town with a population of 2000 in 1878.

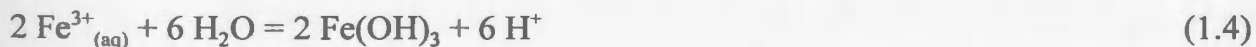
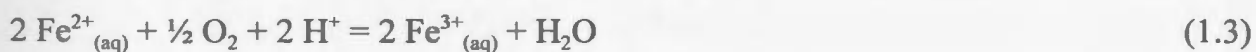
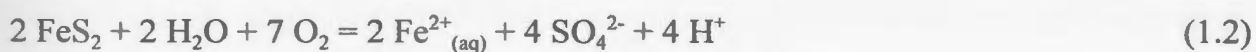
1.4.2.5 Acid Mine Drainage at Betts Cove and Tilt Cove

As previously mentioned, a year's worth of tailings were deposited on land to the southeast of Winsor Lake and covered with topsoil. The purpose of the topsoil was to limit the exposure of the tailings to oxidation which would alter the chemical composition of the tailings and increase the mobility of metals present (Maddox, 2001). With regards to the actual compositions of the tailings, the mean concentrations (ppm)

for a variety of metals in the tailings have been determined using ICP-MS; these were:

Cu = 3546, Zn = 2283, As = 184, Cd = 3.54, Sn = 6.40, Sb = 25.6, and Pb = 114.

One process that increases the mobility of metals present in the tailings is acid mine drainage (Förstner and Wittman, 1979). This process consists of a steep pH decrease in water seeping from mine refuse (*i.e.* tailing piles). There is a slow oxidation of the sulfide components, partially aided by bacteria that produce more H^+ ions, further lowering pH and increasing metal mobility. This acid drainage allows the tailings piles to pass metals into streams for decades. It has been shown that in acidic waters of pH 2.6 and 2.8, the amounts of Mn, Ni, and Co are enriched by factors of 10,000 compared to the natural historic background levels (Förstner and Wittman, 1979). Concentrations of Fe, Cu, and Pb are greater by factors of 2000, 1000, and 500 respectively. The bacterial mediated process of acid mine drainage is shown in the following equations (Siegel, 2002):



Overall Reaction:



Overall, in the reactions above, the sulfur component of pyrite is oxidized to sulfate, H^+ is produced, and Fe^{2+} ions are released. These equations show that atmospheric oxygen is the initiator of the cycle that oxidizes Fe^{2+} to Fe^{3+} and then the ferric ion can oxidize the pyrite which produces additional Fe^{2+} and acidity. Overall, for each mole of iron sulfide oxidized, four moles of acid are produced. This leads to a pH decrease that can go below 4.5 (Drever, 1988). This is not a viable environment for most organisms except specialised algae and bacteria, because most organisms are adapted to waters buffered at a more neutral pH, and because more toxic trace elements are mobilized under these acidic conditions.

These reactions should be operative at Tilt Cove where metals are released, and should allow the metals to reach Winsor Lake where they can enter the stream that outflows from this lake and hence accumulate on Fe-Mn oxide coatings present on stream pebbles. The low pH environment, however, will lead to lower amounts of metals adsorbed to the Fe-Mn oxide coatings than in a higher pH site since metal adsorption decreases with a decrease in pH. At the Betts Cove site, where there is abundant pyrite and other sulfides present in ore bodies or piles in the mine area, acid mine drainage could also be occurring. Similar to Tilt Cove, the metals will enter the lake in the centre of the mine area, and then enter a series of streams and ponds.

As mentioned above, Maddox (2001) examined the trace metal concentrations in on-land and marine deposited tailings. Riggs (2002) examined heavy metal concentrations from the A-soil horizon, for samples taken from the Tilt Cove smelter

area, and samples taken to the east and southeast of the smelter, which is downwind of it. Riggs found that Cu, Ni, As, and Pb, all followed the same pattern of high concentrations around the smelter, and remained high in the direction of the prevailing winds. Zinc concentrations were highest at the point source, and decreased with distance from the smelter. High Cr values in all samples were attributed to bedrock geology.

1.4.3 Robinson's River Study Area

The Robinson's River sampling site is located in the Bay St. George South area (Figure 1.1 and Figure 1.5) in the Humber tectonostratigraphic zone within the Bay St. George subbasin, an extension of the larger Maritimes Basin (Murthy, 1985). The physical topography consists of a gently sloping lowland, 60 m in elevation, surrounded by the Long Range Mountains to the east and the Anguille Mountains to the south (Bell *et al.*, 2001). The coasts are easily eroded and are composed mostly of glaciated sediments, usually around 30 m thick (Shaw and Forbes, 1990). The lowlands are underlain by Carboniferous sandstone, shale, siltstone, and limestone down-faulted against Proterozoic to Ordovician crystalline rocks of the Long Range Mountains (Shaw and Forbes, 1990). Quaternary sediments cover the bedrock, which is predominantly gravel, sand, and mud at the coast, and diamicton inland. Most of this deposition occurred during the Late Wisconsin glaciation.

With reference to Figure 1.5 and Figure 1.6, the dominant lithological unit in this study area is the Robinsons River Formation of the Codroy Group (Knight, 1983). The

Anguille Group consists of a sequence of non-marine siliciclastic rocks, that constitute the oldest strata in the subbasin. The unit includes all Carboniferous strata that conformably underlie the basal Ship Cove Formation of the Codroy Group. The Kennels Brook Formation, which is the lowermost member, consists of red and grey sandstones, pebbly sandstones, conglomerates, and slates with a thickness of 3200 m. Conformably overlying this is the Snakes Bight Formation which comprises a thick sequence of black lutites and gray sandstones 1000 m thick (Baird and Cote, 1964). Above this is the Friars Cove Formation that contains grey sandstones, conglomerates, and shales with some minor carbonates and redbeds. The uppermost unit, the Spout Falls Formation, has a maximum thickness of 2250 m and is composed of red, reddish-grey, and green calcareous, arkosic, and micaceous sandstones in the Anguille Mountain and Bald Mountain locations with conglomerate becoming more abundant northward.

The Codroy Group is a mixed sequence of marine and nonmarine strata (siliciclastic, evaporitic, and calcareous layers), that has a thickness of 4000-6000 m (Knight, 1983). This group is defined as all the lithologies that occur between the basal limestone Ship Cove Formation, and the first deposits of the Barachois Group. This group is divided into four formations; Ship Cove, Codroy Road, Robinsons River, and Woody Cape. The Ship Cove Formation is exposed on Codroy Island, in many areas of the Anguille Mountains and Bald Mountain, and it also outcrops along Fischells Brook and Northern Feeder (Bell, 1984). It is also intersected in gypsum drill holes at Flat Bay, Heatherton, and Highlands River (Knight, 1983). It has a fairly uniform thickness of 18-

20 m and is composed of well laminated, grey limestones and many gypsum molds. Shales and thin sandstones are interbedded with the limestone at the base of the formation in the Fischells Brook area.

The Codroy Road Formation (formerly known as Codroy Shales) is a mixed sequence of fine siliciclastic, carbonate, and evaporitic sedimentary rocks that conformably overlies the Ship Cove carbonates (Knight, 1983). The formation is exposed in the cliffs near Codroy Village, in an area near Ship Cove, in sections at Fischells and Flat Bay. It has a varying composition from north to south with an estimated thickness of 150 m. The evaporite consists of red siltstones and fine sandstones. Carbonates consist of varicolored gypsum, blue grey anhydrite, dark grey to black bituminous dolomites, and fossiliferous, dolomitic, mudstones, and muddy dolomites. Around the Anguille Mountains, the Codroy Road Formation consists mainly of red and grey siliciclastics that have interbedded evaporites containing minor amounts of carbonates.

The Robinsons River Formation is a complex succession of more than 5000 m of terrigenous clastic rocks with small amounts of carbonate and evaporite strata (Knight, 1983). This unit underlies the Codroy and St. Georges Bay lowlands but faulting and folding disrupts the continuity. It is divided into four members. From the lowest they are Jeffrey's Village, Highlands, Mollichignick, and Overfall Brook Members. The former two are mostly located in the St. Georges Bay lowlands, while the latter two are restricted to the Codroy lowlands.

Conformably overlying the Codroy Road Formation is the Jeffrey's Village Member (Knight, 1983). It is well exposed in the St. Georges Bay lowlands along the coast and along some rivers. In salt deposits southwest of Flat Bay, it has a maximum thickness of 2100 m. It mostly consists of red and grey shales, mudstones, siltstones, sandstones, and conglomerates that are interbedded with carbonates and evaporites such as anhydrite, gypsum, halite, and potassic salts. Salt deposits at Robinsons are well bedded and contain interblends of fine grey and red siliciclastics.

The Highlands member is located along the coast south of Crabbes River and eventually continues beneath St. Georges Bay (Baird, 1959). It has a thickness of 884 m and is composed of red, minor grey and yellow sandstones, and red siltstones (Knight, 1983). Conglomerates and pebbly sandstones are present to the east and north. In the St. Teresa region, brown-red conglomerates and pebbly sandstones are found.

The Mollichignick Member is present in the Codroy lowlands and extends eastward as far as the provincial park and it terminates to the south of Bald Mountain (Knight, 1983). It is mostly composed of red siltstones, red to gray micaceous sandstones and stratified sandstones and has a thickness of at least 2275 m.

Finally, the Overfall Brook member is present in the core of a southeast plunging, locally overturned syncline and formed adjacent to the Long Range Fault with a thickness of at least 345 m (Knight, 1983). This member is composed mainly of red, pink, and brown, thick-bedded, massive and crossbedded, pebbly and arkosic sandstones and grits, argillaceous sandstones, and minor conglomerates.

The Woody Cape Formation is the last important area. This area contains green and grey colored mudstones, siltstones, and sandstones that have outcrops that occur only along coastal exposures in the Codroy lowlands having a thickness of about 690 m (Knight, 1983). The mudstones, siltstone, and shales are intercalated with green-grey, mica rich sandstones, grey and black carbonates, and minor red siltstone and sandstone.

Robinsons River originates in the Brow Pond Lentil, then flows through the Barachois Group, the Jeffrey's Village Member, the Codroy Road Formation, and then through the Jeffrey's Village Member again, the Ship Cove Formation and Fischells Conglomerate Member.

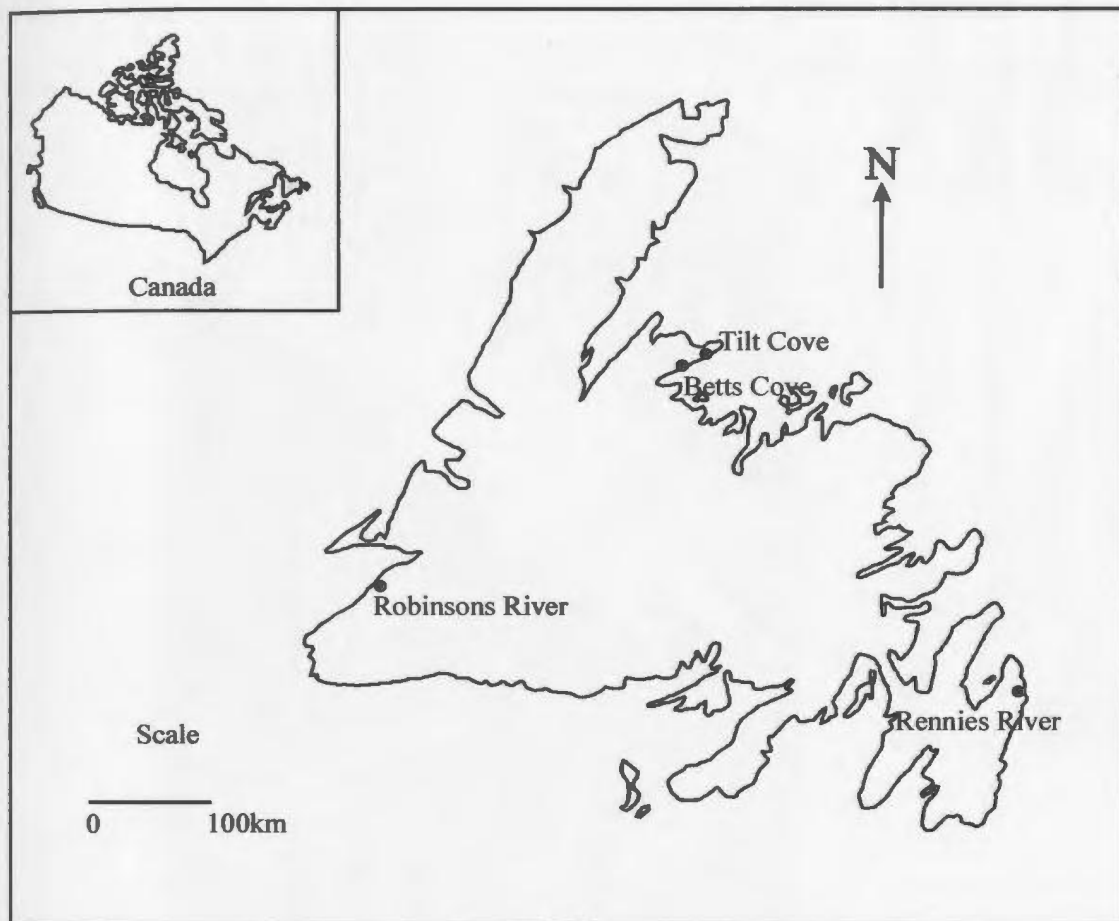
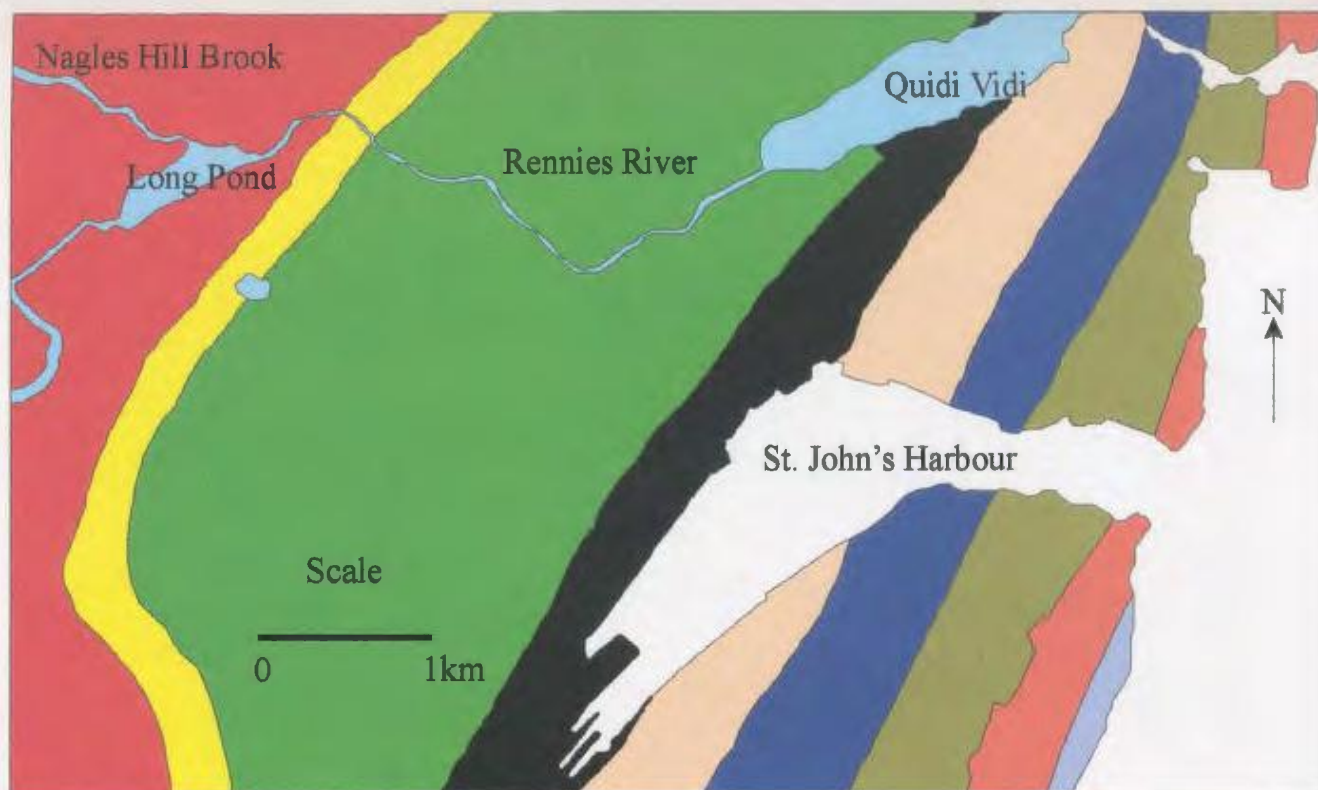


Figure 1.1 Map of Newfoundland showing study areas (modified from Bédard *et al.*, 2000)



Legend










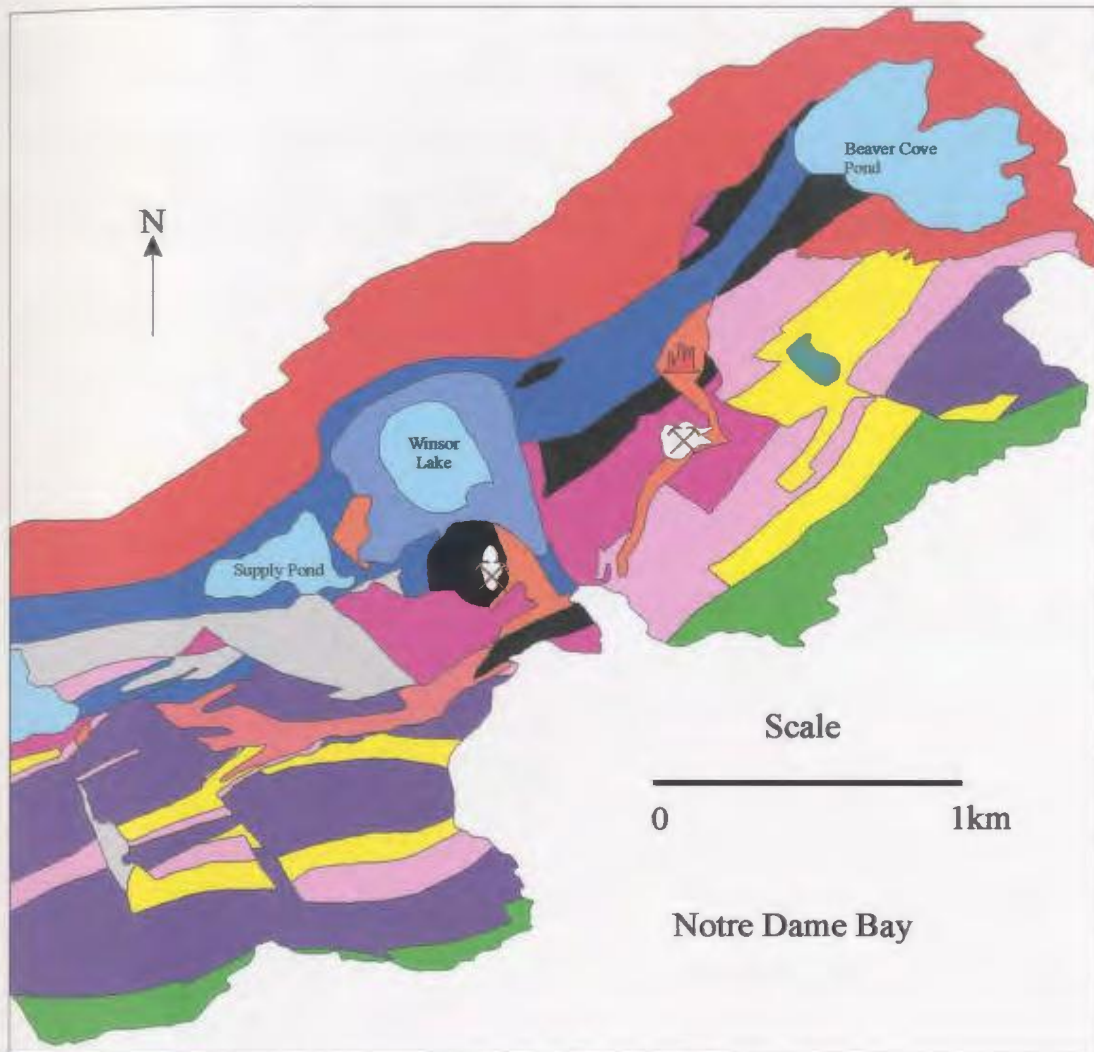
 Hibbs Cove Member	 Renews Head Formation	 Cabot Tower Member
 Trepassy Formation	 Gibbett Hill Formation	 Cape Spear Member
 Fermeuse Formation	 Quidi Vidi Formation	 Skerries Bright Member

Figure 1.2 Geologic map of the St. John's study area (see Chapter 1 for descriptions), (King, 1990).



Legend



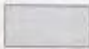







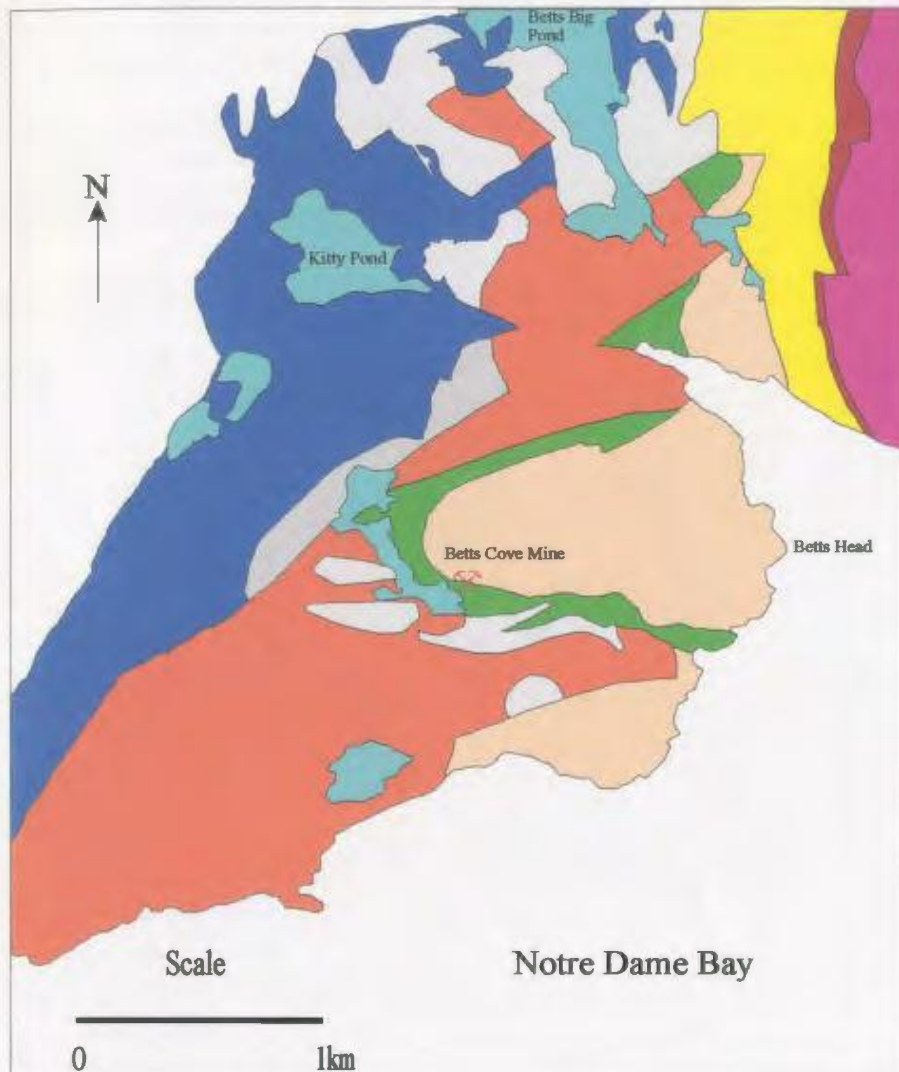
 Serpentine, cumulate peridotite and talc-carbonate schist	 Bobby Cove Formation
 Late intrusive gabbro	 Mafic Sills
 Betts Head Formation	 Cape St. John Group
 Mount Misery Formation	 Quartz + two feldspar + mica porphyritic granitoid
 Scrape Point Formation; volcanic unit; sedimentary unit	 Not Exposed

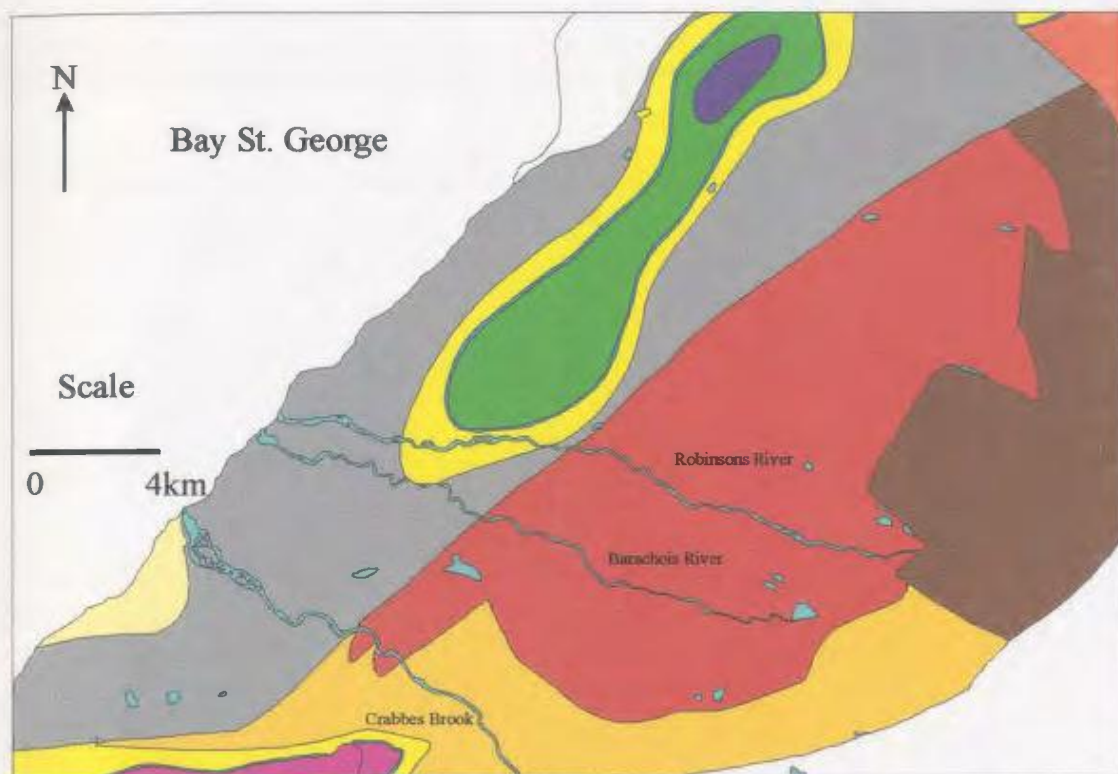
Figure 1.3 Geologic map of the Tilt Cove study area (Bédard *et al.*, 2000).



Legend

 Layered cumulate rocks	 Betts Head bonnitic lavas
 Late intrusive gabbro	 Mount Misery tholeiitic lavas
 Sheeted dykes	 Sedimentary Rocks
 Mixed dykes and lavas	 Scrape Point Formation tholeiitic lava

Figure 1.4 Geologic map of the Betts Cove study area (Bédard *et al.*, 2000).



Legend








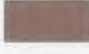


 Pre-Carboniferous Basement	 Jeffreys Village Member
 Spout Falls Formation	 Highlands Member
 Fischells Conglomerate Member	 Robinsons River Formation
 Ship Cove Formation	 Brow Pond Lentil
 Codroy Road Formation	 Undivided Barachois Group

Figure 1.5 Geologic map of the Robinsons River study area (Knight, 1983).

Codroy Group (Middle to Upper Visean)	Woody Cape Formation (690m)	
	Robinsons River Formation	Overfall Brook Member (345m)
		Mollichignick Member (2300m)
		Highlands Member (880m)
		Jeffreys Village Member (1400m)
	Codroy Road Formation (150m)	
	Ship Cove Formation (20m)	
Anguille Group (Tournaisian)	Spout Falls Formation (2250m)	
	Friars Cove Formation (1300m)	
	Snakes Bight Formation (1000m)	
	Kennels Brook Formation	

Figure 1.6 Bay St. George sub-basin stratigraphic column with thickness of each Formation in metres (Murthy, 1985).

2. Experimental, Field Sampling and Laboratory Procedures

2.1 Annual Accretion

The objectives of this part of the study were to determine the factors which govern coating accretion, whether the concentrations of elements change throughout the year with coating accretion, and how element concentrations in the coatings correlate with concentrations in the water.

2.1.1 Annual Accretion Setup

In order to address the first two objectives, clean artificial substrates were placed in the stream upon which Fe-Mn oxide coatings were allowed to “grow.” Three different substrates were used, which provided additional information on coating accretion on different substrates. Based on previous studies (Carpenter and Hayes, 1978, 1980), conventional streak plates used for mineralogical tests were used as a substrate. The second substrate was chosen based on the fact that this study was focussed on Fe-Mn oxide formation on stream pebbles, and thus polished stream pebbles were used which were obtained from a local crafts store. The third substrate was based on a study by Love and Bailey (1992), that examined macroinvertebrate communities on rocks in streams. In this study they placed cement substrates in streams and examined the epilithic invertebrates which grew on these materials. To prepare cement substrates, tennis balls

were cut in half, filled with cement, allowed to set, following which, the concrete was removed from the mould.

As mentioned earlier, the chemical environment is expected to affect the characteristics of the coating. Since the chemical environment is known to change with location in the river, it was necessary that the substrates remain stationary throughout the course of the study. To achieve this, the substrates were attached to building bricks using GE Silicone Sealant, purchased from a local hardware store.

2.1.2 Water Sampling

To meet the first two objectives, various water measurements were taken. These measurements were collected when the substrates were placed and when they were removed from the stream and approximately every 10 days in between. The parameters included pH (Orion Model 290A, Boston, MA), dissolved oxygen (mg/L, Orion Model 835, Boston, MA), and conductivity ($\mu\text{S}/\text{cm}$, Orion Model 835, Boston, MA). The effect of pH and dissolved oxygen levels on coating accumulation were previously mentioned and conductivity provides a measure of the total dissolved ions present in the water. For the pH measurements, calibration was carried out, before entering the field, with two buffer solutions (pH 4.00 and 7.00). Calibration of the dissolved oxygen meter was carried out with an AutoCal™ Air calibration sleeve; the conductivity meter was calibrated with Orion conductivity standard. Measurements were taken in the field by first rinsing the electrode of each meter with deionized water, then taking a water sample

from midstream with a pre-cleaned Corning Snap-Seal™ polyethylene bottle, and finally placing the electrode of each meter separately into each sample and recording the value after the displayed reading stabilized. After the reading was recorded, each electrode was removed from the bottle, and rinsed with deionized water.

In addition to the previously mentioned measurements, water samples were collected for the determination of 46 elemental analytes using a HP 4500+ ICP-MS located in the Department of Earth Sciences. For these analyses, at each of the sampling locations, a new BD Luer-Lok™ 30 ml syringe was rinsed with stream water three times and then 100 ml was filtered using a new Fisherbrand™ 0.45 μm syringe filter into a pre-cleaned Corning Snap-Seal™ polyethylene bottle. These bottles were previously cleaned by placing them in 8N nitric acid (HNO_3) for a minimum of 24 hours. The bottles were then rinsed three times with deionized water and dried in an HEPA filtered air-drying space. Collected water samples were transported to the lab where 2 ml of 8N nitric acid (HNO_3) was added to the 100 ml samples. The samples were acidified to stabilise the solutions (Coish, 2000).

2.1.3 Annual Accretion Study Area

The study area for examining Fe-Mn oxide formation was the Rennies River water system. This system is on the island of Newfoundland, which has a temperate climate consisting of short, cool summers, and long, cold, winters. Previous work on Fe-Mn oxide accretion (Carpenter and Hayes, 1978, 1980; and Cerling and Turner, 1982)

examined the formation of Fe-Mn oxide coatings in Georgia and Tennessee. These US study areas have subtropical climates, with long, hot, humid summers, and short, mild, winters. Thus, Georgia and Tennessee should have much higher chemical weathering rates than Newfoundland, which is expected to create a different chemical environment for coating formation.

Rennies River was chosen as the study site for Fe-Mn oxide formation because it has a wide range of chemical environments due to its flow from a somewhat pristine location through a populated city landscape where pollution on various scales exists and also because it is easily accessible throughout the year. Seven sampling locations were used (Figure 2.1). The first sampling site (S1) was located in Nagles Hill Brook, which is outside of the built-up metropolitan area, approximately 200 m to the west of the Fluvarium in the Pippy Park area. This small stream flows into Long Pond and has a maximum width of approximately 1.5 m and average depth of about 0.25 m. It is the least polluted site in this study area.

Sites S2, S3, and S4 are all located in Rennies River between Prince Phillip Drive and Elizabeth Avenue. Prince Phillip Drive is a busy four lane divided roadway while Elizabeth Avenue is a busy two-lane metropolitan street. Rennies River flows out of Long Pond, which collects drainage from the Pippy Park area and from Leary's Brook. This river flows along Prince Philip Drive, and also collects drainage from a large shopping centre. Therefore, this pond serves as a collection area for metals which then flow into Rennies River. Thus it is expected that the sites in Rennies River should have

much different chemical characteristics than the site at Nagles Hill Brook. Site S3 is about 400 m downstream from S2, and site S4 is approximately 200 m downstream from S3. Since these three sites are located somewhat close together, especially S2 and S3, the coatings are expected to have similar chemical environments and similar compositions. The average depth and width for this section of the river is 7 m and 0.50 m, respectively. The site, S5, is located between Elizabeth Avenue and Carpasian Road, approximately 300 m down river from site S4. Between S4 and S5, there are several culverts that are expected to contribute dissolved metals to Rennies River. Especially notable is a culvert near the bridge on Elizabeth Avenue where the streambed has a distinct black colour which may be due to the oxidation of metals entering the stream environment and forming coatings on media present on the stream bed. Hence, coatings at site S5 are expected to have different compositions compared to sites located upstream.

The final two sampling sites, S6A and S6B, are both located relatively close to Portugal Cove Road, approximately 800 m downstream from site S5. Site S6A is located just above the bridge at the intersection of Portugal Cove Road and Rennies Mill Road. Site S6b is located just below the bridge in an area where a culvert drains an abandoned dump site in the vicinity of the bridge (Coish, 2000). Stream bed material in the S6B area has a distinct reddish orange colour suggesting that a Fe-Mn oxide is being produced. Since both of these sites exist in such chemically different environments, there should be clear differences in the coating accretion and composition, even though, spatially, they are located close together.

Experimental investigations began on February 25, 2002, when the building bricks and attached substrates were placed at midstream in the previously described sampling sites. Eight bricks with attached substrates were placed at each site, with a plan of collecting two sets of substrates every three months for one year. This experimental design was made with a goal of monitoring seasonal variation in the coatings.

2.1.4 Substrate Collection

The Fe-Mn oxide collectors were sampled approximately every three months. This was accomplished by first detaching the substrates from the bricks and then placing them in brown paper sampling bags. Two pebbles from the streambed at each sampling site were also collected at the same time. This was to allow comparisons between relatively “new” and “old” coatings. All samples were brought to the lab and followed a similar sample preparation procedure as Coish (1993, 2000) where coating samples were washed with demineralised water, and dried in an HEPA air filtered drying space. After drying, the samples were placed in pre-cleaned Ziploc® resealable containers. These containers were cleaned by rinsing them three times with deionized water and drying them in an HEPA air filtered drying space. The containers were labelled and stored for later analysis.

2.2 Mineral Exploration/Environmental Monitoring

As previously mentioned in Chapter 1, previous work has been done with Fe-Mn oxides on stream pebbles and mineral exploration/environmental monitoring. Filitpek *et al.* (1981), Carpenter *et al.* (1975, 1978), Robinson (1981), Carpenter and Hayes (1978), and Gulson *et al.* (1992) all used a partial digestion technique, but mentioned problems in partial digestion as a shortcoming of their studies. Hale *et al.* (1984), Thompson *et al.* (1992), and Coish (1993, 2000) all used laser ablation for their analysis but actual concentrations were not determined, leading to a limitation with the technique. Therefore, the goals of this part of the study were: (1) to reassess the role of Fe-Mn oxides as mineral exploration/environmental monitoring tools; and (2) to determine absolute concentrations of the analytes which is necessary if studies using different LA-ICP-MS instruments at different times are to be compared.

2.2.1 Study Areas

During the summer of 2002, Tilt Cove, Betts Cove, and Robinsons River were all sampled for Fe-Mn oxide coatings on pebbles as examples of mineralised and contaminated sites. These three sites, especially Betts Cove and Tilt Cove, were expected to exhibit ranges of pollution in their respective streams and it was anticipated that the Fe-Mn oxide coatings present on these stream pebbles would reflect these variations. Water measurements were taken at each sampling site in a manner similar to Rennies River. Two pebbles were also collected at each site, preferably from the centre of the

stream. The pebbles were collected using the same procedures as the pebbles collected from Rennies River.

As previously mentioned, Tilt Cove and Betts Cove are both located on the Baie Verte Peninsula. At the Tilt Cove site, there were 15 sampling sites (TCS1 to TCS15) (Figure 2.2). TCS1 was taken from the community's drinking water supply, which was a pond located on a hill approximately 1 km to the southwest of the abandoned 19th century smelter (elevation = 90m). This site was chosen to provide information on the source of the stream flowing out of this pond. The prevailing winds in the area at the time the smelter was in operation were from the west and southwest, and therefore concentrations of various metals present in the water may not have been affected by the smelter (Riggs, 2002). It was planned to collect water and pebble samples from the stream that outflows this pond. However upon investigation of the site, it was observed that there was no stream present, and only a rusty pipe through which the drinking water flowed to various homes. Samples were also collected from a pond located 0.5 km to the north of the drinking water supply (elevation = 90 m). This sample (TCS2) was taken along the shore of a lake in the hills to the west of Winsor Lake, again with the goal of obtaining information of the source area of the stream. This pond was approximately 1.2 km west of the abandoned smelter, and similar to the drinking water supply pond, may contain metals released from the smelting process. Pebble and water samples were also taken at random intervals along a stream that flowed out of this pond (TCS3 to TCS8). This stream was about 0.5 m wide, and had an average depth of 20 cm. The samples TCS7 and

TCS8 were taken from an area beneath the hill upon which the pond was located. All of these sampling sites, TCS2 to TCS8, were along a 400 m area that flowed from the sampled pond to Winsor lake and are thought to be the “pristine” sites in this study area.

The remaining sampling sites from this study area, TCS9 to TCS15, were the “polluted” sites. TCS9 was on the southeast shore of Winsor Lake and as previously mentioned, tailings were deposited in this area, therefore water samples from this area are expected to show elevated levels of metals such as Cu, Zn, As, Cd, Sn, Sb, Pb, and other metals that were present at high concentrations in the tailings. Also, since drainage from the smelter area reaches this locality, other metals may show enrichments here, compared to control values. For example, Riggs (2002) reported concentrations of Cu in the slag ranging from 3628 ppm to 80043 ppm, nickel ranged from 0 to 180 ppm, with maximum Zn concentrations of 19519 ppm, As at 929 ppm in the old smelter chimneys, and finally, Pb in the slag ranged from 62-151 ppm. Sampling sites TCS10 and TCS-11 were from a stream that flowed out of Winsor Lake which had a width of about 1 m and depth of about 0.40 m. These sites were located about 100 m apart and the streambed material was covered with a grey coloured precipitate. The sampling site TCS-12, was along the shore of a pond in the area of the West mine. In this body of water, the remains of old buildings and mine equipment were dumped, producing a body of water with no apparent aquatic life. The next site, TCS13 was in a small stream that flowed from the West mine shaft-pond which passed an abandoned mine shaft. The stream was about 0.5 m wide and 0.2 m deep with a distinct light yellow-orange colour on the streambed material. Site TCS14

was at the junction of the stream flowing from Winsor Lake and the stream flowing from the West Mine shaft-pond. Since the water present in both streams should differ chemically, the coatings were expected to reflect this composition. The final site, was TCS15, this was just downstream from site TCS-14.

Another study area which was sampled during the summer of 2002 was Betts Cove which is located approximately 15 km to the southwest of Tilt Cove. In total, there were 22 sampling sites selected, (BCS1 to BCS22), with BCS1 to BCS13 in the abandoned mine area and streams draining from the mine (Figure 2.3). The remaining sites (BCS14 to BCS22) were in a stream which flows out of Kitty Pond, which is approximately 1 km to the north of the old mine site. The mine site is at an elevation of approximately 100 m, and Kitty Pond also lies at approximately 100 m. The first two sampling sites, BCS1 and BCS2, were in a stream and pond, respectively, that were furthest away from the abandoned mine site. The stream had a depth of about 0.30 m and width of 0.50 m, and the stream bed material had grey coloured coating. Sites BCS3 to BCS8 were progressively closer to the mine site, and consisted of a series of streams and ponds. As in the previous study area, water and pebble samples were taken from the streams, and water samples were taken from the ponds. Site BCS9 was collected along the shore of a pond adjacent to the mine area. Sites BCS10 to BCS11 occurred to the northwest of this site (BSC-9). Site BCS10 was a stream that flowed around the gravel dam that separated two ponds. Site BCS11 was slightly to the northwest of site BCS10. The site, BCS12, was along the shore of a pond that is close to the area where the smelter

is thought to have been located. Finally, site BCS13 was a small stream that flowed into the abandoned mine site. In total, these various sampling points were over a distance of 1 km and were expected to be polluted sites in this study area.

Sites BCS14 to BCS22 were in a stream flowing out of Kitty Pond, and are considered to be pristine sites. BCS14 was sampled on the southeastern shore of Kitty Pond whereas, samples BCS15 to BCS22 were collected at random intervals over a distance of 800 m in the stream flowing out of this pond. This stream had a maximum width of 1 m with an average width of 0.60 and depth of about 0.25 m.

As noted in section 1.3.3, the Robinsons River study area is situated within a region of dominantly carbonate geology. Surface waters in contact with calcium carbonate usually have pH values between 7.3 and 8.4 (Drever, 1988). These are somewhat basic and since it has been found that coating formation increases with pH, the coatings in these environments should be thicker (Theobald *et al.*, 1963). In total, there were 15 sampling sites along an 8 km section of Robinsons River (Figure 2.4). This fast flowing river has an average width of 30 m and average depth of 1 m. During the sampling period, heavy rains increased the water level such that it was very difficult to obtain samples from the middle of the river, sampling was therefore completed as close to the middle of the river as possible.

At the first sampling site, RRS1, a small stream, called the Northern Feeder, flowed into Robinsons River. Here, Robinsons River was very fast flowing, and there was a bedrock section of conglomerate exposed containing well-rounded pebbles. The

next two sampling points, RRS2 and RRS3, are slightly downstream from RRS1 and likewise in an area of exposed conglomerate. Sample RRS4 is located approximately 0.5 km downstream from RRS3. RRS5 and RRS6 are approximately 0.5 km and 1.0 km downstream from RRS4, respectively, with RRS6 just above the Robinsons River bridge on the TransCanada highway. RRS7 is just below Robinsons River bridge. Since this bridge is part of a major highway, it was postulated that the input of pollutants from vehicles might be detected in the pebble coatings. Located approximately 1.0 km downstream from RRS7 was RRS8, which was downstream and adjacent to clear-cut areas. When these areas were cut, modern forestry practices were not used and trees on the riverbank were consequently cut. Thus the river bank might have been easily eroded, metals can be readily released from this material and can enter the stream and accumulate on the coatings. RRS9 is 0.5 km further downstream and RRS10 is situated about 0.2 km away from RRS9, in a part of Robinsons River that branches away and flows around a small island. This smaller stream is approximately 5 m wide, and about 0.25 m deep, and is also intersected by a stream flowing from a pond that drains a small wetland. Hence the tributary stream may have acidic waters. RRS11 and RRS12 are approximately 0.8 and 1.2 km downstream, respectively from RRS10. These samples are from the main part of Robinsons River in an area where eroded material from nearby clear-cuts enters the stream. RRS13 and RRS14 are downstream from two former railway bridges. RRS13 is immediately below the larger of the two bridges, whereas RRS14 is downstream from both bridges. The last sampling site, RRS15 is just downstream from a road bridge

connecting the communities of Robinsons and Cartyville and is downstream from land used for agricultural purposes.

2.3 Stream Water Analysis

Concentrations for a wide range of analyte elements, 46 in total, ranging from Li to U, were determined using the HP4500+ quadrupole ICP-MS located in the Alexander Murray Earth Science Building at Memorial University of Newfoundland. Operating conditions are given in Table 2.1.

After the water samples were collected and acidified, they were transported to the lab and placed in cold storage until analysed. Sample preparation for analysis consisted of taking 1 ml of water from the sample and placing it in a 12 ml test tube, and then adding 9 ml of 0.2 N HNO_3 . This dilution is done because the HP4500+ has two modes of detection; pulse counting (PC) mode that measures ions in counts per second (cps) and analog mode that measures the ions current which is cross-calibrated to produce cps. PC mode is used for intensities up to approximately 1,000,000 cps, analog is used for higher ion beam currents. By diluting the samples, detection is maintained in the PC mode.

In addition to the field samples, calibration standards, calibration blanks, reagent blanks, and water reference standards were included in each analytical run. Five calibration standards were used. These are solutions prepared from single element standards (concentration of 1000 ppm) that were purchased from SCP Science (Baie

Table 2.1 HP4500+ quadrupole ICP-MS operating conditions for water analysis.

Plasma Conditions	
RF Power	1250 W
Plasma gas flow	15 l min ⁻¹
Auxiliary gas flow	0.98 l min ⁻¹
Nebuliser gas flow	1 l min ⁻¹
Data Acquisition	
Scanning Mode	Single point per peak
Points per mass	1
Acquisition time per mass	10 s
Average settling time	1.8 ms
Average dwell time	100 ms

D'Urfé, Québec). The original solutions are diluted with 0.2 M HNO₃ to concentrations in the ppb range. They are used to determine the sensitivity (signal/concentration) of the instrument. Calibration blanks are used as a blank for the calibration standards. These were prepared from 8 M HNO₃ that is diluted with deionized water to 0.2 M HNO₃. Reagent blanks are made up of deionized water that undergoes the same sample preparation for ICP-MS analysis as the field samples. Water reference standards were from the United States Geological Survey (USGS) and have accepted elemental concentrations that were used for quality control comparison purposes. Five were used: t129, t137, t143, t145, and t155.

Each analysis for every cycle in the run consisted of a 60 second peri-pump uptake, followed by a 20 second stabilization period, and then data acquisition for 563 seconds. After each tube, there was a rinse with 0.5 M HNO₃ for 3 minutes. Each cycle began with the five calibration standards. After the calibration standards were measured, a flush was inserted to clear away the relatively high concentration calibration standard analytes from the system. Following this, a calibration blank and then a reagent blank were run, followed by the set of “unknown” samples, eight in total. This consisted of field samples, reagent blanks, and reference materials. The field samples contained field duplicates, which are two samples taken at the same sampling point, and split samples, which are field samples that were divided into two aliquots in the laboratory, with the goal of monitoring the analytical precision of the instrument. Field blanks consisted of deionized water that is “sampled” in the field and undergoes the same sample preparation as field samples. Finally, one of the reference materials was used for a comparison of measured values to accepted values, with a different reference material in each cycle. There were a maximum of 10 cycles per run. After the run was completed, concentrations were calculated using a waters/biological package that was developed at Memorial University of Newfoundland by Simon Jackson (Longerich, 2000). Values obtained from field blanks were subtracted from actual field sample concentrations.

The isotopes for which data was acquired in the analyses included: ⁶Li, ⁷Li, ⁹Be, ¹⁰B, ¹²C, ¹⁴N, ²⁵Mg, ²⁷Al, ²⁸Si, ³¹P, ³⁴S, ³⁵Cl, ⁴²Ca, ⁴³Ca, ⁴⁹Ti, ⁵¹V, ⁵²Cr, ⁵³Cr, ⁵⁴Fe, ⁵⁵Mn,

^{56}Fe , ^{57}Fe , ^{59}Co , ^{60}Ni , ^{65}Cu , ^{66}Zn , ^{75}As , ^{79}Br , ^{82}Se , ^{85}Rb , ^{88}Sr , ^{98}Mo , ^{107}Ag , ^{111}Cd , ^{118}Sn ,
 ^{121}Sb , ^{127}I , ^{133}Cs , ^{137}Ba , ^{139}La , ^{140}Ce , ^{201}Hg , ^{205}Tl , ^{208}Pb , ^{209}Bi , and ^{238}U .

2.4 LA-ICP-MS Analysis

After the pebbles were cleaned and dried, they were cut with a rock saw located in the Earth Science Building. To minimize contamination from the rock saw, water was not used to cool the blade and the pieces cut from the pebbles were washed with deionized water and air dried after cutting. After drying they were attached to standard thin section slides using five minute epoxy. Samples were then placed in an HEPA air filtered drying space located in the Department of Earth Sciences at MUN to allow the adhesive to set.

Analysis of the coatings was done at the Great Lakes Institute for Environmental Research at the University of Windsor, Windsor, Ontario. For the pebble chips, two chips from each pebble were analysed. In previous work, individual spots were analysed on the coatings, but the disadvantage of this procedure is that studies have shown that the coatings are heterogenous with large variations on the same coating when done by spot analysis (Coish, 1993, 2000). In an effort to get a better representative sample of the coating, Coish (1993) suggested that a large number of spots should be analysed on each pebble. In this work a traverse was used which should give a better sample of the coating composition because it is in effect a series of points analysed along a line across the pebble chip.

2.4.1 Imaging System and Stage Control

LA-ICP-MS analysis of the samples was observed using a Sony analog camera interfaced to a PC through a video capture card. Real-time imaging, photographs, and spatial measurements were made with Image Pro Plus® (Carlsbad, CA) image analysis software. The motorized stage used was a Prior Scientific® (Rockland, MA) model, that was controlled (x-y-z) by a Stage Pro® module present in the Image Pro Plus® (Carlsbad, CA) image analysis software. Stage movement was controlled using a joystick. The Image Pro Plus® (Carlsbad, CA) software was also used to control the vertical movement; this movement was attained with a Prior Scientific® (Carlsbad, CA) focus drive, which has a resolution of 0.2 μm .

2.4.2 Laser Setup

The laser used for the Fe-Mn oxide analysis was a non-homogenized, high power (~ 1.0 mJ/pulse), frequency quadrupled (266 nm), Continuum® (Santa Clara, CA) Surelite® I Nd-YAG laser. Laser operation used the Q-switched mode and a pulse rate of 17 to 20Hz. The pulse width was 4-6 ns, with a beam diameter of approximately 5 mm.

Figure 2.5 is a diagram of the laser optics system which was designed by Brian J. Fryer and the Metals Research Laboratory of the Great Lakes Institute for Environmental Research (GLIER), and the Department of Earth Sciences at the University of Windsor. One of a series of removable, aluminum disks (beam aperture) with apertures from 1-4 mm in diameter was placed in the beam path. The apertures serve the purpose of

Table 2.2 Incident power of different beam constrictor diameters (Crowe *et al.*, 2003).

Aperture Diameter (UNITS)	Laser Power (UNITS)
none	18.0
4.0	14.5
3.5	13.5
3.0	10.5
2.5	9.0
2.0	6.0
1.5	2.8
1.0	1.1

removing the outer, lower-energy, less homogeneous portion of the laser beam. As the diameter of the aperture is varied, the power of the beam is changed (Table 2.2). Incident beam power was measured with a Melles Griot® (Carlsbad, CA) broadband power/energy metre that was equipped with a large area thermopile, a high density graphite sensor disc. Two 90° solid aluminium (coated for 266 nm) mirrors were used to guide the beam into the laser port of the Olympus® (Markham, ON) BX-51 petrographic microscope. Finally, a Melles Griot® 266 nm coated mirror was used to reflect the beam and an Optics For Research® (Caldwell, NJ) 266 nm 5x objective lens was used for focussing the beam.

Samples were placed in a custom-designed cell that was fabricated from a Lexan cylinder with a screw-top removable lid and a fused silica window. When samples are in the form of standard thin sections, the cell has a volume of 100 ml. Ablation carries

material from the sample cell to the ICP-MS via 4 mm inside diameter plastic tubing. The ablated material was then transported to a standard Thermo Elemental® ICP torch by a mixture of ultra-pure nebuliser Ar gas (BOC®, Windsor) and N₂ gas (BOC®, Windsor). Introduction of the N₂ to the Ar gas was done prior to its entering the sample cell by an Aridus® micro-concentric desolvating nebuliser gas controller. The ratio of Ar to N₂ was 50:1, which gave maximum sensitivity.

The ICP-MS used was a Thermo Elemental® X-7 (Mississauga) quadrupole instrument. This is a high sensitivity instrument (450 million cps ppm⁻¹ on U using solution nebulisation). One of the important advantages of this instrument is that it has a dual mode detector. Previous work by Coish (1993, 2000) used an ICP-MS that only operated satisfactorily in the digital mode. When high count rates were obtained, that were higher than the cut-off limit, the detector would shut off in order to protect it from damage (Longerich *et al.*, 1986). This was a significant problem because when count rates above the cut-off were obtained the element could not be measured subsequently. This is especially important for the monoisotopic element Mn, and the high abundance element Fe, both of which are major elements in the coating being analysed. This was an issue in Coish's second study, in which ⁵⁵Mn could not be measured in the coatings. A dual mode detector switches from PC mode, in which ions are counted, to analog mode, where the ion beam current is converted to a potential. A "cross calibration" must be carried out which allows the conversion of the analog data to an equivalent PC cps signal. Since the Thermo Elemental® X-7 detector is able to use both of these modes, it can offer

the superiority of the PC mode in lower intensity ranges, and the extended dynamic range capability supplied by the analogue mode for higher intensities (Longerich and Diegor, 2001). The Thermo Elemental® X-7 also offers fast switching between two modes of resolution, standard and high. When high resolution is selected, there is a lower sensitivity which maintains the detector in PC mode. Also, the relationship between pulse and analog counts can possibly lead to some loss of precision. An additional reason for using high resolution (lower sensitivity) is that the detector has a dynamic range of 9 orders and if counts go above this, which can easily happen for the major elements Mn and Fe, the detector shuts off to protect itself from damage. This shutoff of the detector takes 100 ms to reset itself and all data is lost during this time interval. The elements that were analysed using high resolution were ^{27}Al , ^{29}Si , ^{43}Ca , ^{55}Mn , and ^{57}Fe .

2.4.3 LA-ICP-MS Data Acquisition

As mentioned in section 2.5, line raster sampling was used for the analysis of the Fe-Mn oxide coatings. The operating conditions for the LA-ICP-MS analysis are given in Table 2.3. After a sample was placed in the sample cell, the cell was allowed to flush for approximately 10 minutes in order to remove residual atmospheric gases. Each run began with two NIST 610 acquisitions, followed by analysis of the samples (8-16 analysis) followed by a repeat of two NIST 610 acquisitions. NIST 610 is a Standard Reference Material (SRM) produced by the National Institute of Science and Technology (NIST)

Table 2.3 LA-ICP-MS operating condition.

Laser	
Model	Continuum Surelite I®
Wavelength	266 nm
Aperture diameter	2.5 mm
Energy per pulse	0.2 mJ
Repetition Rate	20 Hz
Micro-Concentric Desolvating Nebulizer	
Model	Cetac Aridus®
Temperature	70°C
Ar gas flow	2.96 L min ⁻¹
N ₂ gas flow	17 ml min ⁻¹
ICP-MS Plasma Conditions	
RF power	1280 W
Plasma gas flow	15 l min ⁻¹
Auxiliary gas flow	1.02 l min ⁻¹
Nebulizer gas flow	1.05 l min ⁻¹
Data Acquisition	
Scanning mode	Rapid peak hop
Dwell time	10 ms
Points per peak	1
Settling time (average)	2.13 ms

(Rocholl *et al.*, 1997). This is an artificially produced Si-Na-Ca-Al-oxide glass that is doped with sixty-one trace elements at a concentration of approximately 500 ppm and is considered homogeneous (~1%) for many trace elements. Each acquisition started with approximately 60 seconds of background. That is, data was collected while the laser was firing, but with the beam blocked. This is an instrumental “gas” background and not a reagent blank (Longerich *et al.*, 1996). For each element, the background is averaged and subtracted from the averaged gross analyte ablation count rates to produce net count rates. The integration time for the background and the analyte are initially selected by the computer with subsequent optimisation by the operator if needed. After the 60s background, the laser beam was unblocked. Line rasters were used for each analysis, including the NIST 610 reference material. For the Fe-Mn oxide coating samples, places on the pebble with the thickest and most even coatings were selected for ablation. The reference material and the samples were usually ablated for 60 seconds. There was also some depth profiling analysis, in which the laser was turned on and allowed to ablate the Fe-Mn oxide coating at a single spot to obtain information about the coating depth and the variations of analyte concentrations with depth.

A suite of isotopes was chosen that could usefully be applied to all samples. These isotopes consisted ^{27}Al , ^{29}Si , ^{43}Ca , ^{47}Ti , ^{51}V , ^{53}Cr , ^{55}Mn , ^{57}Fe , ^{59}Co , ^{62}Ni , ^{65}Cu , ^{65}Zn , ^{75}As , ^{82}Se , ^{86}Sr , ^{89}Y , ^{107}Ag , ^{111}Cd , ^{118}Sn , ^{137}Ba , ^{139}La , ^{140}Ce , ^{197}Au , ^{202}Hg , ^{206}Pb , ^{207}Pb , ^{208}Pb , ^{209}Bi , ^{232}Th , and ^{238}U . The choice of isotopes for multi-isotopic elements was made to minimise interferences. For example, ^{57}Fe was chosen rather than ^{58}Fe because of the

interference of ^{58}Ni . Polyatomic interferences were also considered for selection. As well signal background ratios were optimised, for example in the choice of ^{53}Cr in place of ^{54}Cr , due to the higher background from interference of $^{40}\text{Ar}^{14}\text{N}$.

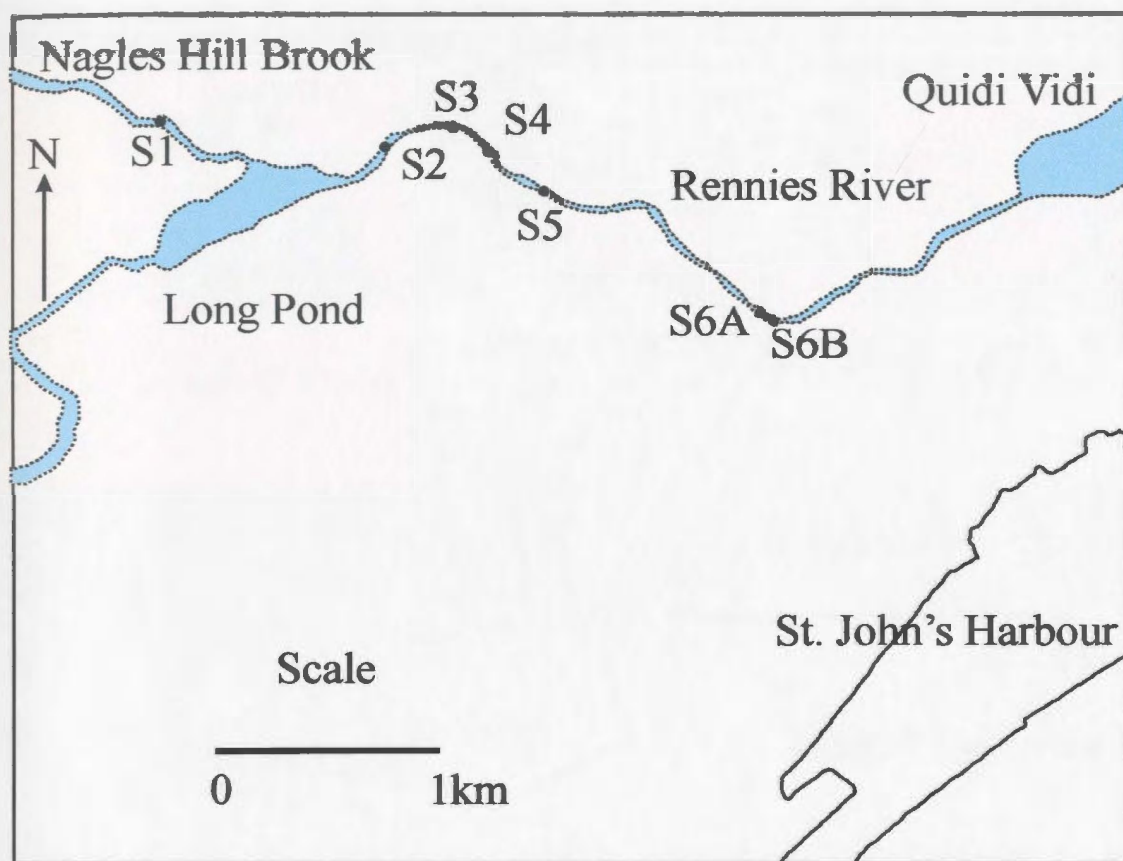


Figure 2.1 Map of the St. John's study area showing sampling locations.

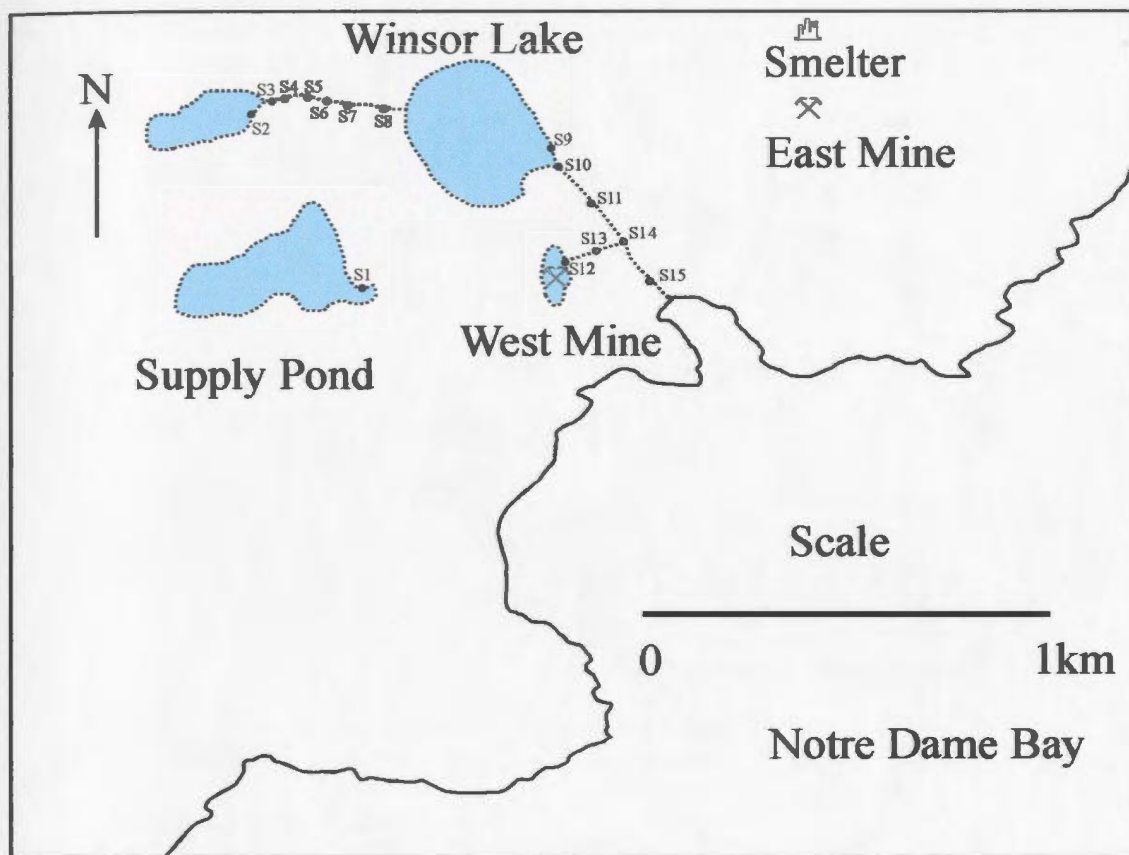


Figure 2.2 Map of the Tilt Cove study area showing sampling locations.

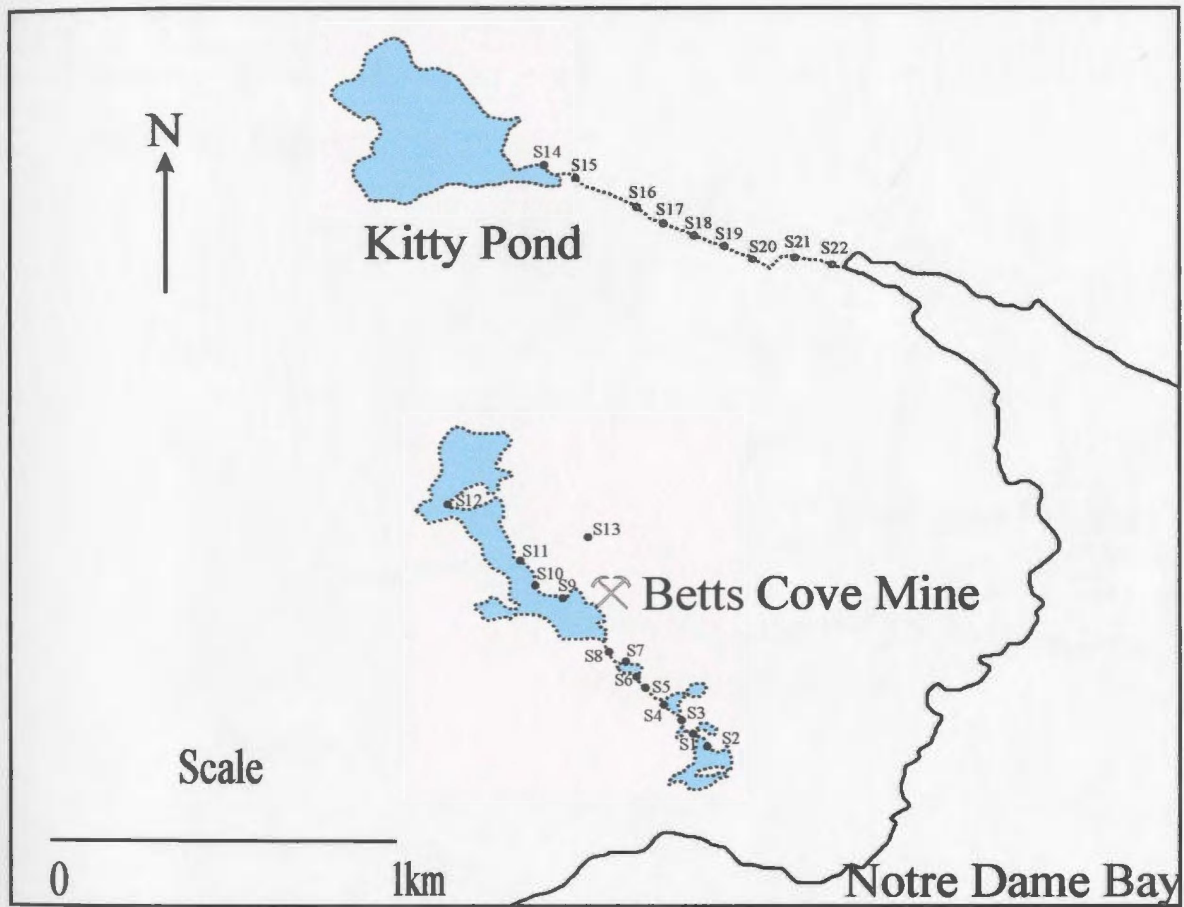


Figure 2.3 Map of the Betts Cove study area showing sampling locations.

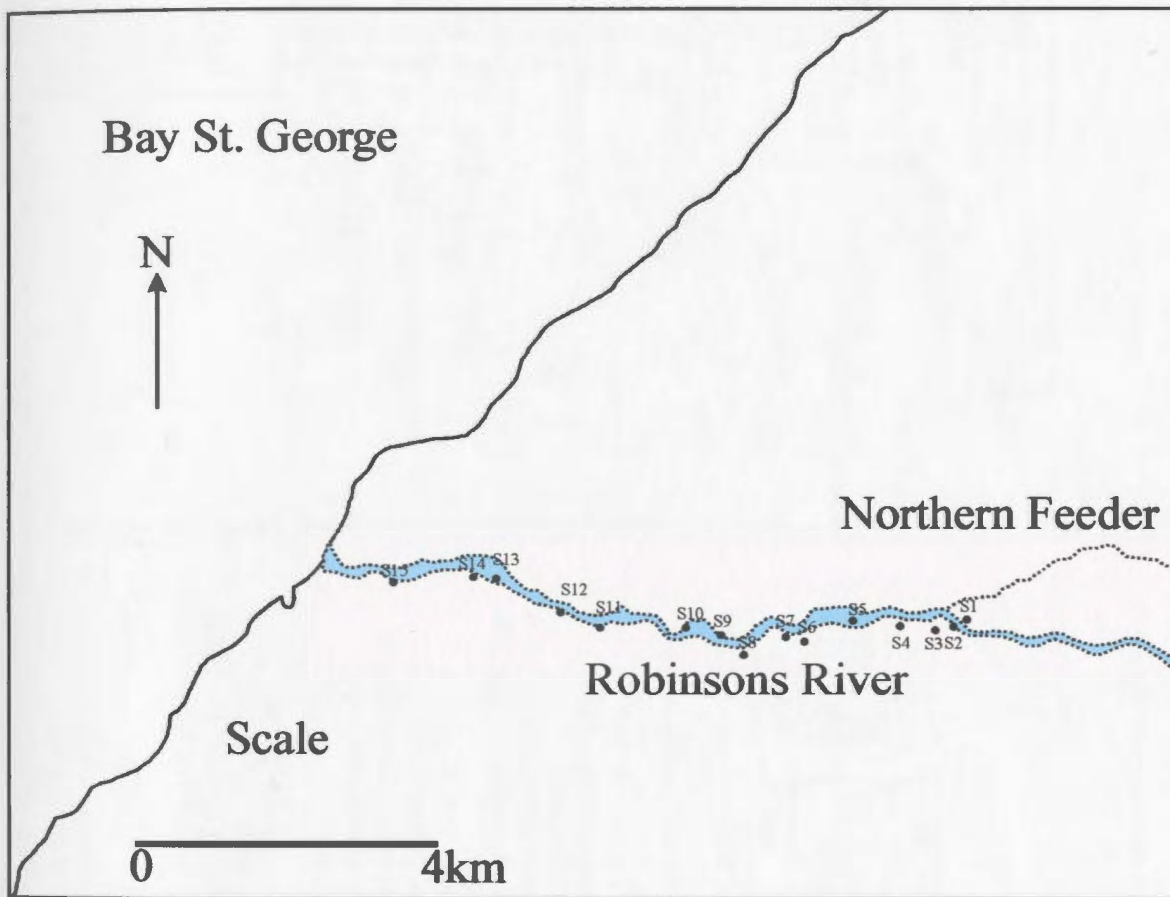


Figure 2.4 Map of the Robinsons River study area showing sampling locations.

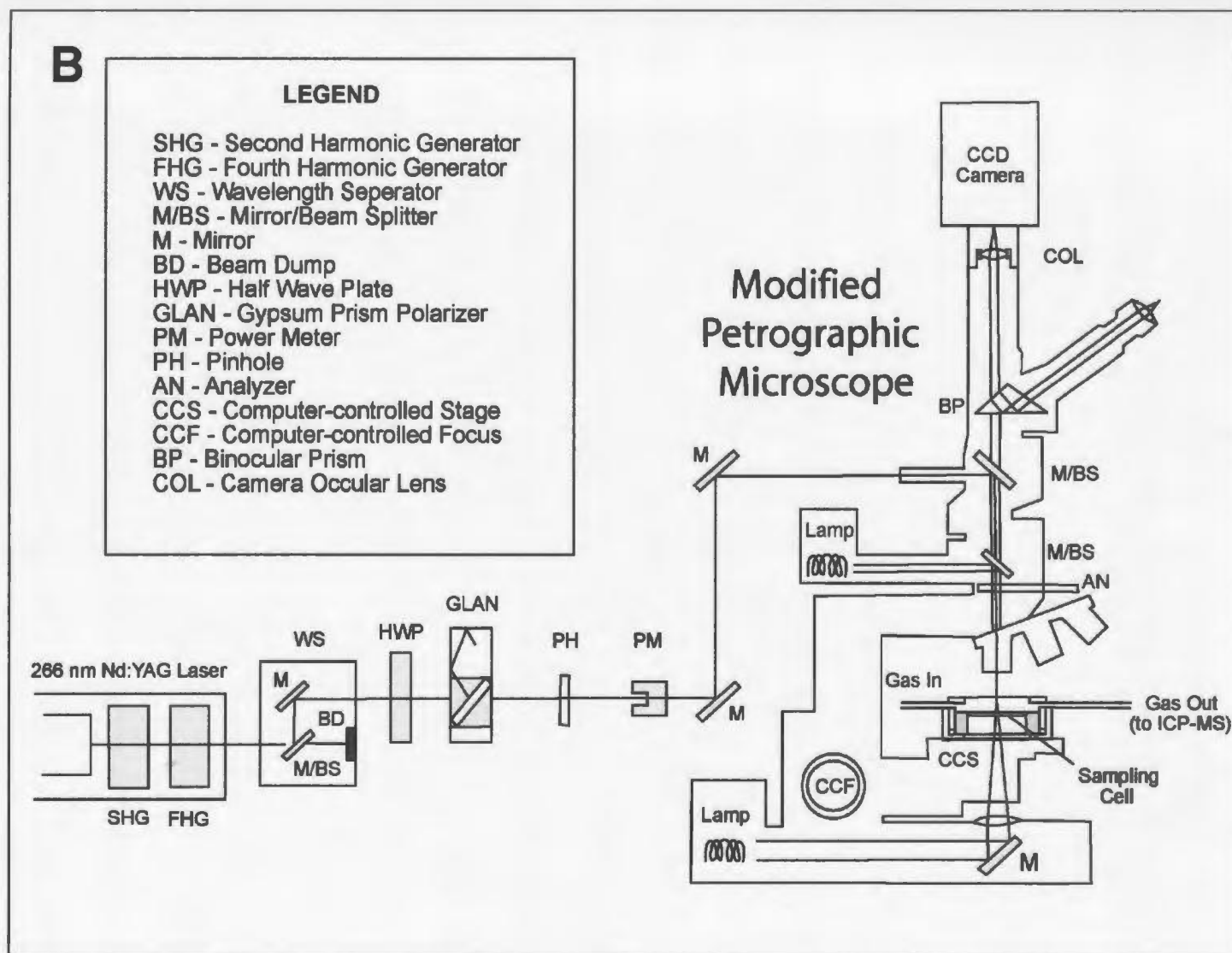


Figure 2.5 LA-ICP-MS schematic (Crowe *et al.*, 2003).

3. LA-ICP-MS Quantification and Data Analysis

3.1 LA-ICP-MS Internal Standard

As previously described, one of the goals of this study was to determine the absolute concentrations of the analytes, a goal which was not accomplished in previous studies using LA-ICP-MS of pebble coatings. This requires a natural occurring internal standard, that is an element (or combination of elements) with a known natural homogeneous distribution throughout the sample and which is also present in the calibration materials at known concentrations. The internal standard corrects for the multiplicative effects of matrix, drift, and quantity (weight or volume) of ablated sample (Longerich, 2001). Examples of natural occurring internal standards for LA-ICP-MS include Si for glass analysis; Ca for seashells, corals, fish otoliths, and fluid inclusions; and S for sulphides (Axelsson *et al.*, 2002; Sylvester, 2001). Elemental concentrations in the internal standard must be known from either direct analysis using another instrument such as the electron microprobe or from known mineral stoichiometry.

3.1.1 EM and SEM Analysis

The electron microprobe (EM) and scanning electron microscope (SEM) were used to study potential naturally occurring internal standards present in iron-manganese oxide coatings that could be used in the quantification of the LA-ICP-MS results. Figure 3.1 is a schematic diagram of an electron microprobe (Reed, 1993).

The electron microprobe located in the Department of Earth Science at MUN is a 1991 Cameca SX-50 with three wavelength dispersive spectrometers (WDS) and one energy dispersive spectrometers (EDS). The WD spectrometer exhibits detection limits as low as 0.01%. Some image acquisition and qualitative analysis were completed using the SEM unit in the Department of Biology at MUN. This system is a Hitachi 5570 SEM with a Tracor Northern 5500 EDS.

3.1.2 EM Results

One of the crucial requirements for quantitative EM analysis is that samples must be flat and polished and positioned perpendicular to the electron beam. For Fe-Mn oxide coating analysis on stream pebbles, this is not possible because the surfaces are rough and rounded and any polishing would remove the coating. Sections of pebbles that appeared reasonably flat and had good coatings were selected for analysis.

Operating conditions for WDS analysis included a beam current of 20 nA, accelerating voltage of 15 kV, and take-off angle of 40°. For EDS analysis, a beam current of 0.1 nA, accelerating voltage of 20 kV and take off angle of 30° were used. Analysis was attempted using WD detection but problems were encountered because of the unfavourable geometry, resulting in the emitted X-Rays not being well focussed on the detector. This problem was due to the rough, non-flat surface topography of the samples (Reed, 1993). Analysis was then attempted in ED mode. Elements, as oxides,

that were detected included: Na_2O , MgO , Al_2O_3 , SiO_2 , SO_3 , K_2O , CaO , TiO_2 , MnO_2 , Fe_2O_3 , and ZnO . The results are given in Appendix 1 from 60 point traverses on each substrate.

Means, standard deviations (SD), and relative standard deviations (RSD) are listed in Table 3.1. For all of the analyses, with the exception of SiO_2 on the polished pebble, RSD values were greater than 10%. One reason for this variability is that the beam was interacting with the substrate and coating, rather than the coating alone. When the electron beam impacts the sample, the electrons spread out into a tear-drop shaped volume (Mason, 1994). The mean depth of penetration is a function of the accelerating voltage and the mean atomic number of the sample. That is, as the accelerating voltage is increased or the mean atomic number is decreased, the beam will penetrate and spread out further into the sample. Depending on the operating conditions and the mean atomic number, the exciting electrons may penetrate anywhere from 1 to 3 μm or more into the sample. For the excited X-Rays that are emitted, some of these will be adsorbed by the sample. The X-Rays produced by higher atomic numbers have higher energies than those produced from lower atomic numbers. This creates an additional difficulty in the data interpretation because X-Rays produced from the low atomic numbers come from nearer the surface than those from higher atomic number analytes. This is not a problem for many geologic samples, which can usually be assumed to be homogeneous vertically and horizontally for a few micrometers. However, Fe-Mn oxide coatings do not have a

Table 3.1 Calculated means (AVG), standard deviations (STD), and relative standard deviations (RSD) of elemental concentrations (%) for traverses done on a streak plate, polished pebble, cement sphere, and pebble collected from site S2 in May, 2002.

Substrate		Streak			Polished		Pebble
Element	AVG	STD	RSD	AVG	STD	RSD	
Na ₂ O	3.0	1.4	49	0.1	0.2	147	
MgO	0.4	0.8	222	0.1	0.2	128	
Al ₂ O ₃	28	6	21	1.1	0.9	86	
SiO ₂	62	7	11	97	3	3	
K ₂ O	3.5	0.9	26	-0.1	0.2	-164	
CaO	0.3	0.2	58	0.05	0.6	1048	
TiO ₂	0.2	0.1	51	0.03	0.08	300	
MnO ₂	0.1	0.2	250	0.06	0.1	215	
Fe ₂ O ₃	2	4	213	1	1.4	134	
SO ₃	0.4	1.0	237	0.2	0.3	162	
ZnO	0.0	0.2	385	0.03	0.2	522	
Total	99	1	1	99	0.7	0.7	
MnO ₂ + Fe ₂ O ₃	2	4	209	1	1	131	
		Cement			Pebble		
Element	AVG	STD	RSD	AVG	STD	RSD	
Na ₂ O	1.1	0.8	72	1.2	1.7	134	
MgO	2.6	2.7	106	1.0	0.7	70	
Al ₂ O ₃	16	10	64	17	5	31	
SiO ₂	40	23	58	40	18	44	
K ₂ O	0.6	0.9	165	3.2	2.4	76	
CaO	10.7	9.1	85	0.20	0.20	100	
TiO ₂	1.2	1.5	129	0.6	1.1	172	
MnO ₂	3.8	7.2	191	8.4	12.9	155	
Fe ₂ O ₃	25	21	83	31	17	56	
SO ₃	0.5	0.5	94	1.2	0.9	76	
ZnO	3.6	5.7	160	0.2	0.3	179	
Total	99	0.8	1	99	0.8	0.8	
MnO ₂ + Fe ₂ O ₃	29	22	78	1	1	131	

uniform thickness or composition (Figure 3.2). When a traverse is completed, one point

could be analysing the coating where it has a thickness of 100 μm , the next point may be analysing a spot where there is no coating present. Even if two points have the same coating thickness, they can have different compositions and thus different penetration depths.

The surface roughness of the samples can also cause analytical problems (Reed, 1993). Even when the surface of the sample appears perfectly smooth when examined using an ordinary petrographic microscope, topographic variation can occur on a horizontal scale of less than 1 μm , and this affects the path length of the emitted X-Rays and exciting electrons. This in turn affects the Z factor, which is a measure of electron penetration, and the absorption factor (A) which are both used in the ZAF correction. For a moderately adsorbing material, the intensity can be reduced by 1% for a 0.2 μm increase in distance travelled by the X-Ray. Emitted X-Rays from low atomic number elements have lower energy than high atomic number elements, and therefore this has a greater effect on the lower atomic number elements.

Results indicate that the streak plate had elevated concentrations of Al_2O_3 and SiO_2 , 28% and 62% respectively; these values are somewhat constant throughout the traverse. Low values of MnO_2 were detected (1%), with a somewhat higher amount of Fe_2O_3 (2%). The polished pebble exhibited elevated concentrations of SiO_2 (97%), and low values of MnO_2 and Fe_2O_3 , 0.06% and 1% respectively. The cement substrate had relatively high amounts of Al_2O_3 (16%), SiO_2 (40%), CaO (10.7%), and Fe_2O_3 (25%).

Finally, the stream pebbles had elevated concentrations of Al_2O_3 , SiO_2 , and Fe_2O_3 ; 17%, 40%, and 28%, respectively. Since there are such high RSD values associated with the data, no useful quantitative information was obtained. This work suggests that determination of an internal standard for Fe-Mn oxide coatings by electron microprobe analysis does not seem to be a viable method.

3.2. LA-ICP-MS Data Reduction

Analysis of geologic samples using LA-ICP-MS produces large quantities of data, much more than conventional techniques such as electron microprobe analysis, due to the fact that time-resolved data are collected for a large number of isotopes. It is important that the analyst carefully examine the time resolved signals during the acquisition and again during data reduction. This requires data reduction software that is able to allow signals to be viewed as a function of time and allow regions of the background and analyte signal to be selected and integrated for concentration calculations.

The program LAMTRACE was used for the data reduction in this work. It is the first widely used program for calculating trace element concentrations and is accompanied by a program CONVERT that reformats ICP-MS instrument software data into a common format for use by LAMTRACE (Achterbergh, 2001). After the data were acquired, the CONVERT program was used to reformat and to integrate the sweeps in each run; sets of 3 sweeps were chosen to be integrated to smooth the data. Converted

files (up to 20 per run) were then loaded into LAMTRACE where signal (cps) versus time graphs were produced. Each run consisted of a maximum 20 analyses with the first two and last two acquisitions of each run being the NIST 610 reference material. Next, the background and signal regions were preselected by the LAMTRACE program, and were accepted or adjusted by the operator. For selection of the background interval, the first initial points of the background were not selected because the system takes a few seconds to stabilize (Longerich, 2001). During the background interval, the laser is on and firing, with the beam blocked. This is done because electrical pick-up by the ion detector of the electrical noise from the laser firing circuits can occur (Longerich *et al.*, 1996). It also thermally stabilizes the laser output energy. As well, points immediately before the laser was unblocked were not included in the background. For the analyte region, initial points were not included because the signal must stabilise to avoid artifacts associated with laser removal of surface contamination (Longerich *et al.*, 1996). After selection of these regions, LAMTRACE calculated the mean net signal by subtracting the mean background intensity (cps) from the mean gross analyte intensity. LAMTRACE then calculated the concentrations of selected elements based on the known NIST 610 concentrations and values for the internal standard. The NIST 610 values are certified for eight elements (Fe, Mn, Ni, Rb, Sr, Pb, Th, U) but only for the entire wafer, and for nine other elements, interim, or uncertain concentrations are reported by NIST. These are termed uncertain concentrations because values were only determined by one method, or

the two comparative methods did not agree within 2% which is required for certification criteria (Rocholl *et al.*, 1997). In this work, for internal standardization, an assumption that $\text{MnO}_2 + \text{Fe}_2\text{O}_3 = 100\%$ was initially applied. Carpenter and Hayes (1980) suggested that at least 99% of the metallic oxides present on these coatings are iron and manganese oxide phases. The chemical composition of the oxide phases was suggested by Drever (1988), Carpenter *et al.* (1975), Chao (1984), and Krauskopf (1995) as MnO_2 and Fe_2O_3 .

In the LAMTRACE program, only one element can be selected for the internal standard. In this work an arbitrary choice of MnO_2 was chosen for the internal standard. Since the program represents the manganese oxide as MnO , 100% MnO_2 was converted to $\text{MnO}\%$. This was done by dividing 100% by 1.2255, which is the ratio of the molecular weights of MnO_2 to MnO . Elemental concentrations were initially calculated based on this internal standard value of 81.599% MnO . The two oxides (Mn and Fe) were then summed to produce a $\text{MnO}_2 + \text{Fe}_2\text{O}_3$ value, and the data were initially normalised to this.

3.3 LA-ICP-MS Optimization

To aid in obtaining high quality analytical results from the LA-ICP-MS analysis, the $\frac{1}{2}$ wave plate setting and the focal height parameters were optimised so that only the coating and not the substrate would be ablated. The $\frac{1}{2}$ wave plate is a control on laser power that is used in combination with a polarizing prism. The polariser allows radiation

that is polarised in one direction to pass through, and rejects the orthogonally polarised component (Jackson, 2001). The function of the wave plate is to rotate the polarisation direction of the laser beam. With no rotation of the $\frac{1}{2}$ wave plate and the laser at full power, the output of the laser is $0.5 \text{ mJ pulse}^{-1}$. When the $\frac{1}{2}$ wave plate is rotated to 90 degrees, the laser beam is fully attenuated ($0.0 \text{ mJ pulse}^{-1}$), and when both the $\frac{1}{2}$ wave plate and prism are removed, the laser power is 1 mJ pulse^{-1} . Using angles of rotation for the $\frac{1}{2}$ wave plate between 0 and 90 degrees allows the operator continuous control over the power between the 0.0 and $0.5 \text{ mJ pulse}^{-1}$.

As focal height is increased, the beam defocusses, producing a larger beam diameter, and hence ablates a larger sample area horizontally, but due to the lower energy density, the beam does not penetrate into the sample as fast. Defocussing of the beam also minimises the change of the beam diameter as the boring depth increases. The depth of ablation pits is a function of the power per pulse, the number of pulses (time), and the beam diameter. To examine the effect of these parameters on LA-ICP-MS analysis of Fe-Mn oxide coatings, a preliminary run was carried out in which a pebble chip, TCS 13.1.2 (study area, site, pebble, chip), was analysed by varying these parameters. There were eight analyses; the first four used a focal height of $200 \mu\text{m}$ with a set of $\frac{1}{2}$ wave plate settings from 140° to 125° . An additional four analyses used a focal height of $400 \mu\text{m}$ and the same set of $\frac{1}{2}$ wave plate settings.

3.3.1 Results of LA-ICP-MS Optimization

Results of the LA-ICP-MS optimization are shown in Appendix 1. Calculated means, standard deviations, and relative standard deviations are listed in Table 3.2. The concentrations determined for the optimization use a 100% $\text{MnO}_2 + \text{Fe}_2\text{O}_3$ internal standard value and include Al_2O_3 , and SiO_2 . These are expected major components of the substrate and can act as a measure of the laser sampling the substrate. Following ablation, observation was made of the rastered areas on the sample (TCS 13.1.2) using a low-power microscope which showed that when using a focal height of 200 μm , the beam would sample the coating and substrate at all $\frac{1}{2}$ wave plate settings used. When the focal height was increased to 400 μm , the beam would penetrate through the coating and into the substrate only when using $\frac{1}{2}$ waveplate settings of 140° or 135°. At $\frac{1}{2}$ waveplate settings of 130° and 125°, there was no observed sampling of the pebble substrate.

Investigation was carried out to study the interaction of operating conditions and concentration of elements determined. For the first analysis, Al_2O_3 and SiO_2 had values of 8.70% and 18.79% respectively, this gradually decreased to 4.19% and 4.83% respectively for the last analysis in the run as $\frac{1}{2}$ wavelength setting and focal height were decreased (Figure 3.3(a)) Lower values of Al_2O_3 and SiO_2 are expected when only the coating is sampled and not the coating and substrate as the coating should have lower concentrations of Al_2O_3 and SiO_2 than the pebble substrate. The final values obtained for Al_2O_3 and SiO_2 may represent clay particles which may be occluded in the coating. This

Table 3.2 Calculated means (avg), standard deviations (std), and relative standard deviations (rsd) of elemental concentrations (ppm) determined by LA-ICP-MS for traverses done on TCS 13.1.2 (* = Concentration in %)

Analysis#	avg	std	rsd
Al ₂ O ₃ *	6.6	1.7	26.3
SiO ₂ *	15.7	7.7	48.9
CaO*	1.45	0.15	10.27
TiO ₂ *	0.15	0.13	84.91
MnO ₂ *	0.09	0.03	34.6
Fe ₂ O ₃ *	100	0.03	0.03
V	101	59.3	58.4
Cr	773	27.5	3.6
Co	257	48.5	18.8
Ni	191	31.2	16.3
Cu	52964	4564	8.6
Zn	9044	462	5.1
As	157	60.8	38.7
Se	2.62	1.76	67.1
Sr	102	6.5	6.4
Y	17.3	18.5	107.2
Ag	1.99	1.49	74.7
Cd	13.1	0.51	3.9
Sn	1.28	1.00	78.5
Ba	69.4	3.55	5.11
La	5.01	0.94	18.8
Ce	13.9	2.06	14.9
Au	<0.013		
Hg	N.A.		
Pb	49.56	7.48	15.09
Pb	45.22	6.62	14.63
Pb	45.71	7.25	15.86
Bi	0.11	0.13	111.2
Th	0.72	0.04	5.56
U	10.50	1.73	16.51

analysis has an Al_2O_3 to SiO_2 ratio of 0.867 which is very close to that of kaolinite clays, 0.848 (Deer *et al.*, 1992). Since organic matter and sediment appeared on the coating, it is reasonable that clay particles could also be present.

The concentrations of other elements in this low MnO_2 -high Fe_2O_3 sample appear to be relatively constant. RSD values less than 20% were obtained for the following elements: CaO, Fe_2O_3 , Cr, Co, Ni, Cu, Zn, Sr, Cd, Ba, La, Ce, Pb, Th, and U. Concentrations for Au and Hg were below the detection limit. It appears that even if some of the substrate is ablated, this has little effect on the calculated concentration of the elements in the coating (Figure 3.3(b)). This is likely due to the excellent adsorbing properties of the coatings for most elements resulting in much higher coating concentrations than substrate trace analyte concentrations.

3.4 LA-ICP-MS Results

As mentioned earlier, calculation of elemental concentrations in the Fe-Mn oxide coatings initially used $\text{MnO}_2 + \text{Fe}_2\text{O}_3 = 100\%$ as the internal standard. This assumed that MnO_2 and Fe_2O_3 were the dominant components in the coating, but it was also observed that some coatings also contained elevated concentrations of Al_2O_3 , and SiO_2 . For example, TCPS 4.1.2 had Al_2O_3 and SiO_2 values of 154.6% and 343.6% respectively. This suggests that Al_2O_3 and SiO_2 were dominant phases in the coating or that ablation of the substrate occurred.

The electron microprobe data indicated elevated concentrations of SiO_2 and Al_2O_3 for all samples, although quantitatively this data is not useful due to high RSD values for most of the elements and the increased depth sampling of the EMP. SEM analyses were carried out on four samples, TCPS 3.1.1-3.2.2 (Table 3.3). These came from the Tilt Cove control area, where most of the pebbles appeared to have a thick black coating. The operating conditions consisted of a beam current of 0.1 nA, an accelerating voltage of 20 kV, and a takeoff angle of 30 degrees. The SEM produced Al_2O_3 values from 43.94% to 7.11%, and the SiO_2 values from 1.63% to 49.7%. Similar to the electron microprobe data, this may be due to interaction with the substrate, an aluminum oxide phase or clay particles present in the coating.

Laser data were also examined to ascertain if Al_2O_3 and SiO_2 are part of the coating. A qualitative examination of intensity (cps) vs. time (s) data was completed for traverses and also for some of the depth profiles. Figure 3.4 shows intensity (cps) vs. time (s) plots of a traverse on TCPS 8.1.2 (Figure 3.4(a)) and TCPS 8.2.1 (Figure 3.4(b)) for the elements ^{27}Al , ^{29}Si , ^{55}Mn , and ^{57}Fe . In Figure 3.4(a) it appears that ^{55}Mn and ^{57}Fe signals are correlated while ^{27}Al and ^{29}Si seem to follow different trends. For the MR14B09 run (Figure 3.4(b)), all four elements follow similar trends along the intensity (cps) vs. time (s) plots. Scatter plots were created for the abundance-normalised background-corrected log-transformed intensity (cps) values for each analysis, and Pearson-R correlation coefficients were calculated. These scatter plots were made to

Table 3.3 Element concentrations (wt%) determined by SEM for three analyses of TCPS 3.1.1-3.2.2.

Sample	TCPS-3.1.1			TCPS-3.1.2		
Element(wt%)	1	2	3	1	2	3
Al-K	26	33	44	17	33	37
Si-K	35	14	11	38	9.9	1.6
Ca-K	5.2	4.5	6.6	6.0	5.7	6.9
Mn-K	11	4.2	19	22	18	22
Fe-K	22	43	19	17	33	31
Ba-L	0.5	1.2	0	0.6	0	1.0
Total	100	100	100	100	100	100

	TCPS-3.2.1			TCPS-3.3.3		
Element(wt%)	1	2	3	1	2	3
Al-K	19	18	36	14	7.1	28
Si-K	50	17	7.7	31	23	35
Ca-K	3.9	5.1	5.5	5.9	15	3.6
Mn-K	5.7	23	3.8	32	42	1.1
Fe-K	21	35	47	15	10	32
Ba-L	0	2.6	0	1.9	2.8	0.5
Total	100	100	100	100	100	100

better observe correlation relationships. Examination of the scatter plots suggested that a transformation of the data should be made (Figure 3.5(a)). Log transformation was tried and it was shown to make the data more closely fit a normal distribution (Figure 3.5(b)).

Pearson-R correlation coefficients were used to measure associations between two random variables (Milton, 1999). It is the most widely used correlation coefficient giving values in the range of +1 to -1. A correlation coefficient of +1 signifies a perfect positive correlation, and a value of -1 signifies a perfect inverse correlation, while a value of 0 indicates that there is no relationship. As a rule of thumb, values from 0 to ± 0.5 are considered weak correlations, values from ± 0.5 to ± 0.9 are considered moderate, and values from ± 0.9 to ± 1.0 are high. Along with the correlation coefficient, a p-value is also calculated. This p-value can be tested to see if the two variables are related but it does not determine if the correlation is of any practical importance (Milton, 1999). The p-value is the probability that an observation is due to chance. So, with a p-value = 0.05, there is a 95% confidence that the observation can be reproduced (Statsoft, 1999).

Figure 3.6(a) shows a strong relationship between ^{55}Mn and ^{57}Fe in the MR14B08 analysis, which is expected since they are expected to comprise 99% of the coating. There also appears to be a strong relationship between ^{27}Al and ^{29}Si , ^{27}Al and ^{55}Mn , and ^{27}Al and ^{57}Fe . Figure 3.6(b) shows a strong relationship between ^{27}Al and ^{55}Mn , and ^{27}Al and ^{57}Fe . Pearson-R correlation coefficients for all four elements for each analysis are given in Table 3.4.

Pearson-R correlation coefficients suggest that the strongest correlation occurs between Mn and Fe for the MR14B08 analysis, although strong correlations also exist between ^{27}Al and ^{57}Fe , ^{27}Al and ^{55}Mn , and ^{27}Al and ^{29}Si . For the MR14B09 run, strong

Table 3.4. Pearson-R correlation coefficients and associated p-values (bottom of cell) for MR14B08 analysis and MR14B09 analysis.

Run	MR14B08			MR14B09		
Element	Al	Si	Mn	Al	Si	Mn
Si	0.773 0.000			-0.060 0.664		
Mn	0.731 0.000	0.428 0.001		0.803 0.000	-0.337 0.012	
Fe	0.796 0.000	0.522 0.000	0.850 0.000	0.719 0.000	0.245 0.072	0.491 0.000

correlations were expected between all four elements, this was based on the intensity(cps) vs. time plot. The strongest correlation was between ^{55}Mn and ^{27}Al , whereas the weakest was between Si and Al. Mn and Fe had a correlation of 0.491 in this analysis, compared to 0.850 in the MR14B08 analysis. These correlation coefficients may be a result of ablation of the substrate, or an $\text{Al}_2\text{O}_3\text{-SiO}_2$ phase that may be separate or included with the $\text{Fe}_2\text{O}_3\text{-MnO}_2$ phase.

In addition to traverses, depth profiling studies were also made. These consisted of ablating a single spot for 240 seconds as subsequent layers of Fe-Mn oxide are ablated. Intensity(cps) vs. time(s) plots were examined for the streak plate samples placed in Rennies River at site SJS6A for 3, 6, 9, and 12 months for the elements ^{27}Al , ^{29}Si , ^{55}Mn , and ^{57}Fe . The goal was to determine how the relative signals of these analytes change as the coating “grows.” In Figure 3.7(a) it can be seen that ^{27}Al has the greatest intensity,

followed by ^{29}Si , ^{55}Mn , and ^{57}Fe . After six months, the ^{55}Mn signal becomes greater than ^{29}Si , and eventually at 9 and 12 months, the signal for ^{55}Mn becomes greater than ^{27}Al . Pictures of the coatings on the streak plates for the above profiles were taken with the optics system of the LA-ICP-MS described in Chapter 2 (Figure 3.8). Figure 3.8(a) shows the coating that accumulated for 3 months, (b) for 6 months, (c) for 9 months, and finally (d) for 12 months.

The coating that formed on the white streak plate after three months in the stream consisted of a light brown staining with darker spots in some areas. When depth profiles were completed on coatings of similar thickness, the coating is quickly ablated and ablation of the substrate occurred. A similar phenomena occurred when rastering. Figure 3.8(b) shows the Fe-Mn oxide coating that had accumulated on a streak plate for 6 months. In some areas the coating has grown from a light brown stain to a thicker dark brown coating. Figure 3.8(c) shows the coating that formed on the streak plate after 9 months; it has now become a dark-brown coating on the substrate, although some areas of exposed streak plate are still visible. After 12 months (Figure 3.8(d)), the coating is almost completely dark brown to black in colour, and the substrate appears to be entirely covered with a coating. This pattern of coating accretion was similar to other substrates that were placed at different sites in Rennies River.

Table 3.5 shows the median concentration of Al_2O_3 , SiO_2 , MnO_2 , and Fe_2O_3 for rasters determined by LA-ICP-MS for streak plate substrates at sites SJS1, SJS6A, and

Table 3.5 Median values (%) of concentrations determined by LA-ICP-MS for streak plates placed in the Rennies River study area at sites SJS1, SJS6A, and SJS6B for 3, 6, 9, and 12 months.

Site	Month	Al ₂ O ₃	SiO ₂	MnO ₂	Fe ₂ O ₃
SJS1	3	65	159	22	78
SJS1	6	40	856	75	25
SJS1	9	21	165	77	23
SJS1	12	16	52	79	21
SJS6A	3	91	352	9	91
SJS6A	6	53	163	82	18
SJS6A	9	14	87	84	16
SJS6A	12	15	80	93	7
SJS6B	3	11	40	0.17	100
SJS6B	6	4	17	0.22	100
SJS6B	9	6	53	14	86
SJS6B	12	7	36	11	89

SJS6B for 3, 6, 9, and 12 months. For all sites, the amount of Al₂O₃ decreases with time, and except for site SJS6B, the lowest amount is detected after 12 months of coating accretion. There is a similar trend apparent for SiO₂, although the highest value occurs at 6 months for site SJS1, and after 9 months for site SJS6B. For the MnO₂ and Fe₂O₃ values, the amounts appear to increase with time for MnO₂, and decrease with time for Fe₂O₃.

Further evidence to support that substrates were ablated comes from a traverse on

a piece of “clean” streak plate using the electron microprobe. This sample had no Fe-Mn oxide coating present on it. Sixty points were acquired on this sample, with the same operating conditions as in previous analyses. Means, standard deviations, and relative standard deviations are given in Table 3.6. From this, it can be seen that the streak plate is composed primarily of Al and Si (87%), followed by K (6%) whereas Na, Mg, Ca, Ti, Mn, Fe, and S are present in only minor amounts. Thus, if ablation of the substrate is occurring, then this would contribute Al and Si to the analysis.

Table 3.6 Means(wt%), standard deviations, and relative standard deviations determined on a 60-point traverse of a streak plate by electron microprobe.

Element	Mean(wt%)	std	rsd
Na	4	0.6	13
Mg	0.4	0.09	25
Al	31	6	18
Si	56	5	9
K	6	0.7	12
Ca	0.2	0.09	44
Ti	0.3	0.09	34
Mn	0.03	0.1	365
Fe	0.3	0.1	46
S	0.06	0.1	188
Total	99	3	3

Based on the above SEM, EM, and LA-ICP-MS evidence, a likely explanation for the significant amounts of Al_2O_3 and SiO_2 is ablation of the substrate. The LA-ICP-MS traverse data suggest that, depending on the sample, the Al_2O_3 and SiO_2 may or may not be incorporated into the $\text{MnO}_2 + \text{Fe}_2\text{O}_3$ phase. Depth profiling using LA-ICP-MS suggests that a reason for high Al_2O_3 and SiO_2 values is that the substrate is being ablated,

and the EM data supports this.

Examination of the literature suggests that Al_2O_3 and SiO_2 can be present in the Fe-Mn oxide coatings. Carpenter and Hayes (1980) report that the Fe-Mn oxide coatings which they examined usually contain 40-50% occluded silt, clay, organic material, and adsorbed water. Since all material in the path of the laser beam is being ablated, the silt and clay portion can contribute Al and Si to the analysis. They concluded that the remainder is 99% Fe and Mn oxides. Filipek *et al.* (1981) derived similar conclusions. They employed a four step sequential extraction scheme on scraped boulder coatings taken from the Magruder Mine area, in Lincoln County, Georgia. The lithogenous fraction ranged from 48-68% of the total, this is also known as the residual crystalline phase, which would be adhered to the surface. Thompson *et al.* (1992) suggested that besides the iron and manganese fraction, aluminum oxide and organic material were also major constituents. Theobald *et al.* (1963) suggested that elevated concentrations of Al_2O_3 were present in a thick white coating collected from the junction of Deer Creek and Snake river in Summit County, Colorado. Analysis of the white coating showed that it contained 64-56% Al_2O_3 , 3.9-7.2% Fe_2O_3 , and 0.04-0.09% MnO_2 .

It appears that ablation of the substrate may be at least partially responsible for the high Al_2O_3 - SiO_2 values, although it is not possible to differentiate whether some of the high values are also due to included clays. Some of the analyses of streak plates taken from site SJS6B showed high values of Al_2O_3 and SiO_2 , even though there was no

apparent ablation of the substrate. Figure 3.9(a)-(d) shows ablated coatings present on a streak plate at site SJS6A after 6 (Figure 3.9(a)) and 9 (Figure 3.9(b)) months. Figures 3.9(c) and (d) shows ablated coatings after 6 and 9 months, respectively, taken from site SJS6B. For the ablated plates from SJS6A, the laser has ablated the coating and some of the substrate. The samples taken from SJS6B show no apparent ablation of the substrate. For the Al_2O_3 and SiO_2 values calculated by the 100% $\text{MnO}_2 + \text{Fe}_2\text{O}_3$ normalisation scheme, values of 81.1 wt% Al_2O_3 and 195.3 wt% for SiO_2 were calculated for the SJS6A 6 month sample, and 20.5 wt% and 118 wt% for Al_2O_3 and SiO_2 respectively for the SJS6A 9 month sample. The ablated streak plates from SJS6B yield Al_2O_3 and SiO_2 values of 2.9 and 14.4 wt% respectively after 6 months; and 6.4 and 43.2 wt% after 9 months.

The above observations strongly suggest that there must be some other source of Al_2O_3 and SiO_2 besides the substrate. For samples where ablation of the substrate is not apparent, elevated concentrations of Al_2O_3 and SiO_2 still occur, although not at as high concentrations as the samples where the substrate was ablated. As mentioned, this may be due to an aluminum oxide phase present in the Fe-Mn oxide coating, or it may be due to adhering sediment, including clays. There may also be some amorphous aluminum and silica present on the coatings (Jenne, 1968). These have been reported to be associated with iron-manganese oxides present in soil environments.

In the case of clay particles occluded on the Fe-Mn oxide coating in oxidizing

environments, adsorption of aqueous elements by iron and manganese oxides appears to be much more important (Drever, 1988).

Since there is a large amount of uncertainty for the Al_2O_3 and SiO_2 values and the concentration of all elements are routinely above 100%, further normalisation was performed on the data. Trace element concentrations were converted to their corresponding oxides value; V_2O_5 , Cr_2O_3 , CoO , NiO , CuO , ZnO , As_2O_5 , SeO_3 , SrO , Y_2O_3 , Ag_2O , CdO , SnO_2 , BaO , La_2O_3 , CeO_2 , Au_2O_3 , HgO , PbO , Bi_2O_3 , ThO_2 , and UO_3 . These concentrations, along with MnO_2 and Fe_2O_3 were added together and the original concentrations were divided by this value to normalise the data. Three oxides, Al_2O_3 , SiO_2 and TiO_2 were eliminated from the normalisation because of elevated and random values which may have been a result sampling of the substrate.

3.5 Stream Water Results

Readings for pH, dissolved oxygen, conductivity measurements and stream water analyte elemental concentrations are shown for all four study areas in Appendix 2. For the water samples taken from Rennies River, monthly water composites were made in which equal weights of the weekly water samples were combined to form a composite sample. These were then subjected to the same sample preparation and analysis procedure as the water samples taken from the other study areas.

Examination of the water data resulted in the elimination of certain elements. ^7Li

was used as ^6Li is included in the parameter set only to allow extra settling time for the large mass jump from U to Li. The elements Be, B, P, and S were omitted from further discussion since most values were below the detection limit. ^{43}Ca was chosen over ^{42}Ca due to the high background caused by $^{40}\text{Ar}^2\text{H}$ at 42 amu. Similarly, ^{53}Cr was chosen over ^{52}Cr because of a high background from $^{40}\text{Ar}^{12}\text{C}$ at 52 amu. If concentrations of C were lower, then ^{52}Cr is recommended since it is more sensitive. Of the three measured isotopes of iron (54, 56, 57), ^{57}Fe was chosen due to a high background from $^{40}\text{Ar}^{14}\text{N}$ at 54 amu and a higher background from $^{40}\text{Ar}^{16}\text{O}$ interference at 56 amu. There is also an isobaric interference caused by ^{54}Cr . Br was also omitted because most values are below the detection limit, this may be due to either its high ionisation potential and thus low sensitivity, or that high backgrounds in St. John's may be derived from road salt and sea spray in the blank; this is true for all of the halogens and St. John's is where the water samples were analysed. Most of the values for Se, Hg and Bi were below detection limits, hence they were not included in further analysis. ^{82}Se had a high background from $^{40}\text{Ar}_2^1\text{H}_2$ and interference from $^{81}\text{Br}^1\text{H}$, resulting in elevated detection limits. Detection limits for ^{201}Hg were also high due to a high background arising from contamination in the Ar gas, and its high ionisation potential (Hirata and Nesbitt, 1995). Considerable amounts of mercury are adsorbed onto the sample introduction system and mass spectrometer making mercury difficult to determine at low concentrations (Knight *et al.*, 1999). For Bi, low concentrations were expected due to its low bulk continental crustal

abundance of 0.06 ppm (Reimann and Caritat, 1998).

3.5.1 Statistical Analysis of Waters Results

The waters data was examined to determine regional differences. Similar to the statistical analysis described in section 3.3.1, the data were log-transformed, and then descriptive statistics, in the form of box plots and scatter plots were used to visually examine the data (Appendix 3). For those elements which had concentrations below the detection limit, the measured value was used in the statistical analysis, even though the RSD is greater than 33% for these analyses. Since the net signal is calculated by subtracting the non-zero background from the gross signal, some samples had negative concentrations. Since these values, along with any values of zero, cannot be log-transformed, they must be set to some value. It was decided that to set these to one half of the detection limit, since values closer to zero will create outliers (Taylor, 2001).

As there are 32 elements, along with temperature ($^{\circ}\text{C}$), dissolved oxygen (mg/L), conductivity ($\mu\text{S/cm}$), and pH readings, a form of variable grouping, multivariate statistics, in particular principle component analysis (PCA), was used. Multivariate statistics analyses the relationships of multiple measurements on an individual sample (Taylor, 2001). Principle component analysis (PCA), also known mathematically as principle component factor analysis (PCFA), is a statistical technique that is both sophisticated and comprehensive (Wyrzykowska *et al.*, 2001). This technique reduces a

large number of variables into a smaller set of dimensions by analysing how the variables are interrelated. Components are produced that account for more of the variance than any other combination.

Before PCFA could be carried out, Pearson-R correlation coefficients were calculated for the data. This was done to reduce the variable to sample ratio, which increases the stability of the PCFA model (Yun, 2002). If two variables have a strong correlation, then using both of them provides no additional information, thus only one of them should be selected. Scatter plots along with the p-values were also examined in order to determine how reliable the Pearson-R correlation values were. Not surprisingly, a strong correlation was found for La and Ce, with a Pearson-R correlation coefficient of 0.989. This was the highest correlation found in the study. Ce was chosen for further data analysis since concentrations were higher, as expected, for this element at all sampling sites.

When PCFA is attempted on a data set, eigenvalues are produced for each Factor. The first Factor explains most of the variance in the data, the second the next greatest variance, and so on. Eigenvalues are the column sum of squares for a component and represent the amount of variance accounted for by a particular component (Hair, 1987). To determine how many Factors to retain, the eigenvalues were examined. This can be done by examining a scree plot, which is a plot of the eigenvalue vs. Factor (Figure 3.10(a)). The plot begins with a steeply sloped line that becomes horizontal. Cattell

(1966) suggested that the cutoff point should be when the slope begins to straighten.

There is also the Kaiser criterion which can be used to determine the number of Factors to retain (Statsoft, 2003). This criterion is based on the principle that only Factors which have an eigenvalue greater than 1 should be kept.

For each Factor, a loading is given for each variable. The absolute value of the loading indicates how much the variable contributes to the Factor, with values ranging from 0 to ± 1 , the sign indicates whether the variable is positively or negatively correlated with the component (Wyrzykowska *et al.*, 2001). Variables that have a low loading on each Factor were eliminated from subsequent refinement of the PCFA.

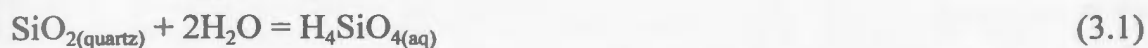
Rotation of the PCFA data space can be applied in order to make each of the Factors more recognizable within the original data set (Systat, 1996). There are Varimax, Quartimax, Equamax, or Orthomax rotations. Varimax, or variance maximizing, maximizes the variance of loadings down through columns of the component loadings matrix (Wilkinson, 1996). It rotates the initial Factor such that a variable will load high on one Factor and as low as possible on all other Factors (Hair, 1987). Quartimax rotation concentrates loadings of many variables onto a strong first Factor. Equamax rotation simultaneously maximizes the variance of loadings down columns and across rows of the component loadings matrix; in most cases, the results lie between those of Varimax and Quartimax. Orthomax results also lie between Varimax and Quartimax, with a gamma parameter that can be set between zero and one; zero represents quartimax rotation, one

represents varimax rotation.

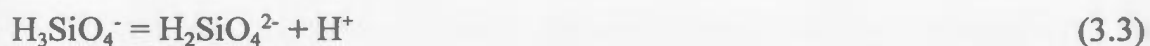
When PCFA was carried out on the waters data, the following elements loaded low on all of the Factors; B, Si, Cl, Ti, V, Cr, Sr, Mo, Ag, Sn, Sb, I, Tl, Pb, and temperature (°C). Thus, these were removed from the PCFA. Most analyses indicated levels of B were below the detection limit, since the calculated values were used for PCFA, there is a high RSD of at least 33% associated with these values; they are not useful for PCFA. Since the data were log-transformed, the standard deviation and not the relative standard deviation becomes constant. This holds true for concentrations greater than several times the detection limit, while for low concentrations, the standard deviation is variable, increasing to infinity at zero concentration. Since many of the values for B are less than 5 times the detection limit, meaningful data was not expected to be extracted from this data. The detection limits for B were high because of its high ionization potential, and from boric acid contamination from other sample preparation procedures used on the HP4500+ (Taylor, 2001). Boron is also known to have memory effects and a low sensitivity.

Silicon concentrations were all well above detection limit but most samples had similar concentrations, which contributed little to the regional classification. The reason for the similar concentrations is that compounds having Si and O are the most abundant materials in rocks, soils and sediments (Krauskopf and Bird, 1995). Silicate minerals make up 90% of the earth's crust and Si has a mean continental crust concentration of

26% (Reimann and Caritat, 1998). Due to the solubility of silica, the global concentration of Si in water is 6 ppm. The dissolution of Si containing minerals follows the reaction below (Drever, 1988);



When the pH is greater than 9, the weak acid, H_4SiO_4 dissociates into H_3SiO_4^- and $\text{H}_2\text{SiO}_4^{2-}$.



The total dissolved silica concentration is a sum of the ionized and neutral species. When pH is greater than 9, the total dissolved silica concentration increases. Since none of the sites had pH values greater than 9, then all sites are expected to have similar concentrations of Si, that being a solution saturated in silica.

Analogous to Br, concentrations of Cl and I are influenced by road salt and sea spray. All four study areas are in coastal locations and three of them are in areas where road salt is used, therefore this is expected to similar analyte concentrations. Also, since road salt and sea spray are present in St. John's, where the water analysis occurred, high

backgrounds are present for all three halogens. Titanium, V, and Cr are all expected to have low solubilities, based on ionic charge and ionic radius properties (Siegel, 2002). This is seen in global background stream concentrations, where values of Ti, V, and Cr are 3 ppb, 0.9 ppb, and 0.7 ppb respectively (Reimann and Caritat, 1998). In this study, concentrations were frequently close to detection limit and thus provide little useful information.

Strontium initially had a moderate loading, but since it is expected to provide similar information as ^{43}Ca , it was discarded from further PCFA. The Pearson-R correlation coefficient between ^{88}Sr and ^{43}Ca is 0.862. Based on ionic charge and ionic radius properties, Mo should be somewhat mobile (Siegel, 2002) but it is found to have a high mobility under oxidizing conditions (Reimann and Caritat, 1998). Molybdenum has a global bulk continental crust concentration of 1 ppm and is usually found in the mineral Molybdenite (MoS_2) and does not substitute into silicates. The median world stream concentration of Mo is 0.5 ppb (Reimann and Caritat, 1998). Most of the concentrations of Mo were only slightly above the detection limit, and therefore this element did not provide useful information for the PCFA.

Silver is commonly associated with lead and zinc ores (Health Canada, 1986a) and is contained in the minerals argentite (Ag_2S), cerargyrite (AgCl), proustite (Ag_3AsS_3), pyrargyrite (Ag_3SbS_3), and silver arsenide (Ag_3As) (Reimann and Caritat, 1998). Silver has a low bulk continental crust concentration of 0.08 ppm and has a medium mobility

under oxidizing conditions and high mobility in acid conditions. In reducing and neutral to alkaline conditions, Ag has a very low mobility. Many of the silver salts such as the chloride, phosphate, sulphide, arsenate, and carbonate salts have a low solubility (Health Canada, 1986a). The median global stream water concentration of Ag for the world is 0.05 ppm (Reimann and Caritat, 1998). Low values were obtained in this study, with most occurring below detection limit, and thus are not expected to contribute any significant information to the waters PCFA.

Tin has a bulk continental crust concentration of 2.5 ppm and is typically found in the minerals cassiterite (SnO_2) and stannite ($\text{Cu}_2\text{FeSnS}_4$) (Reimann and Caritat, 1998). Tin has a very low mobility under most environmental conditions (Siegel, 2002). The estimated median global stream water concentration is <0.01 ppb (Reimann and Caritat, 1998). Similar to Ag, most values for Sn were below or near detection limit and thus provided no practical information. Antimony has a bulk continental crust concentration of 0.2 ppm and is commonly found in the minerals stibnite (Sb_2S_3), kermesite ($2\text{Sb}_2\text{S}_3 \cdot \text{Sb}_2\text{O}_3$), valentinite (Sb_2O_3), and cervantite (Sb_2O_4) (Reimann and Caritat, 1998). Antimony has a low mobility under most environmental conditions but is usually found in the environment as a pure element. Most typically it is associated with sulphides and chlorides (Health Canada, 1999a). Most of the inorganic Sb compounds are insoluble, whereas those that are attached to organic ligands are soluble, but if they form oxides, as antimony trioxide or pentoxide, precipitation occurs. As expected, most of the Sb

concentrations were below detection limits and thus Sb data were discarded.

Thallium has a low to very low mobility in most environments (Plant *et al.*, 1996). It has a bulk continental crustal abundance of 0.36 ppm and some of its typical minerals are crookesite ((CuTlAg)₂Se) and lorandite (TlAsS₂). Except for the Betts Cove samples, all of the remaining samples contained concentrations which were well above the detection limit but concentrations were very similar, which resulted in the low loadings in the PCFA. Lead is the most common of the heavy elements with a bulk continental crust concentration of 8 ppm (Reimann and Caritat, 1998). Some of the common minerals of Pb are galena (PbS), anglesite (PbSO₄), cerussite (PbCO₃), and minium (Pb₃O₄). It is considered to have a low mobility in the environment and has a global median stream concentration of 3 ppb. Except for the Betts Cove polluted sites, the remaining areas had similar concentrations. Detection limits were somewhat high because it has a high presence in the environment due to anthropogenic inputs resulting in high reagent blank concentrations. Lead has been dispersed into the environment through atmospheric inputs (Health Canada, 1992). In 1982, 63% of all Pb atmospheric emissions were a result of leaded gasoline additives. In 1990, leaded gasoline was phased out under the Gasoline Regulations of the Canadian Environmental Protection Act which drastically reduced emissions. Lead is also present in tap water due to dissolution from Pb used in pipes and solders of household and distribution system plumbing systems, as well paints used in the past often were composed of Pb oxides. Soil is also a significant source of

environmental Pb. Since there are high inputs from these common anthropogenic sources, this results in a high reagent blank and poor distinguishing characteristics, because most areas had similar concentrations.

After removal of these elements, there were 4 significant Factors which accounted for 84.2% of the variance with all four Factors having eigenvalues greater than 1 (Table 3.7). The four types of rotation were tried for the analysis, and it was found that for regional separation, no particular rotation of the axis gave better groupings. Variables that loaded high in Factor 1 were Li, Mg, Ca, Mn, Fe, Co, Cu, Zn, Cd, Cs, and conductivity. In Factor 2, the variables that loaded high were Al, Ni, Rb, Ba, and conductivity. Factor 3 shows high loadings of As, Ce, and pH. Factor 4 showed high loadings of U and dissolved oxygen.

When Factor 1 vs. Factor 2 were plotted, the study areas could be regionally differentiated (Figure 3.10(b)). Group 1 consists of the water samples taken from the Betts Cove control site, Group 2 is from the Betts Cove polluted sites, Group 3 are all of the Robinsons River samples, Groups 4 and 5 are from the Tilt Cove control and polluted sites respectively, Group 6 are all of the samples taken for the 12 months from site SJS6B from Rennies River, and finally, Group 7 are all of the samples from SJS2-SJS6A, and Group 8 are all of the SJS1 samples for the whole year.

Table 3.7 Factor loadings and eigenvalues obtained from unrotated PCFA for log-transformed element concentrations in water samples.

Variable	Factor1	Factor2	Factor3	Factor4
Li	0.782	0.284	0.18	0.078
Mg	0.663	-0.436	0.44	-0.244
Al	0.29	-0.679	-0.51	0.304
Ca	0.845	0.193	0.327	-0.068
Mn	0.808	0.434	-0.254	-0.118
Fe	0.691	0.255	-0.198	0.491
Co	0.867	-0.342	0.028	-0.261
Ni	0.487	-0.628	0.256	-0.111
Cu	0.753	-0.56	-0.1	-0.148
Zn	0.855	-0.334	-0.155	-0.132
As	0.184	0.118	0.825	0.083
Rb	0.509	0.695	0.18	0.31
Cd	0.825	-0.376	-0.06	-0.078
Cs	0.749	0.36	-0.018	0.01
Ba	0.326	0.861	0.137	0.111
Ce	0.353	0.405	-0.727	0.338
U	0.111	-0.405	0.477	0.569
Dissolved Oxygen	-0.165	0.428	-0.529	-0.539
Conductivity	0.636	0.679	-0.083	-0.258
pH	-0.334	0.567	0.646	-0.214
Eigenvalue	7.589	4.764	2.992	1.499
%Variance	0.379	0.238	0.15	0.075

3.6 Statistical Analysis of LA-ICP-MS Data

Element intensity (cps) values are given in Appendix 4, calculated element concentrations are presented in Appendix 5. For the calculated element concentrations from LA-ICP-MS, statistical analyses similar to those for the stream water data were

completed (Appendix 6). Specific analytes had concentrations that were less than their detection limits. Detection limits are calculated based upon the variance of the gas blank signal converted to concentration units (Longrich, 2001). The calculation uses the number of blank data points averaged and the sample standard deviation of these values; along with the number of values integrated for the analyte signal. The final part of this calculation converts mean count rates to concentration values, this involves using the sensitivity that is corrected for the multiplicative effects of matrix, drift, and quantity of sample ablated. Concentrations that are below detection limit have RSD's of at least 33%, based on the principle that the standard deviation is defined as three times the uncertainty of a sample with zero analyte is 33%. Analytes that had concentrations above detection limit were used in the statistical analysis. Since concentrations were based on subtracting mean background intensity (cps) values from mean gross analyte intensity values, some concentrations had negative values. These values, along with values of zero cannot be log-transformed, and similar to the waters values, they were set to half of the detection limit. For the LA-ICP-MS data, a variety of transformations were examined such as z-score, assigning ranks to the values, subtracting the mean of the data set from each value, and also dividing each value by the standard deviation of the data set. Again it was found that log transforming the data made a better fit to a normal distribution (Figure 3.11). After log-transformation, box-plots and scatter plots were constructed in order to give a visual representation of the data.

Examination of the data indicated that three analytes should be eliminated from further statistical analysis. These were Se, Au, and Hg. The bulk of the Se and Au concentrations were below detection limit and some of these had negative concentrations. Selenium is widely distributed in the earth's crust at concentrations of 50 ppm and is associated with polymetallic sulphide ores, such as the ones at Tilt Cove and Betts Cove, where it replaces S (Reimann and Caritat, 1998). Therefore Se should have been found at considerable concentrations in the Fe-Mn oxide coatings. High detection limits due to backgrounds of $^{40}\text{Ar}^{1}\text{H}_2$ and ^{82}Kr , and the $^{81}\text{Br}^{1}\text{H}$ interference resulted in Se being omitted from further statistical analysis. Generally, Au is not very abundant in the environment; it has a low bulk continental crustal abundance of 0.003 ppm (Reimann and Caritat, 1998) and a background freshwater concentration of 0.01 ppb (Förstner and Wittman, 1979). Since Au is generally not found in the environment, low concentrations were expected in the coatings. Concentrations could not be calculated for Hg because there was no known value for the NIST 610 reference material. Mercury also presents the problem of a high background arising from contamination in the Ar gas, and a high ionisation potential (Hirata and Nesbitt, 1995). As well, considerable amounts of mercury are easily adsorbed onto the sample introduction system (Knight *et al.*, 1999). Mercury generally showed low signals. Of the three lead isotopes, ^{208}Pb was chosen over ^{206}Pb and ^{207}Pb due to its higher isotopic abundance.

Since there were a large number of variables (30 analytes), and some method of

grouping was needed. Principle component Factor analysis was performed on the LA-ICP-MS data. Pearson-R correlation coefficients were calculated for the data, again with the goal of reducing the variable to sample ratio. The reliability of the Pearson-R correlation was evaluated by examining scatter plots along with the p-value. The highest correlation coefficient was obtained for La and Y , 0.877, with a p-value of 0. Examination of the scatter plots indicated that correlation of some points was not extremely good, therefore data for both analytes were used in the PCFA. In comparison with the waters data, the correlation coefficient for La and Ca was 0.838.

Principle component Factor analysis was attempted on all of the Fe-Mn oxide coating samples. The samples that were used to examine annual accretion were eliminated from the analysis because no regional groupings of the study areas were obtained with these samples. This may be due to varying amounts of MnO_2 and Fe_2O_3 with time, change in the crystallinity of the two phases which affects their adsorption capacity, and changing adsorption rates of various analytes (Jackson, 1998; Carpenter and Hayes, 1980). A separate PCFA was tried on this group of samples, with the goal of differentiating the sampling time.

Certain variables loaded low on all Factors, and these were removed from further PCFA. These were the analytes V, Ag, Sn, Pb, Bi, and U. As mentioned above, V is expected to have a low concentration in stream water due to its low solubility (Siegel, 2002). Its chemical properties and global stream concentration were mentioned in section

3.3.3. Vanadium was not present at high concentrations in the stream environment, which was expected based on their chemical properties. Therefore, V is expected to have low concentrations in the coatings. It was found that V has moderately high concentrations in the coatings. The low loading in the PCFA may be due to the fact that V is found in a wide range of silicate rocks, which may therefore contribute to its poor differentiating abilities. Finally, since V had a low loading in the waters PCFA, a low loading is expected for the LA-ICP-MS data since the adsorbed analytes in the Fe-Mn oxide coatings come from the surrounding waters.

The chemical properties of silver were mentioned in section 3.3.3. Silver had low LA-ICP-MS concentrations in many of the samples, and high RSD's. The low silver coating concentrations are expected, since stream water concentrations were also low. Thus, this element loaded low on the water PCFA. Tin also loaded low in the Factors. Similar to Ag, Sn had relatively high RSD values, although not as high as Ag, and low concentrations, although they were well above detection limits. Tin was also excluded from the waters PCFA. Concentrations of lead were high in the Fe-Mn oxide coatings with low RSD values. Lead has a high concentration in the environment because it has been dispersed into the environment through atmospheric inputs (Health Canada, 1992). These inputs were common in all of the sampled areas, resulting in similar concentrations for lead, and low loadings on all of the Factors; this was also true for the waters data.

Bismuth is a chalcophile element that has a common oxidation state of +3, with

an ionic radius of 110-131 pm, and it has a very low crustal abundance. Concentrations for Bi determined by LA-ICP-MS were the lowest for all of the selected elements, they were accompanied with high RSD values.

Uranium is commonly found in the environment in the +6 state, with an ionic radii of 59-100 pm, and an electronegativity of 1.38 (Reimann and Caritat, 1998). Uranium is a lithophile element with a bulk continental crust concentration of 0.91 ppm and median global stream concentration of 0.04 ppb. It has a high mobility under all conditions except reducing environments. Uranium concentrations were lower than Pb, with similar RSD values.

Vanadium, Sn, and U all have a small ionic radius, generally smaller than that of the elements that were retained for the PCFA (Table 3.8). The exceptions are As, Cr, and Bi, but As and Cr form AsO_4^{3-} and CrO_4^{2-} in water, which obviously increases their ionic radii. The analytes, V, Sn, and U, may not have been adsorbed by the Fe-Mn oxide coatings as well as the other trace elements due to their smaller ionic radius. Brümmer (1986) found that the strength of metal binding increases with ionic radius. Since these smaller ions may not be adsorbed as well as larger ones, this might account for their low loadings on the PCFA.

Rotation of the PCFA data space was tried, and as for the waters data, no rotation gave the better groupings. In total, there were three Factors that were found to be significant. This was based on the Kaiser criterion. These three Factors accounted for

Table 3.8 Elements, along with their main oxidation state in the environment, and ionic radius, that were initially tried in the PCFA (Reimann and Caritat, 1998).

Element	Main Oxidation State	Ionic Radius (pm)
V	+5	49.5-68
Cr	+6	40-58
Mn	+2	80-110
Fe	+3	63-92
Co	+2	72-104
Ni	+2	63-83
Cu	+2	71-87
Zn	+2	74-104
As	+3	47.5-72
Sr	+2	132-158
Y	+3	104-121.5
Ag	+1	81-142
Cd	+2	92-145
Sn	+4	69-95
Ba	+2	149-175
La	+3	117-150
Ce	+3	115-148
Pb	+2	112-163
Bi	+3	110-131
Th	+4	108-135
U	+6	59-100

78.9% of the variance (Table 3.9). Factor 1 consisted of Cr, Mn₂O₃, Fe₂O₃, Cu, Sr, Y, Ba, La, and Ce. Factor 2 consisted of Co, Ni, Zn, As, and Cd. Finally, Factor 3 contained Th. The Factor loadings are listed in Table 3.9. The Scree plot obtained for PCFA is shown in Figure 3.12(a).

Table 3.9 Factor loadings and eigenvalues obtained from unrotated PCFA for log-transformed element concentrations in pebble samples.

Variable	Factor1	Factor2	Factor3
Cr	0.723	-0.261	-0.524
Mn ₂ O ₃	-0.884	-0.354	-0.053
Fe ₂ O ₃	0.677	0.352	-0.271
Co	-0.352	-0.780	-0.183
Ni	0.129	-0.750	-0.566
Cu	0.659	-0.352	0.320
Zn	-0.259	-0.776	0.423
As	0.207	-0.800	-0.210
Sr	-0.658	0.195	-0.302
Y	-0.778	0.168	0.105
Cd	-0.311	-0.865	0.168
Ba	-0.956	-0.095	-0.044
La	-0.854	0.276	0.044
Ce	-0.945	0.055	-0.092
Th	-0.521	0.301	-0.594
Eigenvalue	6.390	3.850	1.52
%Variance	43	25.7	10.2

When the Factor 1 vs Factor 2 and Factor 1 vs. Factor 3 scores were plotted for the LA-ICP-MS data, the study areas could be regionally differentiated (Figure 3.12(b)). These plots produced 9 groups of samples; Betts Cove control (Group 1), Betts Cove polluted (Group 2), Robinsons River (Group 3), and Tilt Cove control sites TCS3-TCS6

(Group 4) and TCS7-8 (Group 5), Tilt Cove Polluted (Group 6), Rennies River SJS6B samples (Group 7), Rennies River SJS6A samples (Group 8), and finally Rennies River samples SJS1-SJS5 (Group 9).

3.6.1 PCFA of Fe-Mn Oxide Formation Data

As mentioned in the above section, the initial PCFA of the LA-ICP-MS data could not define groupings of the samples when the artificial substrates in Rennies River were included in the PCFA analysis, hence they were removed. Statistical analysis of the substrate data was carried out in a similar manner as the waters data and also the LA-ICP-MS data for the collected pebbles. Elements Se and Au, that had concentrations below the detection limit were eliminated from the analysis. Similar reasons as mentioned in section 3.4 result in concentrations below detection limit. Again, Hg concentrations could not be calculated because there is no known concentration in the NIST 610 reference material. In order for the data to better fit a normal distribution, the data were log-transformed (Figure 3.13). Other transformations, like the ones in the previous statistical analysis were attempted, but it was found that a log-transformation worked the best. Box plots and scatter plots were made to visually examine the data.

Pearson-R correlation coefficients were calculated for the data, and it was found that Y and La had a strong correlation coefficient of 0.946. Examination of the scatter plot showed that the points followed an excellent correlation. Both Y and La have similar

crustal abundances of 20 and 16 ppm respectively, they also showed similar concentrations in the Fe-Mn oxide coatings. The correlation coefficient between La and Ce was 0.923, and for Y and Ce it was 0.845, the former showed an excellent correlation in the scatter plot, whereas the latter was not as good. It was decided that La would be eliminated because it showed strong correlations for both Y and Ce.

There were five variables that loaded low on all of the Factors, these were Co, As, Ag, Cd, and Sn. All four of these are chalcophile, except for Sn which is siderophile, but to a lesser extent may be considered lithophile (Rose *et al.*, 1979). As mentioned above, these chalcophile elements are associated with sulfide ore deposits. The study area for this part of the project is in St. John's, where there are no sulfide deposits present, these are only present at Tilt Cove and Betts Cove. Therefore these should not show any distinguishing properties, either temporal or spatial, in these samples.

Cobalt concentrations in the water samples taken from Rennies River were generally low, with all values less than 1 ppb. This was expected, since Co is generally associated with sulphide deposits, and since there are none in this study area, there should be only minor inputs. Concentrations in the polluted sites, SJWS2-SJWS6B were only slightly higher than the non-polluted, so it shows that anthropogenic inputs were minor. Cobalt has a medium mobility under oxidising conditions, and high under acid conditions, and very low under reducing and neutral to alkaline conditions. Rennies River can be considered a neutral environment, with most pH values around 7, so it should have

a very low mobility (Reimann and Caritat, 1998). Cobalt is known to be strongly adsorbed by Fe-Mn oxides (Rose *et al.*, 1979). Therefore most of the Co that is present in solution should be adsorbed onto the Fe-Mn oxide. For the Co concentrations determined by LA-ICP-MS, they were generally high, but RSD values were also high.

Arsenic concentrations in the water samples were generally low, with values less than 1 ppb, which was expected, again due to the lack of sulphide ores in the study area. Concentrations in the polluted sites were only slightly higher than the “pristine” site. Concentrations in the Fe-Mn oxide coatings were generally low, with small differences between concentrations in samples. For Ag, Cd, and Sn, concentrations in water samples were low for both water samples and Fe-Mn oxide coatings. All three of these also exhibited high RSD values.

Like the water and LA-ICP-MS data, rotation of the PCFA data space was tried and no rotation gave better groupings. Based on the Kaiser criterion, there were 2 Factors that were found to be significant (Table 3.10, Figure 3.14(a)). Factor 1 accounted for 61.4% of the variance, and had an eigenvalue of 9.21, the variables that loaded high on this factor were V, Cr, Ni, Cu, Zn, Sr, Y, Ce, Pb, Bi, Th, and U. Factor 2 had an eigenvalue of 2.612 and accounted for 17.4% of the variance; variables that loaded high were MnO₂, Fe₂O₃, and Ba.

Figure 3.14(b) shows the groupings obtained from PCFA of the data obtained from LA-ICP-MS analysis of Fe-Mn oxide coatings that formed on substrates placed in

Table 3.10 Factor loadings and eigenvalues from unrotated PCFA for log-transformed element concentrations in the coatings that formed on the artificial substrates.

Variable	Factor1	Factor2
logV	-0.878	0.276
logCr	-0.888	0.364
logMn ₂ O ₃	-0.332	-0.862
logFe ₂ O ₃	-0.109	0.934
logNi	-0.882	-0.110
logCu	-0.784	-0.075
logZn	-0.763	-0.036
logSr	-0.836	0.070
logY	-0.897	0.151
logBa	-0.452	-0.810
logCe	-0.798	-0.227
logPb	-0.795	-0.072
logBi	-0.900	0.164
logTh	-0.958	0.036
logU	-0.922	0.032
EigenValue	9.21	2.612
%Variance	0.614	0.174

Rennies River. Group 1 consisted of samples from all four sampling periods that were taken from SJS6B; Group 2 were all of the samples taken from the 3 month period; Group 3 were the samples that belonged to those sampled from the 3 month period; finally Group 4 consisted of samples taken from sites that were sampled after 9 and 12 months.

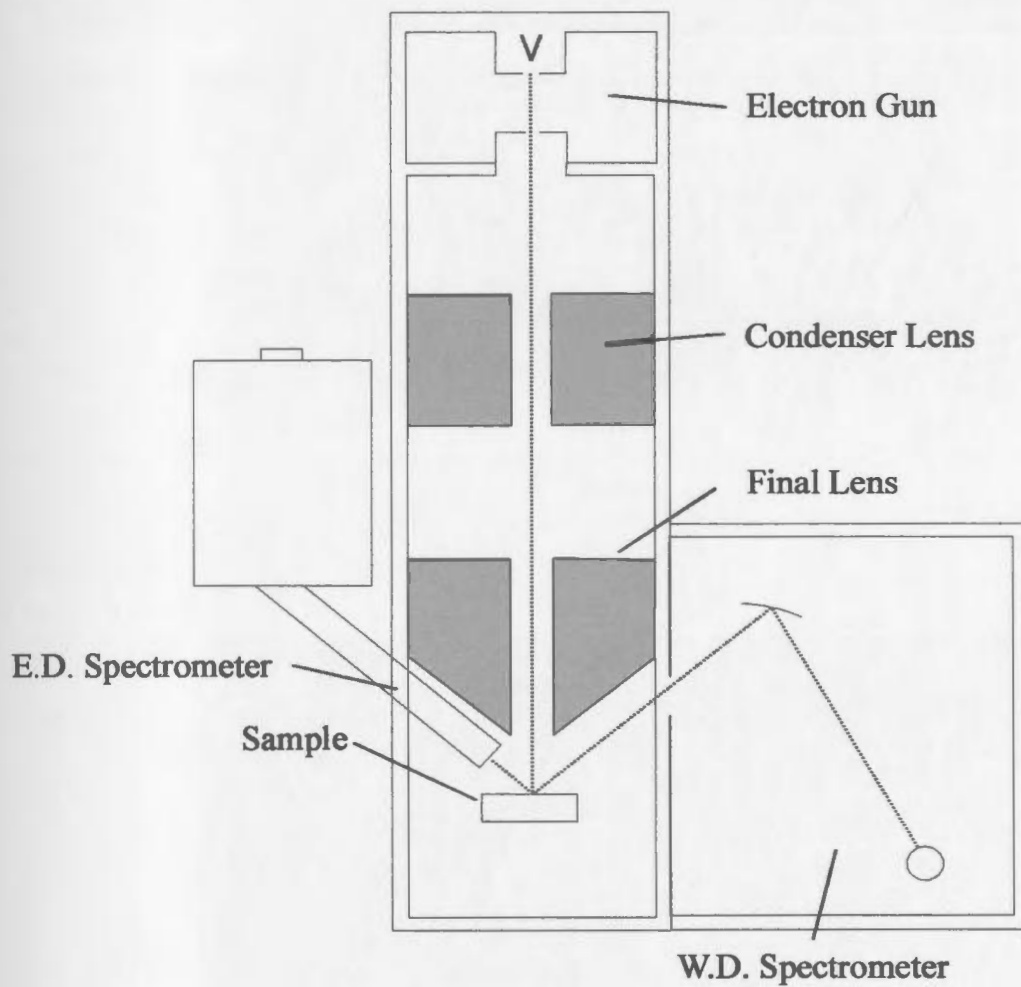
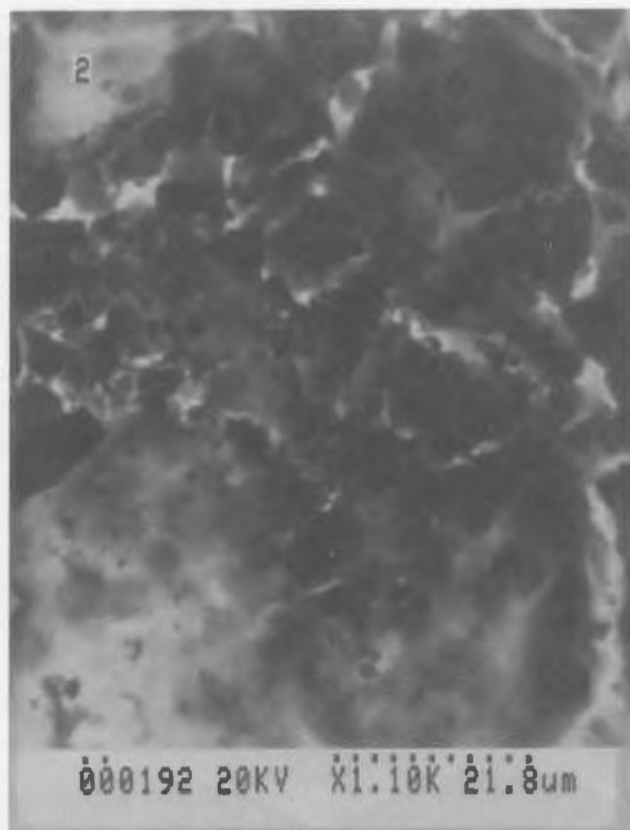


Figure 3.1 Electron microprobe schematic (Reed, 1993).

(a)



(b)



Figure 3.2 Photographs of iron-manganese oxide coatings present on a pebble taken from the streambed at (a) site SJS2 and (b) site SJS6A.

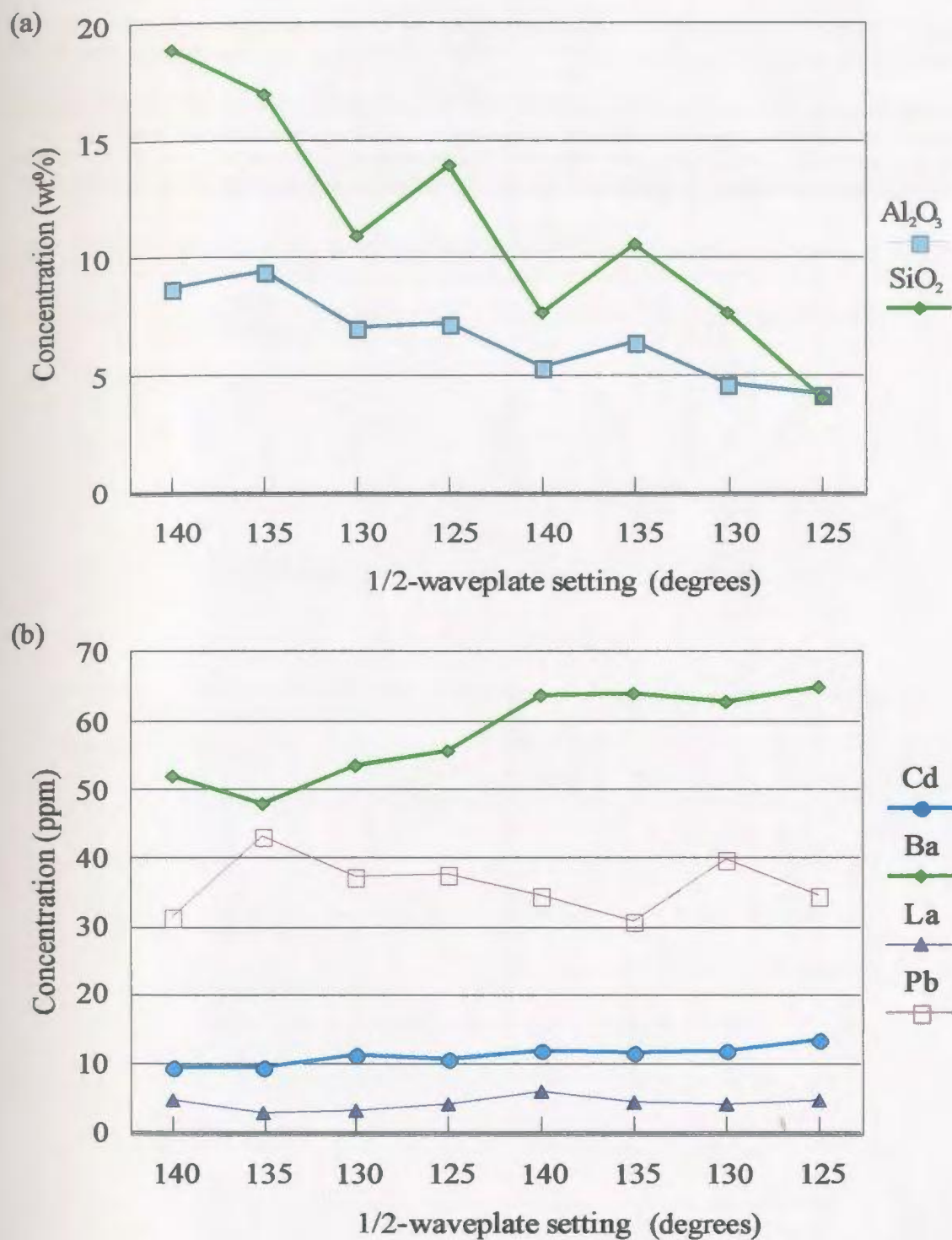


Figure 3.3 Results for the LA-ICP-MS optimisation run with analyses 1-4 done at a focal height of 200 μm and analyses 4-8 done at a focal height of 400 μm for (a) Al_2O_3 and SiO_2 and (b) Cd, Ba, La, and Pb.

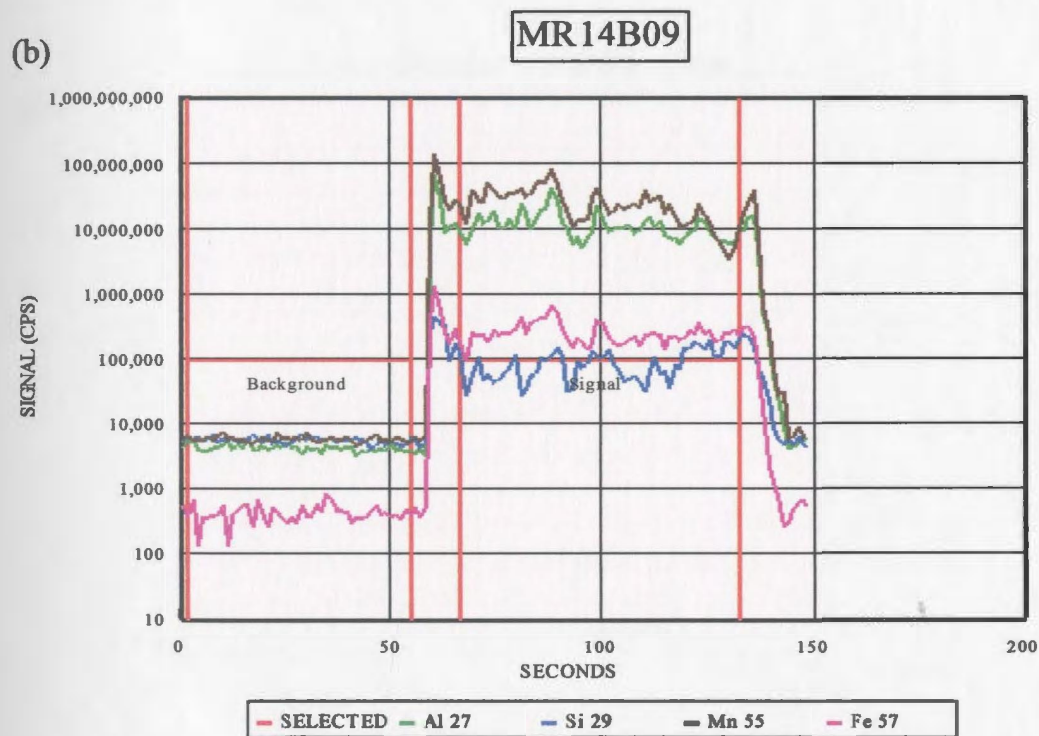
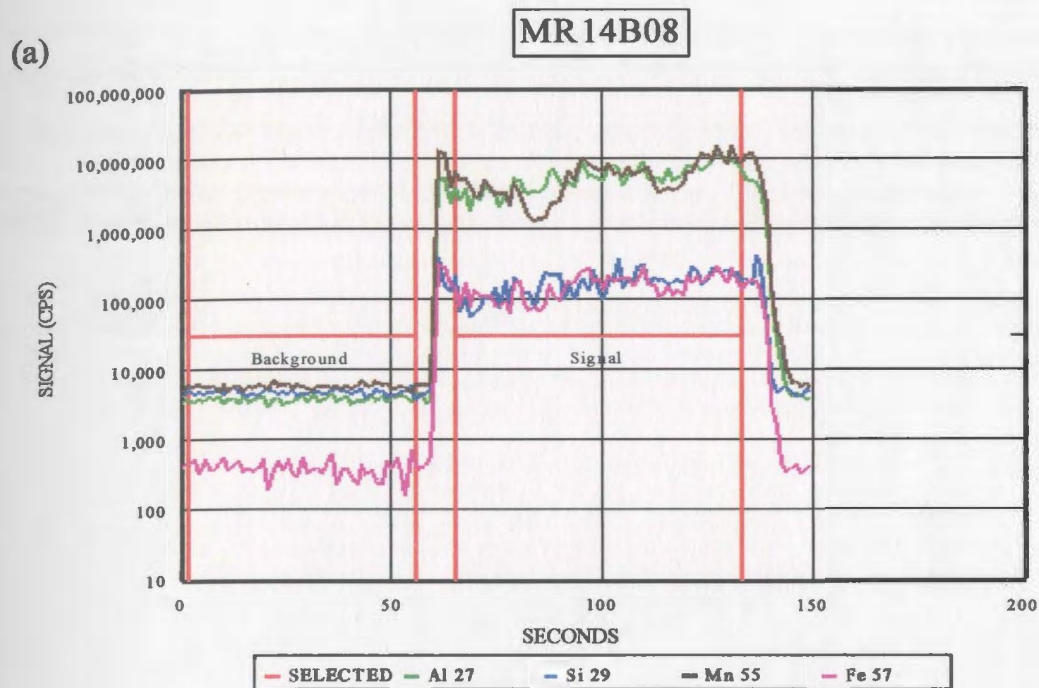
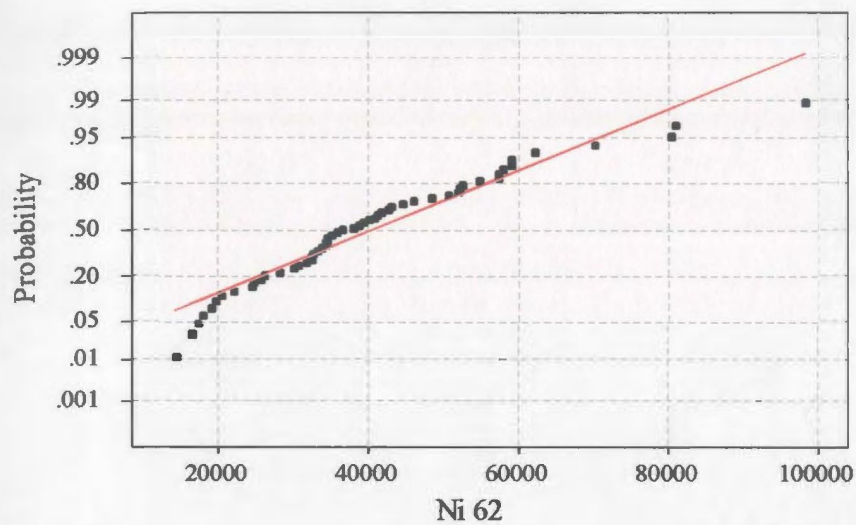


Figure 3.4 (a) TCPS 8.1.2 and (b) TCPS 8.2.1 intensity (cps) vs. time (s) plot for Al, Si, Mn, and Fe determined by LA-ICP-MS.

Normal Probability Plot

(a)

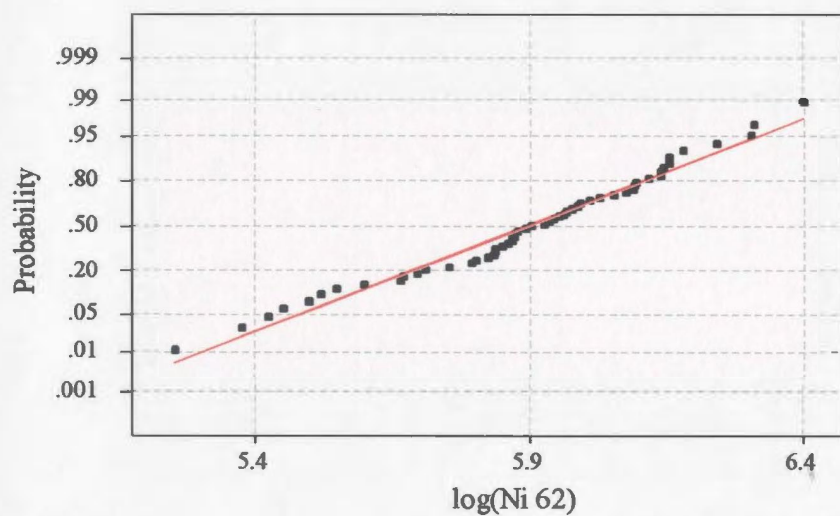


Average: 40544.9
StDev: 17263.1
N: 55

Anderson-Darling Normality Test
A-Squared: 0.904
P-Value: 0.020

Normal Probability Plot

(b)



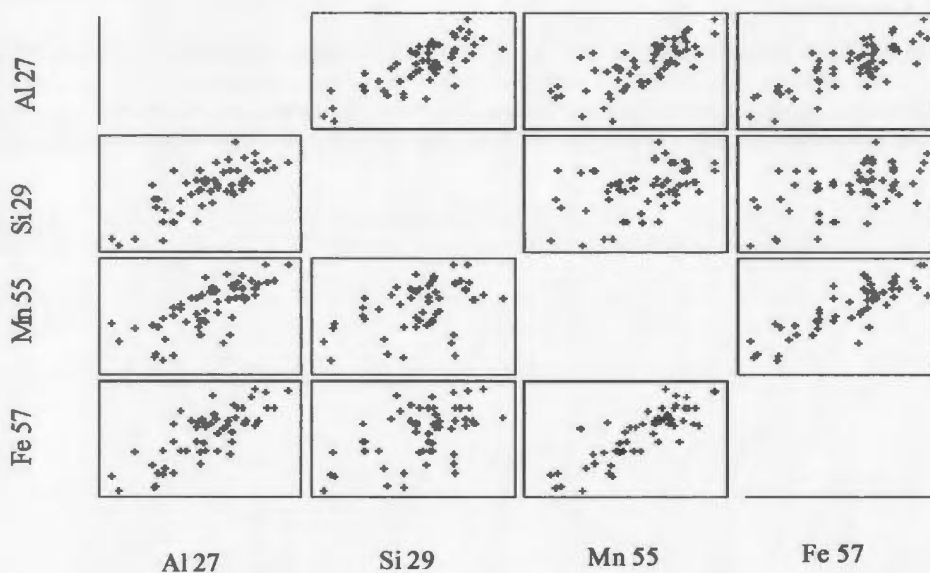
Average: 5.89703
StDev: 0.245174
N: 55

Anderson-Darling Normality Test
A-Squared: 0.522
P-Value: 0.177

Figure 3.5 Normality plot for (a) ^{62}Ni (cps) and (b) log transformed values of ^{62}Ni (cps).

(a)

MR14B08



(b)

MR14B09

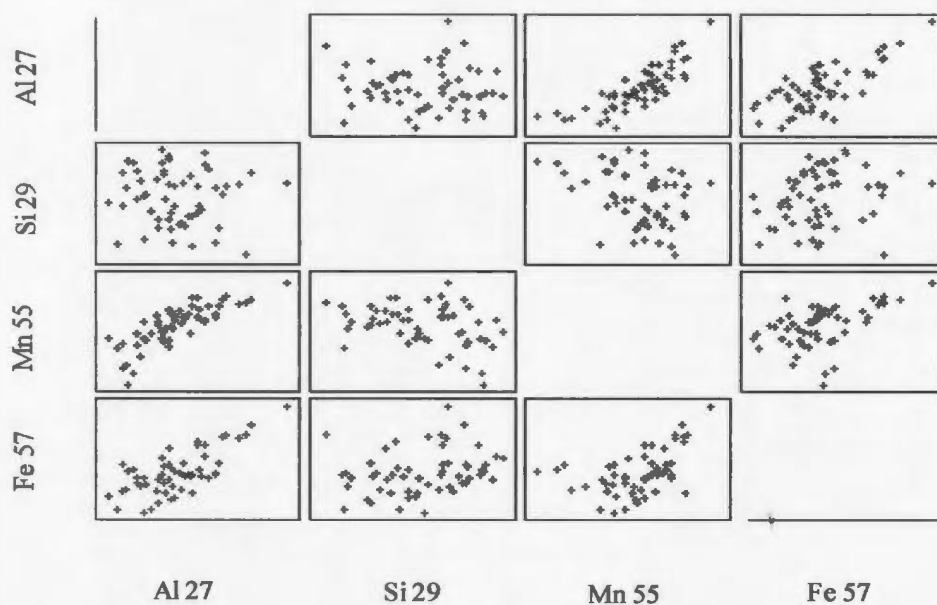


Figure 3.6 Scatter plots for analysis (a) MR14B08, sample TCPS 8.1.2, and (b) MR14B09, sample TCPS 8.2.1 for the analytes ^{27}Al , ^{29}Si , ^{55}Mn , and ^{57}Fe determined by LA-ICP-MS.

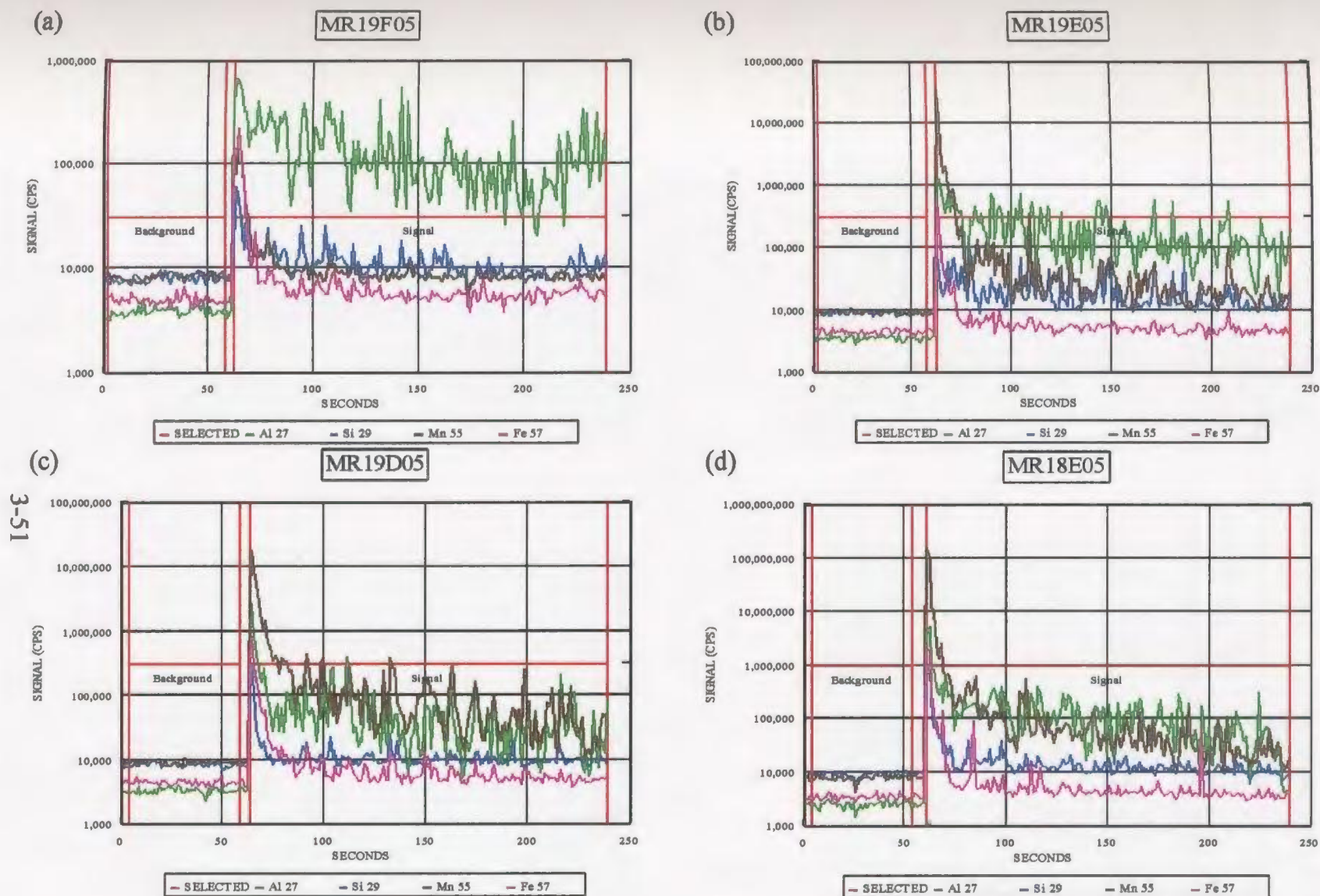


Figure 3.7 Intensity (cps) vs. time (s) plots for the streak plate substrate taken from site SJS6A at; (a) three months, (b) six months, (c) nine months, and (d) twelve months for the elements ^{27}Al , ^{29}Si , ^{55}Mn , and ^{57}Fe determined by LA-ICP-MS.

(a)



(b)



(c)



(d)



3-52

Figure 3.8 Photographs of iron-manganese oxide coatings present on a streak plate substrate taken from site SJS6A at; (a) three months, (b) six months, (c) nine months, and (d) twelve months.

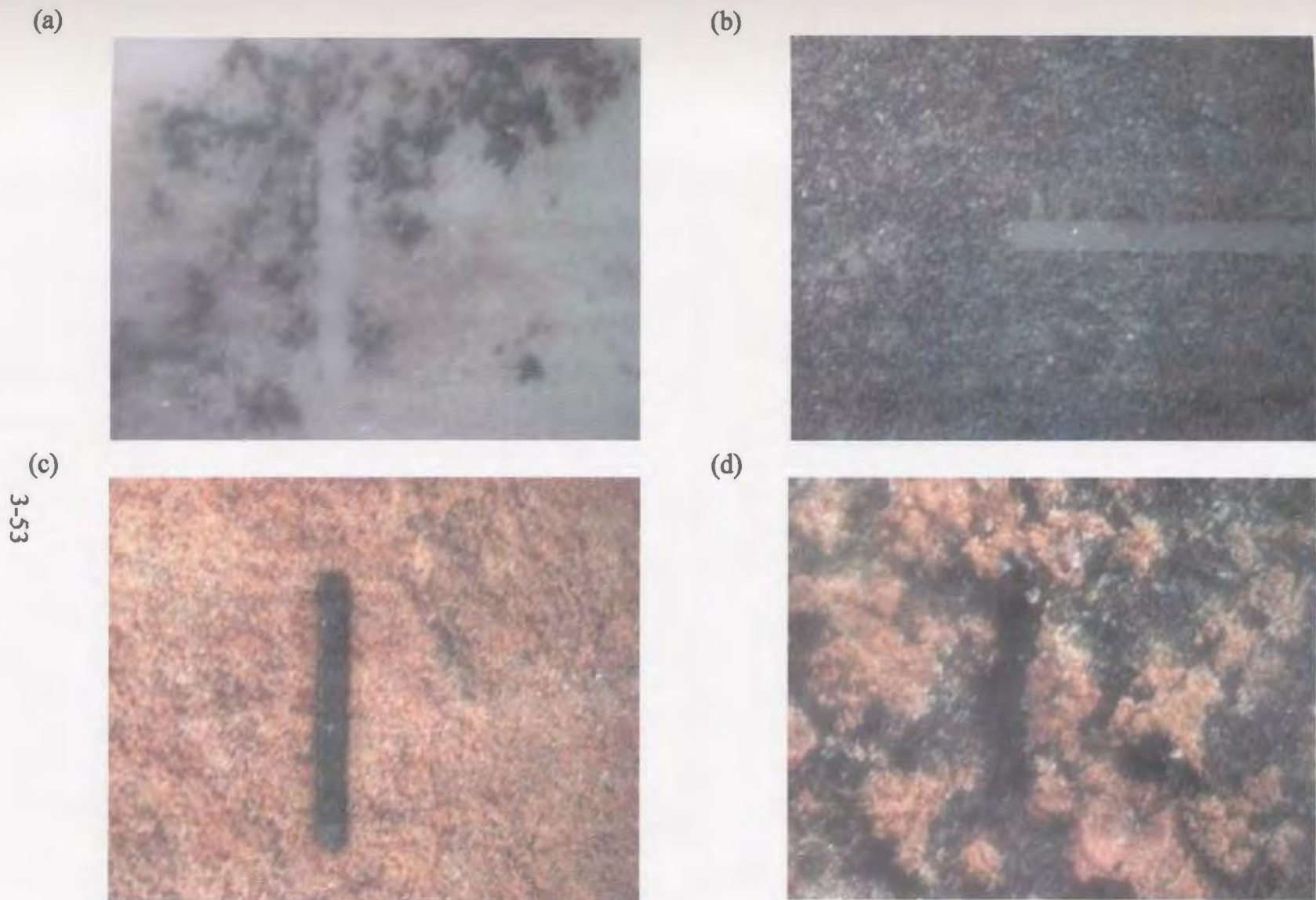


Figure 3.9 Photographs of iron-manganese oxide coatings present on a streak plate substrate taken from site SJS6A after; (a) six months, (b) nine months, and site SJS6B after (c) six months, and, (d) nine months.

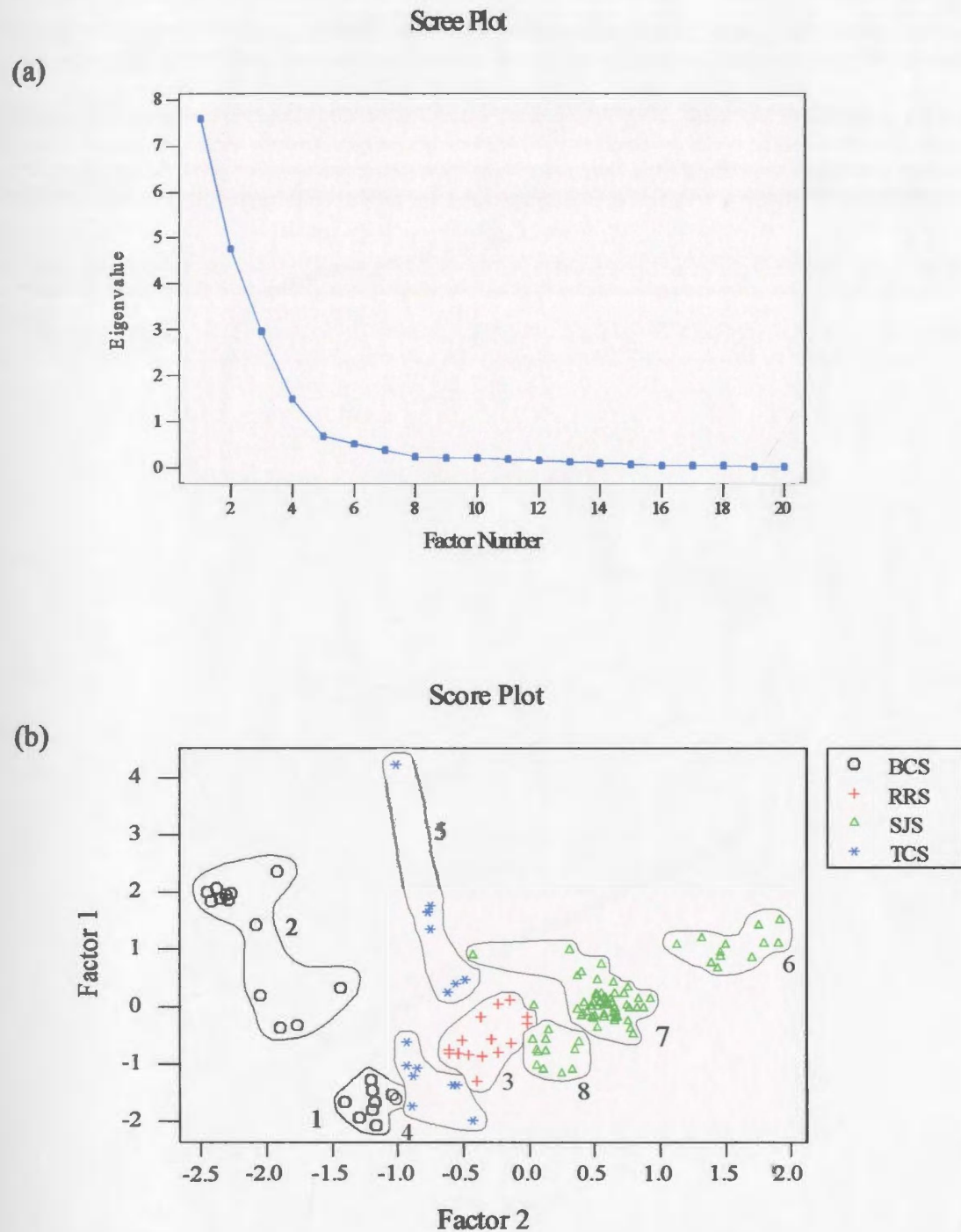


Figure 3.10(a) Scree plot obtained from PCFA of elements in water samples from all four study areas; (b) plot of Factor 1 vs. Factor 2 that were obtained from PCFA of elements in water samples (see text for further description).

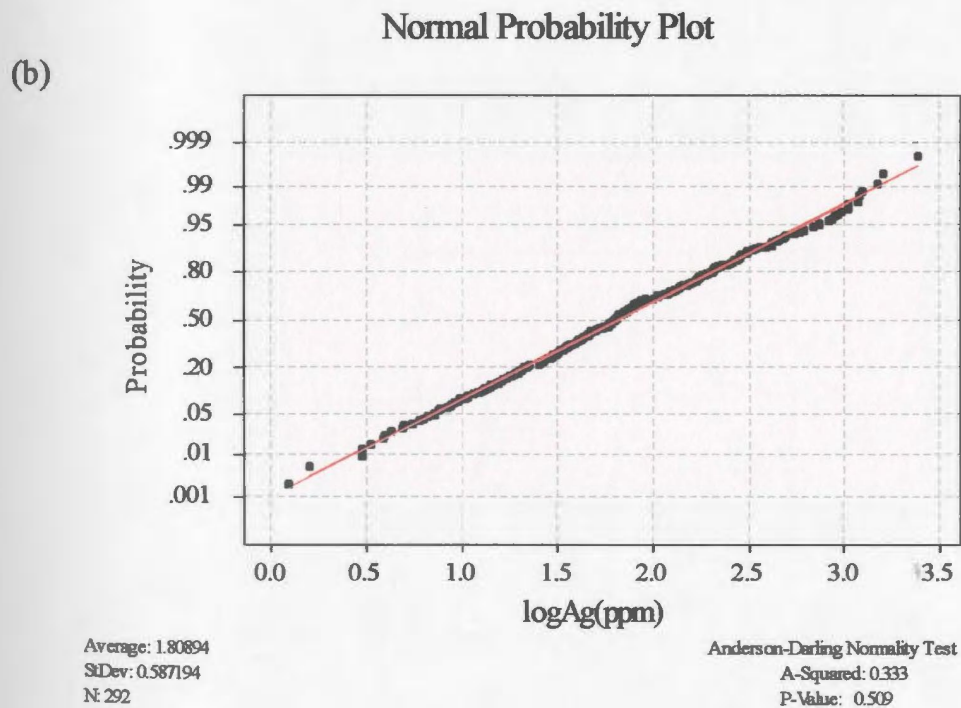
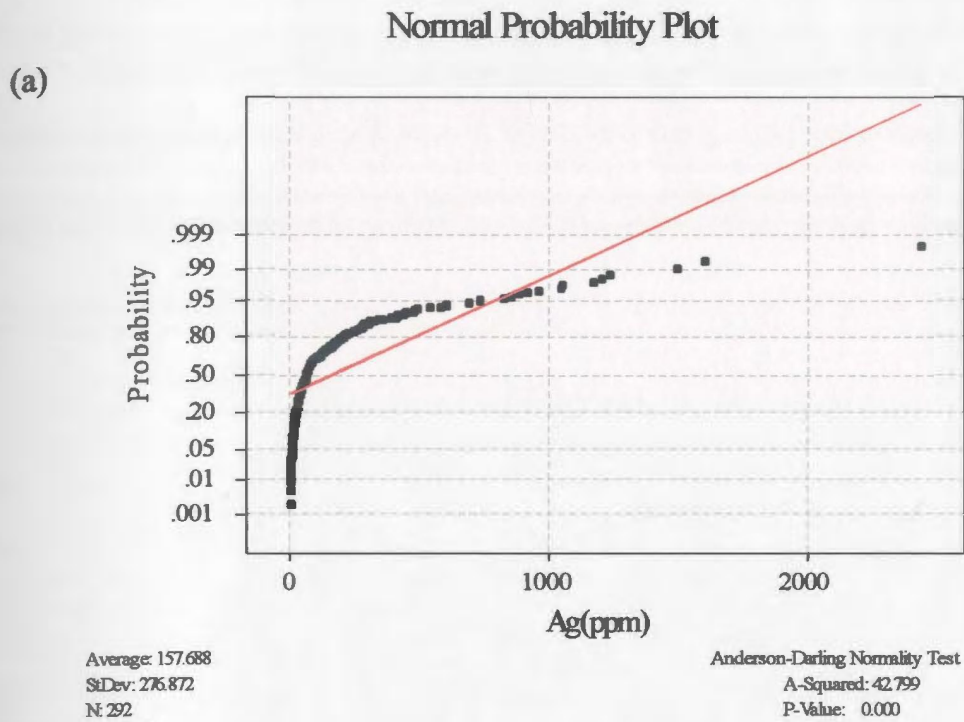
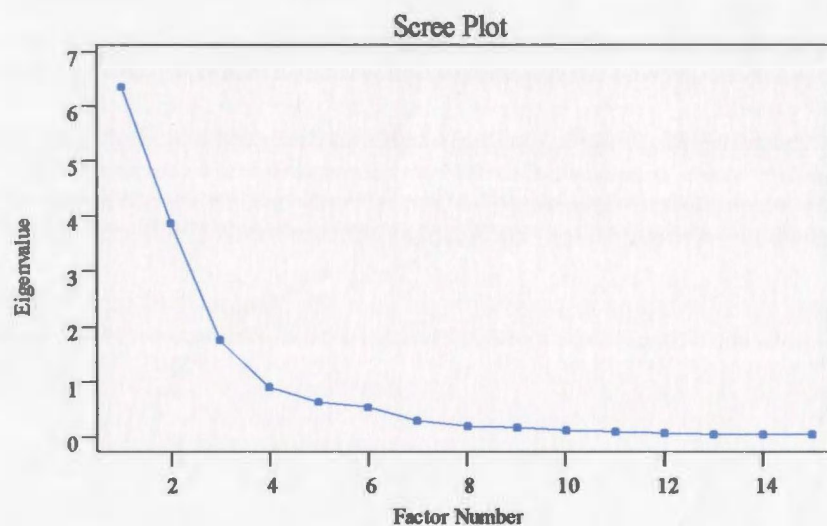


Figure 3.11 Normality plot for (a) Ag (ppm) and (b) log transformed of Ag (ppm).

(a)



(b)

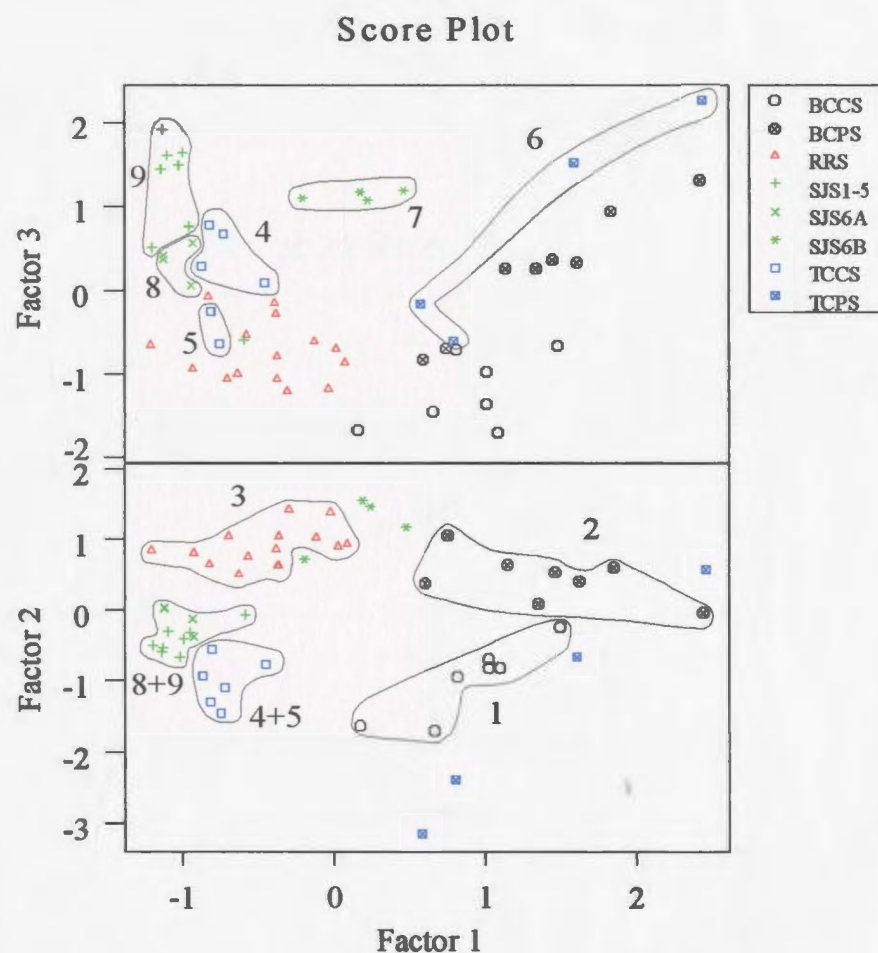
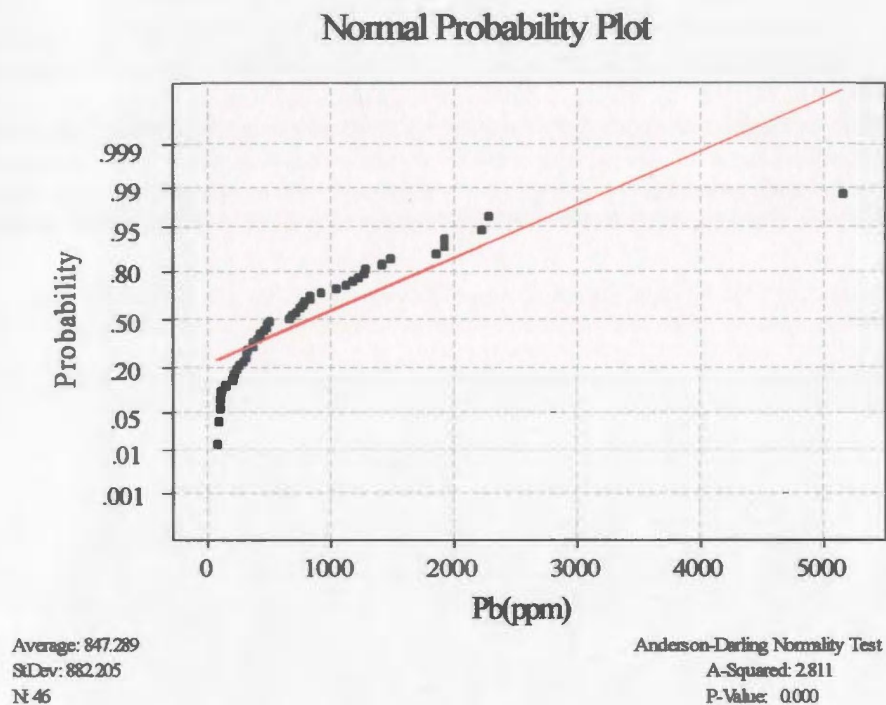


Figure 3.12(a) Scree plot obtained from PCFA of elements in Fe-Mn oxide coating samples from all four study areas; (b) plot of Factor 3 vs. Factor 1 and Factor 2 vs. Factor 1 that were obtained from PCFA of elements in Fe-Mn oxide coatings (see text for further description).

(a)



(b)

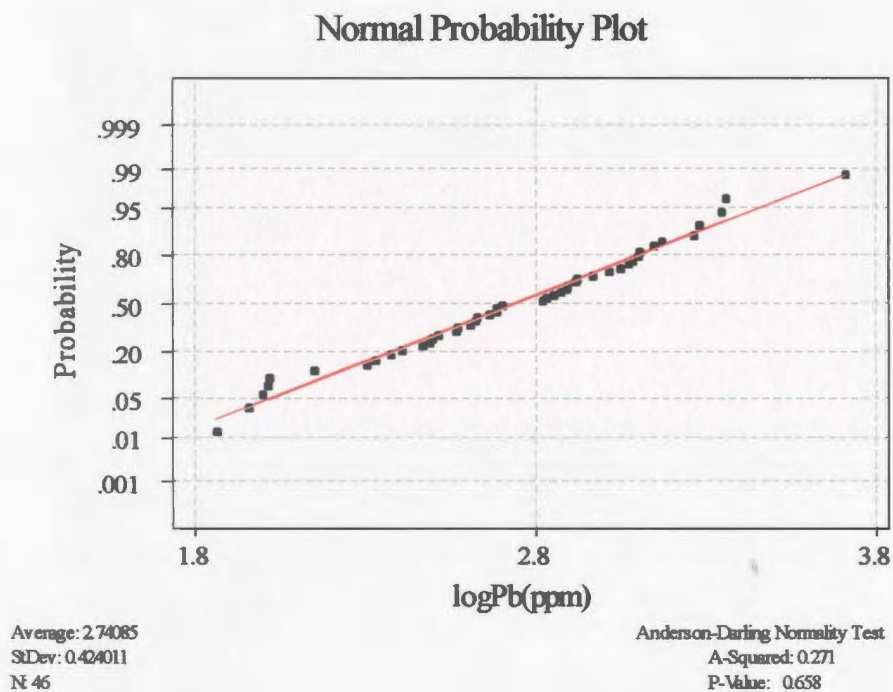


Figure 3.13 Normality plot for (a) Pb (ppm) and (b) log transformed values of Pb (ppb) for LA-ICP-MS analysis of Fe-Mn oxide coating samples on annual accretion samples collected from Rennies River.

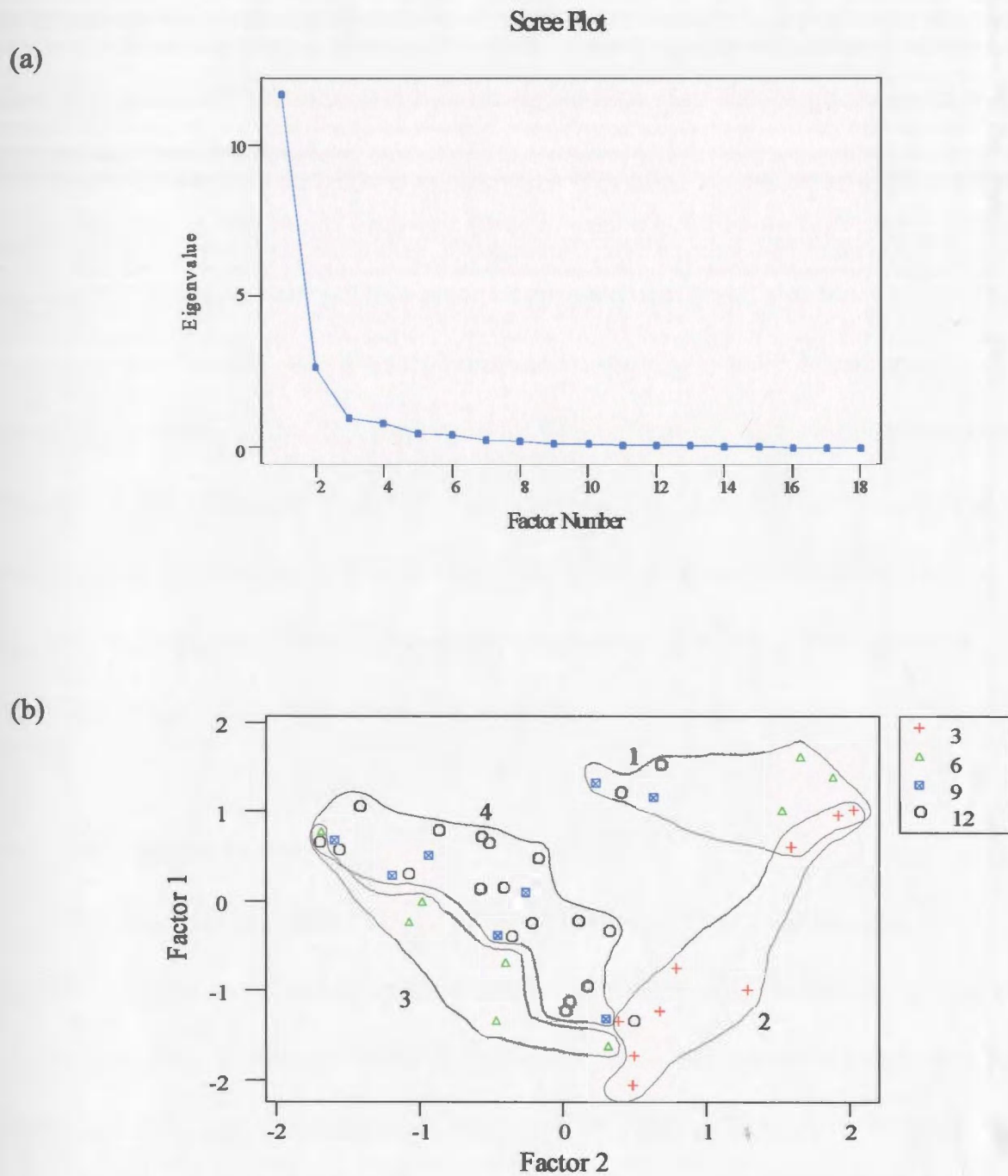


Figure 3.14 (a) Scree plot and (b) plot of Factor 1 vs. Factor 2; both obtained from PCFA of elements in Fe-Mn oxide coatings that formed on the substrates placed in Rennies River.

4. Discussion

4.1 Stream Water PCFA

There were four useful Factors in the regional classification of the study areas based on PCFA of the waters data. Factor 1 consisted of Li, Mg, Ca, Mn, Fe, Co, Cu, Zn, Cd, Cs, and conductivity, all of which correlated positively. Factor 2 contained Al, Ni, Rb, Ba, conductivity, and pH. Aluminum and Ni were negatively correlated in Factor 2, whereas, Rb, Ba, conductivity, and pH were positively correlated. Factor 3 contained As, Ce, and pH in which Ce had a negative loading, whereas As and pH had positive loadings. Factor 4 consisted of U and dissolved oxygen, in which U had a positive loading and dissolved oxygen a negative loading.

4.1.1 Water PCFA Factor 1

The first Factor consists of two groups of elements based on regional concentration patterns. The first group contains Co, Cu, Zn, and Cd and the second group is Li, Mg, Ca, Mn, Fe, Cs, and conductivity. All of these elements are classified as having mobile ions in the environment and all have positive loadings in Factor 1, suggesting that they have similar behaviours in the particular stream environments (Siegel, 2002).

The first subgroup in Factor 1 shows the influence of the Betts Cove and Tilt Cove Copper mines. Of all the study areas, only the Tilt Cove and Betts Cove polluted

areas exhibit real differences by having the highest concentrations of Co, Zn, and Cd at site TCWS13, and the highest Cu concentrations at site BCWS9 (Figure 4.1 and Figure 4.2). All four of these elements have similar chemical properties and are classified as chalcophile elements (Reimann and Caritat, 1998). Chalcophile elements are concentrated in sulfides (Krauskopf, 1995) such as the Betts Cove and Tilt Cove deposits. The common oxidation state for these elements is +2 (Reimann and Caritat, 1998) and they are all considered to be heavy metals, having a density $> 5 \text{ g/cm}^3$ (Jackson, 1998). The densities are all very similar with values for Co, Cu, Zn, and Cd being 8.9, 8.96, 8.65, and 7.133 g/cm^3 , respectively (Reimann and Caritat, 1998). They also have similar electronegativities of 1.88, 1.9, 1.65, and 1.69, respectively. Based on these properties, these elements are expected to exhibit similar behaviour.

In the Tilt Cove study area, Co concentrations at the polluted sites were considerably higher than at the control sites, especially TCWS13 (Figure 4.1). For Betts Cove (Figure 4.2), there is a similar trend, except that polluted sites BCWS10 to BCWS13 are not as elevated in Co compared to the control concentrations as the other polluted sites. For copper, all polluted sites have concentrations greater than at the control sites, especially TCWS13. Betts Cove has the highest concentrations at sites BCWS1 to BCWS9, but BCWS10 to BCWS13 are also considerably higher than the control sites. The pattern for Zn closely follows Cu with concentrations for polluted Tilt Cove sites elevated compared to the control, especially sites TCWS12 to TCWS15, with TCWS13

having the highest concentration. For the Betts Cove study area, Zn concentrations are highest for sites BCWS1 to BCWS9, similarly followed by a decrease at sites BCWS10 to BCWS13, and another decrease at the control sites. Cadmium shows a similar trend to Cu and Zn, and similar to Co.

The concentrations at the Tilt Cove and Betts Cove polluted sites are much higher than at any other areas. All of the Tilt Cove polluted sites except TCWS12 and TCWS13 are downstream from Winsor Lake, TCWS12 and TCWS13 are in the vicinity of the West Mine pond; an area containing buried mine equipment. In Betts Cove, all sampled sites are downstream or in the area of the abandoned copper mine. Sites BCWS1 to BCWS8 are downstream from a pond in the area of the abandoned mine, BCWS9 to BCWS12 is in a network of ponds that were in the mine area, with BCWS12 thought to have been near to the old smelter.

Previous work in the Tilt Cove study area examined the concentrations of elements in on-land mine tailings in which maximum concentrations of Cu = 3546 ppm, Zn = 2283 ppm, and Cd = 3.54 ppm were found (Maddox, 2001). Thus, the tailings could be a possible source of the elevated concentrations in stream water.

In the Betts Cove area, it appears that there is acid mine drainage. Figure 4.2(a) is a line graph of the log of Co, Cu, Zn, and Cd, and pH concentrations vs. Betts Cove sampling site. In the polluted areas, the concentrations correlate with pH such that in areas of lower pH, higher concentrations of all four chalcophile elements are found. The

pH readings reach near neutral values in the control sites, where the concentrations of Co, Cu, Zn, and Cd are significantly decreased. As previously mentioned, the BCWS1 to BCWS8 sites were located in the stream that flowed out of a pond from the mine area, with BCWS1 being furthest away (Figure 4.2(b)). BCWS9 was collected along the edge of a pond where large piles of worked ore were present. All of these samples had the lowest pH, and exhibited the highest concentrations of these four elements. Sites BCWS10 and BCWS11 occurred northwest of the mine area, away from the ore piles. These sites had higher pH concentrations and lower concentrations of these four elements. Site BCWS12 was in the area where it was thought that the old smelter had been located, and here there was a decrease in pH accompanied by an increase in concentrations of these four elements. Finally, site BCWS13 which was from a stream that flowed over a part of the mineralized area; there was a steep increase in pH accompanied by a decrease in elemental concentrations.

Elements that constitute the second group include Li, Mg, Ca, Mn, Fe, Cs and conductivity. These analytes define the same general pattern of enrichment in both the Tilt Cove and Betts Cove polluted sites compared to their control sites (Figure 4.3(a) and 4.3(b)). They also follow this pattern in samples from the St. John's sites where low concentrations were found at site SJWS1 with the highest concentration being found at SJWS6B. This pattern is consistent throughout the whole sampling period for St. John's.

For Li, Ca, Mn, Fe, Cs, and Conductivity, the Tilt Cove polluted and control concentrations have a similar range as the Robinsons River and Rennies River samples.

All of the elements in this second Factor 1 subgroup, except for Fe, are lithophile elements. Iron can be either lithophile, chalcophile, or siderophile (Reimann and Caritat, 1998). Lithophile elements are those that are associated with silicates, siderophile elements are those that preferentially occur with metallic iron which is concentrated in the Earth's iron core, they also occur primarily as oxides (Krauskopf, 1995). Iron is also found in significant quantities as the sulphide pyrite. The reasons for elevated concentrations at the Tilt Cove and Betts Cove polluted sites are probably similar to those for the first group. In Tilt Cove, these elements could be released either from the tailings piles situated southwest of Winsor Lake, or from the body of water situated around the West Mine. Acid mine drainage could be causing the high concentrations in the Betts Cove polluted samples, along with runoff from the mine site.

In Rennies River, all samples show the lowest concentrations at site SJWS1 (Figure 4.4(a)) and the highest concentrations at site SJWS6B (Figure 4.4(b)). All the remaining sites fall in between these extremes. Site SJWS1 was located in Nagles Hill Brook, and was the least polluted site in the study area. Possible pollutant inputs in this area may be coming from the nearby Mount Scio and/or agricultural land. Site SJWS6B occurred at a culvert that drains Kelly Brook which originally was a natural brook that drained a large St. John's residential area (Ford, 1992). It also flows through a site, where

the current Federal Taxation Centre is located (approximately 1 km to the southwest of SJS6B), that up until the mid-1960's, was the city dump (Callahan, 1991). In the 1960's, Kelly's Brook was enclosed in pipe and changed to a trunk storm water system, with a goal of decreasing the quantity of pollutants entering the stream both from runoff and from the dump site (Ford, 1992). Pollutants are still at high levels, and are accompanied by low dissolved oxygen. To remediate these problems, the Quidi Vidi Rennies River Development Foundation opened up the section of Kelly's Brook between Carpasian Road and Rennies River. This exposed the water to the atmosphere in an effort to increase dissolved oxygen in the water. As well, a series of steps were placed in the streambed to further aid in oxygenation by increasing the turbulence. Kelly's Brook also flows through a wetland marsh, which acts as a filter for silt and nutrients such as phosphates and nitrates (Power, 1990).

The first element in this Factor 1 subgroup is Li. Some reasons for increasing concentrations of Li in the SJWS2-6A sites may be due to sources such as lubricants, greases, or batteries (Reimann and Caritat, 1998). These are present in Rennies River and in the surrounding drainage area. At site SJWS6B, similar sources for Li may be present, and since this is an abandoned dump site, more of these sources are likely.

Magnesium exhibits elevated concentrations at Tilt Cove and Betts Cove which are likely due to similar causes as previously mentioned for other elements that are released from mine workings/tailings and mines. Control concentrations for both of these

sites are generally higher than levels obtained in Robinsons River and Rennies River SJWS1 possibly due to the presence of ultramafic rocks at the former sites (Reimann and Caritat, 1998). In Rennies River, increasing concentrations of Mg in the SJWS2 to SJWS6A sites may be due to the use of this element as an alloy with aluminum, for example in beverage containers and electrical equipment, and its use as an anti-corrosion agent in steel structures (Health Canada, 1978). It is expected that the presence of these three pollution sources would be high in a metropolitan area and higher near a buried dump site.

The elevated concentrations of Ca at the Betts Cove and Tilt Cove polluted sites are probably due to the same sources as mentioned for other elements. High concentrations were anticipated in the Robinsons River study area, but this was not observed. The only exception is RRWS11 that had a concentration greater than any of the Tilt Cove and Betts Cove control sites and higher than some of the Betts Cove polluted sites. This location is downstream from a clear-cut area where soil erosion could be producing high Ca concentrations. In addition, sinkholes were observed in the area located about 1.5 km to the east of the sampling site. Low Ca concentrations in the remaining sites could be related to heavy rains that occurred during the sampling period, which may have reduced concentrations by dilution. In Rennies River, Ca concentrations in sites SJWS2 to SJWS6A were about twice as high as SJWS1. This maybe due to release of Ca from concrete bridges. Other potential sources of Ca are from mortar,

stucco, and plaster used in the building industry, and fertilizers (Health Canada, 1987a; Reimann and Caritat, 1998). Sample site SJWS6B, was near a concrete drainage pipe that drained Kelly's Brook, and this likely produced high Ca concentrations. Also there was probable input from the buried dumpsite on Ca concentrations as well.

Manganese concentrations in Tilt Cove and Betts Cove followed similar patterns as other elements and thus reflect similar anthropogenic inputs. At Rennies River, high concentrations of Mn at sites SJWS2 to SJWS6A may be due to anthropogenic inputs from steel, alloys, batteries, fertilizers, wood preservatives, and its use as an antiknock agent (MMT) in gasoline (Reimann and Caritat, 1998). All of these sources are expected to be higher at metropolitan sites. Also, manganese stains were present along certain areas of the streambed near some of the sampling sites, indicating that the groundwater was carrying large amounts of Mn into Rennies River. These sources are responsible for the high concentrations of Mn in Rennies River compared to the other sites. Site SJWS6B shows elevated concentrations, again attributed to the buried dump site.

Iron followed a similar pattern, except that at Tilt Cove, not all polluted sites showed elevated concentrations of Fe. Only sites TCWS13 and TCWS14 exhibited elevated concentrations above the control concentrations; site TCWS13 showed especially high concentrations. This may be because this site is located close to the expected location of the tailings. It may also be due to the low dissolved oxygen concentrations present there. The value is 3.00 mg/L, which is the lowest for all four

study areas, by comparison, the concentrations in the Tilt Cove study area for the remaining sites range from 7.31 mg/L to 9.31 mg/L. Generally, in oxidizing conditions iron is present as Fe(III) which precipitates as oxides or is adsorbed onto surfaces (Health Canada, 1987b). In reducing conditions, such as at site TCWS13, Fe(II) may be present in solution resulting in higher concentrations because of the higher solubility of the reduced state. The sites in Robinsons River also showed somewhat elevated levels of Fe, possibly due to the presence of iron-rich sedimentary rocks. For Rennies River, elevated concentrations of Fe were detected at sites SJWS2 to SJWS6A, with even higher concentrations at SJWS6B. Possible sources of Fe in these polluted sites are from steel and paint pigments (Reimann and Caritat, 1998). The abandoned dump site is expected to contain steel and scrap metal, and thus may result in the high Fe concentrations at site SJWS6B.

Cesium defined a pattern of high concentrations at the Tilt Cove and Betts Cove polluted sites which may be due to the fact that it can be associated with a variety of sulphides (Reimann and Caritat, 1998). It shows enhanced concentrations at sites SJWS2-SJWS6A and even higher concentrations at site SJWS6B which may be due to release from sources such as photovoltaic cells.

Conductivity readings in Tilt Cove had the highest concentrations in the polluted sites, with the highest value at site TCWS13, which is the site which is closest to the tailings piles. At Betts Cove, conductivity concentrations were highest in the polluted

samples, low pH concentrations were also measured in these samples, indicating acid mine drainage. Robinsons River had conductivities that were between those at Tilt Cove and those at Betts Cove control. The only exception is site RRWS15, which had the highest concentrations in the study area. This occurred downstream from an agricultural area, where extensive fertilizers are used, which can release ionic material into the water. At Rennies River, SJWS1 had the lowest conductivity, which was expected since it was selected as the pristine site, concentrations for SJWS2 to SJWS6A were higher, which seems reasonable because they occur in a metropolitan site. Finally, the heavily polluted site, SJWS6B had the highest concentrations, due to drainage from the buried dump site.

4.1.2 Water PCFA Factor 2

Factor 2 consists of Al, Ni, Rb, Ba, pH, and conductivity. Aluminum and Ni both have negative loadings with this Factor, with loadings of -0.679 and -0.628 respectively. Rubidium, Ba, pH, and conductivity have positive loadings in this Factor, with loadings of 0.695, 0.891, 0.567, and 0.679 respectively.

This Factor indicates the importance of pH with regards to the mobility of these ions in the different stream environments. Al and Ni have similar chemical characteristics. Aluminum is a lithophile element which in nature is always found in the +3 oxidation state with an ionic radius of 53-67.5 pm, an electronegativity of 1.61 and a density of 2.698 g/cm³ (Reimann and Caritat, 1998). Nickel is both chalcophile and

siderophile, with a usual oxidation state of +2, an ionic radius of 63-83 pm, an electronegativity of 1.91, and a density of 8.902 g/cm³. Besides the fact that Al and Ni have similar ionic radii and electronegativity, both elements are increasingly soluble in acidic conditions (Reimann and Caritat, 1998). The solubility of Al increases at pH values <5.5. The pH in Betts Cove sites BCWS1 to BCWS9 range from 4.58 to 5.05, increasing to over 6 for the remaining sites, the exception being BCWS12 which has a value of 5.36 (Figure 4.5(a)). In the BCWS1 to BCWS9 locations, there was no apparent life in any of the sampled streams or ponds with a grey coating present on the streambed material. At site TCWS13 in Tilt Cove (Figure 4.5(b)) the pH was 6.59. All the elements in Factor 1 are enriched, with Al showing only a small enrichment. For the remainder of the Tilt Cove polluted sites, Al concentrations are similar to control areas, and the pH values are about 1 unit higher than control sites. For Ni, similar to Al, the Betts Cove polluted sites with pH values <5.5 had the highest concentrations. The remaining sites, including the polluted areas, BCWS10 to BCWS13, all had similar Ni concentrations. There are ultramafic rocks present in the control study area which contain elevated Ni concentrations and thus contribute Ni to the sampled stream in the control area (Maynard, 1983). The Tilt Cove sites all had concentrations which were higher in the polluted compared to control sites. At Robinsons River, no apparent trends were observed.

In the Rennies River sites, site SJWS6B had the lowest Al concentrations, this site also had the highest pH values. There was no apparent trend in the Robinsons River or Rennies River streams for Ni.

As previously mentioned, both Rb and Ba had positive correlations in Factor 2. Barium and Rb have similar ionic radii and electronegativity. Rubidium is a lithophile element with an oxidation state of +1, an ionic radius of 166-197 pm, an electronegativity of 0.82, and a density of 1.532 g/cm³. Barium is a lithophile element with an oxidation state of +2, ionic radius of 149-175 pm, an electronegativity of 0.89, and a density of 3.5 g/cm³. Both are mobile cationic species in the environment (Rose *et al.*, 1979). Compared to Al and Ni, they are not highly influenced by pH. For samples taken from Tilt Cove, concentrations for polluted sites are just slightly above control site concentrations (Figure 4.6(a)) with concentrations for TCWS12 and TCWS13 being close to control concentrations. The same trend is present for the Betts Cove polluted and control sites (Figure 4.6(b)). This may be explained by the fact that Ba is present in barite which is often associated with sulphide ores. When this occurs, Ba has a low solubility resulting in the observed concentrations (Rose *et al.*, 1979). Concentrations for Tilt Cove and Betts Cove polluted sites are in a similar range as Rennies River, whereas for the control sites, concentrations are less than both Rennies and Robinsons River. At Rennies River, Ba concentrations are lowest at SJWS1, and highest for SJWS6B, which has the highest pH

obtained in this study. This is probably related to anthropogenic sources of Ba such as paint, rubber, and electronics (Reimann and Caritat, 1998).

For Rb, Tilt Cove polluted concentrations were only slightly higher than control concentrations (Figure 4.6(a)). Betts Cove polluted site concentrations were also slightly higher than control concentrations (Figure 4.6(b)). This indicates that Rb concentrations are not influenced by pH compared to analytes such as Al and Ni. Betts Cove control concentrations were less than Rennies River, and Tilt Cove sample concentrations were in the same range as Rennies River. The Rennies River data illustrated the pattern of low concentrations at site SJWS1, with the highest concentrations at site SJWS6B. Higher concentrations were found in sites SJWS2 to SJWS6A compared to SJWS1, but the relative difference was small. The concentrations at site SJWS6B were approximately three times those at SJWS1. Anthropogenic sources of Rb include electronics, semi-conductors, and glass (Reimann and Caritat, 1998). The element Rb is generally associated with K, and is found in fertilizers and alloys. Conductivity trends were previously discussed.

4.1.3 Water PCFA Factor 3

Factor 3 consisted of As, Ce, and pH. Arsenic had a loading of 0.825 and was positively correlated with Factor 3. The same was true for pH, which had a loading of 0.646 while Ce was negative correlated with a loading of -0.727. Arsenic is chalcophile,

with oxidation states of +3 and +5, an ionic radius of 47.5-72 pm, an electronegativity of 2.18, and a density of 5.73 g/cm³. Cerium is lithophile with common oxidation states of +3, or +4 in oxidizing conditions. The ionic radius of Ce is 115-148, with an electronegativity of 1.12, and a density of 6.77 g/cm³.

Arsenic showed elevated concentrations in the Tilt Cove polluted area compared to the control site (Figure 4.7(a)). In the Betts cove area, concentrations were slightly lower in the polluted samples compared to the control site, except for site BCWS3, and site BCWS10 (Figure 4.7(b)). Robinsons River had concentrations of As that were similar to Betts Cove polluted and Tilt Cove control and Rennies River. For Rennies River, most of the concentrations at site SJWS1 were the lowest, and SJWS6B were the highest. The differences between the two of these were small. Cerium exhibited concentrations that were lower in the Tilt Cove polluted area than in the control area, except at site TCWS13, but these differences were small (Figure 4.7(a)). At Betts Cove, concentrations were higher in the polluted compared to the control area, except for samples BCWS11 to BCWS13 (Figure 4.7(b)). Robinsons River showed Ce concentrations that were in the same range as Rennies River. At Rennies River, Ce concentrations were lowest at site SJWS1, and for most analytes the concentrations were highest at site SJWS6B. Differences between SJWS6B and SJWS2 to SJWS6A were not significant.

With regards to arsenic at Tilt Cove, high concentrations were expected in the water samples in and around the tailings piles as the piles contained elevated arsenic concentrations (Maddox, 2001). The high concentration of arsenic found at TCWS1 may be due to the low pH at this site (6.45), the lowest pH in this study area. It has been shown that the release of As from minerals is enhanced under acidic conditions (Smedley *et al.*, 1996). Another source of the elevated As concentrations could be the Long Pond East Gold Occurrence, which is located 600 m to the southwest of the supply pond (Figure 1.2). This is hosted by a group of green and red siltstones that are affiliated with a banded hematite-magnetite iron-formation (Bédard, 2000). Low gold concentrations are associated with this in the fine to medium grained pyrite which is disseminated in the green siltstone. Similar findings occur 50 m east of this. Arsenic concentrations for this occurrence ranged from 19 to 283 ppm, with a median value of 76 ppm. For the groups surrounding the supply pond, As concentrations ranged from 1.3 to 7.5 ppm with a median of 3 ppm.

In Betts Cove, high concentrations of As were expected in the polluted sites, because the pH was low and the stream drains an abandoned copper mine. The observed concentration trend for the Betts Cove study area is that there are higher concentrations of As in the control sample sites than in the polluted sites (Figure 4.7(b)). The high As concentrations in the control may be attributed to the Nugget Pond gold occurrence. This gold deposit is located in the only mine that is currently in production in the Betts Cove

ophiolite (Bédard, 2000). The deposit is a disseminated pyrite-gold mineralization which is found within the basal portion of the Sedimentary Member of the Scrape Point Formation. The mineralization is mostly pyrite with minor amounts of chalcopyrite, galena, Ag-telluride, and native silver. The deposit occurs approximately 3.1 km to the Northeast of Kitty Pond with the Scrape Point sedimentary member and Mount Misery Formation extending down to the Betts Cove area (Figure 1.3). Therefore it may be possible that As associated with Nugget Pond could be entering the control sampling sites.

Finally, at Rennies River, site SJWS1 had the lowest As concentrations, and SJWS6B had the highest; sites SJWS2 to SJWS6A had scattered concentrations that occurred between those of SJWS1 and SJWS6B. Potential sources of As into the environment are some metal alloys, wood preservatives, batteries, and paints.

As mentioned previously, Ce showed higher concentrations in the Tilt Cove control sites than the polluted sites, although this difference was small. In Tilt Cove, the mines were in a 400 m thick zone of massive and pillowed basalt and basalt breccia located near the contact between the boninitic and tholeiitic rocks of the Betts Head and Mound Misery Formations (Bédard, 2000). Average Ce concentrations were 1.7 and 3.2 ppm for the low and intermediate-Ti boninite lavas and dykes. For the Mount misery lavas and dykes the average Ce value was 6.1 ppm. In the control area for Tilt Cove, the Cape St. John Group is exposed, along with a serpentinite, cumulate peridotite, and

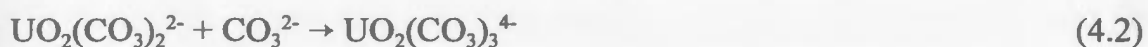
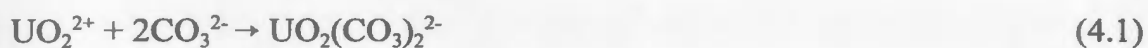
talc-carbonate showing. In the Cape St. John Group lavas, Ce in basalt has an average concentration of 22.2 ppm, and in andesite it has an average concentration of 61.5 ppm. In the peridotite cumulate rock, Ce has a concentration of 0.25, in the talc-magnesite carbonate schist, it has a concentration of 0.19 ppm. High concentrations were determined in TCWS13, which is probably from the tailings. It appears that the Cape St. John Group is contributing Ce to the control water samples in Tilt Cove.

In the Betts Cove area, it appears that pH affects the Ce concentrations. When pH is low in the polluted sites, concentrations of Ce are high. At site 10 where the pH is higher, the Ce concentration decreases. Concentrations at sites BCWS11-13 are similar to control concentrations. With regards to the geology of the area in relation to Ce, both areas have sheeted dykes, mixed dykes and lavas, and late intrusions. The concentrations in dykes were discussed previously. The late intrusions consist mostly of gabbroic rocks with Ce concentrations ranging from 1.02 to 4.28. Therefore, it appears that the high concentrations of Ce in this area can be related to acid mine drainage.

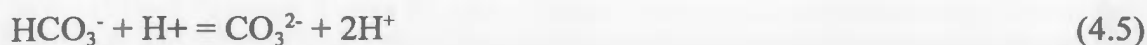
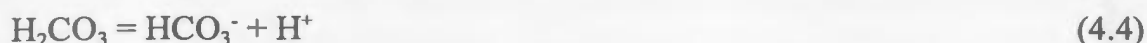
4.1.4 Water PCFA Factor 4

Factor 4 consisted of U and dissolved oxygen. They had loadings of 0.569 and -0.539 respectively. Uranium is found naturally in the +2, +3, +4, +5, and +6 oxidation states (Health Canada, 1999b). The hexavalent form is the most common and is usually associated with oxygen in the form of the uranyl ion, UO_2^{2+} . In the +6 oxidation state, it is

mobile (Siegel, 2002) with a global median stream water concentration of 0.04 ppb (Reimann and Caritat, 1998). Many of the ions of U^{4+} and UO_2^{2+} , such as the hydroxides, have a very low solubility (Krauskopf and Bird, 1995). Uranium compounds in the +6 oxidation state have an increased solubility especially when stable carbonate complexes are formed. A major control on uranium solubility is the amount of CO_2 in the system (Maynard, 1983).



Dissolved oxygen has a negative loading in Factor 4. Dissolved oxygen is consumed by plants and animals by the process of respiration and is produced by plant photosynthesis (Horne and Goldman, 1994). Water contains only a small amount of dissolved oxygen due to its low solubility with the concentration a function of its partial pressure in the atmosphere (0.21 bar). Carbon dioxide concentrations often follow an inverse relationship with dissolved oxygen. Carbon dioxide is a respiration product of plants and animals and provides the major carbon source for photosynthesis. Its solubility in water is 30 times higher than oxygen. Carbon dioxide reacts in the following manner in water:



Dissolved oxygen (DO) concentrations at the Tilt Cove control sites were higher than at the polluted sites, which was expected since no aquatic life was observed in the polluted sites (Figure 4.8(a)). Also, the water in the control sites flowed over a downslope resulting in more aerated water. Betts Cove polluted and control sites were similar, possibly because both were well aerated. Concentrations for Robinsons River were in a similar range as the Tilt Cove polluted sites. This was a much larger, deeper river, where mixing with the atmosphere is not as complete as in smaller streams, leading to lower quantities of dissolved oxygen. For Rennies River, the highest quantities of dissolved oxygen were detected during the spring, late fall, and winter. The lowest quantities were found during the summer and early fall. For the most part, site SJWS1 had the highest DO, whereas site SJWS6B had the lowest. Lower dissolved oxygen contents in the summer could be caused by lower water flow rates. Water is not mixed as well during low flow rates compared to high flow rates (Caissie *et al.*, 1996). Site SJWS1 showed the highest DO levels possibly due to the fact that this is the shallowest, and most well mixed site in Rennies River sample sites. Sites SJWS2 to SJWS6A possibly showed lower concentrations because of raw sewage from drainage pipes which enters near these sites,

an excellent source of carbon, which will consume oxygen producing carbon dioxide. Low dissolved oxygen concentrations have been found at site SJWS6B in the past, but this was before a section of the river was opened between Carpasian Road and Rennies River. Despite this, some of the river is still covered, thus leading to low dissolved oxygen levels at site SJWS6B.

A relationship exists between dissolved oxygen (Figure 4.8(a)) and U concentrations (Figure 4.8(b)). The dissolved oxygen reading from TCWS13 was omitted because it had an extremely low value of 3.00 mg/L, which was much lower than any other area in the sampled sites. Correlation coefficients were calculated with and without this site, and there was a moderate negative relationship between U concentrations and dissolved oxygen levels. The Pearson correlation coefficient for log-transformed concentrations of U (ppb) with dissolved oxygen (mg/L) is -0.623, and when the dissolved oxygen value is removed from TCWS13, the value changes slightly to -0.637. For both of these correlation coefficients, the p-value was 0, suggesting a moderate negative correlation between U and dissolved oxygen. As mentioned previously, dissolved oxygen and carbon dioxide often have an inverse relationship. That is, when dissolved oxygen is high, which means photosynthesis is high, or is at a higher rate than respiration, carbon dioxide will be low. Similarly the inverse is true. In areas of low dissolved oxygen, concentrations of carbon dioxide will be high, which will result in a shift of the U equilibria towards the formation of the $\text{UO}_2(\text{CO}_3)_3^{4-}$ complex, resulting in

higher total U concentrations. Also, the high dissolved U concentrations at Robinsons River may be due to the presence of black shales, which contain high concentrations of U (Maynard, 1983). This area generally had low dissolved oxygen.

4.2 LA-ICP-MS PCFA

Principle component Factor analysis of LA-ICP-MS analyses of Fe-Mn oxide coatings on stream pebbles produced three Factors which resulted in 9 groupings of the samples based on geochemical characteristics (Figure 3.12). Factor 1 consisted of Cr, MnO₂, Fe₂O₃, Cu, Sr, Y, Ba, La, and Ce, Factor 2 was composed of Co, Ni, Zn, and Cd, while, Factor 3 contained Th.

4.2.1 Fe-Mn Oxide Coating PCFA Factor 1

All of the variables that loaded high in Factor 1 have a negative loading except for Cr, Fe₂O₃, and Cu. The elements which have a negative loading are all lithophile elements, and they all positively correlate with MnO₂, whereas elements that have a positive loading in this Factor are lithophile (Cr), chalcophile/siderophile (Fe), or chalcophile (Cu).

Concentration patterns of the waters data in the different study areas were discussed in section 4.1.1 for the elements Mn, Fe, Ba, and Ce. Yttrium was not included in the waters package, therefore no water concentrations were obtained for Y. As

expected, Sr showed a similar pattern to Ca, since the waters data had a correlation coefficient of 0.862 and it is known that Sr replaces Ca in minerals due to similar chemical properties (Reimann and Caritat, 1998). For La, results were not included in the PCFA as La has a high correlation coefficient with Ce of 0.989; they both belong to the rare earth element (REE) group, have very similar chemical and physical properties, and commonly occur together in natural environments (Krauskopf and Bird, 1995). The general trend for the water concentrations of all these negative loading lithophile elements is that elevated concentrations occur in the Tilt Cove polluted sites compared to the control sites, with the maximum concentrations at site TCWS13. Exceptions are La and Ce, with reasons related to the local geology, as previously discussed. For Betts Cove, all except Ba (explanation mentioned above) have higher concentrations in the polluted sites compared to the control sites, all Robinsons River concentrations were higher than the Tilt Cove and Betts Cove control sites. Concentrations at Rennies River follow the general pattern of low concentrations at site SJWS1, with the highest concentrations at SJWS6B.

The negative loading lithophile elements in Factor 1, follow the same general trend as MnO_2 in the various study areas; with higher concentrations in the Tilt Cove control study area compared to the polluted site. The polluted Tilt Cove sites (TCPS10 and TCPS11) have higher concentrations than samples from sites TCPS13 and TCPS14. For the Betts Cove study area, all of the lithophile element concentrations from the

polluted sites are in similar ranges, or slightly less than those taken from the control sites. For the Rennies River data, all concentrations of these large-ion lithophile elements were lowest at site SJPS6B. There were no apparent trends at Robinsons River for these elements.

Pearson correlation coefficients were calculated for the variables that had a negative loading in Factor 1 and the Fe_2O_3 and MnO_2 phases. For Fe_2O_3 and the lithophile elements, the coefficients are; Sr = -0.152, Y = -0.439, Ba = - 0.689, La = -0.397, and Ce = -0.608. The coefficients for these elements with the MnO_2 phase are; Sr = 0.515, Y = 0.567, Ba = 0.880, La = 0.602, and Ce = 0.793. It appears that these lithophile elements are adsorbed by the MnO_2 part of the Fe-Mn oxide coating in preference to the Fe_2O_3 phase.

In addition to Pearson correlation coefficients, concentration trends can be used to show that for the variables which loaded negatively in Factor 1, MnO_2 is a much better adsorber than Fe_2O_3 . At Tilt Cove, Sr and Ba show elevated concentrations in the stream water at polluted sites compared to control sites, and the opposite trend occurs for their coating concentrations (Figure 4.9(a)). At the control sites, MnO_2 ranges from 50.8 % to 72.0 %, whereas in the polluted sites, the MnO_2 ranges from 0.07 % to 13.8 %. The pH and dissolved oxygen concentrations are similar, with the exception of site TCWS13 which has a dissolved oxygen reading of 3.00 mg/L. These trends show that MnO_2

dictates the concentration of these large-ion lithophile elements on Fe-Mn oxide coatings even if water concentrations differ.

In addition to this experimental evidence, the literature on Fe-Mn oxide coatings suggests that the Mn-oxide phase of the Fe-Mn oxide coatings is a better adsorber than the Fe-oxide phase (Jackson, 1998; Rose *et al.*, 1979). It has been estimated that the sorption capacity of Fe-oxides is at least ten times less than that of the Mn-oxides (Suarez and Langmuir, 1976). One possible reason for the better adsorption properties of MnO_2 is its zero point of charge (ZPC), which is the pH at which the surface is uncharged (Rose *et al.*, 1979). This depends on the extent of the dissociation in surface OH^- or H_2O molecules. For the Mn oxides, dissociation at pH 7 is high, therefore the surface of the Mn-oxide will have a strong negative charge. If acid conditions are encountered, H^+ is adsorbed onto the surface. When sufficient H^+ ions are adsorbed, the surface becomes neutrally charged. This pH is termed the zero point of charge. For MnO_2 , this occurs at a pH of 3, although Nicholson (1992) suggested that freshly deposited amorphous manganese oxide has a ZPC at pH between 1.5 and 2.0. Gadde and Laitinen (1974) postulated a ZPC at pH between 1.5 and 1.8 for $\delta\text{-MnO}_2$ and manganese manganite. At a neutral pH, MnO_2 will usually take on a negative surface charge thus being able to adsorb cations from solution, making them poor adsorbers of anions (Zachara *et al.*, 1995) This model has been supported by Whitney (1975), and Jenne (1968). For the iron oxides (*i.e.* Fe_2O_3), the ZPC is between 6.5 and 8.5, so that most Fe-oxides in natural environments

have a positive charge (Rose *et al.*, 1979). In natural pH stream environments, they will be poor adsorbers of cations, but excellent adsorbers of anions.

At Betts Cove, all of the lithophile elements in Factor 1, except for Ba, displayed elevated concentrations in the water samples from the polluted sites compared to the pristine sites (Figure 4.10). Sites BCWS10, BCWS11, and BCWS13 had the lowest Fe-Mn oxide Ba concentrations of the polluted sites. These Fe-Mn oxide concentrations, including MnO_2 , from the polluted sampling sites are slightly less than or in a similar range as the control sites. The exception is Ba, which has lower concentrations in the control sites. These trends further demonstrate the preference of MnO_2 over Fe_2O_3 for adsorption of these lithophile elements. This is especially noted at site BCWS15 where the highest amount of MnO_2 was found, and consequently the highest concentration of all the lithophile elements occurred at this site.

Another variable that could be influencing adsorption in the Betts Cove study area is pH. The polluted study area is a low pH environment, with pH ranging from 4.58 to 5.05 at sites BCWS1 to BCWS9, while at site BCWS10 the pH increases to 6.36. Based on the above discussion of the ZPC of MnO_2 and Fe_2O_3 , the low pH conditions found in sites BCWS1 to BCWS9 should result in a reduced negative surface charge on MnO_2 , and hence its ability to adsorb cations, further increasing the positive charge on Fe_2O_3 , leading to further lowering the capacity of the Fe_2O_3 for the adsorption of cations. Experimental studies have shown that when a pH increase occurs, the concentrations of metals

including Cu, Co, Mn, Zn, and Ni increase on the Fe-Mn oxide coatings (Loganathan and Burau, 1973; Gadde and Laitinen, 1974; Murray, 1975; and Zachara *et al.* 1995).

For the Robinsons River study area, no apparent pattern was observed for the elements that loaded negatively in Factor 1. Water samples collected from Rennies River displayed a similar trend for these elements having the lowest concentrations at site SJWS1, while the highest concentrations occurred at SJWS6B. Exceptions were La and Ce concentrations taken mid-way through the sampling period. For the Rennies River study area, the lowest concentrations of MnO_2 and the negative loading variables in Factor 1 occurred at site SJWS6B. Two exceptions to this pattern are Sr which shows equal concentrations for sites SJPS1 and SJPS6B for the samples taken in May, where La also had a higher concentration in the samples collected in May at site SJPS6B compared to site SJPS1. These low concentrations are related to depleted amounts of MnO_2 on these pebbles collected from site SJPS6B. These samples were extremely iron rich with concentrations of Fe_2O_3 ranging from 86.0 % to 98.0 %. The measured pH at SJPS6B was marginally higher than the other sites, and therefore while adsorption should be favoured at SJPS6B, it was not observed. The trends do display the preferential adsorption on MnO_2 of Sr, Y, Ba, La, and Ce.

As mentioned previously, there were three analytes that had positive loadings in Factor 1 (Cr, Fe_2O_3 , and Cu), possibly suggesting that Cr and Cu are preferentially adsorbed by the Fe_2O_3 phase of the Fe-Mn oxide coating. Pearson correlation coefficients

were calculated to determine the relationship between Cr, Cu, and Fe_2O_3 , and for comparison they were also calculated for MnO_2 . The coefficients of Cr to Fe_2O_3 and to MnO_2 were 0.630 and -0.485 respectively. Similarly, for Cu to Fe_2O_3 and Cu to MnO_2 the coefficients were 0.223 and -0.551 respectively. Thus, there was a weak to moderate positive correlation between Cr, Cu, and Fe_2O_3 . This is likely related to the similar ionic radii of Cr, Fe, and Cu (Table 4.1). Elements that have negative loadings in Factor 1 have larger ionic radii. For the smaller ionic radii elements, this may allow them to be adsorbed preferentially on the surface of Fe_2O_3 .

Table 4.1 Elements that loaded high in Fe-Mn oxide coating Factor 1 along with their common oxidation state in the environment and ionic radius (Reimann and Caritat, 1998).

Element	Main Oxidation State	Ionic Radius (pm)
Cr	+6	40-58
Mn	+2	80-110
Fe	+3	63-92
Cu	+2	71-87
Sr	+2	132-158
Y	+3	104-121.5
Ba	+2	149-175
La	+3	117-150
Ce	+3	115-148

In the Tilt Cove and Betts Cove study areas, the interaction of Cu and Cr with Fe_2O_3 is complex and appears to be the result of a variety of interactions. Iron concentrations in the water samples at the control site had concentrations similar to those

in the polluted sites TCWS10 and TCWS11. The maximum Fe concentration occurred at TCWS13, which was in the stream flowing from a pond at the West Mine.

Concentrations were lower at site TCWS14, but these were the second highest recorded in the study area (Figure 4.11(a)). The amount of Fe_2O_3 in the Fe-Mn oxide coatings was higher at the polluted sites than at control sites (Figure 4.11(a)). Even though low Fe water concentrations were measured at sites TCWS10 and TCWS11, the coatings had high amounts of Fe_2O_3 (62.6% and 54.0% respectively). The coatings at sites TCPS13 and TCPS14, were principally Fe_2O_3 , with concentrations of 88.6 % and 84.2 %. This may be attributed to high concentrations of Fe in the water. Site TCPS13 also showed an extremely low dissolved oxygen value of 3.0 mg/L. This may be too low to allow the precipitation of MnO_2 , resulting in high Fe_2O_3 concentrations (Jackson, 1998).

At Tilt Cove, the Cr concentrations in the water had concentrations at the polluted sites that were in a similar range as at the control sites (Figure 4.11(b)). The maximum Cr concentration occurred at TCWS7, due to the presence of layered cumulate rocks in the control area which have elevated concentrations of Cr and Ni. Chromium concentrations on the pebble coatings followed the trend of higher concentrations in the polluted sites compared to the control sites, which is likely related to the high quantities of Fe_2O_3 present on the coatings. In highly oxidized solutions, when chromium is present in the +6 oxidation state it is found as CrO_4^{2-} and $\text{Cr}_2\text{O}_7^{2-}$ (Rose *et al.*, 1979; Health Canada, 1986b). Since Cr is anionic, it should be adsorbed strongly onto the positive surface of

Fe_2O_3 and rejected from the negative surface of MnO_2 . Other studies have confirmed this model of Cr adsorption (Filipek and Owen, 1979, Zachara *et al.*, 1995). If reduced Cr (Cr^{3+}) is present, it substitutes for Fe^{3+} in the iron-oxides because of similar ionic radii (Jackson, 1998).

The concentrations of Cu in the water samples in the Tilt Cove study area had higher concentrations in the polluted sites compared to the control sites with the highest concentration occurring at site TCWS13 (Figure 4.11(b)). The Fe-Mn oxide concentrations showed a similar trend except that the highest concentration occurred at TCPS11. Adsorption of transition elements is generally favoured on Mn-oxides relative to Fe-oxides, although some studies have found that Fe-oxides are better adsorbers of some elements including Cu (Jackson, 1998; Siegel, 2002). In this study area, adsorption appears to be favoured on Fe_2O_3 compared to MnO_2 , since elevated concentrations of Fe_2O_3 and Cu appear together in the polluted sites. This relationship is also supported by the suggestion that iron-oxides more readily coprecipitate Cu, compared to other transition elements (Förstner and Wittmann, 1979). Also since Cu can form the anionic complexes, CuCl_2^- , and CuCl_3^{2-} , complexes which are similar to that of Cr, Cu can be adsorbed onto the positive surface of Fe_2O_3 .

In the Betts Cove area, water samples taken from the polluted sites have the highest concentration of Fe. The concentrations of Fe are inversely correlated to pH, suggesting the presence of acid mine drainage (Figure 4.12(a)). The pebble coatings in

the polluted sites are almost entirely Fe_2O_3 with compositions from 80.4 wt % at site BCPS4 to 91.0 wt % at site BCPS11. Control site iron oxide compositions ranged from 56.7 % to 86.9 %, and they are generally lower than those at the polluted Betts Cove sites (Figure 4.13(a)). High amounts of Fe_2O_3 at the polluted sites could be related to the low pH in these environments. Whitney (1975) found that iron-oxides precipitated in lower pH environments than MnO_2 . Hence, the pH in the Betts Cove polluted sites could be too low to result in the precipitation of MnO_2 .

Chromium concentrations in the Betts Cove control sites were greater than in the polluted sites for both the water and Fe-Mn oxide concentrations (Figure 4.12(b)). Exceptions were the water samples BCWS3 and BCWS8, and the pebble sample BCPS4. This trend can be explained by the observation of the presence of layered cumulate rocks in the control area, especially in the Kitty Pond area (Bédard *et al.*, 2000). These have high contents of Cr and Ni, therefore high concentrations are present in the water which will be adsorbed onto the iron rich coatings.

Copper concentrations for both the water and pebble samples showed a trend of higher concentrations in the polluted sites compared to the control sites (Figure 4.12(b)). In the water samples, the effects of acid mine drainage are observed in which Cu concentrations in the polluted sites decrease with increasing pH. Copper and Fe_2O_3 appear highly correlated, which may be related to the previous discussion.

There were no apparent trends in the concentrations of Fe in Robinsons River water. Coating compositions of the Fe_2O_3 ranged from a minimum of 17.2% at site RRPS1 to a maximum of 86.2% at site RRPS3. High concentrations of CaO occur in most of the Robinsons River samples. Since these samples were taken in an area of carbonate bedrock, elevated CaO values may indicate ablation of the substrate. At site RRPS10 where a stream draining a small wetland mixes with Robinsons River, coatings were the thickest and darkest in colour, suggesting greater amounts of MnO_2 compared to other sites. Both Cr and Cu concentrations in Rennies River displayed no distinct patterns in either water or pebble samples.

For the water samples from the Rennies River site SJWS1 had the lowest Fe composition, and site SJWS6B had the highest. Coatings present on pebble samples collected at SJPS6B were iron rich (Figure 4.13(a)), and they had the highest Fe_2O_3 composition of the pebbles collected from Rennies River; iron oxide compositions were from 86% to 98%. These high iron concentrations are possibly due to the lower dissolved oxygen at this site, and as previously mentioned, iron-oxides can form at these lower dissolved oxygen concentrations where manganese oxides do not form. Measurements of pH were higher at this site than at other sites in the study area, therefore MnO_2 formation should be favoured (Förstner and Wittmann, 1979). It appears that dissolved oxygen and Fe water concentrations are a controlling factor of whether Fe_2O_3 or MnO_2 forms.

Considering the seasonal trends, the drop in Fe_2O_3 composition at SJPS6B after six months may be due to a decrease in Fe concentrations in the water.

Chromium concentrations at Rennies River displayed the lowest concentrations at site SJWS1, while the remaining sites exhibited higher concentrations. Possible sources of Cr that enter Rennies River include Cr from alloys, pigments, stainless steel, and the combustion of petroleum products (Reimann and Caritat, 1998). No apparent trends are observed in the Cr concentrations of the Fe-Mn oxide coating. It was expected that SJPS6B would have the highest Cr concentration because it was mainly Fe_2O_3 , but this was not observed. The high pH of this site may be contributing to lower Cr concentrations, since this will reduce the positive charge on the Fe_2O_3 surface, and hence lower the quantity of adsorbed CrO_4^{2-} anions.

Copper concentrations in water samples taken from Rennies River showed a slight enrichment in the samples taken from study site SJWS6B compared to the remaining sites (Figure 4.3(b)). The Cu concentrations in the iron-manganese oxide were the lowest at site SJPS6B (Figure 4.13(b)), which was surprising because of the high amounts of Fe_2O_3 present there. Similar to Cr data, this may be related to the higher pH at this locality.

4.2.2 Fe-Mn Oxide Coating PCFA Factor 2

Factor 2 consists of Co, Ni, Zn, As, and Cd, all of which have negative loadings thus suggesting a relationship controlled by similar processes between them. These

elements are similar in that all are chalcophile, hence they are characteristic of sulfide ore deposits. They also have similar ionic radii (Table 4.2).

Table 4.2 Elements that loaded high in Factor 2 along with their common oxidation state in the environment and ionic radius (Reimann and Caritat, 1998).

Element	Main Oxidation State	Ionic Radius (pm)
Co	2	72-104
Ni	2	63-83
Zn	2	74-104
As	3	47.5-72
Cd	2	92-145

The relationship of all five chalcophile elements in Factor 2 are observed in the element trends at the Tilt Cove and Betts Cove study areas. Water concentrations for all five of these chalcophile elements at Tilt Cove showed higher concentrations in the polluted sites compared to the control, an exception is Cd at site TCWS4 which has slightly higher concentrations than some of the polluted sites sampled (Figure 4.14-Figure 4.16).

Iron-manganese oxide coating data show that sites TCPS10 to TCPS11 have concentrations higher than control concentrations, with a maximum occurring at TCPS11. Minimum concentrations for all five chalcophile elements occur at TCPS13, and then an increase in concentrations for all analytes at site TCPS14 (Figure 4.14-Figure 4.16). Nickel exhibits an elevated concentration at TCPS8 possibly due to the exposure of

cumulate rocks around this site that are known to have increased concentrations of Ni (Bédard, 2000). In the polluted sites, concentrations of all five analytes appear to be related to the MnO_2 composition, which ranges from 0.07% at site TCPS13 to 13.8% at TCPS11 (Figure 4.17(a)). Site TCPS11 has the highest MnO_2 , and consequently it has the greatest concentration of all five chalcophile elements, although water concentrations were not at a maximum at this site. Polluted site TCPS13 has the highest concentrations in the water for all five elements, except As. This site has the lowest composition of MnO_2 , resulting in the lowest concentration of all five elements.

It is apparent that the elements in Factor 2 are preferentially adsorbed by the MnO_2 phase of the Fe-Mn oxide coating. Pearson correlation coefficients were calculated for MnO_2 and these five chalcophile elements (Table 4.3). There are low to moderate positive correlations between MnO_2 and the five elements, whereas weak to moderate negative correlations exist for Fe_2O_3 . The positive relationship between the chalcophile elements and MnO_2 may be explained by the process of specific adsorption. In solution, most ions have a shell of water around them that is held by electrostatic attraction due to H_2O dipole (Rose *et al.*, 1979). When specific adsorption occurs, the ions, especially the transition metals or those of high valence or complex electronic structure, easily lose their water molecules because they are more strongly attracted to the oxides, resulting in the ions being strongly adsorbed, even at the zero point of charge. This mechanism of adsorption may explain why levels of MnO_2 in the Fe-Mn oxide coatings, and not other

Table 4.3 Pearson-R correlation coefficients between elements that loaded high in Fe-Mn oxide Factor 2 and the MnO_2 and Fe_2O_3 phases of Fe-Mn oxide coatings.

Element	MnO_2	Fe_2O_3
Co	0.602	-0.341
Ni	0.178	-0.025
Zn	0.415	-0.522
As	0.054	-0.114
Cd	0.539	-0.56

variables such as pH, dissolved oxygen, or water concentrations, control the amount of adsorbed analyte on the coating.

At Betts Cove, all of the elements in Factor 2, with the exception of As, have the greatest concentrations in water at sites BCPS1 to BCPS8, followed by sites BCPS10 to BCPS12, while the lowest concentrations occurred at the control sites (Figure 4.14(b) to Figure 4.16(b)). Similar to Tilt Cove, the Fe-Mn oxide concentration patterns of the chalcophile elements follow the same general pattern as MnO_2 (Figure 4.17(b)). Even though water concentrations are higher in the polluted sites than control, the MnO_2 -poor coatings in the former, result in lower coating concentrations. The low pH environment of the polluted sites also minimizes adsorption by MnO_2 due to its neutralizing effect on the negative surface on the MnO_2 phase.

Again, Robinsons River showed no apparent trend for this set of elements.

Rennies River water concentrations displayed patterns for both Co and As with the lowest

concentration occurring at site SJWS1, and the highest at site SJWS6B, although the difference between these two sites was generally small. Zinc and Cd showed minimum concentrations at site SJWS1. For the Fe-Mn oxide coating concentration data, site SJPS6B, which consisted of coatings that had small amounts of MnO_2 , had the lowest concentrations for most of the elements collected over the study period. Adsorption should have been favoured at site SJPS6B due to higher pH levels present there. This again demonstrates the preferential adsorption of these chalcophile elements by the MnO_2 phase.

4.2.3 Fe-Mn Oxide Coating PCFA Factor 3

Factor 3 consists of Th, which had a negative loading -0.594. Thorium is a lithophile, with a common oxidation state of +4, an ionic radius of 108-134 and has a similar behaviour in the environment as the rare earth elements La and Ce, therefore it should show an affinity for the MnO_2 phase (Reimann and Caritat, 1998). The correlation coefficients of Th with the MnO_2 is 0.342 and with the Fe_2O_3 phase it is -0.023. Thorium displayed only weak positive correlations with MnO_2 , and a small negative correlation with Fe_2O_3 . Even with this weak correlation, Th displayed a pattern similar to the lithophiles in Factor 1 (Figure 18(a)) with lower concentrations at the polluted sites compared to the control site, and with a minimum occurring at site TCPS13. At Betts Cove, concentration trends closely matched those of the lithophile elements, and at

Robinsons River there were no apparent trends. There are no water Th concentrations to compare these trends to because Th is not included in the ICP-MS waters package at MUN, due to the low Th concentration in natural waters and biological systems.

Thorium concentrations are very important for the groupings produced from the PCFA plot of Factor 1 vs. Factor 3 (Figure 3.12). Group 8 and 9 are from the Tilt Cove study area, with sites TCS3, TCS4, TCS5, and TCS6 composing Group 8, and TCS 7 and TCS8 making up Group 9. Samples from Group 9 have higher concentrations of Th than Group 8, which may be related to the presence of the Cape St. John Group in the Group 9 sample area (Bédard *et al.*, 2000). Group 10 consisted of all samples taken from Rennies River site SJS6A. These exhibited the highest concentrations of Th for each 3 month sampling period (Figure 18(b)). These high concentrations may be a result of the exposure of shale in the SJS6A study area. Shale has the highest concentration of Th for the sedimentary rocks present in Rennies River (Rose *et al.*, 1979).

4.3 Fe-Mn Oxide Formation PCFA

As mentioned in Chapter 3, two Factors were maintained for the sample site groupings after PCFA of LA-ICP-MS data of Fe-Mn oxide coatings on artificial substrates placed in Rennies River (Figure 3.14(a)). Factor 1 consisted of V, Cr, Ni, Cu, Zn, Sr, Y, Ce, Pb, Bi, Th, and U; all of which had negative loadings in this Factor. Factor

2 contained the variables MnO_2 , Ba, and Fe_2O_3 . In the Factor 2, MnO_2 and Ba had negative loadings while Fe_2O_3 had a positive loading.

When the two calculated Factors were plotted, four groupings of samples (Figure 3.14(b)) result. Group 1 consisted of samples taken from SJPS6B; these had high abundances of Fe_2O_3 . Group 2 consists of all of the samples taken after three months of coating accretion. Group 3 consisted of samples taken after six months of coating accumulation. Finally, Group 4 contained samples taken between nine and twelve months of Fe-Mn oxide formation. The boundary between Groups 3 and 4 is not well defined, suggesting that coatings formed after 6, 9, and 12 months, are similar in composition. Since none of these groupings were a result of the substrate type, this variable has little effect on Fe-Mn oxide formation.

The common oxidation state, ionic radius, and affinity of all elements in Factor 1 and Factor 2 are given in Table 4.4. For the elements that loaded high in Factor 1, there appears to be no common property. In Factor 2, MnO_2 and Ba both are lithophile elements, with Ba having the largest ionic radius for all of the elements, and both of these have negative loadings on this Factor, thus suggesting a relationship between them.

4.3.1 Group 1

As previously mentioned, the samples collected from Rennies River were separated into four Groups based on element concentrations. Group 1, which consists of

Table 4.4 Elements that loaded high in Factor 1 and Factor 2 for the annual accretion samples along with their common oxidation state in the environment, ionic radius and affinity (Reimann and Caritat, 1998).

Element	Factor	Oxidation State	Ionic Radius (pm)	Affinity
V	1	5	49.5-68	Lithophile
Cr	1	6	58	Lithophile
Mn	2	4	53-67	Lithophile
Fe	2	3	63-92	Siderophile
Ni	1	2	63-83	Chalcophile
Cu	1	2	71-87	Chalcophile
Zn	1	2	74-104	Chalcophile
Sr	1	2	132-158	Lithophile
Y	1	3	104-121.5	Lithophile
Ba	2	2	149-175	Lithophile
Ce	1	3	115-148	Lithophile
Pb	1	2	112-163	Chalcophile
Bi	1	3	110-131	Chalcophile
Th	1	4	108-135	Lithophile
U	1	6	59-100	Lithophile

samples from SJPS6B, were expected to display the highest concentrations of most metals because it has been designated as the polluted site in the Rennies River study area. Since the Fe-Mn oxide coating concentration is partially a result of the amount of analyte in solution, the waters data for the study area was examined. This data showed that only

five of the elements (Mn, Fe, Sr, Ba; and U) which were present in the above two Factors had their greatest concentration at this site. These elevated concentrations did not lead to high analyte concentrations in the Fe-Mn oxide coatings, with the exception of Fe_2O_3 . Site SJS6B also had the highest pH throughout the year, with the pH ranging from 6.89 to 7.56. However this did not lead to increased adsorption and higher concentrations. Examination of the data showed that Group 1 displayed the lowest concentrations of all of the elements throughout the study period (Figure 4.19 and Appendix 5). Minimum concentrations in Group 1, which included all of the samples taken from SJPS6B, may be a result of a high Fe_2O_3 coating (Figure 4.20(a)). In section 4.2.1, it was mentioned that for pebbles collected from the streambed, MnO_2 was a much better adsorber of trace elements, with the exception of Cr and Cu, than Fe_2O_3 . This may also be true for the “fresh” coatings. “Fresh” meaning coatings that accumulated on the artificial substrates for 12 months, as opposed to “mature” coatings that were analysed on pebbles taken from the streambed.

Annual accretion of the elements in the two Factors can also be examined to aid in the interpretation of the element concentration patterns. At site SJPS6B, Fe-Mn oxide coatings had Fe_2O_3 concentrations ranging from 96.8% to 98.8% after 3 months of coating accretion, after which the Fe proportion decreased as the coating aged (Figure 4.20(b)). This decrease in Fe_2O_3 is accompanied by an increase in the relative proportions of MnO_2 . Measurements of pH and dissolved oxygen were measured at this site for an

entire year, and none of the conditions favoured increased deposition of MnO_2 . The most probable mechanism occurring here is that the surface of the precipitated Fe_2O_3 particles are providing an area for MnO_2 precipitation (Whitney, 1975; Cerling, 1982; Hem, 1978; and Jenne, 1968). As the Fe_2O_3 accumulates on the substrate after three months in Rennies River, MnO_2 is able to accumulate, thus leading to higher concentrations of MnO_2 in the later months.

For the remaining elements in the two Factors, the lowest concentration for all of the elements occurred at site SJPS6B during the complete sampling period, with most elements showing the highest concentration after 3 months of coating accretion (Figure 4.21(a)). However this was not the case for all of the analytes (Figure 4.21(b)). It was expected that element trends would follow that of MnO_2 , with increasing concentrations as the coatings aged.

4.3.2 Group 2

As previously mentioned, Group 2 consisted of samples taken after three months of coating accretion. This Group is very similar to Group 1 in that both groups have a high Fe_2O_3 composition. Also, for annual accretion trends, this group displays the highest concentrations of all elements except Ba. This similarity between the groups is seen in the overlap of the two Groups in Figure 3.14. Figure 4.22 shows the accumulation of MnO_2 throughout the year at sites SJPS1 and SJPS6A. After 3 months of accumulation, the

coating contains a small fraction of MnO_2 , being mostly Fe_2O_3 . The fraction of MnO_2 increases sharply in the period from three to six months, and then remains relatively constant to the termination of the sampling at twelve months. Similar to SJPS6B, the increasing amounts of MnO_2 throughout the year is probably due to Fe_2O_3 acting as a surface for MnO_2 precipitation.

Accumulation of other elements in the oxide coating is also higher after three months of accretion, even though MnO_2 amounts are low (Figure 4.23). Based on the PCFA of the “mature” coatings, element concentrations are expected to increase with increasing amounts of MnO_2 . However, Ba is the only element that exhibited this positive correlation with MnO_2 (Figure 4.24(a)). The Pearson correlation coefficient of MnO_2 with Ba was 0.819, indicating a high relationship between the two elements. This is present in Factor 2, with MnO_2 having a negative loading of -0.862, and Ba having a loading of -0.810. Other elements lack any good correlation with MnO_2 (Figure 4.24(b)). For example Sr and MnO_2 have a Pearson correlation coefficient of 0.121.

It may be possible that this coating accretion trend of high trace element compositions of the Fe-Mn coating concentrations is due to ablation of the substrate. Samples taken after three months of accumulation appeared to have the thinnest coatings, therefore ablation of the substrate is more likely. Depth profiles of coatings on streak plates and cement were used to examine this possibility. The issue of high amounts of Al_2O_3 and SiO_2 in streak plate samples was addressed in section 3.3.1, and it was

concluded that ablation of the substrate was almost completely responsible for the elevated concentrations taken after 3 and 6 months of coating accretion. Also, as the coatings aged, Mn intensities increased and lasted longer as the coatings aged (Figure 3.7(a)). The actual intensity (cps) for the depth profiles on the streak plates for the 3 month samples showed that the ^{55}Mn signal remained above background for approximately 25 (s), a longer 120 (s) for the 6 month sample, and even longer for the complete run for the 9 and 12 month samples.

The cement substrate, which was not discussed previously, showed a similar trend (Figure 4.25), except after 12 months of coating formation (Figure 4.25(d)), the signal was shorter in duration than the 6 and 9 month samples. Relative intensities of ^{27}Al , ^{29}Si , ^{55}Mn , and ^{57}Fe for the coatings show a comparable trend to the streak plate, except that for the sample taken after 12 months of coating accretion, ^{27}Al , ^{55}Mn , and ^{57}Fe had similar intensities. The low intensity, short ^{55}Mn signals may be due to the heterogeneous nature of the cement substrate, as seen in Figure 4.26.

The above results indicated that ablation of the substrate occurs for samples taken from Rennies River after 3 and 6 months of coating accretion, and that Al_2O_3 , SiO_2 and possibly TiO_2 are contributed from the substrate. This suggests further investigation of intensity (cps) vs. time (s) data in order to better determine potential contribution from the substrates. Elements examined were those that the PCFA determined were important. Figure 4.27(a)-4.27(d) and Figure 4.28(a)-4.28(d) are intensity (cps) vs. time (s) plots for

streak plate and cement substrates respectively that were placed in Rennies River at site SJPS1 for three months. Intensity concentrations were examined for each analyte.

Two elements, ^{27}Al and ^{29}Si (Figure 4.27(a)) remain well above background levels for the duration of the streak plate depth profile; whereas ^{55}Mn and ^{57}Fe quickly decrease to background concentrations. Five other elements, ^{47}Ti (Figure 4.28(b)), ^{89}Y , ^{140}Ce (Figure 4.27(c)), ^{208}Pb (Figure 4.27(d)), and ^{238}U showed a minor enrichment over background levels. Cement intensity (cps) concentrations for ^{27}Al , ^{29}Si , ^{55}Mn , and ^{57}Fe followed similar trends as the streak plate (Figure 4.28(a)). Contribution from the substrate was also comparable to streak plate trends for ^{47}Ti (Figure 4.28(b)); ^{89}Y , ^{140}Ce , ^{137}Ba (Figure 4.28(c); and ^{232}Th (Figure 4.28(d)). This contribution from the substrate for these elements would be a problem if single spots, instead of rasters, were used for the coating analysis. With rastering, the sample is slowly moved allowing the laser to ablate a line across the pebble surface acquiring data points along the path. Since the laser is only ablating a single point for a short period of time, ablation of the substrate should be minimized, that is, only the coating should be ablated.

Elevated concentrations of Al_2O_3 and SiO_2 after three months are due to ablation of the substrate, as seen in the high intensity ^{27}Al and ^{29}Si signals produced after ablation of the 3 month samples. As the coating became thicker, concentrations decreased, as seen in the 6, 9, and 12 months samples. For the remaining elements, ablation of the substrate was not responsible for high concentrations at 3 months.

Element concentrations for the Fe-Mn oxide coatings may be a function of a particular stream chemistry variable or a property of the Fe-Mn oxide coating. Data for the water samples collected from Rennies River was reexamined, and none of the elements in any of the Factors showed maximum water concentrations for the three month samples, therefore high Fe-Mn oxide coating concentrations are likely the result of some other variable.

Iron-Manganese oxide coating concentrations may also be a function of the water temperature, dissolved oxygen, and pH. Adsorption of metals on Fe-Mn oxide coatings increases with temperature (Trivedi and Axe, 2000). Temperature concentrations at Rennies River increased in the time period from 0 to 6 months, and then decreased (Figure 4.29(a)). From this trend, there appears to be no relation between temperature and coating concentration. Low dissolved oxygen values will prevent the precipitation of MnO_2 , resulting in high Fe_2O_3 concentrations (Jackson, 1998). The dissolved oxygen pattern was the opposite of the pattern for temperature (Figure 4.29(b)). This should have produced high MnO_2 after three months, and then a lower value after 6 months of accretion, while the opposite occurred (Jackson, 1998). The pH values will also determine which oxide phase will form. Iron oxides precipitate at pH values greater than 4.5, whereas manganese oxides require values greater than 8 (Theobald *et al.*, 1963). Oxidation rates of both iron and manganese increase by a factor of 100 for each pH unit increase, with manganese requiring a much higher pH for equivalent rates of oxidation

(Morgan and Stumm, 1964). Measurements for pH are relatively constant for sites SJWS1, SJWS6A, and SJWS6B (Figure 4.29(c)) throughout the sampling period. Dissolved oxygen and pH cannot explain the elevated concentrations of element concentrations after three months of coating accretion.

The coating concentration trends must be due to some other property of the Fe-Mn oxide coating, one of which could be the crystallinity of the structure. Freshly precipitated Fe-Mn oxide “gels” are amorphous and have a high sorption capacity. As the coating ages, the coating crystallizes (Jackson, 1998) resulting in the release of certain adsorbed and coprecipitated metals because they cannot fit into the newly formed crystal structure (Waslenchuk, 1975). Those that have a high probability of being excluded during crystallization are those that have ionic radii that are unable to undergo isomorphous substitution in the newly formed Fe-Mn oxide coating. This may be occurring in the Rennies River samples, but Trivedi and Axe (2000) found that crystallization did not occur in artificial amorphous iron and manganese oxides after six months.

Iron-manganese oxide coatings also contain significant amounts of organic material. Figure 4.30 indicates that there are substantial amounts of organic material on the coatings, which increased with time. This organic material is present on the surface of the coatings, and has the ability to block the coating from adsorbing metals from solution (Jackson, 1998). This may account for the low concentrations found after 9 and 12

months. Organic matter also has the ability to cause reduction of iron and manganese by lowering the Eh and pH (MnO_2 will dissolve at a higher Eh and pH than Fe_2O_3 (Jenne, 1968). This did not occur here because coating thickness did increase with age and also the amounts of MnO_2 increased rather than decreased.

It has been suggested above that metal concentrations of Fe-Mn coatings present on the artificial substrates are not the result of water chemistry, the degree of crystallinity of the coating, or amount of organic matter. They must be related to some property of the MnO_2 and Fe_2O_3 phases. Data analysis of “mature” coatings concluded that MnO_2 was a better adsorber of elements present in solution, except for Cr and Cu, than Fe_2O_3 . For the “fresh” coatings on the artificial substrates, Fe_2O_3 appears to be a much better adsorber of metals because of its high concentrations after 3 months of accumulation being associated with maximum concentrations of all metals except for Ba. Pearson correlation coefficients were calculated between all of the elements in both Factors and MnO_2 and Fe_2O_3 (Table 4.5). The majority of the correlations are weak, with the only strong relationship being between Ba and MnO_2 , which was discussed earlier. Vanadium and Cr defined the strongest relationships with Fe_2O_3 , yet this was only slightly positive. Chromium was expected since it forms an anion in solution and is strongly adsorbed by the positive surface of Fe_2O_3 . Vanadium, which has a similar ionic radius as Cr, at 49.5-68 pm compared to 58 pm (Reimann and Caritat, 1998), and also forms HVO_4^{2-} anions that can be strongly sorbed by Fe_2O_3 (Rose *et al.*, 1979). These results indicate that Fe_2O_3

Table 4.5 Pearson's-R correlation coefficients calculated between elements in Factor 1 and Factor 2 of the artificial substrate PCFA and MnO_2 and Fe_2O_3 .

Element	MnO_2	Fe_2O_3
V	0.121	0.422
Cr	-0.021	0.43
Ni	0.369	-0.042
Cu	0.273	0.002
Zn	0.314	0.046
Sr	0.121	0.117
Y	0.129	0.19
Ba	0.819	-0.654
Ce	0.408	-0.155
Pb	0.366	0.08
Bi	0.161	0.236
Th	0.31	0.132
U	0.309	0.128

did not continue to adsorb all of these elements throughout the twelve month study period, therefore something unique was occurring after three months of coating accretion.

4.3.3 Mature *versus* Fresh Fe-Mn Oxide Coatings

Iron-manganese oxide coatings present on pebbles taken from the streambed are described as "mature" coatings, whereas coatings that accumulated on artificial substrates

are called “fresh.” After three months of coating accretion at site SJS1, concentrations from the “fresh” coatings were higher than the “mature” coatings for all elements except MnO_2 , Ce and Pb (Table 4.6). For the 6 and 9 month samples, more elements from the “mature” coatings had concentrations close to or greater than the “fresh” oxides. After 12 months of coating accretion, all of the elements except MnO_2 , Ba, and Ce had concentrations in the “mature” coatings greater than the “fresh” coatings, although the Ba and Ce “mature” concentrations were only slightly below the “fresh” concentrations. Similar trends were obtained for samples taken at the other sites.

Pearson correlation coefficients were calculated between element concentrations in the water samples and those in the “mature” and “fresh” Fe-Mn oxide coatings with the goal of discovering which coating best reflected water concentrations (Table 4.7). All of the elements except Fe had negative correlation coefficients for the “fresh” coatings. Fewer elements in the “mature” Fe-Mn oxide coatings had negative coefficients, and the relationships were low, whereas for the “fresh” coatings there were a lot of moderate negative relationships. Neither of the coatings appeared to represent stream analyte concentrations well, although the “mature” coatings may be considered slightly better.

4.3.4 Model for Fe-Mn Oxide Formation

The suggested process for metal accumulation is shown in Figure 4.31 (Robinson, 1981). Initial formation of Fe-Mn oxides on stream pebbles begins with precipitation of

Table 4.6 Element concentrations determined by LA-ICP-MS in Fe-Mn oxide coatings present on pebbles (PEB) collected from the streambed and artificial substrates (SUB) located at site SWS1 in Rennies River, St. John's, NL.

	PEB	SUB	PEB	SUB	PEB	SUB	PEB	SUB
Month	3	3	6	6	9	9	12	12
Element								
V(ppm)	184	1813	543	566	243	495	1269	460
Cr(ppm)	185	5760	380	4106	28.9	445	2248	284
MnO ₂ (wt%)	73.3	17.3	66.1	68.4	68.5	74.3	41.4	63.5
Fe ₂ O ₃ (wt%)	20.5	74.4	28.0	23.4	26.0	22.6	54.5	33.7
Ni(ppm)	790	2685	857	3641	539	612	1811	291
Cu(ppm)	2585	15398	2394	10700	1539	3844	7103	1431
Zn(ppm)	20098	20506	18931	32788	15130	6196	5886	5327
Sr(ppm)	190	3231	1505	1175	173	326	496	166
Y(ppm)	471	1159	708	1163	574	434	547	367
Ba(ppm)	6515	19023	13100	14593	10090	12945	8781	10173
Ce(ppm)	2578	2034	1859	1109	1659	893	1231	1308
Pb(ppm)	8479	1891	4703	1895	6864	441	1434	712
Bi(ppm)	2.30	6.64	1.21	4.85	1.18	1.33	1.43	0.40
Th(ppm)	13.3	123	24.8	37.3	15.9	17.4	37.4	6.9
U(ppm)	5.39	43.1	12.6	58.7	6.40	18.0	13.7	8.26

the Fe₂O₃ and MnO₂ phases, metals are precipitated along with this in a coprecipitation process (Jackson, 1998). Metals will initially coprecipitate with just Fe₂O₃ because there is no MnO₂ present since it requires Fe₂O₃ nucleation sites. As the Fe-Mn oxides are precipitated, they begin adsorbing metals from solution. Initially, adsorption accounts for only a small amount of the metals present on the Fe-Mn oxide coating. As the coatings

Table 4.7 Pearson-R correlation coefficients between analyte water and Fe-Mn oxide coating concentrations for samples taken from all sites in Rennies River.

Element	Mature Coating	Fresh Coating
V	0.032	-0.195
Cr	0.637	-0.583
Mn	-0.627	-0.507
Fe	0.756	0.434
Ni	0.037	-0.063
Cu	-0.566	-0.603
Zn	-0.118	-0.426
Sr	-0.492	-0.508
Y	NA	NA
Ba	-0.572	-0.732
Ce	-0.181	-0.342
Pb	-0.402	-0.739
Bi	-0.026	-0.269
Th	NA	NA
U	0.037	-0.334

age, adsorption rates increase, thus leading to a more rapid increase in metal accumulation. Adsorption also increases in rate as the concentration of the given analyte increases in the stream (Robinson, 1981). This is especially important when looking at differences between polluted and “pristine” sites. In summary, the total metal accumulation for Fe-Mn oxide coatings is a result of coprecipitation and adsorption.

4.3.5 Metal Accumulation at Rennies River

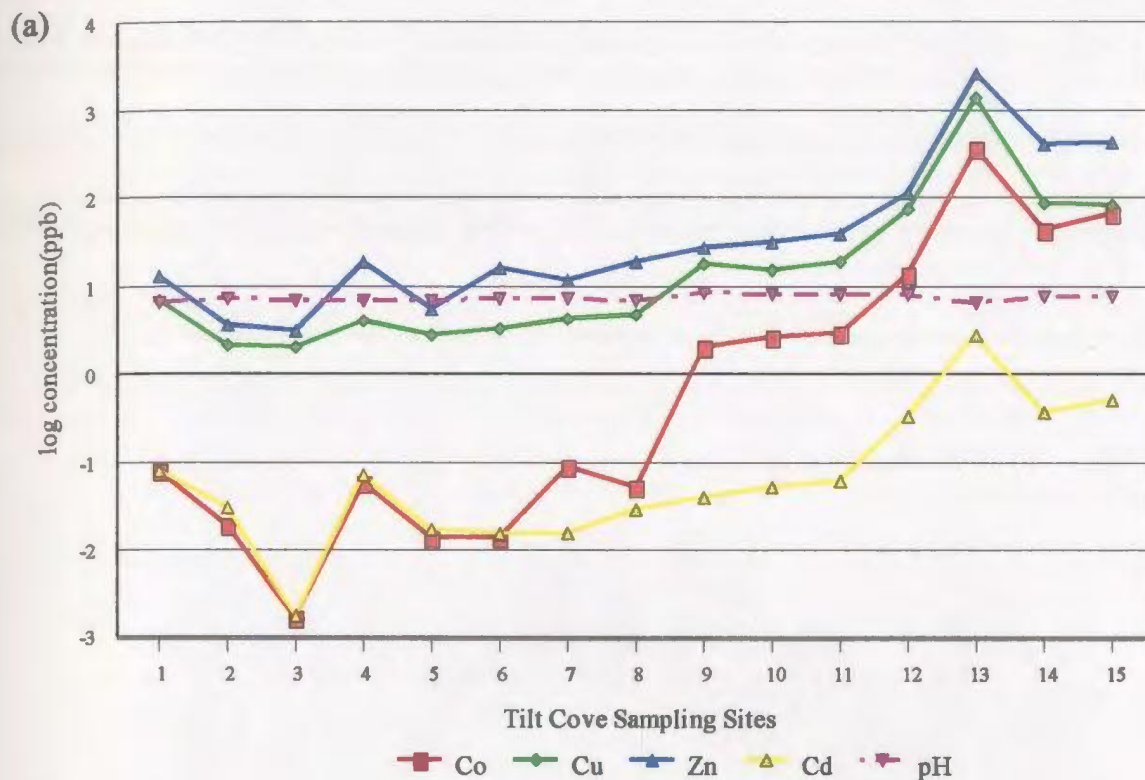
The model for metal accumulation that accounts for the concentration trends for the artificial substrates placed in Rennies River starts with the precipitation of mostly Fe_2O_3 at all sites for the first three months of coating accretion. The process of coprecipitation occurs during Fe_2O_3 precipitation producing elevated concentrations of elements. Based on Figure 4.31, and Robinson's (1981) model of metal accumulation, adsorption probably occurs only to a limited extent after 3 months of coating accretion.

The next part of the metal accumulation process begins with the precipitation of a MnO_2 phase, which should be favoured on a fresh Fe_2O_3 surface. This occurs for the samples taken after 6 months of coating accretion (Group 3, Figure 3.14). The evidence for the occurrence of this step is increased amounts of MnO_2 from 3 to 6 months. From 3 to 6 months, the mass of Fe-Mn oxide coating increases, its colour changes from a light brown staining (Figure 4.30), indicating the elevated amounts of Fe_2O_3 , to a darker colour due to higher amounts of MnO_2 . Elements also coprecipitate with the MnO_2 , but they do so to a lesser extent because all metal concentrations decrease, except for Ba, after 6 months of coating accretion. Barium has the largest ionic radius for all elements in both Factors, and it is possible that Ba is too large to fit into the coprecipitated structure of Fe_2O_3 , but is able to fit into the MnO_2 structure. The actual mass of Fe-Mn oxide increases with time, but the ratio of metal to oxide coating decreases because lower quantities of metals are being coprecipitated with both oxides instead of only Fe_2O_3 ,

MnO₂ thus slows the coprecipitation of metals. This decrease in the rate of coprecipitated metal accumulation in the period from 3 to 6 months produces lower Fe-Mn oxide calculated concentrations, but the opposite occurs for Ba. These low concentrations indicate that adsorption is also at a minimum at this time.

The process of Fe₂O₃ and MnO₂ coprecipitation occurs for the 9 and 12 month samples also (Group 4, Figure 3.14), as there are no major increases in coating concentrations and the coatings appear larger and darker in colour. Some of the coating concentrations increase for the 12 month samples, thus adsorption may be occurring at higher rates for these samples.

In summary, on a clean artificial substrate, coating accretion for the first 3 months constitutes Fe₂O₃ precipitation with coprecipitation of various metals. This first stage provides a surface upon which MnO₂ is able to precipitate for the next 3 months, accompanied by concentrations of metals which decrease because of the lower coprecipitation rates in the MnO₂ phase. This process continues until adsorption may cause an increase in metal concentrations after 1 year of coating accretion.



(b)



Figure 4.1(a) Plot of log concentration (ppb) of Co, Cu, Zn, and Cd, and pH values in water samples from the Tilt Cove sampling sites; (b) photograph of the Tilt Cove study area outlining sampling sites.

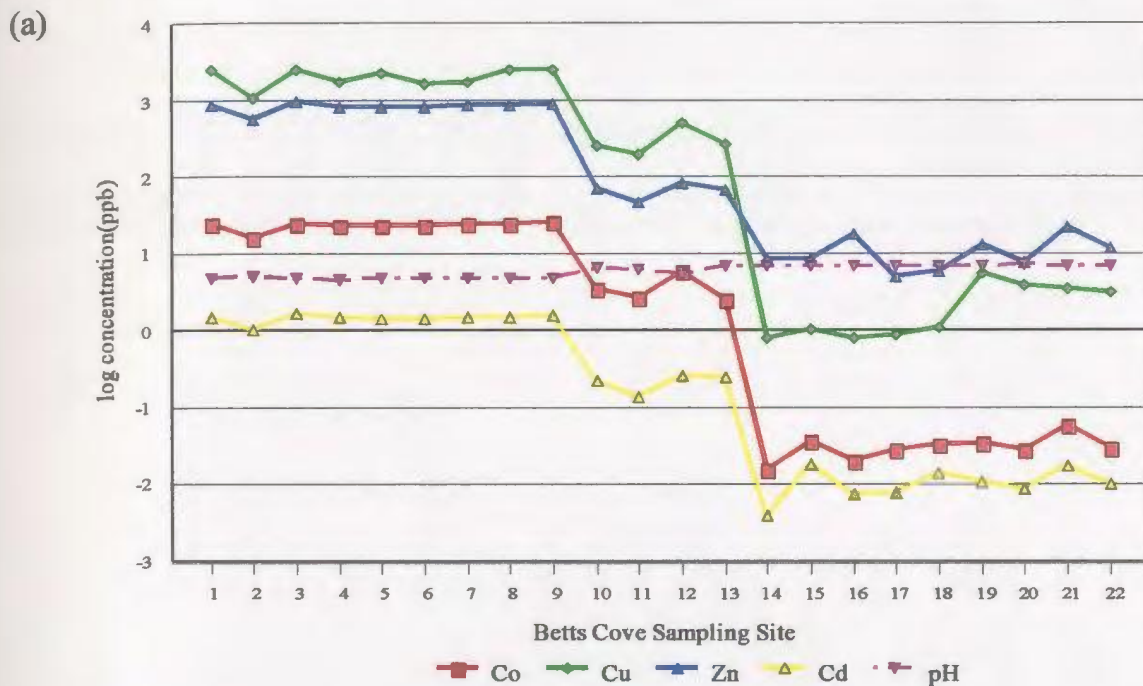


Figure 4.2(a) Plot of log concentration (ppb) of Co, Cu, Zn, and Cd, and pH values of water samples from the Betts Cove sampling sites; (b) photograph of the Betts Cove polluted study area outlining the polluted sampling sites.

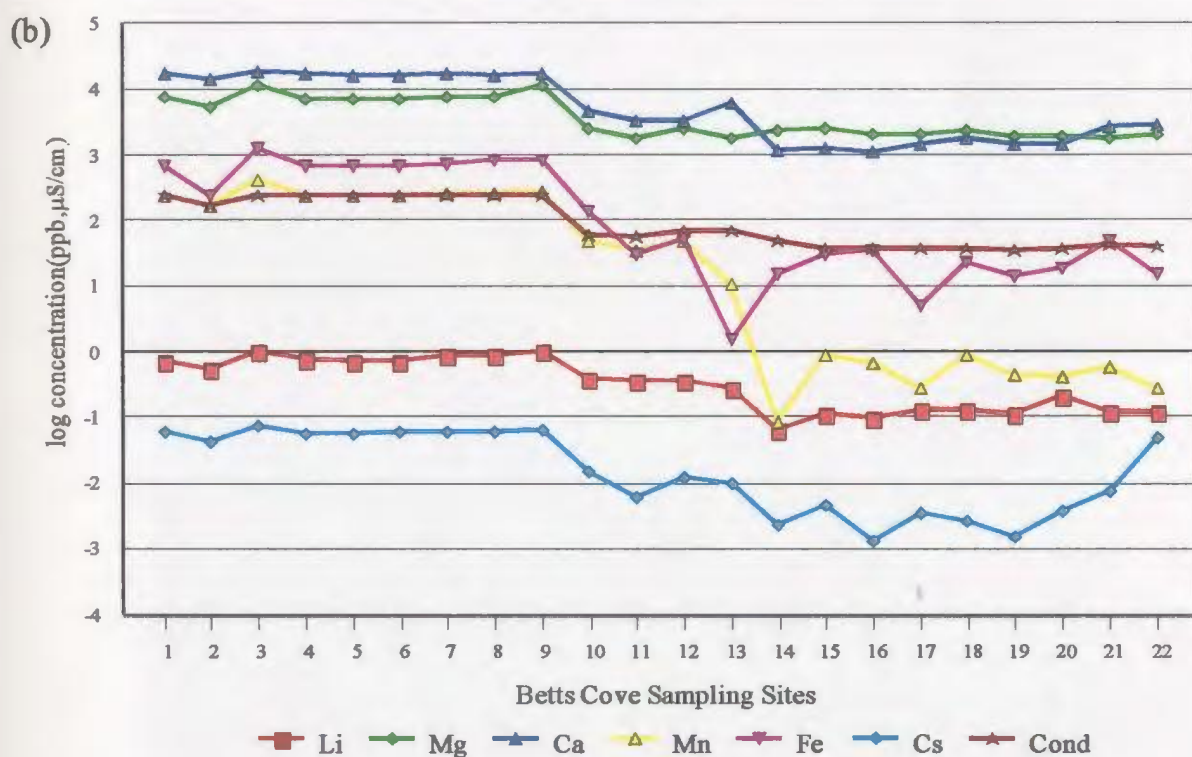
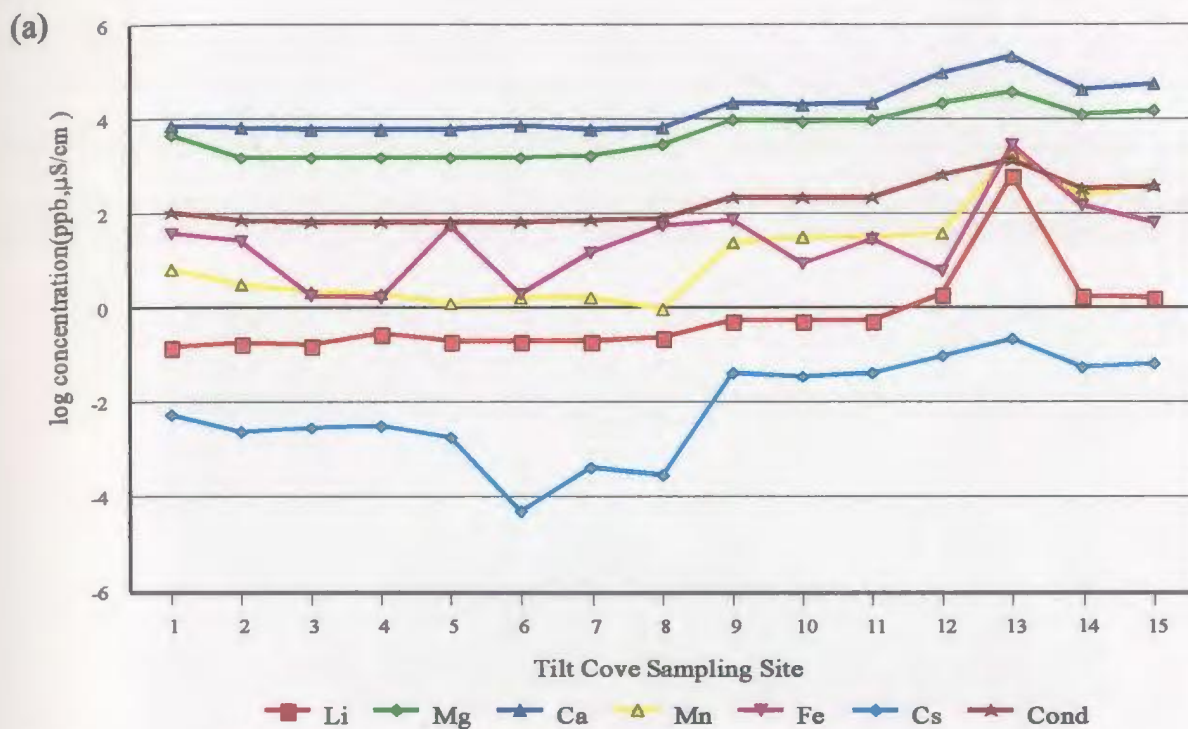


Figure 4.3 Plot of log concentration (ppb) of Li, Mg, Ca, Mn, Fe, and Cs, and conductivity ($\mu\text{S/cm}$) for water samples from the (a) Tilt Cove and (b) Betts Cove study areas.

(a)



(b)



Figure 4.4(a) Sampling site SJWS1 located in Nagles Hill Brook, and (b) site SJWS6B at the outlet of Kelly's Brook.

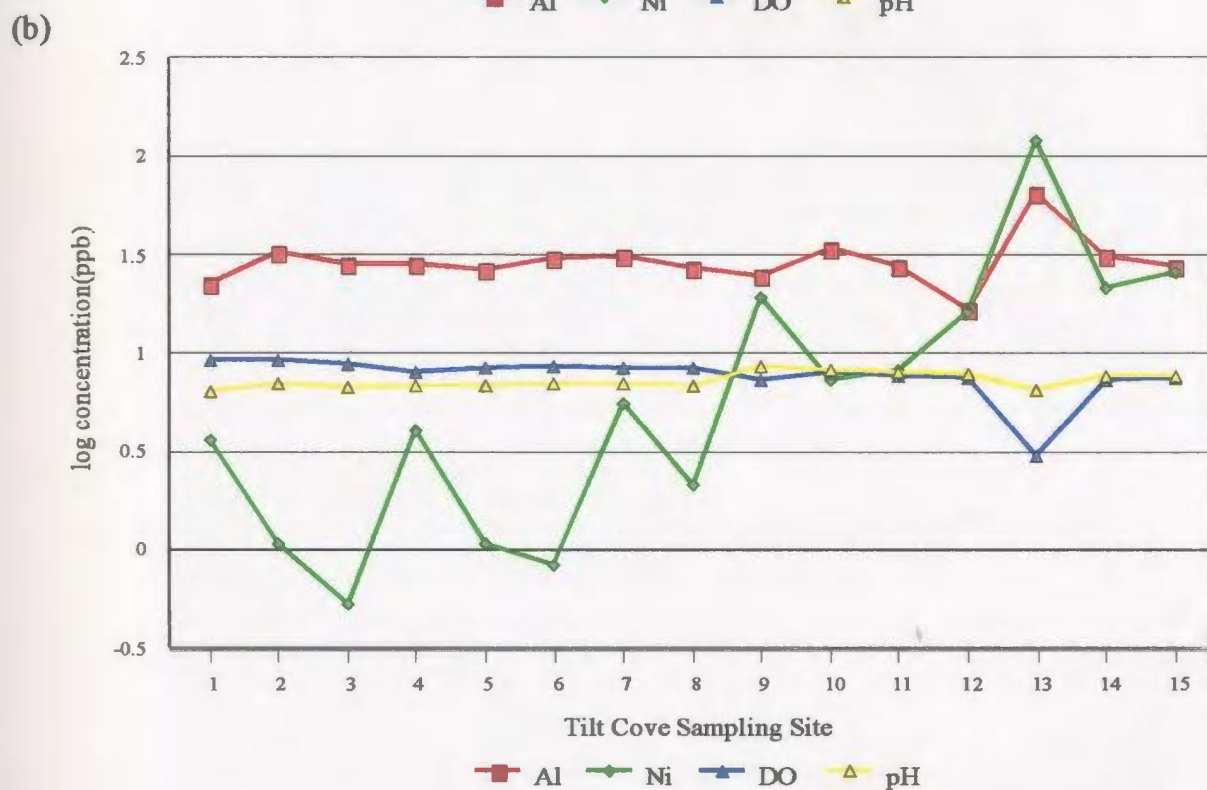
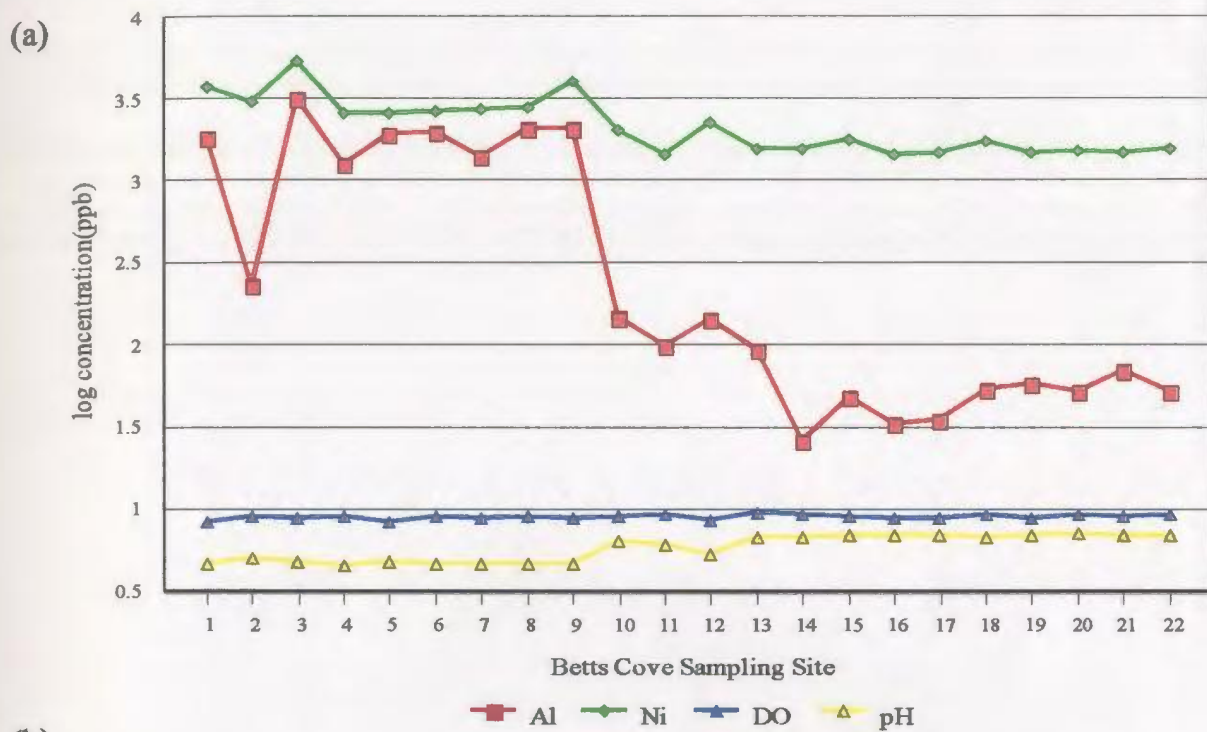


Figure 4.5 Plot of log concentration (ppb) of Al and Ni, pH and dissolved oxygen (mg/L) readings for the (a) Betts Cove and (b) Tilt Cove study areas.

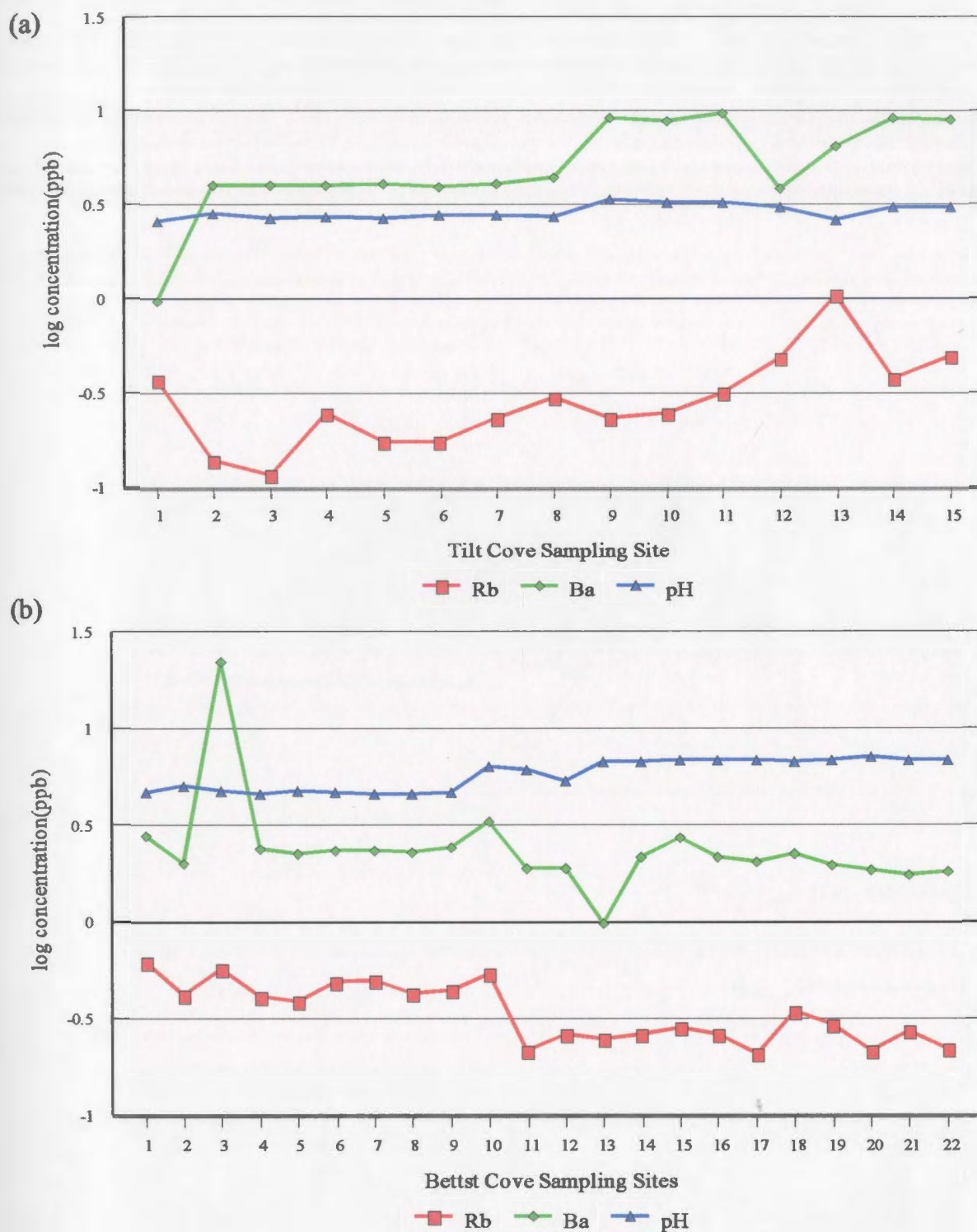


Figure 4.6 Plot of log concentration (ppb) of Rb and Ba, and pH readings for water samples from the (a) Tilt Cove and (b) Betts Cove study areas.

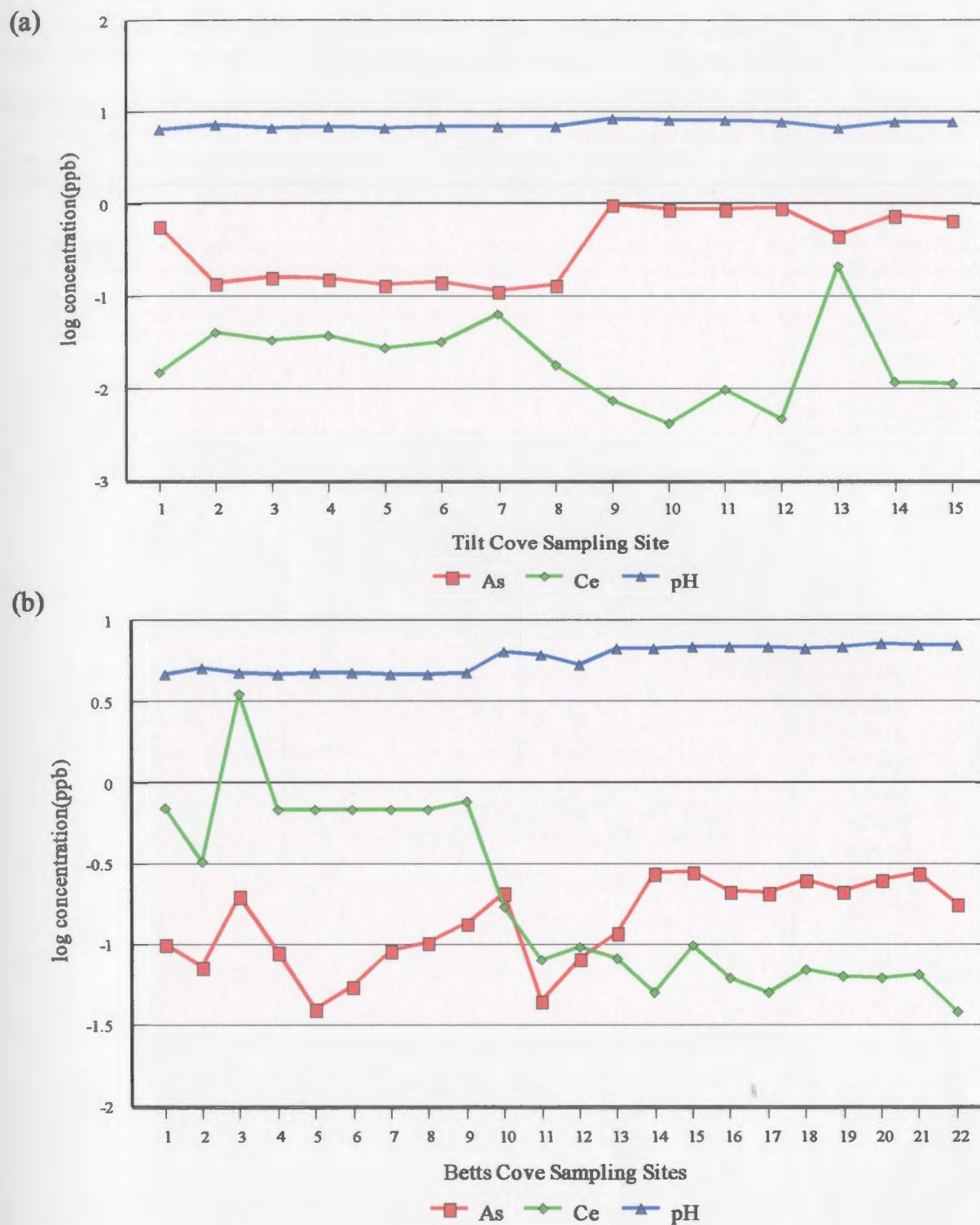


Figure 4.7 Plot of log concentration (ppb) of As and Ce, and pH readings for water samples from the (a) Tilt Cove (b) Betts Cove study areas.

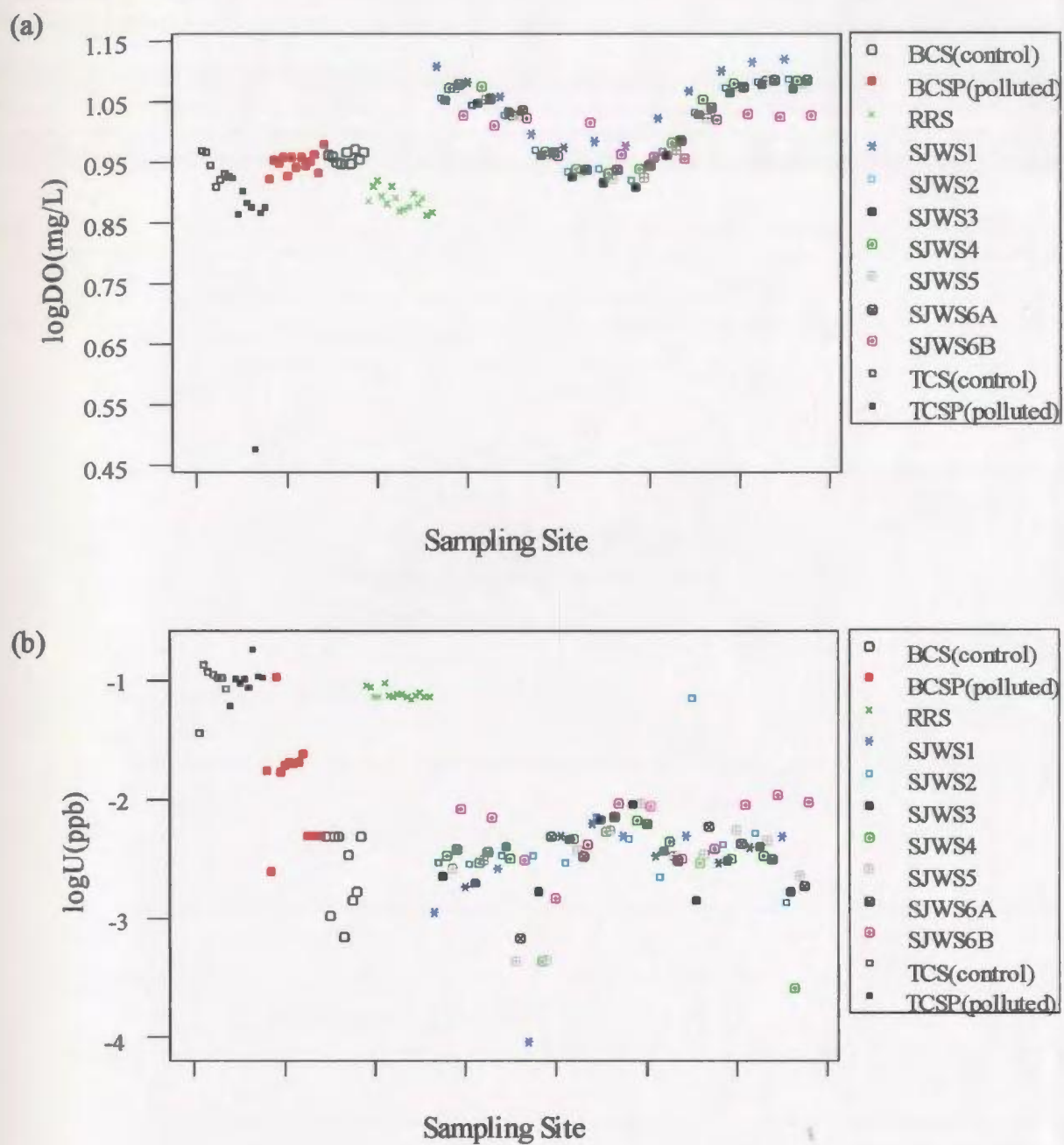


Figure 4.8 Plot of (a) log dissolved oxygen (mg/l) values and (b) log U (ppb) in water samples vs. sampling site for all study areas.

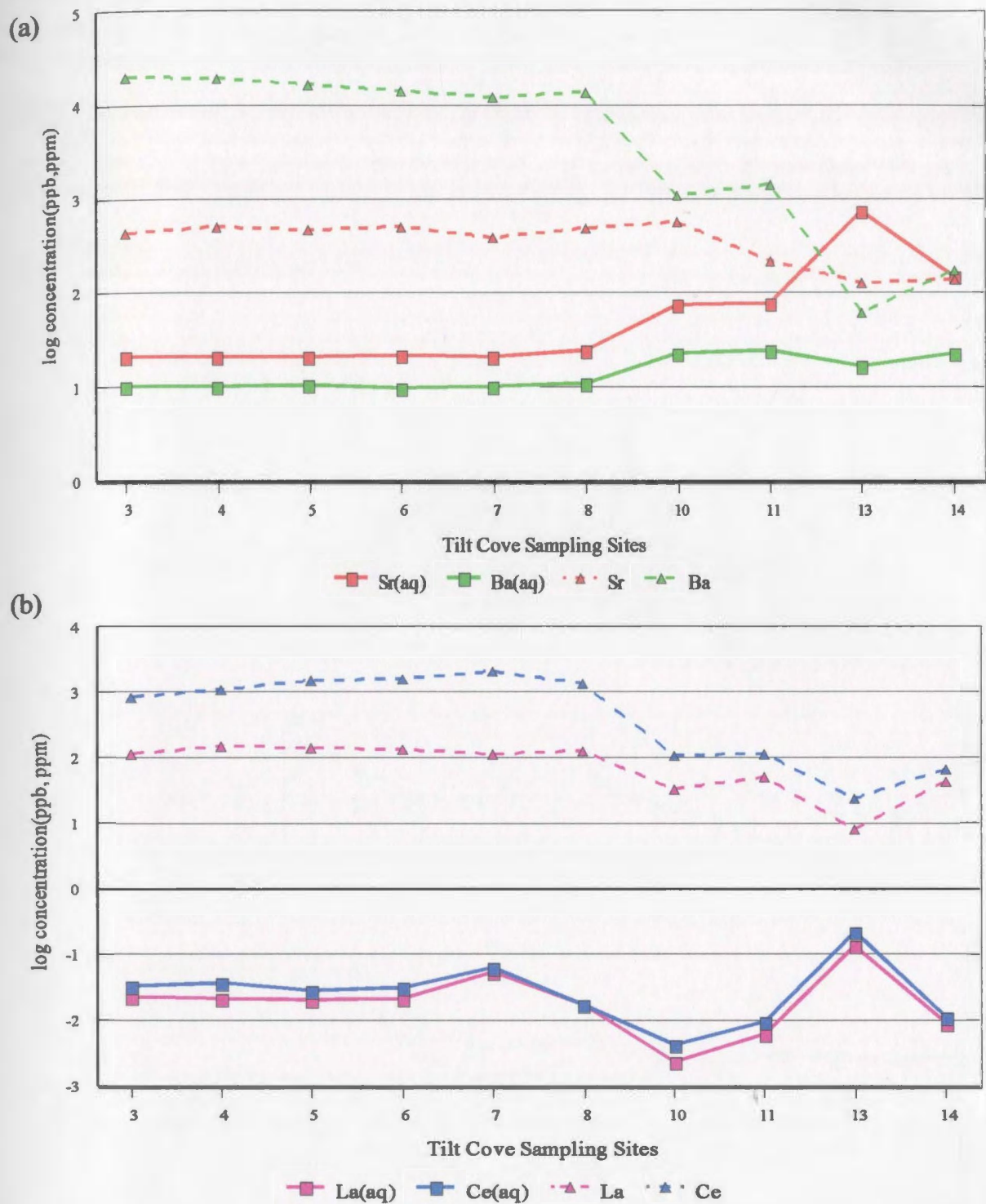


Figure 4.9 Plot of log transformed concentrations from water samples (ppb, solid line) and Fe-Mn oxide coatings (ppm, dashed line) for (a) Sr and Ba and (b) La and Ce from the Tilt Cove study area.

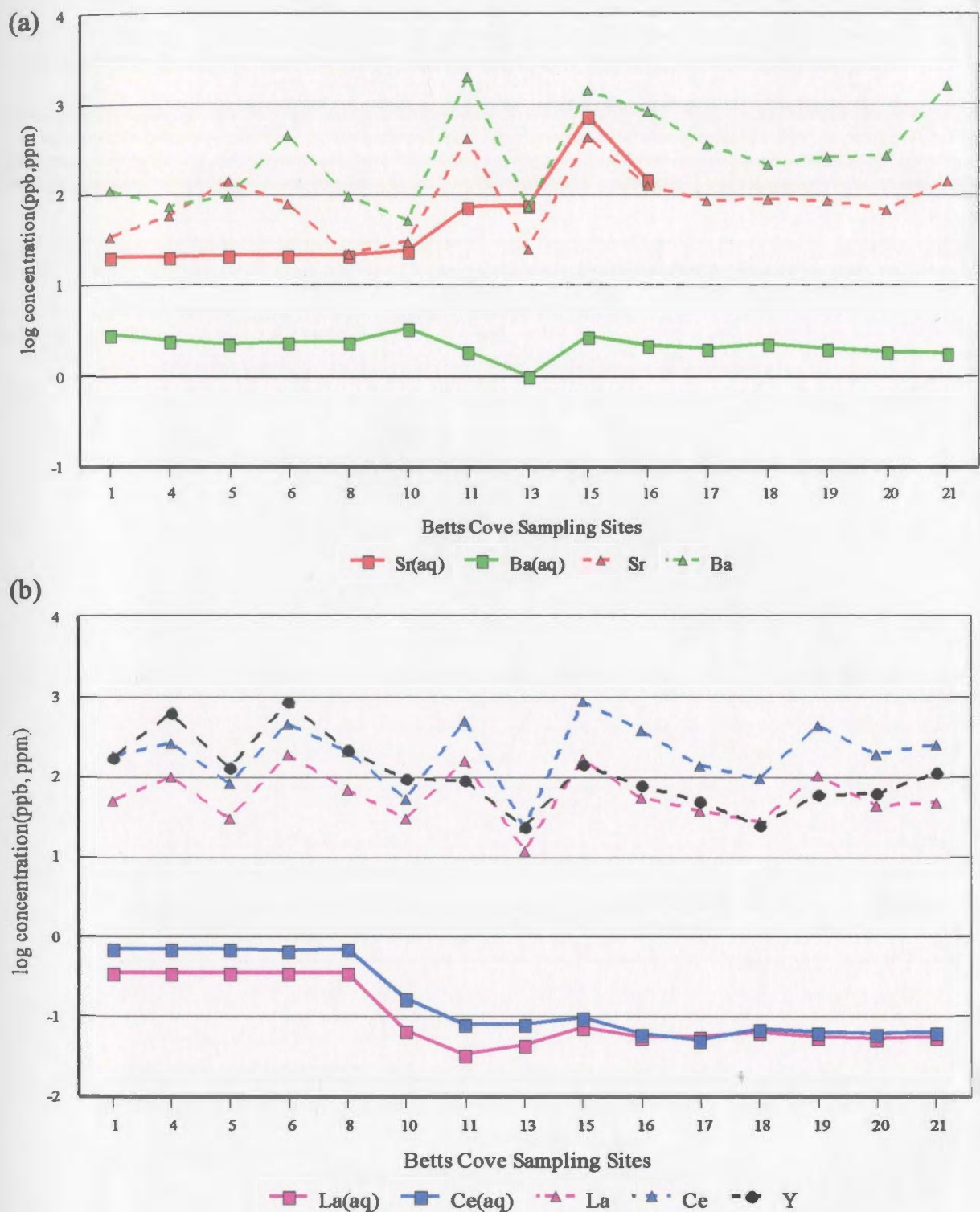


Figure 4.10 Plot of log transformed concentrations from water samples (ppb, solid line) and Fe-Mn oxide coatings (ppm, dashed line) for (a) Sr and Ba and (b) La, Ce, and Y from the Betts Cove study area.

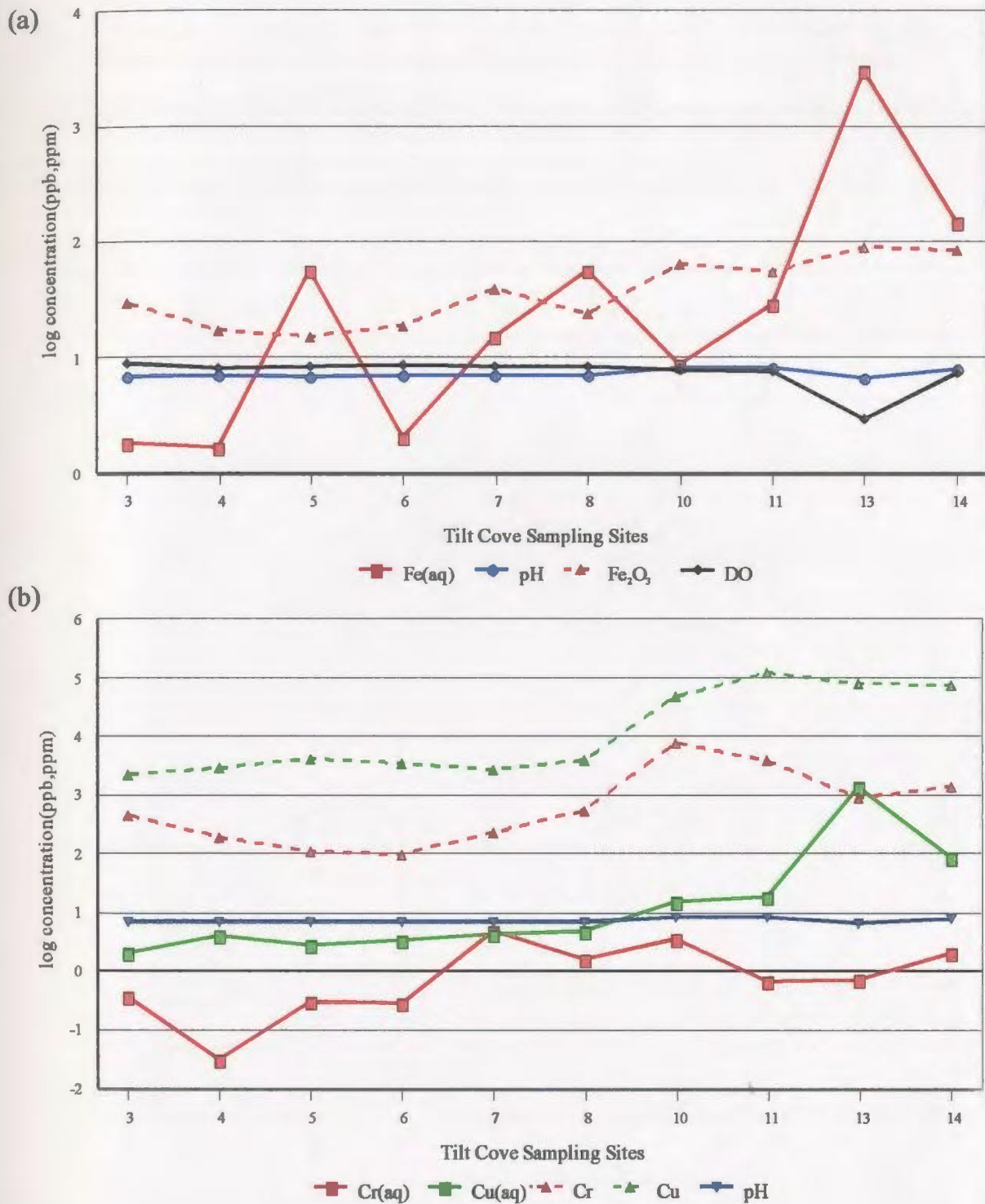


Figure 4.11 Plot of log transformed concentrations from water samples (ppb, solid line) and Fe-Mn oxide coatings (ppm, dashed line) for (a) iron along with pH and dissolved oxygen readings (mg/L) and (b) chromium, copper, and pH(mg/L) for the Tilt Cove study area.

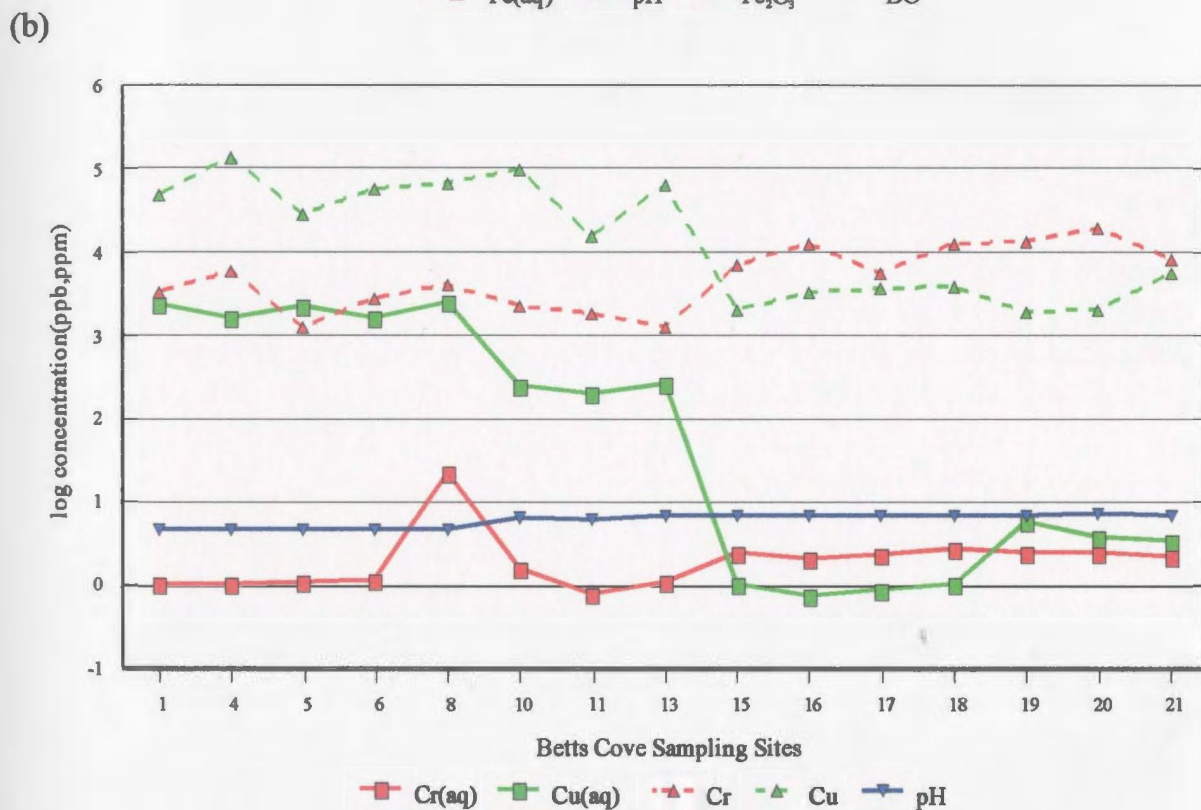
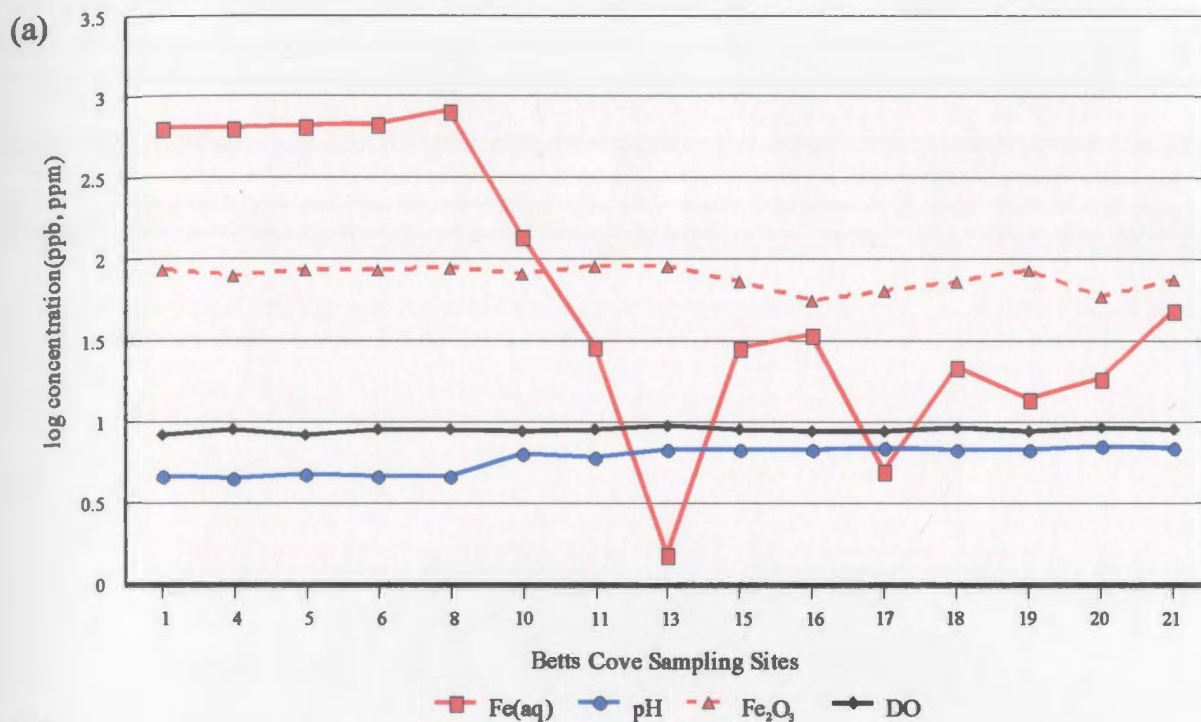


Figure 4.12 Plot of log transformed concentrations from water samples (ppb, solid line) and Fe-Mn oxide coatings (ppm, dashed line) for (a) iron, pH, and dissolved oxygen (mg/L), and (b) chromium, copper, and pH levels from Betts Cove.

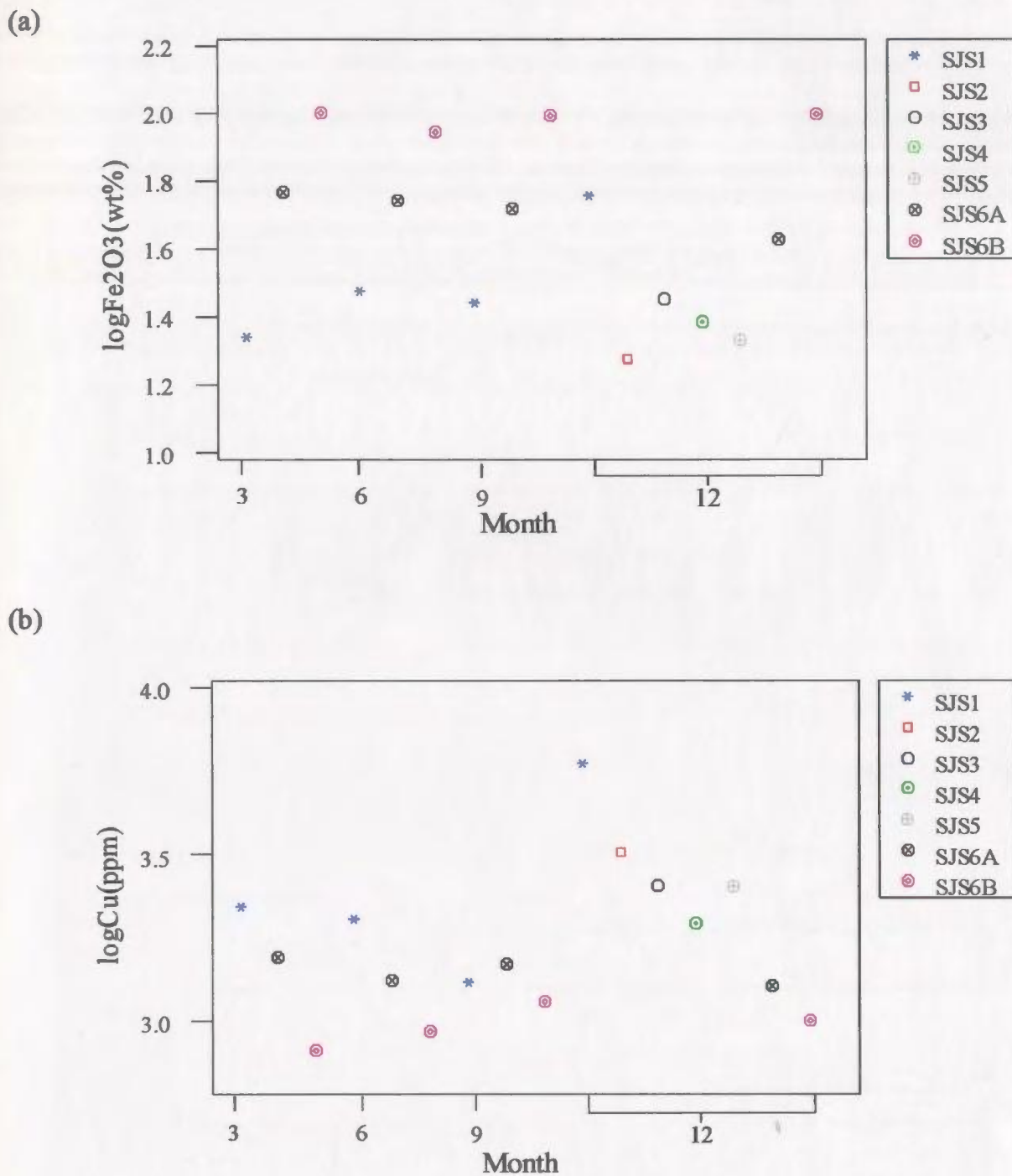


Figure 4.13 Plot of log transformed concentrations of (a) Fe₂O₃ (wt%) and (b) Cu (ppm) on Fe-Mn oxide coatings present on stream pebbles collected from Rennies River at three month intervals from March 2002 to March 2003.

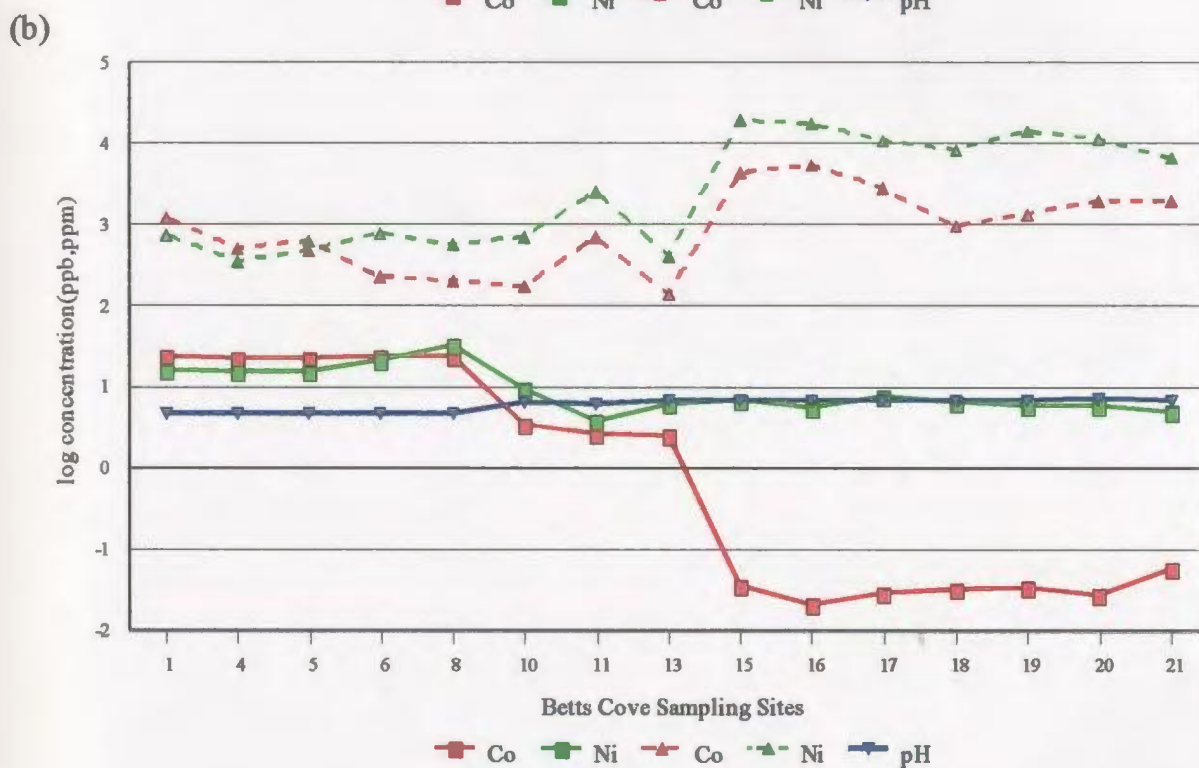
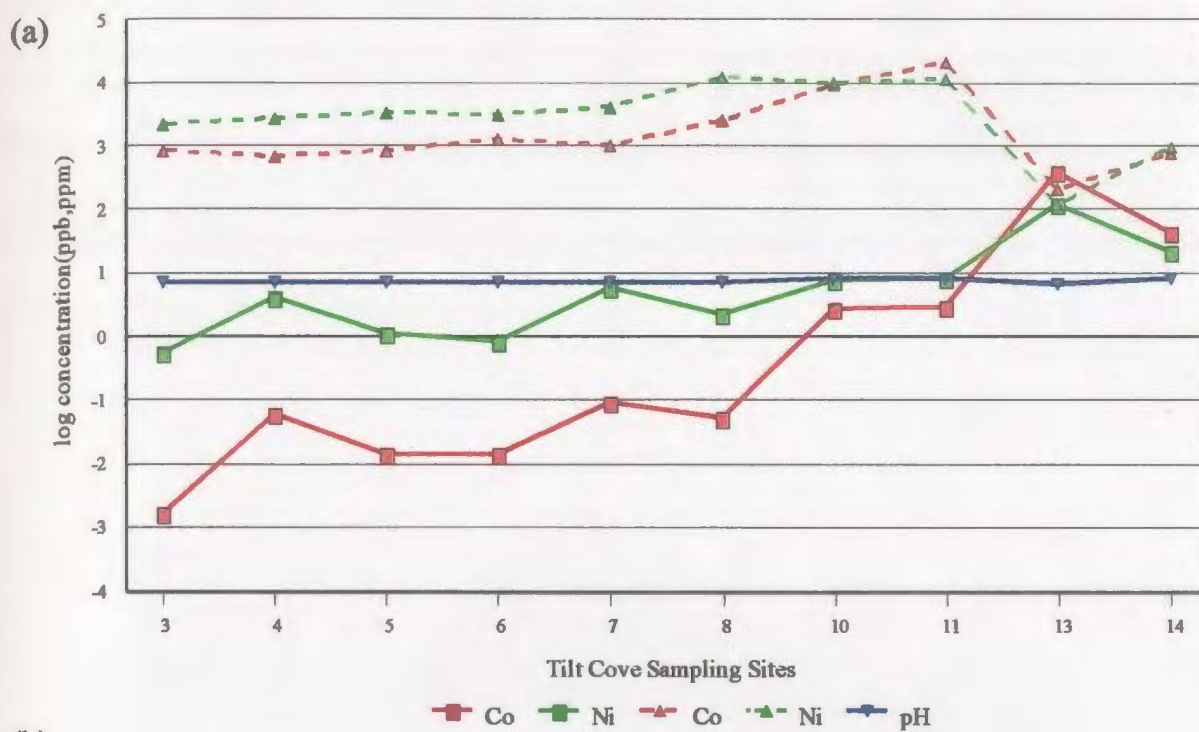


Figure 4.14 Plot of log transformed concentrations from water samples (ppb, solid line) and Fe-Mn oxide coatings (ppm, dashed line) for Co, Ni, and pH levels from (a) Tilt Cove, and (b) Betts Cove.

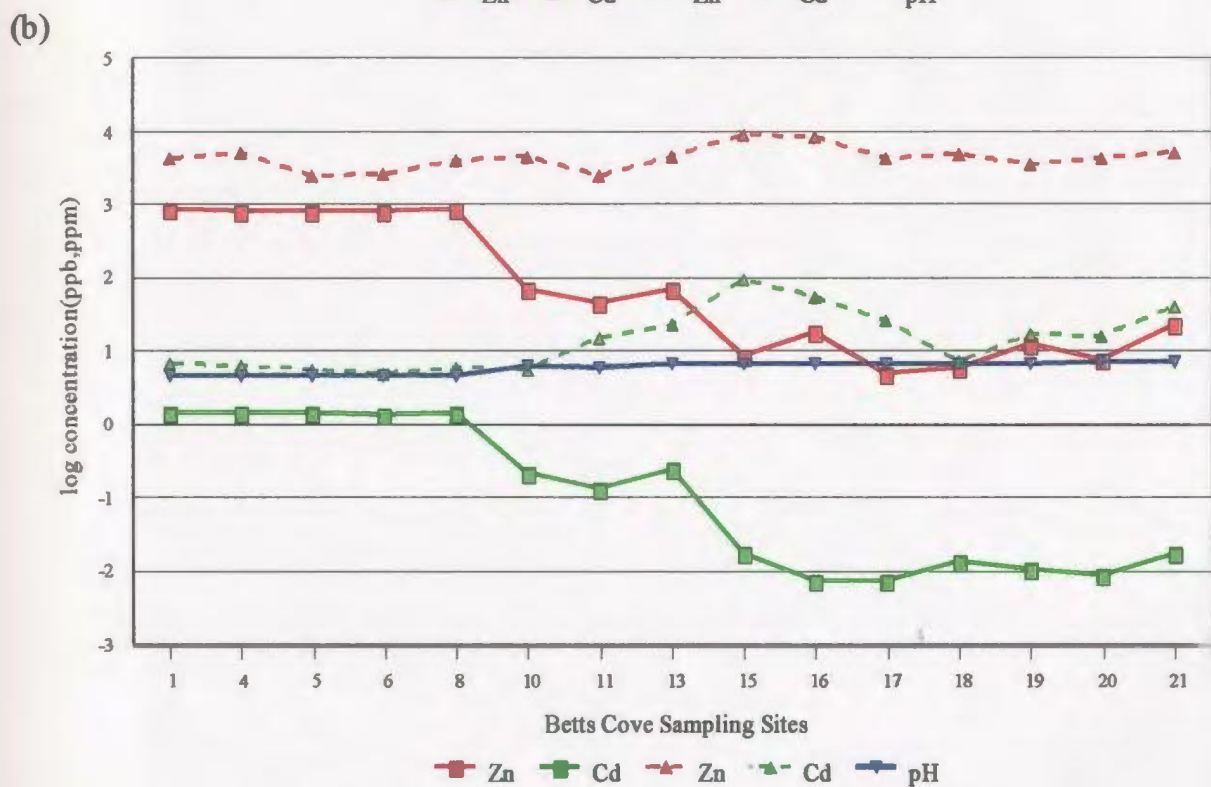
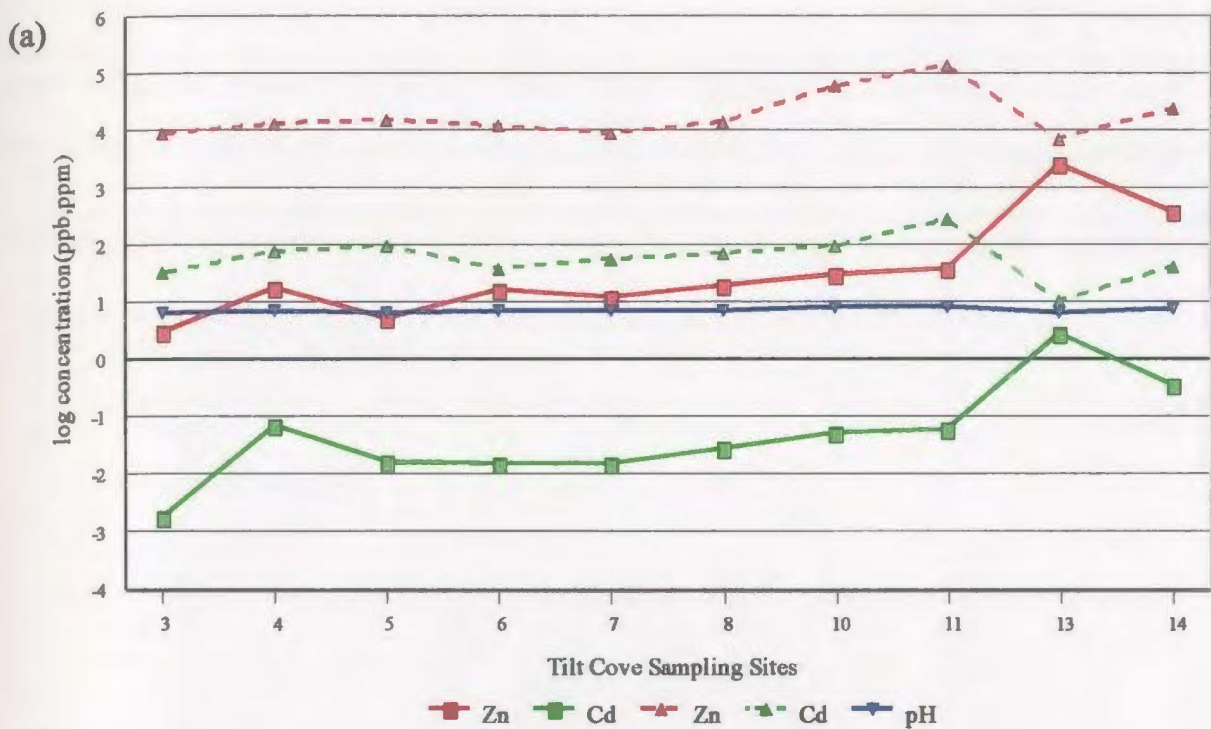


Figure 4.15 Plot of log transformed concentrations from water samples (ppb, solid line) and Fe-Mn oxide coatings (ppm, dashed line) for Zn, Cd, and pH levels from (a) Tilt Cove, and (b) Betts Cove.

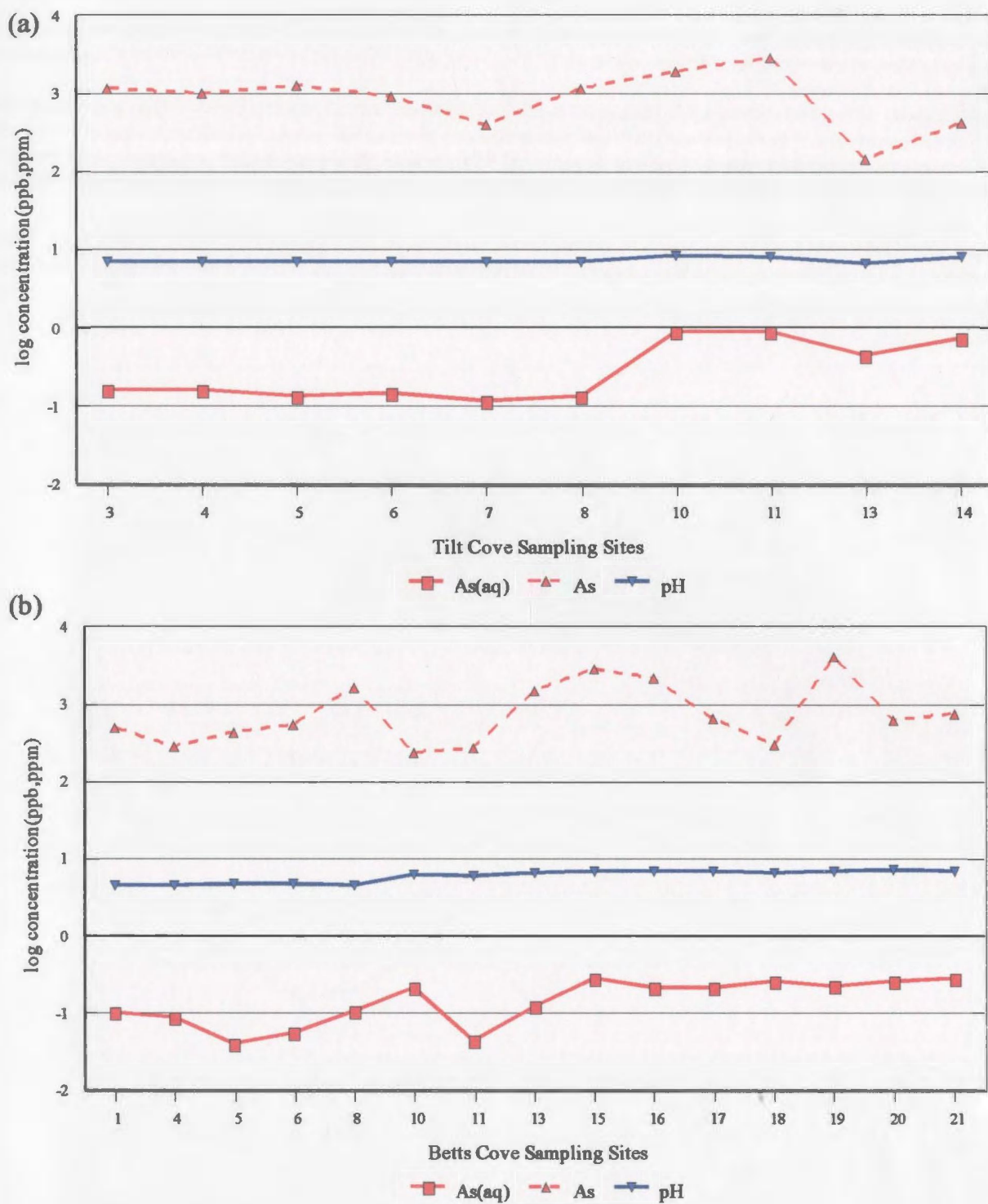


Figure 4.16 Plot of log transformed concentrations from water samples (ppb, solid line) and Fe-Mn oxide coatings (ppm, dashed line) for As and pH levels from (a) Tilt Cove, and (b) Betts Cove.

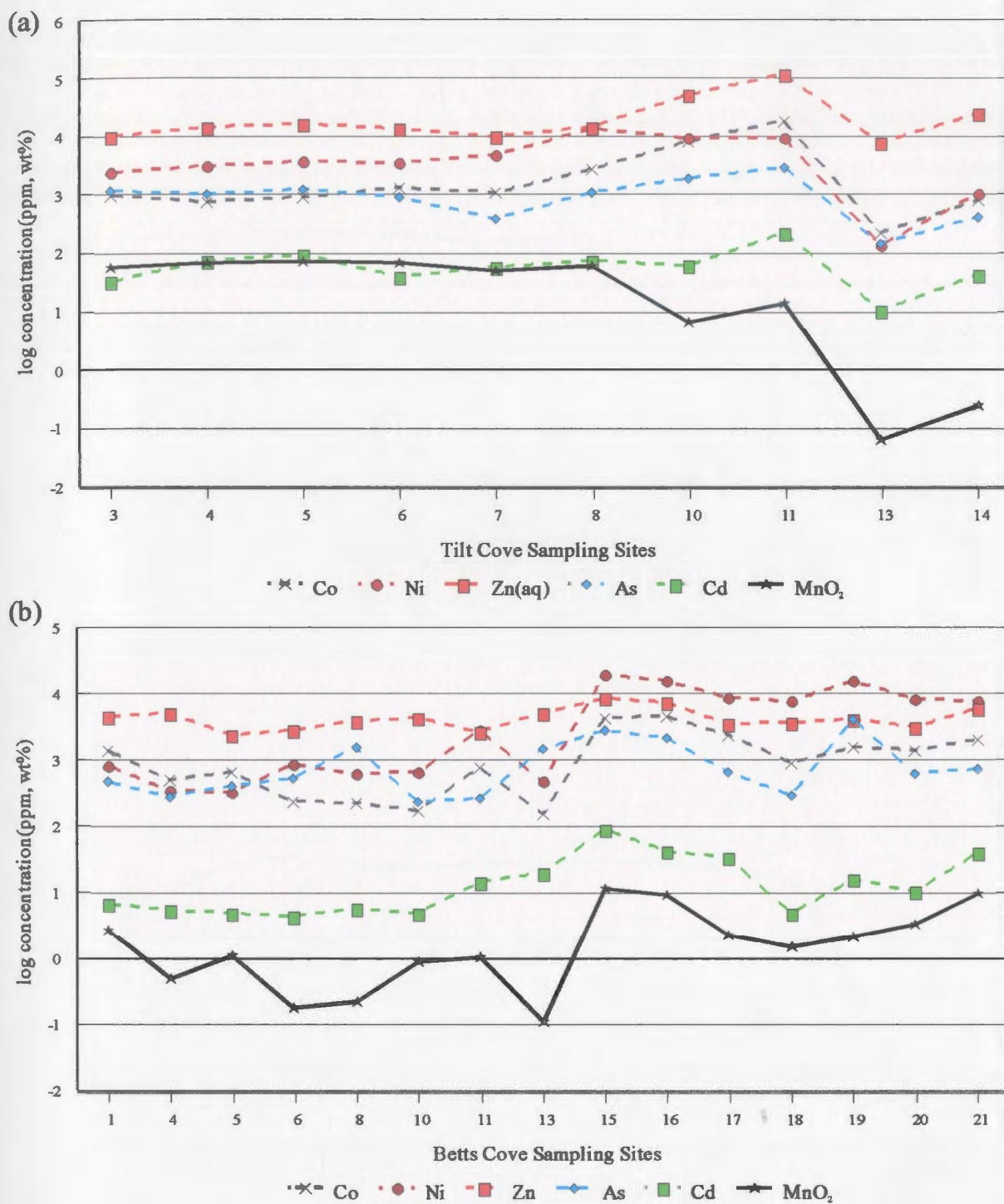


Figure 4.17 Plot of log transformed concentrations of Co, Ni, Zn, As, Cd (ppm), and MnO₂ (wt%) in Fe-Mn oxide coatings from (a) Tilt Cove and (b) Betts Cove.

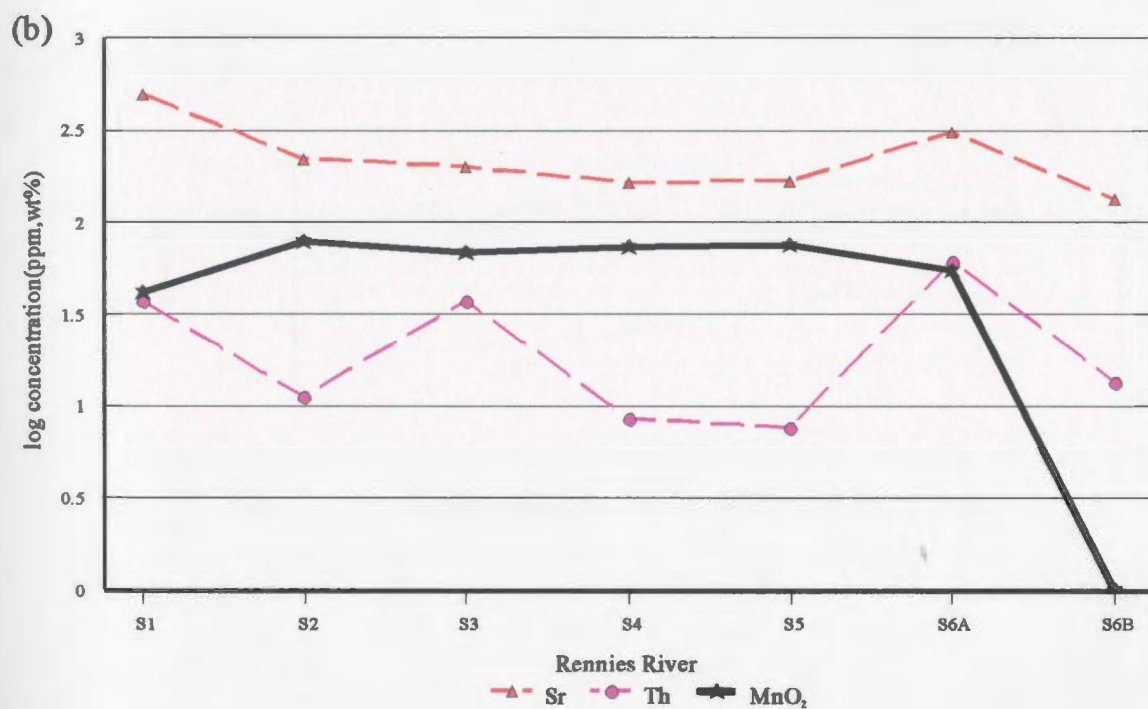
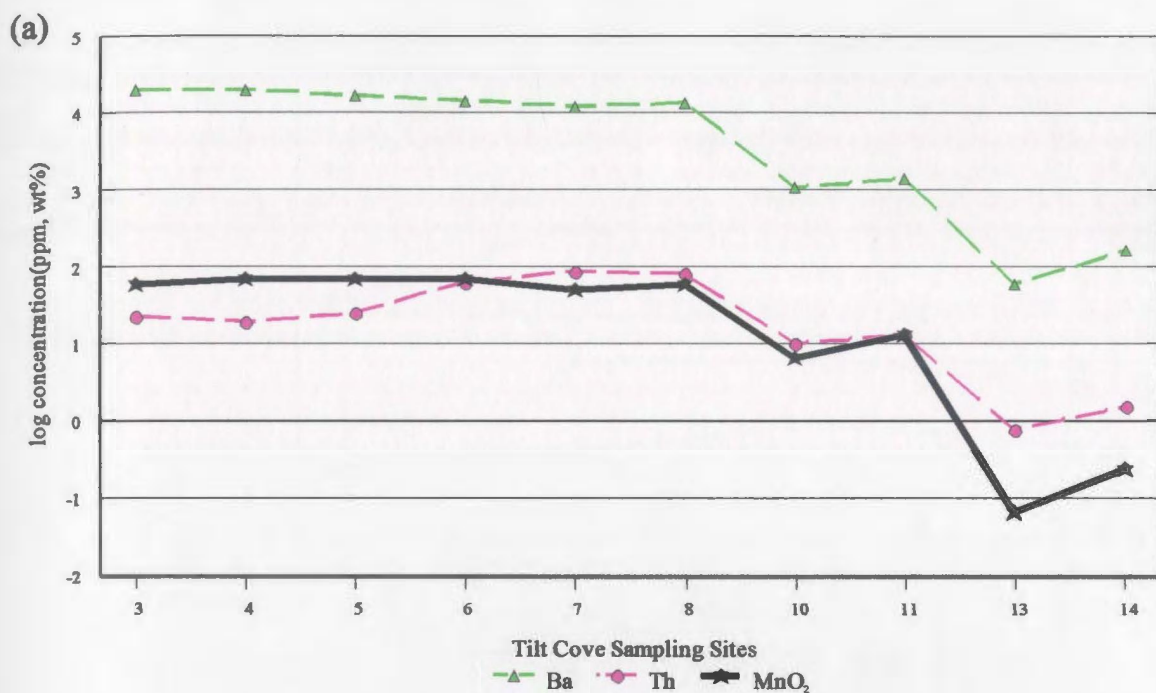


Figure 4.18 Plot of log transformed concentrations from Fe-Mn oxide coating samples (a) Ba, Th (ppm), and MnO₂ (wt%) from Tilt Cove and (b) Sr, Th (ppm), and MnO₂ (wt%) from Rennies River.

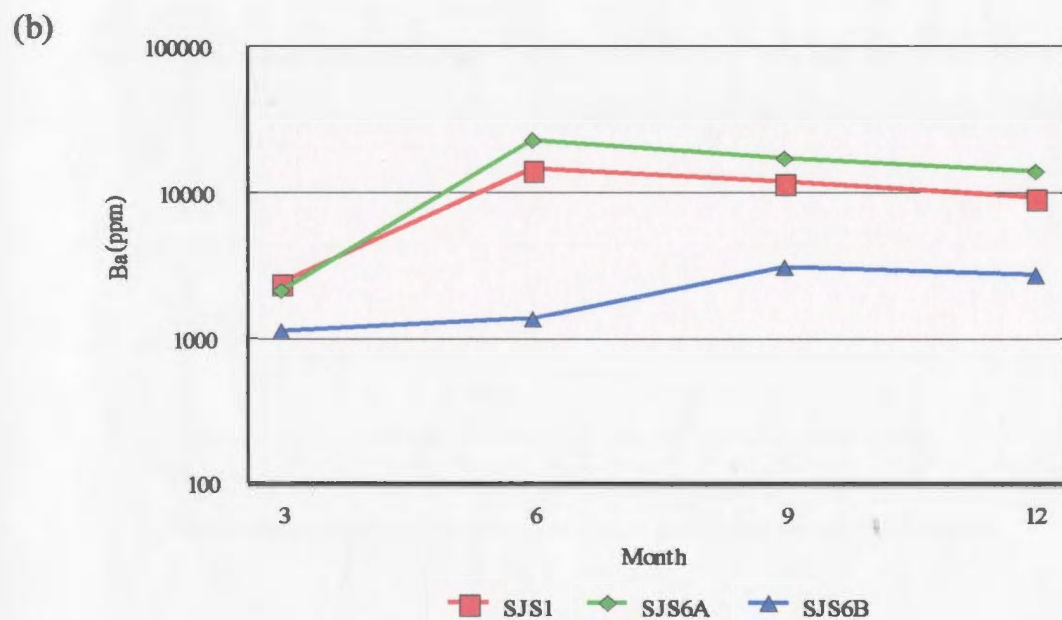
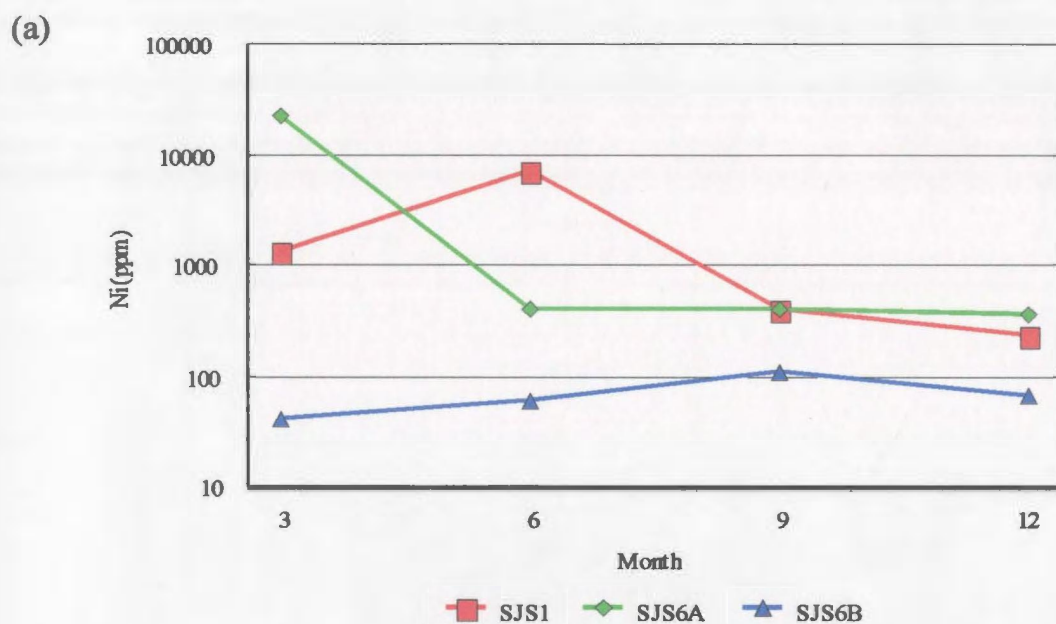
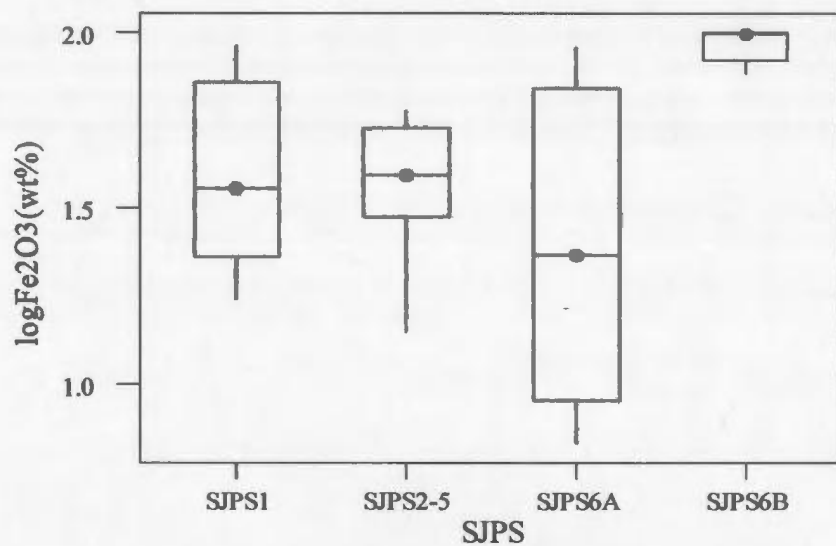


Figure 4.19(a) Plot of Ni(ppm) and (b) Ba(ppm) concentrations for Fe-Mn oxide coatings on artificial substrates taken from Rennies River from March 2002 to March 2003 at three month intervals.

(a)



(b)

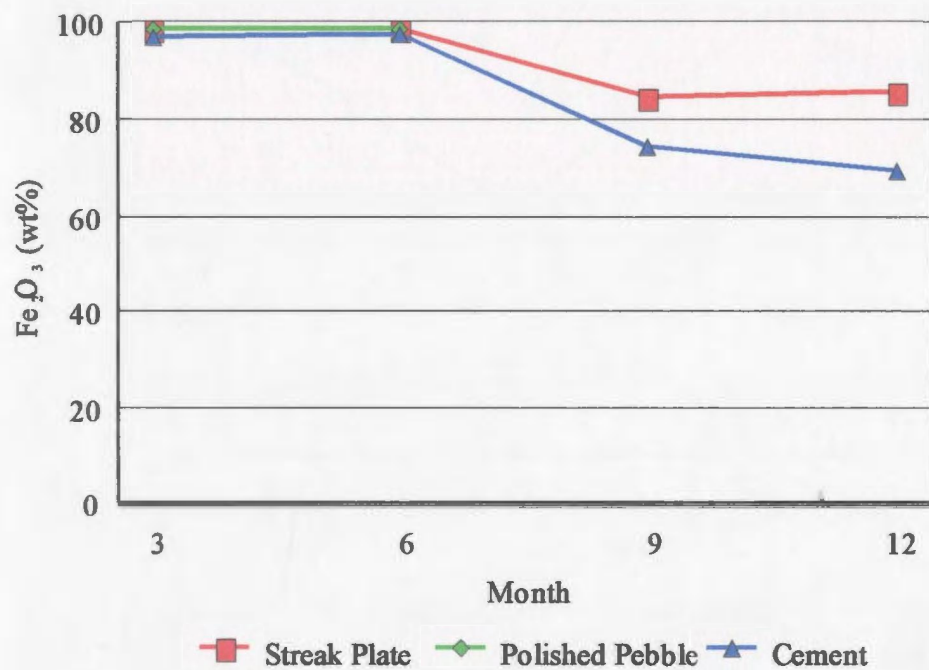
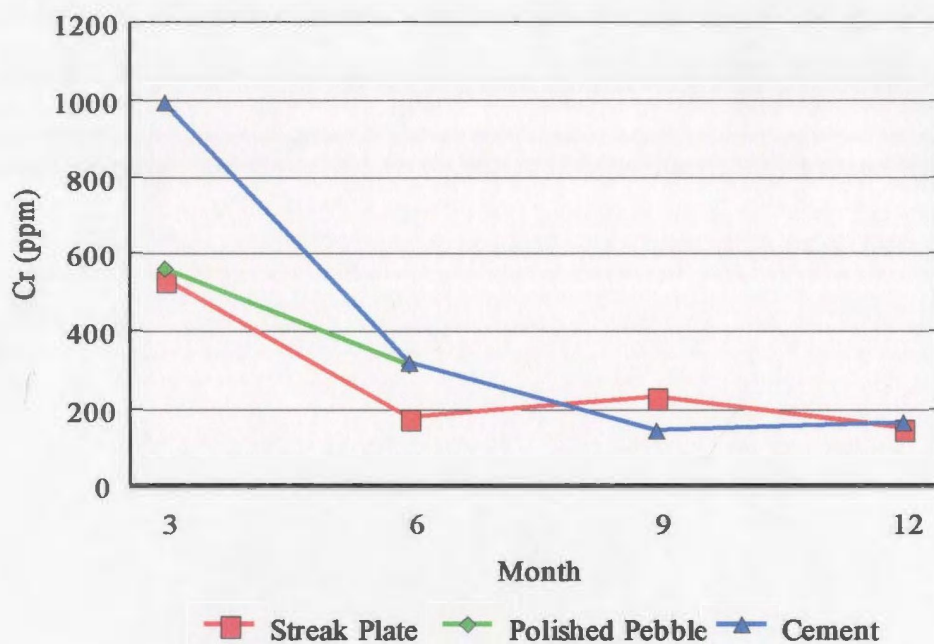


Figure 4.20(a) Boxplot of Fe_2O_3 concentrations (wt%) for Fe-Mn oxide coatings on artificial substrates, (b) Plot of Fe_2O_3 concentrations (wt%) for samples taken from SJPS6B vs. time.

(a)



(b)

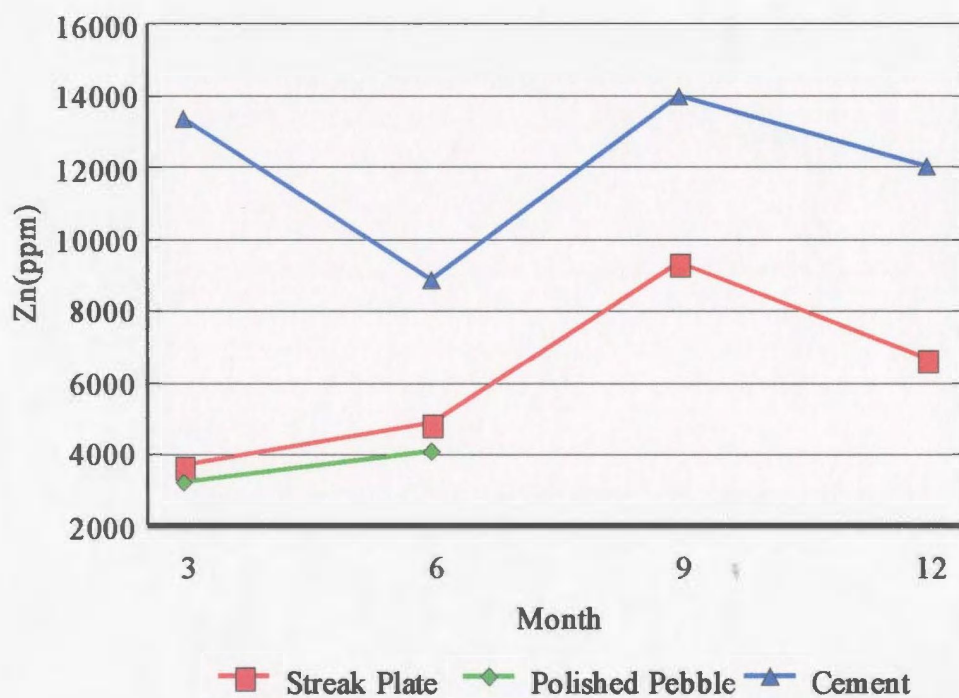


Figure 4.21(a) Plot of Cr concentrations (ppm) and (b) plot of Zn concentrations (ppm) for Fe-Mn oxide coatings on artificial substrates taken from SJPS6B at three month intervals over a 12 month period.

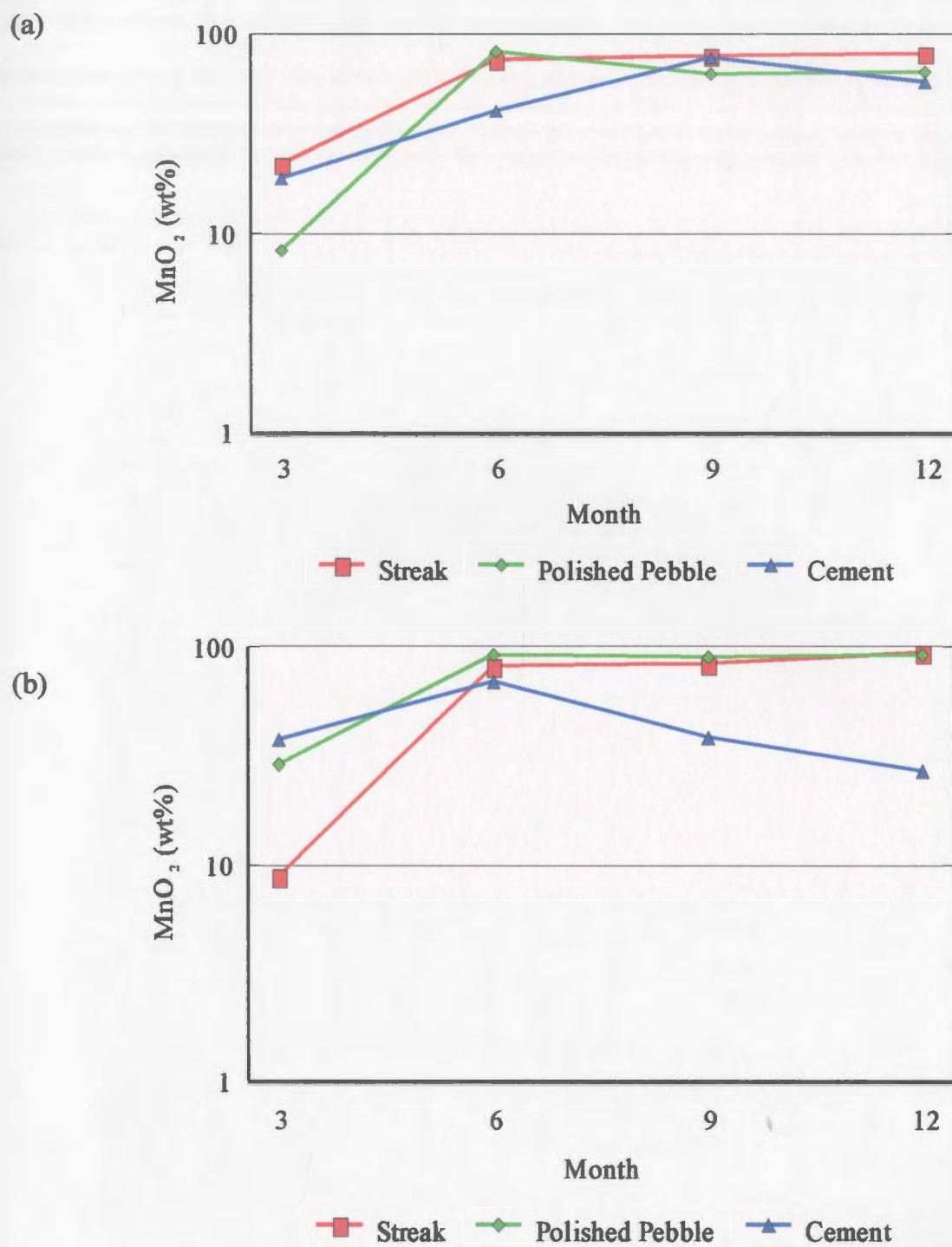
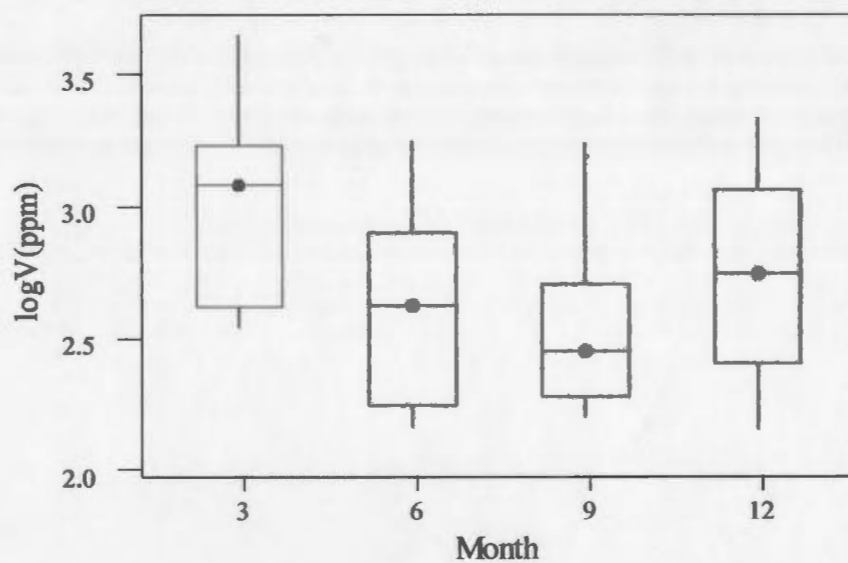


Figure 4.22(a) Plot of MnO₂ concentrations (wt%) for Fe-Mn oxide coatings on artificial substrates taken from SJPS1 for a 12 month period; (b) plot of MnO₂ concentrations (wt%) for samples taken from SJPS6A.

(a)



(b)

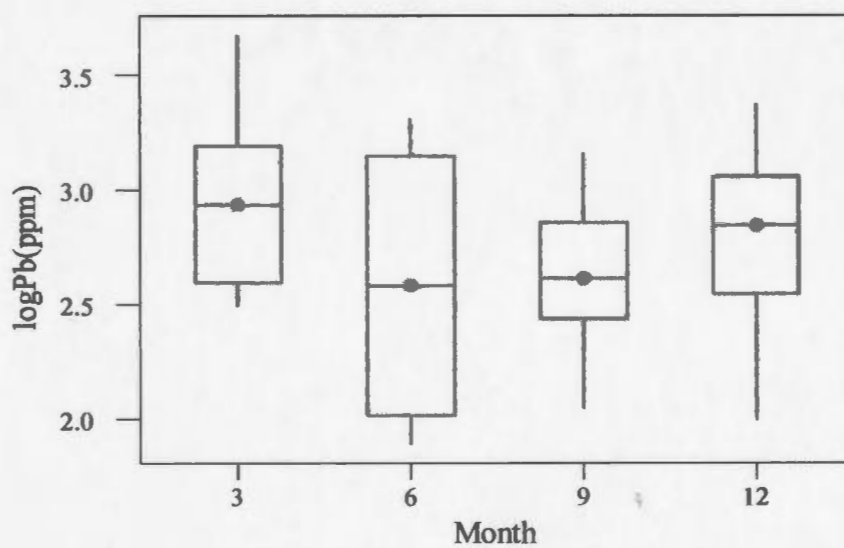
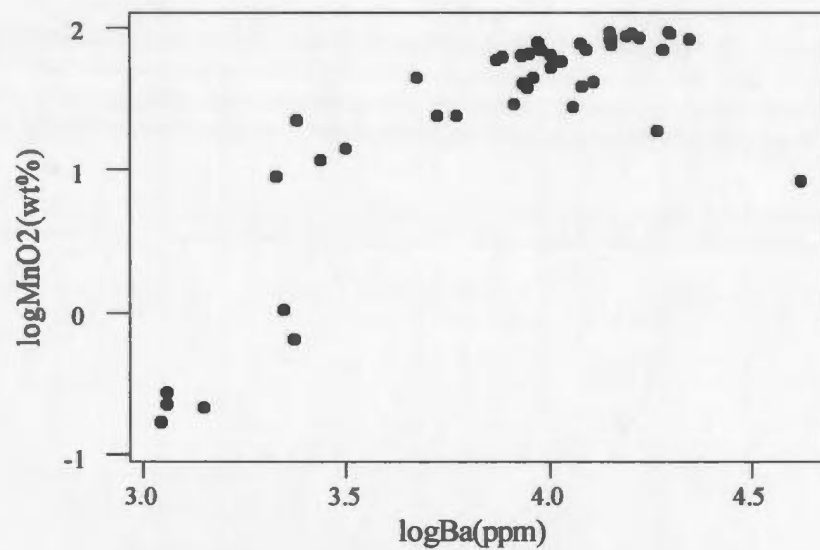


Figure 4.23(a) Boxplot of $\log V$ (ppm) vs. month and (b) $\log Pb$ (ppm) vs. month for artificial substrate samples taken from Rennies River over a 1-year period from March, 2002, to March, 2003.

(a)



(b)

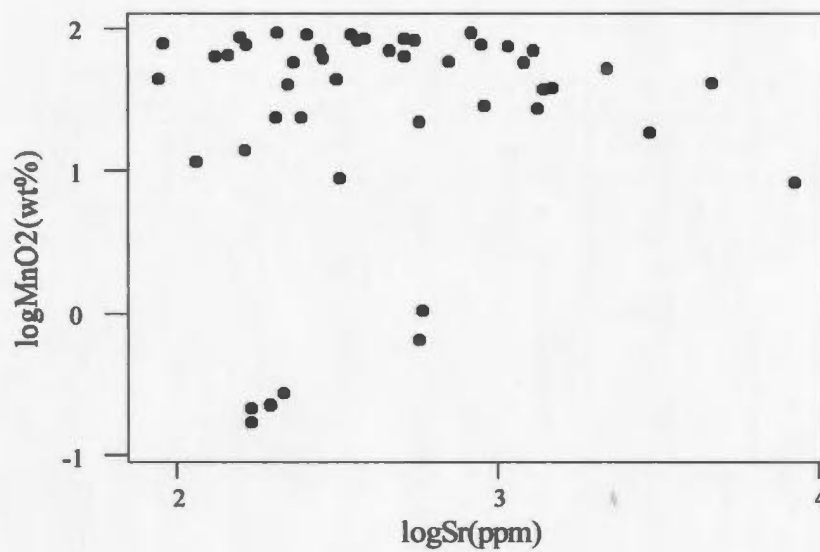


Figure 4.24(a) Scatter plot of $\log \text{MnO}_2(\text{wt}\%)$ vs. $\log \text{Ba}(\text{ppm})$ and (b) $\log \text{MnO}_2(\text{wt}\%)$ vs. $\log \text{Sr}(\text{ppm})$ for artificial substrate samples taken from Rennies River over a 1-year period from March, 2002, to March, 2003.

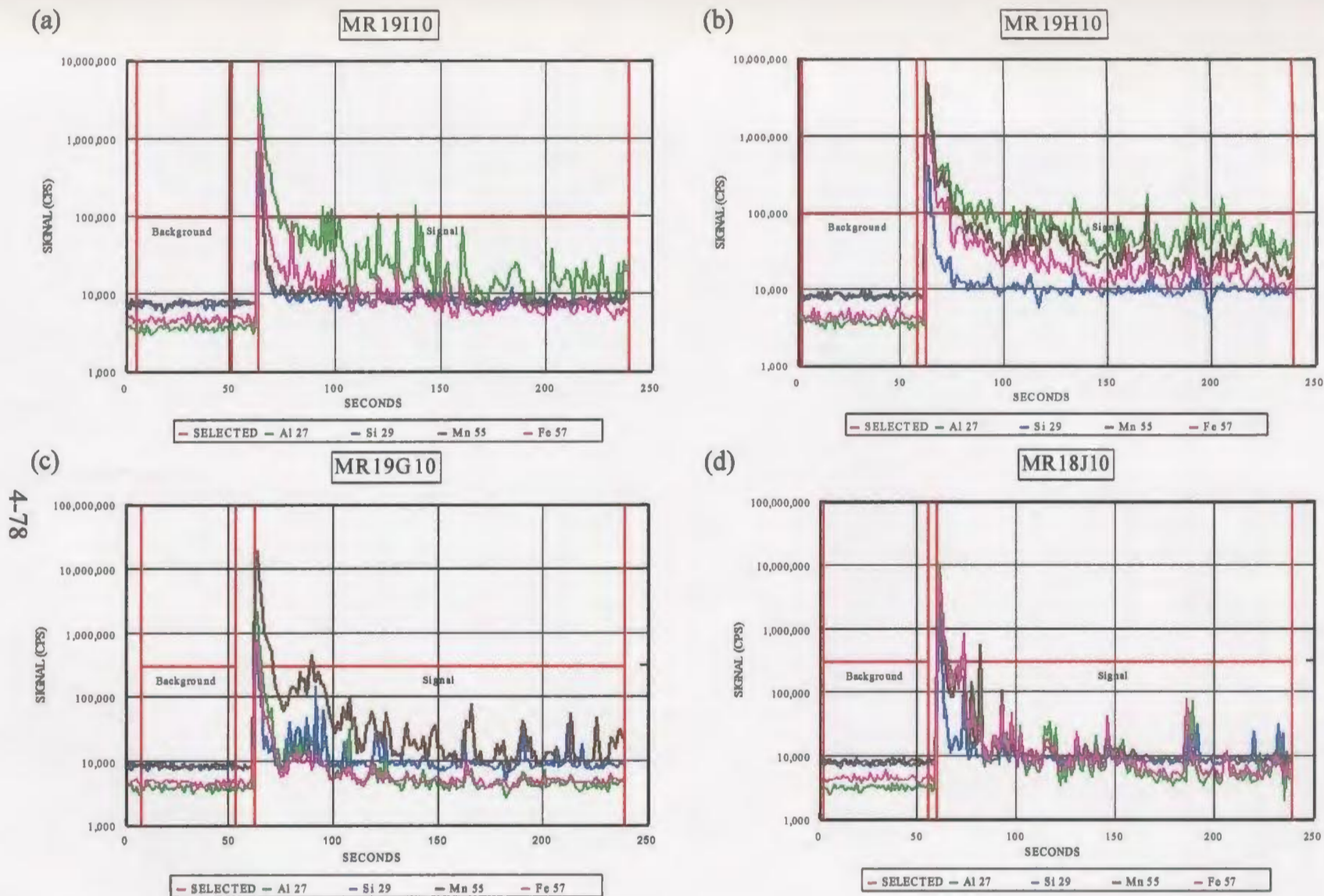


Figure 4.25 Intensity (cps) vs. time (s) plots for the cement substrate taken from site SJS1 at; (a) three months, (b) six months, (c) nine months, and (d) twelve months for the elements ^{27}Al , ^{29}Si , ^{55}Mn , and ^{57}Fe determined by LA-ICP-MS.

(a)



(b)



(c)



(d)



4-79

Figure 4.26 Photographs of iron-manganese oxide coatings present on a cement substrate taken from site SJS6A after 3 months of coating accretion (a) before and (b) after LA-ICP-MS analysis; and from site SJS1 after 6 months of coating accretion (c) before and (d) after LA-ICP-MS analysis.

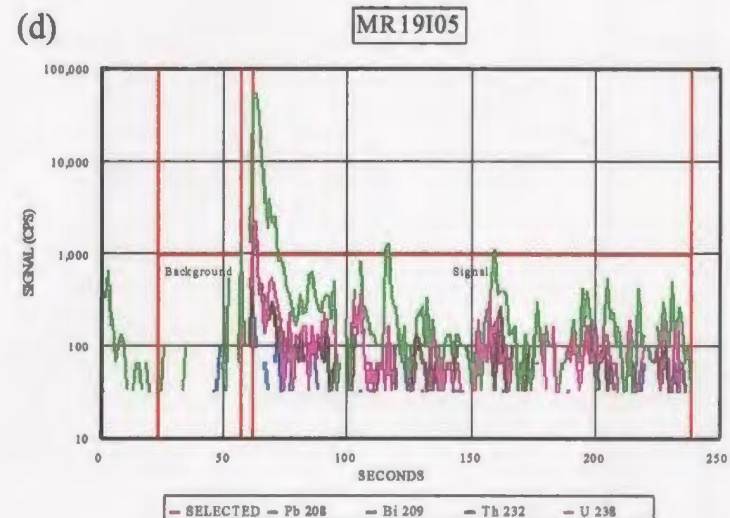
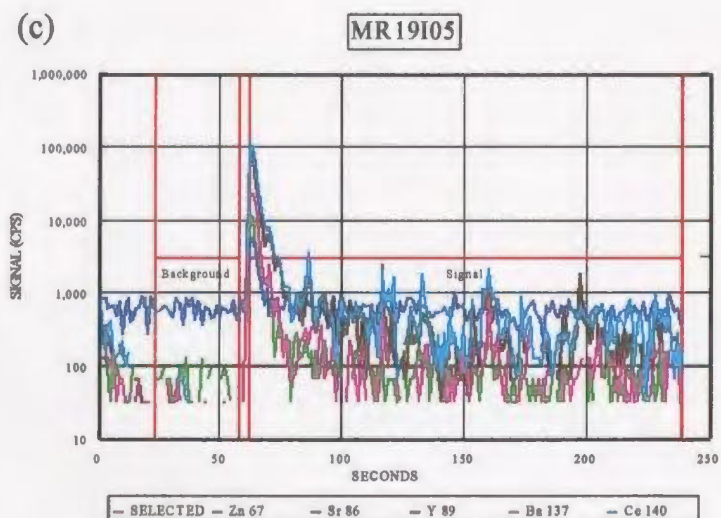
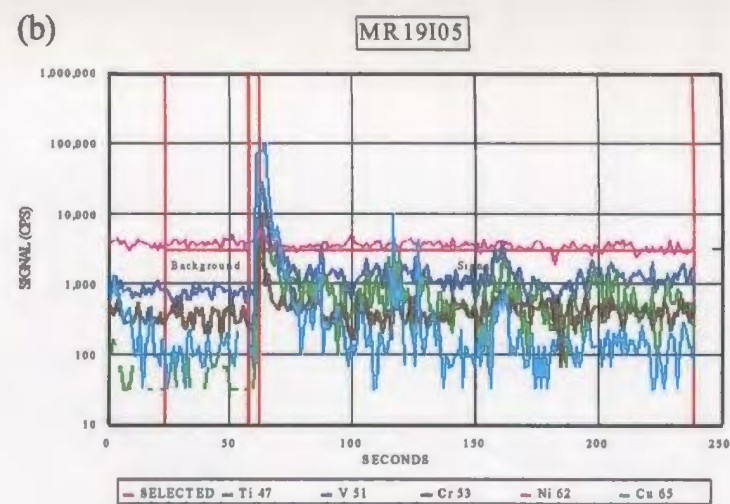
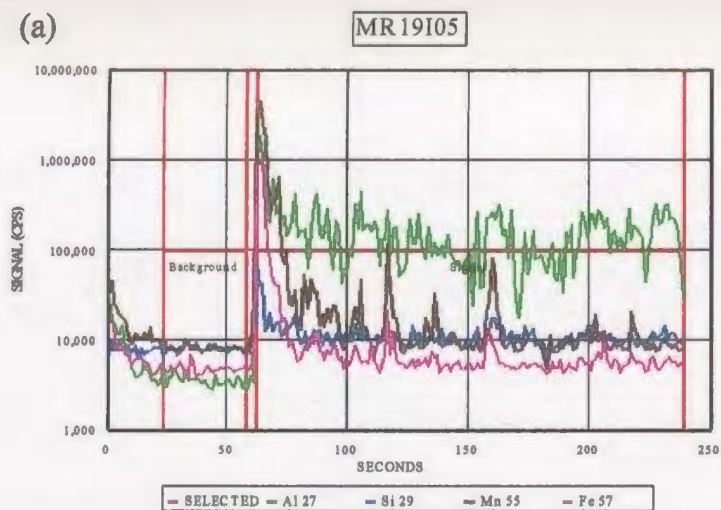


Figure 4.27 Intensity (cps) vs. time (s) plots for the streak plate taken from site SJS1 after three months analyzed by LA-ICP-MS for (a) ^{27}Al , ^{29}Si , ^{55}Mn , and ^{57}Fe , (b) ^{47}Ti , ^{51}V , ^{53}Cr , ^{62}Ni , ^{65}Cu , (c) ^{67}Zn , ^{86}Sr , ^{89}Y , ^{137}Ba , ^{140}Ce , (d) ^{208}Pb , ^{209}Bi , ^{232}Th , and ^{238}U .

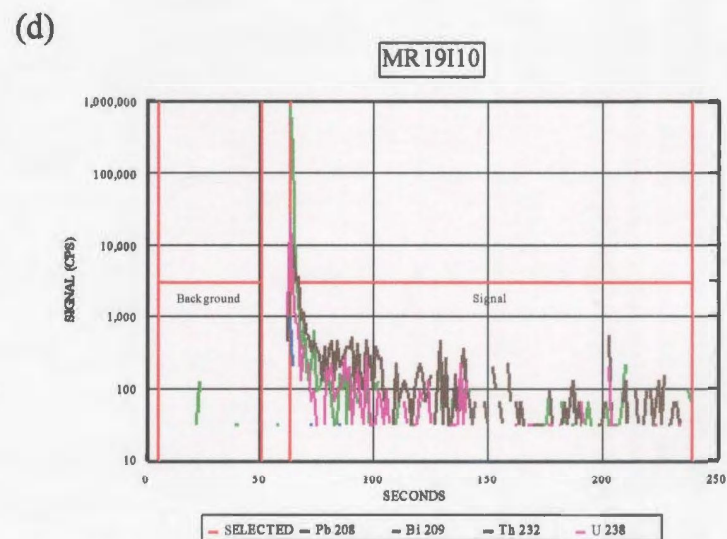
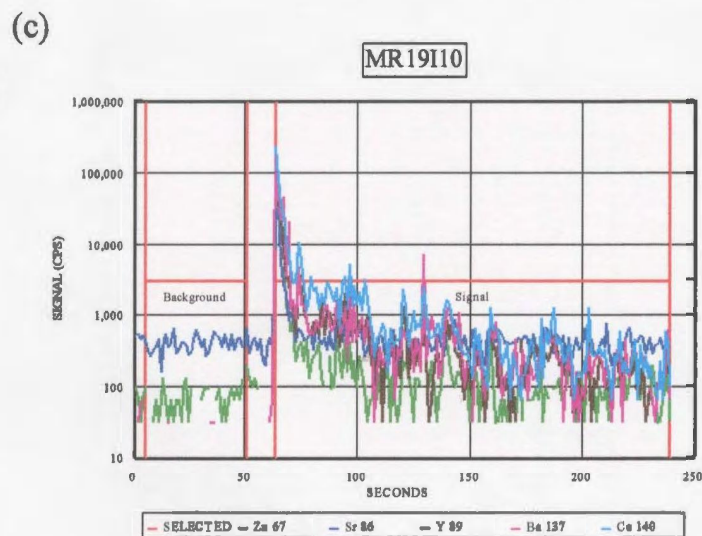
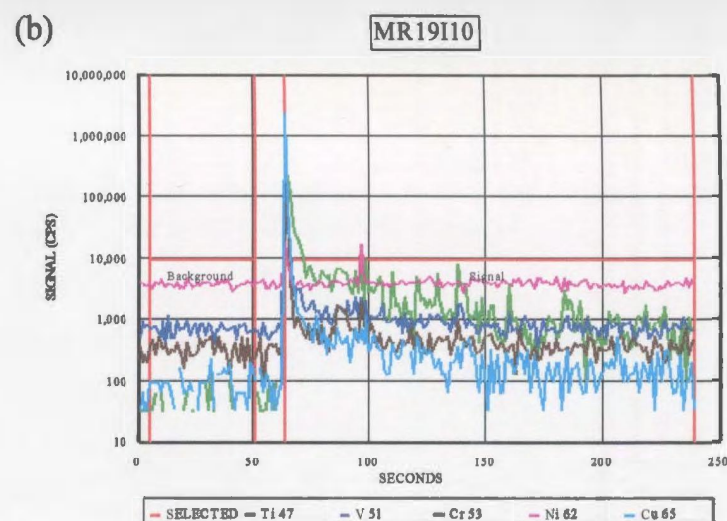
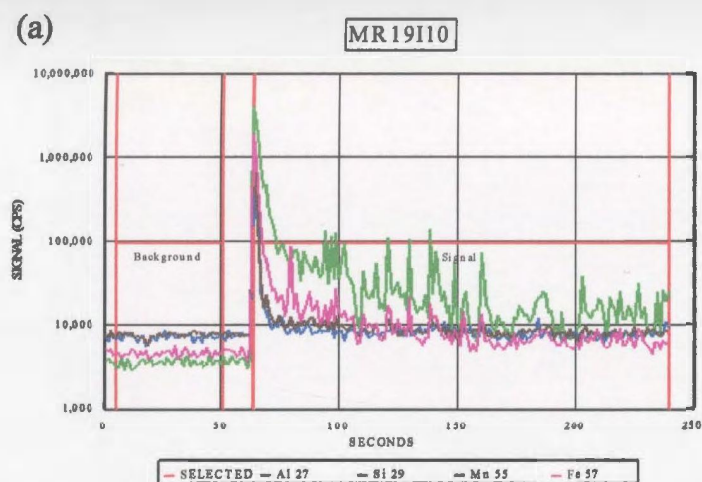
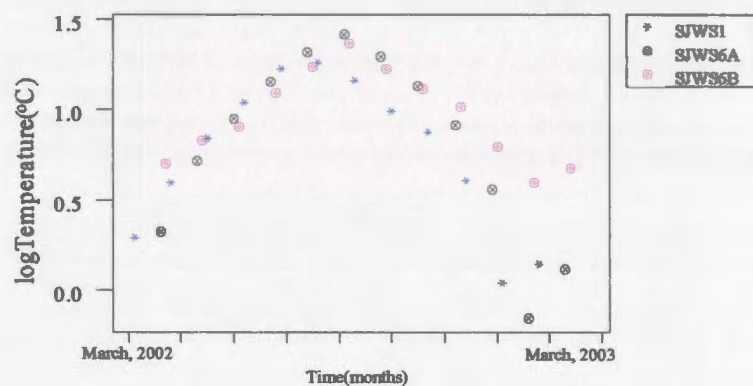
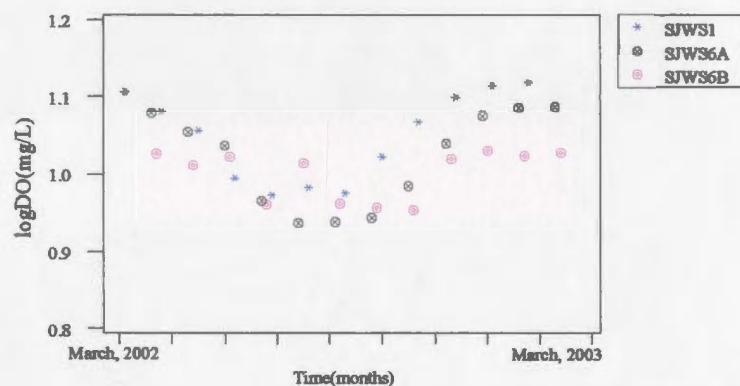


Figure 4.28 Intensity (cps) vs. time (s) plots for the cement substrate taken from site SJS1 after three months analyzed by LA-ICP-MS for (a) ^{27}Al , ^{29}Si , ^{55}Mn , and ^{57}Fe , (b) ^{47}Ti , ^{51}V , ^{53}Cr , ^{62}Ni , ^{65}Cu , (c) ^{67}Zn , ^{86}Sr , ^{89}Y , ^{137}Ba , ^{140}Ce , (d) ^{208}Pb , ^{209}Bi , ^{232}Th , and ^{238}U .

(a)



(b)



(c)

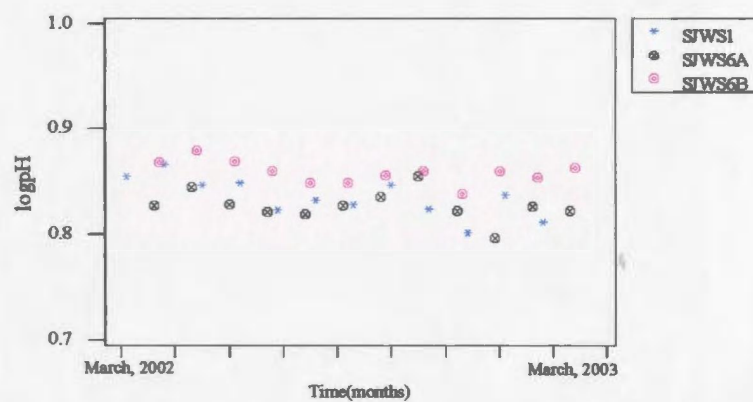


Figure 4.29 Plot of (a) log temperature (°C), (b) log dissolved oxygen (mg/L) and (c) log pH vs. time for water samples taken from Rennies River over a 1-year period from March, 2002, to March, 2003.

(a)



(b)



Figure 4.30 Artificial substrate samples along with pebbles (located on upper right of glass dish) taken from Rennies River at sites (a) SJS1 and (b) SJS6A at three month intervals from March 2002 to March 2003.

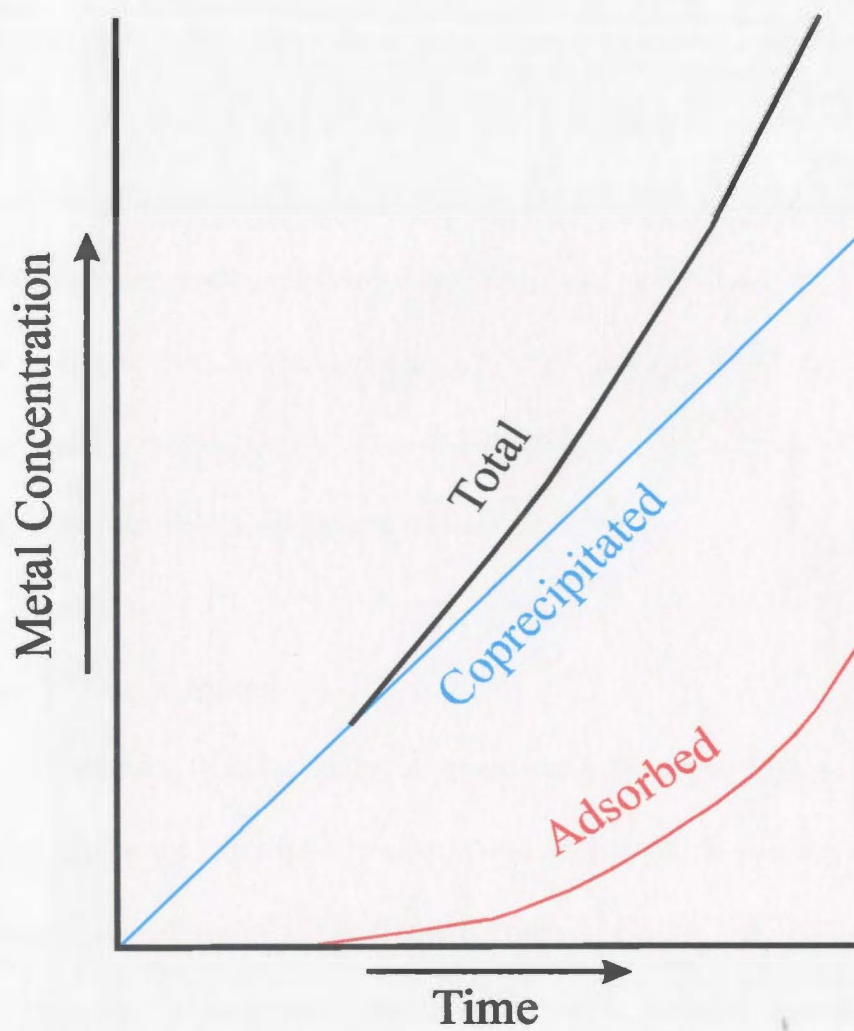


Figure 4.31 Diagram modified from Robinson (1981) that illustrates the proposed model for trace metal scavenging by Fe-Mn oxides in a stream.

5. Conclusions

5.1 LA-ICP-MS

Concentrations of a number of elements in Fe-Mn oxide coatings on pebbles were determined using LA-ICP-MS after a suitable optimization of the instrumental operating parameters for this unique type of sample. The technique required minimal sample preparation, and the sample runs were relatively fast. Data of useful quality was produced, even though the relative standard deviations for some samples were high. Quantitative determination using a single internal standard was not feasible, partially because of sample heterogeneity, but when a data normalisation was used which set the sum of all oxides to 100%, useful results were obtained.

5.2 Stream Water Samples

Multivariate statistical analysis, specifically Principal Component Factor Analysis (PCFA) was performed on both the waters and Fe-Mn oxide coating data. Four Factors were produced for the water's PCFA and a graph of Factor 1 vs. Factor 2 showed that the samples could be separated into eight Groups. Trends for the elements were based on their geochemical characteristics (lithophile, chalcophile, and siderophile), pH, and dissolved oxygen. Elevated elemental concentrations in water, especially for the chalcophile elements contained in Factor 1, indicated that old mining practices and waste

disposal procedures produced long-term pollution at Tilt Cove and more significantly at Betts Cove, where the effects of acid mine drainage is apparent. Anthropogenic inputs were observed in Rennies River where low concentrations of the lithophile elements in Factor 1 were found in one of the more pristine sites on this river. Increasing analyte concentrations were found at sites in the more heavily populated metropolitan area, and with maximum concentrations occurring in a site that drains a former city dump site. Geologic inputs at Tilt Cove and Betts Cove were also identified by their elemental composition.

5.3 Fe-Mn oxide Coatings

PCFA could not be satisfactorily performed on the combined data from “mature” and “fresh” coatings suggesting that these two kinds of samples had very different chemical characteristics. For the “mature” coatings, PCFA produced three Factors, with similar regional groupings to those found in the waters data. Element trends in each study area were based upon the elemental affinity towards the MnO_2 or Fe_2O_3 phase, which is in turn related to ionic radius and chemical affinity (lithophile, siderophile, or chalcophile). Manganese oxide is a strong adsorber of most elements due to its low zero point of charge which produces a negative surface charge in natural stream environments. Only two elements (Cr and Cu) exhibited preferential adsorption onto Fe_2O_3 . These elements have small ionic radii and can form anionic species in solution which are strongly

attracted to a positively charged Fe_2O_3 surface.

Iron-manganese oxide coating concentration trends did not match water trends at all the sites because trace element concentrations in the coatings depended on the following factors: the element concentration in the water, the dissolved oxygen and pH at the sampling sites, and the ratio of MnO_2 to Fe_2O_3 in the coating. When environmental monitoring and mineral exploration is undertaken using these coatings as a sampling media, all of these variables must be considered. Even with these complications, evidence of elemental pollution was clearly displayed in the data from the Tilt Cove and Betts Cove study areas, suggesting that these coatings do indeed reflect long-term environmental conditions. In the control samples from these study areas, the elemental signatures of various bedrock geological members could be observed in the trace element concentration trends in the Fe-Mn oxides. There were no seasonal patterns observed in the Rennies River study area, possibly due to the temperate climate in this area. In this area, water temperature extremes seldom occur, resulting in nearly constant chemical weathering rates with most of the stream chemistry variables remaining constant. The preferential absorption on the manganese oxide was clearly displayed in the high Fe_2O_3 samples taken from Rennies River which exhibited the lowest concentrations of most elements from the entire sampling period. At Robinsons River, natural abrasion of the pebbles in the fast moving stream resulted in very thin coatings that limited the elucidation of element trends.

Samples collected for the annual accretion portion of this study produced a PCFA with two Factors. A graph of these two Factors showed four groupings which were based on location and the time of sampling. Coatings deposited in the initial three months of accretion were primarily Fe_2O_3 containing elevated concentrations of various coprecipitated metals. Manganese oxide concentrations increased after three months and continued to grow for the entire sampling period due to the affinity of manganese for the Fe_2O_3 surface. All of the elements except Ba showed an interesting decrease in concentration with time related to the low adsorption of most trace elements and low coprecipitation within the MnO_2 phase. Barium displayed a positive correlation with MnO_2 related to its large ionic radius. Adsorption rates further increased after 9 months of coating accretion.

Variables that govern element concentrations for “mature” coatings, including element concentration in the aqueous phase, element affinity, dissolved oxygen levels, and pH values, do not appear important in controlling the concentrations in “fresh” coatings. This may be interpreted using Robinson’s (1981) proposed model of accretion in which coprecipitation occurs initially and is predicted to continue for up to 3 years. In this model adsorption starts at a low rate on the precipitated materials and increases exponentially until equilibrium with the stream environment is obtained (Carpenter and Hayes, 1980). Adsorption can continue for longer than three years until an equilibrium is reached between the coating and the stream environment. Trace element concentrations

on “fresh” coatings are a result of both adsorption and coprecipitation. While on “mature” coatings, concentrations will primarily be caused by adsorption. Coprecipitation and adsorption affect element concentrations in significantly different ways.

5.4 Future Work

In order to make the preliminary conclusions of this study more conclusive, more samples from each site would be required. Sampling was limited in this study by both time and cost considerations. The quantitative determination of an internal standard should also be pursued with the possible goal of producing higher quality analytical data.

For both the stream water and Fe-Mn oxide analysis, a larger number of elements could be determined to aid in the detection of further anthropogenic and geologic inputs from the study areas. Water and pebble samples could be taken on a seasonal basis to give a better idea of how coating and water concentrations are related and how both change in different geologic environments.

The different affinities of elements towards the MnO_2 and Fe_2O_3 phases also requires further investigation. Other factors that require examination are the effect of organic matter on metal accumulation and how the crystallinity of the oxide phase is related to adsorption. The processes of adsorption and coprecipitation appear complex, with a more lengthy study needed to address the time-frame and how element concentrations are affected by these processes.

References

- Achterbergh, E.V., Ryan, C.G., Jackson, S.E., and Griffin, W.L., 2001. Laser Ablation-ICP-MS in the Earth Sciences; Appendix 3: Data reduction software for LA-ICP-MS. Mineralogical Association of Canada Short Course Series, 29, pp. 239-243.
- Al, T.A., 1990. The character and setting of gold mineralization associated with the Betts Cove Complex. M.Sc. Thesis, MUN, 143 pp.
- Axelsson, M.D., Rodushkin, I., Baxter, D.C., Ingri, J., and Öhlander, B., 2002. High spatial resolution analysis of ferromanganese concretions by LA-ICP-MS. *Geochemical Transactions*, 3, pp. 40-47.
- Baird, D.M., 1959. Development of gypsum deposits in southern Newfoundland. *Bulletin of the Canadian Institute of Mining and Metallurgy*, 52, pp. 495-502.
- Baird, D.M., and Cote, P.R., 1964. Late Carboniferous sedimentary rocks in southwestern Newfoundland and their relations to similar strata in western Cape Breton Island. *Bulletin of the Canadian Institute of Mining and Metallurgy*, 57, pp. 509-520.
- Balistrieri, L.S., and Chao, T.T., 1990. Adsorption of selenium by amorphous iron oxyhydroxide and manganese dioxide. *Geochimica et Cosmochimica Acta*, 54, pp. 739-751.
- Bédard, J.H., 1999. Petrogenesis of Boninites from the Betts Cove Ophiolite, Newfoundland, Canada: Identification of subducted source components. *Journal of Petrology*, 40, pp. 1853-1889.

- Bédard, J.H., Laurzière, K., Tremblay, A., and Sangster, A., Douma, S.L., and Dec, T., 2000. Betts Cove ophiolite and its cover rocks, Newfoundland. Geological Survey of Canada Bulletin, 550, 76 pp.
- Bell, W.A., 1984. Early Carboniferous strata of St. Georges Bay area, Newfoundland. Geological Survey of Canada Bulletin, 10, pp. 1-45.
- Bell, T., Liverman, D.G.E., Batterson, M.J., and Sheppard, K., 2001. Late Wisconsinian stratigraphy and chronology of southern St. George's Bay, Newfoundland: a reappraisal. Canadian Journal of Earth Science, 38, pp. 851-869.
- Brümmer, G.W., 1986. The importance of chemical speciation in environmental processes: Heavy metal species, mobility, and availability in soils. Springer, Berlin Heidelberg, New York, pp. 169-192.
- Caissie, D., Pollock, T.L., and Cunjak, R.A., 1996. Variation in stream water chemistry and hydrograph separation in a small drainage basin. Journal of Hydrology, 178, pp. 137-157.
- Callahan, B., 1991. Kelly's Brook babbling once again. The Evening Telegram, June 5th.
- Carpenter, R.H., and Hayes, W.B., 1978. Precipitation of iron, manganese, zinc and copper on clean ceramic surfaces in a stream draining a polymetallic sulphide deposit. Journal of Geochemical Exploration, 33, pp. 31-37.
- Carpenter, R.H., and Hayes, W.B., 1980. Annual accretion of Fe-Mn oxides and certain associated metals in a stream environment. Chemical Geology, 29, pp. 249-259.

Carpenter, R.H., Pope, T.A., and Smith, R.L., 1975. Fe-Mn coatings in stream sediment geochemical surveys. *Journal of Geochemical Exploration*, 4, pp. 349-360.

Carpenter, R.H., Robinson, G.D. and Hayes, W.B., 1978. Partitioning of manganese, iron, copper, zinc, lead, cobalt and nickel in black coatings on stream boulders in the vicinity of the Magruder Mine, Lincoln Co., Georgia. *Journal of Geochemical Exploration*, 10, pp. 75-89.

Cattell, R. B., 1966. The scree test for the number of factors. *Multivariate Behavioral Research*, 1, pp. 245-276.

Catto, N. and St. Croix, R., 1998. Urban geology of St. John's, Newfoundland. In: *Urban geology of Canadian cities*. GAC special paper 42, Geological Association of Canada, St. Johns NF, pp. 445-462.

Cerling, T.E., and Turner, R.R., 1982. Formation of freshwater Fe-Mn coatings on gravel and the behavior of ^{60}Co , ^{90}Sr , and ^{137}Cs in a small watershed. *Geochimica et Cosmochimica Acta*, 46, pp. 1333-1343.

Chao, T.T., 1984. Use of partial dissolution techniques in geochemical exploration. *Journal of geochemical exploration*, 20, pp. 101-135.

Chao, T.T., and Theobald, P.K. Jr., 1976. The significance of secondary iron and manganese oxides in geochemical exploration. *Economic Geology*, 71, 1560-1569.

Coish, D.W., 1993. Analysis of Mn and Fe coatings on stream pebbles by laser ablation microprobe-inductively coupled plasma mass spectrometer (LAM-ICP-MS): A tool for environmental monitoring and mineral exploration. Hons. Thesis, MUN.

Coish, D.W., 2000. Applicability of laser ablation and partial dissolution ICP-MS techniques on Mn-Fe-oxide coatings of stream pebbles to mineral exploration and environmental monitoring. M.Sc. Thesis, MUN.

Coish, R.A., Hickey, R., and Frey, F.A., 1982. Rare earth element geochemistry of the Betts Cove ophiolite, Newfoundland: complexities in ophiolite formation. *Geochemica et Cosmochemica Acta*, 46, pp. 2117-2134.

Coonley, L.S. Jr., Baker, E.B., and Holland, H.D., 1971. Iron in the Mullica River and in Great Bay, New Jersey. *Chemical Geology*, 7, pp. 51-63.

Cousineau, B. and Béhard, J.H., 2000. Sedimentation in a subaqueous arc/subarc setting: the Bobby Cover Formation, Snooks Arm Group, Newfoundland. *Precambrian Research*, 101, pp. 111-134.

Crowe, S.A., Fryer, B.J., Samson, I.M., and Gagnon, J.E., 2003. Precise Isotope Ratio Determination of Common Pb Using Quadrupole LA-ICP-MS with Optimized Laser Sampling Conditions and a Robust Mixed-Gas Plasma. Manuscript submitted to the *Journal of Atomic Analytical Spectrometry*, 32 pp.

Deer, W.A., Howie, R.A., and Zussman, J., 1992. An introduction to the rock-forming minerals. Second ed. Addison Wesley Longman Limited, Essex, England, 696 pp.

Dong, D., Hua, X., Li, Y., and Zhonghua, L., 2002. Lead adsorption to metal oxides and organic material of freshwater surface coatings determined using a novel selective extraction method. *Environmental Pollution*, 119, pp. 317-321.

Dong, D., Yu, L., Zhang, B., Hua, X., and Baohua, Y., 2001. Selective chemical extraction and separation of Mn, Fe oxides and organic material in natural surface coatings: application to the study of trace metal adsorption mechanism in aquatic environments. *Microchemical Journal*, 69, pp. 89-94.

Drever, J.I., 1988. *The Geochemistry of Natural Waters*. Second ed. Prentice Hall Inc., New Jersey, 438 pp.

Filipek, L.H., Chao, T.T., and Carpenter, R.H., 1981. Factors affecting the partitioning of Cu, Zn and Pb in boulder coatings and stream sediments in the vicinity of a polymetallic sulphide deposit. *Chemical Geology*, 33, pp. 45-64.

Filipek, L.H., and Owen, R.T., 1979. Geochemical associations and grain-size partitioning of heavy metals in lacustrine sediments. *Chemical Geology*, 26, pp. 105-117.

Ford, R.J., 1992. The effect of Kelly's Brook on the bacteriological water quality of Rennies River. Hons. Thesis, MUN.

Förstner, U., and Wittman, G.T.W., 1979. *Metal Pollution in the Aquatic Environment*. New York, Springer-Verlag, Berlin Heidelberg, 486 pp.

Gadde, R.R., and Laitinen, H.S., 1974. Studies of heavy metal adsorption by hydrous iron and manganese oxides. *Analytical Chemistry*, 46, pp. 2022-2026.

Gulson, B.L., Church, S.E., Mizon, K.J., and Meier, A.L., 1992. Lead isotopes in iron and manganese oxide coatings and their use as an exploration guide for concealed mineralization. *Applied Geochemistry*, 7, pp. 495-511.

Günther, D., Horn, I., and Hattendorf, B., 2000. Recent trends and developments in laser ablation-ICP-mass spectrometry. *Journal of Analytical Chemistry*, 368, pp. 4-14.

Hair, J.F., Anderson, R.E., and Tatham, R.L., 1987. *Multivariate data analysis*. Second ed., Macmillan Publishing, New York, 449 pp.

Hale, M., Thompson, M., and Wheatley, M.R., 1984. Laser ablation of stream-sediment pebble coatings for simultaneous multi-element analysis in geochemical exploration. *Journal of Geochemical Exploration*, 21, pp. 361-371.

Health Canada, 1978. Guidelines for Canadian drinking water quality-supporting documents: magnesium. Government of Canada, Ottawa, 4 pp.
(<http://www.hc-sc.gc.ca/hecs-sesc/water/dwgsup.htm>).

Health Canada, 1986a. Guidelines for Canadian drinking water quality-supporting documents: silver. Government of Canada, Ottawa, 4 pp.
(<http://www.hc-sc.gc.ca/hecs-sesc/water/dwgsup.htm>).

Health Canada, 1986b. Guidelines for Canadian drinking water quality-supporting documents: chromium. Government of Canada, Ottawa, 4 pp.
(<http://www.hc-sc.gc.ca/hecs-sesc/water/dwgsup.htm>).

Health Canada, 1987a. Guidelines for Canadian drinking water quality-supporting documents: calcium. Government of Canada, Ottawa, 4 pp.
(<http://www.hc-sc.gc.ca/hecs-sesc/water/dwgsup.htm>).

Health Canada, 1987b. Guidelines for Canadian drinking water quality-supporting documents: iron. Government of Canada, Ottawa, 4 pp.
(<http://www.hc-sc.gc.ca/hecs-sesc/water/dwgsup.htm>).

Health Canada, 1992. Guidelines for Canadian drinking water quality-supporting documents: lead. Government of Canada, Ottawa, 13 pp.
(<http://www.hc-sc.gc.ca/hecs-sesc/water/dwgsup.htm>).

Health Canada, 1999a. Guidelines for Canadian drinking water quality-supporting documents: antimony. Government of Canada, Ottawa, 9 pp.
(<http://www.hc-sc.gc.ca/hecs-sesc/water/dwgsup.htm>).

Health Canada, 1999b. Guidelines for Canadian drinking water quality-supporting documents: uranium. Government of Canada, Ottawa, 10 pp.
(<http://www.hc-sc.gc.ca/hecs-sesc/water/dwgsup.htm>).

Hem, J.D., 1978. Redox processes at surfaces of manganese oxide and their effects on aqueous metal ions. *Chemical Geology*, 21, pp. 199-218.

- Hibbard, J., 1983. Geology of the Baie Verte Peninsula, Newfoundland. Memoir 2. Mineral Development Division, Department of Mines and Energy, Government of Newfoundland and Labrador.
- Hirata, T., and Nesbitt, R.W., 1995. U-Pb isotope geochronology of zircon: evaluation of the laser probe inductively coupled plasma mass spectrometry technique. *Geochimica et Cosmochimica Acta*, 59, pp. 2491-2500.
- Horne, J.A., and Goldman, C.R., 1994. *Limnology*. Second ed. McGraw-Hill Inc., New York, 576 pp.
- Jackson, S.E., 2001. Laser Ablation-ICP-MS in the Earth Sciences; Chapter 3: the application of ND:YAG lasers in LA-ICP-MS. Mineralogical Association of Canada Short Course Series, 29, pp. 29-45.
- Jackson, T.A., 1998. Environmental interactions of clays; Chapter 5: The biogeochemical and ecological significance of interactions between colloidal minerals and trace elements. Springer, Berlin, pp. 93-205.
- Jenne, E.A., 1968. Controls on Mn, Fe, Co, Ni, Cu, and Zn concentrations in soils and waters: the significant role of hydrous Mn and Fe oxides. *American Chemical Society Advances in Chemistry Series*, 73, pp. 337-387.
- Kanehira, K., and Bachinski, D., 1967. Framboidal pyrite and concentric textures in ores of the Tilt Cove Mine, northeastern Newfoundland. *Canadian Mineralogist*, 9, pp. 124-128.

- King, A.F., 1990. Geology of the St. John's area, Report 90-2. Department of Mines and Energy, pp. 29-62.
- Knight, I., 1983. Stratigraphy, sedimentology, and paleogeography of Mississippian strata of the Bay St. George subbasin, western Newfoundland. Ph. D Thesis, MUN, 430 pp.
- Knight, R., Haswell, S.J., Lindow, S.W., and Batty, J., 1999. Determination of mercury in hair by coupled CVAA-ICP-MS. *Journal of Analytical Atomic Spectrometry*, 14, pp. 127-129.
- Krauskopf, K.B., and Bird, D.K., 1995. *Introduction to Geochemistry*. Third ed. McGraw-Hill, Inc., New York, 647 pp.
- Loganathan, P., and Burau, R.G., 1973. Sorption of heavy metals by a hydrous manganese oxide. *Geochemica et Cosmochimica Acta*, 37, pp. 1277-1293.
- Longerich, H.P., 2000. Inductively Coupled Plasma Chemometrics: Calculation of Sample Concentration from Raw (Gross) Intensities (Count Rates). Personal essay, 17 pp.
- Longerich, H.P., 2001. Laser Ablation-ICP-MS in the Earth Sciences; Chapter 2: Chemometrics. Mineralogical Association of Canada Short Course Series, 29, pp. 21-28.
- Longerich, H.P., 2001. Laser-Ablation Inductively Coupled-Mass Spectrometry (LA-ICP-MS): A Personal Odyssey 1. *Newsletter of the Mineralogical Association of Canada*, 65, pp. 1-6.

Longerich, H.P., and Diegor, W., 2001. Laser Ablation-ICP-MS in the Earth Sciences; Chapter 1: Introduction to Mass Spectrometry. Mineralogical Association of Canada Short Course Series, 29, pp. 21-28.

Longerich, H.P., Jackson, S.E., and Günther, D., 1996. Laser Ablation Inductively Coupled Plasma Mass Spectrometric Transient Signal Data Acquisition and Analyte Concentration Calculation. *Journal of Analytical Atomic Spectrometry*, 11, pp. 899-904.

Longerich, H.P., Strong, D.F., and Kantipuly, C.J., 1986. Progress in evaluation of instrumental and other parameters affecting chemical and isotopic analysis by inductively coupled plasma-mass spectrometry (ICP-MS). *Canadian Journal of Spectroscopy*, 31, 5, pp. 111-121.

Love, S.D., and Bailey, R.C., 1992. Community development of epilithic invertebrates in streams: independent and interactive effects of substratum properties. *Canadian Journal of Zoology*, 70, pp. 1976-1983.

Maddox, W., 2001. Marine and on-land tailings disposal at Tilt Cove, Newfoundland. Hons. Thesis, MUN.

Martin, W., 1983. Once upon a mine: story of pre-confederation mines on the island of Newfoundland. The Canadian Institute of Mining and Metallurgy, special volume 26, Montreal, 98 pp.

Mason, R.A., 1994. Microprobe course. Unpublished course notes. 17 pp.

- Maynard, J.B., 1983. Geochemistry of sedimentary ore deposits. Springer-Verlag, New York, 305 pp.
- Milton, J.S., 1999. Statistical methods in the biological and health sciences. Second ed. McGraw-Hill Companies, Inc., New York, 588 pp.
- Morgan, J.J., and Stumm, W., 1964. Colloid-chemical properties of manganese oxides. *Journal of Colloid Science*, 19, pp. 347-359.
- Murray, J.W., 1975. The interaction of metal ions at the manganese dioxide-solution interface. *Geochimica et Cosmochimica Acta*, 39, pp. 505-519.
- Murthy, G.S., 1985. Paleomagnetism of certain constituents of the Bay St. George sub-basin, western Newfoundland. *Physics of the Earth and Planetary Interiors*, 39, pp. 89-107.
- Neale, E.R.W., Kean, B.F., and Upadhyay, H.D., 1975. Post-ophiolite unconformity, Tilt Cove-Betts Cove area, Newfoundland. *Canadian Journal of Earth Sciences*, 12, pp. 880-886.
- Nicholson, K., 1992. Manganese Oxide-metal adsorption: exploration guide and environmental guide. *Explore*, 78, pp. 10-12.
- Nowlan, G.A., 1976. Concretionary manganese-iron oxides in streams and their usefulness as a sample medium for geochemical prospecting. *Journal of Geochemical Exploration*, 6, pp. 193-210

Plant, J.A., Baldock, J.W., and Smith, B., 1996. Environmental geochemistry and health; the role of geochemistry in environmental and epidemiological studies in developing countries. Geological Society special publication , 113, pp. 7-22.

Potts, P.J., 1993. Analysis of geological materials; Chapter 4: Laboratory methods of analysis. Marcel Dekker, Inc., New York, pp. 123-220.

Power, J., 1990. Kelly's Brook. Quidi Vidi Rennies River Development Foundation Newsletter, 2, pp. 2.

Reed, S.J.B., 1993. Electron microprobe analysis. Second edition. Cambridge University Press, 326 pp.

Reimann, C., and Caritat, P., 1998. Chemical elements in the environment: factsheets for the geochemist and environmental scientist. Springer, Berlin, 398 pp.

Riggs, K., 2002. Heavy metal particulates in soil in the vicinity of the Tilt Cove smelter, Newfoundland. Hons. Thesis, MUN, 2002.

Robinson, G.D., 1981. Adsorption of Cu, Zn, and Pb near sulfide deposits by hydrous manganese-iron oxide coatings on stream alluvium. Chemical Geology, 33, pp. 65-79.

Robinson, G.D., 1984. Sequential chemical extractions and metal partitioning in hydrous Mn-Fe oxide coatings: reagent choice and substrate composition affect results. Chemical Geology, 47, pp. 97-112.

Rocholl, A.B.E., Simon, K., Jochum, K.P., Bruhn, F., Gehann, R., Kramar, U., Luecke, W., Molzahn, M., Pernicka, E., Seufert, M., Spettel, B., and Stummeier, J., 1997. Chemical Characterization of NIST Silicate Glass Certified Reference Material SRM 610 by ICP-MS, TIMS, LIMS, SSMS, INAA, AAS, and PIXE. *Geostandards Newsletter: The Journal of Geostandards and Geoanalysis*, 21, pp. 101-114.

Rose, A.W., Hawkes, H.E., and Webb, J.E., 1979. *Geochemistry in mineral exploration*. Second edition. Academic Press Inc., New York, 657 pp.

Shaw, J., and Forbes, D.L., 1990. Late Quaternary sedimentation in St. Georges Bay, southwest Newfoundland: acoustic stratigraphy and seabed deposits. *Canadian Journal of Earth Sciences*, 27, pp. 964-983.

Siegel, F.R., 2002. *Environmental geochemistry of potentially toxic metals*. Springer, Berlin, 218 pp.

Smedley, P.L., Edmunds, W.M., and Pelig-ba, K.B., 1996. Mobility of arsenic in groundwater in the Obuasi gold-mining area of Ghana: some implications for human health. *Geological Society special publication*, 113, pp. 163-181.

Squires, G.C., 1981. *The distribution and genesis of the Tilt Cove Sulphide deposits*. Hons. Thesis, MUN.

StatSoft, Inc., 1999. *Electronic Statistics Textbook*. Tulsa, OK.
(www.statsoft.com/textbook/stathome.html)

Strong, D.F., 1984. Geological relationships of alteration and mineralization at Tilt Cove, Newfoundland. Newfoundland Dept of Mines and Energy, Report 84-3, pp. 81-90.

Strong, D.F., and Saunders, C.M., 1988. Ophiolitic sulfide mineralization at Tilt Cove, Newfoundland: controls by upper mantle and crustal processes. *Economic Geology*, 83, pp. 239-255.

Suarez, D., and Langmuir, D., 1976. Heavy metal relationships in a Pennsylvania soil. *Geochimica et Cosmochimica Acta*, 48, pp. 589-598.

Sylvester, P.J., 2001. Laser Ablation-ICP-MS in the Earth Sciences; Chapter 13: A Practical Guide to Platinum-Group Analysis of Sulphides by Laser Ablation ICP-MS. Mineralogical Association of Canada Short Course Series, 29, pp. 21-28.

Systat, 1996. Statistics: Systat 6.0 for Windows. Chicago, Illinois. 751 pp.

Taylor, V.F., 2001. Trace element fingerprinting of Canadian wines. M.Sc. Thesis, MUN.

Theobald, P.K. Jr., Lakin, H.W., and Hawkins, D.B., 1963. The precipitation of aluminum, iron, and manganese at the junction of Deer Creek with the Snake River in Summit County, Colorado. *Geochimica et Cosmochimica Acta*, 27, pp. 121-132.

Thompson, M., Hale, M., and Coles, B., 1992. Geochemical reconnaissance using stream sediment pebble coatings and laser ablation ICP-AES. *Trans, Instn, Min. Metall. (Sect. B.: Appl. earth sci.)*, 101, pp. 9-14.

- Trivedi, P., and Axe, L., 2000. Modeling Cd and Zn sorption to hydrous metal oxides. *Environmental Science and Technology*, 34, pp. 2215-2223.
- Upadhyay, H.D., and Strong, D.F., 1973. Geological setting of the Betts Cove Copper deposits, Newfoundland: an example of ophiolite sulfide mineralization. *Economic Geology*, 68, pp. 161-167.
- Veinott, H., 2001. Chapter 14: The use of laser ablation-ICP-MS in the environmental sciences. In: *Laser Ablation-ICP-MS in the Earth Sciences, Short Course Series Volume 29*. Mineralogical Association of Canada, pp. 213-224.
- Waslenchuk, D.G., 1975. Mercury in fluvial bed sediments subsequent to contamination. *Environmental Geology*, 1, pp. 131-136.
- Whitney, P.R., (1975) Relationship of manganese-iron oxides and associated heavy metals to grain size in stream sediments. *Journal of Geochemical Exploration*, 4, pp. 251-263.
- Wilkinson, L., Blank, G., and Gruber, C., 1996. Desktop data analysis with SYSTAT. Prentice Hall Inc., New Jersey, 798 pp.
- Wyrzykowska, B., Szymczyk, K., Ichichashi, H., Falandysz, J., Skwarzec, B., and Yamasaki, S., 2001. Application of ICP sector field MS and principal component analysis for studying interdependence among 23 trace elements in Polish beers. *Journal of Agricultural and Food Chemistry*, 49, pp. 3425-3431.

Yun, M, Longerich, H.P., and Wadleigh, M.A., 2003. The determination of 18 trace elements in lichens for atmospheric monitoring using inductively coupled plasma-mass spectrometry. *Canadian Journal of Analytical Sciences and Spectroscopy*, 48, pp. 171-180.

Zachara, J.M., Gassman, P.L., Smith, S.C., and Taylor, D., 1995. Oxidation and adsorption of Co(II)EDTA^{2-} complexes in subsurface materials with iron and manganese oxide grain coatings. *Geochemica et Cosmochimica Acta*, 59, pp. 4449-4463.

Appendix 1.1:**Elemental Microprobe traverses done on polished pebble collected from site SJS2 in May, 2002.**

Traverse Point	1	2	3	4	5	6	7	8	9	10
Na2O(wt%)	0.2	0.2	0.5	2.0	0.2	-0.0	0.7	-0.1	0.6	0.6
MgO(wt%)	1.2	0.2	0.4	1.4	0.4	0.1	0.7	0.1	0.5	2.5
Al2O3(wt%)	13	2.5	6.4	6.6	1.2	1.6	2.4	1.7	5.1	19
SiO2(wt%)	16	19	44	49	9	9	78	97	80	25
K2O(wt%)	0.2	1.7	3.3	0.7	3.4	0.3	0.4	-0.0	0.3	0.2
CaO(wt%)	20	17	6.5	5.8	4.4	9.3	3.7	0.4	2.2	42
TiO2(wt%)	3.6	2.5	0.6	1.1	0.3	0.6	0.5	0.0	-0.0	0.4
MnO2(wt%)	2.9	3.6	1.6	2.4	16	23	6.4	0.1	0.4	1.0
Fe2O3(wt%)	48	60	40	32	63	53	6.0	0.8	12	9.7
SO3(wt%)	0.2	0.1	1.0	0.7	-0.0	0.0	0.4	0.1	0.3	1.0
ZnO(wt%)	4.1	5.7	5.0	4.0	16.6	16.9	3.3	-0.0	1.1	0.4
Total(wt%)	100	101	101	99	100	99	100	100	100	99
MnO2+Fe2O3(wt%)	51	64	42	34	79	75	12	1.0	12	11

Traverse Point	11	12	13	14	15	16	17	18	19	20
Na2O(wt%)	0.1	0.8	1.2	1.0	2.0	1.4	1.0	0.5	1.0	1.5
MgO(wt%)	0.3	2.6	4.9	2.6	3.6	2.2	3.1	0.7	2.0	1.6
Al2O3(wt%)	2.9	27	27	27	17	27	28	38	24	4.6
SiO2(wt%)	95	33	44	41	42	36	40	12	32	18
K2O(wt%)	0.1	0.4	0.4	0.7	0.4	0.8	0.4	0.1	0.5	0.3
CaO(wt%)	0.7	7.4	7.2	7.6	7.4	10	10	25	8.6	25
TiO2(wt%)	0.1	0.8	1.6	0.8	0.4	0.8	1.0	1.3	0.7	0.9
MnO2(wt%)	-0.1	0.6	1.0	0.9	1.5	1.5	1.2	0.4	1.2	39
Fe2O3(wt%)	1.7	31	14	21	27	22	16	25	34	5.4
SO3(wt%)	0.0	0.8	0.5	0.6	0.4	0.7	0.5	0.4	0.6	0.2
ZnO(wt%)	-0.1	1.0	0.9	1.2	2.0	1.4	1.4	0.2	1.2	12
Total(wt%)	100	100	100	100	99	100	100	99	99	101
MnO2+Fe2O3(wt%)	1.6	31	15	22	29	24	17	25	35	45

Traverse Point	21	22	23	24	25	26	27	28	29	30
Na2O(wt%)	1.1	2.0	3.4	1.5	0.0	1.1	2.1	2.1	1.5	1.2
MgO(wt%)	2.0	3.5	2.1	4.1	0.3	3.5	7.1	3.8	4.8	6.3
Al2O3(wt%)	33	30	26	24	1.3	11	16	11	14	18
SiO2(wt%)	50	34	15	37	97	70	40	34	43	44
K2O(wt%)	5.7	0.3	0.1	0.3	0.1	0.3	0.1	0.3	0.3	0.9
CaO(wt%)	2.5	8.7	5.4	7.9	0.5	3.9	16	21	18	16
TiO2(wt%)	0.1	1.0	0.6	1.0	0.0	0.6	1.6	2.6	4.7	1.7
MnO2(wt%)	0.6	1.2	32	1.8	0.1	0.3	4.7	11	4.6	4.9
Fe2O3(wt%)	5.3	21	22	24	0.9	8.8	9.5	8.7	3.7	6.0
SO3(wt%)	0.1	0.8	1.1	0.4	0.0	0.4	0.4	0.8	2.3	0.6
ZnO(wt%)	1.7	1.6	3.1	1.0	0.3	1.6	5.1	6.0	3.0	2.0
Total(wt%)	100	100	101	99	101	99	100	98	99	100
MnO2+Fe2O3(wt%)	5.8	23	54	26	1.1	9.1	14	20	8.3	11

Appendix 1.1:**Elemental Microprobe traverses done on cement collected from site SJS2
in May, 2002.**

Traverse Point	31	32	33	34	35	36	37	38	39	40
Na2O(wt%)	2.5	0.2	1.0	0.5	0.6	2.1	1.7	1.0	1.6	2.3
MgO(wt%)	5.4	0.2	5.8	1.2	2.5	18	3.5	1.5	1.5	1.9
Al2O3(wt%)	19	0.8	20	5.0	14	10	17	22	19	9.2
SiO2(wt%)	45	97	50	87	23	27	54	32	34	22
K2O(wt%)	1.7	-0.0	0.3	0.2	0.1	0.2	0.4	2.2	0.3	0.1
CaO(wt%)	11	0.3	14	4.9	31	28	16	5.2	7.0	14
TiO2(wt%)	2.1	-0.0	1.4	0.2	8.7	0.4	1.6	0.4	0.3	0.3
MnO2(wt%)	2.0	0.2	2.2	0.5	2.2	1.8	1.8	0.5	0.5	1.2
Fe2O3(wt%)	9.4	0.4	3.2	1.2	20	11	2.8	41	40	56
SO3(wt%)	1.9	0.1	0.7	0.1	0.1	0.3	1.3	0.4	0.4	0.4
ZnO(wt%)	1.6	-0.1	1.8	0.9	0.8	1.8	1.5	1.5	2.0	2.6
Total(wt%)	100	99	99	101	99	99	101	100	100	99
MnO2+Fe2O3(wt%)	11	0.6	5.3	1.7	23	13	4.6	41	41	57

Traverse Point	41	42	43	44	45	46	47	48	49	50
Na2O(wt%)	0.9	0.9	1.2	1.1	0.7	0.3	0.7	3.1	1.2	1.1
MgO(wt%)	2.5	2.2	2.2	2.5	1.2	1.2	1.4	1.6	1.2	1.1
Al2O3(wt%)	24	11	28	15	19	39	30	8.0	14	20
SiO2(wt%)	45	30	49	21	8.9	47	38	23	21	29
K2O(wt%)	0.5	0.4	0.1	0.2	0.1	0.0	0.3	0.1	0.2	0.1
CaO(wt%)	9.6	22	2.3	6.6	25	2.2	2.6	6.9	6.0	4.5
TiO2(wt%)	0.4	1.8	0.2	0.1	4.2	0.2	0.1	0.2	0.1	0.1
MnO2(wt%)	2.7	4.4	0.7	0.5	3.7	0.2	0.4	1.2	1.1	0.7
Fe2O3(wt%)	14	28	18	61	45	11	29	62	61	51
SO3(wt%)	0.3	0.7	0.3	1.1	0.2	0.3	0.4	0.5	0.4	0.5
ZnO(wt%)	2.1	2.8	1.7	1.8	0.5	0.5	1.2	4.1	3.2	1.7
Total(wt%)	100	98	100	100	99	100	99	99	98	100
MnO2+Fe2O3(wt%)	17	32	19	62	48	11	30	63	62	52

Traverse Point	51	52	53	54	55	56	57	58	59	60
Na2O(wt%)	0.9	1.0	0.8	0.7	2.3	-0.3	0.4	0.3	0.9	1.1
MgO(wt%)	2.2	5.1	3.3	1.1	7.3	0.8	0.2	0.6	4.6	1.7
Al2O3(wt%)	31	26	25	10.0	19	5.0	0.7	2.9	34	11
SiO2(wt%)	40	48	39	10	44	19	4	6	47	54
K2O(wt%)	0.3	0.5	0.4	0.2	0.5	0.2	0.3	0.2	0.3	0.6
CaO(wt%)	5.7	9.0	14	38	12	2.2	7.8	2.5	6.0	5.4
TiO2(wt%)	0.2	0.8	1.8	5.9	1.9	0.4	2.1	1.6	0.9	0.4
MnO2(wt%)	0.7	0.8	3.7	1.3	2.3	4.9	14	2.6	0.6	1.0
Fe2O3(wt%)	19	7.2	11	39	9.9	44	68	88	5.6	28
SO3(wt%)	2.7	0.4	0.8	0.2	1.0	0.2	0.1	0.1	0.4	0.7
ZnO(wt%)	0.7	0.9	3.1	1.0	3.5	35	18	11	0.6	1.2
Total(wt%)	99	99	100	100	102	101	100	100	99	99
MnO2+Fe2O3(wt%)	19	8.0	15	40	12	49	81	91	6.2	29

Appendix 1.1:**Elemental Microprobe traverses done on streak plate collected from site SJS2 in May, 2002.**

Traverse Point	1	2	3	4	5	6	7	8	9	10
Na2O(wt%)	3.2	4.9	4.0	3.2	1.8	3.3	2.8	3.6	3.5	9.0
MgO(wt%)	0.2	0.4	0.3	0.1	0.2	0.3	0.0	0.2	0.1	0.5
Al2O3(wt%)	22	26	37	39	25	30	27	36	39	29
SiO2(wt%)	72	59	53	53	67	62	65	56	54	51
K2O(wt%)	4.0	5.1	3.6	3.0	3.8	3.5	3.6	3.3	3.0	5.9
CaO(wt%)	0.2	0.5	0.2	0.2	0.2	0.3	0.2	0.1	0.1	0.4
TiO2(wt%)	0.2	0.2	0.4	0.2	0.1	0.3	0.2	0.2	0.2	0.3
MnO2(wt%)	-0.0	0.3	-0.0	0.1	-0.1	0.0	0.0	0.1	-0.0	0.2
Fe2O3(wt%)	0.3	1.7	1.6	1.7	0.8	0.5	0.6	0.6	0.4	1.8
SO3(wt%)	0.1	0.8	0.4	0.1	0.1	0.1	-0.0	0.1	0.1	1.7
ZnO(wt%)	-0.0	-0.0	0.1	0.1	-0.3	-0.1	0.3	0.1	-0.3	0.2
Total(wt%)	103	98	100	100	99	100	100	100	100	99
MnO2+Fe2O3(wt%)	0.2	1.9	1.6	1.8	0.7	0.5	0.6	0.6	0.3	2.0

Traverse Point	11	12	13	14	15	16	17	18	19	20
Na2O(wt%)	2.6	3.5	2.7	2.8	2.4	2.8	2.4	2.7	2.9	2.6
MgO(wt%)	0.2	0.2	0.2	0.2	0.2	0.2	0.3	0.1	1.0	0.1
Al2O3(wt%)	34	31	37	28	24	33	24	32	25	24
SiO2(wt%)	58	59	54	63	64	59	69	62	60	67
K2O(wt%)	3.0	3.6	3.7	3.4	5.9	3.8	3.7	3.2	3.6	3.4
CaO(wt%)	0.1	0.3	0.3	0.2	0.3	0.1	0.2	0.2	0.2	0.1
TiO2(wt%)	0.3	0.1	0.1	0.2	0.1	0.3	0.2	0.3	0.5	0.3
MnO2(wt%)	-0.0	-0.0	0.1	0.1	0.0	0.1	-0.1	-0.0	0.3	-0.1
Fe2O3(wt%)	0.8	1.5	1.6	0.3	0.7	1.1	0.5	0.5	5.0	0.9
SO3(wt%)	0.4	0.3	0.6	-0.1	0.3	0.1	0.1	-0.0	1.1	0.0
ZnO(wt%)	0.1	0.1	-0.0	0.1	0.3	0.0	-0.0	0.1	-0.2	0.0
Total(wt%)	99	100	100	98	99	100	100	100	98	99
MnO2+Fe2O3(wt%)	0.7	1.5	1.7	0.4	0.8	1.2	0.3	0.4	5.2	0.7

Traverse Point	21	22	23	24	25	26	27	28	29	30
Na2O(wt%)	2.9	2.0	6.0	2.0	1.8	2.6	2.1	4.0	2.4	2.2
MgO(wt%)	0.2	0.2	2.3	0.1	0.2	0.2	0.3	0.8	0.3	0.2
Al2O3(wt%)	27	24	21	30	23	23	22	24	32	24
SiO2(wt%)	64	69	51	65	70	70	70	53	61	68
K2O(wt%)	3.9	3.7	4.5	3.1	4.1	3.3	4.1	6.2	3.5	3.5
CaO(wt%)	0.2	0.2	0.5	0.1	0.3	0.3	0.2	0.3	0.2	0.3
TiO2(wt%)	0.2	0.2	0.2	0.1	0.2	0.2	0.1	0.3	0.4	0.2
MnO2(wt%)	0.1	0.0	0.5	-0.1	-0.1	0.2	0.1	1.5	-0.1	-0.1
Fe2O3(wt%)	1.1	0.6	13	0.4	1.6	0.9	0.6	7.9	1.5	0.5
SO3(wt%)	0.3	0.1	1.2	-0.0	0.1	-0.4	0.3	0.6	0.1	0.1
ZnO(wt%)	0.2	-0.0	0.2	0.2	-0.1	-0.1	-0.2	0.4	0.3	-0.2
Total(wt%)	99	99	98	100	100	100	99	98	101	99
MnO2+Fe2O3(wt%)	1.2	0.6	13	0.3	1.5	1.1	0.7	9.4	1.4	0.3

Appendix 1.1:**Elemental Microprobe traverses done on streak plate collected from site SJS2
in May, 2002.**

Traverse Point	31	32	33	34	35	36	37	38	39	40
Na2O(wt%)	3.5	3.1	3.2	2.3	2.3	2.1	5.3	7.0	2.5	2.1
MgO(wt%)	0.1	0.3	0.1	0.5	0.1	0.1	0.5	0.1	0.1	0.1
Al2O3(wt%)	33	32	24	26	24	23	28	16	23	28
SiO2(wt%)	59	56	65	63	68	69	56	71	69	65
K2O(wt%)	3.0	3.0	3.3	2.9	2.2	4.0	4.1	4.5	3.9	3.6
CaO(wt%)	0.2	0.2	0.7	0.9	0.3	0.3	0.3	0.6	0.3	0.2
TiO2(wt%)	0.2	0.3	0.4	0.8	0.2	0.2	0.3	0.1	0.2	0.1
MnO2(wt%)	0.1	-0.2	0.0	0.1	-0.0	-0.0	0.3	0.2	0.1	0.1
Fe2O3(wt%)	0.5	4.1	2.8	3.0	1.5	0.6	5.5	0.3	0.3	1.3
SO3(wt%)	0.5	0.9	1.1	0.4	0.3	0.3	0.8	1.3	0.7	0.1
ZnO(wt%)	0.1	0.1	0.2	0.5	-0.1	0.0	0.1	0.1	0.4	-0.1
Total(wt%)	99	99	99	100	99	100	100	101	101	100
MnO2+Fe2O3(wt%)	0.6	3.9	2.8	3.1	1.5	0.6	5.8	0.5	0.4	1.4

Traverse Point	41	42	43	44	45	46	47	48	49	50
Na2O(wt%)	2.0	1.7	2.8	2.4	2.0	1.8	3.0	1.5	2.1	4.1
MgO(wt%)	0.1	0.1	0.1	5.8	0.2	0.1	0.2	0.2	0.2	0.5
Al2O3(wt%)	25	22	25	24	25	25	25	26	26	22
SiO2(wt%)	68	71	67	38	67	66	68	66	67	66
K2O(wt%)	3.4	3.3	3.4	1.5	3.0	3.4	3.2	3.1	2.8	3.5
CaO(wt%)	0.3	0.2	0.2	0.2	0.3	0.3	0.3	0.3	0.1	0.4
TiO2(wt%)	0.3	0.4	0.2	0.2	0.3	0.2	0.3	0.3	0.2	0.1
MnO2(wt%)	0.1	0.0	0.1	0.8	0.1	0.1	0.1	0.4	0.0	-0.1
Fe2O3(wt%)	0.3	0.3	0.9	29	0.2	1.9	2.5	0.9	0.2	3.4
SO3(wt%)	-0.0	-0.1	0.2	0.5	0.1	0.2	-0.6	0.4	0.1	0.5
ZnO(wt%)	-0.2	0.1	0.0	0.4	0.2	-0.4	0.2	0.1	0.2	0.1
Total(wt%)	99	99	100	101	98	98	102	99	100	100
MnO2+Fe2O3(wt%)	0.4	0.3	0.9	30	0.3	1.9	2.7	1.3	0.3	3.4

Traverse Point	51	52	53	54	55	56	57	58	59	60
Na2O(wt%)	3.2	1.4	1.6	2.8	2.4	2.0	1.7	1.7	7.5	1.6
MgO(wt%)	0.1	0.2	-0.1	0.1	0.4	0.1	0.2	0.3	0.3	0.2
Al2O3(wt%)	35	48	24	30	35	22	32	40	21	23
SiO2(wt%)	56	46	70	62	61	71	61	55	59	71
K2O(wt%)	3.9	2.2	2.8	3.0	2.6	3.0	2.3	2.2	6.1	2.4
CaO(wt%)	0.2	0.1	0.2	0.1	0.1	0.3	0.1	0.2	0.8	0.2
TiO2(wt%)	0.2	0.1	0.1	0.2	0.1	0.3	0.3	0.0	0.1	0.2
MnO2(wt%)	0.1	-0.0	0.1	0.0	0.0	0.0	-0.0	0.2	0.1	0.0
Fe2O3(wt%)	0.5	0.6	0.6	0.4	0.4	0.4	0.5	0.6	1.2	0.5
SO3(wt%)	0.4	0.5	0.3	-0.1	0.0	0.2	-0.1	0.1	7.4	0.1
ZnO(wt%)	-0.0	-0.2	-0.4	0.2	0.2	-0.3	0.1	-0.0	0.0	0.1
Total(wt%)	100	98	99	99	102	99	99	100	100	100
MnO2+Fe2O3(wt%)	0.6	0.5	0.8	0.4	0.4	0.4	0.4	0.7	1.3	0.6

Appendix 1.1:**Elemental Microprobe traverses done on pebble collected from site SJS2
in May, 2002.**

Traverse Point	1	2	3	4	5	6	7	8	9	10
Na ₂ O(wt%)	1.0	0.4	0.4	1.7	7.2	2.9	0.8	1.2	0.6	3.8
MgO(wt%)	0.6	0.7	0.4	2.1	0.5	0.8	0.7	0.6	1.8	0.3
Al ₂ O ₃ (wt%)	7.6	16	8.9	18	17	13	17	19	16	14
SiO ₂ (wt%)	14	60	55	32	68	26	21	12	67	72
K ₂ O(wt%)	1.2	5.4	1.0	2.6	1.9	1.0	1.2	1.1	3.6	2.4
CaO(wt%)	0.7	0.3	0.5	0.8	0.1	0.5	0.8	0.8	0.0	0.2
TiO ₂ (wt%)	0.6	0.9	0.5	0.3	0.2	0.3	0.3	0.1	0.0	0.9
MnO ₂ (wt%)	72	3.5	17	28	0.9	42	35	34	2.2	1.0
Fe ₂ O ₃ (wt%)	13	14	18	19	2.9	20	26	39	10	3.8
SO ₃ (wt%)	0.9	0.7	1.2	2.6	0.2	1.2	4.7	1.7	0.2	0.6
ZnO(wt%)	1.2	0.3	0.7	0.2	-0.1	0.3	1.1	0.6	0.1	-0.3
Total(wt%)	98	99	98	100	99	98	99	99	100	98
MnO ₂ +Fe ₂ O ₃ (wt%)	85	17	35	47	3.8	61	61	73	13	4.8

Traverse Point	11	12	13	14	15	16	17	18	19	20
Na ₂ O(wt%)	1.7	1.5	2.3	0.4	6.3	0.3	0.3	0.1	1.0	6.2
MgO(wt%)	0.8	0.9	1.1	1.2	1.1	2.6	1.7	3.2	0.9	0.3
Al ₂ O ₃ (wt%)	18	18	13	24	20	19	31	26	8.1	15
SiO ₂ (wt%)	28	12	50	36	54	20	50	42	58	47
K ₂ O(wt%)	1.7	1.0	2.0	7.3	2.4	3.5	9.5	7.4	3.9	0.9
CaO(wt%)	0.4	0.8	0.6	0.3	0.5	0.4	0.0	0.0	0.5	0.2
TiO ₂ (wt%)	0.5	0.1	0.5	0.3	0.7	0.4	0.8	0.6	1.5	0.2
MnO ₂ (wt%)	16	9.4	23	5.5	1.0	2.3	0.3	1.4	2.6	0.6
Fe ₂ O ₃ (wt%)	37	59	12	27	15	56	7.5	22	26	31
SO ₃ (wt%)	2.2	5.2	1.0	1.7	0.7	1.6	0.3	0.2	0.5	0.7
ZnO(wt%)	-0.0	-0.0	0.1	0.1	0.1	-0.5	-0.1	0.1	0.1	-0.1
Total(wt%)	98	98	100	99	99	98	100	100	100	98
MnO ₂ +Fe ₂ O ₃ (wt%)	52.5	68.1	35.0	32.3	15.8	57.8	7.7	24	29	31

Traverse Point	21	22	23	24	25	26	27	28	29	30
Na ₂ O(wt%)	0.6	0.5	0.6	0.5	0.9	0.2	2.9	0.1	0.5	0.4
MgO(wt%)	1.2	0.8	0.5	1.0	0.6	0.5	1.3	1.2	1.7	0.5
Al ₂ O ₃ (wt%)	21	15	13	26	12	14	17	17	17	12
SiO ₂ (wt%)	57	27	41	33	39	34	50	53	37	33
K ₂ O(wt%)	7.0	6.1	2.3	8.5	0.8	6.7	2.7	5.7	3.7	2.7
CaO(wt%)	0.2	0.1	0.2	0.3	0.5	0.3	0.1	0.0	0.1	0.1
TiO ₂ (wt%)	0.4	0.6	0.1	7.1	0.4	0.9	0.1	0.5	0.3	2.4
MnO ₂ (wt%)	0.6	3.8	0.2	0.7	0.5	1.3	0.9	0.5	6.1	6.5
Fe ₂ O ₃ (wt%)	9.3	49	45	24	49	45	25	24	37	46
SO ₃ (wt%)	0.6	1.4	1.5	1.2	1.7	1.1	0.6	0.6	1.2	1.2
ZnO(wt%)	0.2	0.6	0.3	0.5	0.0	0.2	0.1	0.1	0.2	-0.2
Total(wt%)	98	99	99	100	100	99	99	100	99	99
MnO ₂ +Fe ₂ O ₃ (wt%)	9.9	53	45	25	49	47	26	24	43	52

Appendix 1.1:
Elemental Microprobe traverses done on pebble collected from site SJS2
in May, 2002.

Traverse Point	31	32	33	34	35	36	37	38	39	40
Na2O(wt%)	1.0	0.1	0.2	0.0	0.4	0.2	1.9	0.6	0.4	1.0
MgO(wt%)	1.1	0.2	0.2	0.3	0.3	1.8	1.5	2.0	0.6	1.2
Al2O3(wt%)	19	14	17	16	6.06	30	19	19	8.46	18
SiO2(wt%)	24	3.1	13	6.8	71	39	45	32	54	18
K2O(wt%)	2.9	0.3	0.3	1.0	1.0	3.8	3.0	1.1	1.4	1.1
CaO(wt%)	0.2	0.2	0.2	0.2	0.2	0.0	0.2	0.0	0.1	0.1
TiO2(wt%)	0.5	0.0	0.0	0.1	0.3	0.5	0.4	0.2	0.2	0.2
MnO2(wt%)	12	14	28	32	9.7	7.1	10	14	2.9	5.0
Fe2O3(wt%)	43	74	49	52	14	19	19	35	33	58
SO3(wt%)	1.7	2.0	1.8	2.3	0.4	0.8	1.6	1.6	1.5	1.6
ZnO(wt%)	0.3	0.9	0.2	0.5	0.7	-0.1	-0.0	0.0	0.1	1.0
Total(wt%)	99	98	99	99	101	99	97	98	98	97
MnO2+Fe2O3(wt%)	55	88	76	84	24	26	29	49	36	63

Traverse Point	41	42	43	44	45	46	47	48	49	50
Na2O(wt%)	0.4	0.6	-0.0	0.2	0.1	0.5	0.2	0.1	0.6	0.7
MgO(wt%)	1.1	1.3	0.4	0.4	0.4	0.4	0.2	0.6	0.3	0.6
Al2O3(wt%)	12	23	13	14	19	14	12	12	14	10
SiO2(wt%)	54	50	49	30	8.8	29	16	54	35	78
K2O(wt%)	1.6	6.4	2.3	2.0	0.6	0.3	0.7	3.0	2.7	2.8
CaO(wt%)	0.1	0.2	0.1	-0.1	0.2	0.1	0.2	0.2	0.1	0.1
TiO2(wt%)	1.0	0.8	0.4	0.2	0.1	0.3	0.5	0.8	0.7	0.4
MnO2(wt%)	2.1	1.6	2.9	8.7	4.9	5.4	5.3	2.8	3.2	0.4
Fe2O3(wt%)	29	17	35	49	69	53	70	29	48	8.3
SO3(wt%)	0.9	0.5	1.1	1.5	2.3	1.6	1.8	0.7	0.9	0.2
ZnO(wt%)	0.2	0.1	0.5	0.1	0.2	-0.1	0.0	0.4	0.6	-0.1
Total(wt%)	99	99	100	99	97	98	98	99	100	100
MnO2+Fe2O3(wt%)	31	19	37	58	74	59	75	32	51	8.7

Traverse Point	51	52	53	54	55	56	57	58	59	60
Na2O(wt%)	0.8	3.3	3.0	0.2	1.3	6.3	0.5	0.4	0.2	2.2
MgO(wt%)	2.2	3.3	2.5	1.1	0.7	0.8	1.1	0.9	0.9	0.7
Al2O3(wt%)	20	22	15	26	18	17	25	14	18	13
SiO2(wt%)	37	43	52	33	42	60	49	62	57	53
K2O(wt%)	3.6	2.5	2.0	7.3	4.6	0.6	9.1	6.0	5.6	4.9
CaO(wt%)	0.1	0.1	1.0	0.0	0.1	0.1	0.1	0.0	0.1	0.1
TiO2(wt%)	0.3	0.5	0.4	0.2	0.5	0.2	0.3	0.5	0.3	5.3
MnO2(wt%)	2.0	0.9	3.0	1.3	1.7	0.6	0.3	0.7	1.0	0.8
Fe2O3(wt%)	35	26	22	32	32	16	14	17	16	21
SO3(wt%)	1.0	0.4	0.9	1.0	1.0	0.4	0.5	0.2	1.1	0.6
ZnO(wt%)	0.1	-0.1	-0.1	0.3	-0.1	-0.2	-0.0	-0.3	0.7	-0.2
Total(wt%)	99	99	99	99	98	100	99	99	100	99
MnO2+Fe2O3(wt%)	37	27	25	33	34	17	14	17	17	22

Appendix 1.1:**Elemental Microprobe traverses done on polished pebble collected from site SJS2 in May, 2002.**

Traverse Point	1	2	3	4	5	6	7	8	9	10
Na2O(wt%)	0.0	0.8	0.1	-0.1	0.1	0.1	0.1	1.1	0.2	0.3
MgO(wt%)	0.0	0.4	0.2	0.0	-0.0	0.1	0.0	0.6	0.2	0.1
Al2O3(wt%)	0.8	2.9	2.0	0.4	0.6	0.4	0.7	3.2	1.4	2.1
SiO2(wt%)	99	90	94	98	99	98	99	88	97	94
K2O(wt%)	-0.2	0.3	0.0	-0.3	-0.3	-0.4	-0.2	0.3	-0.1	-0.1
CaO(wt%)	-0.2	0.2	0.1	-0.2	-0.2	-0.2	-0.1	3.6	0.1	1.5
TiO2(wt%)	0.0	0.1	0.1	-0.1	-0.0	-0.0	0.1	0.1	0.1	-0.1
MnO2(wt%)	0.1	0.2	0.0	-0.0	0.1	0.0	-0.0	0.2	0.0	0.4
Fe2O3(wt%)	0.6	4.4	2.4	0.2	0.3	0.2	0.9	2.2	0.8	1.4
SO3(wt%)	0.1	0.4	0.1	0.1	0.1	0.1	0.0	0.3	0.6	0.3
ZnO(wt%)	-0.1	0.3	0.2	0.1	-0.1	0.2	0.1	0.2	0.4	-0.0
Total(wt%)	100	99	99	98	100	98	100	99	100	99
MnO2+Fe2O3(wt%)	0.7	4.7	2.4	0.2	0.3	0.2	0.9	2.4	0.8	1.8

Traverse Point	11	12	13	14	15	16	17	18	19	20
Na2O(wt%)	0.1	0.3	0.0	-0.0	0.0	0.1	-0.0	-0.0	0.1	0.1
MgO(wt%)	0.2	0.0	0.1	0.1	0.1	0.4	0.1	-0.1	0.1	0.0
Al2O3(wt%)	1.6	0.1	0.3	0.5	0.4	1.4	0.3	0.3	1.0	0.4
SiO2(wt%)	96	99	98	98	98	95	99	100	97	100
K2O(wt%)	0.1	-0.3	-0.3	-0.3	-0.4	-0.1	-0.4	-0.4	-0.1	-0.3
CaO(wt%)	0.1	-0.2	-0.2	-0.1	-0.1	-0.2	-0.2	-0.2	-0.0	-0.1
TiO2(wt%)	0.0	-0.1	-0.0	0.1	-0.0	0.3	0.1	0.0	0.1	0.0
MnO2(wt%)	0.1	0.3	0.1	0.1	-0.0	-0.1	0.0	-0.1	0.2	0.1
Fe2O3(wt%)	1.9	-0.1	0.1	0.3	0.1	1.2	0.2	0.0	2.3	0.2
SO3(wt%)	0.1	0.0	0.0	0.0	0.0	-0.0	0.1	0.0	-0.0	0.0
ZnO(wt%)	-0.2	-0.1	-0.1	0.1	0.0	-0.3	-0.2	0.2	0.4	0.0
Total(wt%)	100	99	98	99	98	98	99	100	101	100
MnO2+Fe2O3(wt%)	2.0	0.2	0.2	0.4	0.0	1.1	0.2	-0.1	2.5	0.3

Traverse Point	21	22	23	24	25	26	27	28	29	30
Na2O(wt%)	0.2	-0.2	0.7	-0.0	0.2	0.1	0.3	0.2	0.0	0.2
MgO(wt%)	0.1	0.0	0.2	-0.0	0.0	-0.1	0.0	0.0	0.0	0.2
Al2O3(wt%)	0.5	0.2	2.3	0.4	0.5	0.3	1.4	1.0	0.4	0.5
SiO2(wt%)	99	100	90	100	99	98	91	98	99	98
K2O(wt%)	-0.3	-0.3	0.4	-0.3	-0.3	-0.3	0.1	-0.2	-0.3	-0.3
CaO(wt%)	-0.2	-0.2	1.2	-0.2	-0.1	-0.2	0.2	-0.2	-0.2	-0.1
TiO2(wt%)	0.0	-0.0	0.0	0.1	-0.1	-0.1	0.0	0.2	0.0	0.1
MnO2(wt%)	-0.1	0.0	0.4	-0.0	-0.1	0.0	-0.1	-0.0	0.1	-0.0
Fe2O3(wt%)	0.1	0.1	2.6	-0.0	0.3	0.0	5.7	0.9	0.3	0.2
SO3(wt%)	-0.0	0.1	0.6	-0.0	0.0	-0.0	0.2	0.0	0.1	0.1
ZnO(wt%)	-0.1	-0.1	0.1	0.2	-0.0	0.0	-0.2	-0.2	0.3	-0.1
Total(wt%)	99	99	98	100	99	98	98	100	100	99
MnO2+Fe2O3(wt%)	-0.0	0.1	3.1	-0.1	0.3	0.0	5.6	0.9	0.4	0.2

Appendix 1.1:**Elemental Microprobe traverses done on polished pebble collected from site SJS2 in May, 2002.**

Traverse Point	31	32	33	34	35	36	37	38	39	40
Na2O(wt%)	0.1	0.2	0.1	0.2	0.4	0.1	0.4	0.1	0.2	0.0
MgO(wt%)	0.1	0.1	0.2	0.1	0.4	-0.0	0.4	0.0	0.5	0.1
Al2O3(wt%)	1.0	0.3	1.2	1.1	4.2	0.3	2.4	0.6	1.8	0.7
SiO2(wt%)	97	99	97	98	88	99	93	98	95	98
K2O(wt%)	-0.2	-0.3	-0.2	-0.2	0.5	-0.3	0.2	-0.3	0.1	-0.2
CaO(wt%)	-0.2	-0.2	-0.0	-0.1	0.5	-0.2	0.2	-0.2	-0.1	-0.1
TiO2(wt%)	-0.1	-0.0	-0.0	0.0	0.1	0.1	0.1	-0.0	-0.0	-0.2
MnO2(wt%)	-0.1	-0.1	0.1	-0.0	0.2	0.0	0.2	0.0	-0.1	-0.0
Fe2O3(wt%)	0.8	0.2	1.0	0.7	6.0	0.1	3.0	0.2	2.1	0.8
SO3(wt%)	-0.0	0.1	0.3	0.0	0.1	0.0	0.3	0.0	0.1	0.1
ZnO(wt%)	0.2	0.1	0.1	-0.1	0.1	-0.3	-0.1	-0.1	0.2	0.2
Total(wt%)	99	99	100	100	100	98	100	99	99	99
MnO2+Fe2O3(wt%)	0.7	0.1	1.1	0.6	6.2	0.1	3.1	0.2	2.0	0.7

Traverse Point	41	42	43	44	45	46	47	48	49	50
Na2O(wt%)	-0.1	0.1	0.0	0.0	0.1	0.2	0.1	0.0	0.1	0.1
MgO(wt%)	-0.0	0.1	-0.1	-0.0	0.0	0.2	0.3	0.1	0.2	-0.1
Al2O3(wt%)	0.3	0.8	0.5	0.5	0.4	0.4	0.4	0.6	1.3	0.4
SiO2(wt%)	100	99	98	98	98	98	97	97	98	98
K2O(wt%)	-0.4	-0.2	-0.3	-0.3	-0.3	-0.3	-0.3	-0.3	-0.1	-0.3
CaO(wt%)	-0.2	0.0	-0.1	-0.1	-0.2	0.4	0.4	0.0	-0.0	-0.1
TiO2(wt%)	0.1	-0.0	0.1	-0.1	-0.1	0.0	-0.1	0.0	-0.0	0.0
MnO2(wt%)	0.1	0.2	-0.0	-0.0	0.2	-0.0	-0.1	0.1	-0.1	0.0
Fe2O3(wt%)	-0.1	0.3	0.9	0.4	0.3	0.4	0.1	0.8	0.9	0.5
SO3(wt%)	0.1	0.1	0.0	0.1	0.2	1.1	1.5	0.5	0.0	0.1
ZnO(wt%)	0.2	-0.1	0.1	0.2	-0.3	-0.1	-0.1	-0.1	0.2	-0.0
Total(wt%)	100	100	99	98	99	100	99	99	100	99
MnO2+Fe2O3(wt%)	0.0	0.5	0.9	0.4	0.4	0.4	0.1	1.0	0.8	0.5

Traverse Point	51	52	53	54	55	56	57	58	59	60
Na2O(wt%)	0.2	0.1	0.3	-0.0	-0.0	0.2	0.1	-0.0	0.0	0.6
MgO(wt%)	0.2	0.1	0.1	0.1	-0.0	0.3	0.7	0.1	0.0	0.5
Al2O3(wt%)	2.0	1.4	1.2	0.6	0.7	2.2	2.4	1.2	0.3	3.7
SiO2(wt%)	96	98	97	99	98	95	93	98	98	89
K2O(wt%)	-0.1	-0.1	-0.2	-0.3	-0.3	0.1	-0.0	0.1	-0.3	0.9
CaO(wt%)	0.2	-0.1	0.1	-0.1	-0.1	-0.1	0.1	-0.0	-0.1	0.2
TiO2(wt%)	0.0	0.1	0.0	-0.0	0.1	0.1	0.1	0.1	0.0	0.1
MnO2(wt%)	0.1	-0.0	0.1	0.1	0.1	0.2	0.1	0.2	-0.1	0.3
Fe2O3(wt%)	1.3	0.5	0.5	0.3	0.1	2.4	4.1	0.5	0.0	4.6
SO3(wt%)	0.2	0.0	0.2	-0.0	0.1	0.2	0.1	0.2	0.0	0.2
ZnO(wt%)	-0.1	0.2	0.2	-0.1	0.3	0.0	-0.1	0.2	0.0	-0.1
Total(wt%)	100	100	100	100	99	100	100	100	98	99
MnO2+Fe2O3(wt%)	1.4	0.5	0.5	0.3	0.2	2.6	4.1	0.7	-0.1	4.9

Appendix 1.2: LA-ICP-MS Optimization**Concentrations (ppm) obtained by LA-ICP-MS analysis of TCS 13.1.2 with varying focal height and ½ wave plate setting.**

Analysis#	1	2	3	4
Al ₂ O ₃ *	8.7	9.4	7.0	7.1
SiO ₂ *	29	25	15	19
CaO*	1.5	1.5	1.3	1.4
TiO ₂ *	0.29	0.27	0.36	0.09
MnO ₂ *	0.13	0.14	0.10	0.10
Fe ₂ O ₃ *	99	99	99	99
V	163	195	117	139
Cr	814	752	792	769
Co	244	230	242	248
Ni	220	226	170	210
Cu	56944	55988	50612	51233
Zn	9232	8047	8943	9775
As	206	294	126	141
Se	2.65	3.68	2.87	0.00
Sr	99.2	93.6	95.4	95.4
Y	66.0	10.9	7.83	9.69
Ag	1.89	0.57	1.37	1.07
Cd	12.4	12.3	13.2	13.0
Sn	1.39	0.73	0.48	0.76
Ba	70.7	64	63.9	69.3
La	6.28	3.84	3.77	5.00
Ce	17.5	12	11.3	14.2
Au	<.013	<.018	<.011	<.005
Hg				
²⁰⁶ Pb	51.4	65.9	49.5	51.8
²⁰⁷ Pb	44.6	59.8	46.3	48.3
²⁰⁸ Pb	41.4	60.8	47.9	49.6
Bi	0.05	0.08	0.06	0.12
Th	0.69	0.70	0.68	0.75
U	14.1	9.36	9.19	11.5

* = Concentration in wt%

Appendix 1.2: LA-ICP-MS Optimization**Concentrations (ppm) obtained by LA-ICP-MS analysis of TCS 13.1.2 with varying focal height and ½ wave plate setting.**

Analysis#	5	6	7	8
Al ₂ O ₃ *	5.3	6.4	4.7	4.2
SiO ₂ *	9.6	14	9.5	4.9
CaO*	1.62	1.68	1.51	1.46
TiO ₂ *	0.04	0.08	0.05	0.01
MnO ₂ *	0.06	0.09	0.06	0.05
Fe ₂ O ₃ *	100	100	100	100
V	38.3	94.5	46.7	18.6
Cr	777	722	755	799
Co	240	237	385	233
Ni	150	173	230	154
Cu	52637	43564	53095	59645
Zn	9240	9214	8789	9116
As	109	103	164	115
Se	2.50	3.68	5.56	0.00
Sr	110	110	108	103
Y	13.5	10.9	8.97	10.2
Ag	5.55	2.84	1.32	1.28
Cd	13.0	13.3	13.2	14.0
Sn	2.22	3.51	0.65	0.50
Ba	72	75.0	70.1	70
La	6.53	5.01	4.56	5.06
Ce	16.7	13	13	13.0
Au	<0.02	<0.030	<0.004	<0.025
Hg				
²⁰⁶ Pb	45.1	39.7	50.9	42.1
²⁰⁷ Pb	40.5	37.6	46.3	38.4
²⁰⁸ Pb	42.6	35.2	48.0	40.3
Bi	0.06	0.04	0.44	0.06
Th	0.80	0.70	0.74	0.68
U	11.9	8.58	9.74	9.68

* = Concentration in wt%

**Appendix 2.1: Element concentrations in Water Samples (ppb); dp = field duplicate,
* = split sample, () indicates values below detection limit.**

Month						
Sample	TCWS1	TCWS1*	TCWS2	TCWS3	TCWS4	TCWS4dp
Li 6	0.12	(0.18)	0.19	0.15	32.2	0.26
Li 7	0.15	0.19	0.18	0.16	36.9	0.28
Be	(0.02)	(0.05)	(0.11)	(0.04)	(0.02)	(0.32)
B	(4.89)	(8.85)	(7.29)	(3.69)	(2.80)	(3.72)
C (cps)	806755632	920233910	1299124367	909961374	728905598	619419253
N (cps)	114485670	102382645	117780833	111431091	113905934	112027007
Mg	4564	4195	1554	1485	1505	1507
Al	22.5	28.6	32.5	28.6	26.3	28.4
Si	(854)	(965)	(920)	(661)	(560)	(474)
P	(120)	(306)	(286)	(122)	(1464)	(113)
S	(89.0)	(2550)	(371)	(2000)	(173)	(15.8)
Cl	6674	7354	6562	5904	6482	6313
Ca 42	7952	5541	7903	5774	6917	5342
Ca 43	7303	7244	6387	6033	6292	6218
Ti	(0.14)	(0.26)	(0.14)	(0.09)	(0.04)	(0.17)
V	1.62	0.96	0.67	(0.09)	(0.00)	5.67
Cr 52	(2.61)	(4.45)	(7.89)	(2.25)	(18.0)	(18.0)
Cr 53	(1.11)	(1.19)	(1.06)	(0.37)	(0.17)	(0.03)
Fe 54	35.2	(20.8)	(27.4)	(8.76)	(4.66)	(14.5)
Mn	6.52	6.27	3.26	2.09	1.46	2.06
Fe 56	(67.8)	<321	(129)	(16.6)	(31.0)	(25.1)
Fe 57	(38.2)	(23.3)	(26.0)	(1.84)	(9.13)	(1.68)
Co	(0.08)	(0.06)	(0.02)	(0.002)	(0.01)	(0.06)
Ni	3.60	3.25	1.08	(0.53)	(0.86)	4.08
Cu	6.88	7.07	2.14	1.98	2.38	4.08
Zn	12.9	18.5	(3.53)	(3.00)	7.17	18.4
As	0.57	0.55	0.14	0.16	0.15	0.16
Br	(20.8)	(18.0)	(23.6)	(18.5)	(19.5)	(19.7)
Se	(0.13)	(0.17)	(0.09)	(0.09)	(0.09)	(0.09)
Rb	0.93	1.16	(0.35)	(0.29)	(0.39)	0.63
Sr	18.6	17.8	21.5	20.9	21.3	20.8
Mo	0.10	0.07	(0.03)	(0.03)	(0.03)	(0.04)
Ag	(0.03)	(0.02)	(0.02)	(0.01)	(0.02)	(0.03)
Cd	0.08	0.06	0.03	(0.002)	(0.01)	0.07
Sn	0.53	0.50	(0.12)	(0.14)	(0.07)	(0.24)
Sb	0.17	0.16	0.05	0.03	0.03	0.05
I	6.44	7.06	6.93	6.34	6.16	5.88
Cs	(0.01)	(0.002)	(0.002)	(0.003)	(0.004)	(0.003)
Ba	(2.46)	(2.14)	10.1	10.2	10.1	10.1
La	0.01	0.01	0.02	0.02	0.02	0.02
Ce	0.01	0.02	0.04	0.03	0.03	0.04
Hg	(0.01)	(0.003)	(0.01)	(0.01)	(0.01)	(0.01)
Tl	0.15	0.17	0.15	0.12	0.13	0.14
Pb	0.50	0.59	0.18	0.07	0.09	0.42
Bi	(0.004)	(0.001)	(0.01)	(0.01)	(0.01)	(0.001)
U	0.04	0.03	0.14	0.12	0.12	0.11

**Appendix 2.1: Element concentrations in Water Samples (ppb); dp = field duplicate,
* = split sample, () indicates values below detection limit.**

Month						
Sample	TCWS5	TCWS6	TCWS6*	TCWS7	TCWS8	TCWS9
Li 6	0.20	0.21	77.9	0.24	0.29	0.60
Li 7	0.20	0.20	89.0	0.21	0.24	0.55
Be	(0.02)	(0.02)	(0.32)	(0.12)	(0.16)	(0.60)
B	(3.40)	(5.32)	29.3	(9.69)	18.3	28.4
C (cps)	824211761	838943894	774915339	1262388311	1515789803	0
N (cps)	109520926	117533382	112029707	115444439	115974724	124970309
Mg	1450	1488	1591	1597	2810	9774
Al	26.2	30.0	33.0	31.4	26.7	24.5
Si	(561)	(544)	(413)	(824)	(1083)	2659
P	(35.1)	(11.4)	(260)	(395)	(385)	(963)
S	(2000)	(2000)	(502)	(306)	(88.0)	(2291)
Cl	6005	6387	6992	6324	6954	9857
Ca 42	4821	5798	6396	4797	6649	23102
Ca 43	6127	7408	6509	6001	6794	22079
Ti	(0.14)	(0.14)	(0.26)	(0.17)	(0.23)	0.74
V	1.34	(0.55)	0.41	0.60	1.04	(0.26)
Cr 52	(1.33)	(1.06)	(18.0)	(11.7)	(11.6)	54.5
Cr 53	(0.31)	(0.29)	2.05	(4.74)	(1.61)	17.6
Fe 54	(14.5)	(14.5)	(12.4)	(12.2)	(14.0)	66.2
Mn	1.25	1.61	1.78	1.73	0.99	24.6
Fe 56	(157)	(159)	(171)	(67.9)	(23.6)	(164)
Fe 57	(55.5)	(2.07)	(19.8)	(15.0)	(56.0)	(72.9)
Co	(0.01)	(0.01)	(0.11)	(0.09)	(0.05)	2.06
Ni	1.08	0.83	1.06	5.53	2.13	19.0
Cu	2.84	3.23	4.84	4.12	4.76	17.5
Zn	5.39	15.9	14.0	11.8	19.0	27.8
As	0.14	0.14	0.15	0.11	0.14	1.00
Br	(18.4)	(16.2)	(19.1)	(21.9)	(20.6)	(28.3)
Se	(0.06)	(0.09)	(0.18)	(0.09)	(0.09)	0.25
Rb	0.45	0.45	0.79	0.59	0.75	0.59
Sr	21.2	21.7	22.2	21.2	23.9	78.1
Mo	(0.03)	(0.01)	0.004	0.36	0.05	2.46
Ag	(0.03)	(0.03)	(0.71)	(0.03)	(0.01)	(0.03)
Cd	0.02	0.02	0.01	0.02	0.03	0.04
Sn	(0.13)	(0.06)	0.22	0.33	(0.24)	(0.004)
Sb	0.05	0.04	0.04	0.04	0.08	0.50
I	5.98	6.38	6.85	6.38	5.74	8.13
Cs	(0.002)	(0.00005)	(0.06)	(0.0004)	(0.0003)	(0.04)
Ba	10.4	9.88	(12.0)	10.3	11.1	22.9
La	0.02	0.02	0.02	0.05	0.02	0.01
Ce	0.03	0.03	0.03	0.06	0.02	0.01
Hg	(0.01)	(0.01)	(0.01)	(0.01)	(0.01)	(0.01)
Tl	0.14	0.16	0.16	0.14	0.15	0.27
Pb	0.14	0.17	0.26	0.27	0.96	0.10
Bi	(0.01)	(0.01)	(0.01)	(0.01)	(0.01)	(0.01)
U	0.11	0.11	0.11	0.08	0.06	0.10

**Appendix 2.1: Element concentrations in Water Samples (ppb); dp = field duplicate,
* = split sample, () indicates values below detection limit.**

Month						
Sample	TCWS10	TCWS11	TCWS12	TCWS13	TCWS14	TCWS15
Li 6	0.60	0.55	2.04	656	1.81	1.60
Li 7	0.54	0.57	2.08	661	1.79	1.63
Be	(0.45)	(0.32)	(0.32)	(0.07)	(0.32)	(0.32)
B	26.1	(11.6)	(11.0)	971	26.8	(17.7)
C (cps)	0	575471672	671071043	538124724	561127967	885914075
N (cps)	122891237	118691885	114074606	107152301	108247216	116889405
Mg	9025	9756	21252	36792	12095	15141
Al	33.8	27.4	16.6	64.5	31.0	27.6
Si	2182	(309)	(1614)	3213	(711)	(947)
P	(554)	(414)	(627)	(991)	(271)	(318)
S	(1473)	(2093)	18459	40549	8204	8137
Cl	9162	9662	7605	7580	8574	9610
Ca 42	20292	22406	92874	217386	40731	53280
Ca 43	20801	22049	93008	222719	40658	55536
Ti	0.69	0.72	4.76	12.6	2.05	2.66
V	(0.48)	(0.26)	1.19	0.66	(0.35)	0.90
Cr 52	(32.1)	(18.0)	(18.0)	(18.0)	(18.0)	(18.0)
Cr 53	(3.42)	(0.68)	(2.05)	(0.71)	(2.05)	(2.05)
Fe 54	(15.0)	(24.4)	(4.41)	3134	111	90.7
Mn	31.4	33.0	38.8	2043	244	409
Fe 56	(57.8)	(145)	(327)	771	(248)	(103)
Fe 57	(8.73)	(28.6)	(6.20)	3007	(146)	(66.8)
Co	2.66	2.87	13.3	372	43.5	65.8
Ni	7.27	8.24	16.5	119	21.6	25.8
Cu	15.4	18.9	72.9	1364	87.8	81.3
Zn	31.6	38.3	115	2640	398	424
As	0.87	0.86	0.89	0.45	0.74	0.68
Br	(27.9)	(25.5)	(22.7)	(23.9)	(22.7)	(19.8)
Se	(0.15)	(0.10)	3.20	1.37	0.38	0.42
Rb	0.63	0.81	1.22	2.62	0.95	1.26
Sr	72.6	76.4	320	730	145	189
Mo	0.40	0.43	1.74	0.44	0.42	0.42
Ag	(0.03)	(0.03)	(0.03)	(0.03)	(0.03)	(0.03)
Cd	0.05	0.06	0.33	2.77	0.37	0.50
Sn	0.76	(0.23)	(0.20)	0.40	0.29	0.34
Sb	0.47	0.47	1.72	0.46	0.51	0.49
I	8.34	8.65	(1.76)	(1.69)	7.08	6.52
Cs	(0.04)	(0.04)	(0.10)	0.22	(0.05)	(0.07)
Ba	22.2	24.4	9.69	16.4	22.8	22.4
La	(0.002)	0.01	(0.004)	0.14	0.01	0.01
Ce	(0.00)	0.01	0.00	0.22	0.01	0.01
Hg	(0.02)	(0.01)	(0.01)	(0.01)	(0.01)	(0.004)
Tl	0.29	0.26	0.24	0.25	0.29	0.29
Pb	0.08	0.20	0.16	0.22	0.15	0.26
Bi	(0.01)	(0.01)	(0.01)	(0.0001)	(0.01)	(0.01)
U	0.10	0.10	0.09	0.18	0.11	0.11

**Appendix 2.1: Element concentrations in Water Samples (ppb); dp = field duplicate,
* = split sample, () indicates values below detection limit.**

Month						
Sample	TCWS15dp	BCWS1	BCWS1*	BCWS2	BCWS3	BCWS4
Li 6	1.49	0.77	1.10	0.72	1.12	0.70
Li 7	1.53	0.73	0.96	0.55	1.01	0.75
Be	(0.06)	(0.07)	(0.08)	(0.02)	0.21	(0.03)
B	20.9	(2.83)	7.12	5.50	7.32	6.53
C (cps)	1227141841	52910254	63435188	66245614	66304480	66432663
N (cps)	114188583	249466512	269236894	251724384	260690909	264831340
Mg	15660	7284	8190	5313	11599	7068
Al	46.1	1794	2146	227	3170	1256
Si	(1214)	3714	4307	2981	5344	2576
P	(498)	(793)	(2206)	(957)	(1010)	(1069)
S	8983	5348	6696	3922	21847	5178
Cl	9537	3701	4255	3509	3102	3064
Ca 42	56118	17499	20105	15051	19752	17120
Ca 43	56904	16844	17475	14191	18776	17551
Ti	2.93	3.57	3.87	2.28	64.3	3.51
V	0.26	0.20	0.55	0.22	1.22	0.17
Cr 52	(2.39)	(0.53)	0.87	(0.51)	2.83	0.69
Cr 53	(0.67)	1.04	1.29	0.44	3.84	1.05
Fe 54	123	622	745	247	1161	641
Mn	417	244	270	172	412	240
Fe 56	(198)	719	701	(345)	1078	721
Fe 57	(124)	649	747	236	1205	652
Co	67.4	23.9	25.6	15.6	24.8	22.7
Ni	26.6	16.5	24.3	35.7	17.7	15.3
Cu	86.4	2405	2516	1078	2425	1656
Zn	509	853	909	568	960	810
As	0.74	(0.10)	(0.09)	(0.07)	0.20	(0.09)
Br	(24.5)	(3.78)	(57.5)	(12.7)	(57.5)	(2.37)
Se	0.57	0.89	1.44	(0.55)	1.22	0.84
Rb	1.26	0.62	0.69	0.42	0.56	0.41
Sr	187	19.0	20.1	14.5	24.4	18.2
Mo	0.41	(0.001)	0.02	(0.004)	0.06	(0.002)
Ag	(0.03)	(0.01)	(0.02)	(0.003)	(0.02)	(0.001)
Cd	0.50	1.44	1.60	1.00	1.65	1.45
Sn	(0.10)	(0.19)	(0.39)	(0.31)	0.65	(0.09)
Sb	0.48	0.07	0.07	0.04	0.07	0.03
I	6.68	(4.89)	(9.22)	(6.51)	(6.13)	(5.11)
Cs	(0.06)	0.06	0.06	0.04	0.07	0.06
Ba	22.2	2.81	2.75	2.02	22.1	2.40
La	0.01	0.35	0.38	0.18	2.27	0.35
Ce	0.01	0.70	0.72	0.33	3.49	0.69
Hg	(0.004)	(0.03)	(0.03)	(0.03)	(0.03)	(0.03)
Tl	0.24	0.05	0.05	0.03	0.05	0.04
Pb	0.60	2.57	3.13	0.75	1.96	1.50
Bi	(0.002)	(0.01)	(0.002)	(0.01)	(0.002)	(0.01)
U	0.11	0.02	0.03	(0.002)	0.11	0.02

**Appendix 2.1: Element concentrations in Water Samples (ppb); dp = field duplicate,
* = split sample, () indicates values below detection limit.**

Month						
Sample	BCWS5	BCWS6	BCWS7	BCWS7*	BCWS8	BCWS9
Li 6	0.77	0.76	0.75	0.92	0.84	0.92
Li 7	0.71	0.71	0.90	0.91	0.86	0.99
Be	(0.02)	(0.03)	(0.02)	(0.32)	(0.03)	(0.04)
B	4.72	(2.46)	5.98	(2.02)	6.40	6.89
C (cps)	60501572	50035695	63439020	51731802	60921405	67700901
N (cps)	239671771	240075403	252807752	276215868	243755319	260278006
Mg	6942	7104	7490	8459	7571	11576
Al	1904	1943	1394	1519	2063	2076
Si	2533	2592	2690	2895	2742	4034
P	(163)	(200)	(604)	(997)	(134)	(625)
S	4894	5629	5853	6000	6078	7040
Cl	2725	2934	3387	3921	3134	3940
Ca 42	15890	15380	17825	19408	16103	21712
Ca 43	16572	16485	16966	17602	15769	17498
Ti	3.34	3.44	3.54	3.81	5.28	3.59
V	0.25	(0.04)	0.35	(0.04)	0.84	0.12
Cr 52	0.58	(0.51)	0.72	0.59	21.3	1.01
Cr 53	1.07	1.16	1.30	1.27	22.0	1.29
Fe 54	628	649	703	781	798	795
Mn	235	236	254	271	251	269
Fe 56	722	726	715	728	777	743
Fe 57	664	686	723	796	818	800
Co	22.7	23.1	24.1	26.4	23.9	25.5
Ni	15.2	21.3	19.2	19.6	31.9	17.1
Cu	2190	1643	1730	2570	2441	2477
Zn	792	808	856	940	838	890
As	(0.04)	(0.06)	(0.09)	0.17	(0.10)	0.14
Br	(57.5)	(57.5)	(6.93)	(19.6)	(57.5)	(0.70)
Se	(0.59)	0.78	0.96	0.90	1.10	1.22
Rb	0.38	0.49	0.50	0.56	0.43	0.44
Sr	18.1	18.2	18.6	19.6	18.5	19.9
Mo	(0.01)	(0.01)	(0.01)	(0.01)	2.47	0.02
Ag	(0.001)	(0.03)	(0.01)	(0.004)	(0.01)	(0.01)
Cd	1.42	1.38	1.49	1.56	1.45	1.52
Sn	(0.10)	(0.14)	(0.47)	(0.32)	(0.27)	(0.21)
Sb	0.02	0.05	0.03	0.03	0.03	0.02
I	(6.05)	(4.00)	(7.31)	(8.51)	(6.04)	(9.17)
Cs	0.05	0.06	0.06	0.07	0.06	0.06
Ba	2.25	2.37	2.37	2.56	2.32	2.45
La	0.35	0.35	0.35	0.37	0.35	0.39
Ce	0.69	0.68	0.68	0.71	0.69	0.77
Hg	(0.03)	(0.01)	(0.001)	(0.03)	(0.03)	(0.03)
Tl	0.04	0.05	0.05	0.05	0.04	0.05
Pb	1.50	1.55	1.62	1.71	1.65	1.86
Bi	(0.01)	(0.01)	(0.01)	(0.01)	(0.01)	(0.01)
U	0.02	0.02	0.02	0.03	0.02	0.02

**Appendix 2.1: Element concentrations in Water Samples (ppb); dp = field duplicate,
* = split sample, () indicates values below detection limit.**

Month						
Sample	BCWS10	BCWS11	BCWS12	BCWS13	BCWS13dp	BCWS13dp*
Li 6	(0.44)	(0.48)	(0.27)	(0.09)	(0.21)	(0.13)
Li 7	0.39	0.37	0.36	0.28	0.26	0.23
Be	(0.05)	(0.02)	(0.32)	(0.32)	(0.32)	(0.32)
B	9.27	4.06	4.51	(2.56)	(1.37)	4.19
C (cps)	59521321	55436135	59725194	53859778	49166173	54145005
N (cps)	288025133	250430674	258807130	266261849	291516913	255293553
Mg	2449	1732	2509	1736	1807	1625
Al	146	98.2	143	93.1	84.6	88.7
Si	1985	1407	2219	1560	1654	1436
P	(864)	(3200)	(3218)	(3259)	(373)	(3286)
S	(1208)	(1400)	(413)	(1450)	(1.64)	(1450)
Cl	5347	3115	3207	2551	3041	1925
Ca 42	6647	(3214)	(3126)	(4895)	7405	(1921)
Ca 43	4565	3333	3347	6007	6298	6142
Ti	3.31	0.46	0.74	0.66	0.67	0.64
V	0.26	0.20	0.16	0.25	0.08	0.20
Cr 52	1.52	0.75	(0.52)	0.91	1.06	0.87
Cr 53	1.62	0.77	0.59	1.10	1.14	1.02
Fe 54	154	38.5	(37.8)	(14.0)	(35.8)	(19.5)
Mn	49.8	35.1	47.1	10.9	11.6	10.1
Fe 56	(178)	(23.7)	(7.34)	<617	<619	(312)
Fe 57	141	(29.5)	50.3	(1.57)	(32.3)	(2.36)
Co	3.45	2.62	5.79	2.51	2.64	2.36
Ni	9.60	3.75	5.82	6.01	6.38	10.1
Cu	253	196	495	268	276	251
Zn	69.4	46.4	83.6	67.6	108	71.6
As	0.21	(0.05)	(0.08)	0.12	0.20	(0.10)
Br	(13.4)	(3.51)	(4.17)	(1.91)	(22.3)	(57.5)
Se	(0.70)	(0.35)	(0.41)	1.13	1.12	0.91
Rb	0.54	0.22	0.27	0.25	0.24	0.22
Sr	8.82	6.31	5.96	5.65	5.91	5.25
Mo	0.04	(0.01)	(0.01)	0.05	0.05	0.05
Ag	(0.03)	(0.001)	(0.03)	(0.02)	(0.02)	(0.02)
Cd	0.22	0.13	0.25	0.24	0.29	0.22
Sn	0.75	(0.13)	(0.16)	(0.13)	(0.21)	(0.39)
Sb	0.13	0.02	0.02	0.02	0.02	0.02
I	(5.28)	(4.01)	(1.98)	(2.07)	(3.07)	(1.03)
Cs	0.01	(0.01)	(0.01)	(0.01)	(0.01)	(0.01)
Ba	3.31	1.90	1.90	1.00	1.07	1.01
La	0.07	0.03	0.04	0.04	0.04	0.04
Ce	0.17	0.08	0.10	0.08	0.07	0.08
Hg	(0.03)	(0.03)	(0.03)	(0.03)	(0.03)	(0.03)
Tl	0.02	(0.01)	0.03	(0.01)	(0.01)	(0.01)
Pb	1.63	0.68	0.49	0.13	0.12	0.28
Bi	(0.0004)	(0.01)	(0.01)	(0.01)	(0.01)	(0.01)
U	(0.01)	(0.01)	(0.01)	(0.01)	(0.01)	(0.0005)

**Appendix 2.1: Element concentrations in Water Samples (ppb); dp = field duplicate,
* = split sample, () indicates values below detection limit.**

Month						
Sample	BCWS14	BCWS15	BCWS16	BCWS17	BCWS18	BCWS18dp
Li 6	(0.28)	(0.02)	(0.28)	(0.05)	(0.18)	(0.17)
Li 7	(0.06)	0.11	0.09	0.13	0.13	0.09
Be	(0.32)	(0.32)	(0.32)	(0.32)	(0.04)	(0.02)
B	4.47	8.00	4.30	5.34	29.7	6.87
C (cps)	46787845	50243298	44645507	49587018	51723256	59733479
N (cps)	267544080	275907121	234548886	270569966	272783667	283517561
Mg	2266	2544	2002	2015	2244	1945
Al	26.2	47.7	32.7	34.8	53.3	44.5
Si	1547	1755	1414	1460	1714	1531
P	(3280)	17735	3286	3286	3286	(3286)
S	(1450)	(1450)	(1450)	(1450)	(1450)	(1450)
Cl	3413	3975	2356	2888	5861	3118
Ca 42	(719)	(2516)	(2750)	(260)	(726)	(2101)
Ca 43	1141	1281	1094	1403	1785	1572
Ti	(0.11)	1.24	(0.20)	(0.13)	0.47	(0.27)
V	0.14	0.27	0.20	0.21	0.30	0.61
Cr 52	1.83	2.36	1.80	2.20	2.62	2.65
Cr 53	1.98	2.40	2.06	2.29	2.74	2.36
Fe 54	(19.5)	(27.4)	(17.5)	(19.0)	(15.7)	(20.3)
Mn	(0.09)	0.91	0.65	(0.27)	0.90	(0.39)
Fe 56	(311)	(312)	(166)	(305)	(9)	(352)
Fe 57	(15.0)	(28.9)	34.5	(5.08)	(22.0)	(22.9)
Co	(0.02)	(0.04)	(0.02)	(0.03)	(0.03)	(0.01)
Ni	5.00	6.68	5.41	7.50	6.34	5.48
Cu	(0.76)	(1.02)	(0.76)	(0.88)	(1.05)	(0.68)
Zn	(8.26)	(8.58)	17.7	(5.00)	(5.81)	(4.45)
As	0.28	0.28	0.22	0.21	0.26	0.27
Br	(9.15)	(7.28)	(57.5)	(57.5)	(0.55)	(21.6)
Se	(0.02)	(0.36)	(0.04)	(0.07)	(0.35)	(0.61)
Rb	0.27	0.28	0.26	0.21	0.34	0.21
Sr	4.70	5.35	4.57	4.50	5.55	4.92
Mo	(0.01)	0.02	(0.01)	0.02	0.02	0.02
Ag	(0.04)	(0.04)	(0.04)	(0.004)	(0.01)	(0.004)
Cd	(0.004)	(0.02)	(0.01)	(0.01)	(0.01)	(0.003)
Sn	(0.12)	(0.28)	(0.21)	(0.23)	(0.49)	(0.32)
Sb	0.06	0.05	0.08	0.04	0.07	0.03
I	(3.10)	(4.00)	(0.34)	(4.11)	(3.68)	(4.86)
Cs	(0.00)	(0.005)	(0.001)	(0.004)	(0.003)	(0.01)
Ba	2.19	2.75	2.19	2.04	2.27	1.88
La	0.05	0.07	0.05	0.06	0.06	0.06
Ce	0.05	0.10	0.06	0.05	0.07	0.05
Hg	(0.002)	(0.03)	(0.03)	(0.03)	(0.03)	(0.03)
Tl	(0.0002)	(0.002)	(0.05)	(0.002)	(0.01)	(0.05)
Pb	0.16	0.22	0.24	0.11	0.33	0.13
Bi	(0.01)	(0.01)	(0.01)	(0.01)	(0.01)	(0.01)
U	(0.01)	(0.001)	(0.01)	(0.01)	(0.001)	(0.01)

**Appendix 2.1: Element concentrations in Water Samples (ppb); dp = field duplicate,
* = split sample, () indicates values below detection limit.**

Month						
Sample	BCWS18dp*	BCWS19	BCWS20	BCWS21	BCWS22	BCWS22dp
Li 6	(0.28)	(0.28)	(0.08)	(0.28)	(0.01)	(0.24)
Li 7	0.18	0.11	0.20	0.12	0.12	0.14
Be	(0.04)	(0.32)	(0.32)	(0.32)	(0.03)	(0.07)
B	31.8	7.20	6.06	5.03	6.30	11.3
C (cps)	56111619	55692166	51527913	49387907	54604640	57495029
N (cps)	300259583	268644471	266247192	281703015	307098168	332093450
Mg	2515	1858	1897	1750	1979	2147
Al	66.4	58.0	51.7	69.2	51.7	54.6
Si	1913	1472	1488	1446	1541	1655
P	(3286)	(3286)	(3286)	(3286)	(3286)	(3286)
S	(1450)	(1450)	(1450)	(1450)	(1450)	(689)
Cl	6380	2737	2959	2929	2750	3316
Ca 42	(2750)	(381)	(1259)	(3022)	(1818)	(3242)
Ca 43	1772	1460	1473	2750	2799	2700
Ti	0.51	(0.29)	(0.17)	2.29	0.22	0.24
V	0.35	0.35	0.48	0.40	0.28	0.28
Cr 52	7.34	2.59	2.66	2.27	1.77	1.15
Cr 53	13.7	2.44	2.39	2.24	2.13	2.15
Fe 54	7459	(18.5)	(19.0)	(36.8)	(19.0)	(18.5)
Mn	68.6	(0.44)	(0.42)	0.60	(0.27)	(0.23)
Fe 56	1562	(18.7)	(28.0)	(333)	(306)	(298)
Fe 57	7377	(14.0)	(18.5)	48.5	(15.0)	(10.7)
Co	0.26	(0.03)	(0.03)	(0.06)	(0.03)	(0.03)
Ni	7.43	5.95	5.96	4.87	4.51	4.66
Cu	(3.52)	5.66	(3.77)	(3.45)	(3.00)	(3.27)
Zn	587	12.6	(7.76)	22.3	11.7	11.4
As	0.44	0.22	0.25	0.28	0.18	0.15
Br	(57.5)	(16.7)	(23.4)	(37.2)	(57.5)	(57.5)
Se	0.67	(0.21)	(0.50)	(0.45)	(0.51)	0.72
Rb	0.36	0.30	0.22	0.27	0.22	0.23
Sr	5.70	5.60	4.95	6.15	6.06	5.75
Mo	0.23	0.03	0.03	0.02	0.02	0.02
Ag	(0.01)	(0.01)	(0.000)	(0.004)	(0.001)	(0.03)
Cd	0.08	(0.01)	(0.01)	(0.02)	(0.01)	(0.01)
Sn	0.68	(0.39)	(0.36)	(0.25)	(0.36)	(0.47)
Sb	0.09	0.03	0.04	0.04	0.05	0.10
I	(5.08)	(3.57)	(4.08)	(4.26)	(3.13)	(0.02)
Cs	(0.002)	(0.002)	(0.004)	(0.01)	(0.05)	(0.05)
Ba	23.1	1.98	1.87	1.77	1.84	1.90
La	0.06	0.06	0.05	0.06	0.04	0.04
Ce	0.07	0.06	0.06	0.07	0.04	0.04
Hg	(0.03)	(0.03)	(0.03)	(0.03)	(0.03)	(0.03)
Tl	0.02	(0.05)	(0.05)	(0.002)	(0.003)	(0.05)
Pb	0.46	0.30	0.21	0.20	0.24	0.26
Bi	(0.01)	(0.001)	(0.01)	(0.01)	(0.01)	(0.01)
U	(0.01)	(0.003)	(0.001)	(0.002)	(0.01)	(0.01)

**Appendix 2.1: Element concentrations in Water Samples (ppb); dp = field duplicate,
* = split sample, () indicates values below detection limit.**

Month						
Sample	RRS1	RRS1*	RRS2	RRS3	RRS4	RRS5
Li 6	0.51	0.40	0.56	0.23	0.19	0.52
Li 7	0.57	0.47	0.56	0.28	0.24	0.55
Be	(0.32)	(0.32)	(0.32)	(0.32)	(0.32)	(0.32)
B	(6.83)	(4.46)	(5.33)	(2.18)	(1.46)	(3.81)
C (cps)	495522679	218901095	406365085	390861788	350486780	361620901
N (cps)	121930941	118787158	126421475	133029082	119283728	136078509
Mg	1797	1726	1806	696	620	1217
Al	216	204	218	174	175	195
Si	(1096)	(1094)	(1067)	(605)	(558)	(933)
P	(1275)	(1316)	(175)	(1309)	(5.06)	(1309)
S	(2000)	(2000)	(2000)	(2000)	(2000)	(188)
Cl	8048	7569	11034	7508	6727	16156
Ca 42	6981	7818	8714	(1290)	(404)	7556
Ca 43	9071	9386	10198	2870	2411	7814
Ti	2.64	2.90	4.73	1.52	1.57	1.53
V	0.59	0.70	0.81	(0.42)	(0.27)	0.82
Cr 52	(18.0)	(18.0)	(18.0)	(18.0)	(18.0)	(18.0)
Cr 53	(0.34)	(2.02)	(0.24)	(3.34)	(2.05)	(0.19)
Fe 54	348	374	324	171	166	168
Mn	18.5	18.8	18.0	7.06	6.55	14.9
Fe 56	362	386	347	(117)	(170)	(174)
Fe 57	379	389	357	197	192	195
Co	(0.04)	(0.05)	(0.06)	(0.06)	(0.02)	(0.07)
Ni	2.55	2.50	2.15	6.23	0.60	1.63
Cu	6.21	1.84	1.32	4.89	2.34	9.16
Zn	47.8	8.03	70.1	10.2	13.4	29.5
As	0.28	0.29	0.24	0.12	0.13	0.14
Br	(42.6)	(46.1)	(41.5)	(18.8)	(13.7)	(28.5)
Se	(0.09)	(0.09)	(0.07)	(0.07)	(0.01)	(0.16)
Rb	1.38	0.90	1.64	0.87	0.77	1.39
Sr	38.8	38.4	36.8	18.8	17.1	25.4
Mo	(0.05)	0.15	(0.05)	0.15	(0.0002)	(0.05)
Ag	(0.03)	(0.01)	(0.03)	(0.01)	(0.03)	(0.04)
Cd	0.04	0.02	0.12	0.02	0.02	0.04
Sn	0.42	(0.20)	1.90	0.39	(0.17)	0.56
Sb	0.05	0.03	0.06	0.03	0.03	0.03
I	11.60	12.15	9.78	5.12	7.79	8.77
Cs	(0.01)	(0.01)	(0.01)	(0.05)	(0.05)	(0.004)
Ba	19.9	19.0	23.5	8.68	6.28	15.5
La	0.47	0.46	0.42	0.30	0.30	0.30
Ce	0.78	0.76	0.69	0.54	0.54	0.55
Hg	(0.02)	(0.01)	(0.02)	(0.02)	(0.02)	(0.01)
Tl	0.27	0.23	0.60	0.24	0.21	0.88
Pb	0.53	0.26	0.97	0.29	0.28	0.53
Bi	(0.01)	(0.004)	(0.005)	(0.002)	(0.001)	(0.001)
U	0.09	0.09	0.09	0.07	0.07	0.09

Appendix 2.1: Element concentrations in Water Samples (ppb); dp = field duplicate,

*** = split sample, () indicates values below detection limit.**

Month						
Sample	RRS6	RRS6dp	RRS7	RRS7*	RRS8	RRS9
Li 6	0.33	0.28	0.17	0.27	0.18	0.22
Li 7	0.35	0.31	0.19	0.23	0.23	0.26
Be	(0.32)	(0.32)	(0.32)	(0.11)	(0.32)	(0.32)
B	(2.65)	(2.57)	(8.98)	(4.90)	(6.45)	(8.98)
C (cps)	313033675	236356026	210927945	0	215503843	194942854
N (cps)	121729153	117984176	124928129	130714785	126468836	117322146
Mg	704	642	506	487	532	559
Al	196	183	167	167	172	169
Si	(675)	(770)	(252)	(1551)	(117)	(1010)
P	(1309)	(1309)	(1309)	(17.4)	(1309)	(1309)
S	(2000)	(2000)	(2000)	(2000)	(2000)	(2000)
Cl	8406	7782	6169	6181	8186	8341
Ca 42	(1967)	(2645)	(955)	(1080)	(1519)	(1724)
Ca 43	2832	2817	1912	1930	2277	2434
Ti	1.92	1.93	1.74	1.73	1.93	1.69
V	0.63	0.55	(0.27)	(0.37)	(0.33)	(0.30)
Cr 52	(18.0)	(18.0)	(18.0)	(8.90)	(18.00)	(18.00)
Cr 53	(0.05)	(2.05)	(2.05)	(1.09)	(2.05)	(2.05)
Fe 54	197	198	184	175	192	178
Mn	6.82	6.87	5.48	5.52	6.74	6.31
Fe 56	(197)	(242)	(181)	(179)	(144)	(250)
Fe 57	213	215	190	181	202	189
Co	(0.04)	(0.04)	(0.03)	(0.03)	(0.05)	(0.03)
Ni	1.30	1.28	0.66	0.58	1.75	1.54
Cu	3.58	1.76	0.92	1.44	2.64	3.05
Zn	17.7	17.0	5.36	8.48	16.7	63.1
As	0.13	0.13	0.13	0.15	0.14	0.17
Br	(19.4)	(20.4)	(15.1)	(19.5)	(17.6)	(16.4)
Se	(0.09)	(0.09)	(0.06)	(0.09)	(0.13)	(0.06)
Rb	0.86	0.79	0.65	0.69	0.88	0.91
Sr	18.0	17.2	16.3	15.9	20.8	21.7
Mo	(0.01)	(0.04)	(0.01)	(0.01)	(0.02)	(0.005)
Ag	(0.04)	(0.02)	(0.01)	(0.02)	(0.08)	(0.02)
Cd	0.03	0.03	(0.01)	0.02	0.03	0.02
Sn	(0.22)	(0.27)	(0.00)	(0.01)	(0.71)	(0.18)
Sb	0.03	0.02	0.01	0.02	0.03	0.02
I	8.08	8.37	7.89	7.76	8.23	8.08
Cs	(0.05)	(0.01)	(0.01)	(0.01)	(0.01)	(0.01)
Ba	14.9	9.22	5.50	5.63	8.81	8.70
La	0.30	0.30	0.29	0.29	0.30	0.30
Ce	0.54	0.53	0.53	0.53	0.54	0.53
Hg	(0.02)	(0.01)	(0.01)	(0.01)	(0.01)	(0.005)
Tl	0.28	0.24	0.21	0.18	0.28	0.27
Pb	0.46	0.21	0.15	0.18	0.39	0.36
Bi	(0.002)	(0.003)	(0.002)	(0.002)	(0.002)	(0.002)
U	0.07	0.08	0.07	0.07	0.08	0.08

**Appendix 2.1: Element concentrations in Water Samples (ppb); dp = field duplicate,
* = split sample, () indicates values below detection limit.**

Month						
Sample	RRS10	RRS11	RRS12	RRS12dp	RRS13	RRS14
Li 6	0.28	0.65	0.38	0.45	0.33	0.26
Li 7	0.31	0.71	0.36	0.46	0.29	0.29
Be	(0.32)	(0.32)	(0.21)	(0.01)	(0.11)	(0.32)
B	(8.98)	(9.05)	(9.49)	(6.98)	(5.40)	(1.46)
C (cps)	195254903	880882982	0	0	2927596709	0
N (cps)	113676078	117693884	128402111	124696821	157970720	130848588
Mg	636	2632	1082	1019	703	654
Al	167	125	141	140	174	149
Si	(1028)	(529)	(1817)	(1264)	(1331)	(775)
P	(1309)	(1309)	(1309)	(1309)	(246)	339
S	(2000)	(502)	(2000)	(2000)	(2000)	(2000)
Cl	8565	26192	12707	13227	11142	9906
Ca 42	(2563)	19265	6831	6769	6485	(3617)
Ca 43	3306	19300	7835	7346	3404	3198
Ti	1.93	1.90	1.91	1.69	1.94	1.61
V	(0.53)	(0.44)	0.81	0.44	0.35	(0.19)
Cr 52	(18.00)	(18.00)	(18.30)	(3.98)	(14.7)	(8.04)
Cr 53	(2.05)	(3.20)	(2.00)	(0.59)	(1.70)	8.43
Fe 54	170	152	182	162	220	200
Mn	7.59	5.89	7.41	6.65	7.20	5.18
Fe 56	(216)	(183)	(121)	(124)	(79.7)	(245)
Fe 57	198	157	172	178	242	207
Co	(0.03)	(0.04)	(0.03)	(0.02)	(0.04)	(0.09)
Ni	1.38	5.31	1.21	(0.26)	0.99	3.32
Cu	2.55	0.59	0.72	1.27	1.13	2.81
Zn	15.3	5.13	7.12	10.4	11.1	5.88
As	0.12	0.11	0.17	0.14	0.16	0.14
Br	(17.8)	(30.8)	(29.2)	(26.1)	(33.1)	(26.1)
Se	(0.09)	(0.09)	(0.09)	(0.09)	(0.01)	(0.09)
Rb	0.86	1.36	0.80	0.90	0.83	0.69
Sr	24.3	153	68.5	62.8	28.9	27.1
Mo	(0.02)	0.48	(0.03)	(0.02)	(0.01)	0.33
Ag	(0.01)	(0.02)	(0.02)	(0.02)	(0.01)	(0.01)
Cd	0.02	0.02	0.02	0.01	0.02	0.02
Sn	(0.07)	(0.14)	0.77	(0.09)	(0.14)	(0.14)
Sb	0.02	(0.01)	0.02	0.02	0.02	(0.01)
I	5.04	5.32	9.64	8.95	8.24	7.36
Cs	(0.004)	(0.05)	(0.02)	(0.01)	(0.02)	(0.01)
Ba	9.53	28.3	12.3	11.9	10.5	10.7
La	0.33	0.25	0.27	0.26	0.30	0.28
Ce	0.59	0.38	0.47	0.45	0.52	0.48
Hg	(0.002)	0.02	(0.01)	(0.01)	(0.01)	(0.01)
Tl	0.33	1.59	0.54	0.57	0.31	0.34
Pb	0.24	0.15	0.17	0.18	0.16	0.14
Bi	(0.00004)	(0.05)	(0.002)	(0.002)	(0.001)	(0.002)
U	0.07	0.07	0.08	0.07	0.08	0.07

Appendix 2.1: Element concentrations in Water Samples (ppb); dp = field duplicate,

*** = split sample, () indicates values below detection limit.**

Month		March	March	March	March	March
Sample	RRS15	SWS1	SWS1*	SWS2	SWS3	SWS4
Li 6	0.42	0.45	0.49	0.34	0.23	0.19
Li 7	0.43	0.51	0.55	0.40	0.30	0.30
Be	(0.32)	0.02	0.03	0.05	0.05	0.05
B	(7.08)	3.53	8.97	4.82	4.40	6.55
C (cps)	1275685820	12014757	11067120	11843728	12063391	11823001
N (cps)	125098990	12073221	12809471	12508491	12745446	12473161
Mg	1627	1306	1772	1458	1425	1503
Al	135	60.7	43.7	54.5	53.2	48.4
Si	(256)	1623	1924	1723	1663	1705
P	158	94.0	79.0	444	94.0	(94.0)
S	(2000)	309	521	603	577	581
Cl	61093	80092	158764	199794	196305	202696
Ca 42	9857	5531	11985	9866	9298	9861
Ca 43	10464	5715	12359	10097	9637	10040
Ti	2.06	0.26	0.23	0.47	0.34	0.32
V	0.71	0.48	0.23	0.42	0.13	0.22
Cr 52	(18.0)	(0.25)	(0.25)	1.01	0.08	2.52
Cr 53	(2.05)	0.06	0.19	1.16	0.31	2.84
Fe 54	158	15.8	275	72.4	68.3	65.0
Mn	14.0	58.9	168.6	191.3	179.8	187.6
Fe 56	(198)	3.94	(79.5)	(40.8)	(6.18)	39.4
Fe 57	181	33.3	300	90.4	77.8	88.5
Co	(0.04)	0.11	0.24	0.39	0.37	0.40
Ni	0.77	0.90	0.36	0.78	0.65	3.59
Cu	2.37	3.56	5.05	8.15	7.60	8.11
Zn	11.6	14.2	15.7	62.6	52.1	45.5
As	0.14	0.08	0.11	0.13	0.11	0.13
Br	61.4	32.2	46.3	51.2	51.2	52.0
Se	(0.09)	0.03	(0.15)	0.11	0.15	0.02
Rb	1.31	0.52	1.08	0.90	0.82	0.80
Sr	114	17.0	56.5	43.4	41.9	44.7
Mo	0.01	0.03	0.26	0.08	0.06	0.50
Ag	(0.01)	0.0004	(0.10)	0.14	0.13	0.12
Cd	0.04	0.03	0.02	0.08	0.12	0.07
Sn	(0.11)	0.04	1.61	0.19	0.09	0.01
Sb	0.03	0.09	0.08	0.12	0.07	0.07
I	12.1	2.85	4.78	2.78	2.61	3.27
Cs	(0.01)	0.01	0.06	0.02	0.02	0.02
Ba	17.9	10.0	36.3	30.7	29.7	33.1
La	0.29	0.14	0.33	0.71	0.62	0.61
Ce	0.49	0.24	0.44	0.83	0.81	0.77
Hg	(0.01)	(0.02)	(0.02)	(0.02)	(0.02)	(0.02)
Tl	3.26	0.41	0.22	0.47	0.38	0.35
Pb	0.36	0.17	0.13	0.45	0.29	0.27
Bi	(0.001)	(0.01)	(0.01)	(0.01)	(0.01)	(0.01)
U	0.07	0.001	0.003	0.003	0.002	0.003

Appendix 2.1: Element concentrations in Water Samples (ppb); dp = field duplicate,

*** = split sample, () indicates values below detection limit.**

Month	March	March	March	March	April	April
Sample	SWS5	SWS5*	SWS6A	SWS6B	SWS1	SWS1*
Li 6	0.20	0.20	0.41	1.12	0.47	0.47
Li 7	0.30	0.32	0.48	1.20	0.47	0.50
Be	0.06	0.05	0.04	0.05	0.02	0.03
B	6.10	7.02	4.74	18.8	3.51	3.60
C (cps)	11425500	6725103	10642402	12374229	14024959	12159872
N (cps)	13997169	10158055	12761423	12129076	38934271	35924024
Mg	1493	1687	1389	2364	886	946
Al	48.7	55.4	51.8	34.6	49.9	74.0
Si	1783	1888	1673	2388	1038	1192
P	(94.0)	(94.0)	(450)	(500)	(270)	7.58
S	660	733	578	887	79.3	58.5
Cl	212411	195440	172856	319504	43189	46192
Ca 42	10106	9810	8515	23984	2620	3043
Ca 43	10293	10449	8831	24281	2956	3089
Ti	0.31	0.27	0.31	0.26	(0.14)	0.19
V	0.24	1.01	0.27	0.18	0.13	0.23
Cr 52	1.43	2.06	0.35	6.39	(0.15)	(0.15)
Cr 53	1.70	2.46	0.57	6.46	0.02	0.04
Fe 54	62.7	50.3	46.6	1736	(51.2)	(63.5)
Mn	186.4	184.2	153.5	361.2	31.8	33.3
Fe 56	35.5	12.0	1.01	46.4	(60.5)	(55.5)
Fe 57	83.9	81.3	64.6	1737	14.3	23.7
Co	0.40	0.42	0.31	0.57	0.07	0.08
Ni	2.46	3.72	1.86	4.49	0.35	0.47
Cu	8.35	9.50	6.96	11.8	2.47	2.92
Zn	45.4	47.8	36.7	41.1	13.4	17.6
As	0.12	0.10	0.10	0.30	0.07	0.06
Br	54.1	54.3	49.1	85.0	23.9	24.0
Se	0.03	(0.15)	0.02	0.38	(1.40)	1.40
Rb	0.88	0.86	0.74	2.01	0.35	0.43
Sr	46.5	48.9	37.8	120	9.82	9.96
Mo	0.22	0.35	0.07	1.57	0.01	(0.02)
Ag	0.15	0.16	0.10	0.03	0.003	0.01
Cd	0.08	0.09	0.06	0.09	0.01	0.01
Sn	0.02	0.26	0.05	0.06	0.07	0.07
Sb	0.07	0.26	0.08	0.14	0.03	0.03
I	4.05	3.07	3.82	10.3	4.17	1.07
Cs	0.02	0.03	0.02	0.14	0.02	0.01
Ba	32.1	34.4	25.3	80.6	7.61	6.65
La	0.62	0.75	0.47	1.15	0.10	0.14
Ce	0.78	0.91	0.58	1.32	0.16	0.24
Hg	(0.02)	(0.02)	(0.02)	(0.02)	(0.01)	(0.01)
Tl	0.35	0.05	0.33	0.36	2.14	1.13
Pb	0.31	0.30	0.27	0.33	(0.60)	0.18
Bi	0.00003	0.001	0.001	0.0003	(0.01)	0.0001
U	0.003	0.01	0.004	0.01	0.002	0.002

**Appendix 2.1: Element concentrations in Water Samples (ppb); dp = field duplicate,
* = split sample, () indicates values below detection limit.**

Month	April	April	April	April	April	April
Sample	SWS2	SWS3	SWS4	SWS5	SWS6A	SWS6B
Li 6	0.49	0.47	0.47	0.46	0.49	1.73
Li 7	0.51	0.49	0.50	0.48	0.51	1.80
Be	0.05	0.05	0.05	0.04	0.04	0.04
B	5.09	4.75	4.67	4.50	5.72	22.7
C (cps)	14226250	14250944	14138122	13758556	13969747	14457973
N (cps)	42405162	42236926	41904521	37623382	36582205	38272986
Mg	1340	1320	1253	1220	1342	2712
Al	37.0	36.1	48.2	32.0	32.4	7.83
Si	1321	1340	1249	1118	1396	2492
P	(250)	(250)	(250)	(250)	(250)	55.6
S	398	632	297	277	358	563
Cl	145465	142818	121921	132809	147422	270458
Ca 42	7443	7184	6372	6734	7756	27356
Ca 43	7738	7609	6639	7047	7948	27783
Ti	(0.14)	(0.14)	0.02	(0.09)	(1.12)	(0.13)
V	0.16	0.15	0.30	0.17	0.27	0.17
Cr 52	(0.15)	(0.15)	(0.15)	(0.15)	4.16	0.08
Cr 53	0.25	0.24	0.25	0.24	4.42	1.09
Fe 54	39.7	25.5	30.4	25.4	58.2	2339
Mn	159	153	126	140	151	491
Fe 56	24.4	73.0	7.47	(72.5)	43.8	301
Fe 57	64.6	57.4	55.7	51.7	83.7	2379
Co	0.31	0.29	0.24	0.27	0.31	0.60
Ni	0.60	0.50	0.69	0.48	1.99	0.73
Cu	6.44	6.28	5.60	5.51	6.99	11.4
Zn	38.2	40.0	33.5	33.8	34.1	25.2
As	0.09	0.08	0.08	0.10	0.10	0.35
Br	43.9	42.3	39.1	40.8	44.4	83.6
Se	0.05	1.40	0.07	0.09	0.10	0.28
Rb	0.77	0.64	0.62	0.60	0.69	2.40
Sr	34.9	34.2	28.5	32.4	36.4	143
Mo	0.05	0.04	0.03	0.05	0.79	0.55
Ag	0.16	0.12	0.07	0.12	0.10	0.01
Cd	0.05	0.05	0.04	0.05	0.05	0.06
Sn	0.51	0.12	0.06	0.17	0.30	0.32
Sb	0.07	0.06	0.07	0.06	0.09	0.11
I	4.76	4.01	4.01	4.78	5.46	13.2
Cs	0.04	0.04	0.04	0.01	0.02	0.19
Ba	25.5	25.2	20.5	23.5	26.5	96.0
La	0.54	0.53	0.44	0.48	0.51	1.05
Ce	0.73	0.70	0.58	0.64	0.67	1.40
Hg	(0.01)	(0.01)	(0.01)	(0.01)	(0.01)	(0.01)
Tl	5.59	3.98	2.87	3.51	3.43	4.18
Pb	0.08	(0.60)	0.11	0.10	0.13	0.22
Bi	0.0002	0.0002	0.0003	0.0002	0.0005	0.001
U	0.003	0.002	0.003	0.003	0.004	0.01

**Appendix 2.1: Element concentrations in Water Samples (ppb); dp = field duplicate,
* = split sample, () indicates values below detection limit.**

Month	May	May	May	May	May	May
Sample	SWS1	SWS1*	SWS2	SWS3	SWS4	SWS5
Li 6	(0.41)	0.71	(0.56)	0.76	(0.49)	(0.53)
Li 7	(0.46)	(0.58)	(0.54)	(0.62)	(0.52)	(0.59)
Be	(0.06)	(0.06)	(0.07)	(0.07)	(0.05)	0.04
B	8.23	5.99	11.1	7.26	6.76	8.51
C (cps)	50476947	47098546	51479977	45708527	38925120	44976577
N (cps)	206411710	244926284	195592317	228682936	192845635	213161986
Mg	740	809	1149	1227	1119	1292
Al	53.7	57.3	38.1	36.8	34.3	39.7
Si	654	791	800	840	768	975
P	(1700)	(763)	(1700)	(1700)	(1700)	(1700)
S	(4500)	(4500)	(4500)	(4500)	4500	(4500)
Cl	32872	35557	112230	118634	111368	119547
Ca 42	(2000)	(2504)	(3458)	6531	(2103)	6990
Ca 43	2916	2898	7204	7698	7060	7598
Ti	0.54	0.63	0.42	0.53	0.47	0.75
V	0.70	0.18	0.65	0.48	0.42	0.35
Cr 52	(0.28)	(0.37)	(0.40)	0.44	0.19	0.56
Cr 53	0.67	0.61	1.85	1.69	1.47	1.16
Fe 54	(21.0)	(45.6)	(41.9)	62.1	(21.3)	69.1
Mn	17.3	17.8	135	137	126	129
Fe 56	(19.7)	(34.3)	(31.2)	(54.3)	241	(42.6)
Fe 57	(36.1)	(56.4)	79.4	79.8	(55.5)	85.8
Co	(0.03)	0.06	0.31	0.16	0.14	0.19
Ni	1.61	0.88	3.53	1.20	0.91	1.14
Cu	1.45	1.94	2.65	2.55	2.02	3.31
Zn	22.1	26.8	39.4	45.7	31.4	39.7
As	(0.12)	(0.09)	(0.09)	(0.19)	(0.10)	(0.15)
Br	(7.87)	(19.7)	(27.0)	(37.2)	(23.7)	(43.3)
Se	(0.30)	(0.30)	(0.30)	(0.26)	(0.30)	(0.30)
Rb	0.47	0.49	0.83	0.75	0.69	0.81
Sr	8.54	9.02	29.4	32.1	29.6	32.5
Mo	0.06	0.06	0.13	0.12	0.11	0.13
Ag	(0.0003)	(0.01)	0.20	0.16	0.14	0.16
Cd	(0.01)	(0.03)	(0.03)	(0.04)	(0.02)	(0.04)
Sn	0.14	0.11	0.62	0.24	0.16	0.50
Sb	0.05	0.04	0.08	0.07	0.07	0.08
I	11.8	12.6	13.4	15.3	11.8	14.5
Cs	0.01	0.01	0.02	0.03	0.02	0.03
Ba	5.58	8.03	22.4	23.8	22.8	32.7
La	0.15	0.17	0.42	0.43	0.41	0.42
Ce	0.20	0.22	0.56	0.55	0.52	0.54
Hg	(0.02)	(0.003)	(0.02)	(0.02)	(0.02)	(0.02)
Tl	0.25	0.24	0.50	0.49	0.46	0.47
Pb	0.20	0.19	0.46	0.36	0.33	0.43
Bi	(0.01)	(0.01)	(0.01)	(0.01)	(0.01)	(0.01)
U	(0.003)	(0.001)	(0.003)	(0.004)	(0.003)	(0.0004)

Appendix 2.1: Element concentrations in Water Samples (ppb); dp = field duplicate,

*** = split sample, () indicates values below detection limit.**

Month	May	May	June	June	June	June
Sample	SWS6A	SWS6B	SWS1	SWS2	SWS3	SWS4
Li 6	0.60	2.09	0.70	0.59	(0.41)	(0.43)
Li 7	(0.59)	2.02	0.68	0.64	(0.47)	(0.61)
Be	0.03	0.04	0.04	0.03	0.02	(0.004)
B	6.84	25.2	8.92	8.32	6.21	8.86
C (cps)	41459195	42031464	52977146	44976600	39712108	48488762
N (cps)	220768044	216894261	268869076	231162111	212226496	230287866
Mg	1210	2462	943	1329	1207	1317
Al	24.9	10.2	45.9	32.1	26.8	28.2
Si	745	2154	839	859	769	843
P	(1700)	(1700)	(282)	(203)	(1700)	(1700)
S	(4500)	(4500)	(4500)	(4500)	(4500)	(4500)
Cl	104027	209566	40292	117229	103578	114127
Ca 42	4665	23140	5067	7843	(1016)	4832
Ca 43	6930	23640	3692	7813	7000	8072
Ti	0.51	0.84	0.85	0.82	0.61	0.72
V	0.32	(0.19)	0.86	0.22	0.26	0.61
Cr 52	(0.29)	(0.14)	0.48	0.49	(0.04)	(0.25)
Cr 53	1.05	1.38	0.68	1.06	0.85	0.98
Fe 54	63.2	619	67.1	121	55	80
Mn	79.5	445	8.75	148	133	132
Fe 56	(37.9)	664	(51.2)	(68.8)	(11.5)	(41.9)
Fe 57	81.3	618	76.0	129	82.0	92.0
Co	0.07	0.40	(0.05)	0.15	0.14	0.13
Ni	1.13	1.19	1.41	0.96	3.79	0.98
Cu	5.61	5.94	2.73	3.05	3.31	2.67
Zn	25.5	26.7	24.4	31.3	52.7	49.7
As	(0.08)	(0.14)	(0.13)	(0.18)	(0.08)	(0.08)
Br	(22.5)	(81.6)	(35.6)	(52.9)	(18.1)	(29.1)
Se	(0.30)	(0.30)	(0.19)	(0.08)	(0.30)	(0.30)
Rb	0.72	2.40	0.55	0.80	0.73	0.75
Sr	30.0	118	10.8	34.2	31.0	33.3
Mo	0.13	1.57	0.07	0.16	0.14	0.14
Ag	0.09	0.01	0.01	0.13	0.10	0.12
Cd	(0.01)	(0.04)	(0.01)	(0.01)	(0.03)	(0.004)
Sn	0.43	0.42	0.34	0.44	0.28	0.28
Sb	0.08	0.10	0.05	0.10	0.08	0.08
I	16.4	37.4	19.2	23.0	16.6	19.9
Cs	0.02	0.21	0.02	0.03	0.02	0.03
Ba	19.8	82.7	13.0	23.9	23.1	23.3
La	0.26	0.22	0.16	0.38	0.35	0.33
Ce	0.32	0.35	0.18	0.47	0.43	0.39
Hg	(0.02)	(0.02)	(0.02)	(0.02)	(0.02)	(0.02)
Tl	0.40	0.49	0.26	0.39	0.32	0.35
Pb	0.49	0.43	0.40	0.36	0.40	0.35
Bi	(0.01)	(0.003)	(0.01)	(0.01)	(0.01)	(0.01)
U	(0.001)	(0.003)	(0.0001)	(0.003)	(0.002)	(0.0004)

Appendix 2.1: Element concentrations in Water Samples (ppb); dp = field duplicate,

*** = split sample, () indicates values below detection limit.**

Month	June	June	June	June	July	July
Sample	SWS5	SWS5*	SWS6A	SWS6B	SWS1	SWS2
Li 6	(0.40)	(0.45)	(0.56)	1.68	(0.35)	(0.44)
Li 7	(0.53)	(0.51)	(0.54)	1.81	(0.40)	(0.57)
Be	(0.001)	(0.05)	(0.04)	(0.06)	(0.05)	(0.05)
B	11.2	6.34	10.1	27.4	5.72	7.06
C (cps)	48000422	40310005	47726346	51492961	41903373	38477993
N (cps)	216566791	219241429	245912753	227970879	235130646	216452526
Mg	1163	1177	1229	2437	1003	1076
Al	28.2	25.2	36.2	22.8	44.3	56.1
Si	767	743	956	2185	1306	930
P	(1700)	(1700)	(1700)	(1700)	(1700)	(1700)
S	(4500)	(4500)	(93.0)	(4500)	(4500)	(4500)
Cl	99276	98637	112521	234103	31393	92395
Ca 42	(3435)	(3881)	4932	25315	(2135)	(1401)
Ca 43	7087	7108	7630	25938	4306	6591
Ti	0.86	0.63	0.88	1.31	0.63	0.95
V	0.48	0.30	0.76	0.28	0.18	0.31
Cr 52	(0.25)	(0.22)	(0.36)	(0.24)	(0.11)	(0.06)
Cr 53	1.01	1.04	1.19	1.97	0.54	1.02
Fe 54	54	51	(35)	1582	(46.7)	131
Mn	104	77.5	104	432	11.1	163
Fe 56	(32.1)	(32.7)	(22.8)	1489.7	(27.9)	(61.4)
Fe 57	81.0	79.7	(52.7)	1613	75.9	148
Co	0.11	0.07	0.12	0.40	(0.05)	0.12
Ni	2.47	1.48	1.20	3.12	1.65	0.75
Cu	3.62	3.55	2.62	5.10	2.83	2.77
Zn	30.8	70.1	48.3	46.2	18.0	33.9
As	(0.08)	(0.08)	(0.05)	(0.18)	(0.12)	(0.14)
Br	(27.8)	(40.3)	(42.4)	(97.8)	(58.4)	(196)
Se	(0.07)	(0.30)	(0.09)	(0.30)	(0.30)	(0.57)
Rb	0.69	0.77	0.71	2.35	0.52	0.73
Sr	29.0	29.3	30.3	119	11.4	28.2
Mo	0.13	0.13	0.11	0.97	0.07	0.18
Ag	0.09	0.09	0.12	0.01	0.01	0.05
Cd	(0.03)	(0.003)	(0.003)	(0.04)	(0.001)	(0.01)
Sn	0.47	0.67	0.28	0.44	0.41	0.29
Sb	0.07	0.08	0.08	0.11	0.08	0.07
I	17.2	17.3	13.5	40.7	21.8	20.9
Cs	0.02	0.02	0.02	0.19	0.01	0.03
Ba	20.2	19.4	23.0	84.4	7.42	18.7
La	0.30	0.27	0.37	0.70	0.18	0.41
Ce	0.35	0.31	0.46	1.04	0.18	0.65
Hg	(0.02)	(0.02)	(0.005)	(0.02)	(0.02)	(0.02)
Tl	0.30	0.31	0.31	0.33	0.16	0.30
Pb	0.39	0.41	0.33	0.66	0.21	0.49
Bi	(0.01)	(0.01)	(0.01)	(0.01)	(0.01)	(0.01)
U	(0.0004)	(0.01)	(0.01)	(0.001)	(0.01)	(0.003)

Appendix 2.1: Element concentrations in Water Samples (ppb); dp = field duplicate,

*** = split sample, () indicates values below detection limit.**

Month	July	July	July	July	July	July
Sample	SWS3	SWS4	SWS5	SWS6A	SWS6B	SWS6B*
Li 6	0.62	0.71	(0.56)	0.66	1.81	1.93
Li 7	0.67	0.66	0.66	0.75	1.84	1.95
Be	(0.05)	(0.04)	(0.01)	(0.03)	(0.06)	(0.07)
B	7.28	9.81	8.76	7.83	24.8	22.4
C (cps)	39594074	41520362	39738800	39943902	46342229	39524367
N (cps)	229289401	219601300	227065089	222241957	199528883	227694216
Mg	1252	1260	1171	1206	2187	2234
Al	64.3	65.1	57.0	57.0	17.6	15.7
Si	1051	1026	965	1021	1902	1940
P	(1700)	(1700)	(1700)	(1700)	(1700)	(1700)
S	(4500)	(110)	(4500)	(4500)	(4500)	(23.3)
Cl	103488	104878	100341	102356	189015	191602
Ca 42	6245	6755	5401	5555	19103	20294
Ca 43	7494	7558	7128	7473	20678	21041
Ti	1.03	1.12	1.13	1.18	0.89	0.96
V	0.39	0.29	0.31	0.29	0.54	0.23
Cr 52	(0.33)	(0.39)	(0.23)	(0.30)	(0.15)	(0.06)
Cr 53	1.12	1.11	0.92	1.11	1.41	1.13
Fe 54	191	196	151	168	704	722
Mn	210	183	144	96.9	369	372
Fe 56	112	115	82.7	92.4	781	757
Fe 57	200	199	164	177	739	734
Co	0.14	0.12	0.10	0.07	0.33	0.33
Ni	1.34	0.78	2.28	1.36	1.84	0.80
Cu	3.34	3.33	3.40	3.96	3.34	3.67
Zn	31.4	42.2	43.8	47.6	48.2	31.7
As	(0.19)	(0.24)	(0.20)	(0.21)	(0.29)	(0.24)
Br	(37.8)	(46.1)	(28.3)	(60.5)	(81.8)	(78.7)
Se	0.97	(0.49)	(0.23)	(0.31)	(0.42)	(0.48)
Rb	0.77	0.82	0.82	0.89	2.10	2.13
Sr	33.1	32.3	30.8	32.1	98.9	100
Mo	0.20	0.20	0.19	0.21	0.95	0.94
Ag	0.07	0.07	0.06	0.07	0.07	0.01
Cd	(0.02)	(0.03)	(0.01)	(0.01)	(0.04)	0.08
Sn	0.29	0.44	0.26	0.59	0.44	0.32
Sb	0.08	0.10	0.09	0.11	0.13	0.12
I	24.8	25.2	22.3	25.3	31.8	31.2
Cs	0.03	0.03	0.03	0.03	0.19	0.18
Ba	21.8	21.6	23.4	18.3	66.2	66.5
La	0.45	0.48	0.42	0.39	0.32	0.32
Ce	0.69	0.73	0.63	0.58	0.54	0.54
Hg	(0.02)	(0.02)	(0.02)	(0.02)	(0.02)	(0.02)
Tl	0.33	0.32	0.30	0.28	0.30	0.28
Pb	0.52	0.52	0.55	0.51	0.41	0.37
Bi	(0.01)	(0.00005)	(0.0005)	(0.0001)	(0.01)	(0.01)
U	(0.005)	(0.005)	(0.004)	(0.003)	(0.004)	(0.005)

**Appendix 2.1: Element concentrations in Water Samples (ppb); dp = field duplicate,
* = split sample, () indicates values below detection limit.**

Month	August	August	August	August	August	August
Sample	SWS1	SWS1*	SWS2	SWS3	SWS4	SWS5
Li 6	0.65	0.69	0.58	0.66	0.61	0.70
Li 7	0.69	0.76	0.64	0.72	0.64	0.72
Be	(0.01)	(0.003)	0.03	0.04	0.04	0.03
B	5.19	6.49	6.99	11.4	7.13	7.47
C (cps)	36703705	34896844	36505769	36894491	34966874	37523475
N (cps)	210428072	191602210	216281128	219143984	190136197	229370626
Mg	1404	1420	1361	1469	1423	1453
Al	12.6	12.1	27.8	35.1	40.6	33.1
Si	1552	1617	1035	1144	1053	1177
P	(550)	(550)	(550)	(550)	(550)	(550)
S	(225)	(225)	(81.9)	(104)	(225)	(308)
Cl	39035	42384	104939	111556	107351	112014
Ca 42	4863	5383	6688	7874	7118	8557
Ca 43	5988	6134	7906	8650	8517	8502
Ti	(0.19)	(0.10)	0.56	0.74	2.40	1.09
V	(0.09)	0.34	0.41	0.45	0.29	0.49
Cr 52	(0.17)	(0.17)	(0.30)	0.44	0.53	0.48
Cr 53	(0.11)	0.16	0.60	0.76	0.97	0.80
Fe 54	(75.0)	(75.0)	321	347	324	323
Mn	1.37	2.33	98.2	129	90.9	67.4
Fe 56	(79.5)	(79.5)	319	355	299	337
Fe 57	(15.7)	(12.5)	346	362	349	334
Co	(0.02)	(0.03)	0.24	0.16	(0.09)	(0.08)
Ni	0.38	0.60	128	4.03	1.62	1.56
Cu	1.87	4.01	463	14.4	4.96	6.10
Zn	6.25	10.3	213	78.7	21.2	21.5
As	0.14	0.14	0.27	0.22	0.23	0.20
Br	74.9	77.5	71.2	70.4	66.7	72.6
Se	(0.50)	(0.003)	(0.50)	(0.19)	(0.50)	(0.42)
Rb	0.74	0.91	1.05	2.16	1.20	1.29
Sr	16.0	15.9	35.2	39.4	36.6	37.9
Mo	0.07	0.08	0.36	0.28	0.26	0.27
Ag	0.04	0.02	0.16	0.36	0.18	0.16
Cd	(0.01)	(0.01)	0.09	0.13	0.06	0.05
Sn	0.31	0.37	0.72	3.39	1.05	2.07
Sb	0.09	0.08	0.11	0.19	0.09	0.10
I	35.9	37.4	34.9	35.3	34.7	37.0
Cs	0.02	0.02	0.04	0.04	0.04	0.04
Ba	6.7	6.37	18.3	22.5	20.0	19.3
La	0.04	0.05	0.30	0.34	0.30	0.30
Ce	0.04	0.04	0.46	0.49	0.43	0.42
Hg	(0.01)	(0.01)	(0.01)	(0.01)	(0.01)	(0.01)
Tl	0.74	0.88	1.51	1.55	1.44	1.44
Pb	0.13	0.20	33.6	1.71	0.83	0.86
Bi	(0.01)	(0.01)	0.01	0.005	(0.01)	(0.002)
U	0.01	0.01	0.01	0.01	0.01	0.01

Appendix 2.1: Element concentrations in Water Samples (ppb); dp = field duplicate,

*** = split sample, () indicates values below detection limit.**

Month Sample	August SWS6A	August SWS6B	September SWS1	September SWS1*	September SWS2	September SWS3
Li 6	0.67	1.80	0.38	0.47	0.61	0.64
Li 7	0.70	1.84	0.39	0.46	0.63	0.69
Be	0.03	0.02	0.01	(0.01)	0.03	0.03
B	8.20	20.1	5.65	6.28	7.55	7.38
C (cps)	35600830	34299133	34609549	33301813	34353241	34139348
N (cps)	219647950	188318451	196411608	196378215	182528521	200840175
Mg	1406	2005	1124	1153	1216	1269
Al	26.5	8.48	27.7	28.7	34.9	39.6
Si	1063	1740	1597	1620	1400	1475
P	(550)	(550)	(550)	(550)	(550)	(550)
S	(86.6)	(1.72)	(225)	(225)	(225)	(225)
Cl	108530	155746	35423	36746	92162	94200
Ca 42	7202	16731	4020	4236	5873	6393
Ca 43	8281	17572	4599	4710	6713	7040
Ti	0.77	0.24	(0.17)	0.34	0.48	1.51
V	0.42	0.29	0.31	0.26	0.42	0.35
Cr 52	(0.21)	(0.13)	(0.17)	(0.17)	(0.19)	0.35
Cr 53	0.64	0.63	0.26	0.24	0.98	0.89
Fe 54	259	316	(81)	(88)	259	270
Mn	36.3	329	9.28	10.6	166	184
Fe 56	210	299	(58.8)	(62.1)	242	267
Fe 57	282	341	95.3	101	283	290
Co	(0.07)	0.28	(0.06)	(0.07)	0.16	0.16
Ni	1.54	0.96	1.63	1.14	1.69	1.28
Cu	7.49	4.86	3.91	6.08	8.74	6.14
Zn	22.5	21.4	7.79	9.92	32.87	22.91
As	0.18	0.30	0.18	0.18	0.27	0.25
Br	68.1	59.8	53.5	52.2	62.2	62.6
Se	(0.50)	(0.50)	(0.06)	(0.26)	(0.50)	(0.15)
Rb	1.53	2.29	0.86	1.08	1.46	1.32
Sr	37.7	86.4	12.3	12.6	28.9	30.9
Mo	0.26	0.67	0.05	0.09	0.21	0.19
Ag	0.20	0.06	0.05	0.18	0.31	0.20
Cd	0.04	0.05	0.01	0.02	0.05	0.02
Sn	0.41	1.40	0.74	1.26	1.06	1.51
Sb	0.11	0.18	0.06	0.06	0.09	0.09
I	35.9	31.4	23.3	23.2	26.9	26.1
Cs	0.04	0.18	0.01	0.01	0.03	0.03
Ba	17.7	58.8	5.60	6.03	17.7	19.8
La	0.26	0.13	0.08	0.09	0.30	0.33
Ce	0.35	0.20	0.11	0.12	0.50	0.52
Hg	(0.01)	(0.01)	(0.01)	(0.01)	(0.01)	(0.01)
Tl	1.35	1.48	0.72	0.78	1.23	1.22
Pb	0.89	0.65	0.28	0.51	0.78	0.71
Bi	(0.01)	(0.003)	(0.002)	(0.003)	(0.002)	(0.05)
U	0.01	0.01	0.005	(0.001)	0.005	0.01

**Appendix 2.1: Element concentrations in Water Samples (ppb); dp = field duplicate,
* = split sample, () indicates values below detection limit.**

Month	September	September	September	September	October	October
Sample	SWS4	SWS5	SWS6A	SWS6B	SWS1	SWS1*
Li 6	0.64	0.66	0.68	1.78	0.42	0.37
Li 7	0.66	0.70	0.69	1.91	0.41	0.40
Be	0.04	0.03	0.04	0.03	0.02	(0.01)
B	7.66	7.67	6.96	21.7	5.33	5.80
C (cps)	36324255	34979830	34301571	33819855	32340670	32454956
N (cps)	198602203	184535048	213192370	210756404	201032638	180570845
Mg	1298	1287	1268	2071	1011	1036
Al	37.7	39.1	35.7	7.23	40.4	60.0
Si	1521	1526	1429	1970	1710	1736
P	(550)	(550)	(550)	(550)	(550)	1560
S	(206)	(178)	(80.5)	(99.4)	(225)	(225)
Cl	98258	98036	93361	157877	31157	31981
Ca 42	7592	7812	6669	17692	3124	3869
Ca 43	7140	7201	6972	17529	3844	3864
Ti	0.60	0.84	0.62	0.52	0.55	0.65
V	0.31	0.42	0.29	0.15	0.13	0.38
Cr 52	0.41	0.38	(0.21)	(0.19)	(0.17)	(0.05)
Cr 53	0.81	0.76	0.66	0.59	0.30	0.25
Fe 54	287	290	245	392	(89.7)	(90.0)
Mn	169	152	98.7	326	18.3	19.3
Fe 56	297	271	191	362	(79.2)	(93.8)
Fe 57	307	300	270	411	93.0	102
Co	0.16	0.15	(0.09)	0.32	(0.06)	(0.07)
Ni	1.99	1.77	2.46	2.25	1.07	1.66
Cu	8.17	7.63	5.18	5.61	3.52	2.98
Zn	30.82	28.57	29.71	30.69	13.68	9.52
As	0.31	0.27	0.25	0.36	0.13	0.16
Br	65.6	64.5	65.8	64.8	41.2	44.2
Se	(0.37)	(0.22)	(0.20)	(0.42)	(0.12)	(0.50)
Rb	1.39	1.31	1.01	2.26	0.81	0.93
Sr	31.0	30.8	30.7	85.8	10.4	10.9
Mo	0.21	0.21	0.19	1.75	0.05	0.10
Ag	0.27	0.26	0.25	0.03	0.06	0.07
Cd	0.04	0.04	0.03	0.04	0.02	0.02
Sn	1.44	1.29	0.48	0.35	0.40	1.58
Sb	0.09	0.10	0.09	0.10	0.03	0.05
I	27.6	26.4	23.9	27.4	13.8	15.1
Cs	0.03	0.03	0.03	0.18	0.01	0.01
Ba	19.1	18.2	24.3	54.9	5.42	5.55
La	0.32	0.32	0.27	0.21	0.09	0.10
Ce	0.50	0.49	0.40	0.40	0.13	0.14
Hg	(0.01)	(0.01)	(0.01)	(0.01)	(0.01)	(0.01)
Tl	1.24	1.26	1.13	1.36	0.65	0.69
Pb	0.78	0.86	0.71	0.56	0.35	0.58
Bi	(0.001)	(0.0002)	(0.004)	(0.003)	(0.001)	(0.001)
U	0.01	0.01	0.01	0.01	(0.003)	(0.002)

Appendix 2.1: Element concentrations in Water Samples (ppb); dp = field duplicate,

*** = split sample, () indicates values below detection limit.**

Month	October	October	October	October	October	October
Sample	SWS2	SWS3	SWS4	SWS5	SWS6A	SWS6B
Li 6	0.60	0.60	0.55	0.62	0.58	1.89
Li 7	0.58	0.63	0.56	0.65	0.63	1.90
Be	0.03	0.03	0.03	0.03	0.03	0.02
B	6.64	7.29	6.81	7.07	6.92	21.0
C (cps)	33116855	13690844	31345277	33425255	31112518	32274100
N (cps)	201873567	58279132	185248225	197680010	181440700	204624540
Mg	1212	1181	1189	1278	1208	2103
Al	59.7	29.6	35.8	39.1	31.7	14.4
Si	1396	1469	1436	1472	1359	1941
P	(550)	(550)	(550)	1361	(550)	(550)
S	(225)	(4500)	(225)	2685	(225)	(326)
Cl	87067	84405	83150	86372	83188	152384
Ca 42	5719	5352	5439	6975	5129	16792
Ca 43	6450	6386	6452	6629	6426	17191
Ti	0.78	0.47	1.06	1.61	0.71	0.67
V	0.37	(0.02)	0.31	0.34	0.31	0.42
Cr 52	(0.15)	(0.03)	(0.21)	0.55	(0.16)	(0.24)
Cr 53	0.76	(0.25)	0.68	0.88	0.74	0.84
Fe 54	176	199	191	202	195	460
Mn	94.0	104	88.8	85.4	56.6	332
Fe 56	(103)	(140)	180	221	(147)	430
Fe 57	187	196	199	208	214	476
Co	(0.10)	(0.08)	(0.09)	(0.11)	(0.08)	0.37
Ni	0.98	(0.32)	0.93	1.52	2.16	6.39
Cu	3.78	2.88	4.62	6.15	7.49	12.7
Zn	18.7	33.0	19.2	24.4	22.7	71.1
As	0.19	0.16	0.16	0.23	0.21	0.33
Br	50.0	44.8	44.1	60.5	55.3	63.1
Se	(0.06)	(0.34)	(0.09)	(0.11)	(0.50)	(0.50)
Rb	1.11	0.74	1.08	1.38	1.23	2.76
Sr	27.2	29.3	27.5	29.1	28.0	85.6
Mo	0.16	0.23	0.16	0.19	0.25	1.54
Ag	0.07	0.04	0.06	0.13	0.13	0.10
Cd	0.03	(0.002)	0.02	0.04	0.11	0.11
Sn	0.97	(0.01)	2.43	1.36	1.29	2.17
Sb	0.08	(0.01)	0.08	0.09	0.08	0.10
I	18.2	5.59	17.0	18.5	17.8	25.0
Cs	0.02	(0.01)	0.02	0.02	0.02	0.17
Ba	16.5	22.1	16.1	16.8	15.1	54.5
La	0.26	0.29	0.28	0.27	0.25	0.23
Ce	0.41	0.40	0.41	0.41	0.36	0.42
Hg	(0.01)	(0.001)	(0.01)	(0.01)	(0.01)	(0.01)
Tl	1.15	5.77	1.21	1.08	1.14	1.30
Pb	0.50	(0.20)	0.56	0.64	0.79	1.28
Bi	(0.001)	(0.01)	0.005	(0.005)	(0.002)	0.004
U	(0.002)	(0.004)	0.004	(0.003)	(0.003)	(0.003)

Appendix 2.1: Element concentrations in Water Samples (ppb); dp = field duplicate,

*** = split sample, () indicates values below detection limit.**

Month	November	November	November	November	November	November
Sample	SWS1	SWS1*	SWS2	SWS3	SWS4	SWS5
Li 6	0.48	0.62	0.50	0.52	6.90	0.58
Li 7	0.51	0.62	0.54	0.55	7.76	0.62
Be	0.03	0.03	0.04	0.05	0.05	0.05
B	4.82	5.73	6.40	6.51	17.8	7.26
C (cps)	32059877	30875404	31095562	31567214	30593989	30616186
N (cps)	198981695	201717320	191469395	213975306	209535968	202409030
Mg	880	961	1090	1119	1157	1142
Al	66.4	75.2	63.1	64.5	122	65.0
Si	1809	1847	1798	1731	1742	1789
P	(550)	(550)	(550)	(65.0)	(550)	(550)
S	(94.5)	(119)	(103)	(261)	(190)	(225)
Cl	26549	28668	79289	77244	79316	77480
Ca 42	2837	3353	4486	4946	4309	4324
Ca 43	2945	3088	5224	5253	5236	5213
Ti	0.65	0.70	1.05	0.89	0.90	1.00
V	0.60	0.26	0.32	0.28	0.37	0.39
Cr 52	(0.17)	(0.01)	0.35	0.36	(0.23)	(0.23)
Cr 53	0.17	0.31	0.83	0.68	0.78	0.78
Fe 54	(69.2)	(47.4)	(103)	(106)	(90.3)	(81.7)
Mn	45.6	48.1	136	95.5	94.8	89.5
Fe 56	(72.4)	(16.2)	(75.4)	(139)	(72.5)	(58.5)
Fe 57	80.6	98.9	115	116	116	115
Co	0.13	0.13	0.20	0.15	0.22	0.13
Ni	3.23	7.88	4.91	1.54	6.87	1.50
Cu	4.15	10.0	5.79	4.25	11.3	4.84
Zn	23.2	77.5	44.7	23.9	45.2	26.3
As	0.11	0.14	0.14	0.20	0.18	0.14
Br	29.0	32.9	39.8	44.5	43.7	41.3
Se	(0.50)	(0.13)	(0.50)	(0.06)	(0.28)	(0.22)
Rb	0.70	0.88	0.91	0.92	1.92	1.01
Sr	8.80	9.41	21.9	22.1	21.9	21.9
Mo	0.06	0.08	0.17	0.16	0.24	0.17
Ag	0.07	0.12	0.09	0.07	0.17	0.09
Cd	0.02	0.07	0.04	0.03	0.10	0.04
Sn	0.51	0.74	0.77	0.94	4.08	3.91
Sb	0.03	0.05	0.08	0.08	0.10	(0.08)
I	4.52	3.86	6.39	5.75	6.65	6.62
Cs	0.01	0.01	0.01	0.01	0.02	0.02
Ba	14.8	7.36	17.0	15.3	17.2	16.9
La	0.15	0.18	0.40	0.41	0.48	0.46
Ce	0.25	0.29	0.60	0.64	0.73	0.68
Hg	(0.01)	(0.01)	(0.01)	(0.01)	(0.01)	(0.01)
Tl	0.57	0.58	1.05	1.05	0.87	0.94
Pb	0.49	0.97	0.79	0.48	1.02	0.50
Bi	(0.0001)	0.01	(0.002)	(0.003)	0.01	(0.01)
U	(0.01)	(0.003)	0.07	(0.001)	(0.003)	(0.003)

**Appendix 2.1: Element concentrations in Water Samples (ppb); dp = field duplicate,
* = split sample, () indicates values below detection limit.**

Month	November	November	December	December	December	December
Sample	SWS6A	SWS6B	SWS1	SWS1*	SWS2	SWS3
Li 6	0.60	1.66	0.59	0.59	0.71	1.61
Li 7	0.61	1.66	0.50	0.56	0.70	1.57
Be	0.05	0.04	(0.04)	(0.03)	0.04	(0.05)
B	6.85	23.8	(5.97)	(4.94)	(3.93)	(7.50)
C (cps)	30365359	34416356	40917454	38425763	39659035	40984420
N (cps)	201947320	177785552	575800247	0	502899777	565421367
Mg	1141	2224	1002	968	1188	1222
Al	61.5	26.6	59.6	56.2	55.4	61.4
Si	1717	2341	1703	1595	1793	1834
P	(550)	(550)	(189)	(6967)	(9485)	(7908)
S	(225)	1637	(4500)	(2680)	(2925)	(3336)
Cl	78855	171144	32307	31972	138034	133203
Ca 42	4575	17631	(1371)	(743)	(3301)	3984
Ca 43	5246	19086	3528	3448	6715	6874
Ti	0.78	0.97	0.63	0.63	0.89	0.84
V	0.30	0.79	1.01	0.58	1.17	0.78
Cr 52	(0.18)	(0.08)	4.56	(0.16)	(0.01)	(0.08)
Cr 53	0.69	1.05	5.13	0.74	0.97	1.21
Fe 54	(65.0)	1452	46.7	38.1	83.5	81.0
Mn	80.7	352	56.6	60.0	166	142
Fe 56	(72.5)	1237	(35.3)	(48.1)	(70.1)	(104)
Fe 57	99.0	1436	(53.6)	59.0	95.6	102
Co	(0.12)	0.37	(0.09)	(0.14)	0.22	0.21
Ni	1.04	1.60	2.62	0.98	0.61	0.99
Cu	4.13	5.89	2.18	2.91	2.69	3.93
Zn	23.0	30.6	(4.63)	(14.8)	(19.3)	25.3
As	0.16	0.32	0.11	0.10	(0.10)	0.11
Br	39.4	64.7	45.8	58.4	56.8	65.6
Se	(0.02)	(0.50)	(0.18)	(0.18)	(0.18)	(0.18)
Rb	1.03	2.37	0.68	0.75	0.78	0.99
Sr	21.8	89.9	9.41	9.49	26.9	27.2
Mo	0.18	0.73	0.24	0.07	0.28	0.25
Ag	0.08	0.06	(0.01)	(0.01)	(0.03)	(0.03)
Cd	0.04	0.05	0.02	0.03	0.03	0.04
Sn	0.81	0.80	(0.85)	(0.85)	(0.85)	(0.85)
Sb	0.09	0.17	0.10	0.07	0.08	0.09
I	5.73	20.0	12.7	12.2	12.9	11.8
Cs	0.02	0.18	0.01	0.01	0.02	0.02
Ba	16.6	68.0	5.94	6.20	19.4	20.7
La	0.44	0.60	0.12	0.18	0.43	0.46
Ce	0.64	1.09	0.20	0.27	0.66	0.69
Hg	(0.01)	(0.01)	(0.02)	(0.02)	(0.02)	(0.02)
Tl	0.93	1.02	2.10	1.44	4.18	3.56
Pb	0.44	0.63	0.45	0.72	0.54	0.69
Bi	(0.002)	(0.01)	(0.0003)	(0.002)	(0.01)	(0.01)
U	0.01	0.004	(0.003)	(0.001)	0.004	(0.003)

Appendix 2.1: Element concentrations in Water Samples (ppb); dp = field duplicate,

*** = split sample, () indicates values below detection limit.**

Month	December	December	December	December	January	January
Sample	SWS4	SWS5	SWS6A	SWS6B	SWS1	SWS1*
Li 6	(0.49)	1.81	(0.46)	1.79	(0.46)	0.55
Li 7	0.51	1.66	0.48	1.95	0.56	0.58
Be	(0.04)	(0.05)	(0.04)	0.07	(0.03)	(0.02)
B	(5.38)	(7.12)	(6.43)	24.3	(4.52)	(5.73)
C (cps)	41424026	43559946	43453920	38826587	45731147	46501337
N (cps)	505595737	551027141	515214923	585006142	512360857	0
Mg	1237	1314	1298	2465	1337	1309
Al	59.3	61.4	78.7	16.7	58.2	56.8
Si	1861	1965	1917	2434	1557	1565
P	(7881)	(405)	(11285)	(1412)	(8000)	(9875)
S	(2608)	(2250)	(2999)	(3048)	(3704)	(2807)
Cl	141448	148033	149661	368713	61274	64925
Ca 42	3978	5592	9756	24768	(2298)	4195
Ca 43	6848	7243	7130	26565	5108	5335
Ti	0.73	1.16	1.07	1.51	0.57	0.64
V	0.49	1.58	1.51	1.00	0.90	1.19
Cr 52	(0.02)	0.32	0.29	(0.22)	(0.14)	(0.14)
Cr 53	0.97	0.94	0.97	2.56	1.04	0.80
Fe 54	67.8	93.3	107	1467	26.3	27.8
Mn	136	142	131	501	67.9	68.3
Fe 56	(58.6)	(119)	(92.1)	(93.0)	(65.5)	(54.6)
Fe 57	83.6	94.2	115	1530	36.2	(46.9)
Co	0.20	0.19	(0.17)	0.39	(0.09)	(0.08)
Ni	0.58	0.83	1.17	1.04	2.03	2.69
Cu	2.86	2.41	3.69	5.66	6.19	11.3
Zn	(20.5)	(21.7)	(22.9)	28.4	27.5	39.4
As	(0.08)	0.15	(0.10)	0.31	(0.06)	(0.08)
Br	60.1	74.4	80.2	183	(26.2)	(27.6)
Se	(0.18)	(0.04)	(0.18)	(0.18)	(0.18)	(0.20)
Rb	0.83	0.78	0.81	3.02	0.89	0.97
Sr	27.2	28.5	28.7	126	13.8	13.9
Mo	0.25	0.31	0.28	1.51	0.04	0.05
Ag	(0.003)	(0.01)	(0.03)	(0.04)	(0.04)	(0.04)
Cd	0.03	0.05	0.03	0.06	0.04	0.05
Sn	(0.85)	(0.85)	(0.85)	(0.85)	(0.85)	(0.34)
Sb	0.07	0.10	0.08	0.15	0.03	(0.05)
I	12.2	12.2	11.7	22.3	8.66	9.97
Cs	0.02	0.02	0.02	0.24	0.01	0.02
Ba	18.7	19.8	18.7	88.1	8.86	8.83
La	0.47	0.47	0.43	0.53	0.13	0.13
Ce	0.68	0.66	0.62	0.95	0.21	0.21
Hg	(0.02)	(0.02)	(0.02)	(0.02)	(0.02)	(0.02)
Tl	3.21	2.99	2.65	4.44	0.99	0.99
Pb	0.58	0.61	0.53	1.03	0.50	0.65
Bi	(0.0001)	(0.01)	(0.01)	(0.01)	(0.003)	(0.005)
U	(0.003)	0.01	0.004	0.01	0.004	0.003

Appendix 2.1: Element concentrations in Water Samples (ppb); dp = field duplicate,

*** = split sample, () indicates values below detection limit.**

Month	January	January	January	January	January	January
Sample	SWS2	SWS3	SWS4	SWS5	SWS6A	SWS6B
Li 6	0.91	0.51	0.62	0.71	(0.49)	1.62
Li 7	1.17	0.59	0.62	0.72	0.59	1.74
Be	0.06	(0.04)	(0.05)	(0.05)	(0.04)	(0.02)
B	(6.55)	(4.99)	(7.33)	(7.28)	(5.53)	17.1
C (cps)	43575251	43905411	47236175	47713099	45094815	41208865
N (cps)	506872089	526943299	536416660	524979740	568947042	423633498
Mg	1579	1514	1588	1607	1544	2374
Al	84.5	50.8	57.8	53.7	48.2	17.6
Si	1720	1744	1793	1838	1794	1978
P	(811)	(8000)	(8000)	(7070)	(8000)	(8000)
S	(4512)	(2250)	9068	7255	5305	5056
Cl	203936	210052	216869	220304	208344	500000
Ca 42	6262	6288	8903	10432	8189	29032
Ca 43	9622	9654	10172	10124	9783	30533
Ti	1.33	1.00	1.16	1.10	1.02	2.77
V	1.97	1.85	0.82	0.83	0.82	2.89
Cr 52	0.73	0.31	0.42	0.69	0.43	0.51
Cr 53	2.67	1.76	2.17	2.20	2.13	8.60
Fe 54	141	93.0	83.3	107	71.7	1267
Mn	246	228	234	233	226	383
Fe 56	(37.8)	(15.1)	(57.7)	142	(83.6)	309
Fe 57	146	101	(89.0)	129	(89.7)	1354
Co	0.65	0.36	0.36	0.37	0.31	0.43
Ni	21.3	2.70	3.95	5.28	1.45	2.21
Cu	30.0	9.69	14.3	37.5	7.27	12.7
Zn	240	54.1	62.6	106	55.0	43.7
As	0.18	(0.12)	(0.11)	0.19	0.18	0.89
Br	68.1	50.3	90.3	77.9	60.3	161.7
Se	(0.18)	(0.15)	(0.18)	(0.18)	(0.18)	(0.18)
Rb	2.06	1.73	1.47	2.44	1.34	3.85
Sr	39.1	38.4	39.5	39.8	39.1	149
Mo	0.28	0.22	0.23	0.23	0.21	0.85
Ag	0.41	0.19	0.08	0.10	(0.05)	(0.04)
Cd	0.22	0.09	0.08	0.13	0.08	0.14
Sn	(1.02)	2.94	3.17	4.40	(0.77)	(0.56)
Sb	0.13	0.16	0.09	0.12	0.07	0.15
I	10.6	9.75	11.3	12.3	11.0	21.8
Cs	0.03	0.03	0.03	0.03	0.03	0.23
Ba	35.3	29.0	29.7	29.9	29.0	92.2
La	0.51	0.51	0.52	0.51	0.48	0.60
Ce	0.72	0.73	0.73	0.72	0.68	0.85
Hg	(0.02)	(0.02)	(0.02)	(0.02)	(0.02)	(0.02)
Tl	1.55	1.80	1.60	1.41	1.33	3.20
Pb	2.72	0.95	1.04	1.76	1.31	1.43
Bi	(0.02)	(0.01)	(0.005)	(0.01)	(0.001)	(0.01)
U	0.01	0.004	0.003	0.005	0.003	0.01

**Appendix 2.1: Element concentrations in Water Samples (ppb); dp = field duplicate,
* = split sample, () indicates values below detection limit.**

Month	February	February	February	February	February	February
Sample	SWS1	SWS1*	SWS2	SWS3	SWS4	SWS5
Li 6	0.50	0.51	0.43	0.49	0.46	0.74
Li 7	0.46	0.44	0.43	0.48	0.47	0.73
Be	0.03	0.03	0.05	0.06	0.06	0.05
B	4.16	6.18	4.83	5.38	5.93	5.70
C (cps)	83395016	0	79652044	81574866	83611926	66434728
N (cps)	287937752	0	266634934	302908294	283644671	300745612
Mg	972	955	1407	1494	1517	1552
Al	62.4	65.8	54.7	60.4	60.0	61.8
Si	1468	1559	1618	1714	1700	1752
P	(8000)	(8000)	(8000)	(8000)	(1507)	(8000)
S	(1628)	(5000)	(1409)	(2213)	(792)	(1180)
Cl	30982	32651	153788	159527	174347	175817
Ca 42	13171	1604	20811	21458	22697	23550
Ca 43	4312	3495	10379	10911	11184	11427
Ti	0.56	0.57	0.88	0.95	0.89	0.94
V	(0.43)	(0.30)	(0.13)	(0.30)	(0.45)	2.33
Cr 52	(0.22)	(0.27)	(0.14)	0.43	(0.39)	3.96
Cr 53	0.58	0.64	0.63	0.69	0.75	4.39
Fe 54	43.5	42.3	57.2	89.8	78.9	91.2
Mn	60.2	62.1	172	169	169	169
Fe 56	(30.8)	(50.2)	(86.8)	(164)	(128)	146
Fe 57	(39.6)	(54.0)	(88.0)	(114)	(112)	130
Co	0.11	0.14	0.28	0.29	0.30	0.39
Ni	1.28	18.4	(0.47)	1.17	1.05	9.04
Cu	3.90	8.64	2.41	4.08	3.30	5.58
Zn	31.3	36.0	34.2	49.1	37.2	52.6
As	0.12	0.15	(0.08)	(0.09)	(0.12)	0.14
Br	32.8	59.2	59.4	66.4	64.3	74.0
Se	(0.49)	(0.49)	(0.49)	(0.49)	(0.49)	0.49
Rb	0.72	1.10	0.85	1.09	1.15	1.19
Sr	10.7	10.5	35.9	38.2	38.9	39.9
Mo	0.04	(0.02)	0.18	0.21	0.22	0.38
Ag	0.03	0.03	(0.01)	0.02	(0.004)	0.02
Cd	(0.02)	0.02	0.04	0.06	0.03	0.07
Sn	(0.02)	(1.84)	(1.10)	(1.10)	(1.10)	1.10
Sb	0.04	0.06	0.05	0.07	0.07	0.09
I	6.76	8.42	6.98	8.53	8.08	7.94
Cs	0.01	0.01	0.02	0.02	0.02	0.02
Ba	7.21	7.43	27.7	28.5	29.0	29.5
La	0.13	0.14	0.73	0.78	0.77	0.78
Ce	0.22	0.23	0.94	0.99	0.98	0.98
Hg	(0.09)	(0.01)	(0.09)	(0.09)	(0.09)	0.09
Tl	(0.05)	(0.001)	(0.05)	(0.05)	(0.05)	0.001
Pb	0.31	0.62	0.17	0.32	0.26	0.83
Bi	(0.004)	(0.002)	(0.001)	(0.001)	(0.0005)	0.001
U	(0.01)	(0.001)	(0.001)	(0.002)	(0.0003)	0.002

**Appendix 2.1: Element concentrations in Water Samples (ppb); dp = field duplicate,
* = split sample, () indicates values below detection limit.**

Month	February	February
Sample	SWS6A	SWS6B
Li 6	0.55	1.93
Li 7	0.52	1.63
Be	0.05	0.05
B	5.47	26.7
C (cps)	79755352	0
N (cps)	302542214	0
Mg	1555	4809
Al	56.3	14.7
Si	1814	2632
P	(5823)	(8000)
S	(439)	(5000)
Cl	185282	754333
Ca 42	25488	37146
Ca 43	11611	37817
Ti	0.91	2.82
V	(0.06)	1.24
Cr 52	0.35	1.13
Cr 53	0.75	3.60
Fe 54	67.9	2976
Mn	162	731
Fe 56	131	2770
Fe 57	101	3047
Co	0.28	0.50
Ni	0.84	0.92
Cu	2.91	17.6
Zn	39.0	33.6
As	0.10	0.31
Br	75.5	188
Se	0.49	0.49
Rb	0.99	3.46
Sr	40.6	175
Mo	0.19	1.71
Ag	0.01	0.01
Cd	0.05	0.10
Sn	1.10	1.40
Sb	0.07	0.16
I	8.10	30.5
Cs	0.02	0.26
Ba	29.5	114
La	0.71	0.99
Ce	0.89	1.23
Hg	0.09	0.09
Tl	0.05	0.01
Pb	0.22	0.28
Bi	0.01	0.001
U	0.002	0.01

Appendix 2.2: Water sample measurements for pH, dissolved oxygen (mg l⁻¹), conductivity (μS cm⁻¹), and temperature (°C).

Site	pH	D.O	Conductivity	Temperature
TCWS-1	6.45	9.31	101	17.2
TCWS-2	7.08	9.24	71	19.5
TCWS-3	6.77	8.83	68	17.2
TCWS-4	6.88	8.11	68	18.4
TCWS-5	6.81	8.33	69	17.3
TCWS-6	7.04	8.53	69	18.9
TCWS-7	7.02	8.44	71	16.0
TCWS-8	6.89	8.37	82	17.1
TCWS-9	8.53	7.31	225	15.3
TCWS-10	8.14	7.98	226	14.8
TCWS-11	8.13	7.65	227	14.9
TCWS-12	7.79	7.51	676	12.5
TCWS-13	6.59	3.00	1405	7.7
TCWS-14	7.77	7.35	348	13.9
TCWS-15	7.75	3.50	364	14.1
BCWS-1	4.66	8.34	235	18.2
BCWS-2	5.05	8.94	170	17.8
BCWS-3	4.74	8.84	235	17.4
BCWS-4	4.58	9.04	237	17.4
BCWS-5	4.75	8.43	241	17.2
BCWS-6	4.69	9.05	240	17.0
BCWS-7	4.59	8.72	238	18.9
BCWS-8	4.61	9.08	235	17.1
BCWS-9	4.70	8.79	240	16.9
BCWS-10	6.36	8.92	60	18.8
BCWS-11	6.11	9.14	56	18.1
BCWS-12	5.36	8.52	70	18.1
BCWS-13	6.74	9.54	70	12.3
BCWS-14	6.74	9.15	48	16.5
BCWS-15	6.84	9.13	38	16.5
BCWS-16	6.83	8.89	37	17.2
BCWS-17	6.89	8.85	36	17.3
BCWS-18	6.76	9.28	37	15.4

Appendix 2.2: Water sample measurements for pH, dissolved oxygen (mg l⁻¹), conductivity (μS cm⁻¹), and temperature (°C).

Day #	Site	pH	D.O.	Conductivity	Temperature
BCWS-19		6.87	8.88	35	15.1
BCWS-20		7.15	9.36	37	15.2
BCWS-21		6.94	9.02	41	15.3
RRS-1		6.73	7.67	95	19.3
RRS-2		6.71	8.11	83	20.0
RRS-3		6.55	8.29	52	18.9
RRS-4		6.32	7.83	45	19.2
RRS-5		6.48	7.62	92	18.8
RRS-6		6.43	8.15	51	18.8
RRS-7		6.14	7.78	44	19.2
RRS-8		6.11	7.46	50	19.3
RRS-9		6.27	7.42	52	20.2
RRS-10		6.34	7.52	57	19.5
RRS-11		6.43	7.89	72	18.3
RRS-12		6.37	7.65	101	19.0
RRS-13		6.46	7.75	64	19.0
RRS-14		6.43	7.27	65	19.0
RRS-15		6.38	7.35	222	19.5

Appendix 2.2: Water sample measurements for pH, dissolved oxygen (mg l⁻¹), conductivity (μS cm⁻¹), and temperature (°C).

Day #	Site	pH	D.O.	Conductivity	Temperature
5	SWS1	7.12	12.52	467	3.0
	SWS2	6.89	10.42	900	2.9
	SWS3	7.00	10.68	888	2.3
	SWS4	7.03	11.61	895	2.2
	SWS5	6.99	11.55	894	2.5
	SWS6A	6.69	11.78	888	2.6
	SWS6B	7.49	10.52	1588	5.4
12	SWS1	7.29	12.91	495	2.3
	SWS2	6.95	11.40	842	1.9
	SWS3	7.01	11.44	838	2.0
	SWS4	6.97	11.42	842	1.8
	SWS5	6.90	11.07	837	2.0
	SWS6A	6.66	11.83	834	2.1
	SWS6SB	7.60	10.61	1452	5.0
19	SWS1	7.08	13.1	185	1.6
	SWS2	6.61	12.12	588	1.2
	SWS3	6.63	12.18	598	1.2
	SWS4	6.76	12.75	596	1.3
	SWS5	6.65	12.82	597	1.6
	SWS6A	6.80	12.62	600	1.6
	SWS6B	7.12	11.25	1418	5.3
26	SWS1	7.12	12.59	208	0.9
	SWS2	6.80	11.33	539	1.6
	SWS3	6.70	10.78	548	1.7
	SWS4	6.69	11.44	553	1.4
	SWS5	6.76	11.68	555	1.3
	SWS6A	6.75	11.80	556	2.2
	SWS6B	7.23	10.06	1200	4.3
36	SWS1	7.30	11.35	320	2.3
	SWS2	7.00	10.13	1057	1.6
	SWS3	7.10	10.65	1055	1.3
	SWS4	7.05	11.05	1062	1.5
	SWS5	6.99	10.85	1046	1.6

Appendix 2.2: Water sample measurements for pH, dissolved oxygen (mg l⁻¹), conductivity (μS cm⁻¹), and temperature (°C).

Day #	Site	pH	D.O.	Conductivity	Temperature
43	SWS6A	7.07	10.62	1046	2.1
	SWS6B	7.65	9.73	1746	4.6
	SWS1	7.25	11.12	210	4.2
	SWS2	7.12	10.60	550	3.8
	SWS3	7.15	10.75	558	3.8
	SWS4	7.10	10.95	558	4.0
47	SWS5	7.03	10.95	563	4.4
	SWS6A	7.10	11.11	560	4.9
	SWS6B	7.43	10.00	1177	6.9
	SWS1	7.33	11.35	156	4.8
	SWS2	6.95	10.16	528	6.5
	SWS3	7.02	10.95	518	5.4
54	SWS4	7.00	11.36	523	5.9
	SWS5	6.96	10.53	521	7.2
	SWS6A	6.95	10.38	526	6.8
	SWS6B	7.51	9.65	978	8.1
	SWS1	7.42	13.65	145	3.6
	SWS2	6.89	12.49	515	5.3
60	SWS3	7.08	11.99	512	5.1
	SWS4	7.11	13.45	515	5.2
	SWS5	7.09	12.29	511	6.0
	SWS6A	6.85	12.90	516	6.1
	SWS6B	7.60	11.00	960	6.8
	SWS1	7.34	12.63	184	4.9
66	SWS2	6.86	11.78	560	5.2
	SWS3	6.90	11.53	562	5.4
	SWS4	6.82	12.53	567	5.4
	SWS5	6.90	11.88	574	6.1
	SWS6A	7.05	11.67	559	6.1
	SWS6B	7.60	10.81	1030	7.2
66	SWS1	7.33	12.22	208	4.3
	SWS2	6.90	11.58	670	5.9
	SWS3	6.95	11.61	666	4.6

Appendix 2.2: Water sample measurements for pH, dissolved oxygen (mg l⁻¹), conductivity (μS cm⁻¹), and temperature (°C).

Day #	Site	pH	D.O.	Conductivity	Temperature
79	SWS4	6.93	11.63	665	4.7
	SWS5	6.85	11.46	657	6.5
	SWS6A	6.91	11.98	654	7.2
	SWS6B	7.61	11.24	1025	7.1
	SWS1	6.84	11.59	139	6.9
	SWS2	6.46	10.53	451	7.9
	SWS3	6.66	10.95	441	7.5
	SWS4	6.38	10.61	440	7.4
	SWS5	7.09	10.74	442	7.7
	SWS6A	6.72	11.01	451	8.0
85	SWS6B	7.28	10.40	1098	8.1
	SWS1	6.88	10.33	142	9.5
	SWS2	6.48	9.83	450	11.2
	SWS3	6.65	9.89	452	10.2
	SWS4	6.47	9.54	454	10.4
	SWS5	6.50	9.72	454	9.5
	SWS6A	6.60	9.62	455	11.4
	SWS6B	7.26	9.90	1014	8.7
	SWS1	6.80	10.04	151	10.8
	SWS2	6.50	9.69	456	12.5
94	SWS3	6.56	9.78	471	12.1
	SWS4	6.44	9.99	466	12.8
	SWS5	6.44	9.75	460	12.1
	SWS6A	6.63	9.76	453	13.2
	SWS6B	7.13	9.65	890	10.9
	SWS1	7.04	9.51	173	12.6
	SWS2	6.35	9.39	407	14.6
	SWS3	6.48	9.45	411	13.5
	SWS4	6.69	9.30	410	14.1
	SWS5	6.83	9.30	414	15.1
101	SWS6A	6.69	9.15	405	14.5
	SWS6B	7.12	9.20	838	12.1
	SWS1	7.24	9.73	143	11.0
	SWS2	6.35	9.39	407	14.6
	SWS3	6.48	9.45	411	13.5
	SWS4	6.69	9.30	410	14.1
	SWS5	6.83	9.30	414	15.1
	SWS6A	6.69	9.15	405	14.5
	SWS6B	7.12	9.20	838	12.1
	SWS1	7.24	9.73	143	11.0
107	SWS1	7.24	9.73	143	11.0

Appendix 2.2: Water sample measurements for pH, dissolved oxygen (mg l⁻¹), conductivity (μS cm⁻¹), and temperature (°C).

Day #	Site	pH	D.O.	Conductivity	Temperature
115	SWS2	6.43	8.53	407	12.8
	SWS3	6.50	8.37	410	13.1
	SWS4	6.43	8.72	408	14.5
	SWS5	6.69	8.58	402	14.1
	SWS6A	6.69	8.71	390	14.6
	SWS6B	7.36	8.45	880	13.0
	SWS1	7.13	10.26	178	9.2
	SWS2	6.61	9.60	449	13.1
	SWS3	6.65	9.05	452	13.1
	SWS4	6.51	9.09	455	13.9
149	SWS5	6.55	9.04	410	14.8
	SWS6A	6.53	9.33	410	14.9
	SWS6B	7.28	9.24	865	12.8
	SWS1	6.78	8.54	198	16.2
	SWS2	6.08	7.63	489	20.2
	SWS3	6.16	7.54	497	21.0
	SWS4	6.66	7.63	493	21.9
	SWS5	6.63	7.34	494	21.5
	SWS6A	6.67	7.38	491	21.3
	SWS6B	7.15	9.31	715	17.1
156	SWS1	6.50	10.27	108	17.2
	SWS2	6.06	9.54	280	17.9
	SWS3	6.17	9.37	281	18.6
	SWS4	6.48	9.74	284	18.9
	SWS5	6.52	9.85	286	19.5
	S6WSA	6.53	9.95	287	20.0
	S6WSB	6.93	11.32	802	17.1
	SWS1	6.75	10.20	180	17.9
	SWS2	6.36	9.63	444	25.1
	SWS3	6.31	9.00	450	25.1
175	SWS4	6.66	9.01	451	25.3
	SWS5	6.64	9.02	449	25.4
	SWS6A	6.62	9.35	447	26.0

Appendix 2.2: Water sample measurements for pH, dissolved oxygen (mg l⁻¹), conductivity (μS cm⁻¹), and temperature (°C).

Day #	Site	pH	D.O.	Conductivity	Temperature
186	SWS6B	7.00	9.33	890	26.2
	SWS1	6.82	9.01	190	18.0
	SWS2	6.54	7.73	427	24.9
	SWS3	6.55	7.51	434	24.0
	SWS4	6.74	8.02	434	25.0
	SWS5	6.83	7.66	430	25.7
193	SWS6A	6.81	8.03	438	26.0
	SWS6B	7.08	8.99	666	19.7
	SWS1	6.75	9.07	200	17.5
	SWS2	6.50	7.81	440	23.8
	SWS3	6.59	7.50	441	23.9
	SWS4	6.70	8.14	444	24.0
208	SWS5	6.81	7.80	431	25.0
	SWS6A	6.75	8.15	437	25.0
	SWS6B	7.14	9.04	680	19.4
	SWS1	6.69	9.83	154	11.3
	SWS2	6.57	8.83	360	13.6
	SWS3	6.71	8.74	349	13.4
215	SWS4	6.72	9.22	355	14.4
	SWS5	6.85	9.02	360	14.3
	SWS6A	6.95	9.44	355	14.3
	SWS6B	7.17	9.04	670	13.9
	SWS1	6.65	9.85	160	10.5
	SWS2	6.55	8.78	383	13.0
222	SWS3	6.73	8.70	385	13.2
	SWS4	6.68	9.30	389	13.6
	SWS5	6.90	9.08	388	14.0
	SWS6A	7.00	9.38	387	14.1
	SWS6B	7.25	9.01	730	13.7
	SWS1	7.18	10.11	172	10.4
	SWS2	6.76	8.67	383	14.5
	SWS3	6.63	8.50	392	14.2
	SWS4	6.79	8.93	390	14.4

Appendix 2.2: Water sample measurements for pH, dissolved oxygen (mg l⁻¹), conductivity (μS cm⁻¹), and temperature (°C).

Day #	Site	pH	D.O.	Conductivity	Temperature
229	SWS5	6.90	8.70	391	14.7
	SWS6A	7.33	9.14	394	14.9
	SWS6B	7.22	8.49	690	13.7
	SWS1	7.21	11.60	163	8.3
	SWS2	6.82	10.35	364	10.8
	SWS3	6.75	10.28	365	11.0
	SWS4	6.92	10.51	367	11.1
	SWS5	7.00	10.22	367	11.1
236	SWS6A	7.15	10.48	370	11.3
	SWS6B	7.24	9.48	647	11.5
	SWS1	6.75	11.38	136	6.8
	SWS2	6.48	9.06	324	10.1
	SWS3	6.32	9.31	331	9.7
	SWS4	6.53	10.18	327	9.9
	SWS5	6.61	9.27	329	10.0
	SWS6A	6.74	9.63	332	10.0
250	SWS6B	6.97	9.48	685	10.6
	SWS1	6.88	11.83	140	7.2
	SWS2	6.69	11.03	329	7.1
	SWS3	6.42	10.89	334	7.2
	SWS4	6.53	11.84	333	7.2
	SWS5	6.66	10.80	335	7.3
	SWS6A	6.83	11.94	332	7.5
	SWS6B	6.89	10.85	584	10.0
261	SWS1	6.63	11.92	126	4.7
	SWS2	6.44	11.19	340	4.2
	SWS3	6.21	11.15	343	3.9
	SWS4	6.29	11.48	344	4.1
	SWS5	6.40	11.00	347	4.2
	SWS6A	6.55	11.25	345	4.4
	SWS6B	6.66	10.97	700	8.9
270	SWS1	6.41	11.44	140	11.4
	SWS2	6.25	11.61	310	10.6

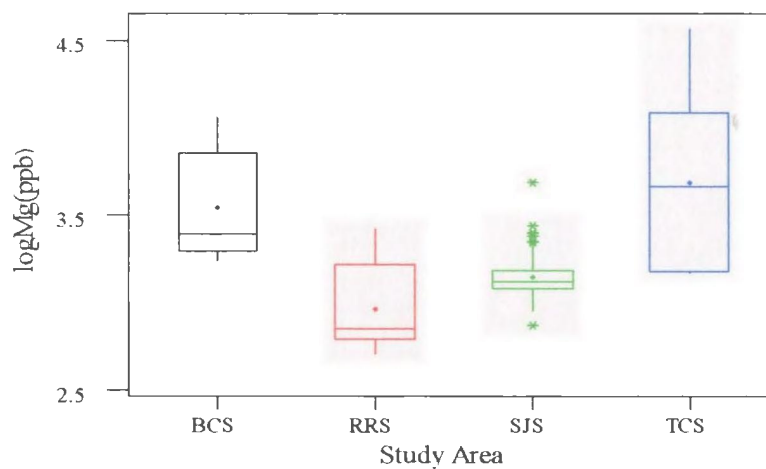
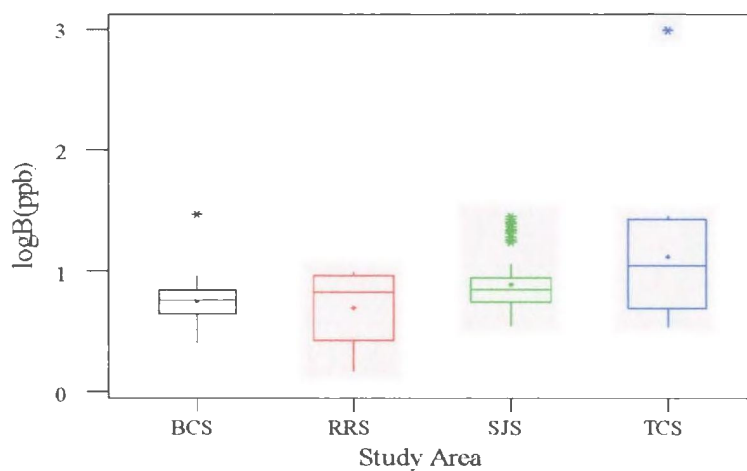
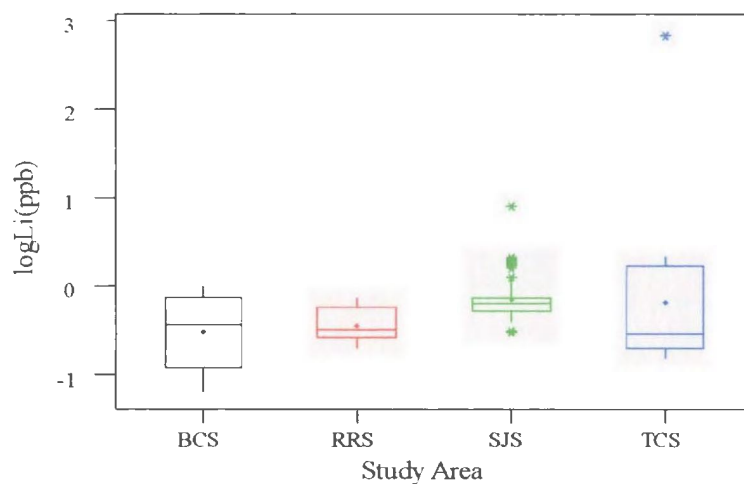
Appendix 2.2: Water sample measurements for pH, dissolved oxygen (mg l⁻¹), conductivity (μS cm⁻¹), and temperature (°C).

Day #	Site	pH	D.O.	Conductivity	Temperature
282	SWS3	6.18	11.42	311	10.6
	SWS4	6.28	11.52	305	10.5
	SWS5	6.30	11.00	306	10.7
	SWS6A	6.43	11.02	310	11.1
	SWS6B	7.03	10.48	770	11.7
	SWS1	6.33	12.12	110	6.3
	SWS2	6.67	11.19	272	5.4
	SWS3	6.40	10.91	278	5.3
	SWS4	6.15	11.39	280	5.2
	SWS5	6.18	11.13	282	5.4
300	SWS6A	6.25	11.15	290	5.2
	SWS6B	7.11	10.22	790	8.5
	SWS1	6.32	13.00	243	1.8
	SWS2	6.55	12.45	540	1.7
	SWS3	6.25	12.33	548	1.9
	SWS4	6.18	12.61	550	2.0
	SWS5	6.22	12.53	551	2.0
	SWS6A	6.27	12.61	553	2.1
	SWS6B	7.35	11.19	1555	4.0
328	SWS1	6.95	13.57	288	1.5
	SWS2	6.86	12.59	756	0.7
	SWS3	6.50	12.52	752	0.6
	SWS4	6.50	12.62	758	0.7
	SWS5	6.55	12.60	760	0.7
	SWS6A	6.73	12.65	761	0.8
	SWS6B	7.10	10.60	3150	3.9
340	SWS1	6.79	12.44	215	0.7
	SWS2	6.70	11.50	530	0.5
	SWS3	6.48	11.47	531	0.5
	SWS4	6.43	11.59	535	0.5
	SWS5	6.55	11.61	535	0.4
	SWS6A	6.69	11.70	540	0.6
	SWS6B	7.15	10.50	2550	4.0
348	SWS1	6.85	12.74	316	1.5
	SWS2	6.73	11.45	888	1.3
	SWS3	6.35	11.40	890	1.2

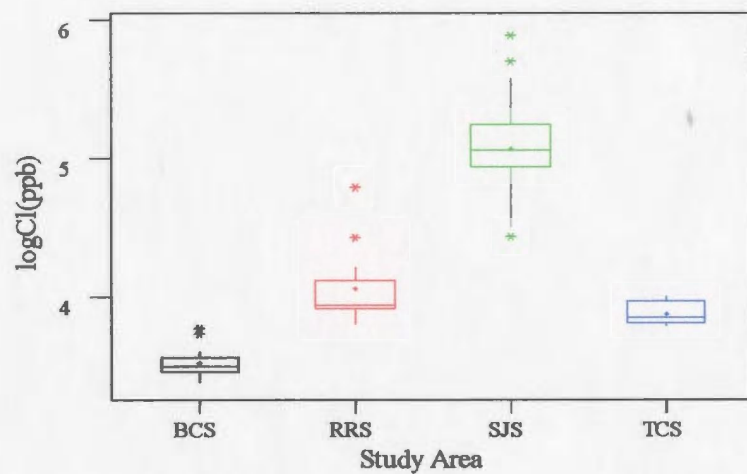
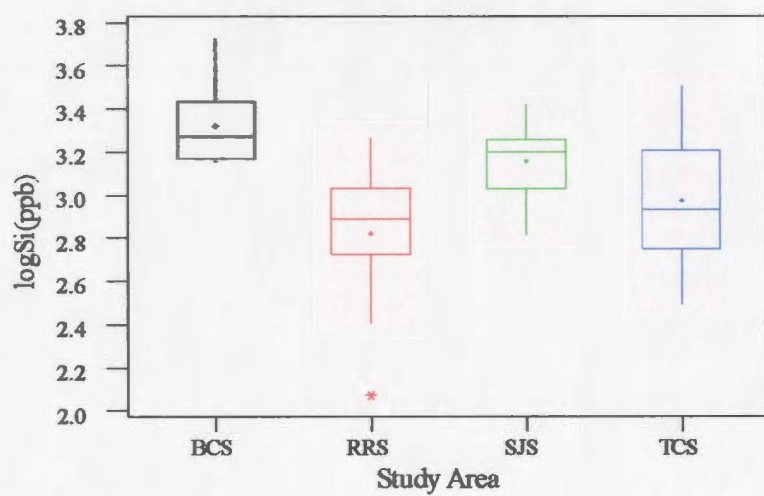
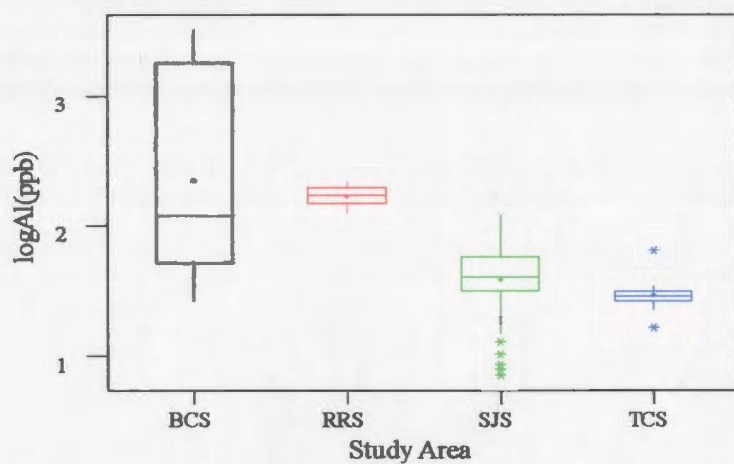
Appendix 2.2: Water sample measurements for pH, dissolved oxygen (mg l⁻¹), conductivity (μS cm⁻¹), and temperature (°C).

Day #	Site	pH	D.O.	Conductivity	Temperature
358	SWS4	6.34	11.53	890	1.2
	SWS5	6.40	11.51	891	1.0
	SWS6A	6.70	11.79	895	1.0
	SWS6B	7.35	10.20	3880	4.3
	SWS1	6.12	13.51	221	1.2
	SWS2	6.60	13.00	662	0.4
	SWS3	6.83	11.99	692	0.3
	SWS4	6.83	12.72	664	0.4
	SWS5	6.90	12.65	693	0.4
	SWS6A	6.90	12.93	698	1.0
365	SWS6B	7.31	11.05	3030	4.6
	SWS1	6.44	13.20	250	1.5
	SWS2	6.30	12.12	563	1.6
	SWS3	6.21	12.03	564	1.7
	SWS4	6.23	12.11	570	1.7
	SWS5	6.29	11.82	571	1.9
	SWS6A	6.35	11.91	576	1.9
	SWS6B	7.17	10.70	2810	5.3

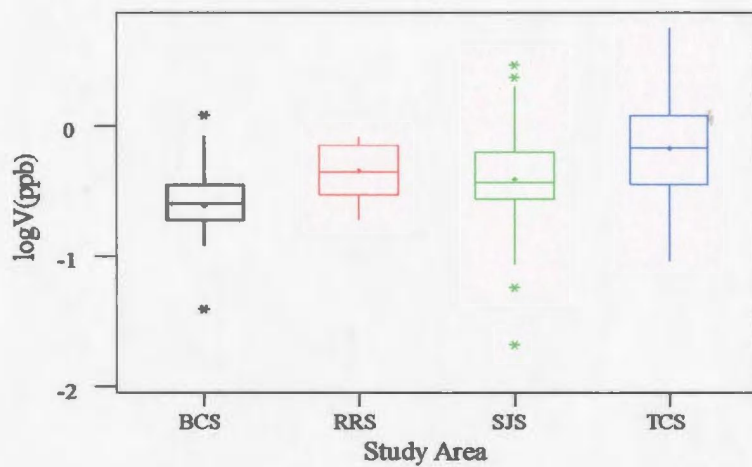
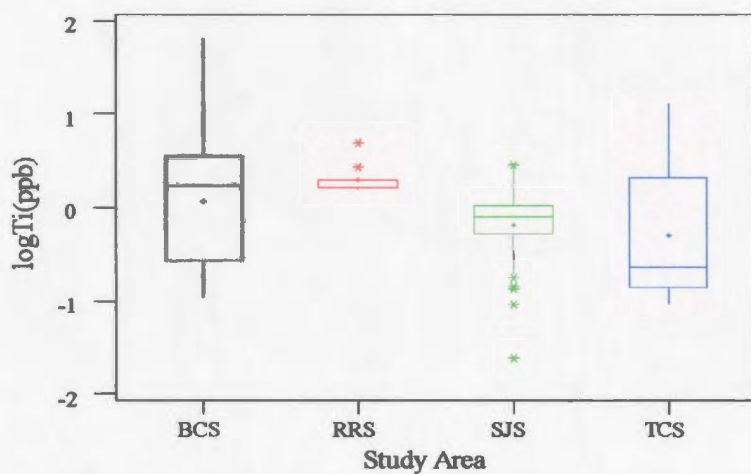
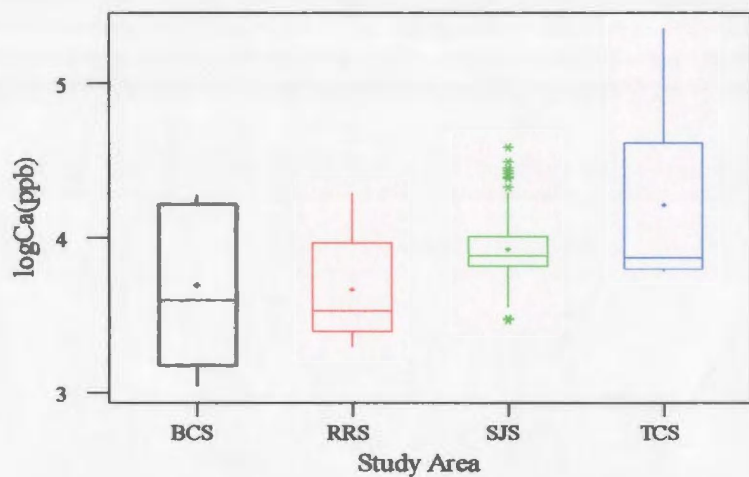
Appendix 3: Box plots of log-transformed analyte concentrations in water samples taken from all four study areas.



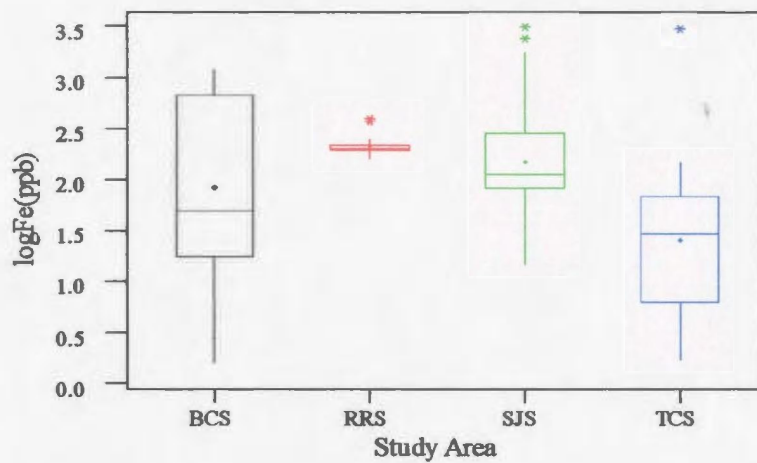
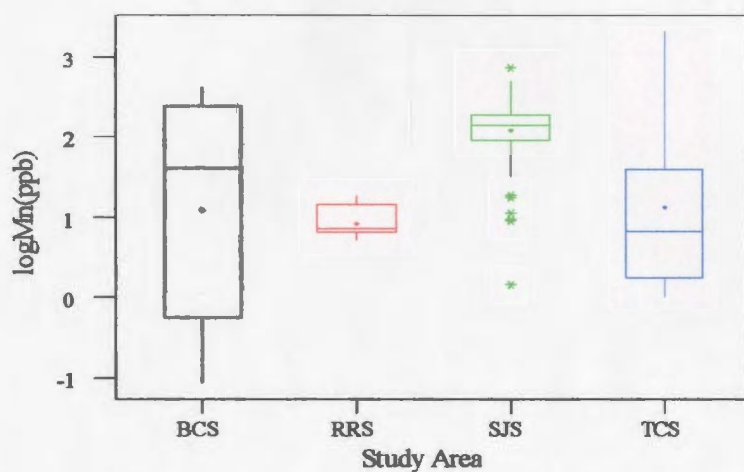
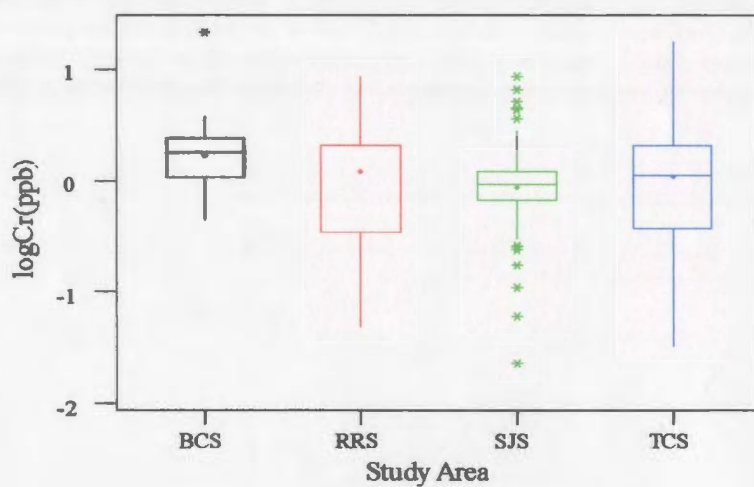
Appendix 3: Box plots of log-transformed analyte concentrations in water samples taken from all four study areas.



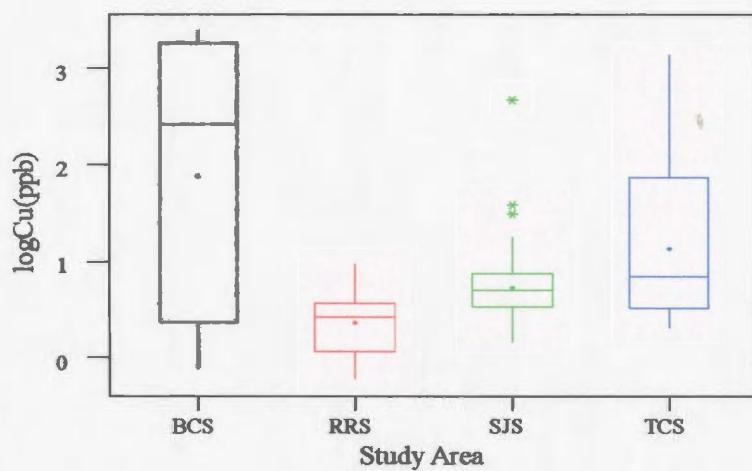
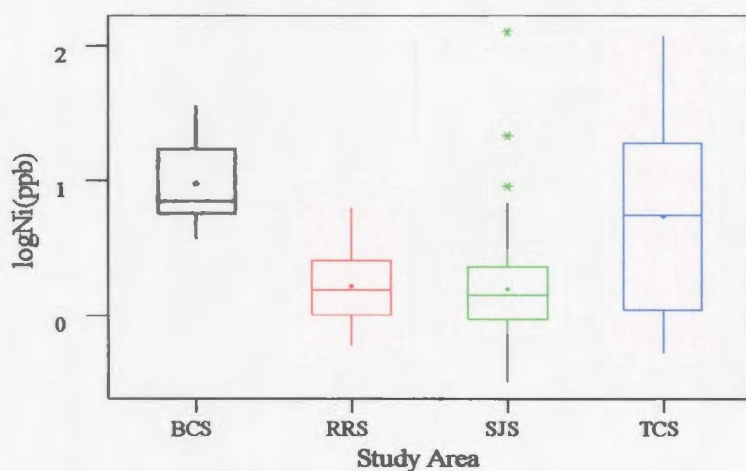
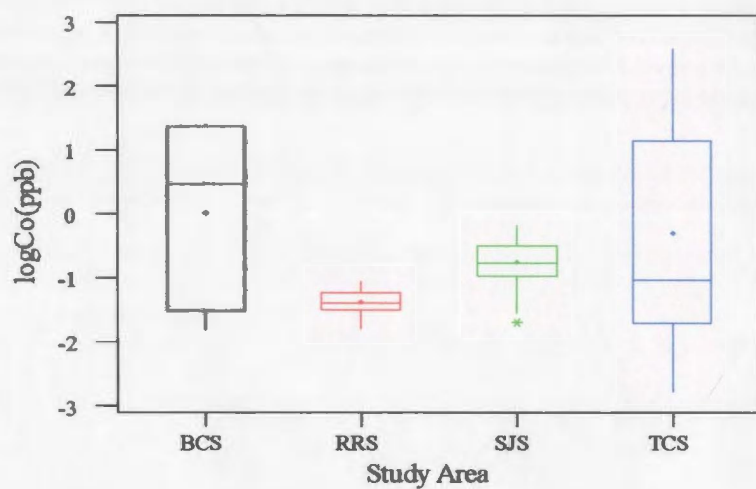
Appendix 3: Box plots of log-transformed analyte concentrations in water samples taken from all four study areas.



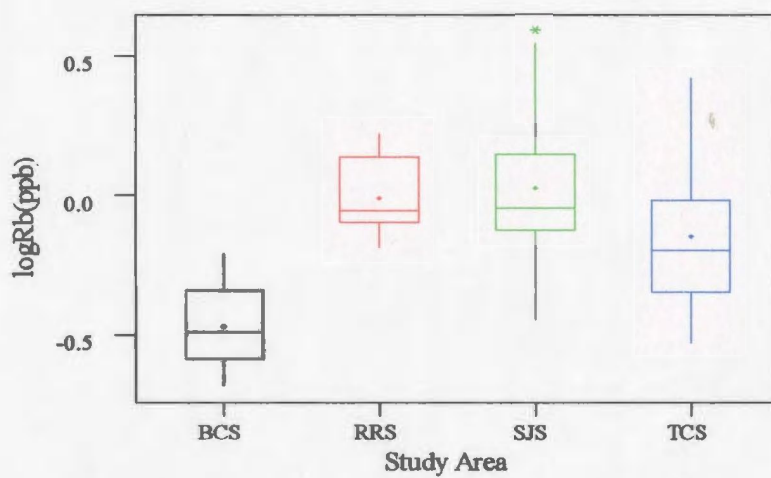
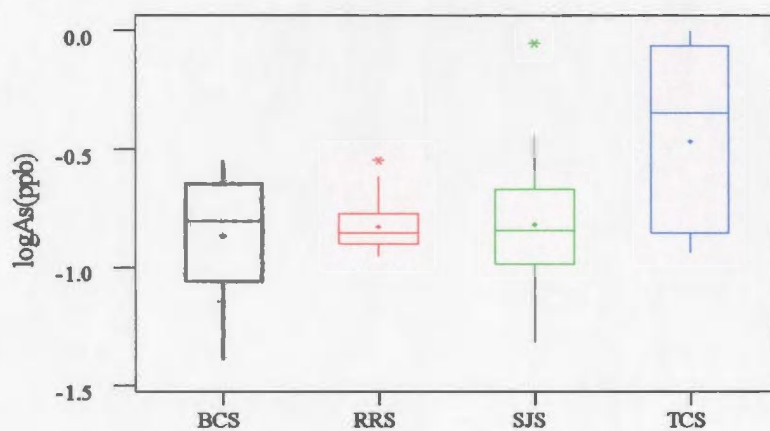
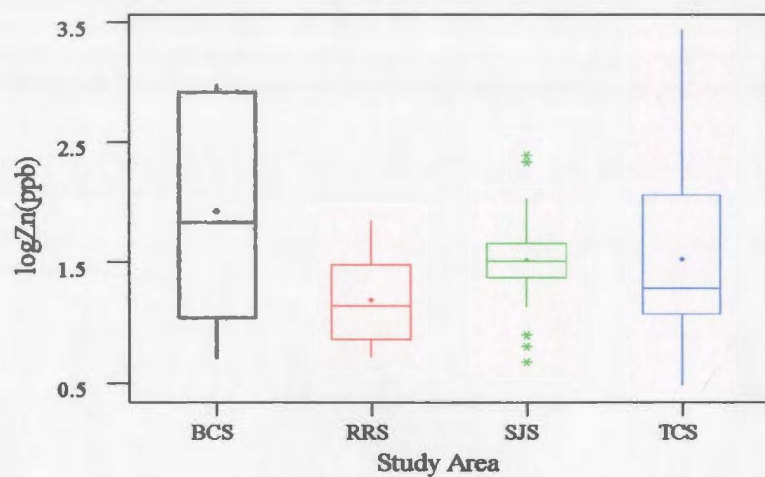
Appendix 3: Box plots of log-transformed analyte concentrations in water samples taken from all four study areas.



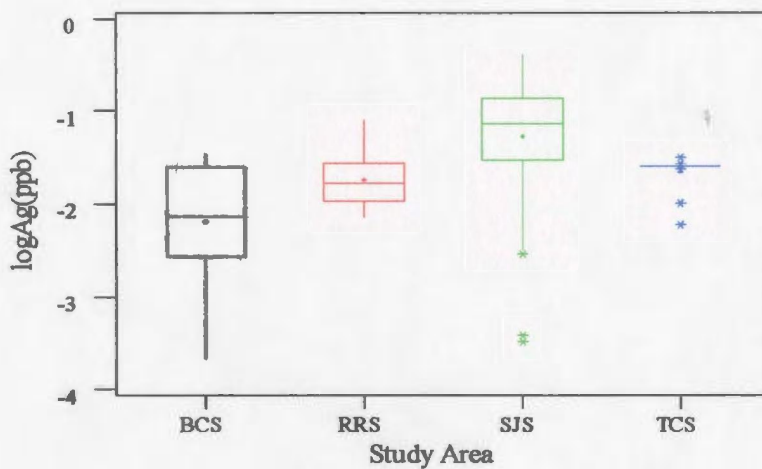
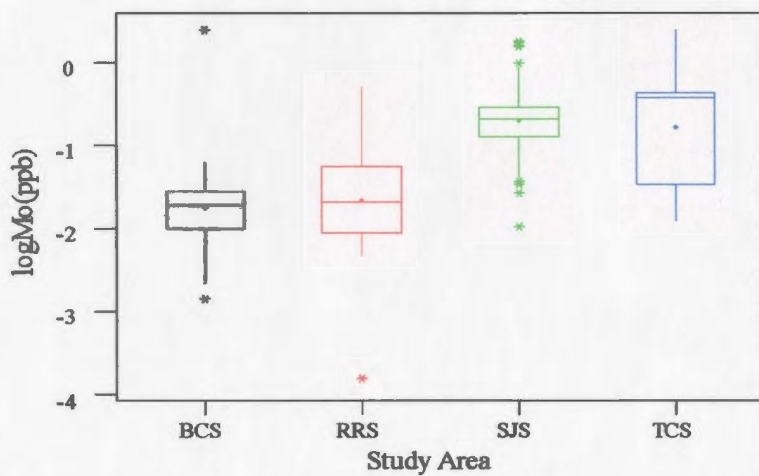
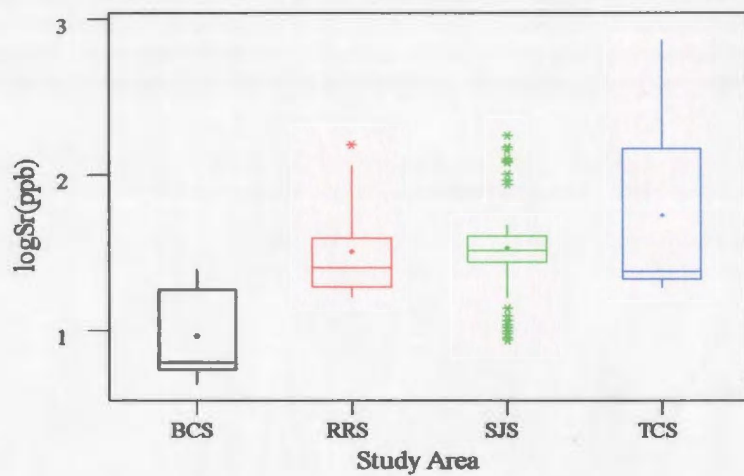
Appendix 3: Box plots of log-transformed analyte concentrations in water samples taken from all four study areas.



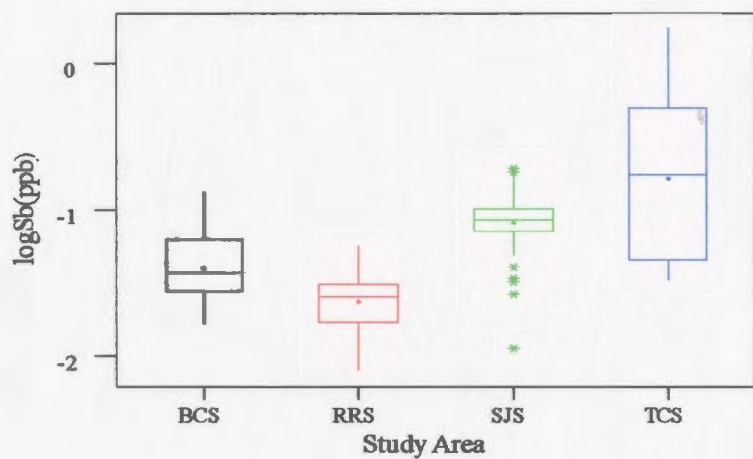
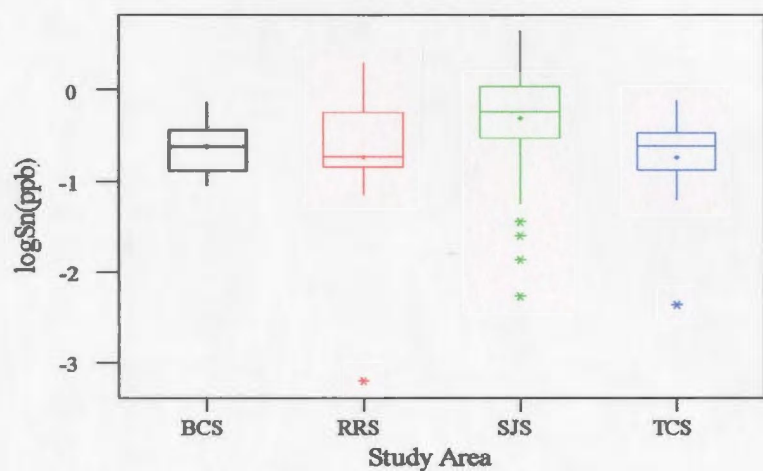
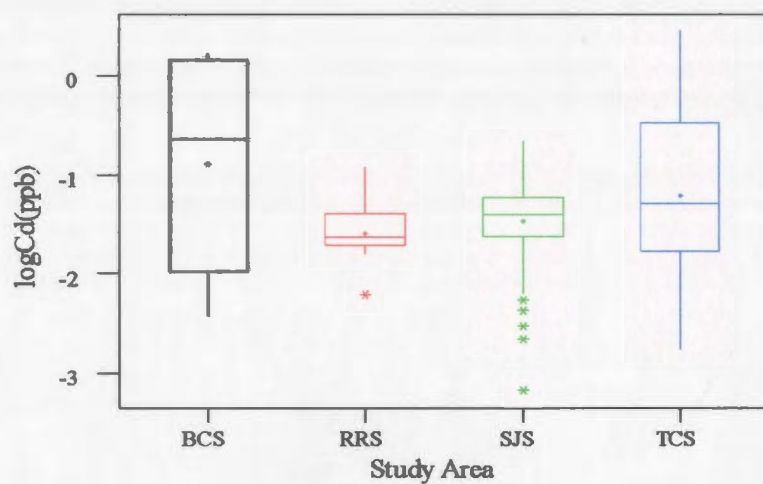
Appendix 3: Box plots of log-transformed analyte concentrations in water samples taken from all four study areas.



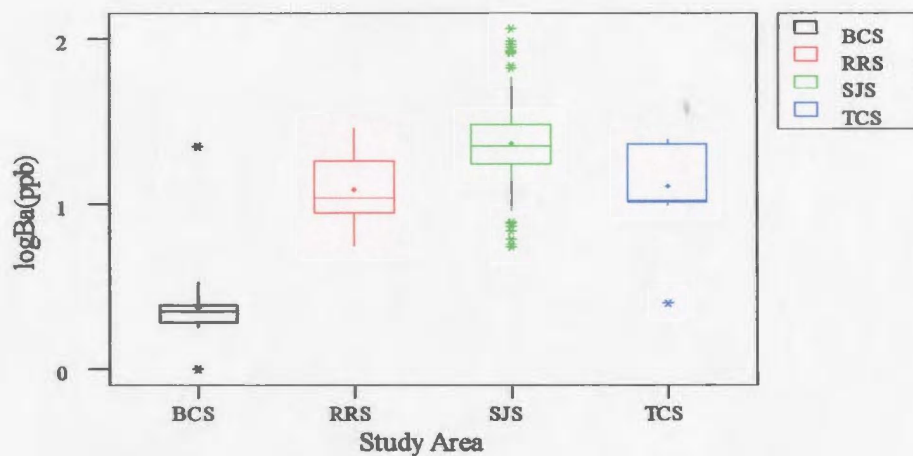
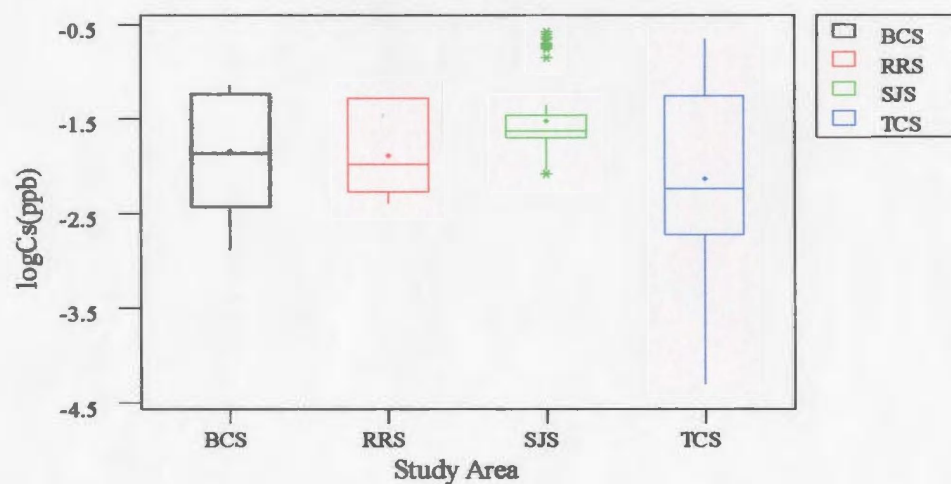
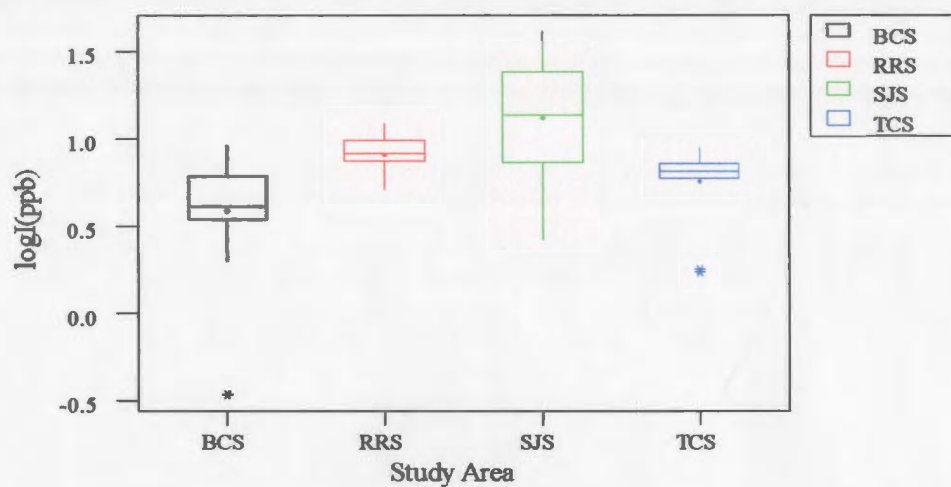
Appendix 3: Box plots of log-transformed analyte concentrations in water samples taken from all four study areas.



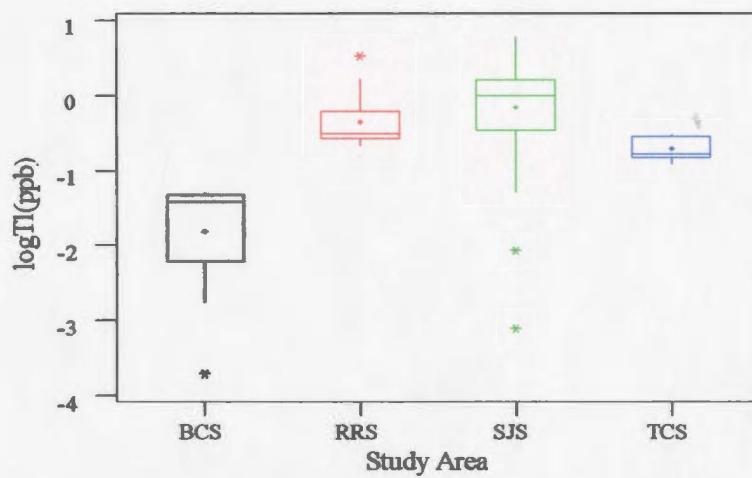
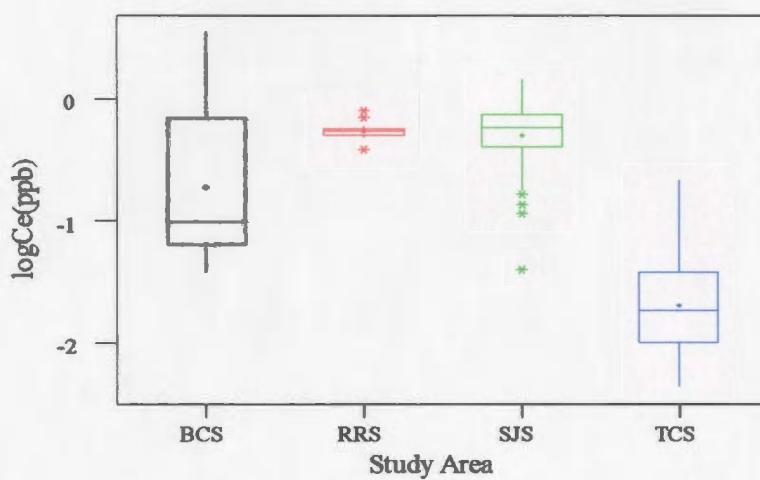
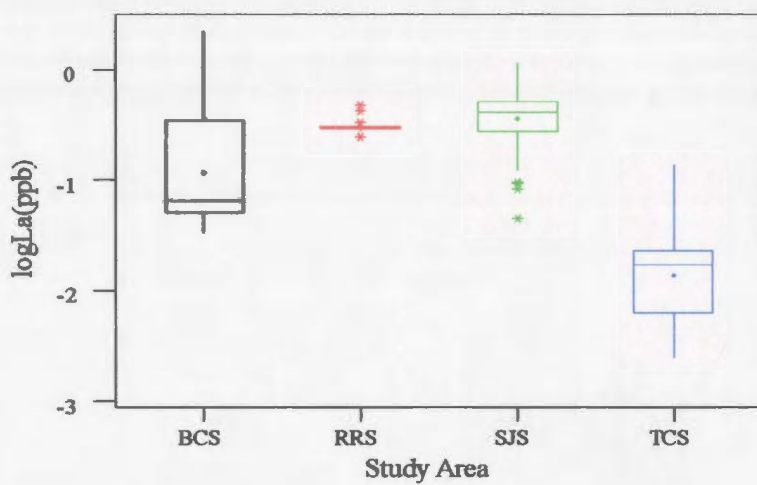
Appendix 3: Box plots of log-transformed analyte concentrations in water samples taken from all four study areas.



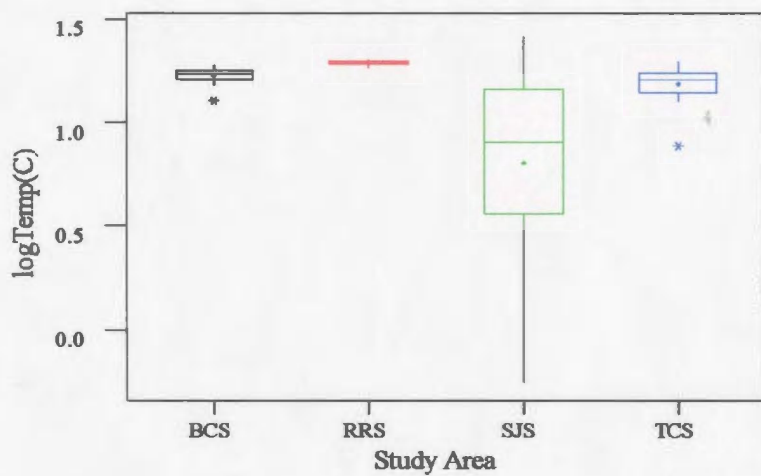
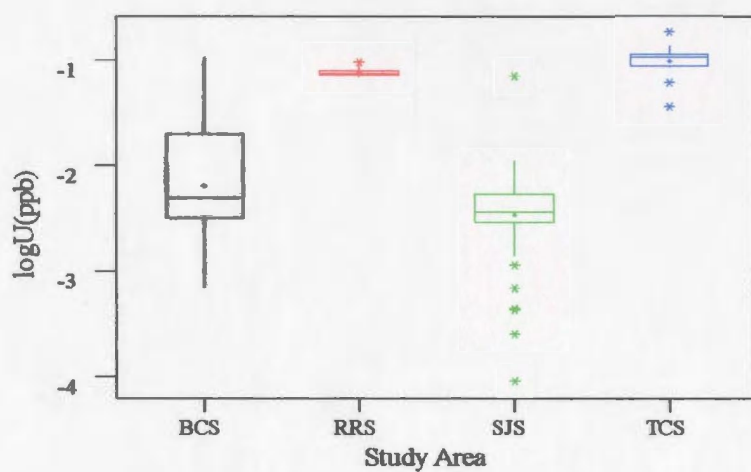
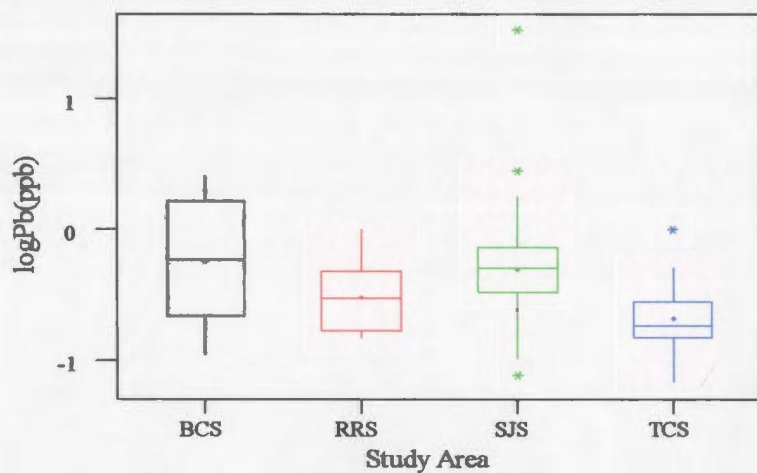
Appendix 3: Box plots of log-transformed analyte concentrations in water samples taken from all four study areas.



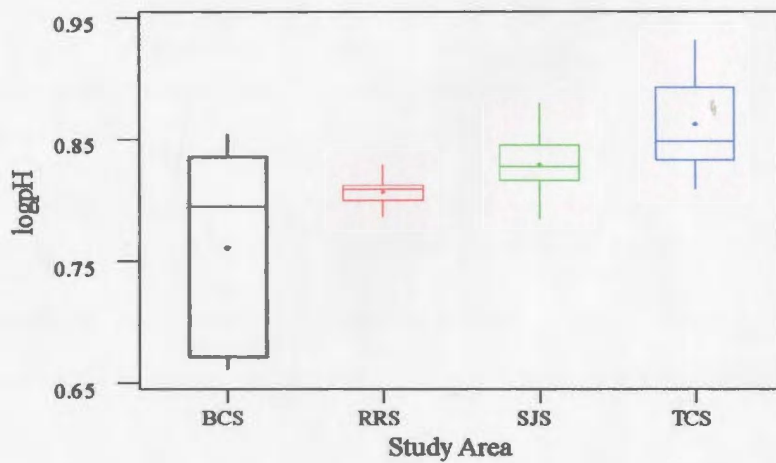
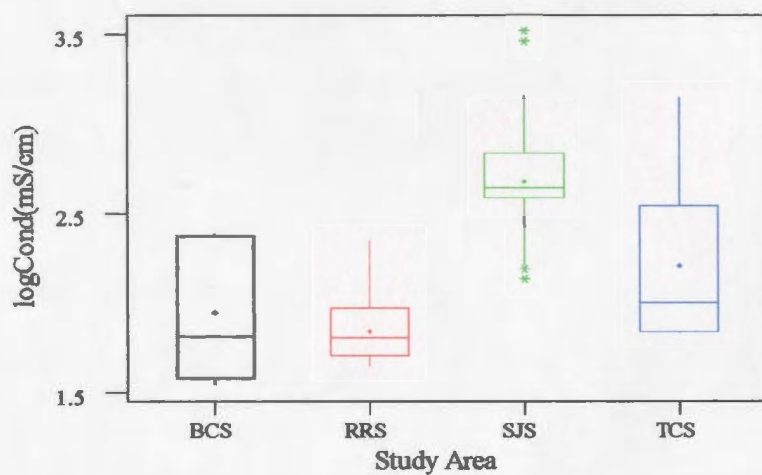
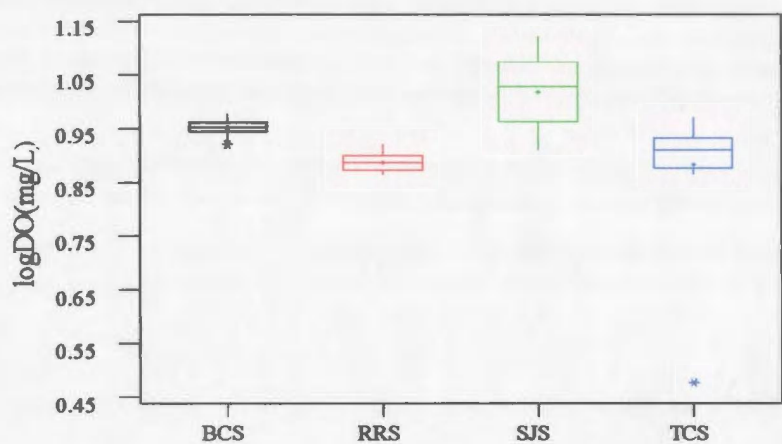
Appendix 3: Box plots of log-transformed analyte concentrations in water samples taken from all four study areas.



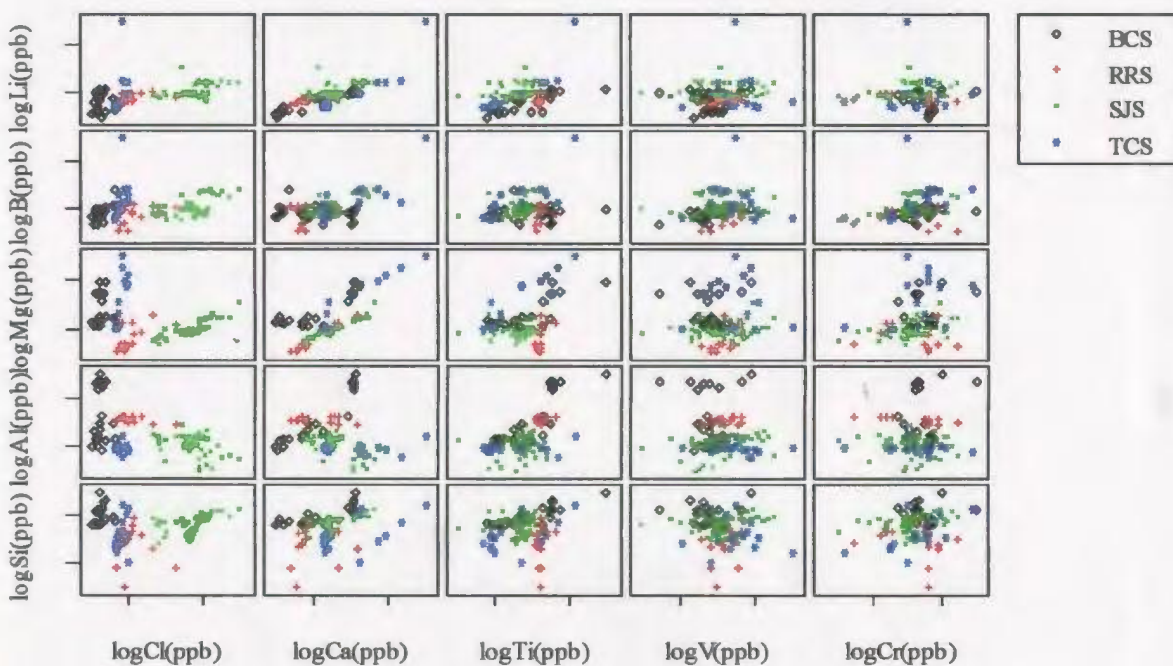
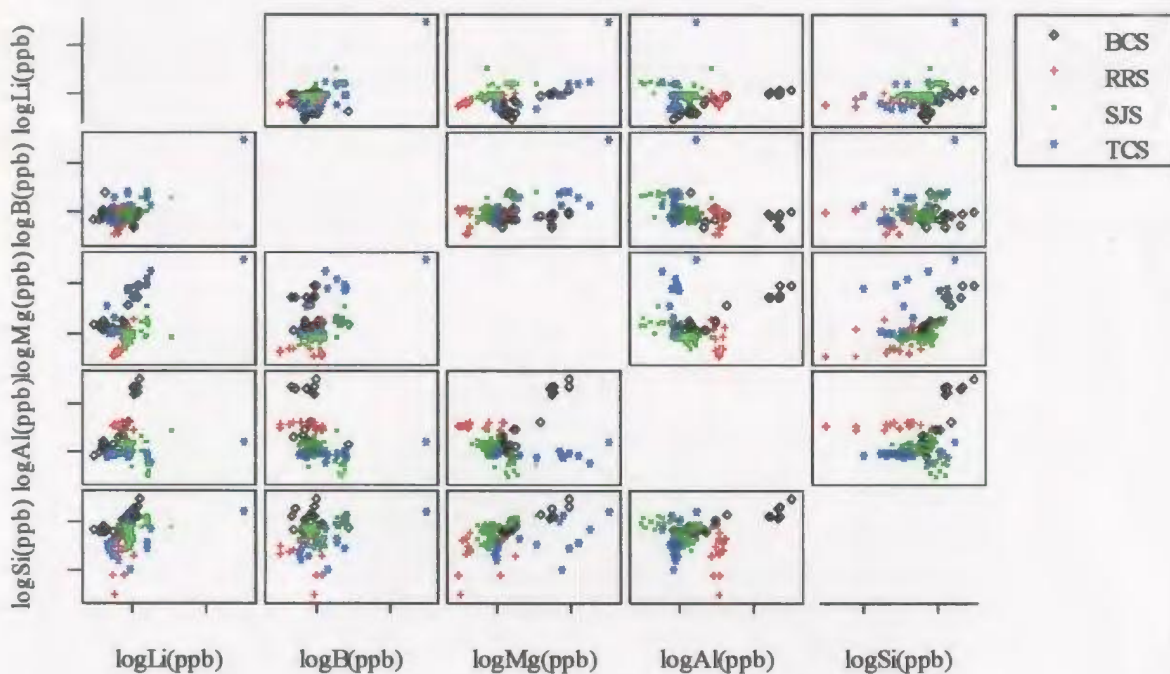
Appendix 3: Box plots of log-transformed analyte concentrations in water samples taken from all four study areas.



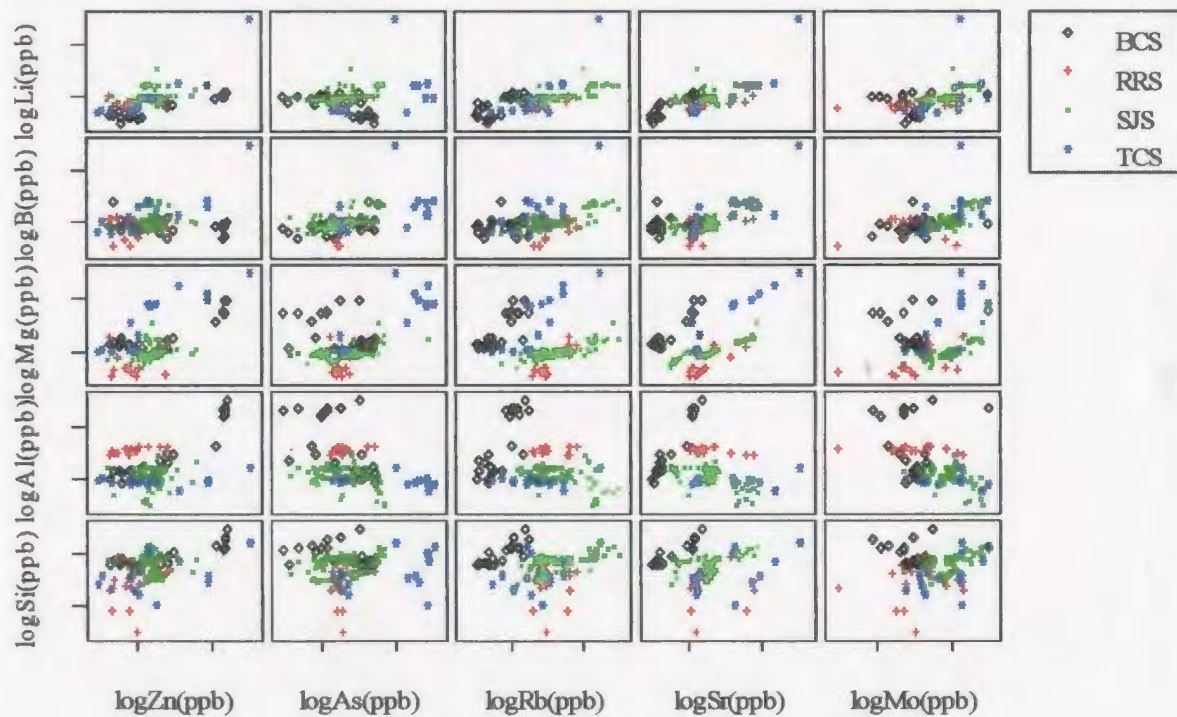
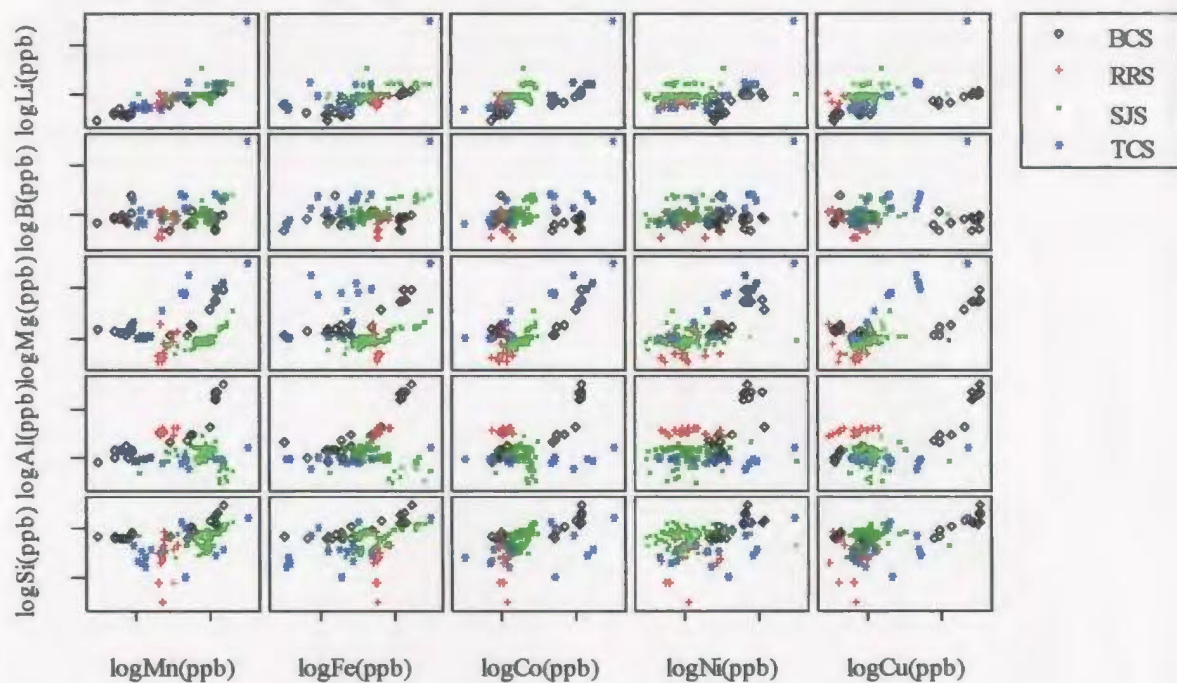
Appendix 3: Box plots of log-transformed analyte concentrations in water samples taken from all four study areas.



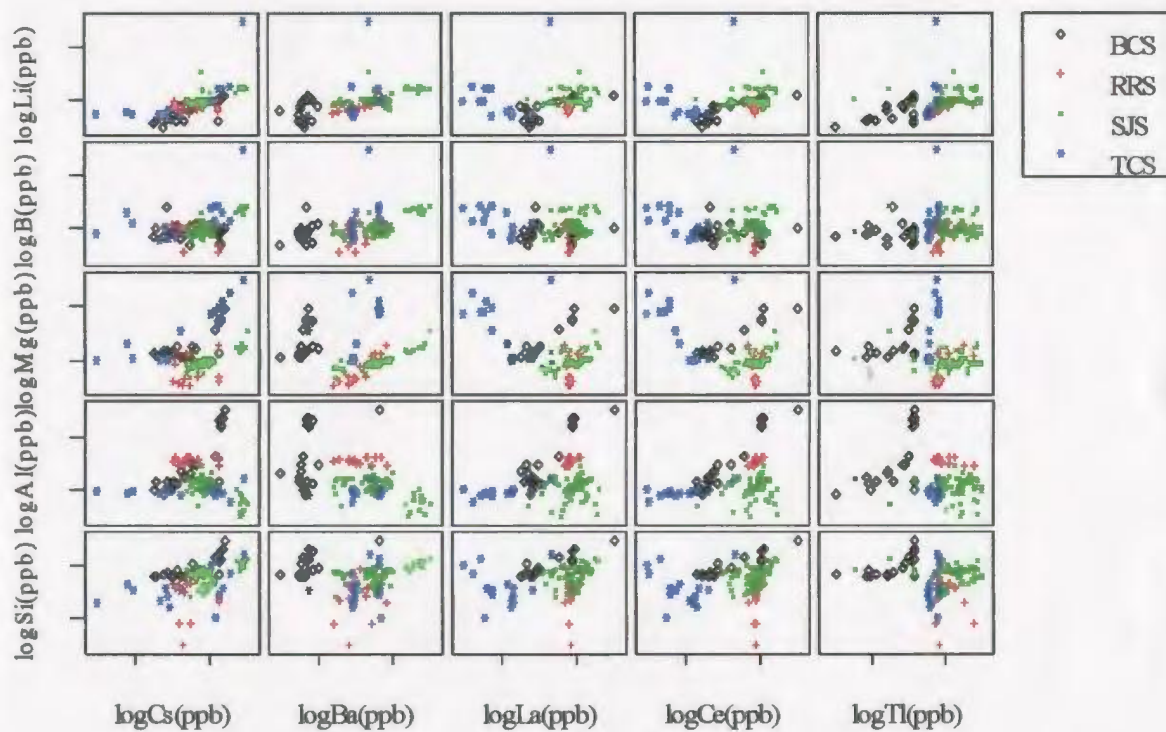
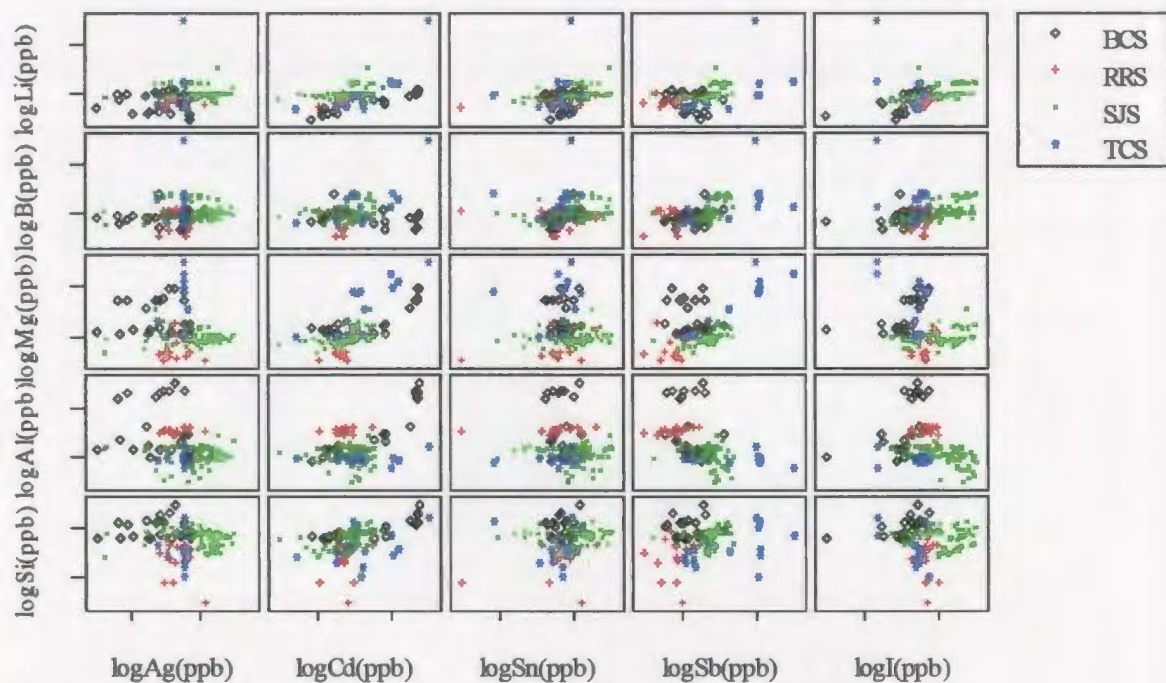
Appendix 3: Scatter plots of log-transformed analyte concentrations in water samples taken from all four study areas.



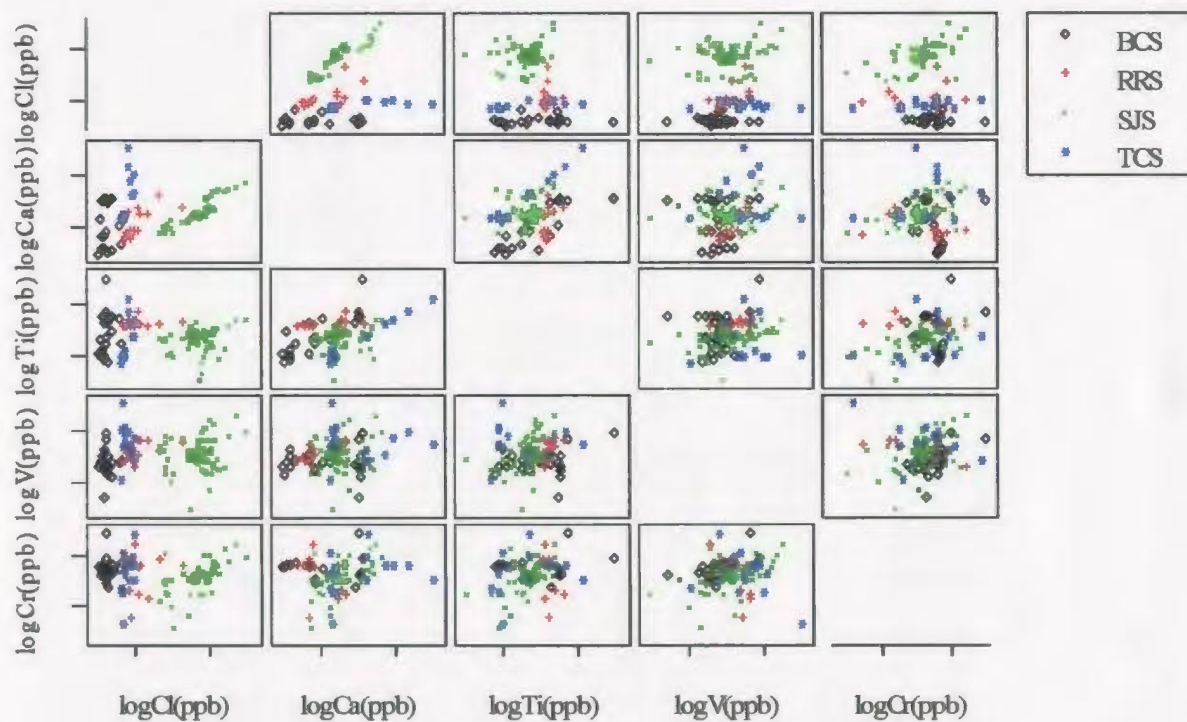
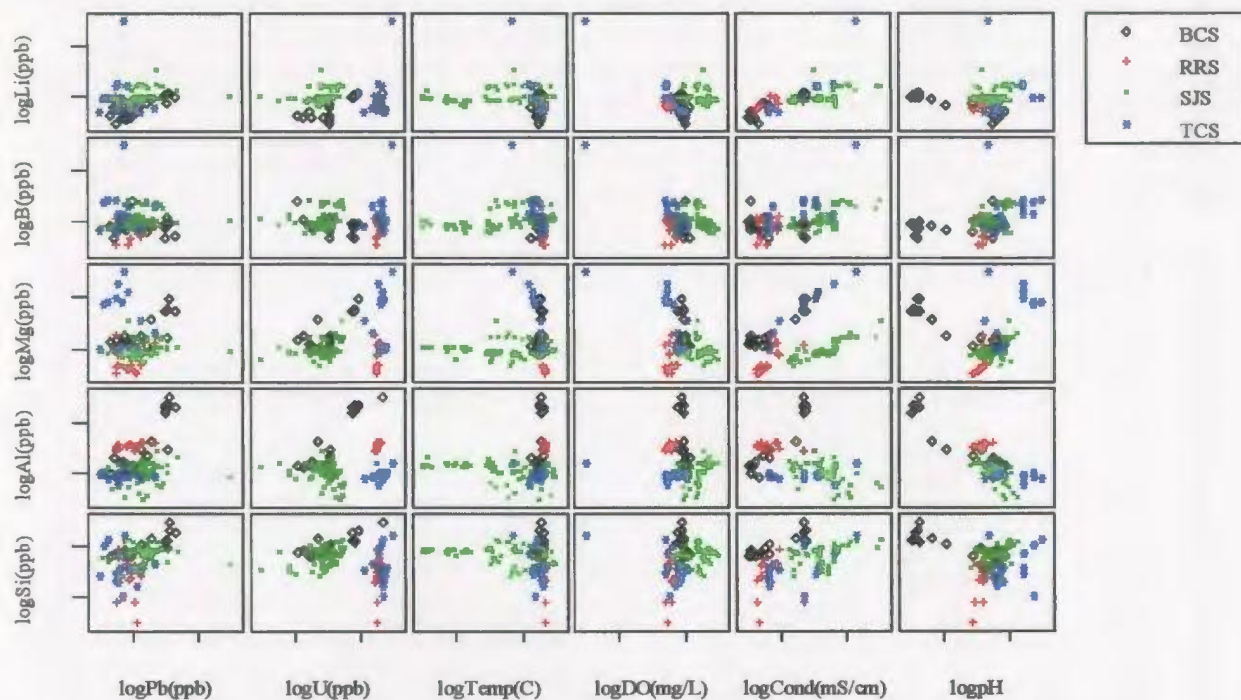
Appendix 3: Scatter plots of log-transformed analyte concentrations in water samples taken from all four study areas.



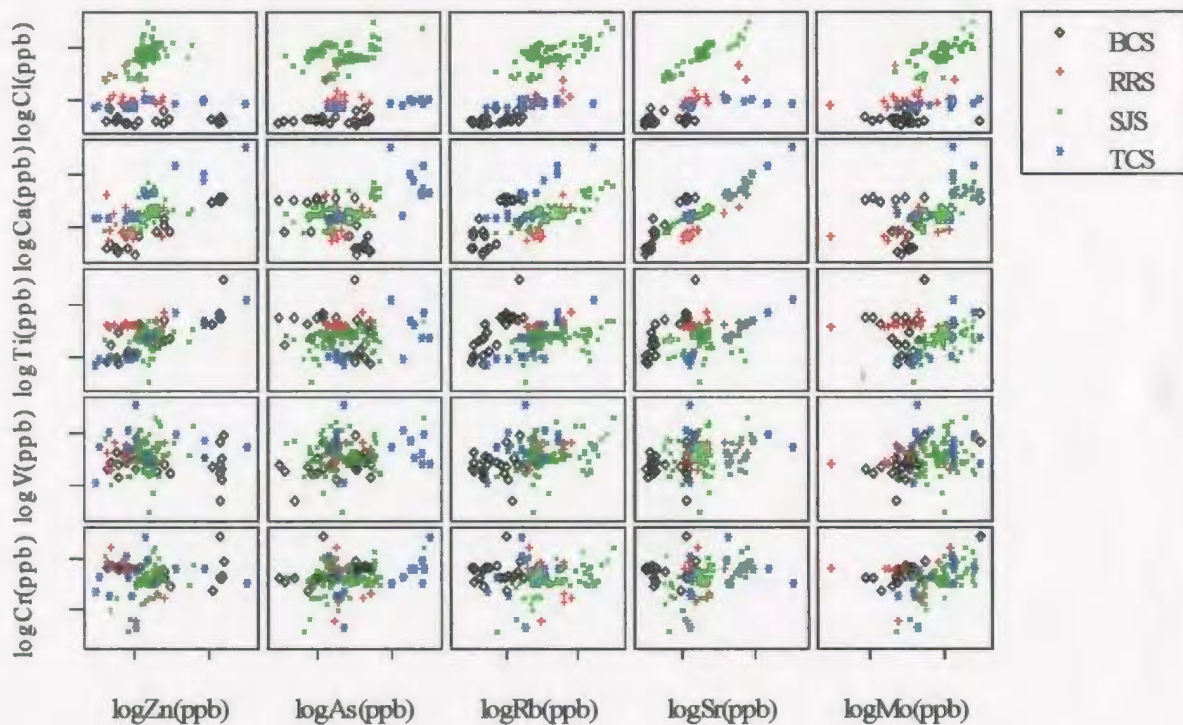
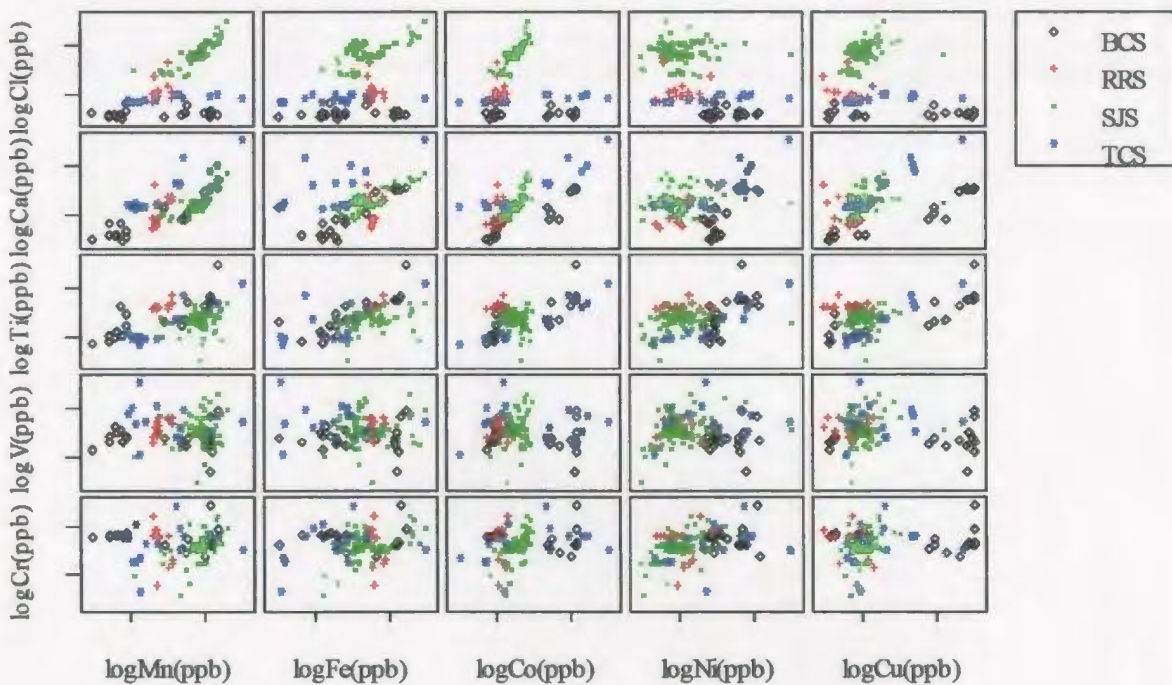
Appendix 3: Scatter plots of log-transformed analyte concentrations in water samples taken from all four study areas.



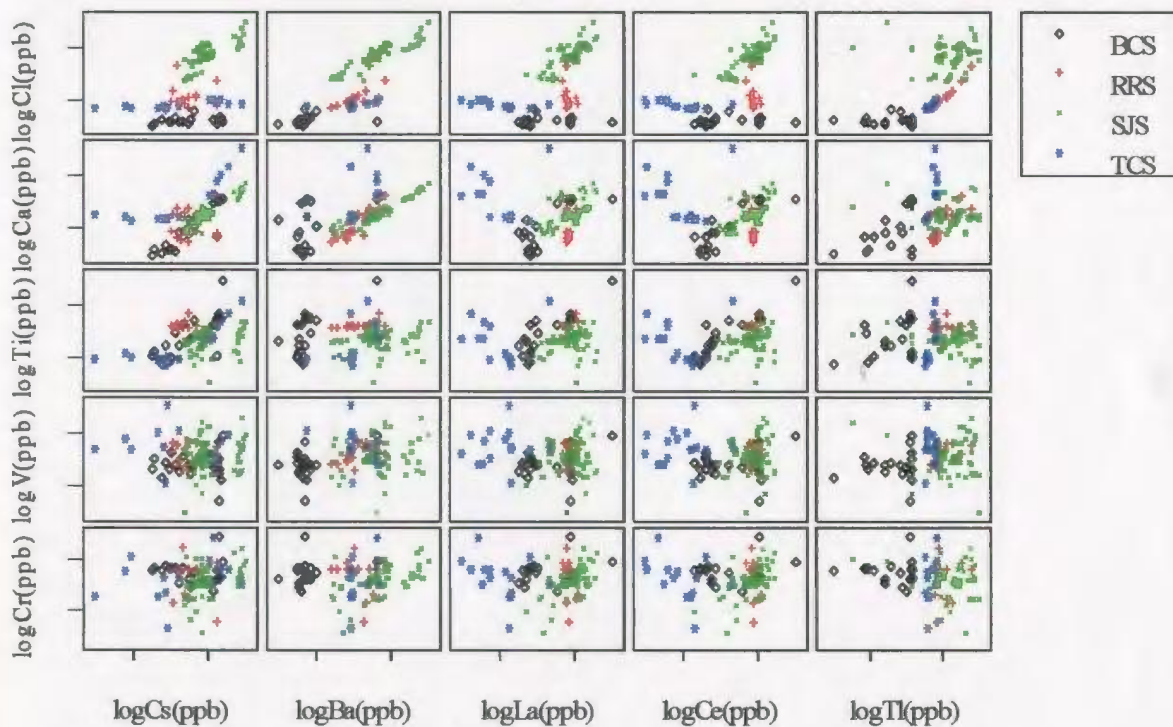
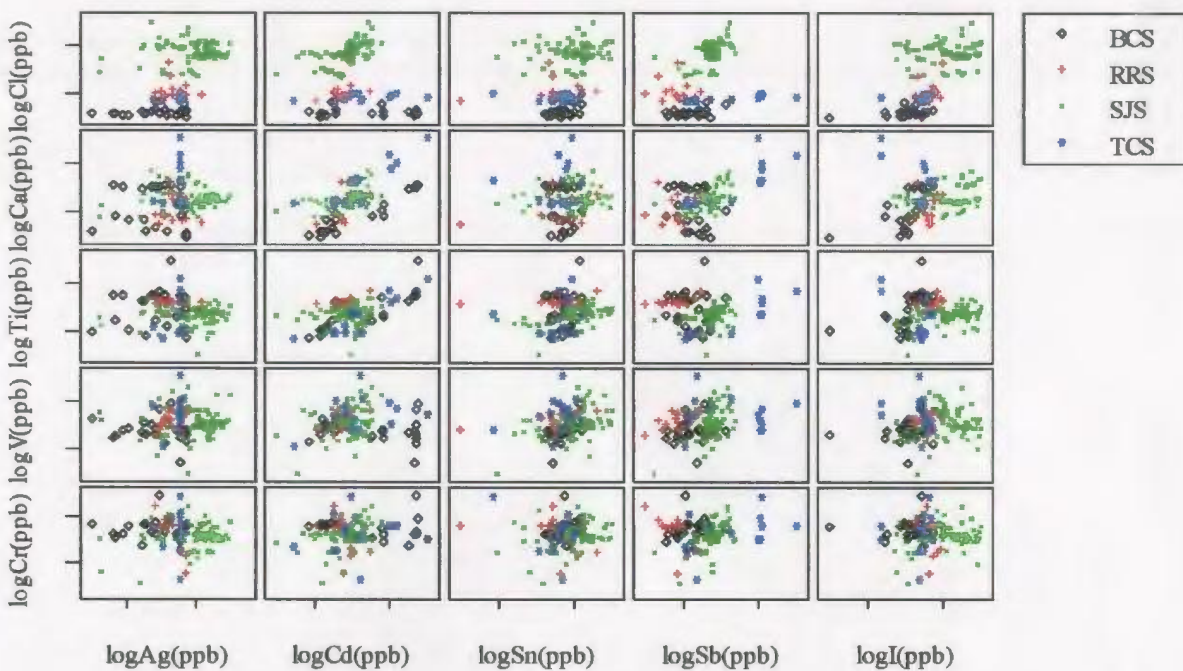
Appendix 3: Scatter plots of log-transformed analyte concentrations in water samples taken from all four study areas.



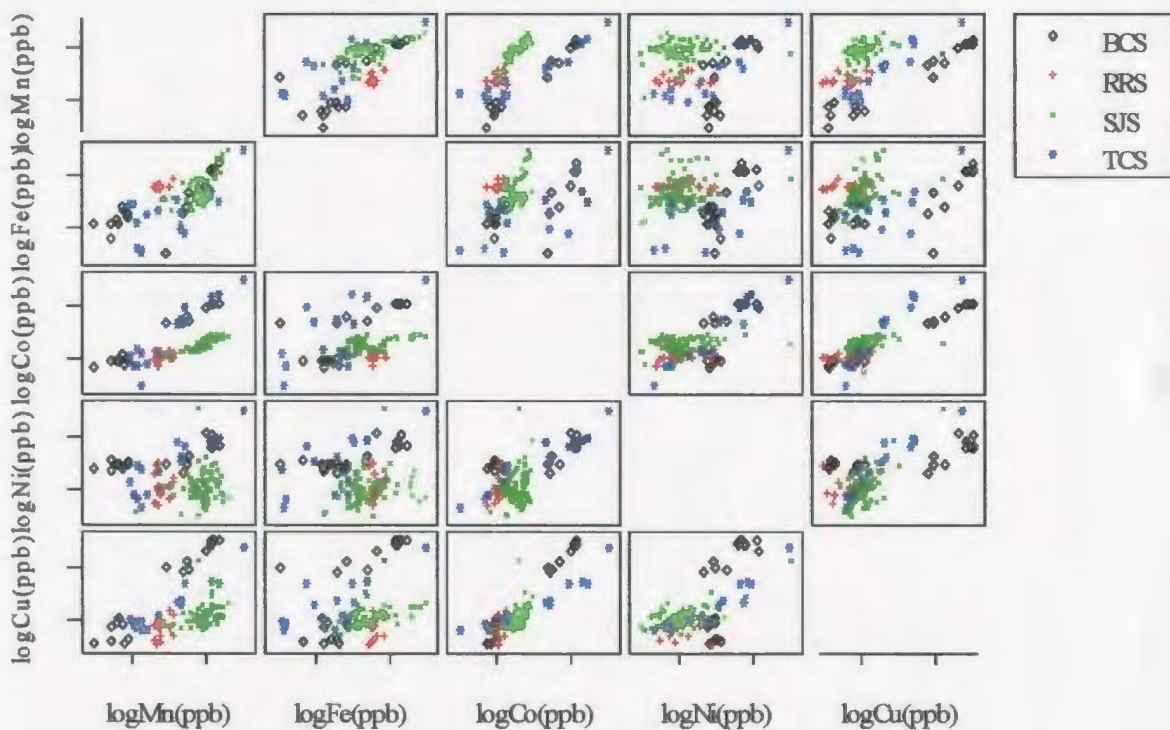
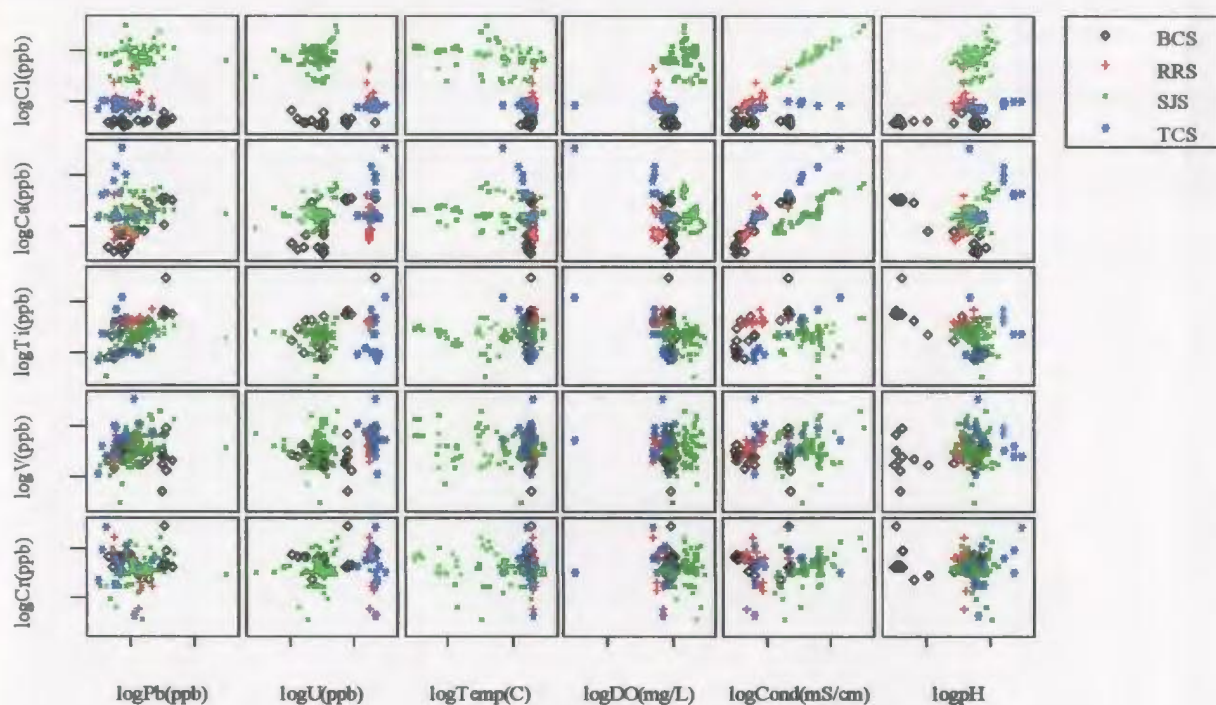
Appendix 3: Scatter plots of log-transformed analyte concentrations in water samples taken from all four study areas.



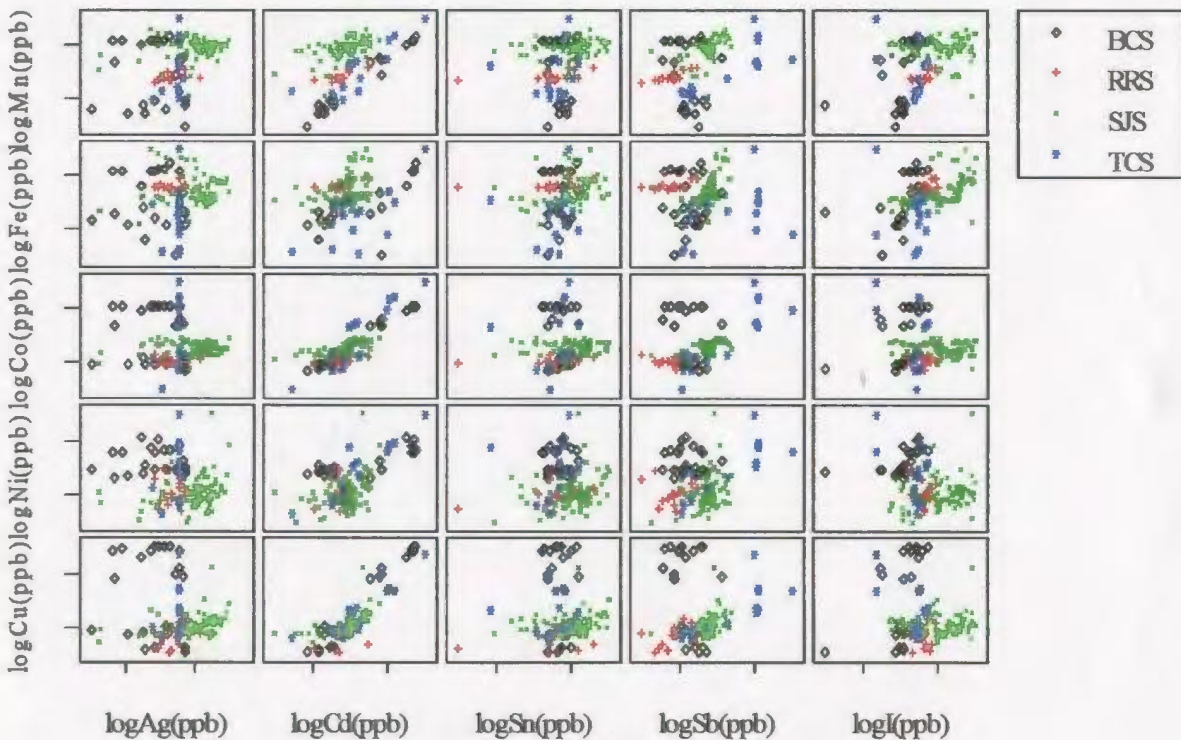
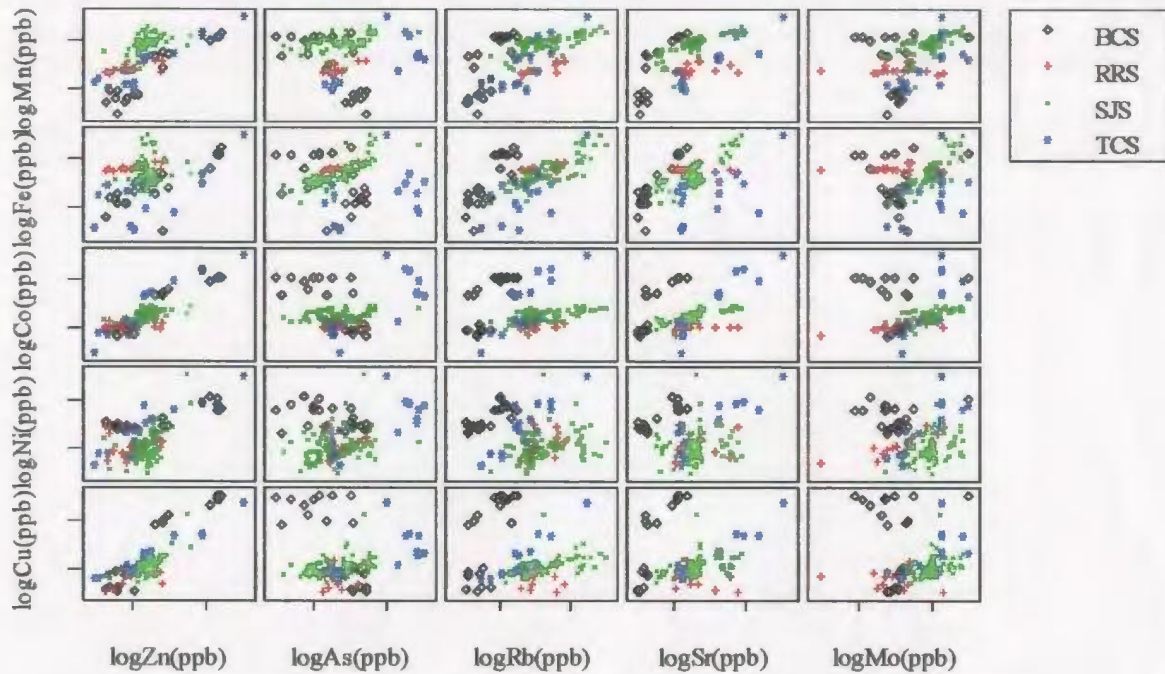
Appendix 3: Scatter plots of log-transformed analyte concentrations in water samples taken from all four study areas.



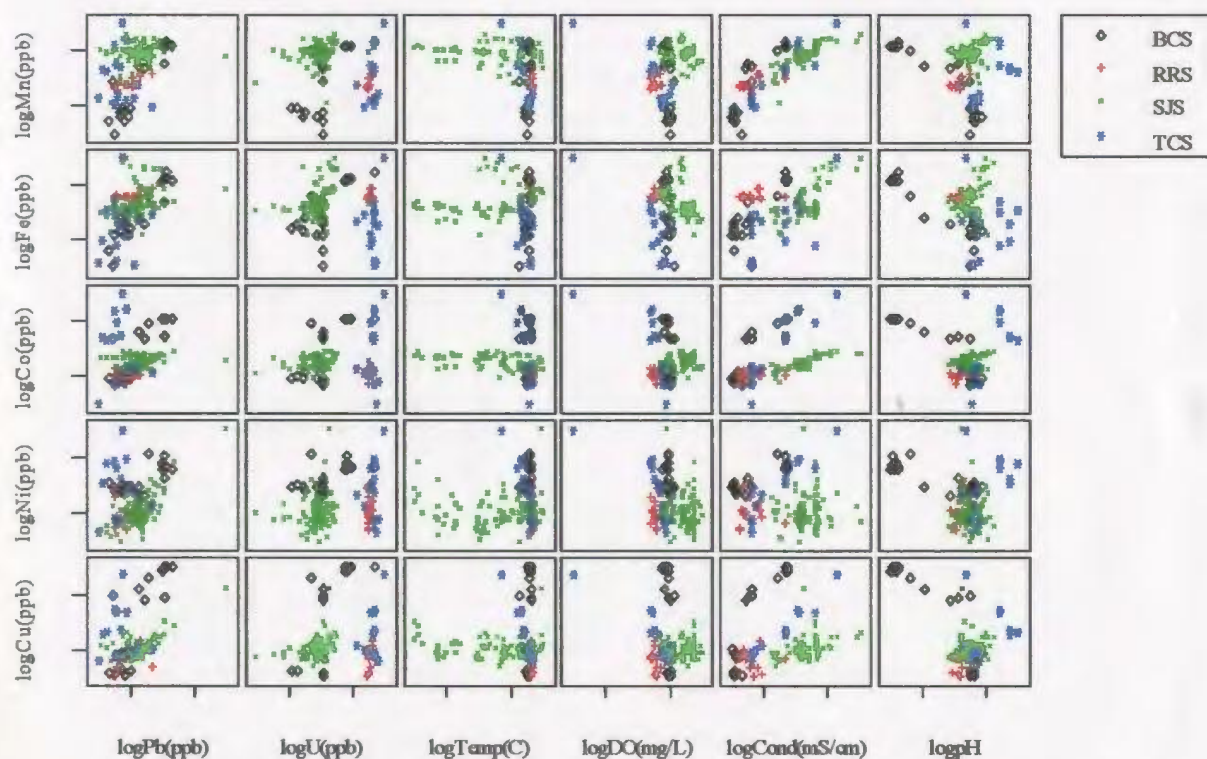
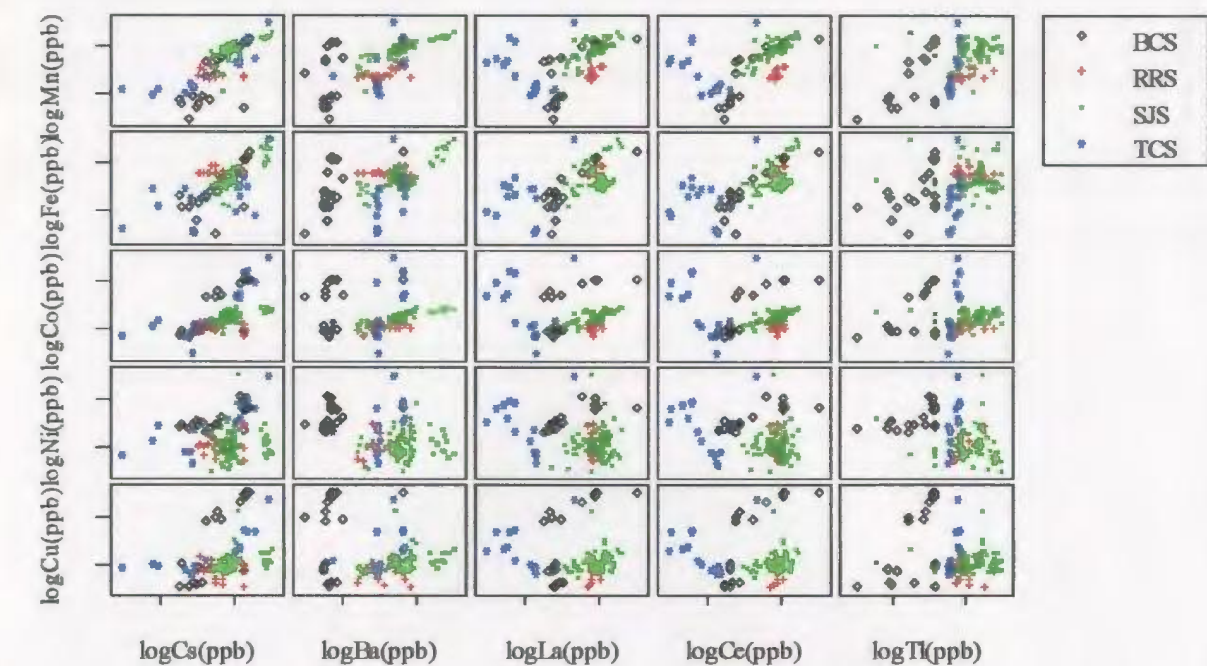
Appendix 3: Scatter plots of log-transformed analyte concentrations in water samples taken from all four study areas.



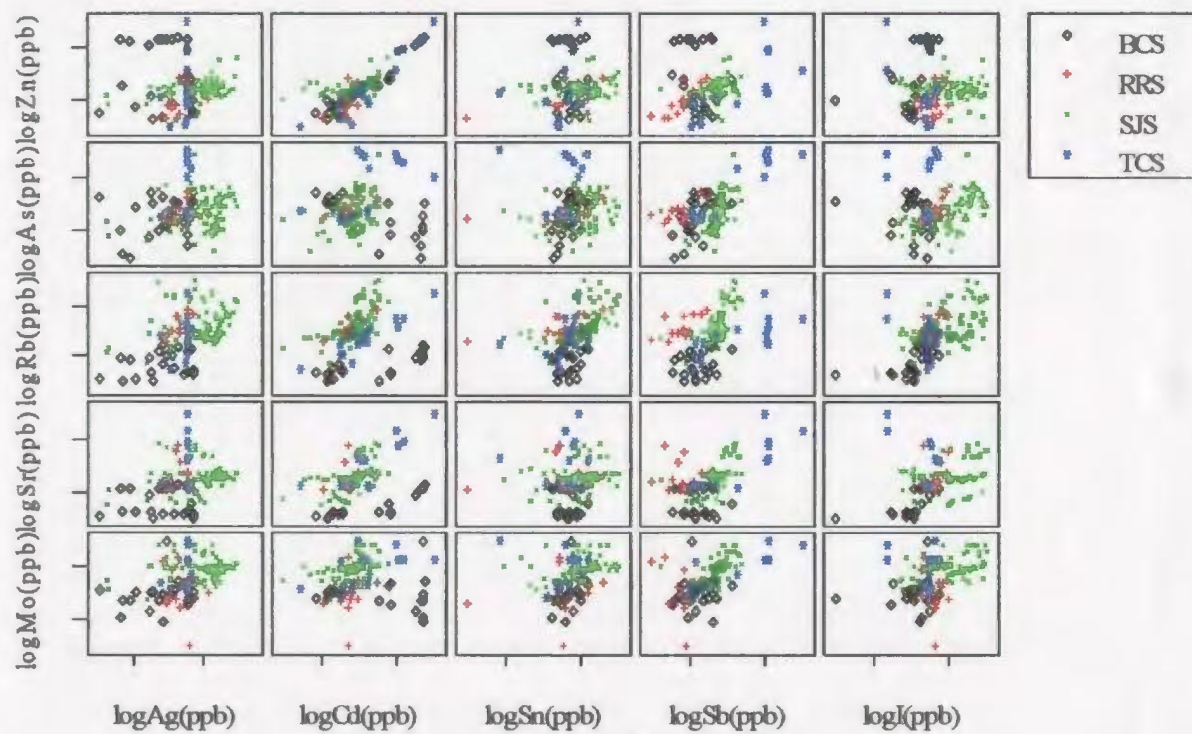
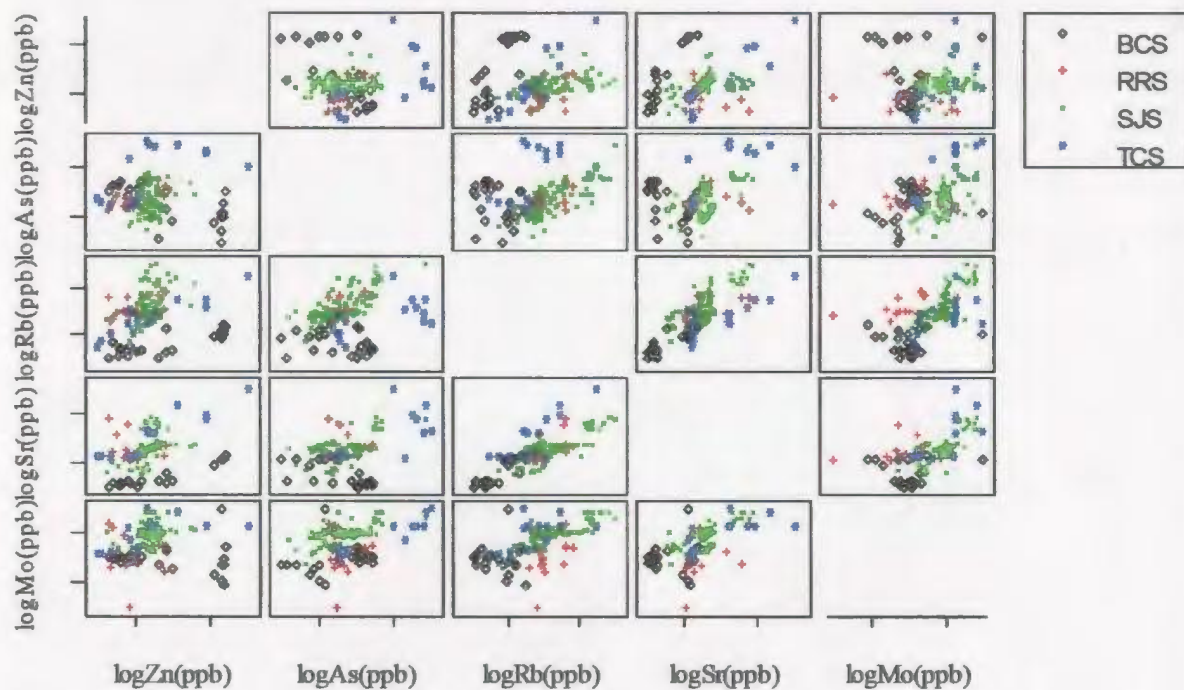
Appendix 3: Scatter plots of log-transformed analyte concentrations in water samples taken from all four study areas.



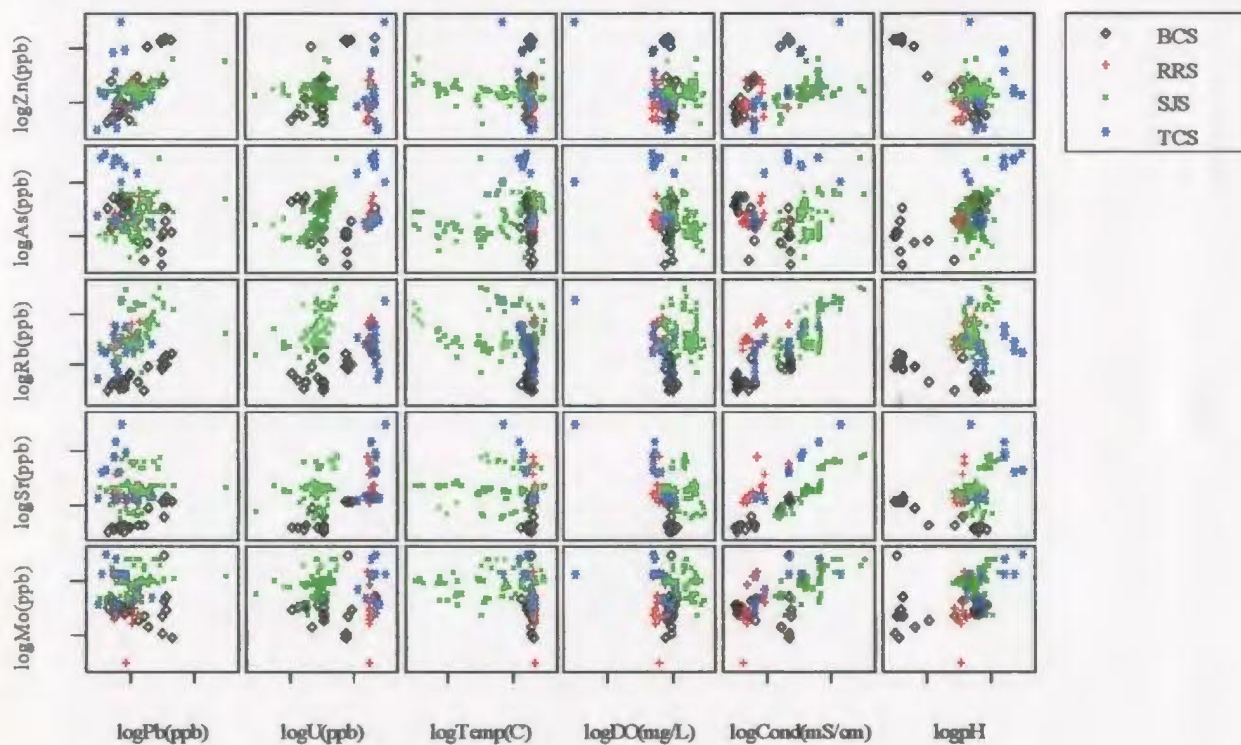
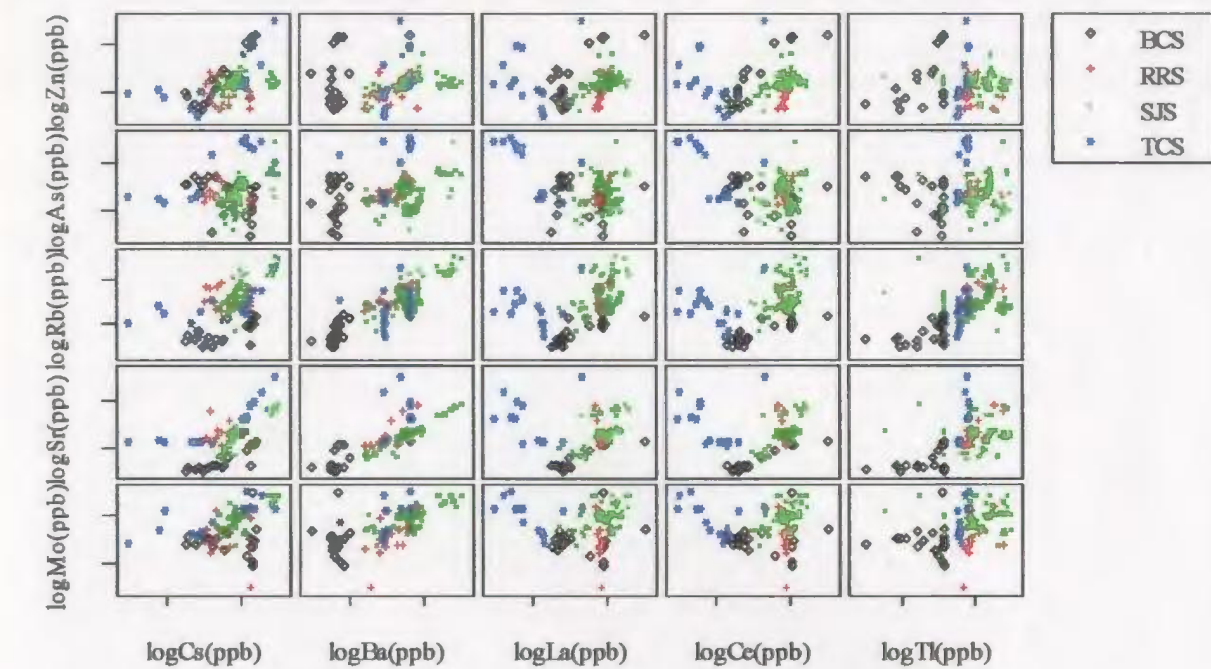
Appendix 3: Scatter plots of log-transformed analyte concentrations in water samples taken from all four study areas.



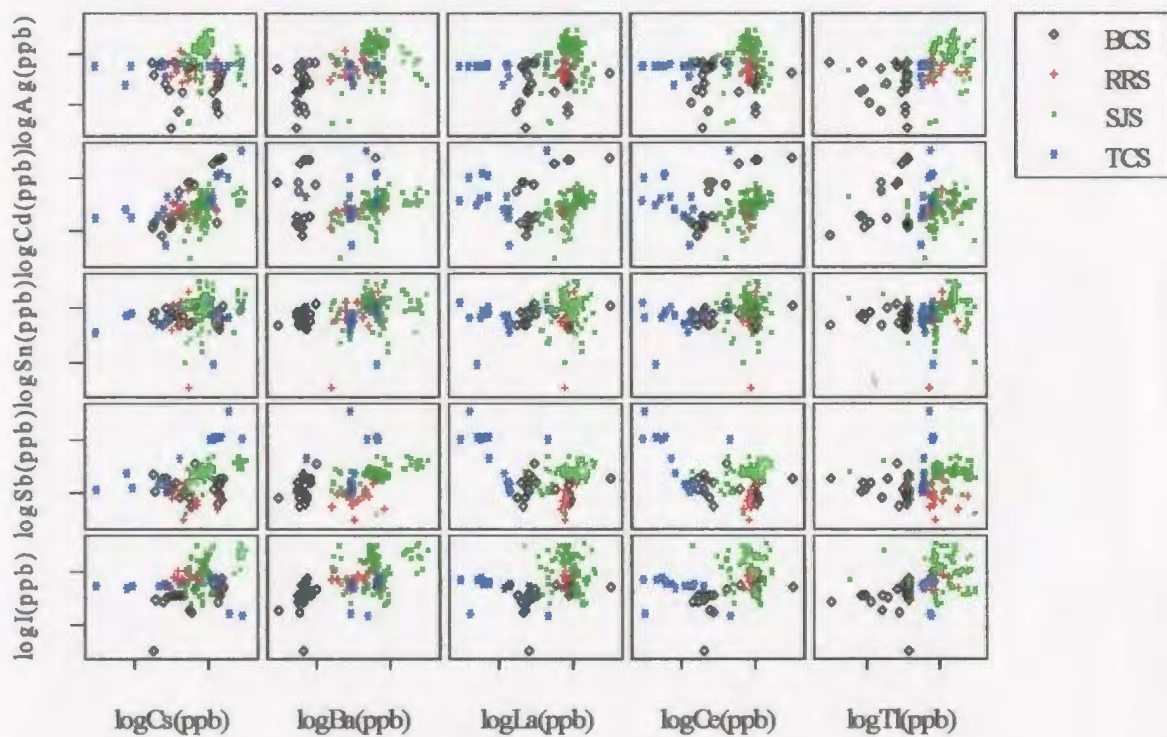
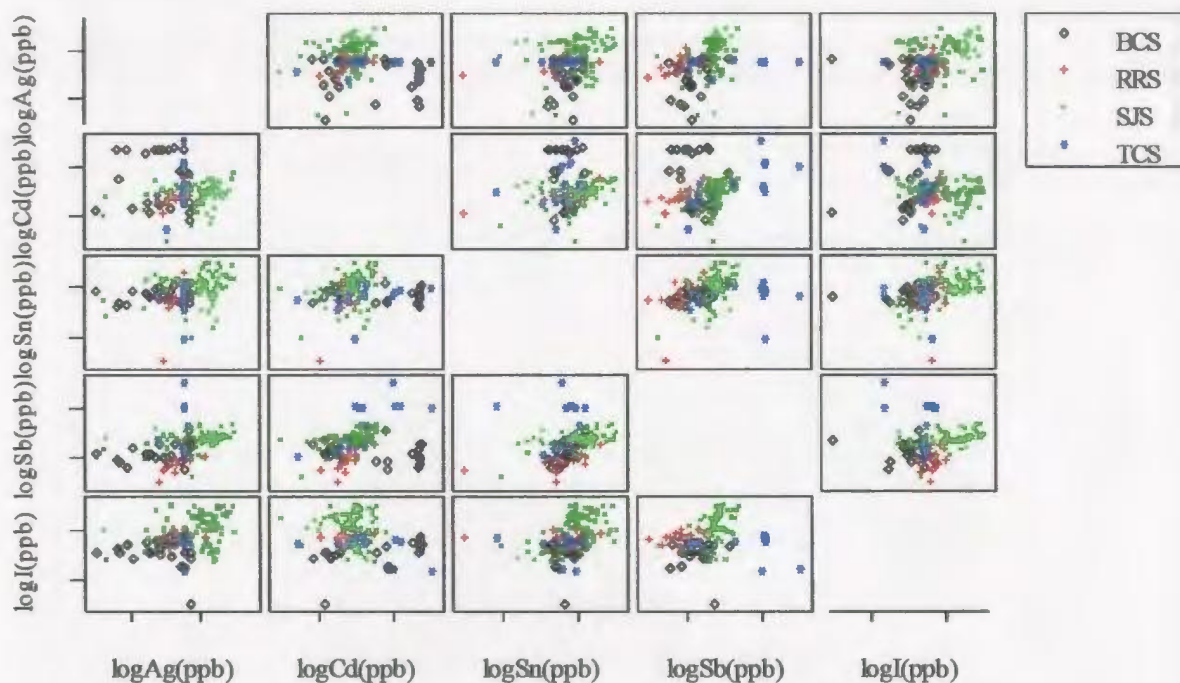
Appendix 3: Scatter plots of log-transformed analyte concentrations in water samples taken from all four study areas.



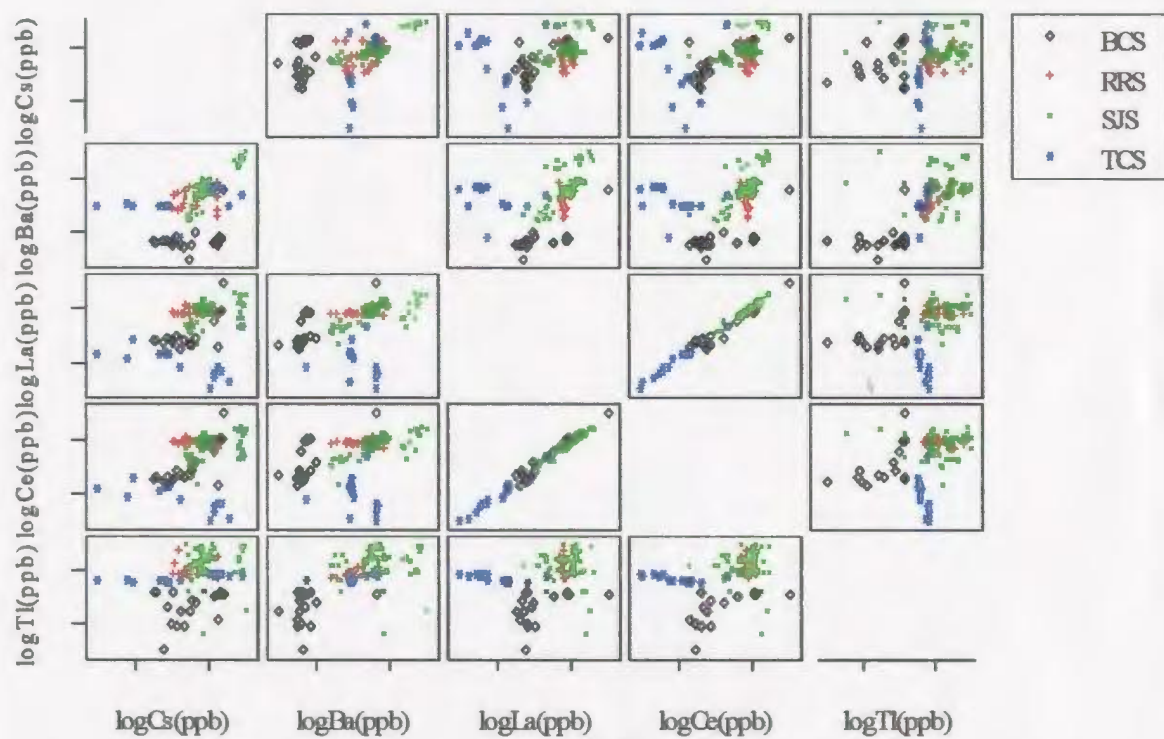
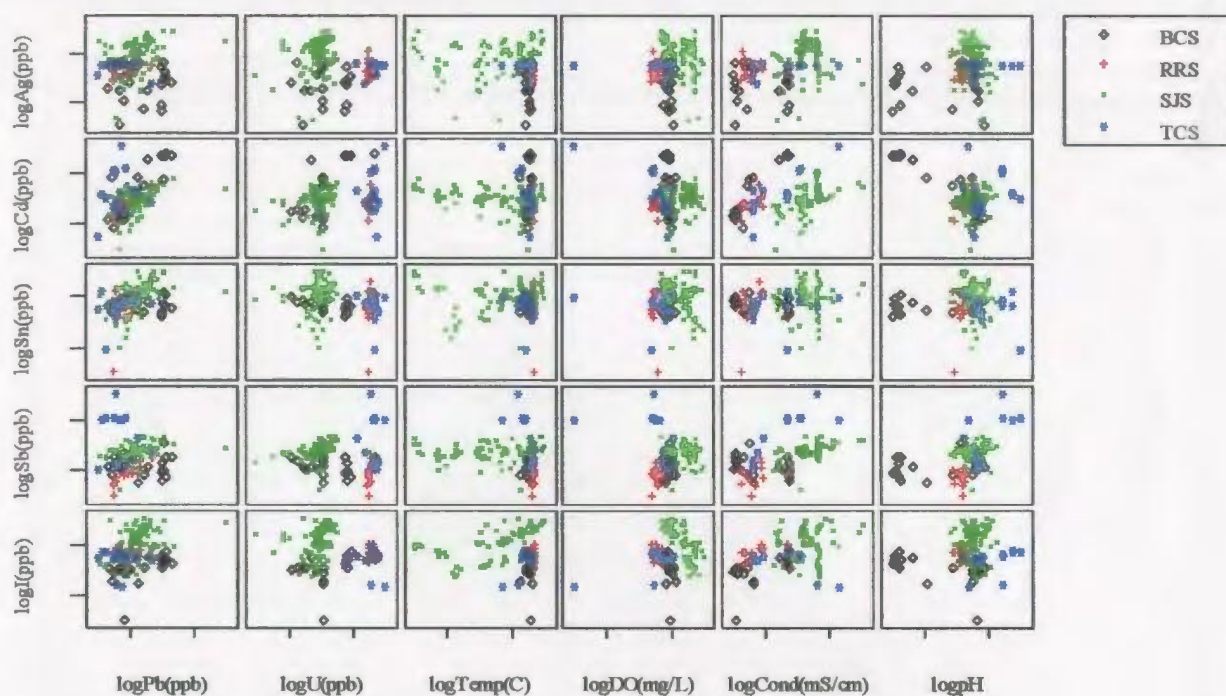
Appendix 3: Scatter plots of log-transformed analyte concentrations in water samples taken from all four study areas.



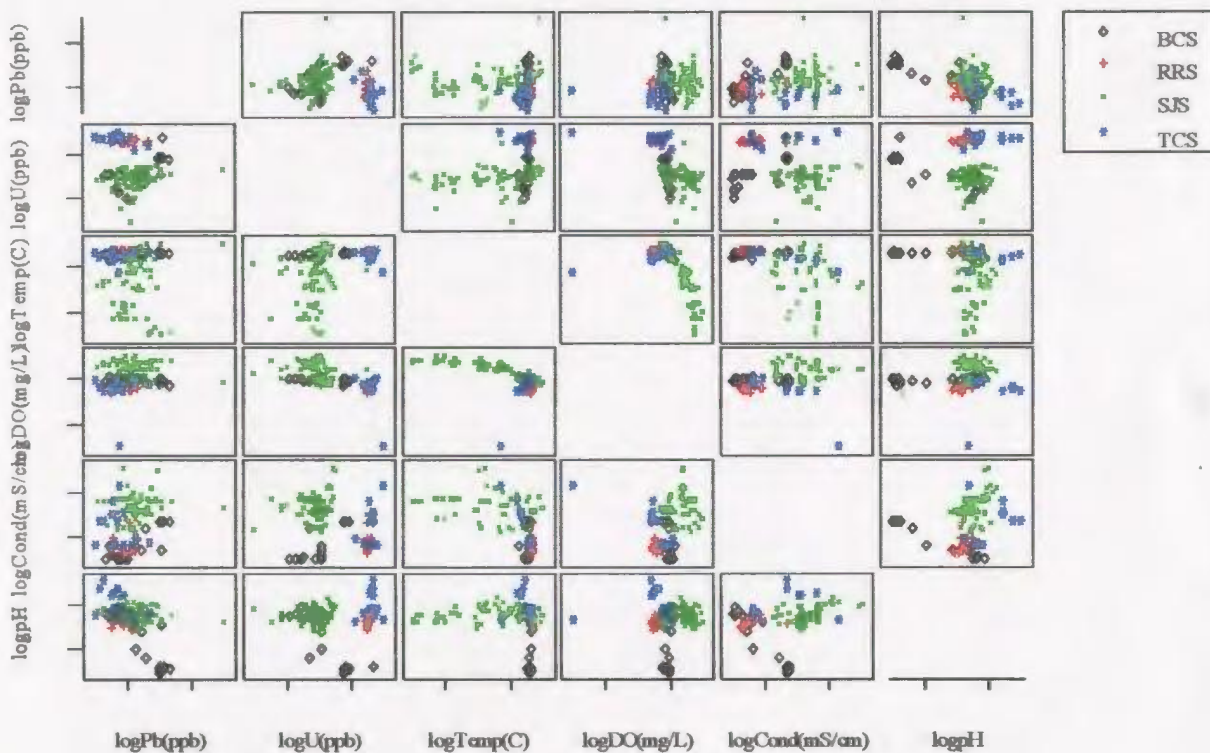
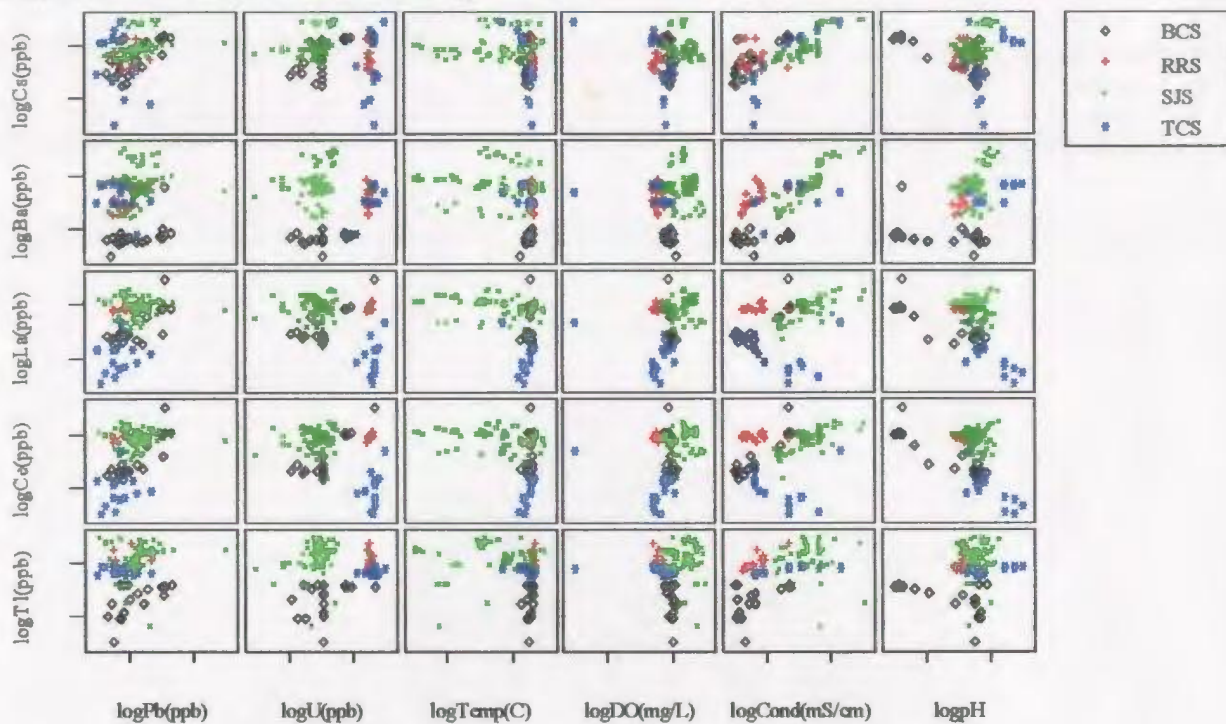
Appendix 3: Scatter plots of log-transformed analyte concentrations in water samples taken from all four study areas.



Appendix 3: Scatter plots of log-transformed analyte concentrations in water samples taken from all four study areas.



Appendix 3: Scatter plots of log-transformed analyte concentrations in water samples taken from all four study areas.



**Appendix 4: LA-ICP-MS intensity (cps) values of all Fe-Mn oxide coated samples;
ND = Not Determined.**

Site	TCS 3.1.1	TCS 3.1.2	TCS 3.2.1	TCS 3.2.2	TCS 4.1.1	TCS 4.1.2
Substrate	Pebble	Pebble	Pebble	Pebble	Pebble	Pebble
Month						
Al 27	5412434	2604474	4996176	5368172	2537649	4234304
Si 29	2454361	946559	3337300	4698944	2545422	3178011
Ca 43	2389065	1162414	801205	1662579	787581	209243
Ti 47	793321	854628	1063312	4580706	718825	1479582
V 51	269850	86690	168049	153660	62246	47653
Cr 53	98577	125953	108536	153774	19909	18750
Mn 55	28907233	34276788	14543928	30966271	13163315	4881421
Fe 57	33436988	7818476	11268035	12011136	5590152	6082158
Co 59	137288	193875	164821	552339	82472	43610
Ni 62	698052	832725	339127	679316	379150	92279
Cu 65	523716	657946	288888	722113	324853	65941
Zn 67	2154974	2277908	1006902	1513790	978573	297872
As 75	95529	44899	75839	72474	39227	8769
Se 82	1144	-28	31	447	500	666
Sr 86	197214	117029	86883	123253	74420	22664
Y 89	53174	33905	34069	52140	25774	22273
Ag 107	12037	7594	28476	25400	11365	1328
Cd 111	35692	11134	2313	3978	6956	2201
Sn 118	8307	4773	6740	20368	5686	6807
Ba 137	5945154	12137202	3750641	8840756	3409528	1703154
La 139	158604	31990	19687	31959	20546	74901
Ce 140	534423	214561	195855	339009	213055	186615
Au 197	6	11	1	7	12	2
Hg 202	830	1839	212	825	325	193
Pb 206	614890	364043	494593	870945	367267	53084
Pb 207	566664	347751	456368	762266	313546	47231
Pb 208	593203	331015	480244	788506	332716	51903
Bi 209	851	364	606	892	490	113
Th 232	16381	2699	4394	5979	3672	16687
U 238	41368	15868	16401	26243	11723	5114

**Appendix 4: LA-ICP-MS intensity (cps) values of all Fe-Mn oxide coated samples;
ND = Not Determined.**

Site	TCS 4.2.1	TCS 4.2.2	TCS 5.1.1	TCS 5.1.2	TCS 5.2.1	TCS 5.2.2
Substrate	Pebble	Pebble	Pebble	Pebble	Pebble	Pebble
Month						
Al 27	1441668	2682049	2905782	3856614	4662121	6307412
Si 29	769970	1307227	2020907	962567	1972002	1455168
Ca 43	586285	2270679	785270	1605178	633896	1601558
Ti 47	267009	1132581	186016	351619	440088	662538
V 51	26393	56686	50897	83401	57697	76604
Cr 53	54512	47508	6852	57994	22325	20714
Mn 55	15714724	51496729	26593344	39279262	12756250	31032455
Fe 57	2467057	6311309	3255547	5528207	7466896	11227466
Co 59	139841	239048	135461	464920	71092	281380
Ni 62	612978	1023345	709104	1138823	420420	908544
Cu 65	369759	936629	785353	822783	497169	1490818
Zn 67	1320383	3560983	2584738	3806623	966061	2251596
As 75	28155	77296	52020	84346	37148	70834
Se 82	363	553	836	1181	662	1290
Sr 86	60865	257172	106295	166627	60234	142715
Y 89	15114	49590	24512	38598	29550	62266
Ag 107	2618	80337	109230	70915	2037	6905
Cd 111	12284	29066	31927	31819	6506	16113
Sn 118	14222	8570	7792	6020	5221	14631
Ba 137	2673222	13980003	5298950	9775425	2347500	5278598
La 139	17308	59176	30302	45868	19730	156379
Ce 140	175498	400111	404705	713344	230646	723382
Au 197	11	228	2	4	3	34
Hg 202	907	725	956	1942	740	1375
Pb 206	257628	686729	366755	768654	263272	617886
Pb 207	205349	621851	341852	713702	230451	567550
Pb 208	201851	668638	315562	722972	235545	578814
Bi 209	260	618	453	1101	672	1846
Th 232	1034	4839	2300	3958	5640	10976
U 238	8096	14450	13063	17518	21381	23323

Appendix 4: LA-ICP-MS intensity (cps) values of all Fe-Mn oxide coated samples;
ND = Not Determined.

Site	TCS 6.1.1	TCS 6.1.2	TCS 6.2.1	TCS 6.2.2	TCS 7.1.1	TCS 7.1.2
Substrate	Pebble	Pebble	Pebble	Pebble	Pebble	Pebble
Month						
Al 27	2274897	3841029	4438838	4494057	6503373	4360727
Si 29	1260407	3353286	941860	1777456	1615083	4990915
Ca 43	509079	511057	1919228	873207	324061	397984
Ti 47	160966	697958	548124	538552	531315	469646
V 51	18555	40924	55140	46124	33151	25573
Cr 53	5892	9632	7161	18182	19940	25424
Mn 55	2037788	11518997	30196937	16687446	9727262	7245757
Fe 57	6231136	3940897	5146832	4879857	12162469	4838835
Co 59	44477	171393	315680	154781	153998	68854
Ni 62	71737	281682	849634	478375	739204	807638
Cu 65	99586	241234	1089018	526758	107132	235746
Zn 67	441934	759285	2640722	1072521	869423	481169
As 75	4246	21894	49780	25975	13704	7802
Se 82	12	389	896	850	56	260
Sr 86	28560	68830	134381	81490	35510	35760
Y 89	7877	33644	40555	34194	52365	43512
Ag 107	1408	11885	1522	9514	186	11629
Cd 111	450	2346	16594	6191	7518	4549
Sn 118	2228	18882	4892	8571	1314	42549
Ba 137	498924	3207245	5022652	2744207	1657743	1823533
La 139	6725	99611	30005	22362	12624	11851
Ce 140	29176	316054	504101	350776	375723	236065
Au 197	2	2	87	-1	-1	2
Hg 202	387	538	982	344	335	500
Pb 206	69997	196865	782129	281740	635431	425583
Pb 207	64877	185319	717668	258339	587504	394666
Pb 208	66922	188814	767967	277521	619936	411519
Bi 209	149	417	3057	633	483	393
Th 232	12091	10261	4446	4018	8103	8852
U 238	3199	14736	16365	11139	18106	11859

**Appendix 4: LA-ICP-MS intensity (cps) values of all Fe-Mn oxide coated samples;
ND = Not Determined.**

Site	TCS 7.2.1	TCS 7.2.2	TCS 8.1.1	TCS 8.1.2	TCS 8.2.1	TCS 8.2.2
Substrate	Pebble	Pebble	Pebble	Pebble	Pebble	Pebble
Month						
Al 27	2784540	16437396	5556781	5740442	11659097	9187527
Si 29	3470358	4236865	2505454	3734548	1847294	652263
Ca 43	513174	1747205	1263598	683181	822569	1131948
Ti 47	1600171	2258984	1296689	822272	1172232	628004
V 51	38568	87354	41137	49958	75774	40425
Cr 53	53164	74882	106783	49318	137508	43882
Mn 55	2072834	45123043	15838890	5908430	24971224	23666907
Fe 57	4502453	24480961	7564417	7507691	11886628	10117244
Co 59	44984	395131	272648	219345	546740	615905
Ni 62	103868	838504	1564882	893495	3784968	2891316
Cu 65	111629	841786	927553	310914	776623	632848
Zn 67	132854	2559611	1529123	439086	2726077	1885406
As 75	3197	29598	23402	8965	119995	75215
Se 82	163	1339	892	254	1182	957
Sr 86	29316	167784	89697	62023	102529	109549
Y 89	50839	118610	54308	18870	64033	72432
Ag 107	8871	177748	21727	3797	9210	7135
Cd 111	662	17976	15016	1737	16436	13535
Sn 118	5121	145143	9231	14793	7419	2709
Ba 137	642829	7260111	2701145	1455104	5327831	3941339
La 139	29811	39384	32464	10887	20268	28932
Ce 140	124160	1727122	333250	76105	388735	517953
Au 197	5	4	4	1	3	-4
Hg 202	184	677	670	238	860	204
Pb 206	109968	1262719	382679	139461	403332	205056
Pb 207	105110	1196018	366705	134382	373891	193069
Pb 208	110534	1220127	368535	134841	393423	198643
Bi 209	613	2091	1245	505	588	510
Th 232	22742	19577	12334	3125	22677	18844
U 238	21971	42630	16321	5901	39115	23412

**Appendix 4: LA-ICP-MS intensity (cps) values of all Fe-Mn oxide coated samples;
ND = Not Determined.**

Site	TCS 10.1.1	TCS 10.1.2	TCS 10.2.1	TCS 10.2.2	TCS 11.1.1	TCS 11.1.2
Substrate	Pebble	Pebble	Pebble	Pebble	Pebble	Pebble
Month						
Al 27	3771937	1501250	2404972	5474362	5085433	5927569
Si 29	5475605	2590176	5773183	12149935	6292550	5265172
Ca 43	602793	14348948	1548732	4453852	920459	1154132
Ti 47	664249	722827	1012516	1994265	1509752	1033392
V 51	216207	103671	191402	364231	275721	269063
Cr 53	1490302	613645	1165766	1786228	990667	902705
Mn 55	2556663	2043304	1092501	4863048	14758813	10118908
Fe 57	23112150	13676433	17611657	39925485	30992683	34255851
Co 59	1423421	816615	748158	3219636	10395664	7759689
Ni 62	1615758	712496	1019991	3053887	4436265	3363828
Cu 65	6345222	3341632	4995628	18333890	35800251	35468763
Zn 67	7114515	3343527	3666103	12664933	33833182	29571983
As 75	82817	44483	52548	141517	223845	412754
Se 82	2024	677	2262	5535	5778	6128
Sr 86	32034	512722	80038	218290	77745	65721
Y 89	7972	7715	7199	40356	20890	28735
Ag 107	2048	3013	34526	20189	11203	61262
Cd 111	10924	8168	5029	22900	100602	89797
Sn 118	3836	2895	8220	13736	16857	11478
Ba 137	252052	147855	182869	757590	971345	652274
La 139	5438	3904	5092	28475	15832	16722
Ce 140	26093	11928	18701	87626	135255	42550
Au 197	49	44	59	115	333	83
Hg 202	1543	1255	1162	2787	1732	822
Pb 206	337449	272504	245760	1180774	1483311	1789334
Pb 207	321972	231649	241140	964942	1387002	1680959
Pb 208	341207	223470	262224	1058417	1585464	1814765
Bi 209	2263	1303	1635	4719	9587	12633
Th 232	1768	659	1193	3679	2405	6533
U 238	4161	2031	3013	11592	17207	31797

**Appendix 4: LA-ICP-MS intensity (cps) values of all Fe-Mn oxide coated samples;
ND = Not Determined.**

Site	FCS 11.2.1	TCS 11.2.2	TCS 13.1.1	TCS 13.1.2	TCS 13.2.1	TCS 13.2.2
Substrate	Pebble	Pebble	Pebble	Pebble	Pebble	Pebble
Month						
Al 27	3796755	3360346	4370515	7131319	3338415	2339879
Si 29	7514140	7220443	1581291	2263300	1862715	1863425
Ca 43	910550	1516719	1609980	2267827	1067271	1083689
Ti 47	999840	1181112	96243	1663067	5614066	233622
V 51	248346	226626	40021	92236	149354	57016
Cr 53	872900	862475	1329529	2489393	1071778	558169
Mn 55	3897234	885462	126300	217705	170609	65599
Fe 57	25708253	24661415	235129262	408157630	140193461	94923604
Co 59	2354604	507205	343482	392797	211722	97049
Ni 62	1735729	883053	199941	221574	211013	57929
Cu 65	16727646	10843532	83967293	200916547	51393579	45771867
Zn 67	13142557	6727619	8508739	13089455	4346422	2776419
As 75	127170	116154	43141	62918	39314	19998
Se 82	4949	5233	1255	3244	1644	1761
Sr 86	58381	53221	197486	226531	121649	74753
Y 89	15110	15129	19603	24137	101002	7530
Ag 107	8515	20450	4914	22099	9394	24474
Cd 111	27570	10906	16046	21905	7823	4802
Sn 118	13338	15841	5207	7243	11781	6736
Ba 137	425796	210487	130240	201221	70378	40485
La 139	15229	10506	13786	15356	9919	5023
Ce 140	31261	29875	50615	87459	20882	24459
Au 197	266	132	1	5	-1	2
Hg 202	2166	4127	139	215	110	100
Pb 206	1027041	1172477	98919	143574	53966	39204
Pb 207	925946	1052944	95020	139353	40624	38104
Pb 208	920671	1113807	96249	145195	49704	37170
Bi 209	6039	8895	83	190	48	52
Th 232	2582	2519	1428	1721	818	531
U 238	6975	4117	41346	80865	16271	23521

**Appendix 4: LA-ICP-MS intensity (cps) values of all Fe-Mn oxide coated samples;
ND = Not Determined.**

Site	TCS 14.1.1	TCS 14.1.2	TCS 14.2.1	TCS 14.2.2	BCS 1.1.1	BCS 1.1.2
Substrate	Pebble	Pebble	Pebble	Pebble	Pebble	Pebble
Month						
Al 27	3201338	2827855	3652824	5876432	14996845	11795482
Si 29	2608519	1791097	3555966	4108668	4508400	3642160
Ca 43	633674	271326	949356	1331466	442359	335400
Ti 47	606466	62452	430862	481246	7614247	1940094
V 51	119392	22488	229300	229945	321132	354566
Cr 53	532749	208541	1424541	1048207	893526	698809
Mn 55	157699	40941	168547	196124	203537	194204
Fe 57	68130191	36163001	48447702	103030924	45317867	32702248
Co 59	342890	164744	205172	393492	110345	78239
Ni 62	379757	158536	323730	502532	140942	102530
Cu 65	22740410	15780652	14839697	41452146	10879306	8508358
Zn 67	7165038	6399983	4439244	12242860	635533	546675
As 75	79784	18779	23611	62086	26760	20297
Se 82	4997	1898	1478	3762	ND	ND
Sr 86	47052	21058	56958	88226	12314	14056
Y 89	22811	11583	13286	25027	40722	33969
Ag 107	9515	22194	11042	12734	18207	6211
Cd 111	14101	7908	8843	25930	1214	915
Sn 118	4828	926	8911	7458	14150	13243
Ba 137	152478	50593	54585	111703	43043	21267
La 139	80417	12074	6769	14244	14646	12971
Ce 140	156077	21251	20065	52073	65254	46450
Au 197	85	20	14	26	1	118
Hg 202	1161	285	586	447	211	115
Pb 206	871942	157827	208628	431019	383183	150618
Pb 207	849561	159228	208240	448131	367779	150321
Pb 208	855574	170608	213904	442026	376003	152731
Bi 209	6884	483	930	1781	427	261
Th 232	1761	453	247	506	7189	3751
U 238	16263	18595	8380	28473	5585	3970

**Appendix 4: LA-ICP-MS intensity (cps) values of all Fe-Mn oxide coated samples;
ND = Not Determined.**

Site	BCS 1.2.1	BCS 1.2.2	BCS 4.1.1	BCS 4.1.2	BCS 4.2.1	BCS 4.2.2
Substrate	Pebble	Pebble	Pebble	Pebble	Pebble	Pebble
Month						
Al 27	18628752	10453502	50823886	46047522	49981083	45748868
Si 29	1199144	1780078	4158682	4046990	4844893	4481876
Ca 43	407914	618749	332410	255255	704578	518988
Ti 47	129838	120645	398064	268300	2072831	4184096
V 51	107354	92090	144128	94053	330970	480646
Cr 53	599455	1081478	916800	826119	784878	747980
Mn 55	40859198	1634802	123156	33609	130992	208512
Fe 57	21373061	30834430	22911380	17815659	21908744	24798764
Co 59	8012556	390566	113261	13788	82309	49671
Ni 62	1950242	173249	35348	36244	43047	81967
Cu 65	32823280	6722600	15909830	13469460	15561323	12515885
Zn 67	2996770	410485	391938	368629	451635	520344
As 75	18225	22048	8848	8524	7877	10200
Se 82	ND	ND	ND	ND	ND	ND
Sr 86	5800	4710	8124	5528	10623	9773
Y 89	37074	19095	64698	54333	67248	61854
Ag 107	1632	3159	10818	2283	22363	12712
Cd 111	19032	1121	585	637	692	571
Sn 118	3766	4760	11478	17047	10495	22005
Ba 137	427413	23868	7649	8696	15962	42433
La 139	16796	9522	16067	11374	13991	9542
Ce 140	147737	49466	54944	42892	52351	38999
Au 197	2	6	8	7	10	8
Hg 202	275	135	272	228	232	159
Pb 206	1526719	438762	311108	268424	250823	190866
Pb 207	1451980	385445	296785	242137	234393	174861
Pb 208	1482828	403994	312950	248351	235157	196657
Bi 209	411	196	305	341	325	343
Th 232	3331	1707	4888	4305	4154	3970
U 238	4160	2276	13844	10208	13848	8647

**Appendix 4: LA-ICP-MS intensity (cps) values of all Fe-Mn oxide coated samples;
ND = Not Determined.**

Site	BCS 5.1.1	BCS 5.1.2	BCS 5.2.1	BCS 5.2.2	BCS 6.1.1	BCS 6.1.2
Substrate	Pebble	Pebble	Pebble	Pebble	Pebble	Pebble
Month						
Al 27	12711148	6345533	2229096	25043931	10316526	15023607
Si 29	6299784	2149740	1297680	5917979	2419310	3250379
Ca 43	2992908	2413805	142055	415151	143001	1466083
Ti 47	367220	286201	865490	1466811	2960236	291225
V 51	354054	152207	109491	404028	59025	81365
Cr 53	397656	234930	71752	644429	366949	491700
Mn 55	215518	987779	136777	323962	21072	70689
Fe 57	45558538	29008339	9033813	40213117	15968830	31641543
Co 59	169904	468428	31574	124502	18185	46510
Ni 62	91873	54638	34057	237333	47149	15434
Cu 65	6755656	4597953	933286	12658409	5513345	8257962
Zn 67	526752	199737	55381	494000	183541	296934
As 75	45329	24550	2735	10994	11651	27184
Se 82	4400	1750	196	5903	4216	8022
Sr 86	68930	106949	3977	15282	11451	170407
Y 89	19880	13638	6127	27705	58693	189530
Ag 107	22045	1790	2843	11800	4541	12443
Cd 111	1287	897	859	645	674	911
Sn 118	18378	35849	3472	8581	15213	21349
Ba 137	60837	20770	5061	33952	148697	196649
La 139	10566	4091	1213	11288	13646	91447
Ce 140	39342	16841	4053	34255	58189	229287
Au 197	7	4	1	12	3	8
Hg 202	129	118	99	156	42	38
Pb 206	756276	441564	66110	358780	205152	407372
Pb 207	679033	402151	64294	316836	202985	399921
Pb 208	784895	420182	64873	331800	204176	371687
Bi 209	227	212	37	345	255	447
Th 232	1848	1099	433	2426	39797	118598
U 238	4761	2999	717	8494	8914	21876

**Appendix 4: LA-ICP-MS intensity (cps) values of all Fe-Mn oxide coated samples;
ND = Not Determined.**

Site	BCS 6.2.1	BCS 6.2.2	BCS 8.1.1	BCS 8.1.2	BCS 8.2.1	BCS 8.2.2
Substrate	Pebble	Pebble	Pebble	Pebble	Pebble	Pebble
Month						
Al 27	14415052	12174927	18755446	17736064	61637990	31046812
Si 29	2412886	1327995	2929550	3099193	3781871	3518342
Ca 43	122288	71987	1720593	653083	276515	512441
Ti 47	502733	209650	321029	383752	367646	192598
V 51	124564	39072	65064	166392	147267	239958
Cr 53	465451	401564	872973	1370402	1520548	1140906
Mn 55	60174	17341	144448	200052	78915	175119
Fe 57	35394625	6377008	19803721	82440491	42867146	92576535
Co 59	37880	11926	34195	88151	43728	109891
Ni 62	209666	142902	244136	250132	142475	275318
Cu 65	8459106	5139378	7398868	11618069	21740369	27934021
Zn 67	200913	117876	322762	805729	686342	1119686
As 75	13718	4647	6843	61316	135905	554043
Se 82	6708	1331	2769	9360	14246	54686
Sr 86	2619	1879	5634	5096	6872	9878
Y 89	35010	24376	29463	33177	91574	56398
Ag 107	5658	3628	1646	33367	47869	36034
Cd 111	477	169	826	1720	1404	2321
Sn 118	3487	1707	1821	33161	9879	20485
Ba 137	11149	7973	20351	44766	37534	32763
La 139	12234	8864	10096	14659	35478	34225
Ce 140	37830	24113	85677	57558	102185	93491
Au 197	5	3	5	15	6461	328
Hg 202	-3	102	50	339	569	1031
Pb 206	351202	94093	134650	423683	488515	1095956
Pb 207	329715	86824	121765	385949	451785	980182
Pb 208	344561	93971	131117	402276	471273	976796
Bi 209	175	134	149	454	637	2027
Th 232	8214	4429	3306	6478	10866	5296
U 238	9221	4080	6501	8100	22256	13420

**Appendix 4: LA-ICP-MS intensity (cps) values of all Fe-Mn oxide coated samples;
ND = Not Determined.**

Site	BCS 10.1.1	BCS 10.1.2	BCS 10.2.1	BCS 10.2.2	Slag 1.1.1	Slag 1.1.2
Substrate	Pebble	Pebble	Pebble	Pebble	Pebble	Pebble
Month						
Al 27	9005686	4444834	12242830	10119635	6973345	1516928
Si 29	2234115	1231217	4786956	5899109	2765496	737865
Ca 43	223554	194133	1782755	1604205	622580	124521
Ti 47	260679	227951	847870	886809	3083490	443180
V 51	162217	109292	271412	287205	167777	40801
Cr 53	454637	327335	1099947	666427	201076	20512
Mn 55	142965	45775	515007	685538	73872	13440
Fe 57	84173936	104270781	26287341	27448783	27780449	3337573
Co 59	45818	34041	38304	100388	78802	18891
Ni 62	56451	26724	201508	200040	244683	55549
Cu 65	34902954	27288512	16105102	16804440	2716811	969194
Zn 67	430017	357778	713688	756903	260525	31320
As 75	48352	35550	6331	7409	4003	1277
Se 82	63867	48885	1473	2168	433	-260
Sr 86	9839	13333	7527	19645	551999	103735
Y 89	24533	9231	17346	16385	26992	6512
Ag 107	5403	3136	8146	100469	276	82
Cd 111	1640	1127	995	1082	351	29
Sn 118	3894	7065	10293	6405	4688	560
Ba 137	32200	28569	13166	20577	726881	179540
La 139	13423	5763	6335	7086	44876	9517
Ce 140	27208	14465	16348	18331	130926	23152
Au 197	47	45	15	22	2	3
Hg 202	391	347	260	168	95	-24
Pb 206	582774	392675	406491	454103	280286	19215
Pb 207	491102	360955	376117	421273	236871	57672
Pb 208	531971	351081	397311	424559	243923	24189
Bi 209	1257	2016	342	341	211	35
Th 232	2667	2101	2169	1974	8765	2451
U 238	2146	1232	1776	1539	3388	1131

**Appendix 4: LA-ICP-MS intensity (cps) values of all Fe-Mn oxide coated samples;
ND = Not Determined.**

Site	Slag 1.2.1	Slag 1.2.2	BCS 11.1.1	BCS 11.1.2	TCS 11.2.1	TCS 11.2.2
Substrate	Pebble	Pebble	Pebble	Pebble	Pebble	Pebble
Month						
Al 27	7696729	3436547	1866166	10082242	4886105	3791185
Si 29	4879973	2232222	2401444	19352460	1982560	1076222
Ca 43	1289057	1843116	102194	815983	487658	69359
Ti 47	2786727	1625468	1816917	8906860	384104	75295
V 51	167221	136116	48415	344251	273559	88107
Cr 53	249318	175012	66798	1260455	638082	208314
Mn 55	76853	378041	74667	670512	95353	25387
Fe 57	21862840	48627023	3420021	25574872	154624908	109967918
Co 59	48393	156969	26901	432260	59107	14287
Ni 62	143885	335125	101481	1952998	54587	29075
Cu 65	6411031	18571557	403870	1020576	15234402	6935074
Zn 67	404529	529855	46539	523654	715026	246122
As 75	7767	34180	2441	11684	36593	11466
Se 82	1828	2004	503	141	10754	8430
Sr 86	217407	240789	26095	141075	4834	2803
Y 89	24714	50147	3665	20657	16500	8679
Ag 107	1139	4078	9828	268017	15225	2308
Cd 111	1059	1993	445	4651	714	471
Sn 118	3953	9376	3161	48688	7896	1465
Ba 137	492666	406887	131024	817814	12131	8171
La 139	52682	38162	9224	52686	4954	4446
Ce 140	157789	91863	32028	205865	29753	14175
Au 197	14	10	3	9	21	3
Hg 202	307	192	67	-2	126	137
Pb 206	567555	1586839	22737	151880	1342077	1308069
Pb 207	489709	1308952	22295	94319	1195777	1205971
Pb 208	540861	1321605	18206	87091	1296330	1248438
Bi 209	417	4180	8	169	1136	140
Th 232	16032	10522	3367	14035	2634	1067
U 238	6585	7358	1680	11755	4412	1571

**Appendix 4: LA-ICP-MS intensity (cps) values of all Fe-Mn oxide coated samples;
ND = Not Determined.**

Site	BCS 13.1.1	BCS 13.1.2	BCS 13.2.1	BCS 13.2.2	BCS 15.1.1	BCS 15.1.2
Substrate	Pebble	Pebble	Pebble	Pebble	Pebble	Pebble
Month						
Al 27	3541400	4316569	19697256	1770882	6197826	4959339
Si 29	3602526	5396120	3094277	2433302	6150749	4146262
Ca 43	333423	579951	726573	758154	1405006	437817
Ti 47	810478	1385088	431780	159797	422606	490387
V 51	203713	221418	261795	234443	158225	112488
Cr 53	583284	580344	778619	100316	737599	399066
Mn 55	113829	107502	86150	61304	1890535	1529345
Fe 57	63760272	95085197	69493980	130806452	11259582	9203260
Co 59	58445	62383	40354	161720	393023	320572
Ni 62	171509	180949	268217	154083	1451406	1188888
Cu 65	24562505	27244301	89911570	38336341	782855	188973
Zn 67	729126	675942	2433778	2944729	505091	306593
As 75	80789	62558	329389	319658	23260	24900
Se 82	27521	38061	30398	332766	5159	1612
Sr 86	8615	47857	14965	6209	69843	42900
Y 89	7176	9011	51654	1197	12350	7613
Ag 107	17525	14857	45082	205512	26001	19915
Cd 111	3474	3360	11998	21536	4694	5541
Sn 118	19986	13815	7595	32423	20282	12462
Ba 137	40554	150988	41447	15750	267525	370213
La 139	3995	7132	20723	971	22636	9671
Ce 140	11145	19597	44537	1825	111259	86171
Au 197	88	77	38	325	5	-0
Hg 202	464	562	1452	3308	524	512
Pb 206	162545	341657	308844	1132452	361479	388941
Pb 207	144672	309561	298246	1025235	337684	359242
Pb 208	151689	328433	310586	1083336	355135	367405
Bi 209	2706	3163	1909	23452	839	678
Th 232	1857	2748	6107	325	2708	978
U 238	980	1243	5084	292	4226	1946

**Appendix 4: LA-ICP-MS intensity (cps) values of all Fe-Mn oxide coated samples;
ND = Not Determined.**

Site	BCS 15.2.1	BCS 15.2.2	BCS 16.1.1	BCS 16.1.2	BCS 16.2.1	BCS 16.2.2
Substrate	Pebble	Pebble	Pebble	Pebble	Pebble	Pebble
Month						
Al 27	2633168	2056761	2081665	2578980	4406448	2593984
Si 29	5880316	3117823	2491354	3849895	2504097	2282693
Ca 43	557966	475504	1162090	2206821	2195190	1326290
Ti 47	203606	156099	582538	222420	541268	299086
V 51	110698	70297	104312	169742	187604	109881
Cr 53	1424723	598822	591888	1060452	819036	1553929
Mn 55	3119679	2015661	250303	241562	7960310	2659449
Fe 57	23004001	16052773	8122382	9928904	12665845	8756462
Co 59	529103	316511	62102	162919	1670354	582893
Ni 62	3506960	1835528	298190	323582	4551511	1994179
Cu 65	94999	80556	170468	215818	161598	175231
Zn 67	1214369	618971	183542	120619	1549013	550663
As 75	139285	111883	14686	16676	180427	62639
Se 82	4355	4058	20	427	203	276
Sr 86	24065	26859	8355	11868	27721	9966
Y 89	15139	9587	3939	2794	12985	5506
Ag 107	5891	7839	84318	8235	6411	21973
Cd 111	16085	8582	743	472	27569	5481
Sn 118	15889	7148	6503	6722	46783	12028
Ba 137	162034	100590	35072	25178	476929	144811
La 139	26131	16700	3379	1593	10824	5424
Ce 140	174485	165620	9494	4989	346326	83019
Au 197	10	6	2	2	3	2
Hg 202	429	424	163	45	224	281
Pb 206	804574	636841	75759	53607	2415475	972048
Pb 207	725464	590875	80194	49913	2254694	897819
Pb 208	784432	600052	75468	51268	2386897	954912
Bi 209	1964	1628	326	381	2875	1487
Th 232	3614	2689	592	512	2305	1294
U 238	3197	2750	287	92	628	299

Appendix 4: LA-ICP-MS intensity (cps) values of all Fe-Mn oxide coated samples;
ND = Not Determined.

Site	BCS 17.1.1	BCS 17.1.2	BCS 17.2.1	BCS 17.2.2	BCS 18.1.1	BCS 18.1.2
Substrate	Pebble	Pebble	Pebble	Pebble	Pebble	Pebble
Month						
Al 27	6025756	5319048	2966456	3180229	3243666	3477651
Si 29	4212275	5698500	4692006	3490774	3007134	7461547
Ca 43	1677484	3344726	2193573	2078886	693470	2655315
Ti 47	2497043	379840	618588	677265	36478	266111
V 51	433911	261310	173658	161576	60674	159274
Cr 53	1246795	1720798	527663	314964	502478	2052694
Mn 55	22301594	571202	470840	236437	153125	383275
Fe 57	38453326	21920139	11392245	11235275	9494196	17317285
Co 59	3792704	132379	307427	106542	47976	101076
Ni 62	9855908	997043	804140	678496	432558	785609
Cu 65	456399	156981	844191	378859	172109	370664
Zn 67	3703093	362920	224908	191165	107476	155555
As 75	164043	33619	9090	8459	5626	1641
Se 82	1085	553	967	845	17	191
Sr 86	42926	12028	20708	7185	4539	14183
Y 89	27905	4125	5557	4933	609	1240
Ag 107	13447	1821	17859	9134	48941	17058
Cd 111	60161	1107	752	2302	209	347
Sn 118	12368	8213	31695	5054	1667	9875
Ba 137	2370390	25195	77216	15868	15759	15973
La 139	28764	4322	3979	17417	871	1028
Ce 140	261436	10273	17830	21987	1787	3397
Au 197	1	6	2	0	0	-1
Hg 202	343	110	62	87	115	60
Pb 206	2994668	186589	117739	67825	16054	16166
Pb 207	2841626	181287	101059	65592	14669	19013
Pb 208	2987978	201078	110751	65053	15857	13928
Bi 209	1204	608	272	322	47	96
Th 232	4237	787	2505	930	98	180
U 238	1124	525	1487	208	219	172

**Appendix 4: LA-ICP-MS intensity (cps) values of all Fe-Mn oxide coated samples;
ND = Not Determined.**

Site	BCS 18.2.1	BCS 18.2.2	BCS 19.1.1	BCS 19.1.2	BCS 19.2.1	BCS 19.2.2
Substrate	Pebble	Pebble	Pebble	Pebble	Pebble	Pebble
Month						
Al 27	2512178	451503	655715	1119554	5180915	5782464
Si 29	8590259	1152637	6206574	7500305	4247865	4516371
Ca 43	4997312	497604	154688	389743	1362259	1729497
Ti 47	546891	121341	38314	97102	1225045	1968597
V 51	154493	907410	33752	67997	961469	962672
Cr 53	1414096	922872	1871060	4859228	3225005	3349536
Mn 55	290636	350933	197856	157726	2032734	1879948
Fe 57	14744360	13226204	15539047	9438019	64790418	56501340
Co 59	136272	64603	121682	170628	510355	312402
Ni 62	1053934	219653	1951814	1977291	1616135	1827016
Cu 65	323918	61661	90844	229981	938032	255176
Zn 67	355516	548486	262072	453324	586980	631236
As 75	4474	15117	6936	7912	674310	573493
Se 82	353	305	-22	431	1378	1217
Sr 86	20700	6540	4013	6544	43255	31533
Y 89	4206	4449	841	1446	28072	35749
Ag 107	27330	5618	3212	11366	57688	18967
Cd 111	614	589	582	1155	4516	5209
Sn 118	29128	1205	988	10532	8238	31892
Ba 137	44844	56992	20768	18030	158040	175838
La 139	6200	14588	958	17816	39240	43265
Ce 140	34748	23066	2674	7752	444303	562607
Au 197	6	-0	-0	3	2	3
Hg 202	332	4	74	77	96	194
Pb 206	48771	29181	37821	102035	1154063	1272305
Pb 207	44423	27990	34057	61015	1102838	1204270
Pb 208	44861	27688	35323	62123	1115306	1251730
Bi 209	365	115	79	271	1627	2987
Th 232	993	684	319	514	15609	19671
U 238	450	150	181	569	1653	1794

**Appendix 4: LA-ICP-MS intensity (cps) values of all Fe-Mn oxide coated samples;
ND = Not Determined.**

Site	BCS 20.1.1	BCS 20.1.2	BCS 20.2.1	BCS 20.2.2	BCS 21.1.2	BCS 21.1.2
Substrate	Pebble	Pebble	Pebble	Pebble	Pebble	Pebble
Month						
Al 27	2396732	2791491	1221094	861536	3935809	5646901
Si 29	3355471	3379444	6674783	2453758	3406527	3248990
Ca 43	2719249	2123230	3124844	504792	462509	799764
Ti 47	313223	340721	181766	188909	2558340	2239315
V 51	147849	142917	78982	55131	477190	600520
Cr 53	547711	617812	3637977	1241650	117648	303603
Mn 55	635273	472542	342975	745852	4749568	12143668
Fe 57	10423894	10926108	14357647	5808419	19595202	34286558
Co 59	101892	70865	157527	500508	627359	466819
Ni 62	434437	392902	1170700	1124196	1066265	3475017
Cu 65	178183	91644	90141	82612	1058577	2356291
Zn 67	123470	160408	241937	178080	597443	1162764
As 75	6800	13008	14780	16602	24263	100163
Se 82	89	277	262	598	608	1212
Sr 86	3955	4194	11998	8954	21577	36964
Y 89	4479	4245	2050	3636	15836	30911
Ag 107	2899	1558	10558	12518	6584	2176
Cd 111	1024	868	872	637	9624	38078
Sn 118	4914	5333	4745	5475	7405	3450
Ba 137	30151	33524	20759	53887	381453	643074
La 139	3931	3783	2095	4529	8738	21225
Ce 140	28301	18815	22013	70217	77420	171413
Au 197	11	-4	1	1	4	5
Hg 202	59	87	55	139	123	174
Pb 206	98779	87554	48188	196446	363364	554978
Pb 207	89503	89292	45064	189933	333632	590926
Pb 208	92351	84321	47443	195668	357222	524219
Bi 209	114	159	214	484	160	287
Th 232	517	936	881	1971	1079	2209
U 238	558	541	172	268	361	736

Appendix 4: LA-ICP-MS intensity (cps) values of all Fe-Mn oxide coated samples;
ND = Not Determined.

Site	BCS 21.2.1	BCS 21.2.2	RRS 1.1.1	RRS 1.1.2	RRS 1.2.1	RRS 1.2.2
Substrate	Pebble	Pebble	Pebble	Pebble	Pebble	Pebble
Month						
Al 27	5804241	3102604	2880459	739456	2329136	7614056
Si 29	3316035	1887035	14185185	3006456	3155864	4786267
Ca 43	311908	523279	10718567	7989889	5762413	14239314
Ti 47	1155393	1037216	4716551	880042	3039810	1245471
V 51	253407	194481	150356	34403	304104	550262
Cr 53	2199430	721850	130325	29475	45510	24351
Mn 55	229421	115160	13944557	2157611	460708	2193336
Fe 57	16494157	7065163	5021227	1208780	16732377	17713787
Co 59	94691	79956	78651	35009	51319	100872
Ni 62	494280	185241	225487	51271	85629	13094
Cu 65	245136	82930	851859	379068	168333	202770
Zn 67	264725	83658	553466	145985	180368	202917
As 75	14096	3264	5301	1607	1153	2928
Se 82	381	286	813	92	-171	677
Sr 86	5670	40998	244931	130892	79620	2980559
Y 89	2074	2542	212170	65092	49096	92932
Ag 107	3029	4991	8287	7209	8307	18657
Cd 111	495	169	3153	1364	506	795
Sn 118	5165	4144	18694	31445	7712	15639
Ba 137	14736	71903	3885896	526453	113661	575549
La 139	1478	1305	279287	82391	43627	75962
Ce 140	11521	3110	1303791	328447	245384	209721
Au 197	0	9	34	45	2	5
Hg 202	42	115	737	269	283	158
Pb 206	42525	20071	64586	53435	30508	100590
Pb 207	37194	19412	59815	53945	17948	86829
Pb 208	41918	19415	57770	59685	22948	88430
Bi 209	150	68	999	456	57	155
Th 232	555	877	11776	3284	5875	1310
U 238	350	236	8641	2006	2199	732

**Appendix 4: LA-ICP-MS intensity (cps) values of all Fe-Mn oxide coated samples;
ND = Not Determined.**

Site	RRS 2.1.1	RRS 2.1.2	RRS 2.2.1	RRS 2.2.2	RRS 3.1.1	RRS 3.1.2
Substrate	Pebble	Pebble	Pebble	Pebble	Pebble	Pebble
Month						
Al 27	701920	2212501	2869017	897614	2548772	3730059
Si 29	4505965	2265253	3897815	2720888	3252625	3126993
Ca 43	172673	294351	314214	186824	319218	396090
Ti 47	1874749	1758696	651840	453466	958935	1553304
V 51	60351	138890	113406	49379	119103	191600
Cr 53	45016	105622	66516	33528	58693	119347
Mn 55	319519	2026028	2976513	352959	114175	232139
Fe 57	4319628	9076722	8979857	2432356	9296175	13857929
Co 59	31997	88649	48425	48139	19085	73183
Ni 62	77777	102031	141321	22965	66395	133048
Cu 65	146078	158060	49849	58376	38538	66100
Zn 67	109704	237782	262137	32965	128264	245753
As 75	1560	3217	2489	1226	1144	1658
Se 82	543	726	-320	592	-49	-50
Sr 86	19140	39936	50538	20575	25366	39283
Y 89	6012	217548	11358	14567	9878	11775
Ag 107	6850	15881	3205	8167	2120	3736
Cd 111	711	1473	1716	131	242	418
Sn 118	10650	13230	5418	5974	4190	7099
Ba 137	163728	577499	1005255	381092	206048	368507
La 139	28345	27798	27784	24648	19954	29304
Ce 140	51742	94445	70371	61408	50150	49533
Au 197	30	3	3	2	9	591
Hg 202	264	143	365	107	200	105
Pb 206	83884	70992	27701	24334	34227	37902
Pb 207	77941	58105	25185	18390	31443	35001
Pb 208	82446	62554	25492	20433	39903	38742
Bi 209	267	200	234	1852	112	148
Th 232	2837	18387	7207	8739	4625	6277
U 238	1161	34453	2248	3670	1195	1637

**Appendix 4: LA-ICP-MS intensity (cps) values of all Fe-Mn oxide coated samples;
ND = Not Determined.**

Site	RRS 3.2.1	RRS 3.2.2	RRS 4.1.1	RRS 4.1.2	RRS 4.2.1	RRS 4.2.2
Substrate	Pebble	Pebble	Pebble	Pebble	Pebble	Pebble
Month						
Al 27	2851304	1678853	3422398	3862555	3085190	3631411
Si 29	2876689	1771612	5568016	6296303	2809584	4931953
Ca 43	1692797	206548	326424	396020	3323448	1999498
Ti 47	5010444	594899	3041076	486187	18493276	2923276
V 51	328698	81478	131594	53807	338150	190217
Cr 53	83566	29891	28017	6377	442230	401585
Mn 55	7775203	284888	886971	555160	325050	632325
Fe 57	17379427	6437235	12518480	4997126	13420194	19058427
Co 59	163136	40916	17830	20790	63708	102962
Ni 62	104506	72121	19867	8058	128469	180669
Cu 65	121425	144861	260982	26660	124164	97313
Zn 67	876111	131823	216242	103519	106825	165957
As 75	7900	1058	5813	2500	4573	4201
Se 82	254	187	259	48	111	392
Sr 86	172732	17722	47843	55604	19534	27537
Y 89	37119	8997	8980	2928	50084	15636
Ag 107	7254	14037	17309	7571	6083	3942
Cd 111	2458	328	443	270	291	419
Sn 118	11713	24203	14887	4120	11584	13941
Ba 137	2329506	261801	1015801	448215	88878	229730
La 139	73906	14283	19020	4365	9690	16261
Ce 140	293321	32924	98405	54852	43871	182752
Au 197	3	165	3	0	8	6
Hg 202	560	250	144	235	196	139
Pb 206	128676	43779	100154	54624	32129	72108
Pb 207	125351	35228	98306	51575	27805	58057
Pb 208	133306	36300	100780	57078	31820	70221
Bi 209	756	136	579	128	85	172
Th 232	6681	3346	10527	3766	1275	3207
U 238	2001	1163	3390	2097	1021	2172

Appendix 4: LA-ICP-MS intensity (cps) values of all Fe-Mn oxide coated samples;
ND = Not Determined.

Site	RRS 5.1.1	RRS 5.1.2	RRS 5.2.1	RRS 5.2.2	RRS 6.1.1	RRS 6.1.2
Substrate	Pebble	Pebble	Pebble	Pebble	Pebble	Pebble
Month						
Al 27	542009	1436316	3873963	3808252	5596915	1896667
Si 29	626587	961495	2823522	10800729	8303016	1267002
Ca 43	238912	293224	294530	421313	615904	355850
Ti 47	91985	900827	1264646	4387622	932887	249894
V 51	66860	70615	195550	149785	159111	106478
Cr 53	6660	9328	28375	27526	108684	61816
Mn 55	6176877	13826214	1612393	1162613	933716	2499412
Fe 57	4459299	7634527	30807920	11446146	16676469	17313981
Co 59	98124	178730	87764	51509	59552	106804
Ni 62	35854	85073	132360	44464	63405	33684
Cu 65	72289	79227	1899295	75141	59759	100798
Zn 67	347118	583234	440073	232579	684252	229927
As 75	5525	6623	13543	16198	1320	3515
Se 82	145	-61	-137	1805	-137	1071
Sr 86	28385	55968	28840	114749	843753	59992
Y 89	25212	19024	24459	123502	6829	11440
Ag 107	1992	1150	1982	16021	1335	3091
Cd 111	2968	2112	497	1177	481	718
Sn 118	2454	3530	2457	6404	12050	8726
Ba 137	2398316	5566261	959497	900141	10839914	434208
La 139	46265	66958	31634	1424911	8359	28791
Ce 140	129109	197577	115282	2842614	39466	99603
Au 197	4	10	3	1	77	-1
Hg 202	421	986	286	190	307	201
Pb 206	42636	41893	73614	112417	159501	100969
Pb 207	38833	36127	66710	66359	157732	87099
Pb 208	38588	37158	69760	106149	155901	100515
Bi 209	313	132	297	371	113	225
Th 232	17616	2826	9516	356566	1613	2442
U 238	984	1805	2731	11618	1074	2701

**Appendix 4: LA-ICP-MS intensity (cps) values of all Fe-Mn oxide coated samples;
ND = Not Determined.**

Site	RRS 6.2.1	RRS 6.2.2	RRS 7.1.1	RRS 7.1.2	RRS 7.2.1	RRS 7.2.2
Substrate	Pebble	Pebble	Pebble	Pebble	Pebble	Pebble
Month						
Al 27	3141965	1480523	2546555	5928477	4347027	3833675
Si 29	8847725	1980224	2720974	5809592	5395819	4154466
Ca 43	1059278	883883	1116756	2321294	8248766	3931005
Ti 47	2592752	1007934	305608	4226189	12745830	5479629
V 51	121918	109762	149066	557121	776527	472626
Cr 53	33968	28671	19576	124016	198320	121800
Mn 55	1023935	1085406	2488095	1777357	5324250	10364310
Fe 57	8187216	6804407	15383671	46822332	46698717	32115559
Co 59	40497	107745	119500	398367	414148	721725
Ni 62	24863	31478	20721	150282	204754	232879
Cu 65	35141	18588	71547	569286	203362	935722
Zn 67	220985	120065	161814	841641	753223	1044987
As 75	3935	6590	7310	20162	21473	15821
Se 82	481	303	640	2083	489	678
Sr 86	415184	190370	314139	399008	262264	361701
Y 89	6993	7511	11856	70535	88827	47685
Ag 107	1551	1034	3877	247598	263729	61883
Cd 111	559	420	744	7339	3565	4588
Sn 118	6061	9845	7085	60509	24421	58105
Ba 137	1299795	295895	663431	1547674	1632027	2725263
La 139	26702	24013	34319	169231	123704	83233
Ce 140	105649	140393	124715	756249	499061	376978
Au 197	-0	2	28	14	16	12
Hg 202	127	53	119	1161	245	1210
Pb 206	140501	107041	132297	591772	245928	293127
Pb 207	131801	97261	116089	545116	241781	321238
Pb 208	126977	102545	118130	629531	260980	302142
Bi 209	374	629	235	1395	448	611
Th 232	9265	9751	1939	13777	6710	7074
U 238	6315	3307	2121	10614	5609	5788

Appendix 4: LA-ICP-MS intensity (cps) values of all Fe-Mn oxide coated samples;
ND = Not Determined.

Site	RRS 8.1.1	RRS 8.1.2	RRS 8.2.1	RRS 8.2.2	RRS 9.1.1	RRS 9.1.2
Substrate	Pebble	Pebble	Pebble	Pebble	Pebble	Pebble
Month						
Al 27	2654418	2123861	2736876	3352554	11135309	4668142
Si 29	4486030	5675386	4212965	4633468	6559146	2791389
Ca 43	1002538	404769	5307915	5813534	4187644	644952
Ti 47	1697163	184957	7126674	5270779	18746862	4006511
V 51	323352	33047	322912	353081	1538132	519875
Cr 53	202380	13538	543927	442674	394514	156985
Mn 55	1620818	94316	850795	1249459	4026908	1515014
Fe 57	25439636	3103363	18665189	19477159	104327432	38203212
Co 59	146420	25223	71643	82018	207394	72548
Ni 62	161578	16382	148068	153161	234544	90415
Cu 65	1414951	100543	123209	75663	290588	88188
Zn 67	407062	59171	178393	160702	422128	200634
As 75	10667	2694	1649	2725	191028	53879
Se 82	1745	430	424	806	2145	272
Sr 86	148231	99483	65071	108280	347879	95064
Y 89	22117	6510	35550	42719	309108	68361
Ag 107	37125	8555	2496	1660	5378	4117
Cd 111	1338	160	711	763	2143	580
Sn 118	76963	5002	8987	7132	16703	12310
Ba 137	675449	815386	294730	428091	1817332	638874
La 139	39888	14681	11329	15202	460055	153632
Ce 140	202180	39614	47946	71017	990478	309003
Au 197	-0	2	3	1	119	2
Hg 202	573	192	202	108	319	228
Pb 206	85415	45061	34878	36995	343804	124758
Pb 207	75891	43831	30597	34456	291920	105153
Pb 208	83382	50043	33212	35792	311297	112444
Bi 209	539	91	168	142	1037	374
Th 232	7439	2197	1055	985	67010	22391
U 238	6158	1669	1438	1153	46306	9753

**Appendix 4: LA-ICP-MS intensity (cps) values of all Fe-Mn oxide coated samples;
ND = Not Determined.**

Site	RRS 9.2.1	RRS 9.2.2	RRS 10.1.1	RRS 10.1.2	RRS 10.2.1	RRS 10.2.2
Substrate	Pebble	Pebble	Pebble	Pebble	Pebble	Pebble
Month						
Al 27	1633836	913110	5139222	8107471	3853178	7187761
Si 29	3725887	2777644	2027856	4065745	4312840	4967590
Ca 43	3789636	2757455	1715405	2218523	5158425	11972528
Ti 47	1767485	354414	3369606	6608987	7570351	1765957
V 51	241999	72159	404149	449293	189740	461978
Cr 53	1840522	101991	203134	221493	91217	182266
Mn 55	950015	611845	41253602	32385493	6634089	12052767
Fe 57	21360704	10035520	45754840	48559609	15467090	29507099
Co 59	70890	52587	484895	354277	134877	196759
Ni 62	175598	145611	507297	356912	108896	152438
Cu 65	98166	55160	308947	254086	83553	102840
Zn 67	128993	95982	1305816	1243127	233732	448080
As 75	2232	1429	62082	47553	7442	13790
Se 82	188	26	1620	834	871	1542
Sr 86	73665	26788	317414	393297	931562	3908531
Y 89	13346	5491	87432	68375	72106	131414
Ag 107	1737	3489	16628	19812	2661	69874
Cd 111	369	264	8815	7823	1140	2570
Sn 118	3285	2909	32203	20356	9336	11755
Ba 137	264844	128334	8505227	6741896	1211752	2084363
La 139	20348	12508	248151	173164	50657	114220
Ce 140	57697	49154	3123300	1319107	304338	372174
Au 197	2	3	2	4	3	0
Hg 202	100	116	911	780	269	517
Pb 206	98483	59384	221428	132168	64313	133122
Pb 207	90608	56603	205299	126328	58222	128114
Pb 208	96941	56958	213390	130112	60143	127777
Bi 209	278	189	710	485	240	566
Th 232	2211	2286	60772	37880	12266	3875
U 238	2142	1158	10328	10983	6802	4066

**Appendix 4: LA-ICP-MS intensity (cps) values of all Fe-Mn oxide coated samples;
ND = Not Determined.**

Site	RRS 11.1.1	RRS 11.1.2	RRS 11.2.1	RRS 11.2.2	RRS 12.1.1	RRS 12.1.2
Substrate	Pebble	Pebble	Pebble	Pebble	Pebble	Pebble
Month						
Al 27	7013142	2404916	6758242	8478529	7457037	8759368
Si 29	7001358	2830912	4234189	5133564	8457281	7677812
Ca 43	6068003	1088898	3893408	653231	1343945	1755010
Ti 47	4258263	3335494	1227882	726015	8520448	11543076
V 51	339878	1050139	112428	59515	547063	499688
Cr 53	145540	192849	50231	17033	117418	143274
Mn 55	4412486	621177	1378890	1427575	1075521	1222283
Fe 57	33571963	45082704	17314477	9816469	35056307	25026627
Co 59	180257	62224	49680	41756	197443	82808
Ni 62	100459	76698	54683	58508	124429	79230
Cu 65	106096	117813	208785	81486	251270	186988
Zn 67	665991	255903	413274	500545	635206	424583
As 75	19736	1794	3987	2882	9976	15229
Se 82	-807	-728	1157	726	225	432
Sr 86	447613	51217	1086900	357721	200651	166248
Y 89	159794	12938	21655	11347	61742	94652
Ag 107	1310	3969	2612	2596	20423	4189
Cd 111	4578	2202	1942	1690	1279	624
Sn 118	10817	10987	6290	2958	24180	19080
Ba 137	2088780	162946	2197832	4458730	1631929	2103581
La 139	47640	5573	50559	21362	94957	52910
Ce 140	247178	23379	118678	67142	272901	190215
Au 197	0	7	6	5	11	6
Hg 202	227	268	360	227	333	156
Pb 206	151479	26949	127742	64551	242427	217462
Pb 207	135032	601457	114346	55420	213167	1288070
Pb 208	157371	28406	124241	56983	224047	205592
Bi 209	441	79	399	227	1260	772
Th 232	3040	1053	6059	1935	25342	28392
U 238	3443	564	3983	1753	11301	13929

**Appendix 4: LA-ICP-MS intensity (cps) values of all Fe-Mn oxide coated samples;
ND = Not Determined.**

Site	RRS 11.2.1	RRS 11.2.2	RRS 13.1.1	RRS 13.1.2	RRS 13.2.1	RRS 13.2.2
Substrate	Pebble	Pebble	Pebble	Pebble	Pebble	Pebble
Month						
Al 27	2685082	3534110	1277721	1012655	684204	875126
Si 29	3986648	4003996	1297796	2885243	6394663	4548869
Ca 43	3435494	5206950	1450727	380556	421706	526872
Ti 47	3703299	8349510	1708204	531684	350150	481103
V 51	232477	450347	115572	91010	36878	64889
Cr 53	89797	144194	62056	19108	15319	20934
Mn 55	1545927	1958004	686096	1587644	809859	1475892
Fe 57	13232551	27974338	8900014	9066579	5069353	7032876
Co 59	133118	71649	41974	61622	76983	74177
Ni 62	81355	255150	41003	27838	13079	41544
Cu 65	119274	178858	57406	398230	95587	196339
Zn 67	168193	299081	75433	109320	218305	172330
As 75	6552	25604	2583	4567	2151	7703
Se 82	188	812	-1024	250	-1221	237
Sr 86	793286	338542	36549	53515	66460	100225
Y 89	28984	63681	21945	15363	10938	10779
Ag 107	8959	7627	5536	16481	20783	7018
Cd 111	1229	1959	484	682	520	832
Sn 118	22911	18995	4831	45920	4618	8477
Ba 137	466687	514663	135172	293225	472118	435274
La 139	115880	91538	21606	28679	21018	24529
Ce 140	328773	238640	151465	200907	71828	92302
Au 197	4	0	2	10	2	19
Hg 202	267	268	149	253	295	283
Pb 206	109526	184403	42462	95250	39265	75574
Pb 207	107018	168431	36636	79179	41310	68574
Pb 208	99900	168792	38742	89994	36435	68390
Bi 209	500	2851	483	440	252	170
Th 232	36468	30115	35206	5072	2406	3114
U 238	5989	9787	2487	2847	1402	1576

Appendix 4: LA-ICP-MS intensity (cps) values of all Fe-Mn oxide coated samples;
ND = Not Determined.

Site	RRS 14.1.1	RRS 14.1.2	RRS 14.2.1	RRS 14.2.2	RRS 15.1.1	RRS 15.1.2
Substrate	Pebble	Pebble	Pebble	Pebble	Pebble	Pebble
Month						
Al 27	1463341	4531285	1643495	2567105	2700104	4534436
Si 29	1317416	3935782	1422547	4042158	4979552	3546705
Ca 43	1792958	7925235	531452	1170119	412218	952338
Ti 47	170302	857232	1325637	4302182	2795239	2869738
V 51	25819	103275	142065	294208	134310	295889
Cr 53	8131	455616	46494	87283	104769	174014
Mn 55	165607	732011	1187984	3415332	443141	2241966
Fe 57	1670997	6385375	13893795	28463173	12465923	26858150
Co 59	14230	54257	43634	158443	25785	89889
Ni 62	28394	138121	32769	64633	33533	101921
Cu 65	80110	85481	84125	105404	35709	261553
Zn 67	37525	96260	199714	482959	78495	323555
As 75	524	722	6118	14235	4103	11742
Se 82	-220	520	3330	873	-519	1980
Sr 86	40606	135582	103308	205885	104077	183801
Y 89	1887	6124	720768	36928	15800	42808
Ag 107	17585	3469	3986	22467	13192	23137
Cd 111	320	462	2956	2560	264	1601
Sn 118	6596	55837	3860	8478	7914	12935
Ba 137	78001	238572	559861	1209111	245062	897098
La 139	2926	10114	34663	70169	25103	94361
Ce 140	13600	38253	97979	231352	73056	308044
Au 197	34	3	3	1	3	5
Hg 202	114	220	166	288	59	196
Pb 206	14310	39785	104296	196145	57865	149926
Pb 207	14824	36364	102507	166061	49714	132012
Pb 208	14813	37829	101756	171725	52649	140001
Bi 209	98	108	458	522	705	1308
Th 232	391	714	36866	10015	16812	24668
U 238	272	740	19568	6966	5485	10121

**Appendix 4: LA-ICP-MS intensity (cps) values of all Fe-Mn oxide coated samples;
ND = Not Determined.**

Site	RRS 15.2.1	RRS 15.2.2	RRS 15.3.1	RRS 15.3.2	RRS 15.4.1	RRS 15.4.2
Substrate	Pebble	Pebble	Pebble	Pebble	Pebble	Pebble
Month						
Al 27	2188588	2797244	2590468	3942950	5175327	4653561
Si 29	2122070	2477906	2303751	4039094	6494287	7940149
Ca 43	248473	446783	705469	1105459	3168850	1551089
Ti 47	1662647	3503775	4175790	2417198	1410098	1317804
V 51	110962	143327	213273	291252	337186	146170
Cr 53	67693	91362	193236	2504009	246665	195950
Mn 55	701695	1117402	2855496	3006694	13144758	3477915
Fe 57	9132218	17559823	33888965	33102993	36590481	21155608
Co 59	25661	77300	111024	233166	381490	219153
Ni 62	34307	108057	76503	179749	169295	87679
Cu 65	56521	354794	104843	293057	145901	99817
Zn 67	79461	119839	370743	487667	1148782	378835
As 75	5744	4103	21316	18569	51937	13022
Se 82	338	484	533	329	1794	988
Sr 86	53472	47276	161809	233289	826506	302663
Y 89	108996	29842	22370	31733	48254	25628
Ag 107	4722	4568	11147	38440	6061	7971
Cd 111	264	454	1978	2484	12671	3737
Sn 118	9127	18911	6582	17495	26176	6464
Ba 137	345789	303688	858758	939631	4002227	1560075
La 139	4061866	37395	63584	88666	124842	44173
Ce 140	7715612	147893	218285	310876	612730	182494
Au 197	5	3	8	2	5	0
Hg 202	99	225	231	176	254	130
Pb 206	49065	45182	103265	127168	238953	66663
Pb 207	46036	43682	91336	107369	219780	64847
Pb 208	46919	46425	97864	112374	250947	62699
Bi 209	2520	512	1662	3631	1059	655
Th 232	36582	14290	14446	23303	11120	7335
U 238	4836	5068	5008	6962	7795	3580

**Appendix 4: LA-ICP-MS intensity (cps) values of all Fe-Mn oxide coated samples;
ND = Not Determined.**

Site	S6B	S6B	S6B	S6B	S6B	S6B
Substrate	Streak	Streak	Streak	Cement	Cement	Cement
Month	12	12	12	12	12	12
Al 27	1574820	969114	206639	1834118	1421943	257390
Si 29	1661581	3071264	536580	6652948	3985949	450763
Ca 43	278859	1220568	162450	7881163	4727495	665625
Ti 47	137233	906042	148685	1158354	1215394	169756
V 51	36232	85419	14506	364760	447368	21183
Cr 53	61201	97260	15090	267143	187844	21759
Mn 55	319471	23918521	1756488	66306917	29541725	1597604
Fe 57	61632370	94831291	15175716	205170827	134394759	11795396
Co 59	14632	197427	31529	717353	258917	130489
Ni 62	8423	114564	20221	268236	181809	20736
Cu 65	232345	450560	78844	1108616	752816	49834
Zn 67	759724	4968783	540689	14838931	8634156	666405
As 75	18482	39822	4499	100646	72719	4553
Se 82	215	1893	411	3231	2126	-114
Sr 86	43788	152754	20010	537030	383351	34957
Y 89	76820	112163	15587	279265	251966	19330
Ag 107	1495	33097	8882	44396	83128	14123
Cd 111	1911	10205	926	37182	23501	1309
Sn 118	10938	10887	3358	62109	24523	14422
Ba 137	324644	5625092	446633	15983117	7235187	556296
La 139	115154	154678	23693	386371	346956	25999
Ce 140	154886	242188	35642	545193	404843	33535
Au 197	3	4	1	5	-1	-1
Hg 202	77	1402	193	3340	1683	224
Pb 206	41974	223826	52824	239400	173206	14319
Pb 207	40653	202005	19638	263333	151792	13777
Pb 208	44176	220550	20057	223498	167614	14912
Bi 209	140	232	60	422	539	45
Th 232	1242	1922	467	4584	2809	729
U 238	3363	2484	400	6845	4588	460

**Appendix 4: LA-ICP-MS intensity (cps) values of all Fe-Mn oxide coated samples;
ND = Not Determined.**

Site	S6B	S6B	S6A	S6A	S6A	S6A
Substrate	Pebble	Pebble	Streak	Streak	Streak	Pol. Peb.
Month	12	12	12	12	12	12
Al 27	8526305	10621412	704796	1531279	188496	686363
Si 29	8529717	9281167	972823	3867820	379993	2562453
Ca 43	1686820	1774224	ND	ND	ND	ND
Ti 47	2953289	3110520	122911	443215	40230	146979
V 51	320688	359917	10449	36616	4769	21868
Cr 53	242397	274411	7334	41855	8600	30884
Mn 55	1886714	1856627	14994718	46351630	1904291	19673970
Fe 57	212496586	192517867	7351058	24732615	1482451	15353867
Co 59	145933	197306	228711	608210	26132	393832
Ni 62	152437	274357	54175	125548	9883	75334
Cu 65	1030093	1688297	384170	392985	62456	390956
Zn 67	5115220	5472181	691918	1860376	122769	831582
As 75	56615	54941	3624	10145	427	5585
Se 82	4001	3320	46	183	-5	1245
Sr 86	212099	197518	29976	91365	7674	52991
Y 89	278638	248949	51296	118070	4956	71493
Ag 107	46593	93995	3047	235082	11990	46049
Cd 111	6448	6844	1949	11423	1309	3499
Sn 118	76536	75233	13474	9688	3334	32107
Ba 137	2027849	1827375	2824438	5493891	206459	3622058
La 139	805506	617261	100035	263941	12537	157292
Ce 140	2428907	2100167	197364	527980	24997	302926
Au 197	3	5	4	2	1	1
Hg 202	1528	1662	1092	4226	90	1566
Pb 206	1034607	2521553	37309	85428	7054	68932
Pb 207	944020	2228605	33078	82867	6504	58691
Pb 208	1001366	2338416	31930	84712	6095	65773
Bi 209	1569	1848	63	146	28	78
Th 232	13350	18012	504	1370	275	918
U 238	6964	8723	981	3873	287	981

**Appendix 4: LA-ICP-MS intensity (cps) values of all Fe-Mn oxide coated samples;
ND = Not Determined.**

Site	S6A	S6A	S6A	S6A	S6A	S6A
Substrate	Pol. Peb.	Cement	Cement	Cement	Pebble	Pebble
Month	12	12	12	12	12	12
Al 27	1222331	1887467	5201170	219507	5438207	6826770
Si 29	4899054	4196380	7426048	388317	4602260	6147823
Ca 43	ND	ND	ND	ND	ND	ND
Ti 47	513869	2227432	4903278	274450	4478205	6608119
V 51	35568	112577	208571	9096	139339	193828
Cr 53	56787	362149	717344	32235	68709	87034
Mn 55	51791235	6348306	2374151	438492	11563399	32336280
Fe 57	26758373	62007014	102460483	3419128	80402078	110106177
Co 59	843760	156684	365475	17016	334744	562015
Ni 62	214442	122132	169043	11599	84376	147364
Cu 65	562524	221756	368403	37077	222003	447200
Zn 67	2486477	2606514	4653340	238649	1246977	3975590
As 75	10322	4344	7516	290	11771	20524
Se 82	974	1086	1740	-395	844	2048
Sr 86	118789	153616	245624	13949	60689	117495
Y 89	154910	174720	225359	9537	104394	192546
Ag 107	72222	4082	10934	5382	10469	15028
Cd 111	11346	4750	10653	415	2431	9048
Sn 118	29744	9333	16531	2414	12422	15910
Ba 137	8661982	1901135	1831651	165857	2564885	7404674
La 139	323350	300989	334617	15372	169389	379388
Ce 140	575175	480857	538001	23191	532768	1057572
Au 197	8	1	7	-1	2	9
Hg 202	3691	2250	1753	151	736	1413
Pb 206	74894	139569	312728	35068	930814	776389
Pb 207	69721	120917	306335	27813	867634	733275
Pb 208	73490	126522	305776	32027	896487	775979
Bi 209	103	274	605	20	452	228
Th 232	1506	8291	17692	1001	10733	12428
U 238	2021	4365	8198	427	2642	4060

Appendix 4: LA-ICP-MS intensity (cps) values of all Fe-Mn oxide coated samples;
ND = Not Determined.

Site	S5	S5	S5	S5	S5	S5
Substrate	Streak	Streak	Streak	Pol. Peb.	Pol. Peb.	Cement
Month	12	12	12	12	12	12
Al 27	1693505	1353136	377511	387362	2773382	4768862
Si 29	3793672	1905052	236983	3766476	7725957	10540542
Ca 43	ND	ND	ND	ND	ND	ND
Ti 47	1362462	872787	49361	72419	1135764	5829361
V 51	95224	60621	2039	14182	100478	267324
Cr 53	63615	39904	1973	36234	90883	487825
Mn 55	6570824	5554920	384016	29430544	43208624	24095564
Fe 57	49819412	67161630	1257821	14301666	82716077	128488069
Co 59	200711	156563	9065	497676	1035224	722181
Ni 62	34291	30326	1357	62020	90892	367636
Cu 65	191504	178944	5068	278597	591336	597825
Zn 67	436447	337935	14175	905425	1806115	18693950
As 75	5687	6539	340	9714	17300	15169
Se 82	101	319	-536	488	1786	2695
Sr 86	39151	22791	2166	83045	368547	186317
Y 89	75478	51346	3024	54813	211174	287998
Ag 107	4273	9789	227	13377	69336	134429
Cd 111	933	586	73	4229	4419	22082
Sn 118	10486	41152	1141	8947	38153	38973
Ba 137	1475664	1145612	79596	5270017	6453056	3125340
La 139	126180	97197	4078	121036	405165	526702
Ce 140	276495	217564	9461	247328	794079	895637
Au 197	10	3	-2	3	9	4
Hg 202	616	638	38	1546	2954	7036
Pb 206	266316	282470	4681	49709	407193	443004
Pb 207	246354	238695	4544	37328	375000	414253
Pb 208	259627	236393	3944	38303	376119	426453
Bi 209	305	163	8	114	567	980
Th 232	3374	1619	201	726	15423	20665
U 238	2500	1806	270	940	4362	9747

**Appendix 4: LA-ICP-MS intensity (cps) values of all Fe-Mn oxide coated samples;
ND = Not Determined.**

Site	S5	S5	S5	S5	S4	S4
Substrate	Cement	Cement	Pebble	Pebble	Streak	Streak
Month	12	12	12	12	12	12
Al 27	925739	60335	2200559	4279421	1342574	1261224
Si 29	12498280	197286	1313487	3661501	3438049	1384756
Ca 43	ND	ND	ND	ND	ND	ND
Ti 47	1227585	41663	328316	2635902	543874	204071
V 51	54078	3130	131920	197537	48861	73351
Cr 53	56519	5041	200470	130975	53679	27900
Mn 55	4098842	393060	54659251	76671973	10586642	19797580
Fe 57	23916018	1273506	96138589	121478145	48846100	88639921
Co 59	200809	23417	1142926	1638344	716154	394080
Ni 62	84119	20220	160386	271044	51957	47550
Cu 65	374370	12564	931372	2008346	433063	202393
Zn 67	2167619	27024	5497508	5689449	589283	847630
As 75	4806	245	72681	67751	4809	10828
Se 82	806	109	2869	2189	187	-109
Sr 86	268916	6476	86162	126039	59994	31544
Y 89	44806	3901	214226	247235	98021	65026
Ag 107	11575	2330	100088	86159	41543	19965
Cd 111	2822	95	19241	17544	1537	2249
Sn 118	120090	1458	24745	181509	38072	87829
Ba 137	984075	87296	12686204	18239345	2084674	3282116
La 139	123952	5956	451086	558243	201831	133854
Ce 140	294344	12988	1402493	1594308	428592	322457
Au 197	3	1	6	3	2	3
Hg 202	1112	135	2231	2614	491	770
Pb 206	87107	23699	1368272	1651088	151618	251896
Pb 207	84256	20719	1293071	1534020	143054	225248
Pb 208	84987	21925	1281558	1621991	144744	245928
Bi 209	581	7	143	216	154	70
Th 232	3730	117	1318	5775	2299	1150
U 238	2131	103	2070	2786	1863	1046

Appendix 4: LA-ICP-MS intensity (cps) values of all Fe-Mn oxide coated samples;
ND = Not Determined.

Site	S4	S4	S4	S4	S4	S4
Substrate	Streak	Pol. Peb.	Pol. Peb.	Cement	Cement	Cement
Month	12	12	12	12	12	12
Al 27	60865	622222	1641536	3760740	4571121	54729
Si 29	103464	1702728	6521257	7587889	5732418	393791
Ca 43	ND	ND	ND	ND	ND	ND
Ti 47	10822	178628	284672	2333955	3550107	139563
V 51	2966	26400	81869	237747	328641	2918
Cr 53	964	16862	60223	113834	209130	4220
Mn 55	394641	41733680	72612060	25670498	56714863	713082
Fe 57	2053730	24304893	109966779	94568490	102049175	1792166
Co 59	8103	475989	1202430	586853	941506	27445
Ni 62	924	99484	91917	219950	430415	11818
Cu 65	4056	403278	625114	430614	857549	16042
Zn 67	16173	1875196	2297717	4784028	18010128	50783
As 75	166	16100	26425	12231	25389	181
Se 82	47	180	1434	1599	1808	-60
Sr 86	193	64893	121381	136367	331616	6444
Y 89	1273	69604	142103	182023	273663	5227
Ag 107	251	10822	34201	32305	70593	1799
Cd 111	63	7571	7824	7266	34087	92
Sn 118	2898	10193	23747	36379	21532	1047
Ba 137	79139	7892212	11466026	2887315	8081009	92882
La 139	3401	157591	338289	258825	449565	7858
Ce 140	10332	313940	791703	566927	780736	12430
Au 197	1	6	8	1	6	1
Hg 202	156	3155	1696	5978	7537	12
Pb 206	6543	104343	313576	353840	283413	3027
Pb 207	4628	96163	288087	319689	236952	3173
Pb 208	4387	107001	296478	342173	249261	2194
Bi 209	-2	86	142	518	745	8
Th 232	38	790	1681	7665	20310	267
U 238	47	637	1555	7538	9253	168

**Appendix 4: LA-ICP-MS intensity (cps) values of all Fe-Mn oxide coated samples;
ND = Not Determined.**

Site	S4	S4	S3	S3	S3	S3
Substrate	Pebble	Pebble	Streak	Streak	Streak	Pol. Peb.
Month	12	12	12	12	12	12
Al 27	3061398	1421660	944342	1097709	162455	1143796
Si 29	1516908	515697	673442	946394	210910	3490099
Ca 43	ND	ND	ND	ND	ND	ND
Ti 47	1280822	204098	149000	262976	20939	170090
V 51	116749	54824	40420	51681	4231	60544
Cr 53	47177	21867	22649	37515	3087	61846
Mn 55	39234582	30252486	8323044	7138810	651253	30374094
Fe 57	90291287	52441892	56159975	63199729	4614733	88787896
Co 59	621089	338966	165632	120894	11588	543824
Ni 62	139475	113886	21625	10025	2036	59230
Cu 65	863595	406247	363247	112520	28619	475967
Zn 67	3178751	2625910	274739	273060	42020	834449
As 75	56459	24619	5529	5192	422	14011
Se 82	1344	1064	-347	-452	-323	842
Sr 86	65978	45922	11837	12378	-64	47901
Y 89	173709	89388	33018	38710	2238	80961
Ag 107	20058	15939	5845	5903	6075	18353
Cd 111	6049	9312	7618	838	81	3387
Sn 118	10629	7662	7075	8123	1159	16823
Ba 137	9054894	5200644	1679928	1306153	120755	4767839
La 139	353869	204275	67207	67797	4429	175305
Ce 140	853768	555977	161193	156349	16015	422809
Au 197	3	3	6	2	2	2
Hg 202	3470	2095	410	567	66	1560
Pb 206	1095640	893699	173130	231943	19919	259319
Pb 207	1044446	816462	161318	218941	15914	242322
Pb 208	1035974	886345	173805	223283	14374	254004
Bi 209	267	130	38	84	7	87
Th 232	3656	934	797	1363	78	688
U 238	1614	801	1276	1423	160	729

**Appendix 4: LA-ICP-MS intensity (cps) values of all Fe-Mn oxide coated samples;
ND = Not Determined.**

Site	S3	S3	S3	S3	S3	S3
Substrate	Pol. Peb.	Cement	Cement	Cement	Pebble	Pebble
Month	12	12	12	12	12	12
Al 27	726184	1729074	976334	353965	2155127	2175796
Si 29	5320995	2936919	1456031	588446	2679331	5500849
Ca 43	ND	ND	ND	ND	ND	ND
Ti 47	130941	1787429	502501	404593	1284814	173939
V 51	46890	124317	56690	23860	127802	41966
Cr 53	35540	121136	64158	57067	164396	30683
Mn 55	11155546	16571095	8261608	2534073	22421979	33256397
Fe 57	44140348	54929914	31743352	5736014	90388843	42694656
Co 59	306050	271732	190153	122300	534271	496697
Ni 62	35664	134526	75530	43632	95476	121940
Cu 65	176674	180836	146089	134927	992053	325415
Zn 67	474799	5223664	527283	646552	1322883	2613131
As 75	9397	9356	4975	788	43057	15906
Se 82	953	371	-192	-72	1172	681
Sr 86	19129	120634	47855	32068	64106	49308
Y 89	33027	70588	34331	10818	103574	84756
Ag 107	21546	13464	24244	10871	81063	14072
Cd 111	560	5262	930	1146	3209	9919
Sn 118	18034	6265	5657	6967	34973	22082
Ba 137	1515914	1938541	1124751	746119	4905789	8619323
La 139	60573	127210	66013	18823	231375	221727
Ce 140	172237	311245	151413	27473	573653	451864
Au 197	-0	-1	0	0	5	29
Hg 202	899	6959	1994	611	5032	1060
Pb 206	138270	175925	107183	10236	392858	423889
Pb 207	129090	149529	97731	9822	368592	366455
Pb 208	141476	171426	95635	8430	383554	404264
Bi 209	46	153	70	19	269	960
Th 232	553	4411	2073	1264	3331	11377
U 238	351	4080	1543	743	1839	2466

**Appendix 4: LA-ICP-MS intensity (cps) values of all Fe-Mn oxide coated samples;
ND = Not Determined.**

Site	S2	S2	S2	S2	S2	S2
Substrate	Streak	Streak	Streak	Pol. Peb.	Pol. Peb.	Cement
Month	12	12	12	12	12	12
Al 27	2475010	1776625	382677	569320	2238345	4591893
Si 29	3500738	2447395	379151	2969750	3828968	3532162
Ca 43	ND	ND	ND	ND	ND	ND
Ti 47	1130545	1015125	89859	469869	551825	2755236
V 51	104838	71045	8970	23317	83602	337052
Cr 53	247723	48343	7812	37796	97618	209087
Mn 55	22045462	2660104	483149	12128588	13876329	18309152
Fe 57	70486264	51837698	4706799	12116194	70352189	73940362
Co 59	304137	153499	17135	283146	341958	312543
Ni 62	136190	17992	4939	38663	57570	180760
Cu 65	585771	82587	39957	492097	357870	231501
Zn 67	1077438	213963	33576	367455	482433	10720041
As 75	9700	3503	431	4726	6851	16143
Se 82	375	592	-463	131	640	1393
Sr 86	49819	43884	5353	34283	59370	190218
Y 89	84796	58921	4431	30498	71487	192737
Ag 107	16982	5038	1366	19106	12149	10798
Cd 111	4029	371	62	961	1588	15056
Sn 118	44555	12116	95220	9130	12266	11165
Ba 137	1723807	430906	63324	2277322	1831233	2506527
La 139	148416	103731	7280	67267	141641	324551
Ce 140	379592	211009	17754	198915	305226	513698
Au 197	1	4	-1	1	7	3
Hg 202	1161	233	-26	434	575	5640
Pb 206	454745	293138	15572	40347	122355	229940
Pb 207	422655	269604	15400	39750	132457	321785
Pb 208	413267	269927	13666	40238	127785	225639
Bi 209	361	333	20	60	331	1244
Th 232	3796	2831	329	739	4830	8992
U 238	3481	2272	237	402	1173	10000

**Appendix 4: LA-ICP-MS intensity (cps) values of all Fe-Mn oxide coated samples;
ND = Not Determined.**

Site	S2	S2	S2	S2	S1	S1
Substrate	Cement	Cement	Pebble	Pebble	Streak	Streak
Month	12	12	12	12	12	12
Al 27	9112939	226466	2956961	3101754	854870	1721116
Si 29	6668135	808529	2672215	2515584	895190	1711600
Ca 43	ND	ND	ND	ND	ND	ND
Ti 47	6520803	190185	858230	774579	300617	235308
V 51	511407	22157	78502	92541	22189	50972
Cr 53	590213	20807	60770	77623	26160	62333
Mn 55	31285556	1191390	63701791	34070220	17788227	28341083
Fe 57	143912854	5535157	67031162	61410636	25777352	56689386
Co 59	297681	29542	1214668	982615	348671	686417
Ni 62	360425	32008	257795	174370	45877	55268
Cu 65	717665	43497	1615137	925537	118384	286913
Zn 67	16411844	298830	5893177	2509909	473922	890889
As 75	23128	729	25811	26251	4378	9088
Se 82	2644	499	2562	1757	-4	575
Sr 86	316323	15937	109883	82902	16949	32545
Y 89	301677	5373	206722	126351	41193	65537
Ag 107	135511	10509	127188	62810	5660	22585
Cd 111	18378	1621	20315	6361	1293	1891
Sn 118	68359	66764	39351	162355	5805	33929
Ba 137	3163292	93700	10297652	5989971	1661606	4060497
La 139	445561	9054	484270	235362	83099	120229
Ce 140	872828	17979	1820146	1359862	223221	375320
Au 197	4	-1	4	2	5	7
Hg 202	4099	74	2996	1426	903	1774
Pb 206	673135	14259	637398	1391167	72488	164359
Pb 207	609463	12770	598927	1232205	63726	148780
Pb 208	603620	11269	623493	1279948	66931	155738
Bi 209	1786	27	337	228	57	106
Th 232	23284	427	3345	3414	822	1511
U 238	20224	437	2619	1462	1418	2444

**Appendix 4: LA-ICP-MS intensity (cps) values of all Fe-Mn oxide coated samples;
ND = Not Determined.**

Site	S1	S1	S1	S1	S1	S1
Substrate	Streak	Pol. Peb.	Pol. Peb.	Cement	Cement	Cement
Month	12	12	12	12	12	12
Al 27	419281	751207	846296	1427792	3318325	114367
Si 29	290535	3137860	1151850	2498938	6930455	422935
Ca 43	ND	ND	ND	ND	ND	ND
Ti 47	27615	967695	136149	2314225	2323000	54242
V 51	2327	34499	45065	67545	224308	7591
Cr 53	2846	29618	32245	251855	141560	8161
Mn 55	469480	8556166	18118511	4692016	14491626	68558
Fe 57	1619529	34764370	51585597	20298278	71716107	4128840
Co 59	14233	437984	647632	601787	476570	27652
Ni 62	8118	19947	33994	153830	259961	7632
Cu 65	9100	96686	250881	881332	455755	40536
Zn 67	32406	252497	445561	1748263	7901161	23151
As 75	146	3710	7004	2444	9627	507
Se 82	-427	1092	893	383	1854	-391
Sr 86	2262	20843	31112	138702	131066	6227
Y 89	1888	35870	46305	38110	123928	2666
Ag 107	706	3833	9320	63135	39332	6592
Cd 111	64	452	868	1890	8703	54
Sn 118	1076	8367	7071	43581	91436	2993
Ba 137	84826	1171847	2448126	1027229	2107554	21082
La 139	3395	70304	100484	42141	208521	4948
Ce 140	8003	199157	268183	80713	422368	11122
Au 197	2	1	7	0	3	2
Hg 202	-33	504	983	1844	4352	39
Pb 206	4357	106880	143071	14278	285452	13678
Pb 207	3405	99729	124446	11331	254871	14882
Pb 208	4746	99216	134217	13662	287407	15226
Bi 209	11	56	47	223	299	15
Th 232	137	808	589	8552	7373	196
U 238	259	590	736	3418	7991	230

Appendix 4: LA-ICP-MS intensity (cps) values of all Fe-Mn oxide coated samples;
ND = Not Determined.

Site	S1	S1	S6B	S6B	S6B	S6B
Substrate	Pebble	Pebble	Streak	Streak	Streak	Cement
Month	12	12	9	9	9	9
Al 27	2045364	2330120	2327602	2469920	56226	1505666
Si 29	2563255	4837775	8745947	5843814	74690	7945347
Ca 43	ND	ND	ND	ND	ND	ND
Ti 47	1174316	2086842	1396117	1628671	22006	688904
V 51	78139	122925	142622	182296	2457	459725
Cr 53	83021	354714	138604	315686	2669	286576
Mn 55	10767259	4642657	27520724	18498654	23791	85098835
Fe 57	49881732	70642301	155011465	168991186	2347443	241444701
Co 59	252081	822766	244088	292578	3119	710794
Ni 62	47329	296176	141148	152964	1074	534273
Cu 65	263926	1069011	855655	847262	10432	1615865
Zn 67	435267	422775	7343744	6928035	26343	24260457
As 75	5455	7340	70486	58127	403	128294
Se 82	289	1611	5238	3977	-138	6911
Sr 86	65074	77102	210436	270315	3741	534959
Y 89	54389	59978	213470	215858	2965	230219
Ag 107	11164	153732	12431	29488	1449	43154
Cd 111	1389	898	20244	18863	55	59182
Sn 118	19893	51665	23820	28649	1419	68532
Ba 137	1678745	1167028	5334086	4784051	23567	18462007
La 139	97263	94915	284480	304928	3839	310884
Ce 140	235234	167890	399398	515250	6158	474730
Au 197	5	1	1	-1	3	9
Hg 202	557	407	770	931	90	5254
Pb 206	286764	178112	375087	759061	5644	356420
Pb 207	260919	165429	306259	600907	5376	315807
Pb 208	266997	174163	298576	915703	5067	329215
Bi 209	177	178	444	533	10	688
Th 232	3609	3952	4421	4758	81	2931
U 238	1659	1958	6794	5049	50	12554

**Appendix 4: LA-ICP-MS intensity (cps) values of all Fe-Mn oxide coated samples;
ND = Not Determined.**

Site	S6B	S6B	S6B	S6B	S6B	S6B
Substrate	Cement	Cement	Pebble	Pebble	Streak	Streak
Month	9	9	9	9	6	6
Al 27	1820552	210565	5656907	9343993	672349	1244615
Si 29	4987410	719236	4298835	6151526	826138	2082764
Ca 43	ND	ND	ND	ND	ND	ND
Ti 47	1407257	141422	1758805	1800405	84588	151944
V 51	229804	26756	165487	203693	33711	67459
Cr 53	211237	21388	157093	112783	52578	118466
Mn 55	49513986	2022486	1395936	2234441	100184	308162
Fe 57	269095310	12802970	112344292	122448604	270689177	972911147
Co 59	647518	109561	195221	376461	196353	46237
Ni 62	210979	67928	105541	140543	28259	36179
Cu 65	3724507	324932	668856	935245	253542	363793
Zn 67	15099366	501895	1957078	2779792	822122	2840238
As 75	107552	3853	32617	29905	15282	46418
Se 82	4154	340	1704	1586	280	1319
Sr 86	519832	37798	99312	93595	65234	224652
Y 89	299458	14967	107167	104659	94704	251121
Ag 107	212899	28645	51512	79709	15457	22477
Cd 111	31888	1023	2441	6528	1900	7220
Sn 118	48848	11427	28285	214630	4310	20427
Ba 137	15501131	616547	868330	933600	653691	1778604
La 139	390069	22103	259487	157793	141698	368696
Ce 140	554321	34938	208651	209218	327042	437226
Au 197	1	3	4	4	2	3
Hg 202	2937	166	1431	1191	365	1112
Pb 206	479270	25816	214273	434127	31777	74857
Pb 207	268710	23258	205496	417694	27212	71129
Pb 208	270229	26920	217330	406496	32052	71966
Bi 209	286	245	298	1886	77	109
Th 232	5148	477	3466	4991	523	1175
U 238	5625	625	2417	3663	1555	2131

**Appendix 4: LA-ICP-MS intensity (cps) values of all Fe-Mn oxide coated samples;
ND = Not Determined.**

Site	S6B	S6B	S6B	S6B	S6B	S6B
Substrate	Streak	Pol. Peb.	Pol. Peb.	Cement	Cement	Cement
Month	6	6	6	6	6	6
Al 27	145937	666888	592493	2311548	3835584	563446
Si 29	313834	2600736	3158538	4796174	6450732	954590
Ca 43	ND	ND	ND	ND	ND	ND
Ti 47	28278	193900	406720	1478848	2169262	324531
V 51	10383	53177	38476	235561	362530	28583
Cr 53	16059	99783	81691	240224	384422	120708
Mn 55	148295	173455	118496	1017278	1195301	466598
Fe 57	155421130	457642975	231576958	982422367	1095319658	144028470
Co 59	14823	126418	43980	193035	525289	116743
Ni 62	3541	45062	18396	110094	138692	62981
Cu 65	94873	344997	212650	620186	1811877	155876
Zn 67	450778	1335632	517321	5739745	6282712	945301
As 75	6481	23779	12405	44575	54902	6015
Se 82	34	1251	318	1511	3038	606
Sr 86	37194	125966	73873	746408	897270	164479
Y 89	33341	177470	102090	328161	342769	42256
Ag 107	7181	90259	22463	89070	90515	15323
Cd 111	1328	3610	1116	15132	16596	1894
Sn 118	6223	21904	10324	27455	51858	8642
Ba 137	300962	853414	376883	3556745	4088057	676133
La 139	47749	270144	158034	483447	509650	64597
Ce 140	66594	301160	186300	580120	661892	83317
Au 197	5	12	5	-1	4	1
Hg 202	-13	650	434	1893	1680	151
Pb 206	10593	54516	31613	98915	195938	27640
Pb 207	9222	49193	30205	112575	314233	31496
Pb 208	10400	53318	28532	113934	175786	31087
Bi 209	19	570	86	228	525	84
Th 232	140	718	870	4652	8169	1384
U 238	320	717	453	4080	6117	739

**Appendix 4: LA-ICP-MS intensity (cps) values of all Fe-Mn oxide coated samples;
ND = Not Determined.**

Site	S6B	S6B	S6B	S6B	S6B	S6B
Substrate	Pebble	Pebble	Streak	Streak	Streak	Pol. Peb.
Month	6	6	3	3	3	3
Al 27	1457701	4542501	915999	1572947	599838	1382933
Si 29	2167141	6147105	1075048	1852136	628546	5651426
Ca 43	ND	ND	ND	ND	ND	ND
Ti 47	1389902	3120629	195958	453619	150126	1254832
V 51	60580	163675	40410	86586	18891	137005
Cr 53	66468	158796	97936	141911	21352	247964
Mn 55	3215667	22782198	41734	106279	104526	156923
Fe 57	237165764	660514633	179955850	353441857	131592610	409511015
Co 59	73578	338518	10264	45436	11534	273484
Ni 62	41270	211202	8037	18571	14328	187105
Cu 65	161979	1078461	140633	394991	76791	1266336
Zn 67	1309246	5495724	430956	727734	259941	977245
As 75	10586	41547	8454	15081	3959	18217
Se 82	1056	2693	47	1704	-305	1994
Sr 86	100345	265922	43186	86116	31109	122867
Y 89	70851	177510	73304	153459	41948	127349
Ag 107	13230	37898	1577	2864	22233	71503
Cd 111	2005	27949	957	1916	804	2061
Sn 118	8855	43300	6038	16170	6179	134282
Ba 137	1043851	4847746	295930	603452	229183	743107
La 139	88997	398515	117146	298755	83485	224990
Ce 140	207683	763662	151301	385075	99585	325590
Au 197	17	1	-3	3	1	2
Hg 202	549	1095	79	81	13	448
Pb 206	400698	2045220	75548	206496	33054	196125
Pb 207	336383	1703655	64617	214099	27209	162679
Pb 208	362584	1722370	94768	191012	29812	182545
Bi 209	270	581	67	147	53	266
Th 232	2589	7071	816	1554	449	1555
U 238	1480	5454	923	5951	390	1680

**Appendix 4: LA-ICP-MS intensity (cps) values of all Fe-Mn oxide coated samples;
ND = Not Determined.**

Site	S6B	S6B	S6B	S6B	S6B	S6B
Substrate	Pol. Peb.	Cement	Cement	Cement	Pebble	Pebble
Month	3	3	3	3	3	3
Al 27	852634	3980510	3343712	433883	3755890	3740609
Si 29	3229924	5895931	6818365	656096	6777004	4895780
Ca 43	ND	ND	ND	ND	ND	ND
Ti 47	402196	3038710	2115594	307062	2428600	3449224
V 51	56099	318992	409343	36132	331800	218992
Cr 53	121990	1121232	697581	70084	474690	247471
Mn 55	107602	2235852	1184155	97051	540301	945412
Fe 57	313223096	895800200	1295091596	128774937	1203744759	697030807
Co 59	44017	142583	723901	31945	197853	177018
Ni 62	30070	221471	316729	19985	107151	151032
Cu 65	465791	681944	968434	127933	1012426	641328
Zn 67	480025	7761374	10645527	477465	4113572	1943970
As 75	11186	38349	51834	4168	63532	34420
Se 82	1194	3015	3620	930	5763	2171
Sr 86	83690	967588	853905	74694	298146	191063
Y 89	116294	291691	508056	46366	432409	272565
Ag 107	23992	41571	198449	13769	80059	57051
Cd 111	821	18989	21020	1533	9752	4861
Sn 118	25740	64397	79836	10321	181113	72109
Ba 137	535801	3716521	3752753	379273	2250389	1520839
La 139	187022	471036	887397	86555	721467	468794
Ce 140	245676	628236	1082568	111122	949278	586957
Au 197	1	1	9	0	5	3
Hg 202	429	812	1115	78	700	520
Pb 206	130520	549201	515026	53379	1166174	2049024
Pb 207	120007	515802	439046	37212	1058076	1866794
Pb 208	127250	386286	470373	44124	1153330	2115011
Bi 209	198	878	2552	128	707	635
Th 232	1278	10385	5913	816	5771	6579
U 238	982	5050	4255	496	4408	3241

**Appendix 4: LA-ICP-MS intensity (cps) values of all Fe-Mn oxide coated samples;
ND = Not Determined.**

Site	S6A	S6A	S6A	S6A	S6A	S6A
Substrate	Streak	Streak	Streak	Pol. Peb.	Pol. Peb.	Cement
Month	9	9	9	9	9	9
Al 27	835060	1039987	82920	518187	494617	954288
Si 29	1808245	1947524	112545	2982080	3993058	2051206
Ca 43	ND	ND	ND	ND	ND	ND
Ti 47	198910	344047	10976	131829	100863	1182888
V 51	20081	30532	1286	16393	11984	44272
Cr 53	14080	25702	5354	14594	9570	110645
Mn 55	30923887	13046894	359890	15472531	19217269	2650012
Fe 57	14762024	22652326	638460	12226975	9143018	18811570
Co 59	481725	278635	6402	218181	267718	64150
Ni 62	104755	40200	9628	42944	44601	45016
Cu 65	272345	193849	50130	142621	205189	125454
Zn 67	1949569	613294	35570	893792	713230	975082
As 75	6944	5253	161	4269	3628	1985
Se 82	-1149	-141	-615	693	276	555
Sr 86	108981	44951	782	63277	39618	84002
Y 89	57583	43459	1125	29895	38276	54353
Ag 107	15684	11671	361	37934	61604	51192
Cd 111	7503	1115	42	1873	1298	1148
Sn 118	7205	12428	21374	260699	1299376	29573
Ba 137	4220810	2793386	65420	3460669	3215605	742760
La 139	132036	79189	2311	66226	83575	90932
Ce 140	284220	179894	5147	150795	179580	144864
Au 197	3	3	1	1	0	1
Hg 202	2059	781	-1	556	698	714
Pb 206	58032	109221	23986	59934	34235	44981
Pb 207	57114	99600	22884	56373	32447	43015
Pb 208	56028	100321	22176	54632	33360	42440
Bi 209	104	97	6	67	32	137
Th 232	694	2824	53	622	367	4006
U 238	1224	1187	74	593	487	2000

Appendix 4: LA-ICP-MS intensity (cps) values of all Fe-Mn oxide coated samples;
ND = Not Determined.

Site	S6A	S6A	S6A	S6A	S6A	S6A
Substrate	Cement	Cement	Pebble	Pebble	Streak	Streak
Month	9	9	9	9	6	6
Al 27	3284305	95092	2709366	3301402	319784	1765954
Si 29	11649764	422952	2258387	4007202	543831	1383532
Ca 43	ND	ND	ND	ND	ND	ND
Ti 47	3797672	47453	1957850	1720182	65395	316182
V 51	149129	5185	74133	59084	5824	18169
Cr 53	420731	6553	30508	31589	3799	34378
Mn 55	6115304	142713	17863432	5361608	3331346	6363673
Fe 57	70870426	1793642	67852838	55521797	5746237	5994450
Co 59	129959	11078	409656	172184	44690	67695
Ni 62	166655	7647	65400	38376	18943	13663
Cu 65	456628	56939	307096	138161	32421	104912
Zn 67	3302938	108888	2483261	627494	156921	289178
As 75	7515	251	15138	5355	1473	1806
Se 82	1879	297	1782	482	55	136
Sr 86	173846	5172	100715	32605	13967	22018
Y 89	164883	3788	102947	72720	11255	16945
Ag 107	36966	6545	17279	7681	1733	7039
Cd 111	4201	142	5849	1501	295	453
Sn 118	54421	7257	21928	11557	914	4393
Ba 137	1693665	37208	3217423	872623	949953	1369701
La 139	219360	5414	170646	77624	18639	29107
Ce 140	402754	11221	567887	447491	52363	63236
Au 197	3	-0	-1	3	1	8
Hg 202	1495	-78	769	157	276	289
Pb 206	265199	5531	3235769	1525838	15458	21641
Pb 207	250152	5667	2894025	1422869	13517	19755
Pb 208	294406	5248	3030756	1513465	14084	20536
Bi 209	524	4	722	420	18	283
Th 232	12817	102	5264	10359	272	1087
U 238	5935	182	2089	3423	460	2086

**Appendix 4: LA-ICP-MS intensity (cps) values of all Fe-Mn oxide coated samples;
ND = Not Determined.**

Site	S6A	S6A	S6A	S6A	S6A	S6A
Substrate	Streak	Pol. Peb.	Pol. Peb.	Cement	Cement	Cement
Month	6	6	6	6	6	6
Al 27	222487	120990	864980	1380667	1686571	44921
Si 29	233987	4086992	3932002	1901091	5871797	174208
Ca 43	ND	ND	ND	ND	ND	ND
Ti 47	23997	157575	182837	1512766	2205453	45652
V 51	1511	4892	20677	75733	104330	2820
Cr 53	2772	3650	27990	121255	167167	3225
Mn 55	382308	5684815	40385814	10272039	12780812	373865
Fe 57	345412	3565456	16341893	31268433	28956283	967975
Co 59	6145	34018	274238	203525	327540	21574
Ni 62	3238	21051	92244	118350	227150	20998
Cu 65	2068	52845	249977	526515	654725	137943
Zn 67	18055	306600	1391498	947566	2698369	83341
As 75	114	1016	7001	3305	5195	122
Se 82	291	543	806	173	111	192
Sr 86	1648	52624	257740	127655	253452	6041
Y 89	1482	9110	59466	61198	60249	2602
Ag 107	140	3825	18394	83288	101363	11290
Cd 111	64	976	3187	1204	5670	179
Sn 118	667	6772	66280	147577	63044	1576
Ba 137	67167	1092173	8392123	2271532	3719986	74458
La 139	2058	20894	143414	81209	77367	2236
Ce 140	5375	37798	266022	115030	132955	4201
Au 197	-2	3	4	4	2	2
Hg 202	68	416	2340	1584	1412	64
Pb 206	1297	12228	61626	85335	51077	4001
Pb 207	1409	11455	58797	80246	65830	3558
Pb 208	1373	13471	60543	81489	50018	3781
Bi 209	8	16	82	187	250	18
Th 232	144	862	693	3902	6779	268
U 238	153	200	832	4103	5032	190

**Appendix 4: LA-ICP-MS intensity (cps) values of all Fe-Mn oxide coated samples;
ND = Not Determined.**

Site	S6A	S6A	S6A	S6A	S6A	S6A
Substrate	Pebble	Pebble	Streak	Streak	Streak	Pol. Peb.
Month	6	6	3	3	3	3
Al 27	4312871	8982743	591960	299385	144512	167661
Si 29	3366447	9720707	826934	379330	81589	3574721
Ca 43	ND	ND	ND	ND	ND	ND
Ti 47	2776895	11704738	634309	228771	54171	148636
V 51	152655	230935	16531	7591	570	7042
Cr 53	64178	141154	38029	15938	3174	19814
Mn 55	23483892	8546836	352326	84835	4534	23035
Fe 57	101935526	111318914	19678013	6682032	247150	4117102
Co 59	826877	335427	7355	6976	907	62173
Ni 62	87325	125111	182756	339432	19601	13524
Cu 65	302041	274704	70517	44624	2314	77494
Zn 67	2690765	1999248	116026	97997	2806	39543
As 75	45048	14772	545	269	-20	1058
Se 82	1910	1536	-684	-797	-218	-66
Sr 86	88493	103759	15441	1577	367	3872
Y 89	144986	116746	18182	9644	615	1876
Ag 107	23926	15311	11087	4524	353	13526
Cd 111	3236	2407	107	95	35	38
Sn 118	13294	48177	3348	3271	78	6185
Ba 137	6018157	2755863	92237	18941	3409	36246
La 139	248212	173842	20933	9226	617	3373
Ce 140	610882	454834	31941	14697	907	5759
Au 197	6	2	-0	3	-2	1
Hg 202	968	160	218	127	22	44
Pb 206	420238	213431	32047	15575	652	44402
Pb 207	389859	198020	30262	13654	548	13628
Pb 208	400435	212340	34973	14502	635	8371
Bi 209	162	305	51	284	3	445
Th 232	5066	16416	801	468	94	1443
U 238	3034	4562	951	483	84	158

Appendix 4: LA-ICP-MS intensity (cps) values of all Fe-Mn oxide coated samples;
ND = Not Determined.

Site	S6A	S6A	S6A	S6A	S6A	S6A
Substrate	Pol. Peb.	Cement	Cement	Cement	Pebble	Pebble
Month	3	3	3	3	3	3
Al 27	788828	4440411	5603849	346955	8183996	5115249
Si 29	3634133	5701548	6604559	276551	2810642	3472613
Ca 43	ND	ND	ND	ND	ND	ND
Ti 47	318291	3789033	4342533	280290	834026	2230388
V 51	26868	239369	334597	11468	547273	219926
Cr 53	245876	444161	535222	29454	159136	87956
Mn 55	3487097	8866040	14477334	745213	73718261	11743430
Fe 57	18689918	106801031	135616932	3957703	431950927	164868922
Co 59	222509	135397	207216	11922	2860683	717315
Ni 62	84782	236755	303810	24563	514229	204779
Cu 65	762917	374092	366352	15969	1293863	461556
Zn 67	352284	26677232	35649556	1209840	12893776	3027707
As 75	1402	8655	14488	421	180426	42270
Se 82	142	1770	2382	-427	11036	2784
Sr 86	69034	319943	454914	27726	408783	100147
Y 89	32436	377443	495005	13107	725123	186805
Ag 107	55750	53384	23362	4237	68878	24482
Cd 111	1057	56037	77806	3037	24814	3774
Sn 118	32786	37668	30341	2747	33321	8300
Ba 137	715449	2286914	3124355	177354	16575928	2869607
La 139	58951	696078	998660	20578	1179564	254923
Ce 140	96293	927582	1406083	37349	3202053	690859
Au 197	1	3	3	2	6	4
Hg 202	1301	13228	10177	627	1644	487
Pb 206	59273	185210	261315	6888	1821659	693170
Pb 207	53177	172010	254157	4919	1664613	667769
Pb 208	54619	176888	276455	5383	1715218	663816
Bi 209	109	544	720	31	568	434
Th 232	1875	14394	18005	922	5394	4185
U 238	650	8015	10992	649	6292	2671

**Appendix 4: LA-ICP-MS intensity (cps) values of all Fe-Mn oxide coated samples;
ND = Not Determined.**

Site	S1	S1	S1	S1	S1	S1
Substrate	Streak	Streak	Streak	Pol. Peb.	Pol. Peb.	Cement
	9	9	9	9	9	9
Al 27	357907	550473	59439	780388	687556	2119966
Si 29	1073913	1185147	121646	2783935	6567039	5245149
Ca 43	ND	ND	ND	ND	ND	ND
Ti 47	40088	49107	5044	192488	365692	3064279
V 51	3591	5848	1803	19403	20218	69032
Cr 53	1778	8353	699	23500	23374	383419
Mn 55	7164663	4587148	597951	9624067	3870872	15235359
Fe 57	8731076	10893433	577338	22641306	20430610	37579181
Co 59	115612	102054	14345	208873	127555	273064
Ni 62	13354	28699	1626	41407	31655	205919
Cu 65	80836	141990	7474	209861	258694	451995
Zn 67	161429	152439	19380	295759	180388	2638178
As 75	2002	1519	114	3894	2861	4624
Se 82	-616	-863	-993	297	611	812
Sr 86	11400	9058	-4	30397	18159	156374
Y 89	12112	18682	1448	23795	18953	88371
Ag 107	1205	2203	370	25966	23709	13707
Cd 111	558	769	248	1555	828	4657
Sn 118	2542	8693	930	12523	15118	23251
Ba 137	1244342	443551	75843	1018913	456511	2368404
La 139	17582	23979	2663	38814	21613	101127
Ce 140	40786	66817	8387	95780	48951	198193
Au 197	1	3	1	4	15	0
Hg 202	501	396	51	596	440	3730
Pb 206	18837	35899	1502	47339	68083	48545
Pb 207	16575	33336	1201	42643	62613	44306
Pb 208	17771	34228	1246	44277	72539	44283
Bi 209	9	43	4	109	67	290
Th 232	232	348	37	934	765	11296
U 238	417	756	127	1030	1359	5010

**Appendix 4: LA-ICP-MS intensity (cps) values of all Fe-Mn oxide coated samples;
ND = Not Determined.**

Site	S1	S1	S1	S1	S1	S1
Substrate	Cement	Cement	Pebble	Pebble	Streak	Streak
Month	9	9	9	9	6	6
Al 27	791897	34341	2715397	5936092	139155	334213
Si 29	2084902	257866	609431	2079928	1166762	2121393
Ca 43	ND	ND	ND	ND	ND	ND
Ti 47	456124	12645	245229	610681	44975	108317
V 51	15605	744	48680	80108	3792	6840
Cr 53	31165	673	7557	12887	8062	260039
Mn 55	10084728	310672	22691689	80268593	603520	5292134
Fe 57	13726532	663957	77304314	124597579	2262889	6304324
Co 59	224360	92149	658188	1488798	37136	60175
Ni 62	78752	3454	100428	429944	84396	109466
Cu 65	270745	31121	321871	895683	457247	384917
Zn 67	399111	23273	1902894	7516231	211428	596058
As 75	2853	156	21779	37921	1425	1781
Se 82	428	-293	754	3291	-252	-116
Sr 86	95708	4381	30650	180674	12829	28410
Y 89	35939	1281	117198	276234	7484	20207
Ag 107	5922	15812	3301	6399	5618	4581
Cd 111	1108	119	3782	28966	1690	2090
Sn 118	9632	15564	15321	36436	11357	10638
Ba 137	1354299	68612	2665170	10368465	98920	952961
La 139	55706	1655	133936	356106	12637	43702
Ce 140	101293	4338	546754	1380429	10376	60009
Au 197	5	-1	4	6	5	9
Hg 202	1288	64	4585	2415	139	1391
Pb 206	30095	1211	2187732	4942560	27566	47574
Pb 207	27008	1366	2141973	4727053	27906	46815
Pb 208	27875	1329	2237357	4924858	27489	44861
Bi 209	52	-0	163	1144	53	90
Th 232	1530	41	3991	5177	269	490
U 238	1240	114	1772	4777	668	1144

**Appendix 4: LA-ICP-MS intensity (cps) values of all Fe-Mn oxide coated samples;
ND = Not Determined.**

Site	S1	S1	S1	S1	S1	S1
Substrate	Streak	Pol. Peb.	Pol. Peb.	Cement	Cement	Cement
Month	6	6	6	6	6	6
Al 27	50980	238738	411347	1722981	1224580	136726
Si 29	121224	2290650	3042958	4808322	1897710	160383
Ca 43	ND	ND	ND	ND	ND	ND
Ti 47	19030	78580	111198	2899255	1791085	230137
V 51	611	7474	9646	47823	40672	4469
Cr 53	1407	7648	12600	154126	196295	30419
Mn 55	177439	2826433	14498009	2062885	2570200	111921
Fe 57	410734	6454340	9767742	25528699	18391158	1947874
Co 59	3036	66398	160324	357115	95390	4882
Ni 62	5656	46547	156814	184310	88529	15367
Cu 65	8164	252217	982697	235348	187704	115573
Zn 67	25943	324204	1386285	966795	638662	104430
As 75	68	1177	3034	2226	2271	73
Se 82	-332	-138	973	539	-89	226
Sr 86	989	19339	69923	154564	292729	7888
Y 89	1243	10879	36184	50696	38024	3421
Ag 107	125	12983	4576	24195	6067	5354
Cd 111	105	1735	5922	1620	1197	120
Sn 118	410	11984	15485	16559	7979	542
Ba 137	39539	374155	2622222	639161	712074	46370
La 139	2183	21100	89570	62781	87486	4633
Ce 140	3450	39635	104497	110257	154663	9648
Au 197	-0	5	12	7	7	2
Hg 202	100	446	3415	1169	964	31
Pb 206	1454	83864	82855	43331	58696	2850
Pb 207	1390	486819	78497	46359	55901	3264
Pb 208	1311	103011	92039	44103	59042	2981
Bi 209	8	90	103	311	268	38
Th 232	94	247	576	10725	7136	1012
U 238	57	490	668	3994	2604	247

Appendix 4: LA-ICP-MS intensity (cps) values of all Fe-Mn oxide coated samples;
ND = Not Determined.

Site	S1	S1	S1	S1	S1	S1
Substrate	Pebble	Pebble	Streak	Streak	Streak	Pol. Peb.
Month	6	6	3	3	3	3
Al 27	2383575	4176924	202444	874437	178951	709662
Si 29	3424064	7112216	220571	356958	79769	10871400
Ca 43	ND	ND	ND	ND	ND	ND
Ti 47	2768569	4341226	82488	192432	15599	342634
V 51	49564	112757	5022	9826	1019	34807
Cr 53	141224	26794	5532	13644	1851	41583
Mn 55	29040054	21682360	96735	2001603	97484	93938
Fe 57	62255172	78689725	5524320	22675854	1074438	6499165
Co 59	540144	725780	23187	41944	2326	30398
Ni 62	246001	163907	15454	26439	-10403	118288
Cu 65	642294	409655	159410	111490	7058	259645
Zn 67	3296837	2571232	119465	137393	6138	89601
As 75	16990	17390	609	1136	83	5395
Se 82	2267	1733	-283	592	-806	-226
Sr 86	171201	650755	5705	23616	980	100310
Y 89	116263	143633	8430	28703	1972	6513
Ag 107	7272	3280	6698	2594	149	9661
Cd 111	14479	7123	1199	500	45	723
Sn 118	16836	30436	7311	23139	5328	8304
Ba 137	4549248	4031765	24179	119072	5357	550672
La 139	183594	143480	7990	23552	1447	15046
Ce 140	562182	672144	13172	54351	3079	23107
Au 197	11	12	6	9	1	4
Hg 202	2248	444	183	849	-67	469
Pb 206	1019662	2093920	27278	49434	2803	48784
Pb 207	949484	1944996	24164	52378	2451	50323
Pb 208	972773	2066640	24001	47741	2244	49514
Bi 209	445	202	45	73	7	214
Th 232	2907	5857	404	840	79	1063
U 238	3434	3369	466	774	107	507

**Appendix 4: LA-ICP-MS intensity (cps) values of all Fe-Mn oxide coated samples;
ND = Not Determined.**

Site	S1	S1	S1	S1	S1	S1
Substrate	Pol. Peb.	Cement	Cement	Cement	Pebble	Pebble
Month	3	3	3	3	3	3
Al 27	394388	2252437	1815947	88166	5243388	3504408
Si 29	5576128	3422774	2455072	126049	1754642	922729
Ca 43	ND	ND	ND	ND	ND	ND
Ti 47	296550	3105226	2592460	96118	970727	695391
V 51	17396	73625	43050	2321	67690	35913
Cr 53	75488	300715	215453	12007	10201	10561
Mn 55	106861	1931851	735397	13317	72045219	30700334
Fe 57	6740575	30658979	38229831	1247795	93797893	62217166
Co 59	30285	74138	144641	1679	981678	490850
Ni 62	40204	114588	126997	8428	500127	186996
Cu 65	214507	602607	150397	51976	2039513	362721
Zn 67	115439	2212845	2956315	47285	8951140	2723438
As 75	2792	2960	2121	18	23658	15034
Se 82	-3	442	499	-436	2820	1808
Sr 86	72621	231380	133143	4830	129333	61236
Y 89	7374	69472	80142	1563	207599	119975
Ag 107	8915	12792	50347	2132	10166	1595
Cd 111	506	3549	3376	128	43702	13146
Sn 118	30004	7283	9174	1930	46503	20543
Ba 137	396924	1785718	702123	26068	5632980	2209618
La 139	18069	88390	91546	1983	288773	133661
Ce 140	23351	164692	184253	3893	1886414	1108299
Au 197	8	1	4	1	-0	34
Hg 202	365	4103	5341	39	2789	1868
Pb 206	57305	40933	57697	1950	6155499	3236137
Pb 207	55010	37394	58626	3784	5527328	3231357
Pb 208	55573	56743	54857	12968	5708698	3229241
Bi 209	212	345	357	10	1489	708
Th 232	502	11087	10239	320	4983	3415
U 238	316	6829	4170	239	2330	2472

Appendix 5:**Median values of concentrations determined by LA-ICP-MS for Fe-Mn oxide coating samples; ND = Not Detected, () indicates concentrations below detection limit.**

Site	TCS3	TCS4	TCS5	TCS6	TCS7	TCS8	TCS10	TCS11
Substrate	Pebble	Pebble	Pebble	Pebble	Pebble	Pebble	Pebble	Pebble
Months								
CaO(wt%)	7.49	7.39	7.22	9.58	6.18	8.93	16.4	5.01
V(ppm)	945	556	406	507	452	449	1799	1457
Cr(ppm)	569	254	141	120	296	682	8291	3965
MnO2(wt%)	58.6	70.1	72.0	69.0	50.8	61.8	6.60	13.8
Fe2O3(wt%)	29.2	17.0	14.8	18.5	38.9	24.1	62.6	54.0
Co(ppm)	948	738	907	1318	1078	2770	7992	18478
Ni(ppm)	2379	3011	3673	3462	4617	13512	9144	9509
Cu(ppm)	2471	3001	4593	3626	2794	4246	44780	103722
Zn(ppm)	9770	14486	16476	13138	9584	14615	52716	116981
As(ppm)	1140	998	1216	895	390	1119	1853	2880
Se(ppm)	(2.54)	(10.0)	(11.9)	(10.5)	(8.79)	13.2	46.4	72.8
Sr(ppm)	425	493	468	501	378	481	558	217
Y(ppm)	212	219	222	258	616	406	66.6	103
Ag(ppm)	52.2	49.3	107	40.7	150	35.5	29.6	63.8
Cd(ppm)	32.3	75.0	95.0	39.4	56.9	72.1	60.8	219
Sn(ppm)	22.4	53.1	29.0	38.6	172	33.7	23.4	39.9
Ba(ppm)	19406	19096	16387	13886	11787	13263	1056	1425
La(ppm)	112	149	142	131	117	125	33.4	52.3
Ce(ppm)	821	1074	1485	1578	2116	1338	106	112
Au(ppm)	(0.40)	0.19	(0.03)	(0.08)	(0.06)	(0.07)	1.02	2.38
Pb(ppm)	1467	1230	1414	1292	2661	1134	1332	3321
Pb(ppm)	1338	1078	1270	1210	2439	1032	1313	3112
Pb(ppm)	1364	1065	1298	1264	2609	1108	1384	3089
Bi(ppm)	1.97	1.43	3.39	3.35	3.81	3.20	10.5	25.4
Th(ppm)	22.9	19.9	25.5	62.2	88.1	84.0	10.0	13.8
U(ppm)	59.7	44.7	50.1	48.8	97.5	71.7	16.4	26.9

Appendix 5:**Median values of concentrations determined by LA-ICP-MS for Fe-Mn oxide coating samples; ND = Not Detected, () indicates concentrations below detection limit.**

Site	TCS13	TCS14	BCS1	BCS4	BCS5	BCS6	BCS8	BCS10
Substrate	Pebble	Pebble	Pebble	Pebble	Pebble	Pebble	Pebble	Pebble
Months								
CaO(wt%)	1.84	3.45	2.30	3.84	8.69	2.20	1.70	6.08
V(ppm)	107	542	1363	2600	2165	930	718	1378
Cr(ppm)	1111	1668	4292	7004	1557	3579	5289	2583
MnO2(wt%)	0.07	0.25	2.87	0.52	1.17	0.19	0.23	0.91
Fe2O3(wt%)	88.6	84.1	86.8	80.4	85.2	86.0	87.7	81.3
Co(ppm)	228	812	1382	500	677	247	232	171
Ni(ppm)	136	1008	846	353	334	892	639	663
Cu(ppm)	86151	76820	55331	134477	28762	61534	67962	99690
Zn(ppm)	7598	25101	4628	5122	2435	2795	4013	4246
As(ppm)	141	411	490	289	424	544	1617	237
Se(ppm)	4.42	24.2	ND	ND	(37.0)	107	111	127
Sr(ppm)	126	138	34.4	57.9	143	77.8	22.1	30.6
Y(ppm)	15.6	76.2	168	626	131	869	217	92.8
Ag(ppm)	8.16	23.5	22.0	71.0	47.7	49.7	65.6	25.0
Cd(ppm)	10.3	41.9	6.96	5.59	5.18	4.67	6.12	5.09
Sn(ppm)	5.35	8.47	30.3	85.6	47.9	53.5	29.7	17.4
Ba(ppm)	61.1	168	111	72.3	94.6	450	94.6	52.1
La(ppm)	8.23	43.5	50.8	98.0	30.6	190	68.2	30.8
Ce(ppm)	24.1	65.9	178	262	81.6	443	206	52.1
Au(ppm)	(0.01)	(0.13)	(0.04)	(0.12)	(0.02)	(0.08)	0.71	0.21
Pb(ppm)	42.0	452	1338	1335	1361	1504	1033	1196
Pb(ppm)	38.6	471	1237	1306	1172	1409	969	1077
Pb(ppm)	37.5	462	1228	1274	1235	1407	1006	1147
Bi(ppm)	0.05	2.27	0.97	1.80	0.75	1.96	1.44	1.79
Th(ppm)	0.79	1.59	14.5	32.1	7.91	289	19.6	8.30
U(ppm)	18.3	27.6	11.4	63.6	11.0	67.4	26.6	4.53

Appendix 5:**Median values of concentrations determined by LA-ICP-MS for Fe-Mn oxide coating samples; ND = Not Detected, () indicates concentrations below detection limit.**

Site	SLAG	BCS11	BCS13	BCS15	BCS16	BCS17	BCS18	BCS19
Substrate	Pebble	Pebble	Pebble	Pebble	Pebble	Pebble	Pebble	Pebble
Months								
CaO(wt%)	7.84	3.67	1.47	7.83	23.0	28.5	21.3	5.75
V(ppm)	1730	2016	725	1790	2193	2403	1859	2863
Cr(ppm)	1319	2374	1609	8053	12286	5267	12326	17946
MnO2(wt%)	0.35	1.08	0.11	11.8	9.72	2.36	1.59	2.23
Fe2O3(wt%)	82.6	91.0	90.1	73.4	56.7	64.0	73.8	86.9
Co(ppm)	556	767	159	4320	4626	2357	911	1543
Ni(ppm)	1509	2832	475	19947	15635	8844	7782	15966
Cu(ppm)	57852	19234	72022	2182	2738	3260	3190	2170
Zn(ppm)	2907	2674	5000	8888	7486	3495	3676	4079
As(ppm)	274	275	1519	2778	2175	657	297	4168
Se(ppm)	(33.2)	(211)	(90.4)	(7.77)	(22.2)	(7.68)	(9.25)	(10.4)
Sr(ppm)	2208	409	25.1	420	128	84.4	88.1	86.4
Y(ppm)	203	89.2	24.0	145	79.6	50.4	25.2	60.7
Ag(ppm)	5.32	217	63.9	151	147	47.5	138	86.1
Cd(ppm)	5.53	14.7	20.8	92.9	44.7	34.4	5.02	16.9
Sn(ppm)	22.5	64.2	27.8	114	91.8	68.9	40.8	42.7
Ba(ppm)	2971	2005	74.6	1404	808	350	217	258
La(ppm)	297	158	12.0	167	54.7	38.4	27.0	106
Ce(ppm)	680	489	24.1	867	379	134	94.1	441
Au(ppm)	(0.02)	(0.39)	0.11	(0.02)	(0.03)	(0.07)	(0.05)	(0.01)
Pb(ppm)	1989	943	439	3611	4025	758	209	1552
Pb(ppm)	2112	870	406	3270	3775	693	194	1306
Pb(ppm)	1810	840	421	3350	3915	763	202	1316
Bi(ppm)	1.80	0.52	5.15	8.36	8.23	2.50	0.91	3.41
Th(ppm)	77.0	42.9	5.06	24.6	11.0	17.0	4.17	24.1
U(ppm)	24.3	28.1	1.73	18.3	2.35	5.95	1.68	3.23

Appendix 5:**Median values of concentrations determined by LA-ICP-MS for Fe-Mn oxide coating samples; ND = Not Detected, () indicates concentrations below detection limit.**

Site	BCS20	BCS21	RRS1	RRS2	RRS3	RRS4	RRS5	RRS6
Substrate	Pebble	Pebble	Pebble	Pebble	Pebble	Pebble	Pebble	Pebble
Months								
CaO(wt%)	35.0	4.69	64.8	9.13	9.04	20.8	4.87	18.5
V(ppm)	2171	4697	1261	2634	2525	1931	1268	2039
Cr(ppm)	20504	9729	189	1440	856	1525	113	457
MnO2(wt%)	3.50	10.4	6.19	15.3	3.14	4.95	32.9	11.3
Fe2O3(wt%)	58.7	75.0	17.2	69.1	86.2	71.4	54.0	67.6
Co(ppm)	1402	2039	222	1034	820	473	866	675
Ni(ppm)	8344	7652	326	1484	1297	568	523	439
Cu(ppm)	1776	6249	1516	2579	718	816	988	509
Zn(ppm)	3160	5884	1152	4564	4251	2826	5060	3778
As(ppm)	625	763	31.7	176	82.0	182	262	155
Se(ppm)	11.9	11.3	(35.1)	(1.09)	(5.14)	(1.80)	(18.7)	(9.45)
Sr(ppm)	68.1	139	599	530	373	334	322	4264
Y(ppm)	63.8	115	376	593	199	130	301	150
Ag(ppm)	49.7	35.5	28.3	153	32.6	93.7	12.8	13 7
Cd(ppm)	11.1	40.6	5.25	20.8	6.90	4.50	12.8	5.33
Sn(ppm)	44.2	41.9	31.5	150	50.6	66.6	18.2	59.1
Ba(ppm)	273	1572	1541	7138	3914	4830	14446	8307
La(ppm)	42.7	47.0	321	623	317	109	525	352
Ce(ppm)	186	252	1009	976	563	832	1044	836
Au(ppm)	(0.05)	(0.24)	(0.14)	(3.92)	(0.08)	(0.06)	(0.17)	0.09
Pb(ppm)	744	884	153	690	438	568	322	1132
Pb(ppm)	705	922	132	543	413	531	300	1033
Pb(ppm)	673	821	130	581	488	585	280	919
Bi(ppm)	1.41	1.04	1.15	4.40	1.95	1.68	2.22	2.86
Th(ppm)	9.35	8.39	28.6	214	76.7	65.9	178	111
U(ppm)	4.29	2.29	8.17	76.5	14.8	20.3	10.5	31.9

Appendix 5:**Median values of concentrations determined by LA-ICP-MS for Fe-Mn oxide coating samples; ND = Not Detected, () indicates concentrations below detection limit.**

Site	RRS7	RRS8	RRS9	RRS10	RRS11	RRS12	RRS13	RRS14
Substrate	Pebble	Pebble	Pebble	Pebble	Pebble	Pebble	Pebble	Pebble
Months								
CaO(wt%)	18.9	38.2	24.4	24.3	22.6	24.9	17.5	43.4
V(ppm)	2175	2136	2441	1165	1212	2784	1666	1393
Cr(ppm)	381	1537	780	397	374	615	337	391
MnO2(wt%)	10.5	3.19	4.02	31.8	6.43	4.36	14.0	5.20
Fe2O3(wt%)	63.7	56.6	70.3	39.3	64.3	68.8	65.4	48.8
Co(ppm)	1044	583	338	616	378	615	1043	369
Ni(ppm)	419	614	629	552	290	496	426	426
Cu(ppm)	1221	2286	465	430	739	971	3005	738
Zn(ppm)	2868	2112	1070	2283	3201	2424	3099	1843
As(ppm)	196	139	462	224	107	231	213	129
Se(ppm)	(20.5)	(3.14)	(9.98)	(8.46)	(5.35)	(30.5)	(16.3)	(11.7)
Sr(ppm)	974	598	361	2162	2402	873	1027	848
Y(ppm)	211	258	253	288	159	296	315	153
Ag(ppm)	284	84.1	9.73	23.4	10.9	34.2	138	58.4
Cd(ppm)	11.8	3.43	2.38	9.94	12.8	6.26	11.3	8.58
Sn(ppm)	80.0	79.8	16.8	25.9	23.4	66.7	87.2	65.3
Ba(ppm)	3560	2170	1527	6468	6521	3448	4294	2713
La(ppm)	260	156	419	288	191	336	425	207
Ce(ppm)	774	519	639	1314	473	716	1262	440
Au(ppm)	(0.05)	(0.06)	(0.01)	(0.07)	(0.06)	0.14	(0.09)	(0.07)
Pb(ppm)	655	220	347	192	412	611	785	433
Pb(ppm)	632	193	316	185	443	538	680	325
Pb(ppm)	636	216	350	187	405	571	691	393
Bi(ppm)	1.42	1.50	1.23	0.90	1.45	3.89	4.80	1.78
Th(ppm)	21.5	29.6	79.6	80.0	19.2	147	82.5	37.1
U(ppm)	12.8	15.8	20.1	14.2	11.5	30.9	23.8	13.5

Appendix 5:**Median values of concentrations determined by LA-ICP-MS for Fe-Mn oxide coating samples; ND = Not Detected, () indicates concentrations below detection limit.**

Site	RRS15	RRS15	SJS1	SJS6A	SJS6B	SJS1	SJS6A	SJS6B
Substrate	Pebble	Pebble	Pebble	Pebble	Pebble	Pebble	Pebble	Pebble
Months			3.00	3.00	3.00	6.00	6.00	6.00
CaO(wt%)	7.96	11.5	ND	ND	ND	ND	ND	ND
V(ppm)	2277	1355	184	1081	413	541	1404	327
Cr(ppm)	1005	1035	30.4	298	420	381	585	244
MnO2(wt%)	6.48	11.1	73.3	39.3	0.55	66.2	42.5	11.9
Fe2O3(wt%)	83.2	75.1	20.5	55.9	98.0	28.0	52.9	86.0
Co(ppm)	422	1030	1808	3113	213	2877	2688	364
Ni(ppm)	522	474	788	711	152	858	554	221
Cu(ppm)	1201	562	2583	1849	1003	2396	1590	1136
Zn(ppm)	1643	3120	20083	19931	4886	18938	17557	8932
As(ppm)	230	332	191	725	203	291	529	190
Sc(ppm)	9.14	14.0	28.7	8.71	20.2	18.0	(8.95)	(10.0)
Sr(ppm)	778	1200	190	346	200	1500	381	305
Y(ppm)	315	174	471	941	423	708	667	291
Ag(ppm)	77.2	37.4	9.74	70.4	58.6	17.0	73.8	40.8
Cd(ppm)	3.87	15.8	74.8	22.6	8.20	45.2	16.5	24.4
Sn(ppm)	81.2	38.3	58.2	24.0	88.7	68.3	115	31.8
Ba(ppm)	2989	4832	6512	10451	1385	13100	13989	3506
La(ppm)	426	320	484	1083	575	693	860	392
Ce(ppm)	1045	829	2579	2136	540	1858	1744	613
Au(ppm)	(0.07)	(0.14)	(0.02)	(0.01)	0.10	(0.04)	(0.07)	(0.01)
Pb(ppm)	537	368	8756	1852	1512	4928	1101	1601
Pb(ppm)	475	306	8907	1779	1295	4364	1024	1348
Pb(ppm)	463	304	8482	1743	1527	4692	1071	1410
Bi(ppm)	6.57	4.45	2.30	1.05	0.67	1.21	1.08	0.82
Th(ppm)	210	63.3	13.3	14.3	8.36	24.7	61.9	11.5
U(ppm)	48.1	16.3	5.40	7.09	3.40	12.5	16.3	5.20

Appendix 5:**Median values of concentrations determined by LA-ICP-MS for Fe-Mn oxide coating samples; ND = Not Detected, () indicates concentrations below detection limit.**

Site	SJS1	SJS6A	SJS6B	SJS1	SJS2	SJS3	SJS4	SJS5
Substrate	Pebble	Pebble	Pebble	Pebble	Pebble	Pebble	Pebble	Pebble
Months	9.00	9.00	9.00	12.00	12.00	12.00	12.00	12.00
CaO(wt%)	ND	ND	ND	ND	ND	ND	ND	ND
V(ppm)	243	729	437	1265	353	501	408	433
Cr(ppm)	28.9	264	231	2232	211	421	114	349
MnO2(wt%)	68.5	44.2	1.80	41.5	77.0	68.2	72.2	74.2
Fe2O3(wt%)	26.0	48.4	97.1	54.4	17.8	27.3	23.0	20.2
Co(ppm)	2695	2025	471	5336	3090	2175	1630	2802
Ni(ppm)	539	393	202	1797	606	461	433	400
Cu(ppm)	1539	1727	1408	7054	3798	3063	2338	3002
Zn(ppm)	15128	16381	4702	5883	16769	11903	15256	16821
As(ppm)	309	278	178	249	298	494	545	523
Se(ppm)	(17.4)	5.66	(20.8)	13.6	(9.52)	(9.84)	(11.5)	(14.0)
Sr(ppm)	173	372	124	496	219	202	163	168
Y(ppm)	574	810	187	546	515	469	541	547
Ag(ppm)	10.7	73.8	74.7	634	196	157	50.7	170
Cd(ppm)	31.0	28.1	7.27	11.5	35.7	28.9	29.8	40.3
Sn(ppm)	42.4	86.4	122	228	241	81.6	22.2	129
Ba(ppm)	10089	9444	971	8792	15523	19889	17260	21025
La(ppm)	553	828	310	766	842	880	888	974
Ce(ppm)	1659	2681	224	1232	2978	1487	1654	1924
Au(ppm)	(0.04)	(0.01)	(0.05)	(0.02)	0.14	(0.19)	(0.02)	(0.03)
Pb(ppm)	7144	12574	350	1541	2303	1217	2549	2212
Pb(ppm)	6990	12083	353	1462	2242	1089	2397	2085
Pb(ppm)	6864	12824	327	1436	2267	1190	2434	2237
Bi(ppm)	1.18	3.85	1.38	1.43	0.70	2.11	0.55	0.31
Th(ppm)	15.9	84.5	7.34	37.4	11.3	36.7	8.65	7.63
U(ppm)	6.40	19.4	3.53	13.6	4.22	6.99	3.08	3.77

Appendix 5:**Median values of concentrations determined by LA-ICP-MS for Fe-Mn oxide coating samples; ND = Not Detected, () indicates concentrations below detection limit.**

Site	SJS6A	SJS6B	SJS1	SJS6A	SJS6B	SJS1	SJS6A	SJS6B
Substrate	Pebble	Pebble	Streak	Streak	Streak	Streak	Streak	Streak
Months	12.00	12.00	3.00	3.00	3.00	6.00	6.00	6.00
CaO(wt%)	ND	ND	ND	ND	ND	ND	ND	ND
V(ppm)	1020	404	760	1197	343	523	436	145
Cr(ppm)	368	221	634	2036	538	4083	468	178
MnO2(wt%)	54.5	1.02	21.6	8.38	0.17	66.1	78.9	0.21
Fe2O3(wt%)	40.6	95.4	73.1	85.6	98.8	21.8	16.9	98.8
Co(ppm)	2034	137	2410	635	98.3	3536	1624	401
Ni(ppm)	519	170	1574	26477	52.1	7836	511	77.1
Cu(ppm)	1527	1210	15509	5068	1130	42863	1991	763
Zn(ppm)	14680	6132	17778	14283	3725	35456	9278	4835
As(ppm)	277	171	262	120	190	506	196	227
Se(ppm)	6.21	(189.0)	(5.00)	(6.40)	(267)	(19.9)	(14.1)	(5.87)
Sr(ppm)	309	132	634	280	198	1091	413	199
Y(ppm)	737	228	1188	1278	493	1086	439	356
Ag(ppm)	46.1	45.2	450	438	7.26	370	92.8	33.5
Cd(ppm)	22.7	6.02	120.2	(8.46)	6.64	141	12.4	8.62
Sn(ppm)	43.0	42.4	633	194	30.2	684	46.4	13.2
Ba(ppm)	14150	1077	2512	2229	1215	14187	23899	1546
La(ppm)	1064	509	869	1018	700	1563	586	425
Ce(ppm)	2369	1204	1227	1117	675	1058	1156	574
Au(ppm)	(0.01)	(0.26)	(1.07)	(0.11)	(1.12)	(0.12)	(0.19)	(0.09)
Pb(ppm)	2987	998	2152	1313	409	1882	396	81.1
Pb(ppm)	2938	921	2051	1237	396	1969	374	71.1
Pb(ppm)	3052	957	1924	1290	446	2035	383	77.6
Bi(ppm)	1.54	1.13	4.06	16.7	0.38	4.48	2.80	0.18
Th(ppm)	61.0	13.4	52.1	60.8	5.48	34.5	18.7	1.93
U(ppm)	12.0	4.67	38.6	41.6	9.40	54.2	25.9	3.22

Appendix 5:**Median values of concentrations determined by LA-ICP-MS for Fe-Mn oxide coating samples; ND = Not Detected, () indicates concentrations below detection limit.**

Site	SJS1	SJS6A	SJS6B	SJS1	SJS2	SJS3	SJS4	SJS5
Substrate	Streak	Streak	Streak	Streak	Streak	Streak	Streak	Streak
Months	9.00	9.00	9.00	12.00	12.00	12.00	12.00	12.00
CaO(wt%)	ND	ND	ND	ND	ND	ND	ND	ND
V(ppm)	157	286	229	265	1072	586	543	1154
Cr(ppm)	138	177	233	243	972	287	302	536
MnO2(wt%)	75.1	80.9	14.0	77.4	43.3	43.3	56.0	39.2
Fe2O3(wt%)	22.0	14.9	84.3	20.2	53.7	54.2	40.7	57.6
Co(ppm)	2537	2733	264	2805	1869	1370	4089	1877
Ni(ppm)	379	501	143	293	480	145	333	327
Cu(ppm)	2928	1864	933	1128	2334	2502	2629	2173
Zn(ppm)	5939	13883	9318	5346	6714	3877	7182	6480
As(ppm)	168	188	236	143	201	205	190	255
Se(ppm)	(10.9)	(3.64)	(10.8)	(9.87)	(8.66)	(211.6)	(5.17)	(17.4)
Sr(ppm)	189	436	189	104	361	101	261	253
Y(ppm)	433	437	228	312	679	429	662	756
Ag(ppm)	33.7	86.2	15.3	53.9	63.5	42.3	181	62.2
Cd(ppm)	16.7	31.9	20.3	9.70	15.4	42.3	13.1	8.61
Sn(ppm)	100	59.8	16.8	63.4	142	48.9	272	184
Ba(ppm)	12972	17969	3439	10206	5115	9997	11565	9290
La(ppm)	461	698	258	495	983	621	1056	1042
Ce(ppm)	895	1142	300	1082	1673	1051	1760	1706
Au(ppm)	(0.35)	(0.07)	(0.03)	(0.06)	(0.02)	(0.60)	(0.02)	(0.02)
Pb(ppm)	507	552	369	461	2411	1345	916	2139
Pb(ppm)	459	521	310	413	2365	1266	833	1895
Pb(ppm)	442	518	390	426	2383	1331	867	1927
Bi(ppm)	0.49	0.69	0.37	0.37	3.09	0.51	0.69	2.21
Th(ppm)	8.07	18.2	4.72	6.80	33.4	12.9	13.9	29.4
U(ppm)	11.4	7.36	4.18	8.29	19.8	9.59	7.82	17.5

Appendix 5:

Median values of concentrations determined by LA-ICP-MS for Fe-Mn oxide coating samples; ND = Not Detected, () indicates concentrations below detection limit.

Site	SJS6A	SJS6B	SJS1	SJS6A	SJS6B	SJS1	SJS6A	SJS6B
Substrate	Streak	Streak	Pol. Peb.	Pol. Peb.	Pol. Peb.	Pol. Peb.	Pol. Peb.	Pol. Peb.
Months	12.00	12.00	3.00	3.00	3.00	6.00	6.00	6.00
CaO(wt%)	ND	ND	ND	ND	ND	ND	ND	ND
V(ppm)	141	150	4492	1536	370	291	144	211
Cr(ppm)	98.6	153	7164	5533	563	234	105	315
MnO2(wt%)	90.1	11.1	7.15	26.8	0.22	77.4	88.7	0.27
Fe2O3(wt%)	6.54	85.8	78.2	65.8	98.6	16.1	7.53	98.8
Co(ppm)	2015	149	3642	9752	423	2190	978	242
Ni(ppm)	444	85.1	9461	1007	289	1735	451	95.4
Cu(ppm)	2602	659	30606	19734	2684	10890	1301	971
Zn(ppm)	9638	6661	19117	13277	3206	20436	10066	4065
As(ppm)	131	196	1976	535	166	153	107	225
Se(ppm)	(5.8)	13.5	(0.05)	(9.87)	(38.7)	(11.8)	(3.13)	(12.0)
Sr(ppm)	235	131	8446	997	227	611	941	251
Y(ppm)	484	195	934	720	395	523	249	486
Ag(ppm)	294	18.9	898	1732	105	223	69.5	123
Cd(ppm)	27.0	10.8	87.7	13.4	4.51	61.4	22.2	7.48
Sn(ppm)	51.8	15.1	1623	725	151	220	149	33.2
Ba(ppm)	15231	2925	39911	8481	1252	14885	21362	1252
La(ppm)	818	225	1826	1002	531	894	468	597
Ce(ppm)	1188	243	1893	1184	542	919	678	508
Au(ppm)	(0.19)	(0.08)	(0.07)	(0.03)	(0.01)	(0.05)	(0.05)	(0.03)
Pb(ppm)	218	144	4810	4270	359	1516	205	104
Pb(ppm)	210	135	4979	1677	307	7450	201	96.1
Pb(ppm)	209	147	4749	1176	346	1920	222	96.2
Bi(ppm)	0.45	0.28	22.5	43.5	0.60	2.08	0.33	0.75
Th(ppm)	5.33	3.06	113	228	4.76	10.3	13.5	3.27
U(ppm)	8.49	4.53	40.0	19.9	3.05	11.3	3.43	1.44

Appendix 5:**Median values of concentrations determined by LA-ICP-MS for Fe-Mn oxide coating samples; ND = Not Detected, () indicates concentrations below detection limit.**

Site	SJS1	SJS6A	SJS1	SJS2	SJS3	SJS4	SJS5	SJS6A
Substrate	Pol. Peb.	Pol. Peb.	Pol. Peb.	Pol. Peb.	Pol. Peb.	Pol. Peb.	Pol. Peb.	Pol. Peb.
Months	9.00	9.00	12.00	12.00	12.00	12.00	12.00	12.00
CaO(wt%)	ND	ND	ND	ND	ND	ND	ND	ND
V(ppm)	495	178	461	562	437	170	248	168
Cr(ppm)	445	115	284	543	274	83.9	221	187
MnO2(wt%)	61.0	85.9	63.7	67.8	62.6	83.2	82.0	88.0
Fe2O3(wt%)	36.1	9.48	33.8	28.9	34.7	13.5	14.7	8.26
Co(ppm)	2825	2177	4610	2739	2396	1936	2774	2571
Ni(ppm)	613	406	227	421	266	253	277	561
Cu(ppm)	4663	1681	1434	4526	1839	1412	1715	2304
Zn(ppm)	6209	12067	4142	5798	5442	8295	7598	9605
As(ppm)	235	146	174	199	271	212	192	134
Se(ppm)	(3.27)	(24.5)	(5.9)	(9.88)	(25.1)	(5.00)	(1.25)	6.86
Sr(ppm)	326	395	167	318	151	180	582	288
Y(ppm)	435	358	367	444	366	294	510	531
Ag(ppm)	364	371	39.5	119	99.4	39.9	117	205
Cd(ppm)	20.0	17.7	5.79	12.4	9.32	21.9	18.3	28.3
Sn(ppm)	176	4749	46.8	66.4	75.9	28.1	54.3	101
Ba(ppm)	8316	21233	9739	13310	11042	16846	15401	17303
La(ppm)	465	621	621	745	568	526	816	927
Ce(ppm)	819	1005	1310	1441	1079	855	1152	1274
Au(ppm)	(0.07)	(5.87)	(0.04)	(0.01)	(0.01)	(0.02)	(0.01)	(0.01)
Pb(ppm)	846	330	778	460	775	340	528	244
Pb(ppm)	771	320	714	516	723	312	472	223
Pb(ppm)	810	316	713	506	786	326	482	246
Bi(ppm)	1.29	0.41	0.40	1.30	0.32	0.23	0.98	0.35
Th(ppm)	17.4	5.18	6.95	22.5	4.68	3.27	27.2	6.15
U(ppm)	18.0	3.89	4.51	4.77	2.22	1.89	6.71	4.99

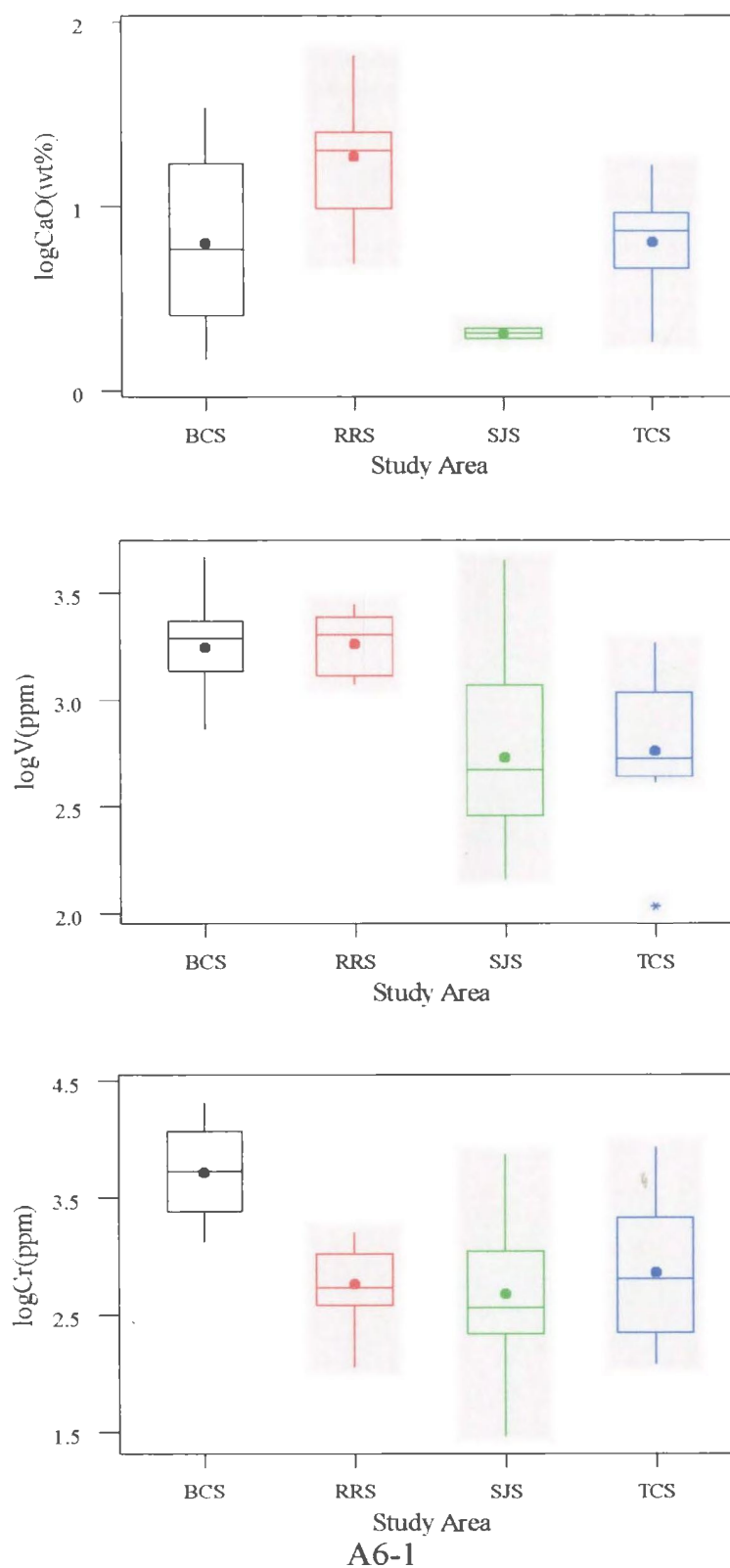
Appendix 5:**Median values of concentrations determined by LA-ICP-MS for Fe-Mn oxide coating samples; ND = Not Detected, () indicates concentrations below detection limit.**

Site	SJS1	SJS6A	SJS6B	SJS1	SJS6A	SJS6B	SJS1	SJS6A
Substrate	Cement	Cement	Cement	Cement	Cement	Cement	Cement	Cement
Months	3.00	3.00	3.00	6.00	6.00	6.00	9.00	9.00
CaO(wt%)	ND	ND	ND	ND	ND	ND	ND	ND
V(ppm)	1715	1662	471	1767	1208	422	508	1751
Cr(ppm)	5458	2224	991	5184	1448	321	1757	3505
MnO2(wt%)	16.3	29.0	1.03	38.2	64.9	0.63	73.1	35.5
Fe2O3(wt%)	70.4	48.6	96.7	53.4	28.5	97.7	22.2	56.1
Co(ppm)	2241	713	367	6127	2553	346	2556	1452
Ni(ppm)	2447	1127	248	3625	1638	125	1260	1388
Cu(ppm)	8204	1747	860	6178	6327	1309	3783	4070
Zn(ppm)	81830	196384	13377	32665	25928	8857	19391	45689
As(ppm)	206	185	166	240	161	198	146	243
Se(ppm)	5.02	(2.94)	4.18	0.00	0.00	5.25	0.00	29.45
Sr(ppm)	3055	1274	672	5079	1423	660	1000	1598
Y(ppm)	1733	2181	405	1536	625	376	677	1750
Ag(ppm)	521	137	80.2	306	715	71.3	76.6	729
Cd(ppm)	83.8	294	21.0	36.7	37.6	17.6	25.3	41.0
Sn(ppm)	121	98.5	47.4	220	723	26.8	104	461
Ba(ppm)	17983	7640	2424	13226	19893	2577	12756	12418
La(ppm)	1717	3234	547	2079	656	444	709	2066
Ce(ppm)	2433	3182	512	2518	809	412	1003	2554
Au(ppm)	(0.004)	(0.01)	(0.09)	0.19	0.01	0.00	0.07	0.00
Pb(ppm)	763	695	393	1000	501	111	303	1338
Pb(ppm)	782	679	344	982	542	159	275	1318
Pb(ppm)	864	691	310	1026	490	109	261	1466
Bi(ppm)	6.28	2.25	1.33	6.93	1.84	0.33	1.30	3.79
Th(ppm)	264	83.3	9.50	311	53.7	7.40	62.9	130
U(ppm)	90.8	30.8	3.65	75.5	36.1	3.97	22.1	42.6

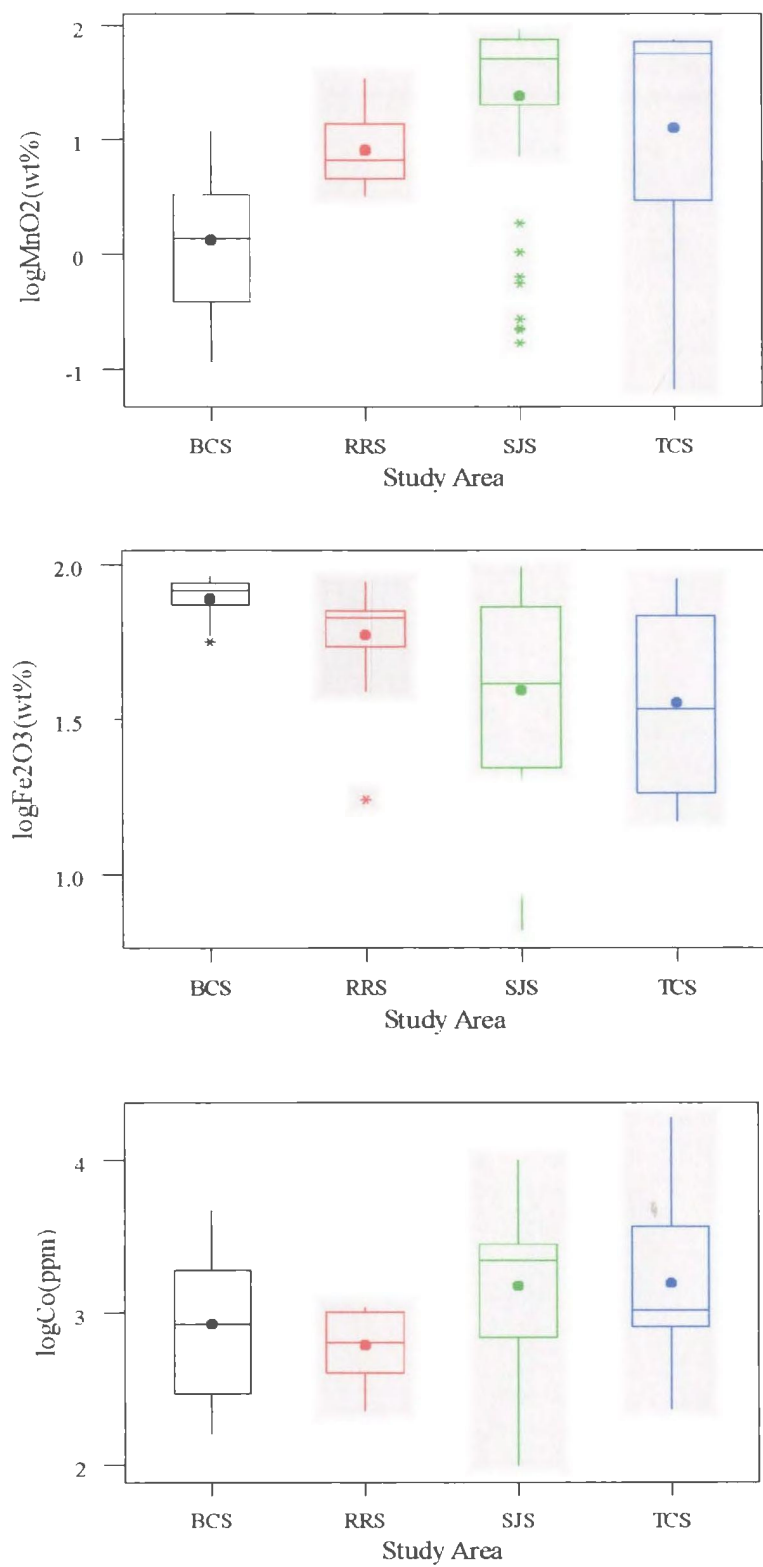
Appendix 5:**Median values of concentrations determined by LA-ICP-MS for Fe-Mn oxide coating samples; ND = Not Detected, () indicates concentrations below detection limit.**

Site	SJS6B	SJS1	SJS2	SJS3	SJS4	SJS5	SJS6A	SJS6B
Substrate	Cement	Cement	Cement	Cement	Cement	Cement	Cement	Cement
Months	9.00	12.00	12.00	12.00	12.00	12.00	12.00	12.00
CaO(wt%)	ND	ND	ND	ND	ND	ND	ND	ND
V(ppm)	278	1745	2157	998	1145	1313	1878	443
Cr(ppm)	145	2927	1368	768	439	1353	4749	168
MnO2(wt%)	23.2	52.0	52.6	60.0	65.7	46.8	25.1	21.6
Fe2O3(wt%)	74.4	37.9	37.3	35.0	27.8	41.7	66.3	69.5
Co(ppm)	386	7214	1191	2016	2148	3173	2303	313
Ni(ppm)	207	2309	976	876	864	1360	1298	154
Cu(ppm)	1665	10408	1771	1588	1926	4982	2772	708
Zn(ppm)	13992	58042	77248	28646	43146	79419	46792	12012
As(ppm)	238	209	289	235	205	270	205	233
Sc(ppm)	10.47	18.66	12.94	0.00	17.80	15.65	25.53	6.12
Sr(ppm)	235	1286	745	571	505	2296	1430	263
Y(ppm)	161	749	997	519	765	1058	2024	210
Ag(ppm)	52.8	551	171	144	110	295	51.2	39.8
Cd(ppm)	26.2	47.4	70.6	23.5	53.4	68.6	68.0	24.1
Sn(ppm)	21.1	451	88.4	36.5	66.5	849	74.4	19.6
Ba(ppm)	6426	10720	7467	9127	9935	10023	11750	5402
La(ppm)	177	869	1260	751	896	1935	2623	235
Ce(ppm)	192	1323	1681	1307	1307	2790	3129	222
Au(ppm)	0.00	0.01	0.01	0.01	0.01	0.01	0.01	0.00
Pb(ppm)	157	707	1096	849	722	1164	1381	101
Pb(ppm)	115	636	1289	747	638	1112	1363	102
Pb(ppm)	110	694	1084	798	668	1163	1382	98.0
Bi(ppm)	0.21	2.55	5.09	0.77	1.49	6.36	3.22	0.30
Th(ppm)	2.43	109	62.4	32.6	41.7	80.5	129	2.67
U(ppm)	3.63	44.4	41.2	16.9	18.4	28.6	43.9	2.94

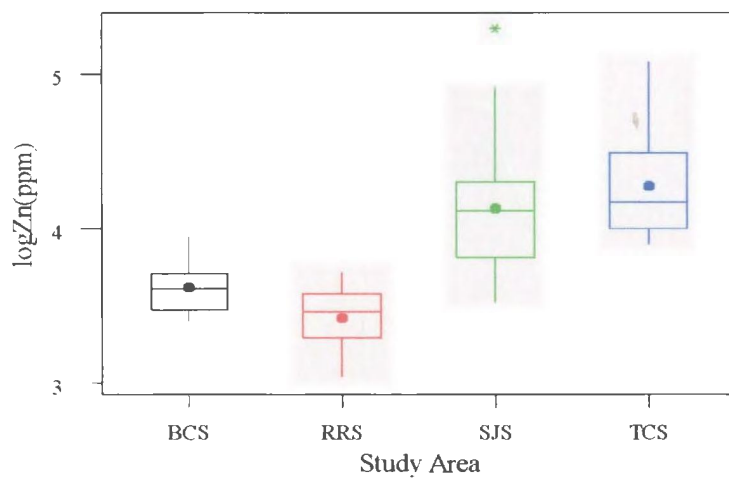
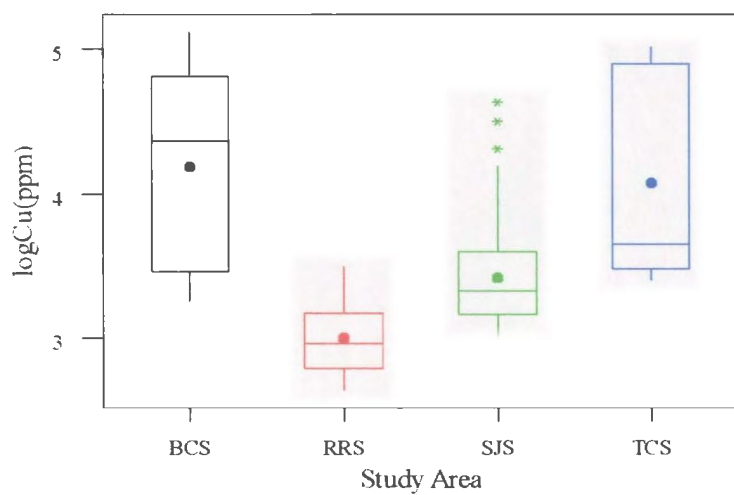
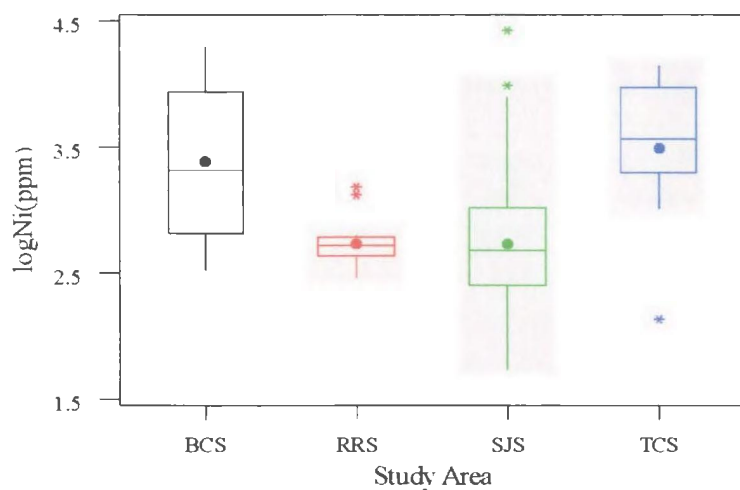
Appendix 6: Box plots of log-transformed analyte LA-ICP-MS concentrations in stream pebble Fe-Mn oxide coating samples taken from all four study areas.



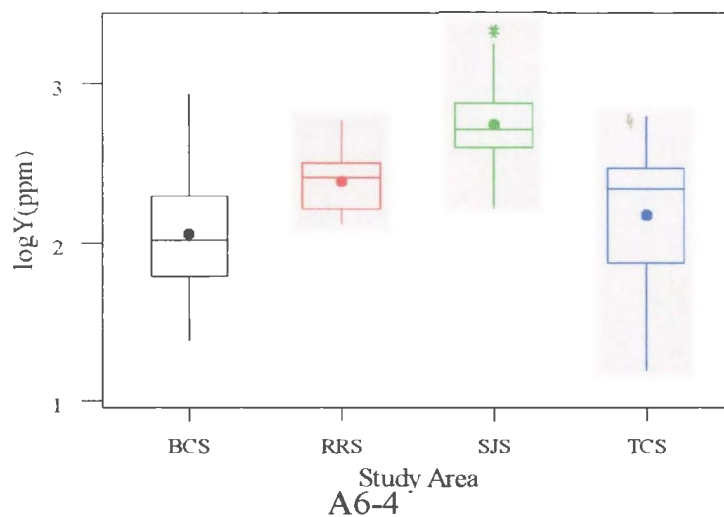
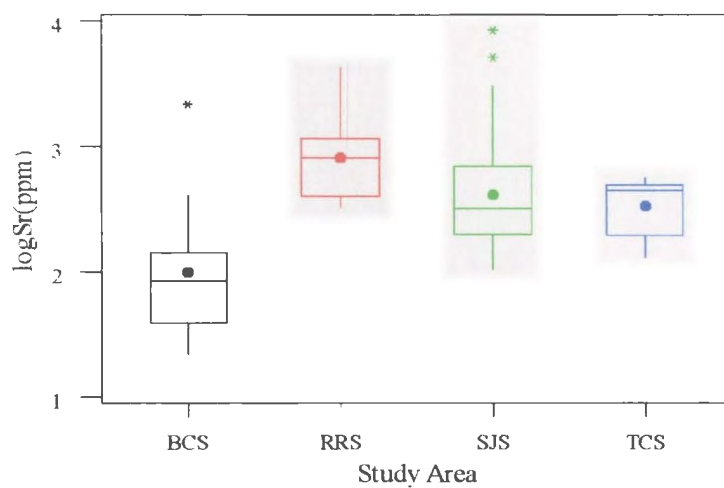
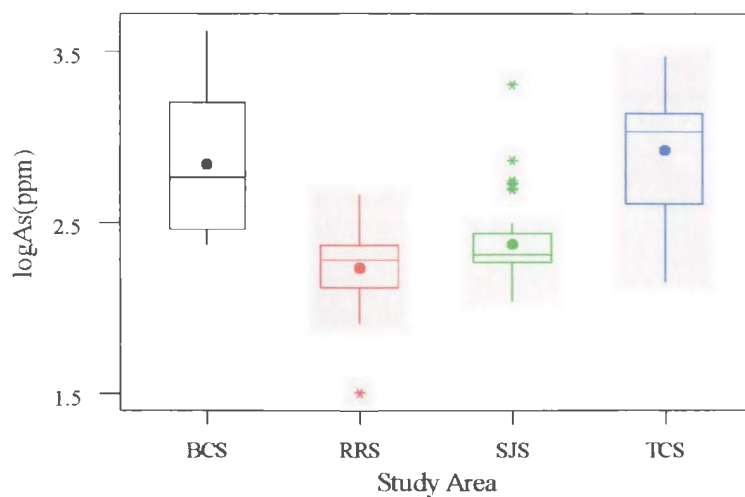
Appendix 6: Box plots of log-transformed analyte LA-ICP-MS concentrations in stream pebble Fe-Mn oxide coating samples taken from all four study areas.



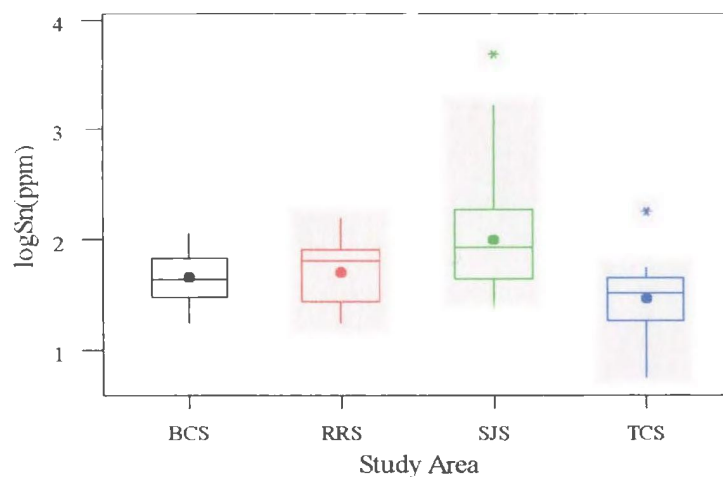
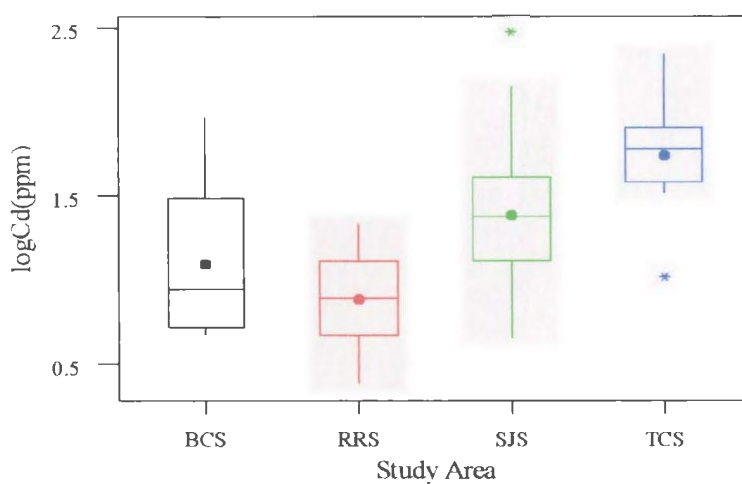
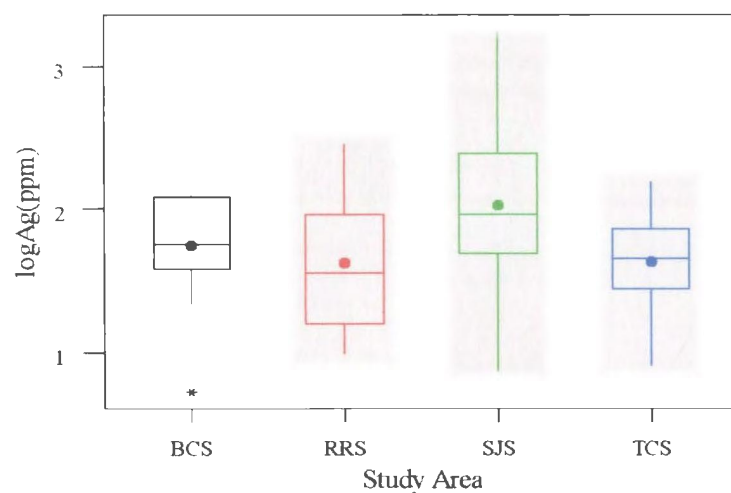
Appendix 6: Box plots of log-transformed analyte LA-ICP-MS concentrations in stream pebble Fe-Mn oxide coating samples taken from all four study areas.



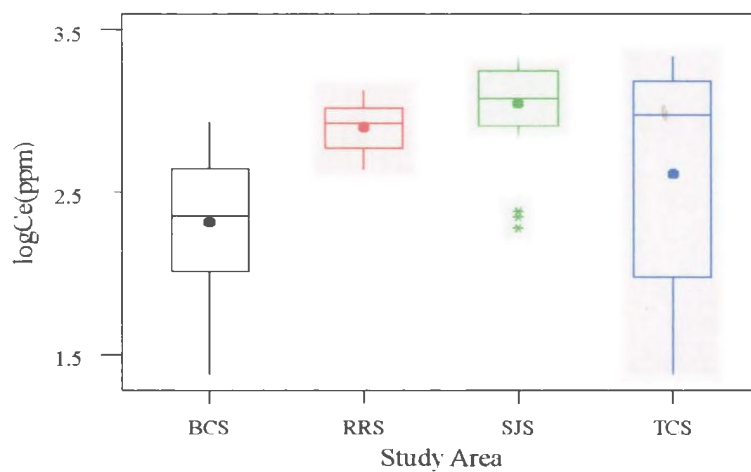
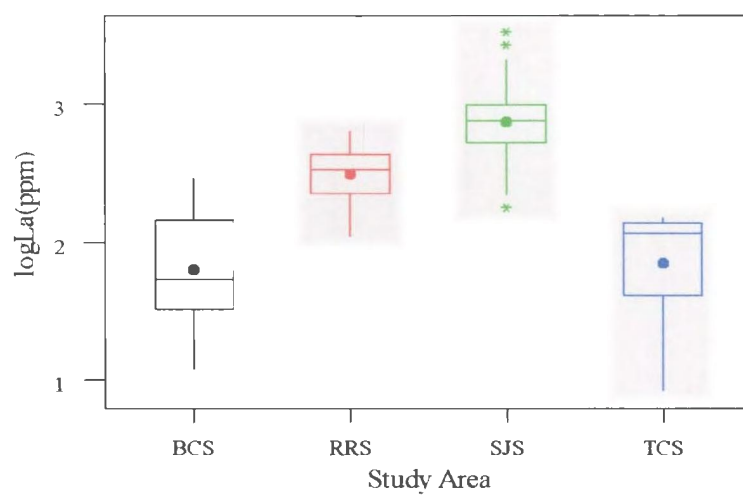
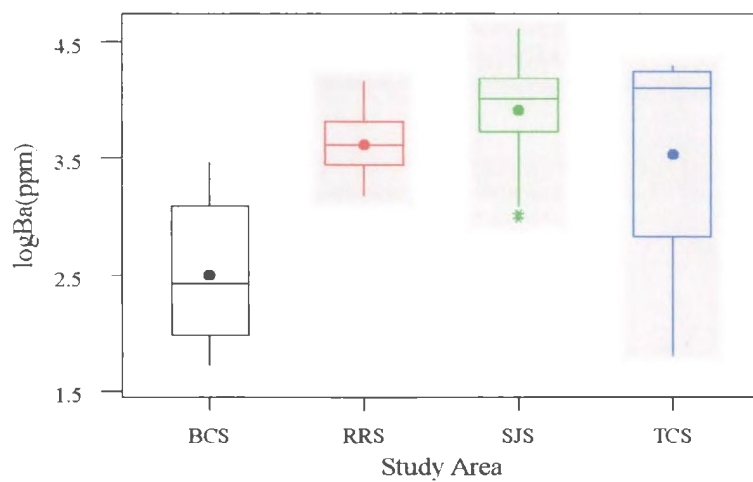
Appendix 6: Box plots of log-transformed analyte LA-ICP-MS concentrations in stream pebble Fe-Mn oxide coating samples taken from all four study areas.



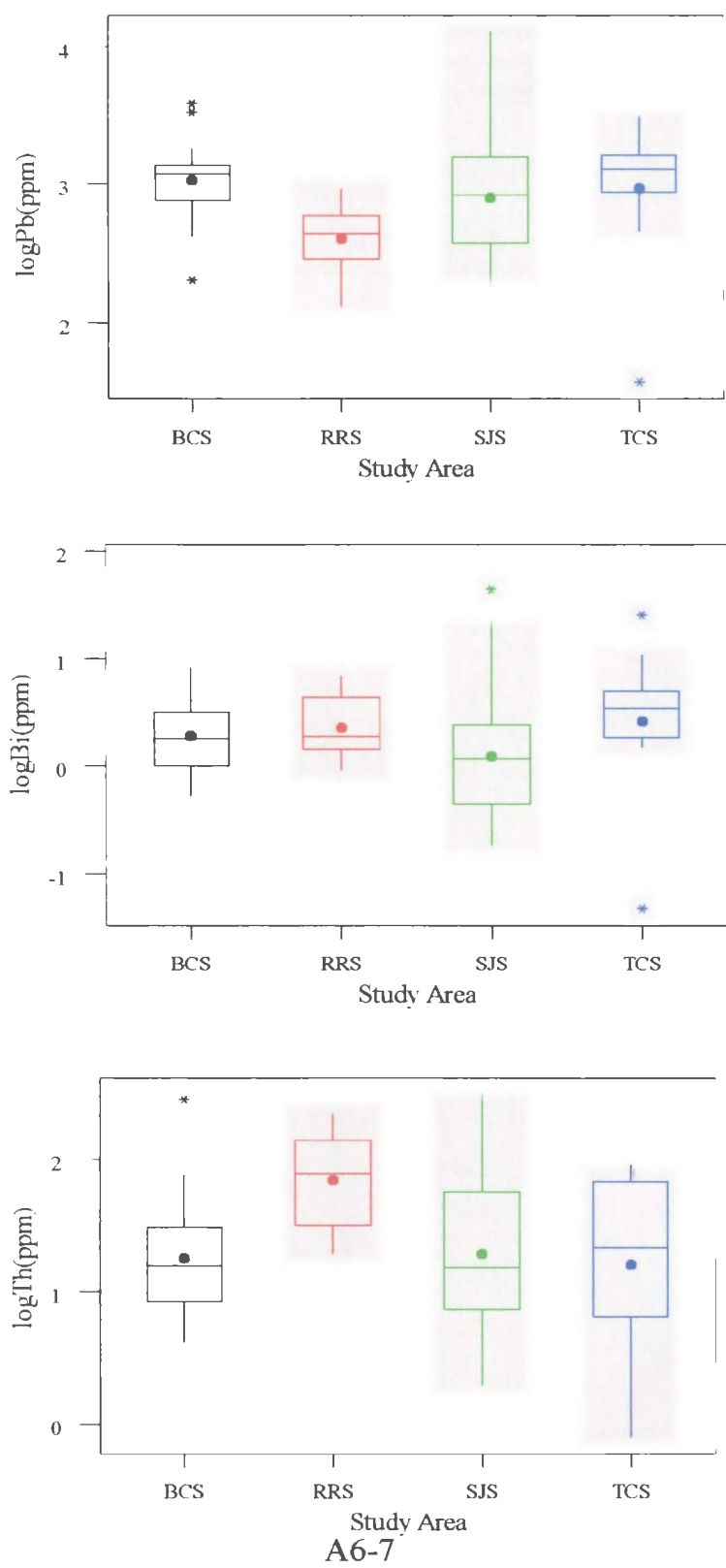
Appendix 6: Box plots of log-transformed analyte LA-ICP-MS concentrations in stream pebble Fe-Mn oxide coating samples taken from all four study areas.



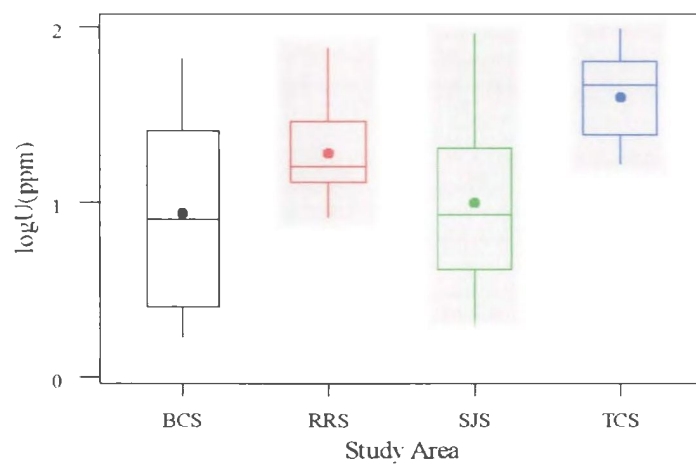
Appendix 6: Box plots of log-transformed analyte LA-ICP-MS concentrations in stream pebble Fe-Mn oxide coating samples taken from all four study areas.



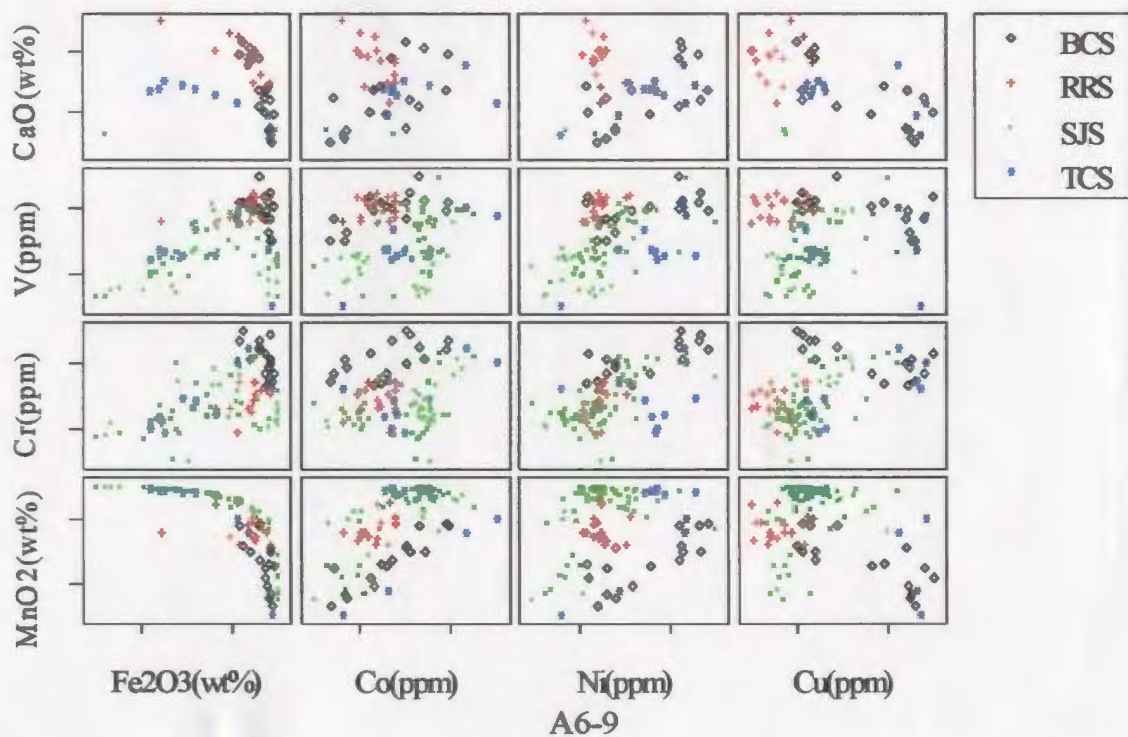
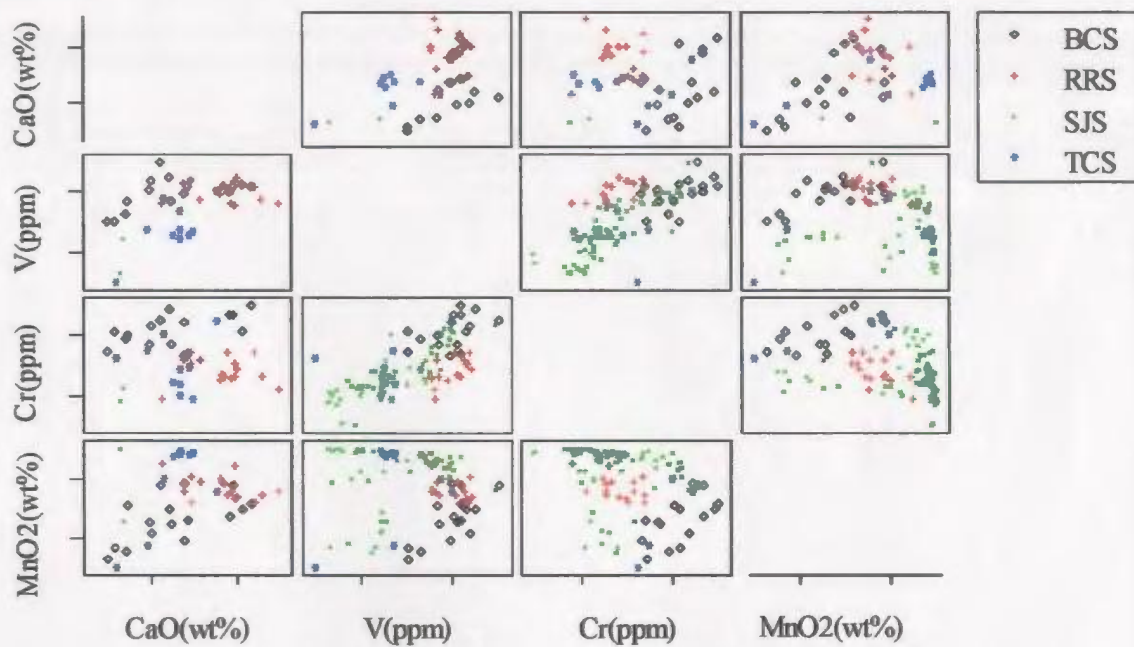
Appendix 6: Box plots of log-transformed analyte LA-ICP-MS concentrations in stream pebble Fe-Mn oxide coating samples taken from all four study areas.



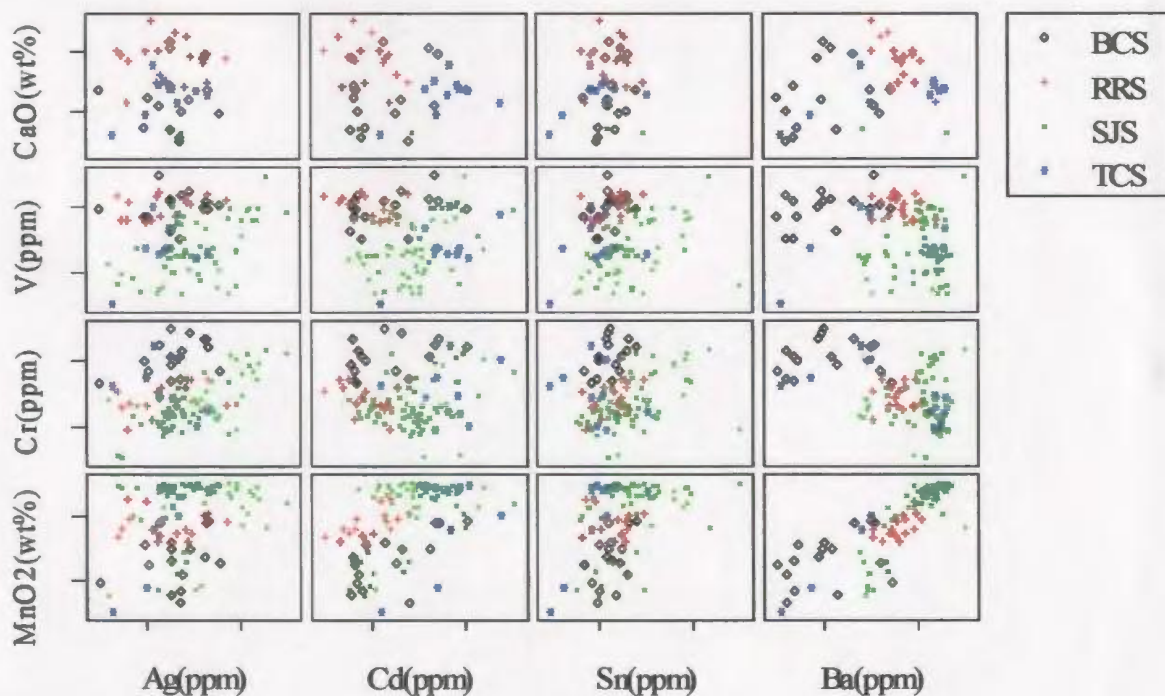
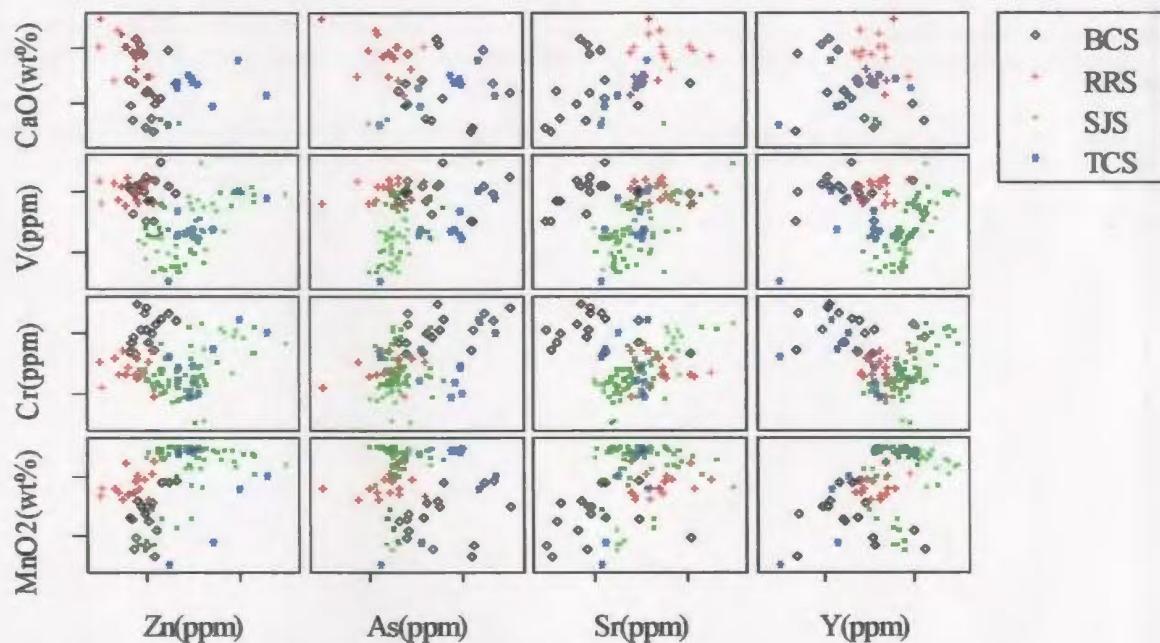
Appendix 6: Box plots of log-transformed analyte LA-ICP-MS concentrations in stream pebble Fe-Mn oxide coating samples taken from all four study areas.



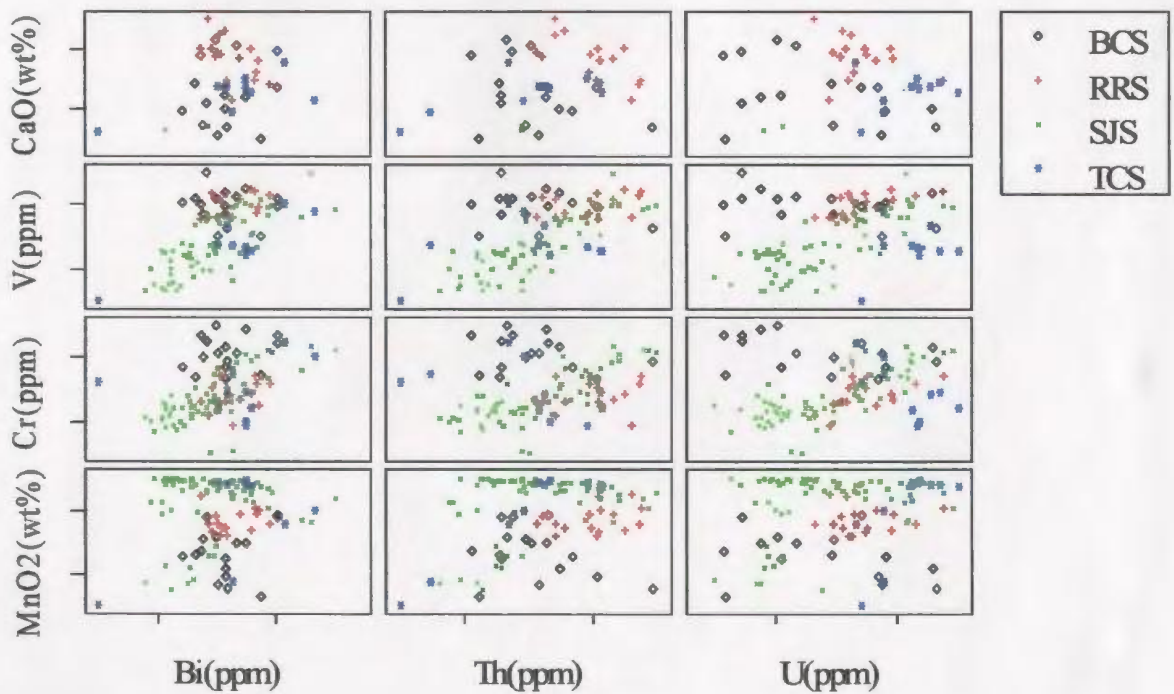
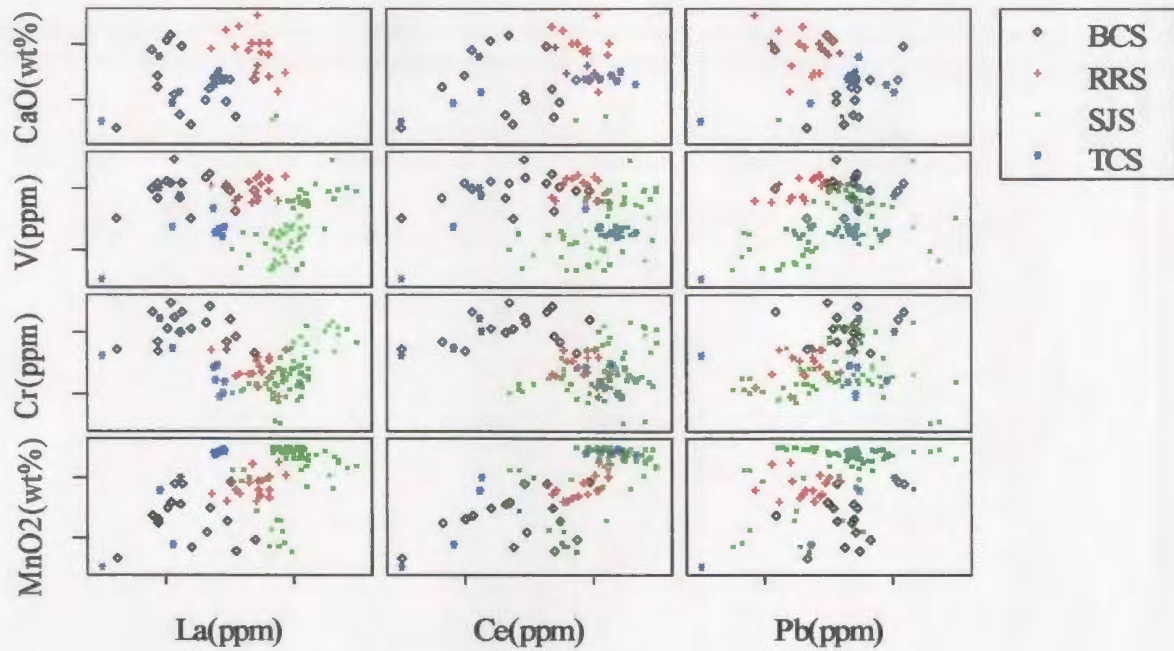
Appendix 6: Scatter plots of log-transformed analyte LA-ICP-MS concentrations in stream pebble Fe-Mn oxide coating samples taken from all four study areas.



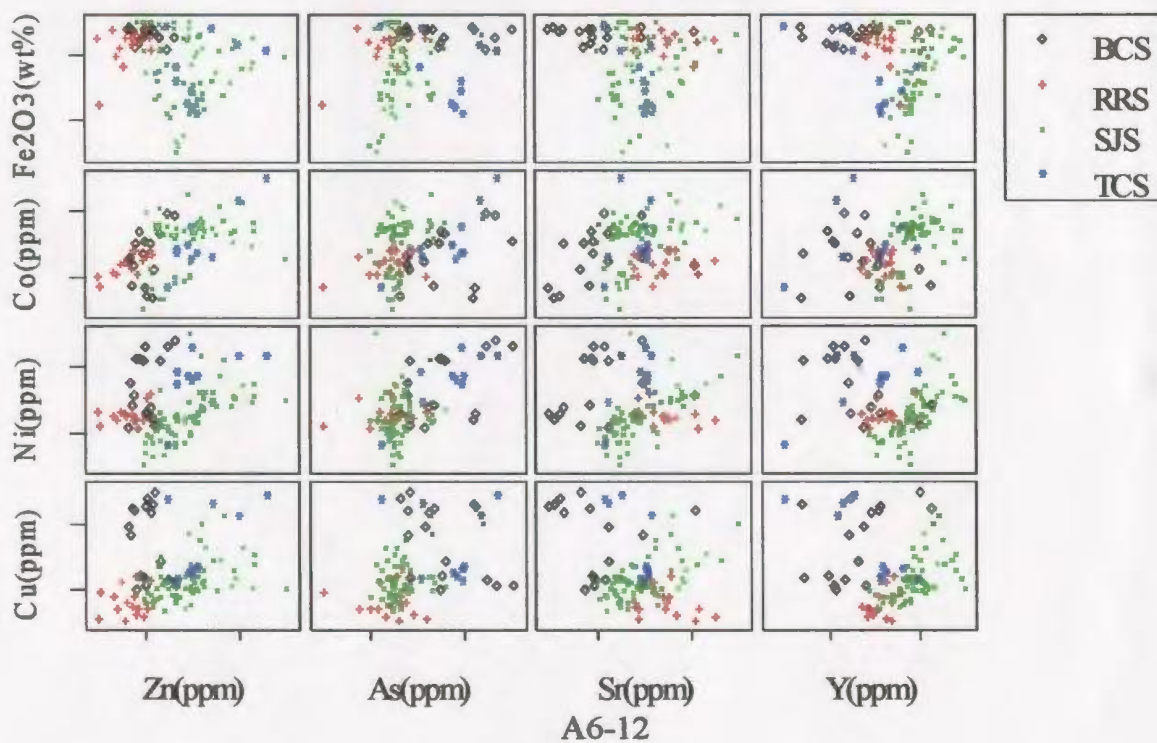
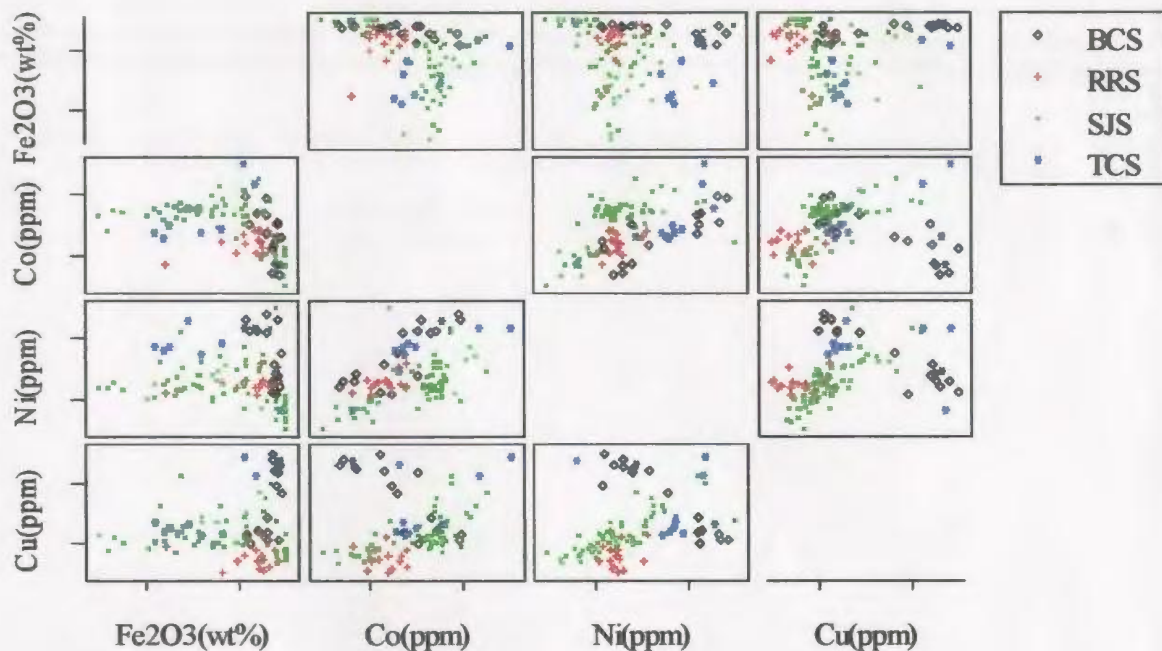
Appendix 6: Scatter plots of log-transformed analyte LA-ICP-MS concentrations in stream pebble Fe-Mn oxide coating samples taken from all four study areas.



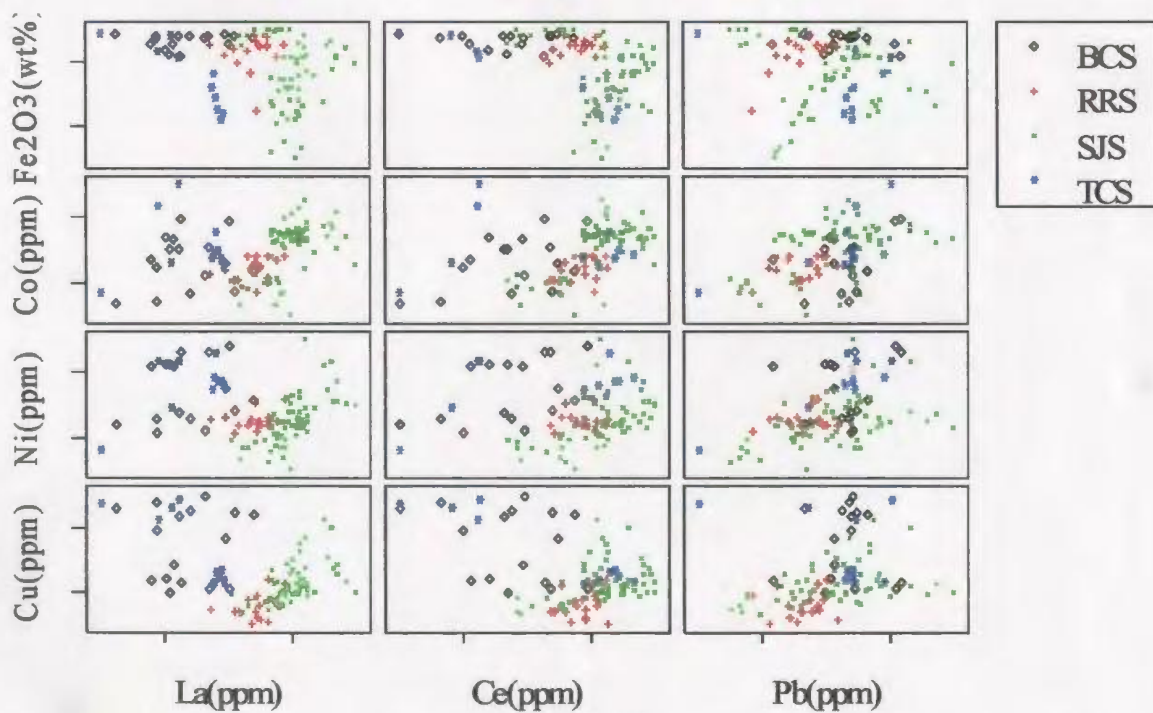
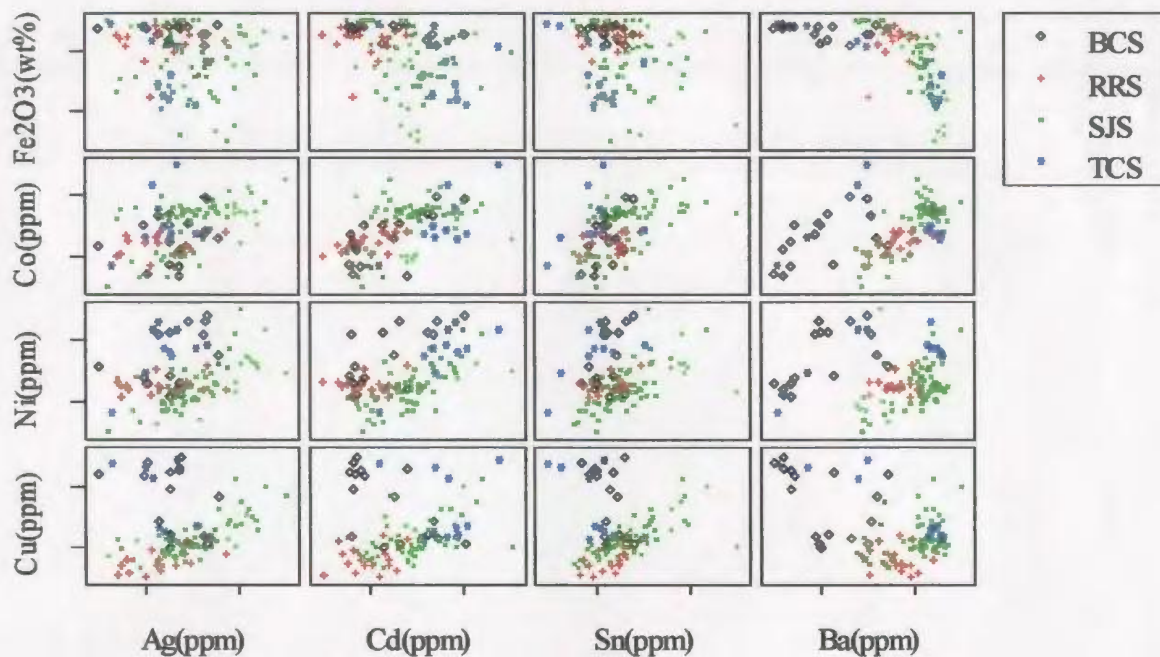
Appendix 6: Scatter plots of log-transformed analyte LA-ICP-MS concentrations in stream pebble Fe-Mn oxide coating samples taken from all four study areas.



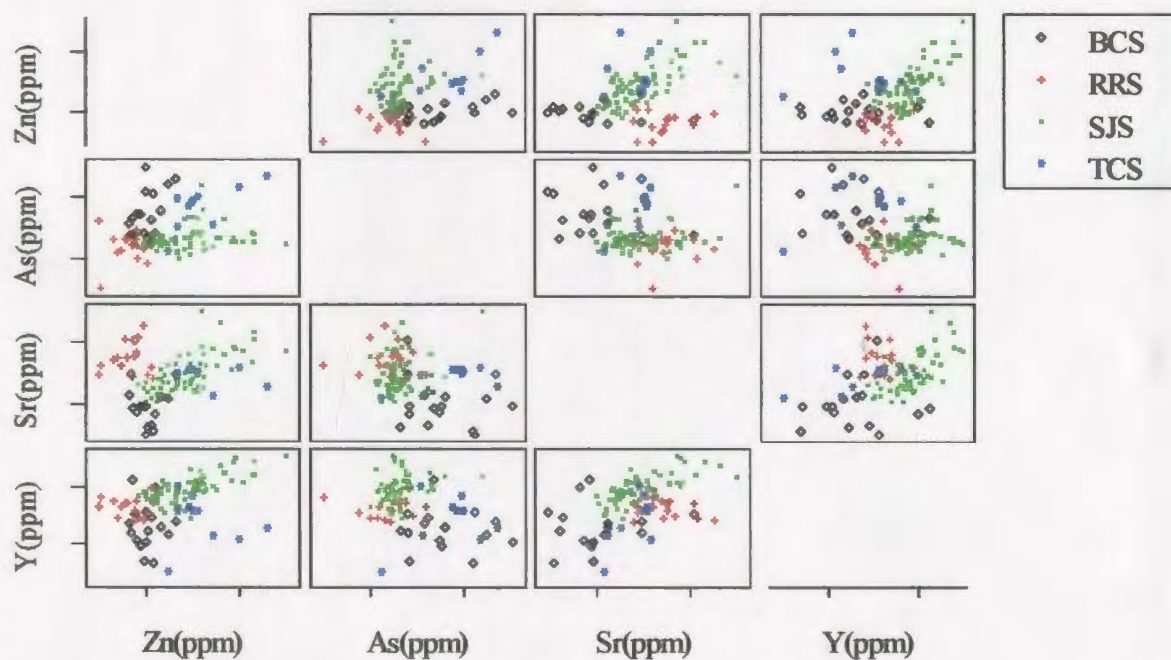
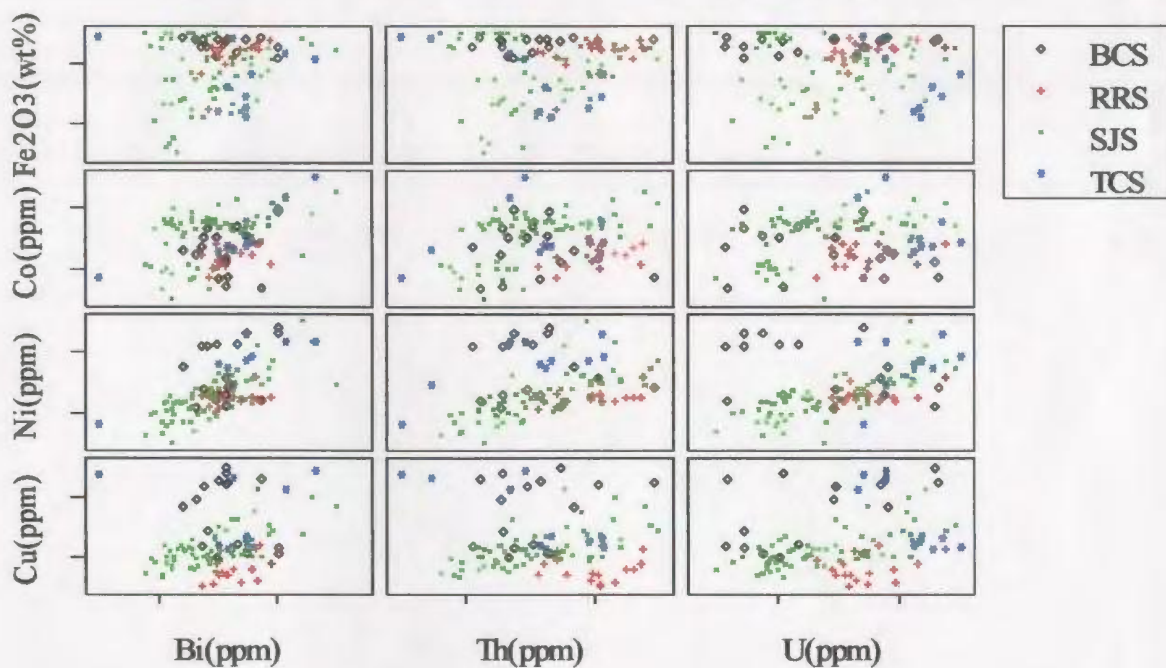
Appendix 6: Scatter plots of log-transformed analyte LA-ICP-MS concentrations in stream pebble Fe-Mn oxide coating samples taken from all four study areas.



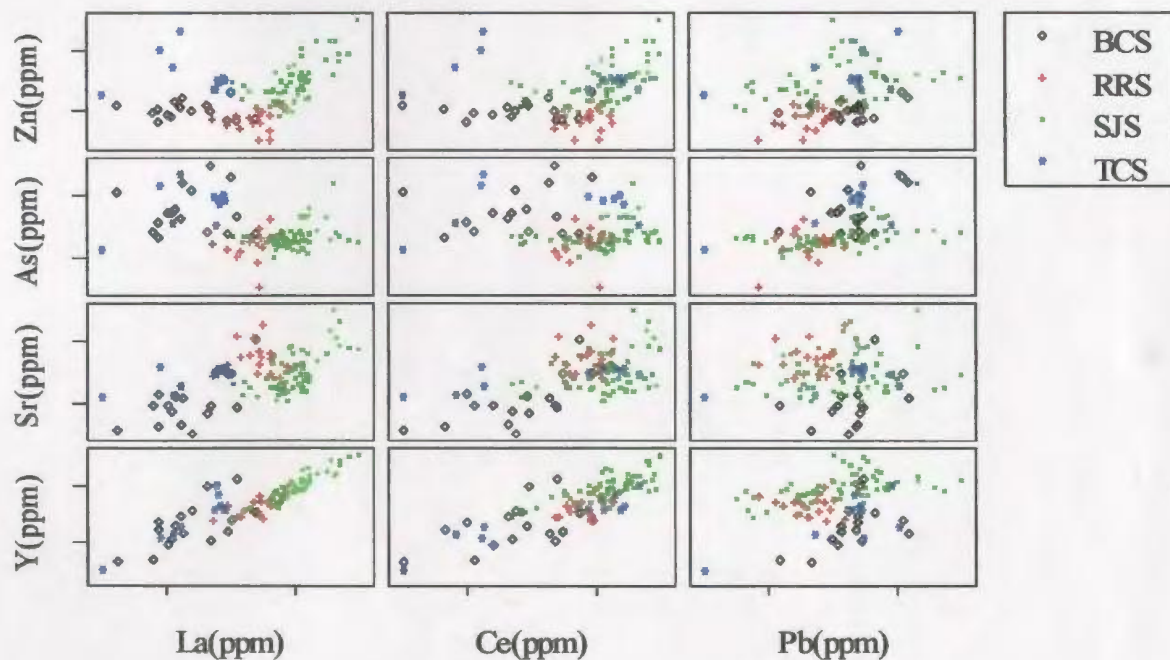
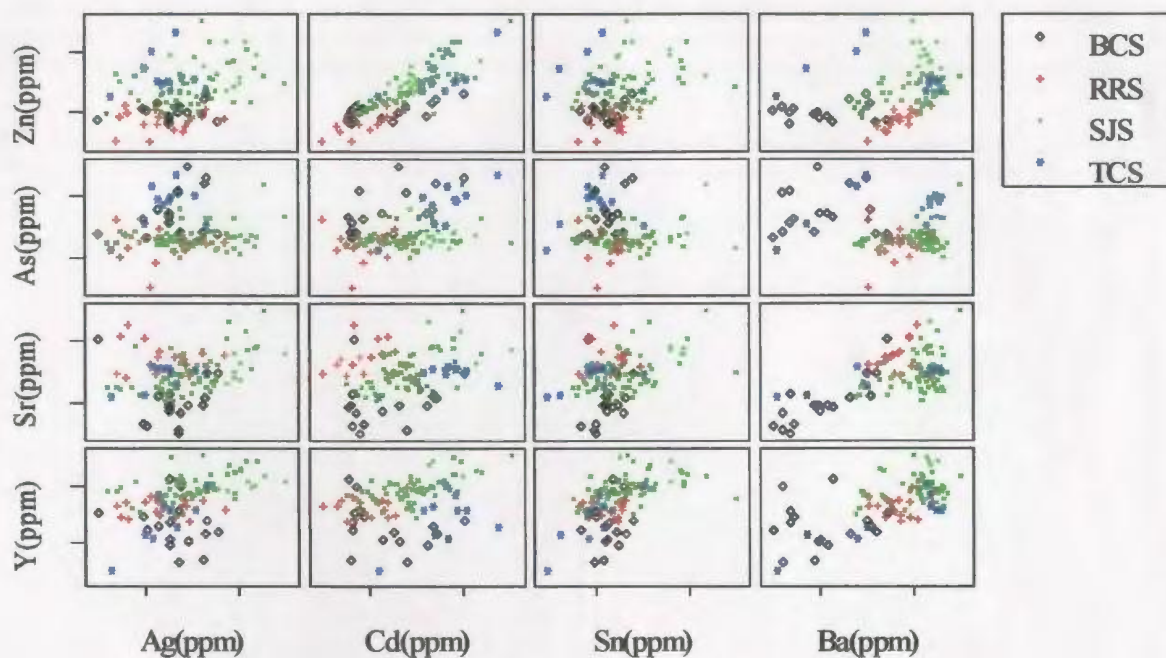
Appendix 6: Scatter plots of log-transformed analyte LA-ICP-MS concentrations in stream pebble Fe-Mn oxide coating samples taken from all four study areas.



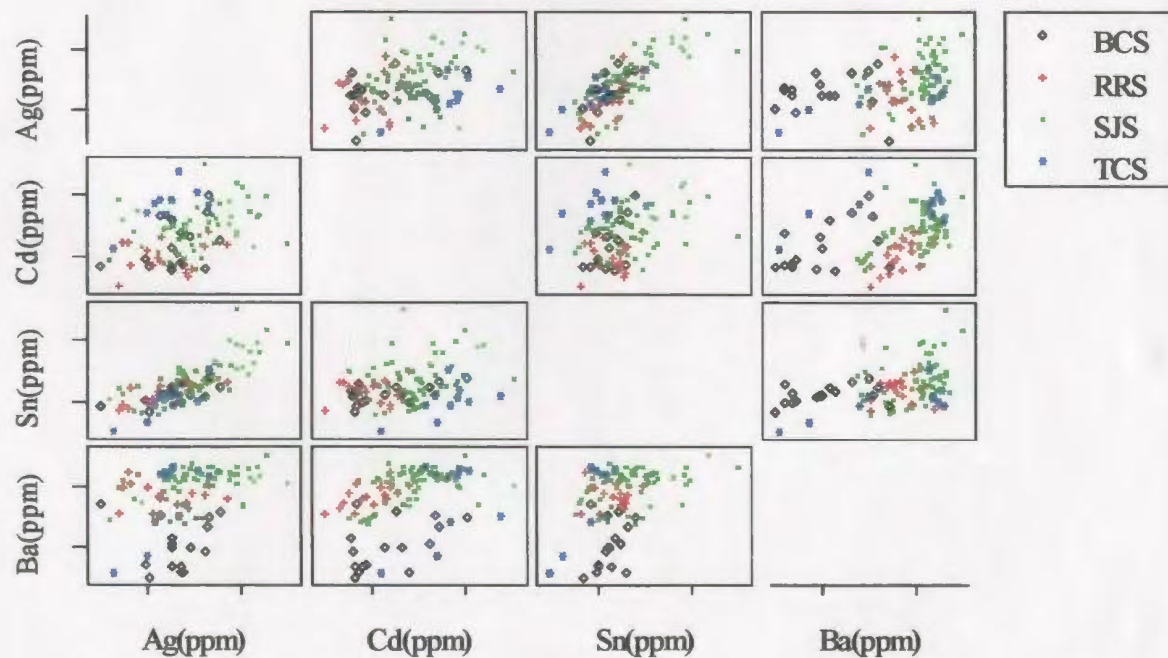
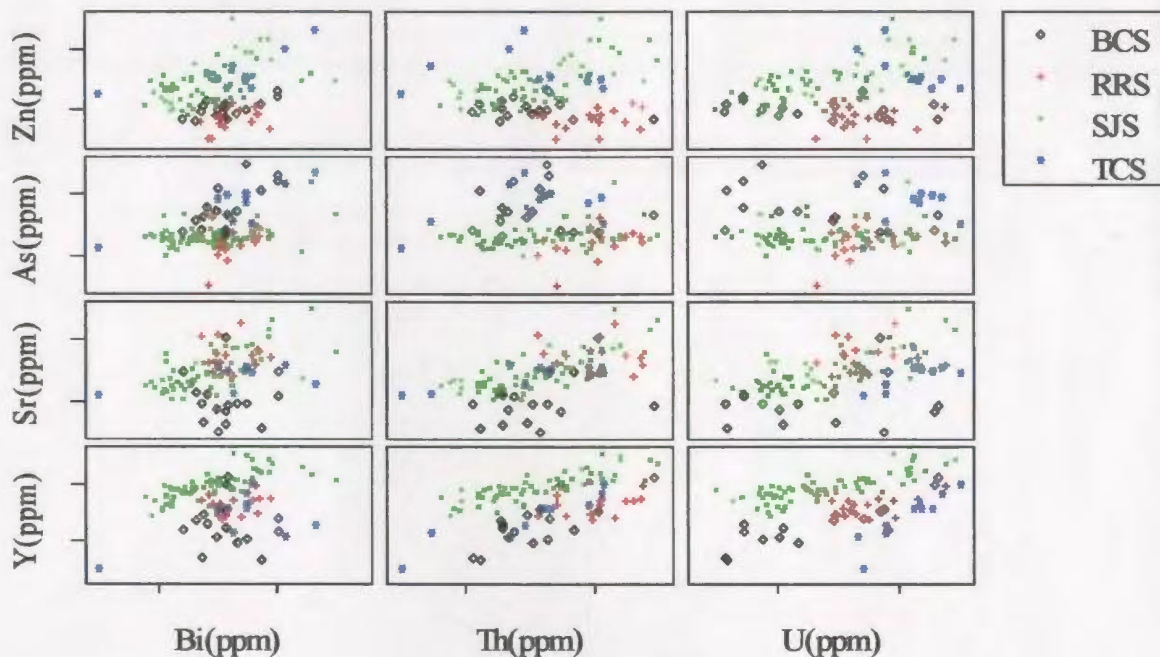
Appendix 6: Scatter plots of log-transformed analyte LA-ICP-MS concentrations in stream pebble Fe-Mn oxide coating samples taken from all four study areas.



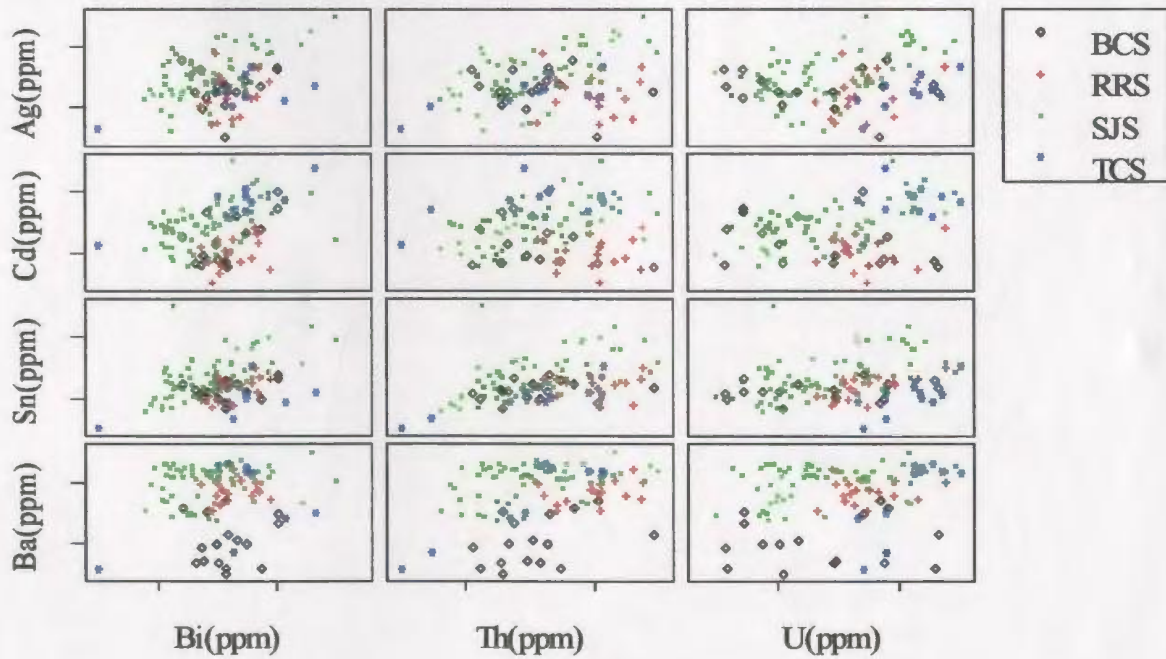
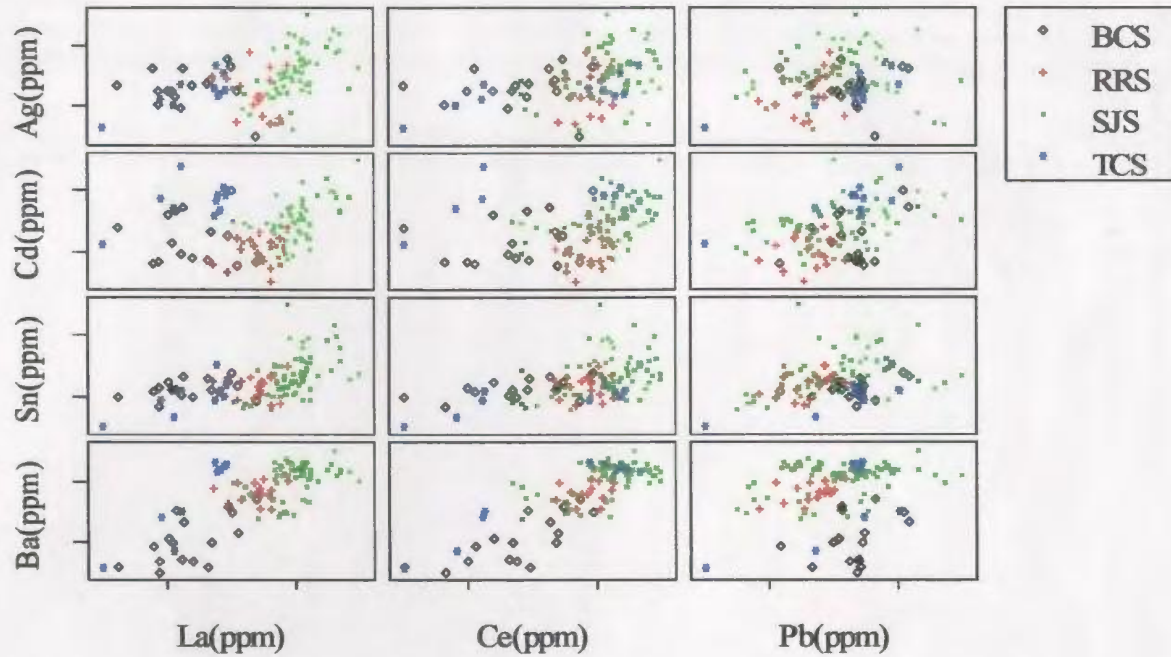
Appendix 6: Scatter plots of log-transformed analyte LA-ICP-MS concentrations in stream pebble Fe-Mn oxide coating samples taken from all four study areas.



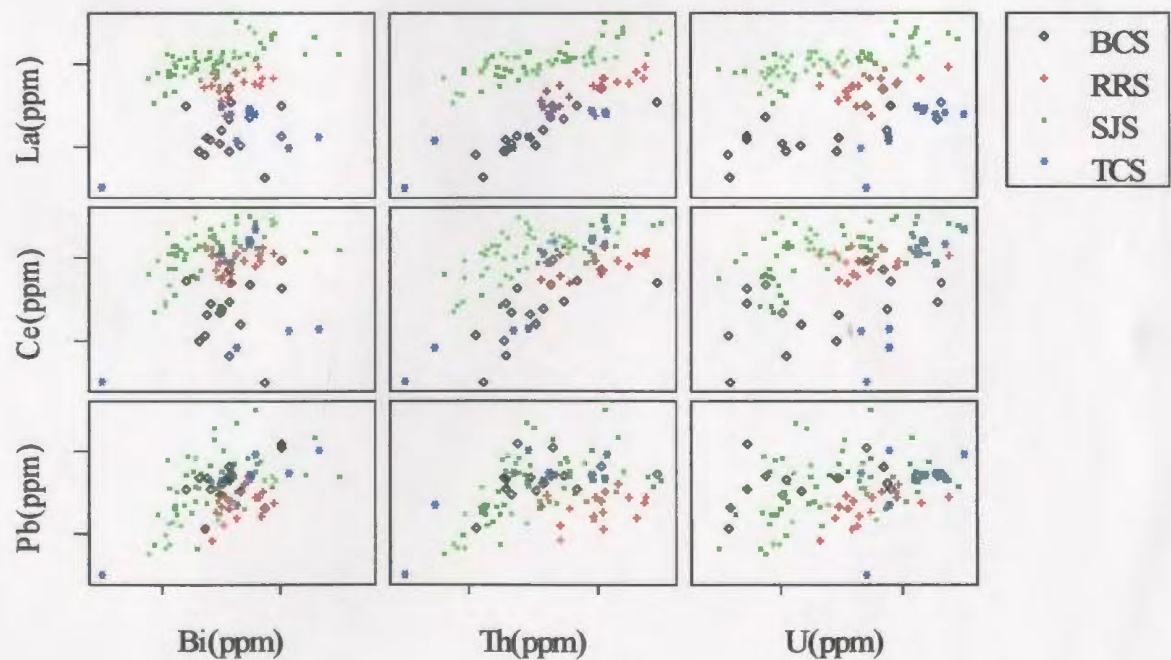
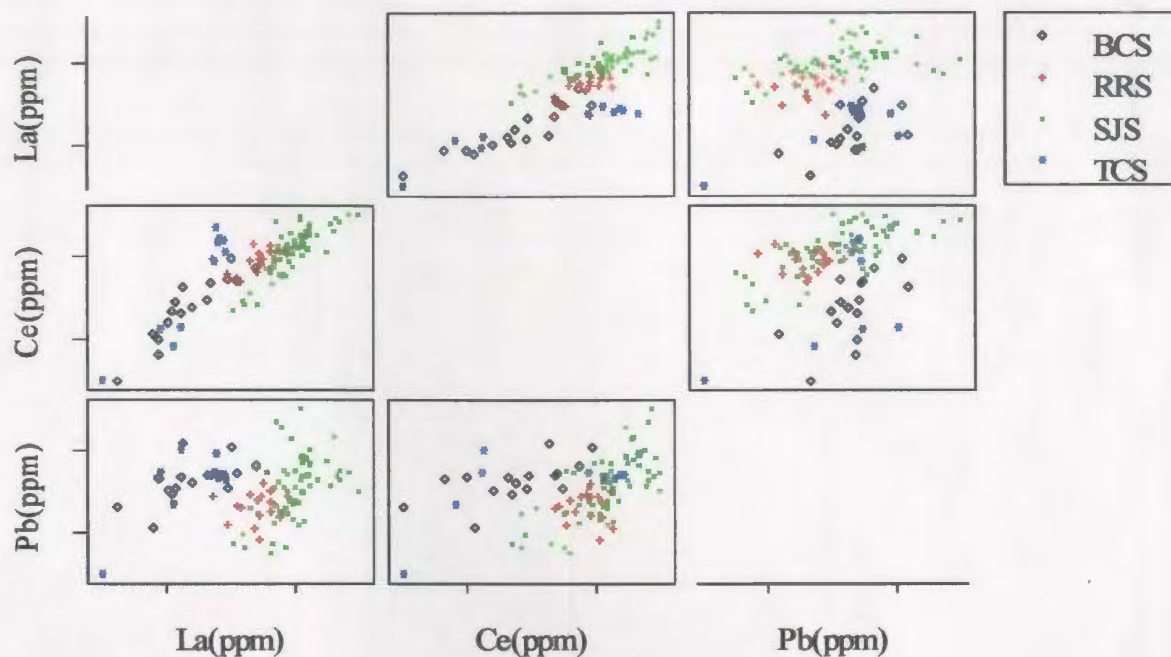
Appendix 6: Scatter plots of log-transformed analyte LA-ICP-MS concentrations in stream pebble Fe-Mn oxide coating samples taken from all four study areas.



Appendix 6: Scatter plots of log-transformed analyte LA-ICP-MS concentrations in stream pebble Fe-Mn oxide coating samples taken from all four study areas.



Appendix 6: Scatter plots of log-transformed analyte LA-ICP-MS concentrations in stream pebble Fe-Mn oxide coating samples taken from all four study areas.



Appendix 6: Scatter plots of log-transformed analyte LA-ICP-MS concentrations in stream pebble Fe-Mn oxide coating samples taken from all four study areas.

